The University of Nottingham
UNITED KINGDOM · CHINA · MALAYSIA

Humphreys, Nicholas David. (1995) High cross wind gust loads on ground vehicles from moving model experiments. PhD thesis, University of Nottingham.

Access from the University of Nottingham repository:
http://eprints.nottingham.ac.uk/11923/1/283406.pdf

Copyright and reuse:

The Nottingham ePrints service makes this work by researchers of the University of Nottingham available open access under the following conditions.

- Copyright and all moral rights to the version of the paper presented here belong to the individual author(s) and/or other copyright owners.
- To the extent reasonable and practicable the material made available in Nottingham ePrints has been checked for eligibility before being made available.
- Copies of full items can be used for personal research or study, educational, or not-for-profit purposes without prior permission or charge provided that the authors, title and full bibliographic details are credited, a hyperlink and/or URL is given for the original metadata page and the content is not changed in any way.
- Quotations or similar reproductions must be sufficiently acknowledged.

Please see our full end user licence at:
http://eprints.nottingham.ac.uk/end_user_agreement.pdf

A note on versions:

The version presented here may differ from the published version or from the version of record. If you wish to cite this item you are advised to consult the publisher's version. Please see the repository url above for details on accessing the published version and note that access may require a subscription.

For more information, please contact eprints@nottingham.ac.uk

High Cross Wind Gust Loads on Ground Vehicles from Moving Model Experiments.

by Nicholas David Humphreys, BSc.

Thesis submitted to the University of Nottingham
for the degree of Doctor of Philosophy.

October 1995.

Abstract.

The environmental wind tunnel at Nottingham University has been extended so that realistic mean hourly atmospheric boundary layers can be generated at sufficient scale to allow aerodynamic tests of sharp edged vehicles to be undertaken.

A moving model rig owned by British Rail Research was installed perpendicular to the flow near the end of the working section. As part of this project an automatic refiring mechanism was developed allowing some 2000 transits of vehicles incorporating an internal balance and data logger to be made across the working section with a realistic mean hourly atmospheric boundary layer present. The quality of the data from the moving model rig was assessed.

Moving model rig tests and static model tests of a 1/50th scale lorry and 1/45th railway container vehicles have been conducted and extreme value forces and moments relevant to the gust time that overturn a vehicle were calculated. These are the first measurements to have been made using a realistic mean hourly ABL and modelling the vehicle's movement. This thesis assesses the usefulness of the normalised extreme force parameter in determining the extreme forces that a full scale moving vehicle experiences.

It was found that the normalised extreme force parameter remains invariant with model time scale for the range of times considered. Further for both the moving model rig tests and the static tests the value of unity that this parameter takes for yaw angles above 30 degrees implies quasi steady behaviour without additional body induced unsteadiness. At lower yaw angles, however, some body induced unsteadiness is evident. These conclusions are compared with predictions from existing numerical models and previous experimental tests.

The measured lift force from the static tests compared with the moving model rig tests at 90 degrees yaw angle, i.e. with the moving model stationary, shows a large difference. This is not understood and two concerns are expressed: the effect of the slot, through which the supports of the moving model travel, beneath the vehicle, may be altering the pressure in this region; or it could be due to a Reynolds number effect caused by the small underbody height above the ground.

Acknowledgements.

The author gratefully acknowledges the continuous support and technical advice of Dr. C.J. Baker as the supervisor of the author and of the work presented in this thesis.

The project was aided significantly by the enthusiasm, expertise and quality of workmanship of many technical staff of Nottingham University. In particular Mr. R. McClelland, Mr. N. Hardy and Mr J. Trigg are gratefully acknowledged.

The staff of the Aerodynamics Unit, British Rail Research are acknowledged for their advice on the rebuilding of the moving model rig and data acquisition and analysis considerations. In particular I would like to thank Mr. R.G. Gawthorpe, Mr. T. Johnson, Mr. D. Harrison, Mr D. Gillot and Mr. F.S. Harris.

The author would like to thank Dr. S.A. Coleman and Dr. N. Cherry, representing BMT Fluid Mechanics Ltd, for their technical support on the application of Wind Engineering methods. Also I would like to thank Dr. S.A. Coleman for his help in the initial stages of this project when previously at Nottingham University.

The rig assembly and data acquisition from which the results shown in this thesis have been computed were supported by SERC, grant GR/F 15388, British Rail Research and BMT Fluid Mechanics Ltd. The railway vehicle container tests were additionally funded by the German State Railways, DB.

Also acknowledged are the contributions from the liaison with the linked project at Cranfield College of Aeronautics, namely Mr R. Cairns and Dr. K. Garry with the technical support of Dr. J.P. Howell, Rover Group Ltd, UK.

Finally, I would like to thank Lorraine Curotto for the many hours spent in the preparation of this thesis and for the continued support that has made the completion of this thesis possible.

Contents.

Notation.

$1/a$	dispersion - used in extreme value analysis.
A	reference area of vehicle.
C	force or moment coefficient.
F	force.
G	gust value.
h	reference height of vehicle.
h_W	height of water measured by manometer.
h_{cm}	lorry model height of centre of mass.
H	reference wind height.
i	dummy label applied to a member of a set.
I	turbulence Intensity.
l	length
${}^{x}L_u$	longitudinal (or streamwise) turbulence length scale.
Mode	mode used for extreme value distribution.
M	moment.
N	number of data.
n	frequency.
p	static pressure.
p_O	total pressure.
t	static temperature.
Re	Reynolds number.
$S(n)$	spectral density.
St	Strouhal number.
$S.D.$	standard deviation (square root of variance)
t	time.
u	streamwise wind speed.
v	vehicle speed.

V	resultant of wind and vehicle speeds.
v	voltage.
X	horizontal non dimensional point of action.
$X(n)$	aerodynamic admittance.
Y	vertical non dimensional point of action.
z	height above ground level.
z_0	surface roughness length (m).
μ	absolute viscosity of air.
ν	kinematic viscosity of air, μ/ρ.
ρ	density of air (unless suffixed otherwise).
σ	standard deviation (root mean square).
ψ	yaw angle.

Subscripts.

A to E	force balance calibration coefficients.
L	lift.
P	pitch.
R	roll.
S	side.
u	streamwise wind velocity.
Y	yaw.
f	full scale
F	force
m	model (as measured in wind tunnel).
w	water
1 to 5	channels 1 to 5.
x, y, z	Cartesian co-ordinates used for the description of the wind.
	x streamwise (+ve in direction of wind), y lateral, z vertical.

Superscripts.

–	mean value.
∧	extreme value.
$F'(t)$	first derivative of force with time.
$u'(t)$	first derivative of wind speed with time.

List of Tables.

List of Figures.

1. Introduction.

Large ground vehicles are at risk from accidents from occasional very high cross winds. In the United Kingdom, hundreds of these vehicles, often moving, have been involved in accidents caused by extreme gusts present during short periods of relatively infrequent high mean wind speeds. For example 371 accidents of this kind happened, and were subsequently reported, within only a few hours on the 25th January, 1990 (Baker and Reynolds (1990)) and the frequency of such events since, in the UK, of this magnitude has been at least once every year to date (1995).

At some exposed sites such as on major span bridges the incidence of high wind speeds is much more common and traffic control is usually applied, consequently reducing the number of accidents. However accurate accident prediction methods are needed in order to set appropriate and not onerous traffic restrictions.

This thesis is concerned with the determination of the extreme gust loads that large ground vehicles, such as high sided articulated lorries and trains moving through a high cross wind, are likely to experience. This information is needed in order to calculate the risk of a vehicle having an accident using either Wind Engineering techniques, for an overturning accident, or sophisticated numerical models specifically developed for ground vehicles. The latter models such effects as vehicle suspension and considers other types of accident, say, due to course deviation.

The type of wind gusts mainly considered in this thesis are those due to the continuous turbulence of the Earth's atmospheric boundary layer and lack of convective currents. Other types of gusts that are important to these large vehicles, but not considered in detail in this thesis, are those due to vehicles passing large objects, e.g. bridge pillars, which in effect cause gusts on vehicles as they pass. In a high cross wind the resultant wind velocity is of a similar magnitude to the vehicle speed and therefore the vehicle experiences relatively high levels of turbulence intensity with a large resultant component perpendicular to the vehicle's direction of motion. This is distinct from the case of vehicles experiencing very common, low cross winds in which the main considerations are vehicle handling and more often passenger comfort criteria rather than safety. A vehicle travelling quickly through a low cross wind experiences a resultant low turbulence flow with only a small cross wind component. The assessment of likely loads on ground vehicles due to low cross winds are not considered in this thesis.

The determination of extreme forces and moments experienced by a ground vehicle moving through a particular environment is an important issue and therefore a common problem for engineers involved in either the design of new bridges and exposed roads as well as the vehicle designers. The accepted practice, to date, has been to conduct extreme value analysis of data obtained from a wind tunnel test of a strain gauged model vehicle in which the mean hourly atmospheric boundary layer (ABL) is modelled. There are three main practical difficulties in the application of such methods for ground vehicles :

1. Modelling both the ABL and the vehicle at the same scale due to the available wind tunnel size for the former and Reynolds number considerations for the latter.

2. Modelling the vehicle movement - not only are the underbody flow and the development of vortices around the vehicle distorted, but from the frame of reference of the vehicle the approaching ABL is skewed; additionally the actual wind conditions seen by the vehicle are a function of both the vehicle speed and the wind conditions.

3. The wind conditions encountered by vehicles vary across a wide range due to the terrain variations.

Whilst these uncertainties may have an effect upon the known mean forces and moments, the effect upon their extreme values, which are means calculated over the short gust periods, could be much greater. Central to the problem is the determination of the model time scale which is used for determining the equivalent full scale gust time period for an atmospheric boundary layer modelled in the wind tunnel. Usually the magnitudes of these extreme values increase dramatically as the gust period decreases.

Due to these difficulties, previous tests have not been undertaken successfully which cover all these criteria. These previous tests fall generally into the following categories:

1. Large scale model wind tunnel tests with the vehicle mounted static in steady flow.

2. Adequate modelling of the ABL, in an environmental wind tunnel, but with a small scale static vehicle mounted on a turntable.

3. Moving model tests, in a wind tunnel, with simple turbulence modelling of inadequate very small lengthscale.

4. Ambitious large scale model or full scale tests, outside, using either the ambient wind conditions or the exhaust from gas turbine - ejector configurations of large area ratio. The former tests generally suffer due to lack of control and knowledge of the ambient conditions at the time of a test run and the latter tests suffer from inadequate high cross wind modelling characterised by extremely small turbulence length scales.

This thesis describes the installation of a moving model rig, owned by British Rail Research, in Nottingham University's environmental wind tunnel perpendicular to the flow direction. The moving model rig was previously installed at Cranfield Institute of Technology and was built specifically for measuring the wind loads on a scale BR Advanced Passenger Train (Baker(1986b)). Static and moving model tests were conducted at Nottingham University including the simulation of a realistic mean hourly atmospheric boundary layer. Side and lift forces and pitching, yawing and rolling moments were measured on scale sharp edged high sided road and rail vehicles. The conventional static tests were conducted with the model mounted on a turntable and further moving model tests were conducted with a simulated 5m high escarpment with and without 3m high wind fences.

The vehicle types tested were a 1/50th scale high sided articulated lorry, figure 1.1, and a 1/45th scale German Railway container mounted, but not fixed, to a railway wagon, figure 1.2. Consideration of the size, bluffness and weight of these vehicles show that these types of ground vehicles are at significant risk from high cross winds. Indeed this is demonstrated by the number of these vehicle types that experience accidents caused by high cross winds ((Baker and Reynolds (1990) and Peters (1992a). Further, these specific vehicle types were chosen because they have been the subject of previous wind tunnel tests and accident risk assessment and therefore there exists a wealth of information for comparison with the tests described in this thesis. These previous tests, conducted by many authors, have used a conventional static mounting arrangement with both steady and turbulence flow simulations using a range of scales and wind tunnels.

The main aim of the work described in this thesis was as follows :

1. Determine the mean forces and moments and the extreme forces that a moving scale high sided bluff vehicle experiences for a few typical situations in a simulated realistic mean hourly atmospheric boundary layer typical of high winds. These would be the first such measurements to have been made.

2. Investigate the effect of the realistic mean hourly ABL on these forces by comparison with previous results of the same vehicle types in tests using low turbulence and turbulence simulations characterised by small length scales.

3. Determine the extreme loads for various model time scales and investigate the use of a normalised extreme force parameter for determining the full scale extreme loads for various vehicle speeds and geographical situations from limited wind tunnel test data.

The work covered by this thesis is structured in the manner described in the following paragraphs.

In order to understand the nature of the wind loads measured in these tests comparisons have been made with numerical models that had previously been developed, that predict in the time, amplitude and frequency domain, high cross wind forces on vehicles. In Chapter 2 these models are discussed and compared with the results from previous experimental tests. Two further sections deal with the results from the same vehicle types as tested in this thesis and also the results of previous tests undertaken by British Rail Research using the moving model rig on different vehicle types.

Chapter 3 discusses the physical principles of the aerodynamic forces on a ground vehicle including a review of bluff body aerodynamics. Further, Chapter 3 includes a review of the currently available knowledge of the atmospheric boundary layer, particularly at small heights and discusses these with respect to moving ground vehicles.

Chapter 4 describes the experimental equipment and in particular the development of the moving model rig and the extension of Nottingham University's environmental wind tunnel in order to accommodate the rig and increase the length of the upstream fetch. The latter was necessary in order to develop an atmospheric boundary layer characterised by large turbulence length scales. The methods used to analyse the results from these tests including Wind Engineering methods, are detailed in Chapter 5. Also

discussed is the interpretation of the mean hourly atmospheric boundary layer simulated in the wind tunnel and its relation to the available wind data recorded at sites in the UK.

The development of the mean hourly atmospheric boundary layer simulation is described in Chapter 6 and the results compared with target values for an open countryside simulation at 1/50th scale.

The static turntable tests are described in Chapter 7 of both vehicle types. Mean and extreme aerodynamic loads, the latter for a range of model time scales, are presented. The results are compared with previous static tests of these vehicle types by other authors. A first series of moving model tests again using both vehicle types are discussed in Chapter 8 in which problems of over prediction of extreme gust forces due to mechanical noise are highlighted. This led to a successful redevelopment of the moving model release mechanism and the mounting of both the live vehicle and the data acquisition equipment.

Chapter 9 describes a second series of moving model tests, using the revised rig, in which the influence of the mechanical noise on both the aerodynamic mean and the extreme loads was investigated. Aerodynamic tests were conducted of the 1/50th scale lorry using the flat ground simulation and also a 5m full scale equivalent high escarpment simulation with and without slatted 3m high wind fences. The mean and extreme aerodynamic loads that the moving model vehicle experiences are determined for these tests. Further, the extreme aerodynamic loads are determined for a range of model time scales and the use of the normalised extreme force parameter assessed. The results of these tests are comprehensively examined and compared to the static tests of Chapter 7 and from tests undertaken by other authors.

Chapter 10 lists the conclusions from the work presented in this thesis.

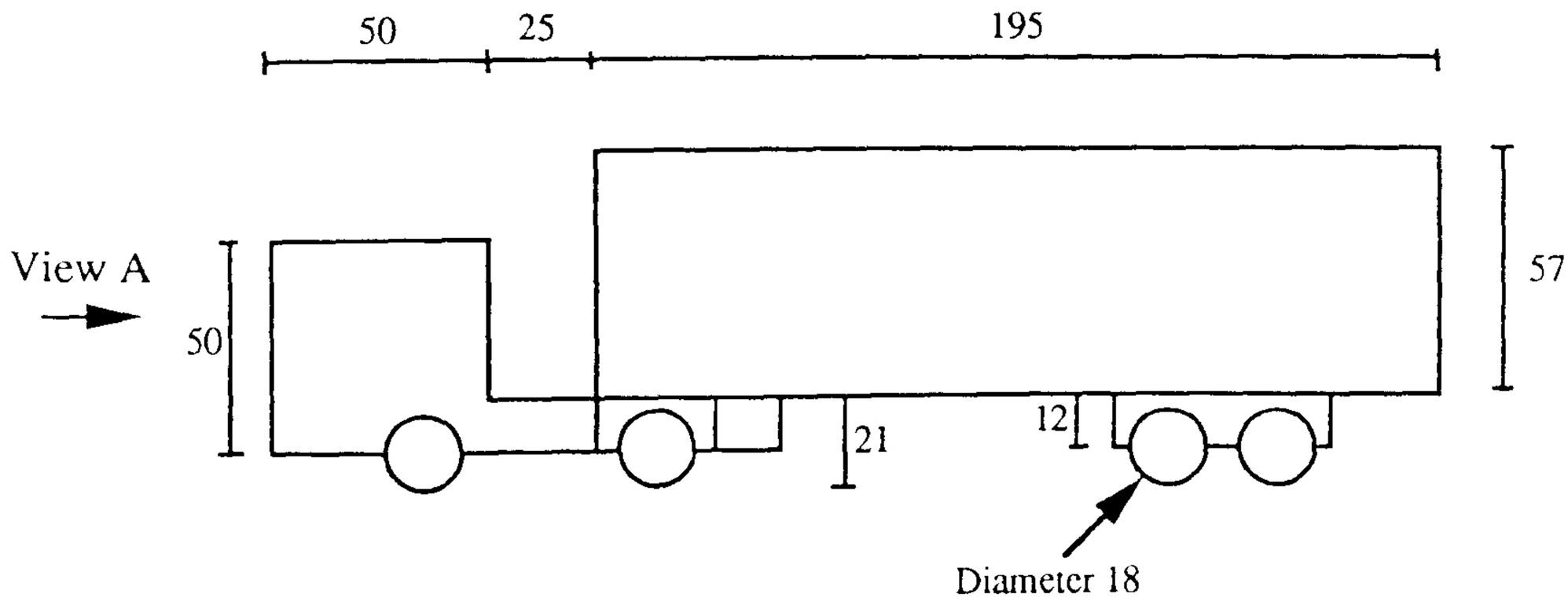

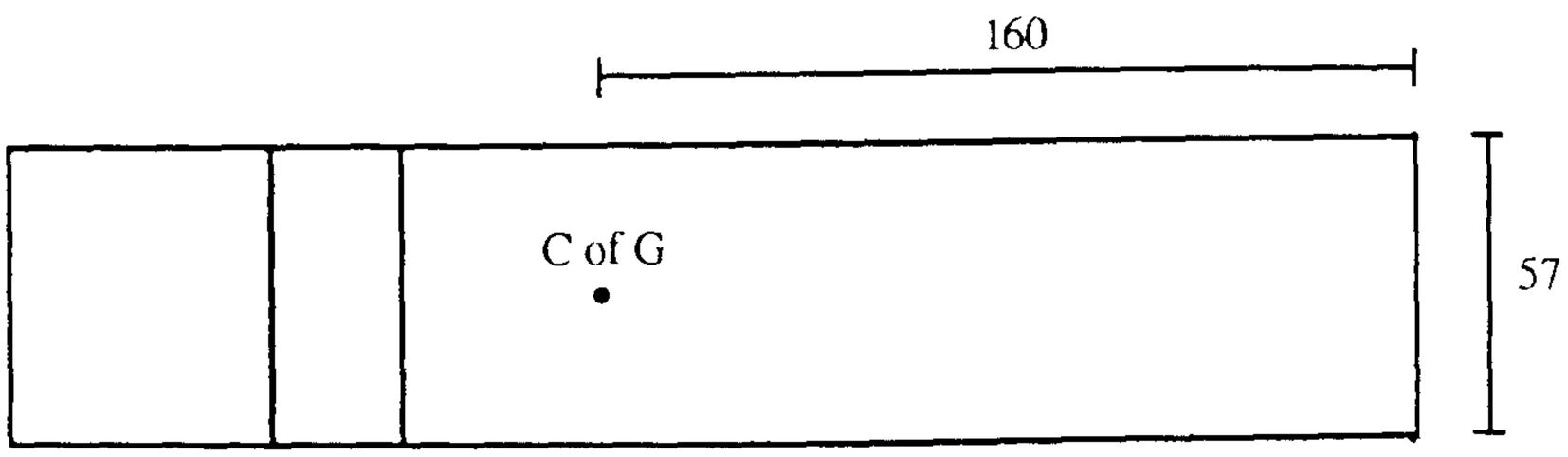

Plan

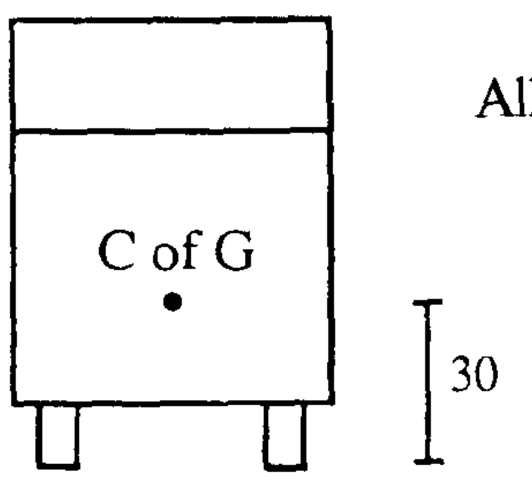

View A

All cab edges are of 5mm radii.

Figure 1.1 $^{1}/_{50}$ th scale high sided articulated lorry model geometry. Dimensions in mm.

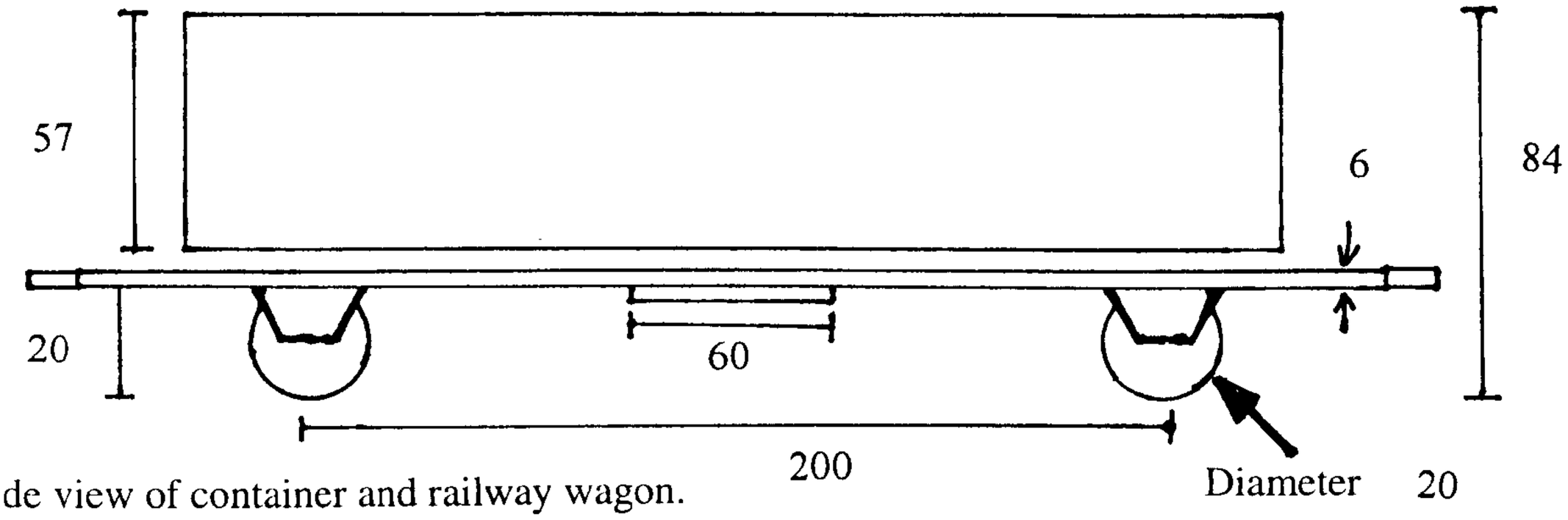

Side view of container and railway wagon.

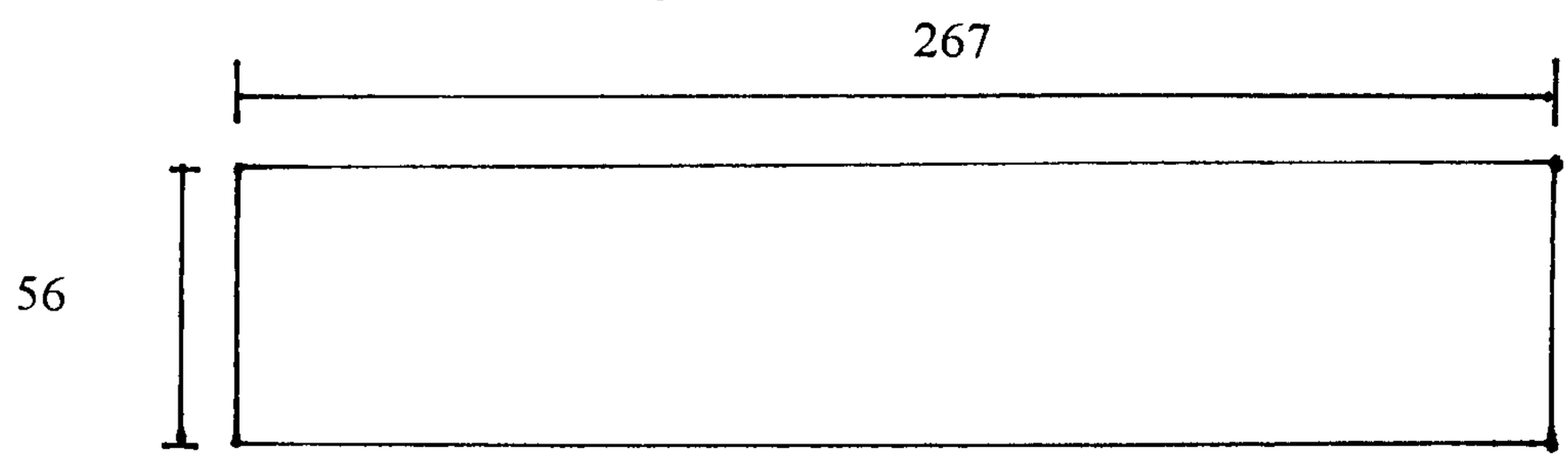

Plan view of container.

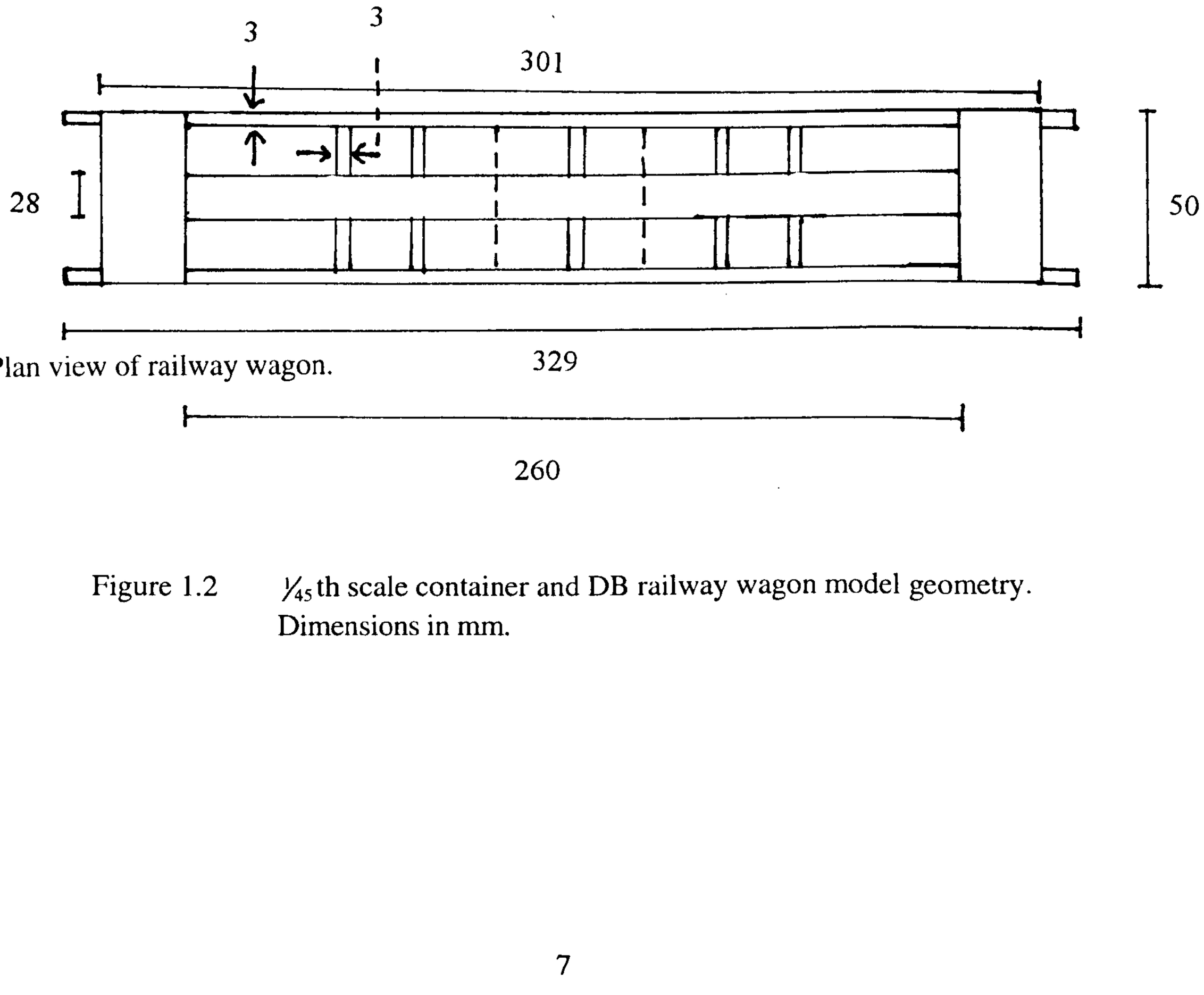

Plan view of railway wagon.

Figure 1.2 $\frac{1}{45}$th scale container and DB railway wagon model geometry. Dimensions in mm.

2. Review of Numerical Models and Experimental Testing Techniques.

This chapter reviews the tests and numerical models undertaken in order to determine the risk of a vehicle accident due to high cross winds. Firstly section 2.1 reviews the numerical methods for analysing the extreme loads on such a vehicle and the methods for evaluating the nature and predicting the risk of a subsequent accident. These prediction methods require knowledge of the aerodynamic force and moments for a specific vehicle present at the extreme wind conditions. Section 2.2 reviews the attempts by many authors to acquire such data using a wide variety of test techniques and further, predictions using these analytical methods are compared with the experimental data.

Central to discussing the gust loads on an object are the use of extreme values. In the context of this work an extreme value is the most likely maximum value for a given observation time of the calculated mean of a parameter over the time period of the gust. It is the convention to calculate extreme values corresponding to an observation time of one hour and this should be assumed throughout this thesis unless stated otherwise. For a ground vehicle, the gust time is taken to be the shortest time which corresponds to a gust that produces a correlated, and therefore, significant force on the vehicle and is usually around 1 to 5 seconds depending on the vehicle's size.

The following definitions are used throughout this thesis.

Referring to figure 2.1, for a vehicle moving at constant speed v, encountering a cross wind of mean wind speed $\overline{u}$, with a direction relative to it φ, the resultant mean wind speed, $\overline{V}$, experienced by the vehicle is given by :

$$\overline{V} = \left(\overline{u}^2 + v^2 + 2\overline{u}v\cos\varphi\right)^{1/2} \qquad 2.1$$

In this chapter the yaw angle ψ, defined to be that between the vehicle's track and the resultant wind direction - see figure 2.1, is used extensively. In a conventional wind tunnel test with the model vehicle mounted static on a turntable the yaw angle is simply that between the direction it is aligned relative to the wind tunnel's centre line as shown in figure 2.2. For a static wind tunnel test this is usually interpreted as a vehicle moving perpendicular to a cross wind and therefore corresponding to a vehicle speed to mean wind speed ratio defined by :

$$\psi = \tan^{-1}\left(\frac{v}{\overline{u}}\right) \qquad 2.2$$

The definition of the resultant extreme wind speed, $\hat{V}$, is given by :

$$\hat{V} = \left(\hat{u}^2 + v^2 + 2\hat{u}v\cos\varphi\right)^{1/2} \qquad 2.3$$

where $\hat{u}$ is the extreme wind velocity. This definition neglects the difference in the lateral turbulence structure compared to the stream wise direction but is used in much of the work reviewed in this thesis and is discussed further in Chapter 3.

The mean and extreme force coefficients, $\overline{C}_F$ and $\hat{C}_F$ respectively, used in this chapter, for a moving ground vehicle, are defined as :

$$\overline{C}_F = \frac{\overline{F}}{\frac{1}{2}\rho A\overline{V}^2} \qquad 2.4$$

$$\hat{C}_F = \frac{\hat{F}}{\frac{1}{2}\rho A\hat{V}^2} \qquad 2.5$$

where $\overline{F}$ and $\hat{F}$ are the corresponding mean and extreme force values on the vehicle of size characterised by its reference area, A and ρ is the density of the ambient air. There is no absolute convention for the vehicle's reference area but usually the frontal area is used. It should be assumed that this convention is used throughout this chapter unless it is stated otherwise. The definitions for the moment coefficients vary, depending upon the assumed point of rotation, and are defined for particular tests.

The sign convention for the force and moment directions adhered to in all the work reviewed in this Chapter is shown in figure 2.3.

2.1 Vehicle high cross wind analysis methods.

This section reviews the methods developed specifically for analysing the effects of high cross winds on ground vehicles and further those for calculating the subsequent accident risk.

The accident prediction methods described here are those of Baker (1986a), Baker (1987), Baker (1988), Baker (1991c) and Baker (1993). Also, reviewed in this section are the methods of analysing unsteady aerodynamic forces on ground vehicles which were developed in Cooper (1984) and Baker (1991b).

Starting with Baker (1986a), this considered three accident criteria, defined as follows :

1. Overturning accidents, when one wheel vertical reaction falls to zero.

2. Side slip accidents, when the lateral deflection exceeds 0.5m.

3. Rotational accidents, when the angular deflection exceeds 0.2 radians.

Treating the vehicle as a rigid body including tyre - road friction but neglecting suspension and driver interaction effects, Baker developed a method for predicting the necessary aerodynamic force needed to cause each of the above accidents. This in turn was related to the oncoming wind and vehicle velocity by use of a set of correlations of the six aerodynamic force and moment coefficients as a function of yaw angle. In the worked example such parametric correlations were derived from the results of a set of low turbulence, static, 1/12th scale wind tunnel tests of a Leyland Atlantean double decker bus conducted at Cranfield Institute of Technology, Garry (1984). One of the limitations of this numerical model was that gusts had to be assumed to be sharp edged, i.e. sudden, so that the yaw angle did not vary as the vehicle entered the gust. Also it was assumed that the above accident criteria must be exceeded in the first 0.5s of entering a gust before the driver had time to apply a necessary corrective action to avoid an accident. By considering various wind and vehicle speeds Baker concluded that an overturning accident was much more likely than the other types for this vehicle type. Baker notes that the experimental data on which this model is calibrated were perhaps not too accurate due to Reynolds number effects observed during flow visualisation checks and that the predicted centre of pressure appeared to be higher than the bus's roof so that doubt was cast particularly on the side force and rolling moment coefficients. However as to be expected for this rear engined vehicle the centre

of pressure was above and in front of the vehicle's centre of gravity. At the time this was the only complete set of data available for a high sided vehicle.

Baker (1988) calibrated the numerical model of Baker (1987) with experimental data from a range of 1/10th scale vehicle types from Stewart (1977). It should be pointed out that data were only available for a yaw angle of 30 degrees and so the correlations for the force coefficients with yaw angle were based on modifying the Atlantean bus data previously used so that it fitted Stewart (1977). Whilst again the calibration of the numerical model was in doubt the results proved interesting. These results, giving the first accident type to be predicted for the lowest accident wind speed for each vehicle type, for a range of vehicle speeds and wind directions are as follows :

1. Cars - for yaw angles less than 45 degrees side slip accidents were predicted with rotation accidents taking over for the larger yaw angles.

2. Coaches - for yaw angles less than 90 degrees overturning accidents were predicted with rotation accidents again taking over at larger yaw angles.

3. Rigid large vans - overturning accidents were predicted for all yaw angles.

4. Articulated tractor trailer combinations - again only overturning was predicted.

Recommendations were produced from these results for operations across exposed road bridges for the various vehicle types. As was the current practice (Seven Bridge, Orwell Bridge) at the time, vehicle speeds were lowered when wind gusts exceeded certain levels and vehicles were stopped altogether at higher values. An important feature of these results was that they indicated that no account should be taken of wind direction, which was against the then current practice of setting limits based wind direction. It should be noted, though, that the predicted accident wind speeds from the numerical model were somewhat higher than those used in practice for traffic control.

Baker (1988) extended the numerical model to include road curvature and camber and also to produce the results in terms of accident risk - the number of hours a year that the accident wind speed is exceeded. Additionally a model of driver interaction during the onset of a gust was included. Further, Baker undertook wind tunnel tests of a high sided lorry specifically for calibrating this numerical model. These tests are described in detail in section 2.2.1.1 but briefly all six mean forces and moments across the yaw angle range were measured on a 1/25th high sided articulated lorry in low turbulence

flow. Again it was found that for the high sided lorry entering a sharp edged gust only overturning accidents were predicted and also, as tentatively suggested in Baker (1987), their likelihood was not a strong function of the actual vehicle speed.

Baker (1991b) reviews various analytic methods which describe the interaction between the wind force on a body in the frequency domain, from the field of Wind Engineering, that are applicable to the prediction of forces on ground vehicles in a high cross wind. Firstly considering the side force fluctuations, and considering the mean and fluctuating forces, $\overline{F}_S$ and $F_S'(t)$, to be due to similar mean and fluctuating components of the wind velocity, $\overline{u}$ and $u'(t)$, i.e. buffeting by the turbulence in the wind, using the factor k_S which is a function of yaw angle and vehicle geometry,

$$\overline{F}_S + F_S'(t) = \tfrac{1}{2}\rho A k_S\left[\overline{u} + u'(t)\right]^2 \qquad 2.6$$

the following expression can be derived:

$$S_S(n) = \frac{4\overline{F}_S^{\,2}}{\overline{u}^2} S_u(n) \qquad 2.7$$

where $S_S(n)$ is the side force spectral density and $S_u(n)$ is the wind velocity spectral density. The expression in equation 2.7 is the quasi-steady case for wind induced bluff body forces. Further Baker notes that a similar equation could be written for the lift force but this may be inappropriate if additional effects are present which are known to exist for bluff bodies, e.g. vortex shedding (section 3.1). A complete description of the forces on bluff body therefore incorporates the aerodynamic admittance function, $X(n)$, and is defined to be, considering the side force :

$$S_S(n) = \left|X_S(n)\right|^2 \left\{\frac{4\overline{F}_S^{\,2}}{\overline{u}^2} S_u(n)\right\} \qquad 2.8$$

A similar expression may be written for the lift force, relating the lift force spectral density to the streamwise wind spectral density.

From experimental test data the aerodynamic admittance can be found, and compared with the quasi - steady expression. Section 2.2 describes these comparisons for the test data under discussion.

Baker (1991b) also reviews the contributions described in Cooper (1984) which are as follows.

Cooper (1984) developed correlations of the mean hourly boundary layer as experienced by a moving vehicle perpendicular to cross wind described in terms of the mean hourly atmospheric boundary layer. Briefly a random-process model was developed culminating in calculations of the following quantities for a range of yaw angles, vehicle speed / wind speed and length of the vehicle / streamwise turbulent lengthscale :

1. The resultant wind velocity spectrum, as experienced by the vehicle was calculated to be translated to higher frequencies as the vehicle's speed increased. The expression calculated, assuming that the lateral turbulence length scales were a factor of 0.42 of the stream wise component.

$$\frac{nS_v(n)}{\sigma_u^2} = \frac{\left(4\left(nL_u/\overline{V}\right)\right)}{\left(1+70.8\left(nL_u/\overline{V}\right)^2\right)^{5/6}}\left\{\frac{\overline{u}}{\overline{V}}+\left[1-\frac{\overline{u}}{\overline{V}}\right]\left[\frac{0.5+94.4\left(nL_u/\overline{V}\right)^2}{1+70.8\left(nL_u/\overline{V}\right)^2}\right]\right\} \qquad 2.9$$

where L_u is the compound turbulence lengthscale and is related to the longitudinal length scale ${}^xL_u$ by :

$$L_u = \left[\frac{\overline{u}}{\overline{V}}+0.353\left(1-\frac{\overline{u}}{\overline{V}}\right)\right]^{1/2} {}^xL_u \qquad 2.10$$

This is considered further in Chapter 3 as part of the review of the required wind tunnel testing conditions for a moving ground vehicle.

2. The side force aerodynamic admittance, for a vehicle of length L and height H was calculated to be of the following form :

$$\left|X_S(n)\right|^2 = f\left(\frac{nL}{\overline{V}}, \frac{v}{\overline{u}}, \frac{H}{L}, \frac{L}{{}^xL_u}\right) \qquad 2.11$$

The results of the side force aerodynamic admittance for the side force using Cooper's theory are shown in figure 2.4 for a vehicle of characteristics L/H = 5.0, in fact similar to the dimensions of the lorry and DB container under discussion in this thesis. The

most noticeable general feature is that the aerodynamic admittance is attenuated at high frequencies which is due to the filtering effect of the vehicle's finite length. At the lower frequencies and for the lower values of $L/^{x}L_u$ the aerodynamic admittance takes the value of unity. This corresponds to the quasi steady situation for gusts which are correlated across the vehicle's length. The frequency at which the attenuation is marked implies the minimum time duration of gusts that give rise to the quasi steady perturbations for gusts correlated across the vehicle. It is seen for all cases considered that, approximately, $Ln/V = 0.1$ and referring to Baker(1991b) this corresponds to gust periods of between 1 and 5 seconds for vehicle lengths varying between 4m (car) and 20m (rail vehicle). Also referring to figure 2.4 it is seen that for high values of $L/^{x}L_u$ that the aerodynamic admittance is less than unity showing the effect of lack of correlation across the vehicle's length.

Comparisons of the calculated side force aerodynamic admittance with experimental data are discussed in detail in section 2.2. for a range of vehicle types but briefly this function compared favourably with the evaluated quantity from the only available experimental data at the time, the 1/5th scale moving model Advanced Passenger Train data of Cooper (1981).

3. It was shown that for speeds of over 40m/s significant excitation of the vehicle's suspension may occur with the turbulence intensity increasing approximately with the square of the speed of the cross wind.

Baker (1991b), also Baker and Robinson (1988), extends these methods further into the amplitude and time domains so that comparisons can be made with the model of Baker (1988).

1. In the amplitude domain the relationship between the extreme force and mean force values that are usually of interest and the aerodynamic admittance calculated using Cooper's theory are developed using the methods of Greenway (1979). Considering the side force case in which the extreme value is formed from a gust time, t seconds, in an observation period of T seconds, the ratio of the extreme to mean values are given as :

$$\frac{\hat{u}}{\overline{u}} = 1 + \frac{\sigma_{ut}}{\overline{u}}\left[2\ln(\nu_u T\right]^{1/2}, \qquad \frac{\hat{F}_S}{\overline{F}_S} = 1 + \frac{\sigma_{St}}{\overline{F}}\left[2\ln(\nu_S T\right]^{1/2} \qquad 2.12$$

where σ_{ut} and σ_{St} are the root mean square values of the ensemble of values formed over the gust times, that is filtering the data at a frequency of 1/t :

$$\sigma_{ut} = \left\{ \int_0^\infty S_u(n) \left(\frac{\sin(n\pi t)}{n\pi t} \right)^2 dn \right\}^{1/2}, \qquad \sigma_{St} = \left\{ \int_0^\infty S_S(n) \left(\frac{\sin(n\pi t)}{n\pi t} \right)^2 dn \right\}^{1/2} \qquad 2.13$$

also the zero crossing rates, ν_u and ν_S, of these ensemble of values are given by

$$\nu_u = \left\{ \int_0^\infty S_u(n) n^2 \left(\frac{\sin(n\pi t)}{n\pi t} \right)^2 dn \right\}^{1/2} \Big/ \sigma_{ut}$$

$$\nu_S = \left\{ \int_0^\infty S_S(n) n^2 \left(\frac{\sin(n\pi t)}{n\pi t} \right)^2 dn \right\}^{1/2} \Big/ \sigma_{St} \qquad 2.14$$

It is seen therefore that the extreme wind and extreme side force values can be found from knowledge of the aerodynamic admittance and the mean values. Baker (1991b) undertakes this calculation for an observation time of one hour for the case of a typical large commercial vehicle which is characterised by L/H = 5.0 and a gust time of around 3 seconds. The resulting extreme side force and extreme wind velocities were presented in the following ways:

a) Figure 2.5 shows the unsteady side force parameter calculated for various mean wind and vehicle speeds plotted against the ratio of the vehicle's length to the streamwise turbulence lengthscale, where,

$$\text{unsteady side force parameter} = \left(\frac{\hat{F}_s}{\overline{F}_s} - 1 \right) \Big/ \left(\frac{\hat{u}}{\overline{u}} - 1 \right) \qquad 2.15$$

It is seen that for small values of $L/^xL_u$, this parameter takes a value approaching 2.0. This value of 2.0 can be shown to be that corresponding to the quasi steady case by repeating the calculation using a value of unity for the aerodynamic admittance across all frequencies. (Baker and Robinson (1988)). The results show that in order to replicate gusts of more than 3s on full scale vehicles which behave in a quasi - steady

manner, then wind tunnel testing needs to be conducted with the streamwise turbulence length scale much larger than the vehicle's length.

b) Figure 2.6 shows the results in terms of the normalised extreme side force parameter, where,

$$\text{normalised extreme side force parameter} = \hat{C}_s / \overline{C}_s \qquad 2.16$$

Figure 2.6 shows that the normalised extreme side force parameter was relatively insensitive to values of $L / {}^{x}L_u$ taking values between 0.85 and 0.95. Further this suggests that measurements of this parameter in the wind tunnel may not be too sensitive to the streamwise turbulence length scale modelled.

2. In the time domain, Baker developed Cooper's theory with and without corrections for vehicle length effects. In Cooper's theory it was assumed that the vehicle length must be much shorter than the streamwise turbulence lengthscale. Remembering that the intention was to compare this with work done earlier (Baker 1986a, 1987 and 1988) and that if a model of a vehicle entering a sharp edged gust was required, this assumption in Cooper's theory would not hold. As a vehicle enters a sharp edged gust the wind velocity will change over the vehicle's length. The developed model appeared to give physically realistic results when compared to the previous analysis and further large pitching and yawing transients were predicted.

Baker (1991c), using the various numerical methods, considers other effects that are due to the interaction of the aerodynamic forces and the vehicle system :

1. Suspension excitation using the method of Cooper (1987), a development of Cooper (1984).

2. Overturning using the methods of Baker (1987), Baker (1988) and Cooper (1987).

3. Course deviation using the methods of Baker (1987 and Baker (1988).

Also included in this paper are worked examples of calculating the accident risk using the methods of ESDU (1982) and Cook (1985).

In Baker (1993), a version of the same numerical model of Baker (1988) was developed considering the forces and wind in the frequency domain, using the methods developed from Wind Engineering in Cooper (1984), Baker (1991b) and Baker (1991c). The force on the vehicles, described in the frequency domain as the force spectral density, was calculated from the streamwise wind velocity spectral density and the side force aerodynamic admittance. This latter quantity is determined from either a theoretical model or experimental data. A vehicle transfer function was then defined and used to predict the behaviour of the vehicle in terms vehicle displacement. The method is compared with the earlier time domain program of Baker (1988) by specifying a sharp edged gust as the wind spectrum. It was found that the method gave good agreement for cases where the centrifugal forces present in the calculation were not important, that is for cars and vans. One of the other main conclusions was that the method predicted similar results over a wide range of vehicle speeds as noted in Baker (1988). One of the shortcomings of this model, also present in the original time domain model, but more clearly seen in the frequency domain model, was that the only unsteady effect modelled was that of buffeting in the defined side force aerodynamic admittance. Therefore the possible interesting lateral oscillation due to vortex shedding was not included. Baker notes, though, that the mean lift forces are much smaller than the side force and therefore this omission may not be too important on the overall predictions. Comparisons of the aerodynamic admittance for the side and lift forces from experimental tests with Cooper's quasi - steady predictions are shown in section 2.2.

Finally it should be mentioned that established methods are available in the field of Wind Engineering in order to determine the extreme values that relate to the full scale case for a given geographical site and observation time, for either the wind velocity or the force on a static structure from wind tunnel experiments. Chapter 5 describes these methods. If the prime objective is the overturning of a ground vehicle, neglecting other effects, e.g. suspension or driver interaction, then these methods may be used directly. Noting that the numerical models of Baker, described in this section, predict overturning as the most likely for large high sided vehicles, these methods may be adequate for the vehicles being studied in this thesis.

2.2 Experimental techniques.

This section describes the results from experimental tests conducted in order to determine the forces and moments on large high sided vehicles in high cross winds. The first two sections deal specifically with tests that this work may be considered a direct development and are as follows. Section 2.2.1. describes the results of tests that have used the same vehicle model or a scale replica as used for tests described in this thesis and therefore direct comparisons with the results of this thesis can be made. Section 2.2.2 deals with a comprehensive set of tests undertaken of the BR Advanced Passenger Train during the late 1970s and early 1980s. These tests are considered important to the work of this thesis as they include tests of the British Rail Research moving model rig when sited at the College of Aeronautics, Cranfield Institute of Technology (now Cranfield University) for which the rig was specifically designed. Static conventional tests were undertaken at the same facility. Together with the results obtained from other scale tests of this vehicle using another moving model rig and other static wind tunnel turbulence simulations, these form a comprehensive set of data. In section 2.2.3, the results of tests, by many researchers, of other high sided vehicles are described. Finally section 2.2.4 reviews the results obtained from some of the exotic facilities that have been used for the low yaw angle low cross wind tests as these offer alternative approaches to the moving model rig used in this thesis.

Further discussion of the results described in this chapter are included in Chapters 7, 8 and 9 where comparisons are made with the results of this thesis.

2.2.1 Vehicle types tested and described in this thesis.

2.2.1.1 The high sided lorry.

Baker (1988) measured all forces and moments of a 1/25th scale replica of the 1/50th scale lorry in low turbulence using a 6 component internal force balance. This was done with the vehicle mounted statically in British Rail Research's 1.4m by 1.1m wind tunnel situated at the Derby College of Higher Education. (This is now Derby University and the tunnel has been resited at the main London Road, Derby site of British Rail Research). The Reynolds number of these tests, based on the vehicle's height, were 2.4 $\times 10^5$ with a blockage of 6% at high yaw angles. The results of these were corrected using the MIRA blockage correction, ESDU (1980).

Coleman (1990) measured forces and moments on the same 1/50th scale lorry, using the 5 component force balance described in this thesis, both in low turbulence flow and with grid generated turbulence of longitudinal length scale 0.15m and a turbulence intensity of 10.5%. The Reynolds numbers of these tests were $0.85 - 0.88 \times 10^5$ based on the vehicle's height. The model was mounted on a bridge deck representing a 3 lane motorway including a realistic 1.5 degree of road camber (sloping down towards the oncoming wind) in Nottingham University's 2.4m by 1.2m environmental wind tunnel. The results of this work were also described further in Coleman and Baker (1989, 1992 and 1994).

The mean force and moment coefficients, using the vehicle's frontal area for the reference area, of Baker (1988) and Coleman (1990) are shown in figure 2.7. The mean side force coefficients show a general agreement regardless of the test conditions and turbulence simulation with the turbulence simulation producing slightly higher values at all yaw angles. Similarly the mean lift force coefficients show a similar trend but this time showing a large variation. Considering the results of Coleman (1990), the results of the tests using the turbulence simulation show much larger values than the low turbulence results at yaw angles above 30 degrees, indicating the sensitivity of the lift force to the turbulence simulation. However the low turbulence tests of Baker (1988) show even greater values at yaw angles above 30 degrees being much larger than the similarly low turbulence results of Coleman (1990) and indeed larger than the results of Coleman (1990) using the turbulence simulation. In Coleman (1990) this was attributed to the difference in vehicle camber, as the tests in Coleman (1990) were with the vehicle tilting towards the wind at a camber of 1.5 degrees compared to the flat ground simulation of Baker (1988). Coleman (1990) further undertook some tests at zero camber and it was found that the magnitude of the lift force coefficients were up to 80% of the values measured in Baker (1988). The rest of the difference between the lift coefficients, Coleman (1990) suggests, may be due to adverse camber in the mounting of the larger vehicle, Baker (1988). It was noted (Baker (1989)) that the mounting supports of this larger vehicle were prone to bending during wind tunnel tests.

The moment coefficients for the lorry are defined to be about the vehicle's centre of gravity with the lorry's height used for the reference height and are therefore formed from the pure side and lift forces as well as the moments measured about the balance centre. Briefly, the mean moment coefficients showed that points of actions were aft and above the lorry's centre of gravity (in fact similar to the characteristics of an aeroplane - due to the large area of the tail fin). The differences between the mean moment coefficients of Baker (1988) and Coleman (1990) were large and only in part

explained by the differences in the side and lift force contributions. Further investigation showed that these moments were very sensitive to small differences in the points of action of the side and lift forces which show themselves as real differences in the moments measured about the balance centre. These differences in the actual moments about the centre of gravity of the vehicle are therefore probably real and indicate the sensitivity of these parameters to small differences in the experimental simulation.

The normalised extreme side and lift coefficients and the unsteady side and lift force parameters calculated in Coleman (1990) for yaw angles of 60 and 90 degrees are shown in table 2.1. These were obtained using the time scaling based upon the vehicle scale and the ratio of the mean wind speed in the tunnel to a value of 30m/s, this being taken to be the full scale mean hourly extreme wind speed. The sampling period of 0.12s was taken to be equivalent to a 3 second gust. The effect of the factor of 8 in the mismatch the simulated turbulence longitudinal length scale between that in the wind tunnel and that of the Earth's atmospheric boundary layer was not included. It should be pointed out that the wind tunnel suffered from a low frequency oscillation thus giving two peaks in the wind velocity spectrum. The longitudinal length scale quoted in Coleman (1990) was based upon a best fit von Karman spectrum to the turbulence distribution created by the grid ignoring the sharper peak corresponding to a much larger lengthscale. This low frequency oscillation, however, may be more important when considering the correlation of the gusts across the vehicle and so little correction to the time scale may be needed for the effect of turbulence length scale mismatch.

Referring to table 2.1 it is seen that the normalised extreme side force parameter takes a value of unity and the unsteady side force parameter takes a value just under 2.0 indicating quasi steady unsteadiness according to Cooper's theory. However similar comparisons for the extreme lift force values indicate that only for a yaw angle of 60 degrees is this true and that these values are much higher for the experiments at a yaw angle of 90 degrees, indicating that some extra unsteady force is present. Coleman (1990) investigated this further by examining the force measurements in the frequency domain. One of the main effects noted, for the yaw angle of 90 degrees only, was that the lift force spectrum was dominated by a peak at around 35Hz which corresponded to a Strouhal number similar to that expected for vortex shedding in the wake of a square cylinder (Vickery (1966)), see Chapter 3. This explains the departure from Cooper's quasi steady theory noted in the examination of the unsteady lift force parameters at this yaw angle. The aerodynamic admittance function for the lift and side forces at yaw angles of 30 and 90 degrees, shown in figures 2.8 and 2.9, demonstrate

this effect. It is seen that the aerodynamic admittance derived from the experimental tests agree with Cooper's theory, bearing in mind the experimental errors, except for the lift force aerodynamic admittance case at the yaw angle of 90 degrees. This had values greater than unity at some frequencies, in the spectrum, demonstrating the departure from the quasi steady state.

Included in Coleman (1990) were tests in which various slatted wind fences were fitted to the bridge deck, shielding the lorry to some extent. These had a dramatic effect in reducing the mean force and moment coefficients and the normalised extreme forces were also reduced a little. (These results are presented in Chapter 9 and compared with the results the tests described in this thesis). It was noted from wind velocity and vehicle force spectral measurements that the effect of the slatted wind fences was to reduce the low frequency energy, due to the breaking up of the lateral correlation and increasing the high frequency energy across the range corresponding to the vehicle's suspension modes. Coleman included calculations of the accident risk for the various fences and compared the results with the numerical model of Baker (1991c); see section 3.3. These were also published in Coleman and Baker (1992).

Coleman (1990) also undertook mean and unsteady static pressure measurements on the surface of the vehicle and flow visualisation tests in order to investigate the flow mechanisms that give rise to these effects. Due to the comprehensive nature of the tests Coleman was able to relate the results both to other experimental work in the general field of bluff body aerodynamics and also to the numerical models described in section 2.1. Coleman (1990) develops a comprehensive description of the flow field around the vehicle and the mechanisms causing the macroscopically recorded forces and moments for both turbulent and smooth oncoming flow.

2.2.1.2. The DB railway container.

These tests concern forces and moments of containers loaded on railway wagons but not attached to them. The main objective was to find the maximum rolling moment about the lee bottom corner of the container, about which it may be caused to rotate, due to the resultant of the vehicle's motion and an extreme wind gust. The reference area and height for these vehicles were defined to be the container's frontal area and the container's width respectively with the container's length being used for the characteristic length in the Reynolds number definition. The rolling moment coefficient was defined to be about the lee bottom corner the container. The mean value was formed from the contributions of the mean side and lift forces and the rolling moment

measured about the balance centre. The extreme rolling moment was formed from extreme value analysis of the ensemble of rolling moments, each corresponding to a equivalent full scale 3 second gust, formed from the simultaneously measured side and lift forces and the rolling moment.

Peters (1989) describes mean value measurements of all 6 forces and moments on static 1/3rd scale railway container vehicles in the low turbulence using the 6m by 6m DNW facility (German - Dutch wind tunnel). The container and wagons tested were modelled on 3 (full scale dimensions) types; a 40 foot (12.2m) long container, 2.6m by 2.5m in section with and without 0.7m high side fences fitted to the truck and a similar 20 foot long container without side fences. Note that only the 40 foot container versions were used in the tests described in this thesis. These tests at DNW were conducted at high Reynolds numbers of between 13.9 and 30.9 $\times 10^6$ but had a very large blockage of 6% at high yaw angles but no correction appears to be have applied. In Peters (1992) these results are compared with further 1/7th scale low turbulence tests of the same vehicle using the 5.8m by 3.9m FKFS wind tunnel. (Forschungs-institut fur Kraftfahrzeugwesen und Fahrzeugmotoren, Stuttgart). Again the blockage was fairly high at 3% and no correction appears to have been applied. The Reynolds numbers of these tests varied between 5.4×10^6 and 8.7×10^6, a little lower than the DNW tests.

Kronke and Sockel (1992) describes the mean and extreme force and rolling moment measurements of a statically mounted 1/75th scale railway vehicle with the 20 foot long container already described. This was chosen as the tests of Peters (1989) indicated that these were most at risk. Three different atmospheric boundary layer simulations using a 2m by 2m wind tunnel at MTI Arsenal, Vienna, with an available fetch of 8m, for boundary layer growth, before the 3m test length. One of the ABL simulations had no roughness blocks and therefore corresponded to a very smooth flow of turbulence intensity 5% and the results were similar to the previous low turbulence tests of Peters (1989 and 1992). The other two ABL simulations had a similar longitudinal integral length scale of 0.3m which is approximately half the full scale value at these model scales. The longitudinal turbulence intensities for these cases were 15% and 22% at a reference height of 0.05m, corresponding to a full scale value of 3.75m, near to the height of the roof of the vehicles. The area blockage of the rests was very small at 0.16% but so was the Reynolds number of 2.5×10^4. A rather simple extreme value analysis of the results was conducted, based on the 99% fractile of the results gathered, using data filtered at 10Hz with the extreme values calculated for an equivalent full scale value of 3s using the resultant train - wind speed as the velocity scale and including the mismatch in integral longitudinal length scale (in the manner described in

Chapter 3 of this thesis). This was done for a comprehensive set of train and wind speeds. The accident criterion used here was that of the extreme rolling moment of a container should not exceed the value needed to lift the container at the windward side when it is empty. The results were then reinterpreted giving the maximum allowable train speed as a function of wind speed and turbulence intensity.

Figures 2.10 and 2.11 show comparisons of the mean side and lift force coefficients for the 40 foot container mounted on a wagon fitted with side fences, from Kronke and Sockel (1992). The trends shown are representative of the tests with side fences and those using the model equivalent 20 foot container. Generally the mean side force coefficients agree with some possible systematic Reynolds number effect in the low turbulence results. The comparisons of the lift force coefficients show large variations. The low turbulence tests of Peters (1989) and (1992) show a systematic Reynolds number effect with the results of Kronke and Sockel (1992) being consistent with this.

From Kronke and Sockel (1992) the mean and the extreme normalised lee bottom corner container rolling moment coefficients from the equivalent 20 foot tests for the three simulated atmospheric boundary layer are shown in figure 2.12 and 2.13. These show results broadly similar to the results for the lorry tests described in section 2.4.1, a value of around 1.0 or less for the high yaw angles but a larger value is indicated for the lower yawing angles. However there seemed to be a trend of larger values with increasing roughness of the fetch and hence turbulence intensity at the reference height. The calculated maximum allowable train speed was found to be very much reduced for the higher turbulence simulations.

These results are described further in Chapter 7 and compared with the results of the tests described in this thesis.

2.2.2 The BR Advanced Passenger Train.

The determination of accident risk for the BR Advanced Passenger Train (APT) was pursued vigorously by British Rail Research due to the low weight of these vehicles, made possible by its monocoque aluminium construction. Further, the leading and trailing coaches of the prototype and the intended (never built, as the project was scrapped by the UK Government) service types were unpowered passenger vehicles with a similar weight to the inner passenger vehicles. These vehicles, as well as the inner carriages, were therefore at risk from the wind. (The electric power cars of these trains were to be positioned, unusually, in the centre of the train). Unless stated, all

results described in this review concern the leading vehicle of the APT as this was identified to be at greater risk of overturning (Cooper(1977)). Figure 2.14 shows the leading vehicle of the service version, APT-S, although it should be noted that the profile of the initially built gas turbine powered leading vehicle of the experimental, APT-E, and the prototype, APT-P, were similar with only detail changes.

The initial tests used conventional low speed wind tunnel tests. The first series were of the initial experimental vehicle, APT-E and were 1/24th scale (Rigby (1973)) at yaw angles of 40 degrees and 90 degrees and 1/5th (Cooper(1977)) for yaw angles up to 30 degrees. More model tests were undertaken of the very similar APT-P or APT-S and, unless stated otherwise, for the yaw angle range of 0 to 90 degrees. For the APT-P these were 1/5th scale (Cooper(1978)) and 1/25th scale (yaw of 0 to 40 degrees tested, Cooper(1982)), plus for the APT-S, 1/50th scale (Baker(1981a)) and 1/35th (Baker(1983a)). The side and lift force coefficients and lee rail rolling moment coefficients were calculated and the agreement is good with the range of Reynolds numbers, based on vehicle height, ranging from 1.5×10^5 to 16×10^5 and are shown in figure 2.15. These comparisons were also described in Baker and Gawthorpe (1983).

The first series of moving model tests were conducted on an outdoor test track nearly 1km in length and a height of 1m at the Proof and Experimental Establishment at Pendine, Wales. (Cooper (1979). The 1/5th scale model of the APT-P built from Kevlar was tested. This scale being chosen as it gave a match equivalent to a full scale rural mean hourly ABL based on the longitudinal turbulence length scale of around 7m measured from available wind data measured at the site at the model scale reference height.

Due to the lack of control of the atmospheric conditions at the track height and vibration of the model travelling along the track, a large variation was found in the results but these dynamic tests always gave mean side and lift forces less than the static tests of Cooper (1978). However analysis of the side force aerodynamic admittance function was conducted and found to agree with the quasi unsteady theory of Cooper (1984), see figure 2.16. Cooper however points out that there was a large standard error (S.D./mean) of 38% in the measured data and therefore much more reliable data is required to test the theory.

After the analysis of the Pendine tests it was decided to design and build a high specification moving model rig for use with 1/50th scale APT-S models to be installed perpendicular and crossing the College of Aeronautics' 2.4m × 1.2m environmental

wind tunnel at Cranfield Institute of Technology in which a mean hourly atmospheric boundary layer was modelled (Johnson (1981)). This rig was the one now installed at Nottingham University and described in Chapter 4 of this thesis. The rig, principally designed by R.K. Cooper, was developed by means of building a short prototype track section (Harrison (1982)). The aim was to ensure that any mechanical noise present in the measured signal would be at a sufficiently high frequency that it could be removed by analogue filtering. Tests were conducted, between November 1980 and February 1981, with the live vehicle taking each of the carriage positions, using both a flat ground and an embankment simulation - with and without slatted fences. Further static tests were conducted with the vehicles mounted on a turntable - using the same ABL. (Baker (1981a) and Baker (1986b)). Tests were conducted corresponding to the full yaw angle range.

Typical time histories of the measured and filtered side and lift forces and all the three moments for a typical set of flat ground and embankment simulation using the moving model rig are shown in figures 2.17 and 2.18. It is noticed, particularly for the lift and pitch measurements, that for the embankment simulation aerodynamic equilibrium was not reached with these values still increasing as the vehicle reaches the end of the test section in the wind tunnel. This however was thought to be due to the non uniformity of the flow across the working section gap in the tunnel, all round the working section, to allow the vehicle and the data acquisition cord to pass, and that the embankment aided the non uniformity of an already diverging flow. The presence of the slot for the model supports to pass was also a concern and is discussed further in Chapter 4. Generally the operation of the rig was successful and provided high quality data from which the mechanical noise, present only above 50Hz, could be removed. However the interpretation of the ensemble of mean forces and moment coefficients averaged over each run was difficult due to the inadequate modelling of the mean hourly atmospheric boundary layer which was characterised by a longitudinal length scale some eight times too small. In Baker (1986b) the results are interpreted as an ensemble of means, each corresponding to approximately a 3 second gust without any integral length scale correction but instead interpreting the atmospheric boundary layer generated as a gust simulation. In terms of the longitudinal length scale interpretation this was reasonable but the lateral correlation of the gusts was not considered. The Reynolds number, based on the vehicle's height was quite low, taking the value of 6×10^4, and whilst this was of concern for these well rounded vehicles, specific Reynolds number tests did not show too much variation probably due to the turbulence present in the flow - see Chapter 3.

Next to be shown, from Baker (1981a), Baker (1986b) and Baker (1991a), are the mean side and lift forces and the calculated lee rail rolling moments from the ensemble of runs for these various tests. Figure 2.19 compares the level ground moving, the embankment moving and the equivalent flat ground static tests, using the simulated ABL, for the leading vehicle. It is seen that for the level ground simulation moving tests, the side force coefficient decreases, the lift force increases and the lee rail rolling moment remains similar when compared with the static tests. Further, comparing the moving embankment tests with the moving level ground tests showed that the side force and lee rail rolling moment coefficients tended to increase for the embankment simulation whilst the lift force coefficient remained similar.

Due to the poor mean hourly atmospheric boundary layer simulation at Cranfield, a further static tests series was conducted of the 1/50th scale APT-S in Oxford University's environmental wind tunnel with a conventional mean hourly ABL with a relatively large turbulence length scale of $L / {}^{x}L_{u} = 0.9$ and are described in Baker 1983b. The Reynolds number, based on the vehicle's height for these tests was 5×10^{4}, very similar to the Cranfield tests. Figure 2.20 shows these results compared to the static Cranfield tests with $L / {}^{x}L_{u} = 3.8$ for the ABL modelled and an average of the much earlier steady flow tests, figure 2.15, of this vehicle. It is seen that, compared to the steady flow results, the longer turbulence length scale simulation tended to increase the values of all the coefficients whilst the short length scale simulation tended to decrease the coefficients.

Robinson (1988) investigated the effect of turbulence length scale further by numerical modelling and wind tunnel tests using various grid turbulence simulations on a 1/50th scale idealised train shape, I.T., similar though to the APT's profile. The tests were conducted in Nottingham University's environmental wind tunnel and, as to be expected using the grid turbulence, the ratio of the vehicle's length to the longitudinal turbulence length scale was less than unity varying from $L/{}^{x}L_{u}(H) = 3.2$ to 6.3. The results however showed the same trend as the APT tests in turbulent flow compared to the steady flow results. Robinson further developed a numerical model that could reproduce a similar trend but not the absolute magnitudes.

2.2.3 High cross wind tests of other high sided vehicles.

Stewart (1977) undertook tests using a moving model rig of a range of 1/10th scale commercial vehicles with a sheared wind velocity profile present. The limitations of the tests, in terms of high cross wind conditions, were that the test condition corresponded

to a single yaw angle of 30 degrees and that the turbulence length scale modelled corresponded to ${}^{x}L_{u}$ =0.15m, a factor of thirty too small. However all the moments as well as side and lift forces were measured. Mean coefficients were produced from the data that corresponded to steady state conditions after the initial transient of the vehicle entering the gust. The results for the articulated lorry agreed reasonably well with the tests of Baker (1988), see figure 2.7, considering the large differences in test condition. The largest differences being for the lift and rolling moment where Stewart's data predicted much lower values. The effect of rounding of the vehicle edges was also investigated and the results showed a large reduction of the side and lift force coefficients with rounding but that the yawing moment tended to increase.

Garry and Cooper (1986) took static and 'moving' wind tunnel tests in steady flow of a range of commercial vehicles. The 'moving' tests were undertaken with the models rotating on a turntable at low and high rotation rates in an attempt to simulate the change of direction of the resultant wind as the vehicle encounters a gust. The quantities measured were side and drag force and yawing moment and interpreted from these were the phase lag of these quantities for different yaw rates. Of significance were the conclusions that showed that there existed significant phase lag even at the lowest turntable rotation speeds indicating that the forces on the vehicle do not respond in a quasi - steady manner to the wind fluctuations even at low frequency. However the magnitudes of the coefficients determined appeared to be independent of the yawing rate.

Comperthwaite (1986) conducted conventional static low turbulence wind tunnel tests of a variety of tractor trailer combinations but for yaw angles only up to 20 degrees. However all six forces and moments were measured and the results were in reasonable agreement with Baker (1988). The effect of rounding of the vehicle corners was also investigated.

Howell (1986) undertook static wind tunnel and moving model results for a short magnetically levitated (mag-lev) vehicle with a simple short turbulence lengthscale simulation. The results showed that the side and lift force coefficients for the moving tests were both lower than the static tests. The side force results therefore agree with the results of the British Rail Research APT tests at Cranfield, see section 2.3, but the lift force coefficients show the opposite trend.

Tzeremopoulos (1981) and Coleman (1990) describe the results of measuring the forces and moments on each vehicle of a very common British Rail two car multiple

unit train of similar geometries with curved roofs and blunt noses at the front and rear. The tests of Tzeremopoulos were at 1/25th scale and of a Reynolds number of 2.5×10^5 based on the vehicle's height, in British Rail Research's wind tunnel, already described in section 2.1, using steady flow. Coleman (1990) describes tests of 1/50th scale vehicles tested in the smooth and grid turbulence flow at identical conditions to the lorry tests described in detail in section 2.2. The Reynolds number of these tests were somewhat lower at around 0.8×10^5 based on the vehicle's height. In Coleman (1990) it was pointed out, that for the high yaw angle tests, that the separation line positions were not stable and exhibited large variations with change of geometries indicating a Reynolds number effect. However at the low yaw angles the results from all 3 simulations agreed reasonably well.

2.2.4 Other cross wind test facilities.

Bearman and Mullarkey (1994) describe results from a novel facility in which drag, side force and yawing moments were measured of various 1/8th scale car shapes in which an unsteady wind has been produced using a pair of oscillating aerofoils situated upstream of the model. Tests were limited to yaw angles up to 20 degrees. Spectral analysis of the longitudinal wind velocity showed that it had a spectrum of corresponding to a realistically sized turbulence length scale that a moving vehicle of the scale tested in the tunnel would encounter, with length scales ranging from 2 to 20 times the vehicle's length. The advantage of this facility is that the tunnel need only be quite short and that large vehicle scales may be tested and hence realistic Reynolds numbers obtained. In these tests the working section of the tunnel was 0.91m × 0.91m and had a length of 4.5m. A Reynolds number of 4.5×10^5 based on the vehicle length was obtained and the tunnel blockage was 1.1% based on the model frontal area. The short comings were that the oscillating aerofoils needed to be driven in resonance due to both the power available to drive them and the inertia of the system. The unsteady wind therefore consists of sinusoidal transverse gusts superimposed on a mean flow and therefore does not have the stochastic nature of a conventionally grown boundary layer. Tests were also conducted with the vehicle in steady flow and in turbulence using conventional grid methods, the latter though, as expected from such a facility, produced length scales very much less than the vehicle's length and with a characteristic turbulence lower than the Earth's ABL at small heights above the ground.

From these tests, for these various gust simulations, the aerodynamic admittance functions were calculated for the side force and yawing moment data and compared with predictions form quasi - steady theory, described in section 2.1. It was found that

these aerodynamic admittance functions calculated for these scale car tests showed no significant amplification above the quasi - steady prediction, i.e. values above unity. Further the values of the aerodynamic admittance calculated for the lower frequency gusts were less and therefore in general agreement with Garry and Cooper (1986) for the lower frequency gusts. Therefore the phase lag of side force and yawing moment as a vehicle encounters a gust seem to produce a lower values for the magnitude of these quantities than predicted by quasi - steady theory.

Finally described in the two remaining paragraphs are the progress on two facilities currently under development :

Cairns (1994) undertook the design and building of a new moving model test rig situated on the site of the original British Rail Research's moving model test rig, perpendicular to the 2.4m × 1.2m environmental wind tunnel at Cranfield University. This facility was specifically for the testing of 1/5th scale cars, at speeds up to 20m/s, and only the velocity profile of the wind can be modelled with the turbulence scales being too small for a high cross wind simulation. To date there have been many problems concerning the rigidity of the track and the model vehicle, its mounting and the measurement system (Garry et al (1994)) due to the large scale of the vehicles being tested. The advantage of this facility is the large Reynolds numbers that can be simulated although questions regarding acquiring aerodynamic equilibrium of the measured forces and moments in the short number of vehicle lengths of the working section width, at this scale, remain unresolved.

Dominy and Docton (1994) describes the results of a scale prototype of a proposed rig in which the cross wind is simulated by a cross jet at 30 degrees to the flow form the main jet simulating the vehicle's direction of travel. The static vehicle is situated at the intersection of the jets and by controlling the jets independently, transient effects, such as vehicles suddenly experiencing gusts due to passing a bridge pillar, can be simulated. To date the prototype has been used to simulate a vehicle entering a sharp edged gust. The positioning of the second jet means that this rig will be limited in producing resultant gust yaw angles of up to 30 degrees. The advantage of this rig is that it is relatively easy to operate, it can produce transient gusts at reasonably large Reynolds numbers, based on car length, of the order 6×10^5.

Table 2.1 Full scale equivalent 3 second gust hourly extreme values for 1/50th scale high sided lorry in grid turbulence from Coleman (1990).

Yaw angle	60 degrees	90 degrees
Normalised extreme side force parameter.	0.98	0.97
Unsteady side force parameter.	1.91	1.85
Normalised extreme lift force parameter.	1.15	1.53
Unsteady lift force parameter.	3.75	7.62

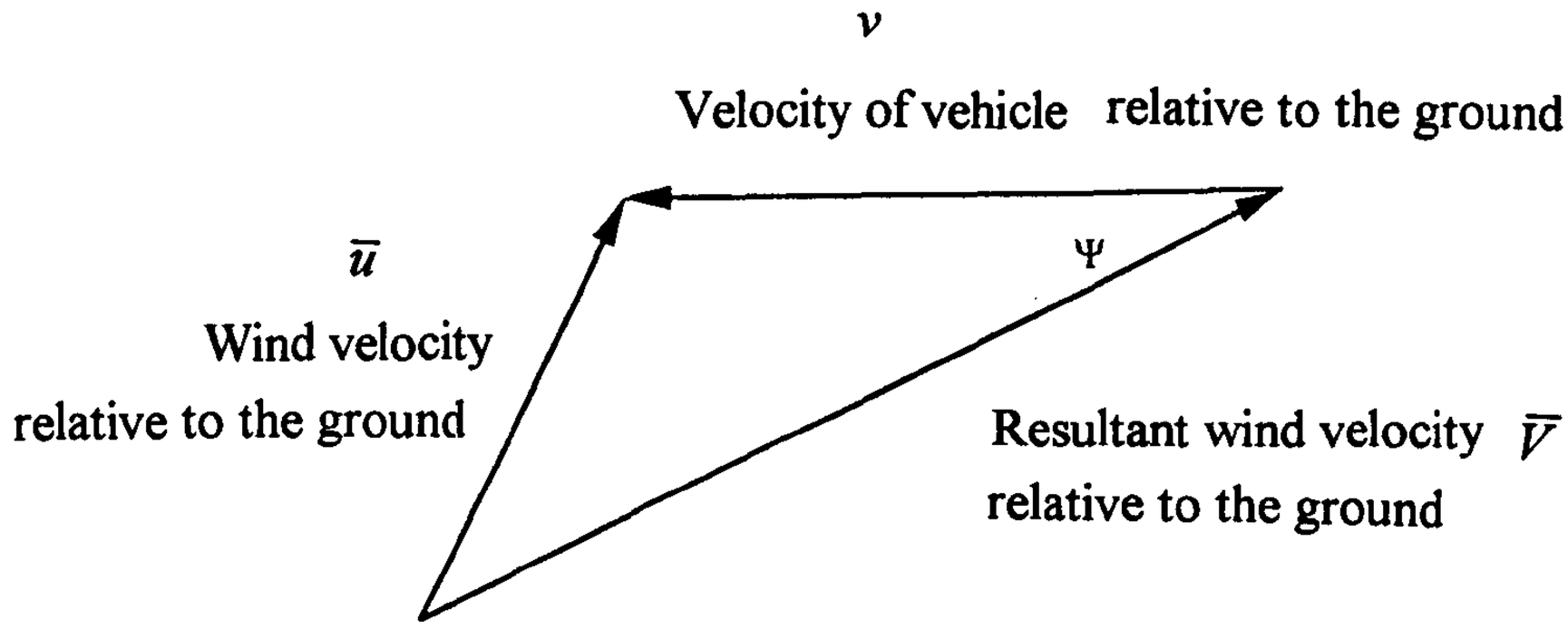

Figure 2.1 Definition of yaw angle Ψ, for a cross wind acting on a moving vehicle.

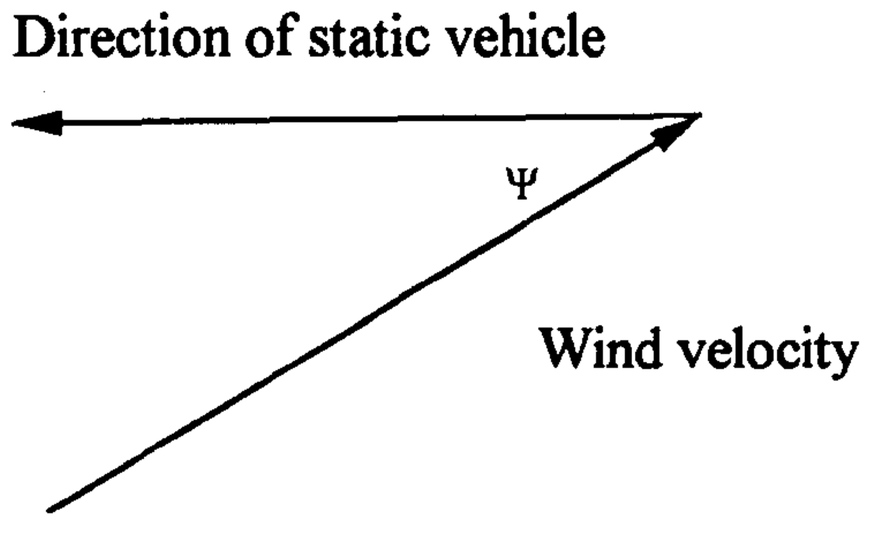

Figure 2.2 Definition of yaw angle Ψ, for a static wind tunnel simulation.

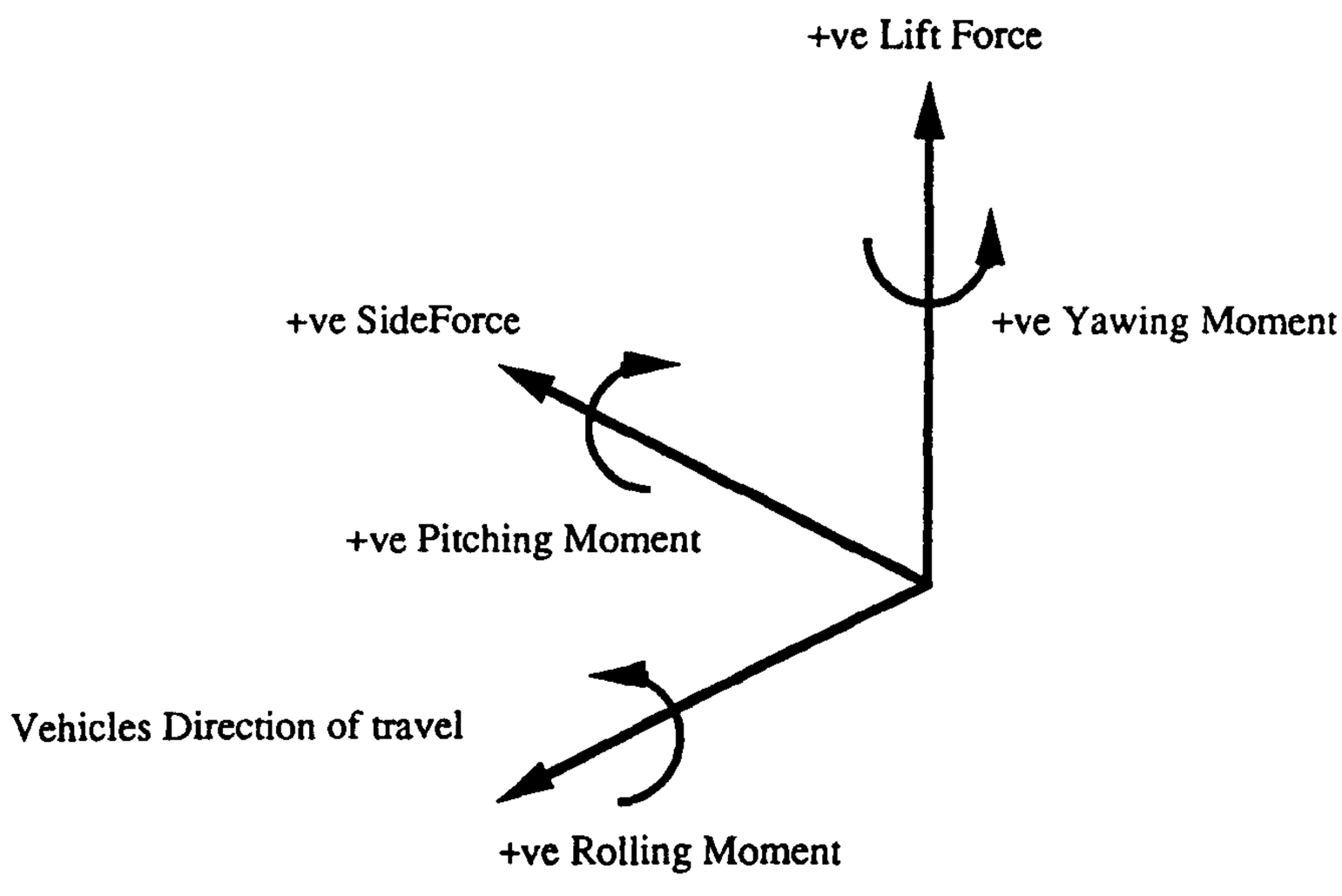

Figure 2.3 Relative force and moment sign convention.

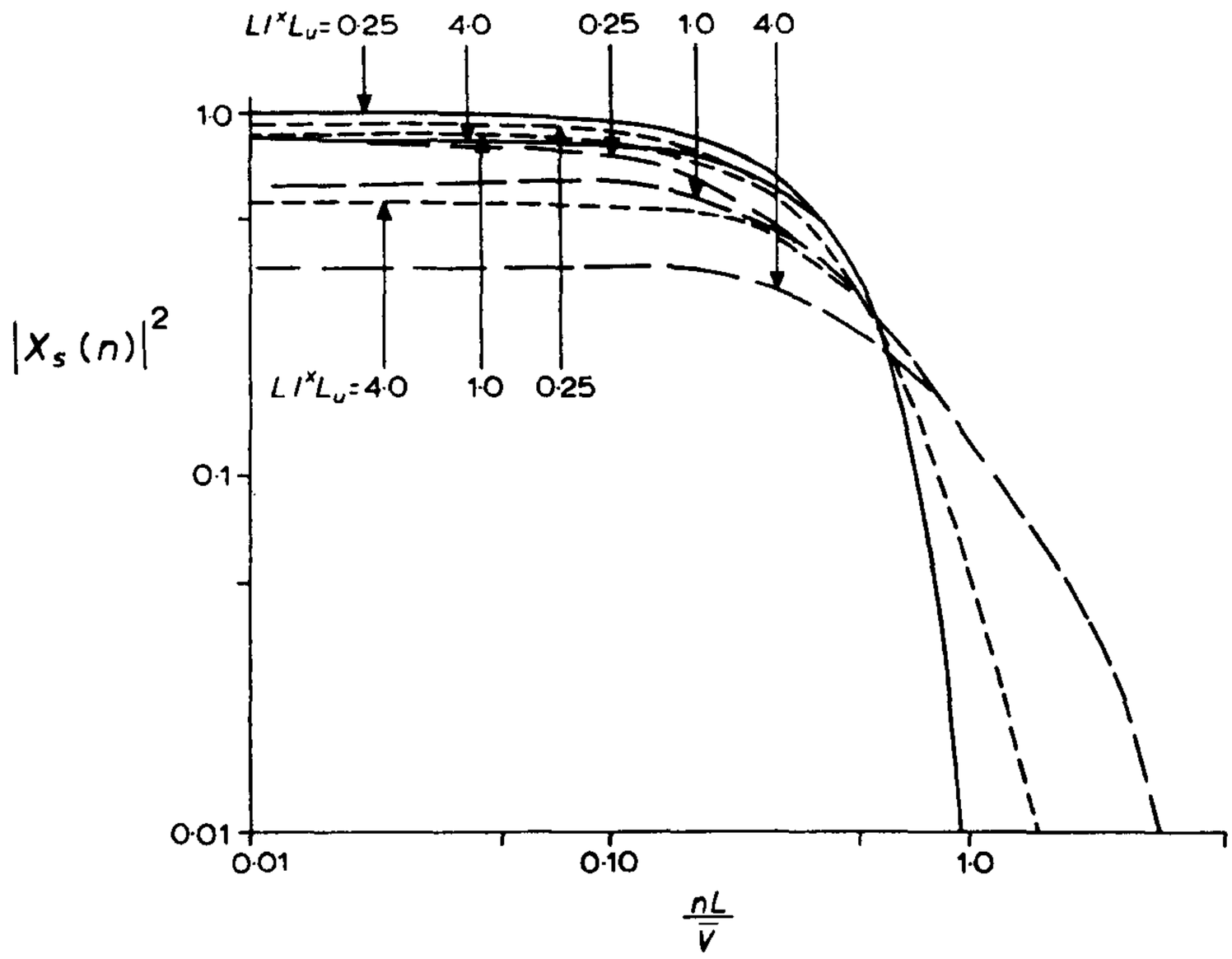

From Baker (1991b)

Figure 2.4 Aerodynamic admittance for side force using Cooper's method (L/H = 5.0).

——, $v/\bar{u} = 4{\cdot}0$; - - -, $v/\bar{u} = 1{\cdot}0$; ——, $v/\bar{u} = 0{\cdot}0$.

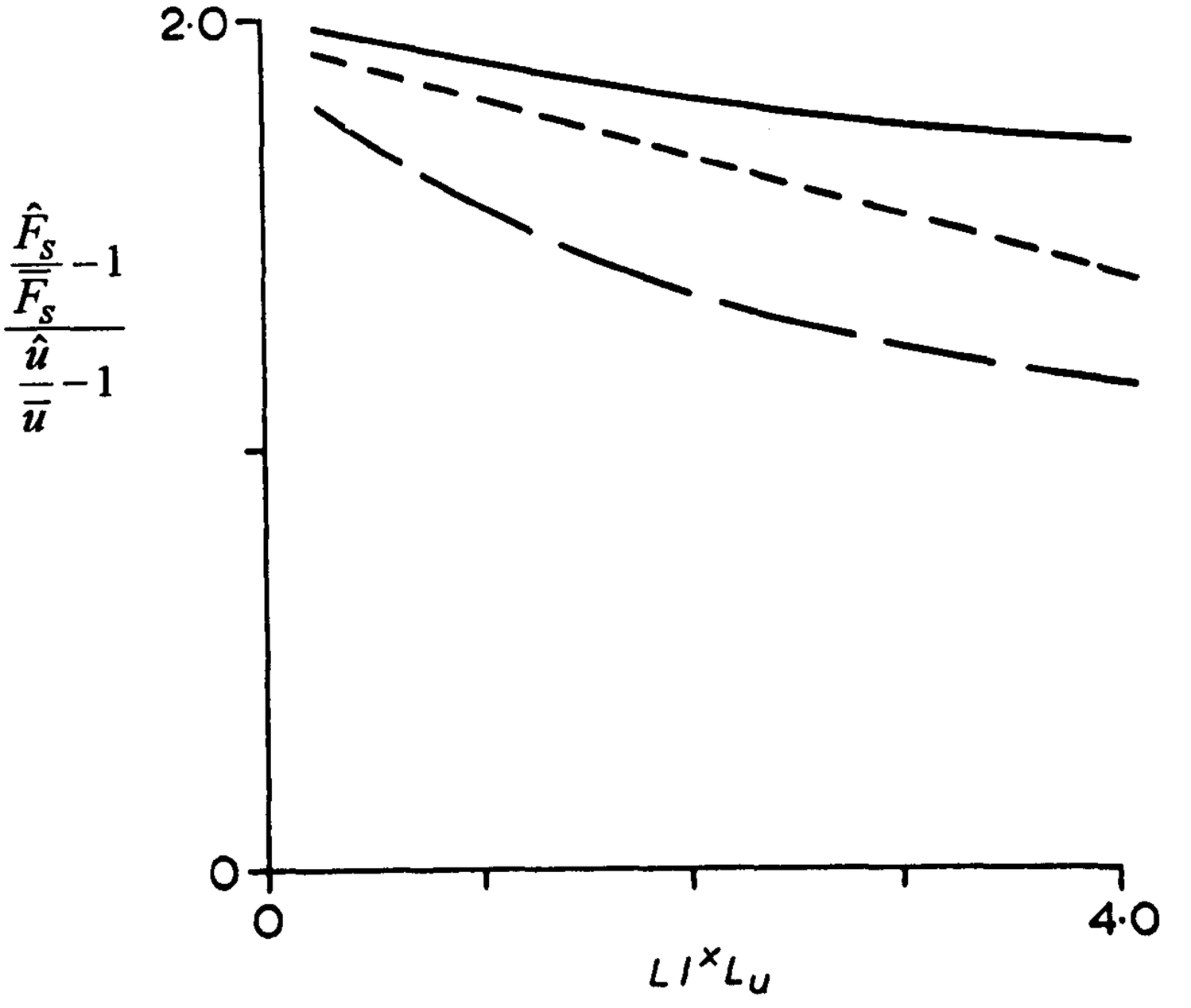

From Baker (1991b)

Figure 2.5 $(\hat{F}_s/\bar{F}_s - 1)/(\hat{u}/\bar{u} - 1)$ against $L/^xL_u$; $L/H = 5{\cdot}0$; $\sigma_u/\bar{u} = 0{\cdot}2$; $\bar{V}T/L = 5000$, $\bar{V}\tau/L = 5$.

——, $v/\bar{u} = 4{\cdot}0$; - - -, $v/\bar{u} = 1{\cdot}0$; ——, $v/\bar{u} = 0{\cdot}0$.

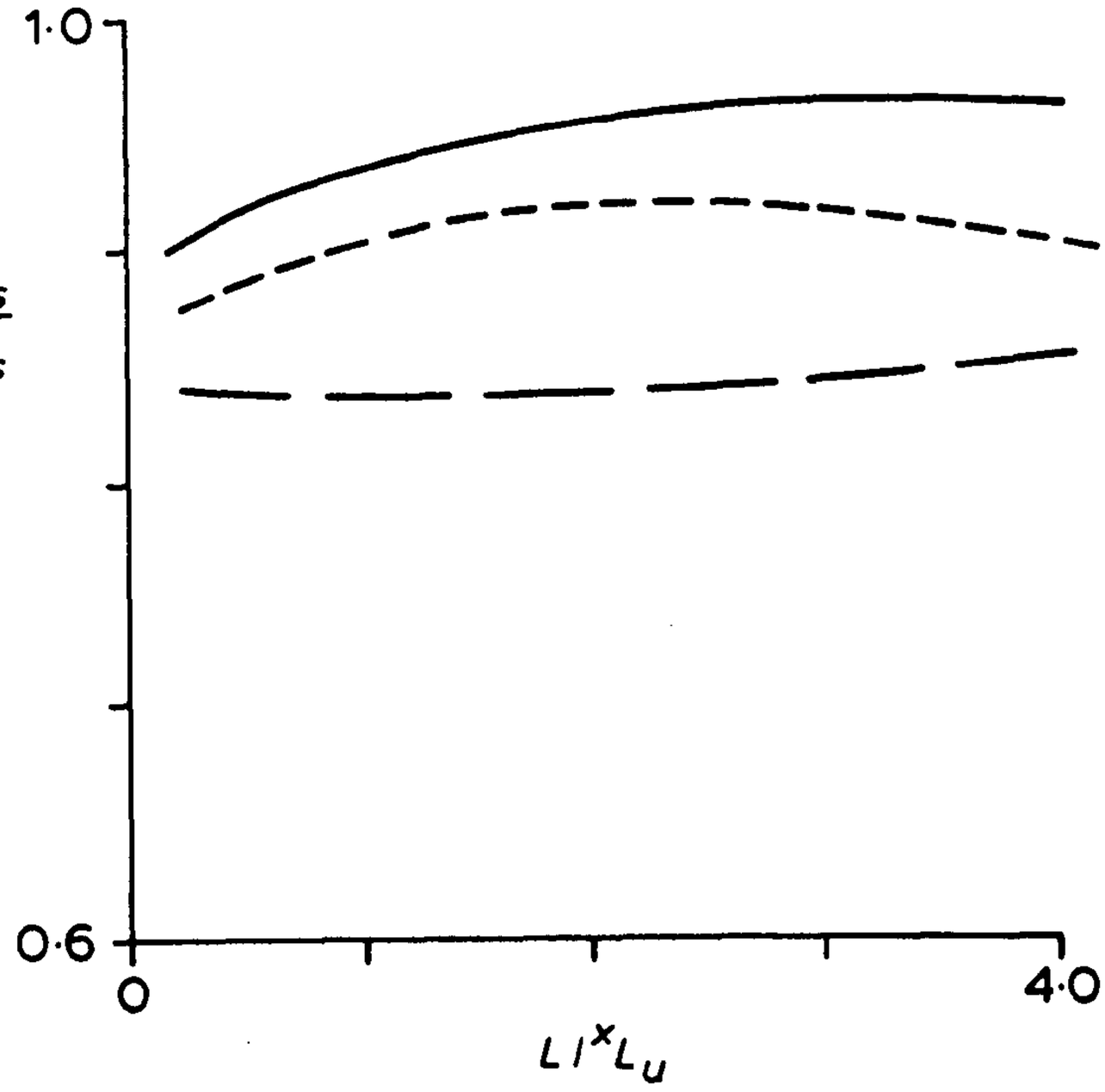

From Baker (1991b)

Figure 2.6 $\hat{C}_s/\bar{C}_s$ against $L/^xL_u$; $L/H = 5{\cdot}0$; $\sigma_u/\bar{u} = 0{\cdot}2$; $\bar{V}T/L = 5000$, $\bar{V}\tau/L = 5$.

— $v/\bar{u} = 4{\cdot}0$, -- $v/\bar{u} = 1{\cdot}0$, ——, $v/\bar{u} = 0{\cdot}0$.

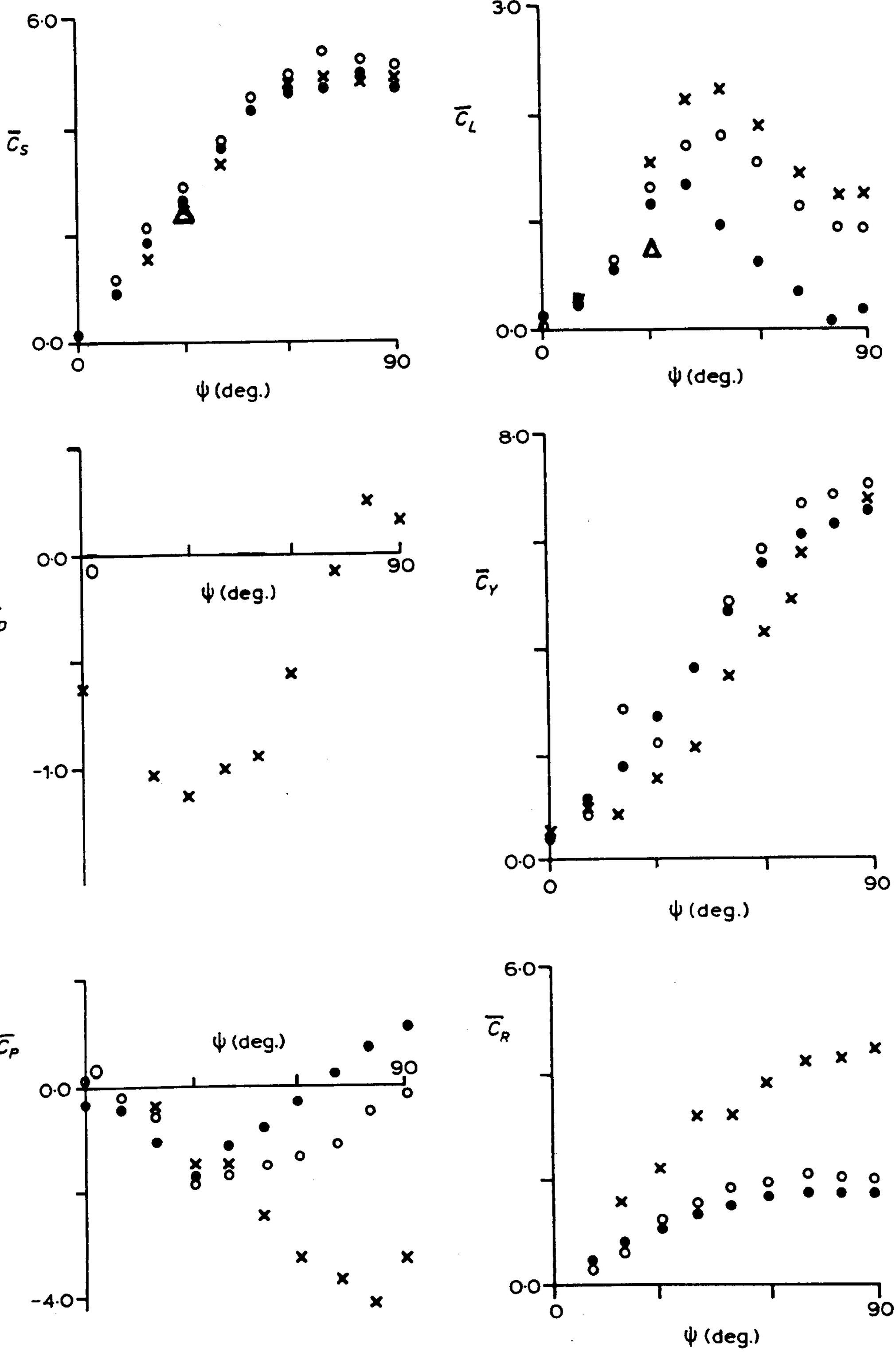

Figure 2.7 Articulated lorry force and moment coefficient data (static tests).

×, 1/25 th scale, low turbulence, $\bar{V}H/\nu = 2{\cdot}4 \times 10^5$;

●, 1/50 th scale, low turbulence, $\bar{V}H/\nu = 0{\cdot}85 \times 10^5$;

o, 1/50 th scale, $L/^xL_u(H) = 2{\cdot}06$, $\sigma_{u0}(H)/\bar{u}(H) = 0{\cdot}106$, $\bar{V}H/\nu = 0{\cdot}88 \times 10^5$.

From Baker (1991b)

Also Δ, 1/10th scale, similar articulated lorry model from Stewart (1977). Moving model tests, $L/^xL_u = 10$, $\bar{V}H/\nu = 6.9 \times 10^5$.

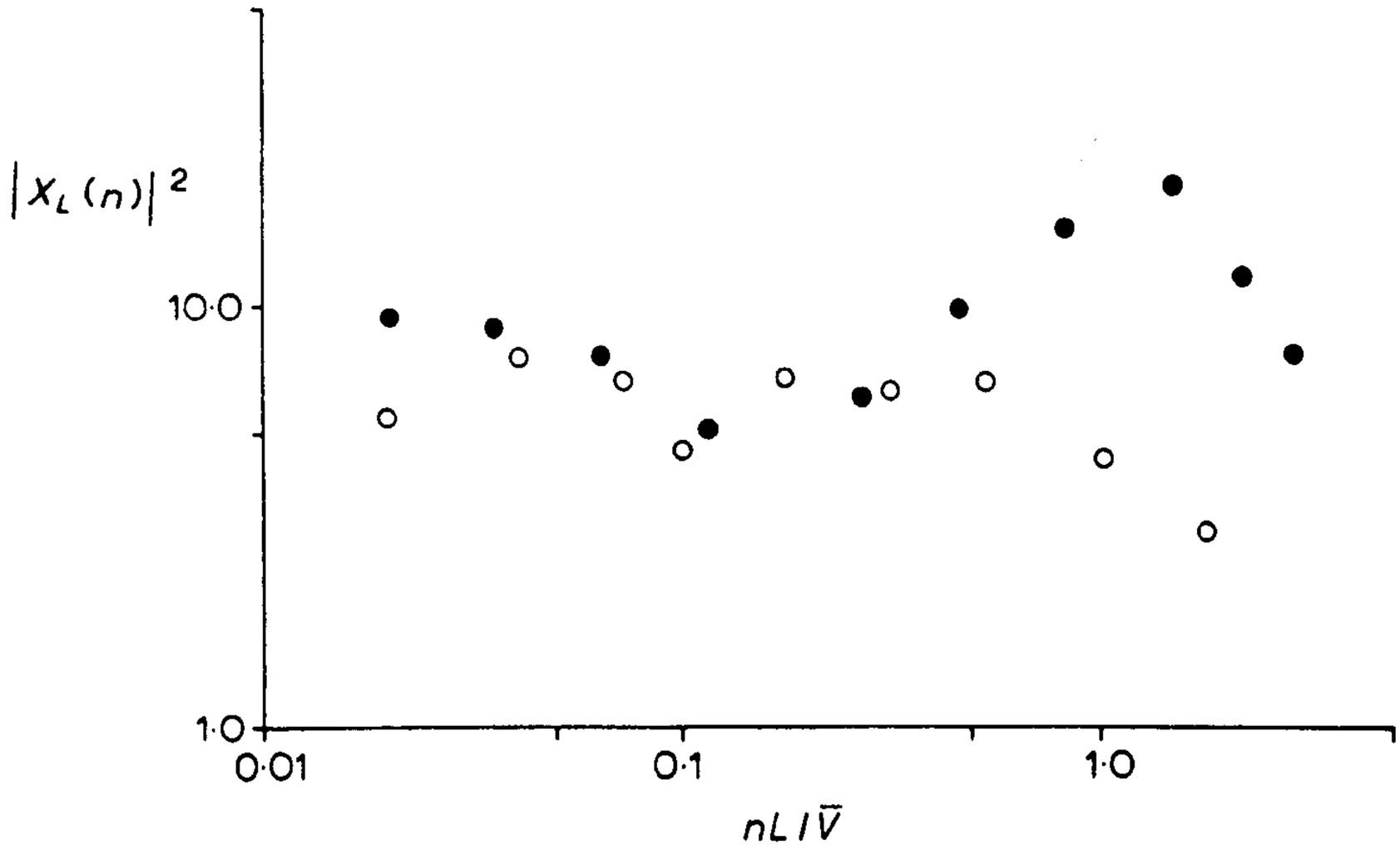

From Baker (1991b)

Figure 2.8 Experimental data for $|X_L(n)|^2$; 1/50 th scale Lorry , Coleman (1990)

●, $L/^xL_u = 2{\cdot}0,\ v/\bar{u} = 0{\cdot}0,\ L/H = 5{\cdot}0,\ \psi = 90°$;

o, $L/^xL_u = 1{\cdot}0,\ v/\bar{u} = 0{\cdot}0,\ L/H = 2{\cdot}5,\ \psi = 30°$.

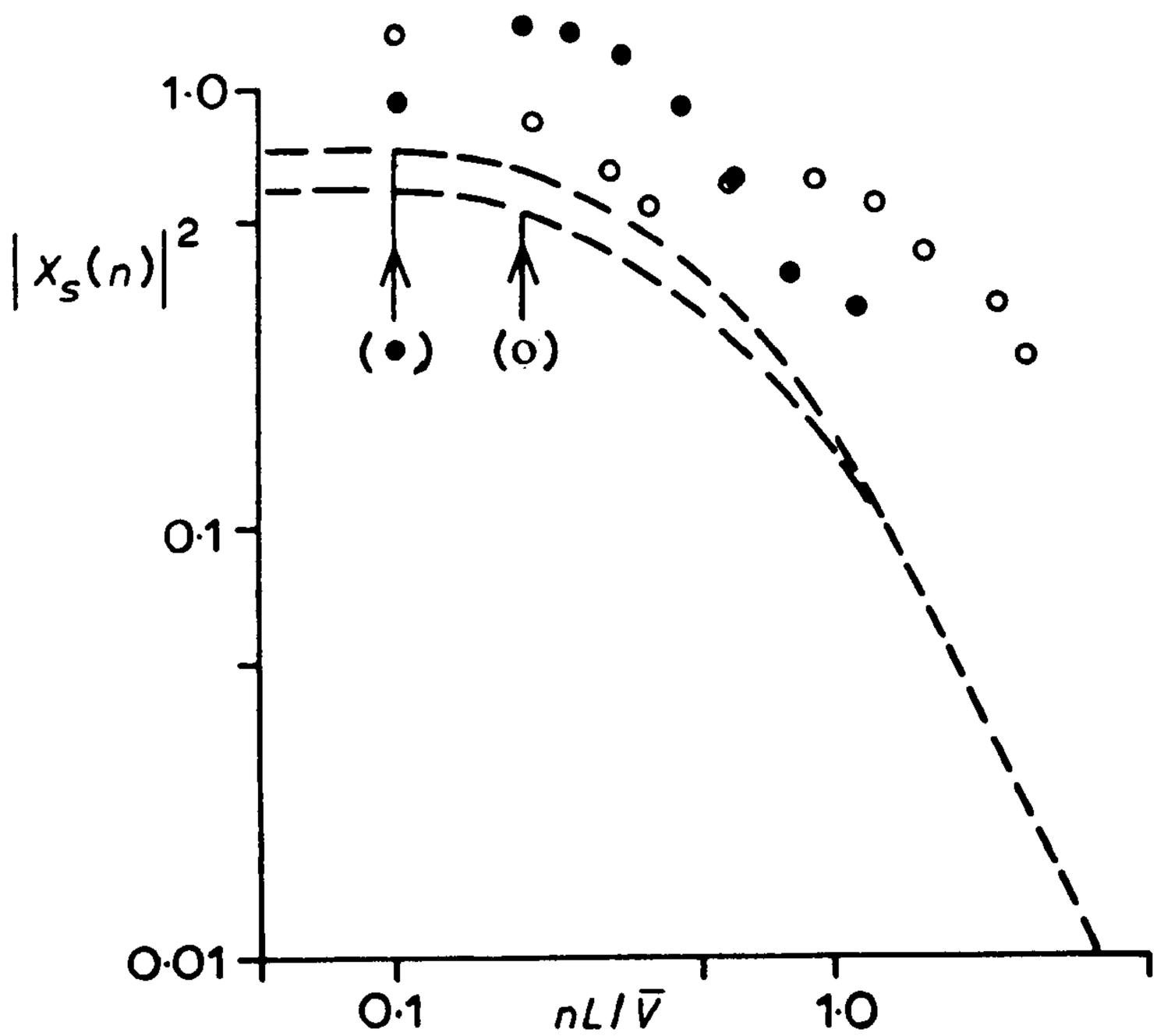

From Baker (1991b)

Figure 2.9 Comparison of theoretical and experimental results for $|X_s(n)|^2$;

Experimental results ●, $L/^xL_u = 1{\cdot}0,\ v/\bar{u} = 0{\cdot}0,\ L/H = 2{\cdot}5,\ \psi = 30°$.

o, $L/^xL_u = 2{\cdot}0,\ v/\bar{u} = 0{\cdot}0,\ L/H = 5{\cdot}0,\ \psi = 90°$,

Theoretical prediction - - -.

Experimental results obtained from 1/50 th scale Lorry , Coleman (1990)

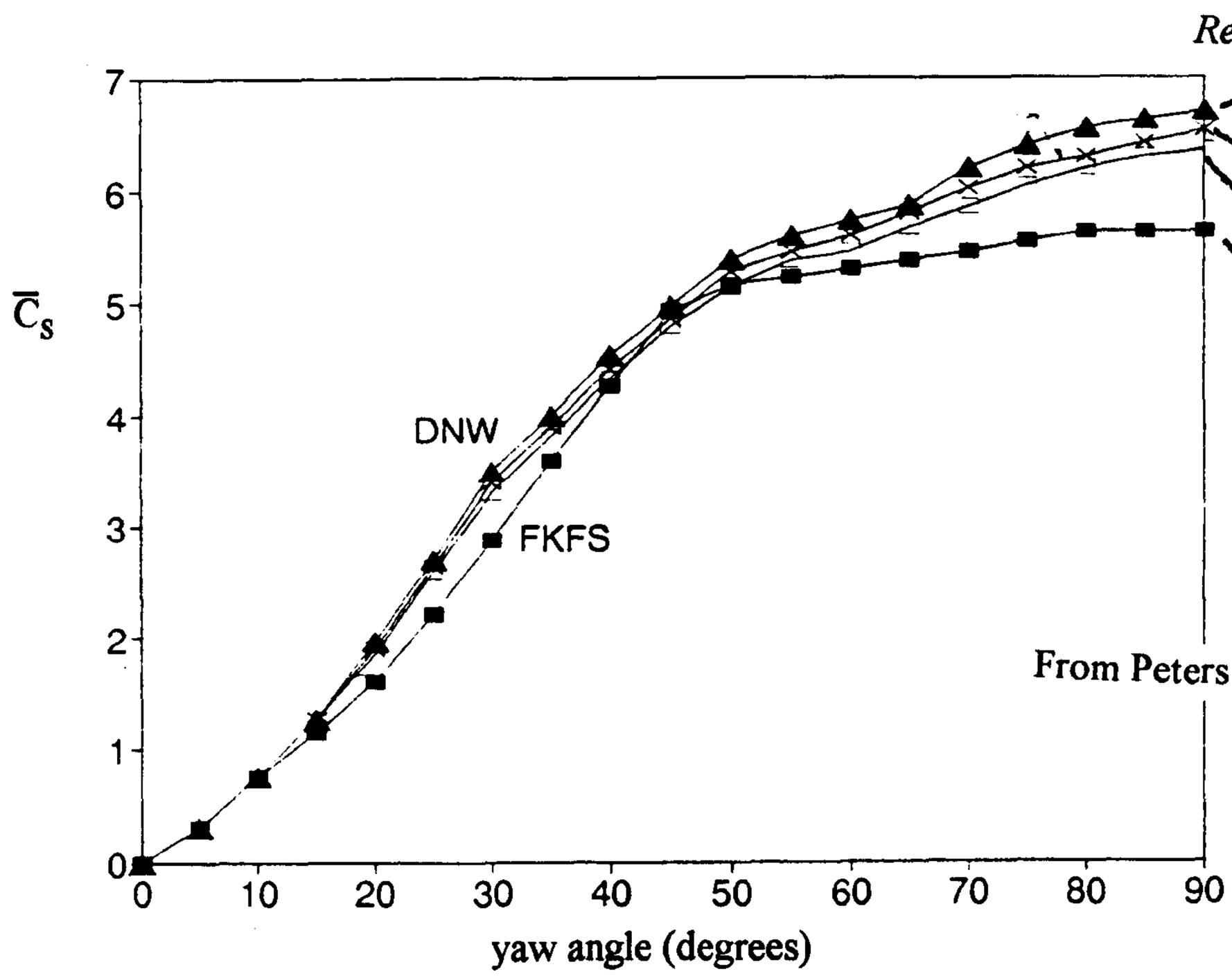

Figure 2.10 Mean side force coefficient C_S, as a function of yaw angle and Reynolds number Re, for various scale model D.B. container wind tunnel tests.

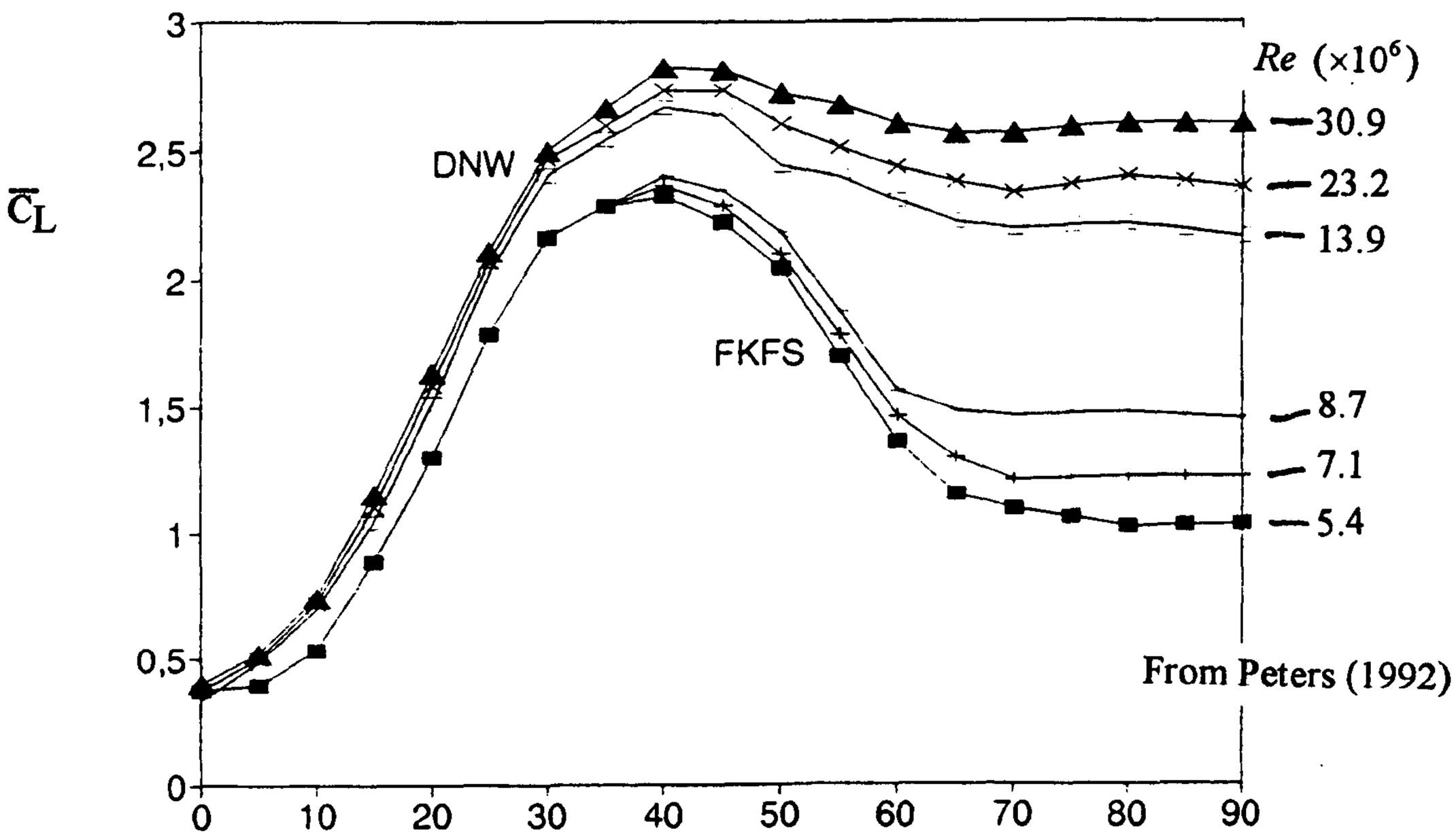

Figure 2.11 Mean lift force coefficient C_L, as a function of yaw angle and Reynolds number Re, for various scale model D.B. container wind tunnel tests.

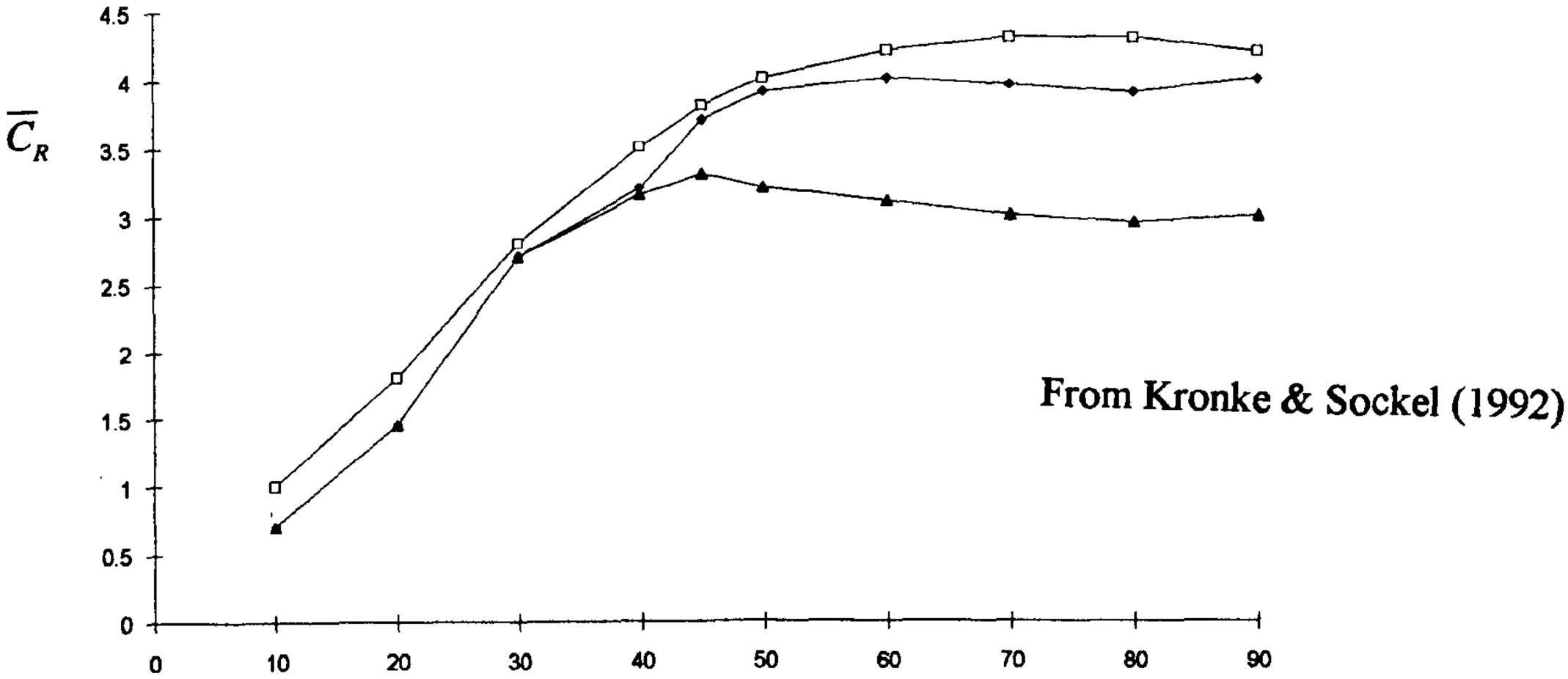

Figure 2.12 Mean rolling moment coefficient versus yaw angle for 1/75 th scale D.B. container tests.

Turbulence Intensity		Spectral decay power exponent
▲	5 %	0.07
□	15 %	0.14
◆	22 %	0.23

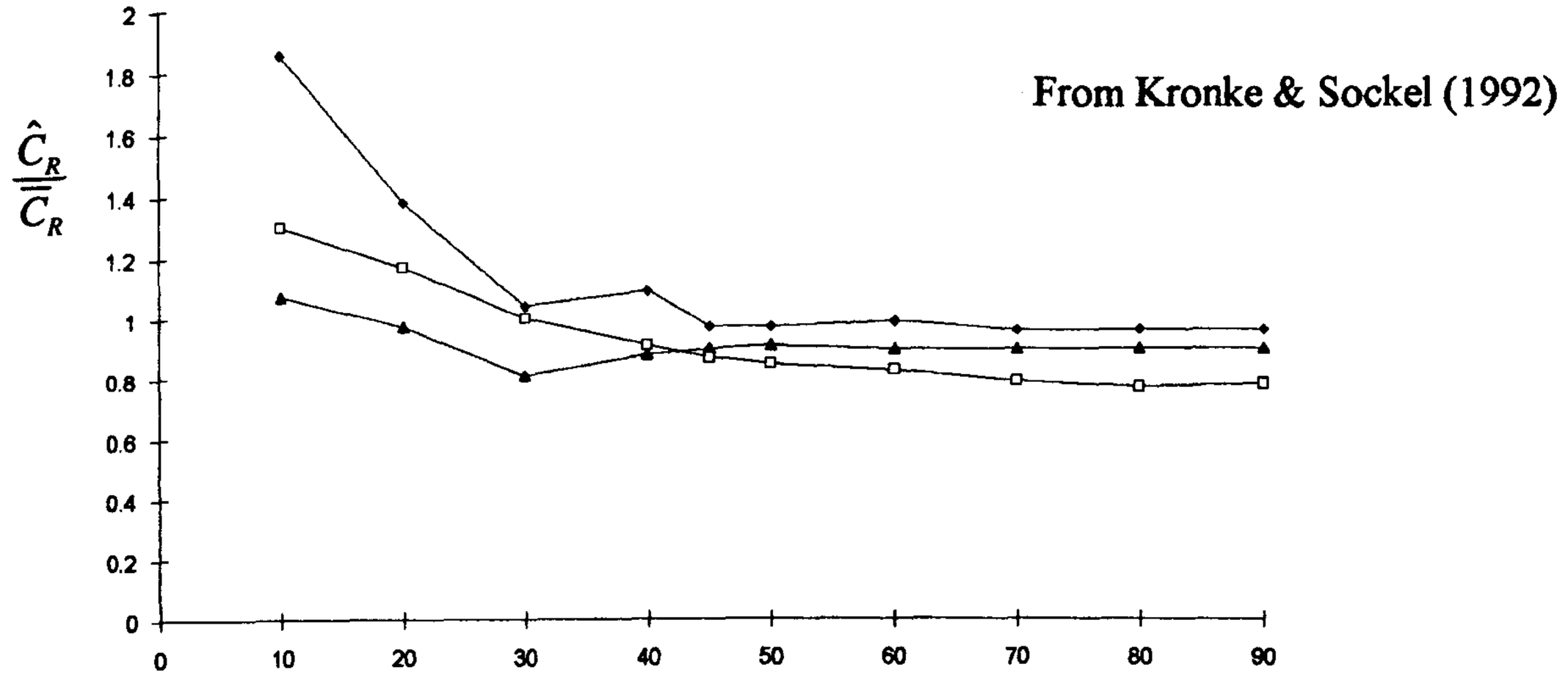

Figure 2.13 Normalised extreme rolling moment parameter versus yaw angle for 1/75 th scale D.B. container tests.

Turbulence Intensity		Spectral decay power exponent
▲	5 %	0.07
□	15 %	0.14
◆	22 %	0.23

Front Profile

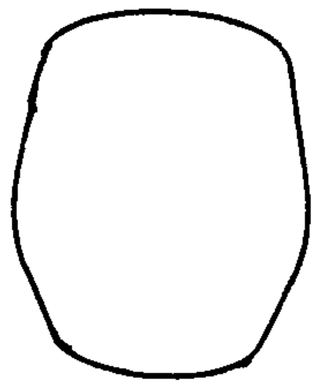

Side Profile

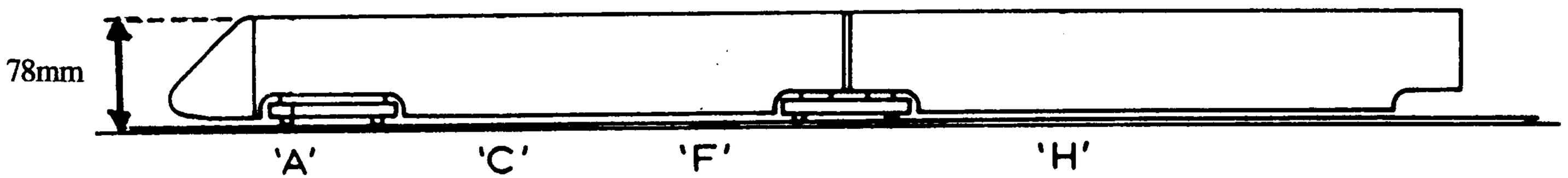

Figure 2.14 $^{1}/_{50}$ th scale APT - S model geometry.

From Baker (1986)

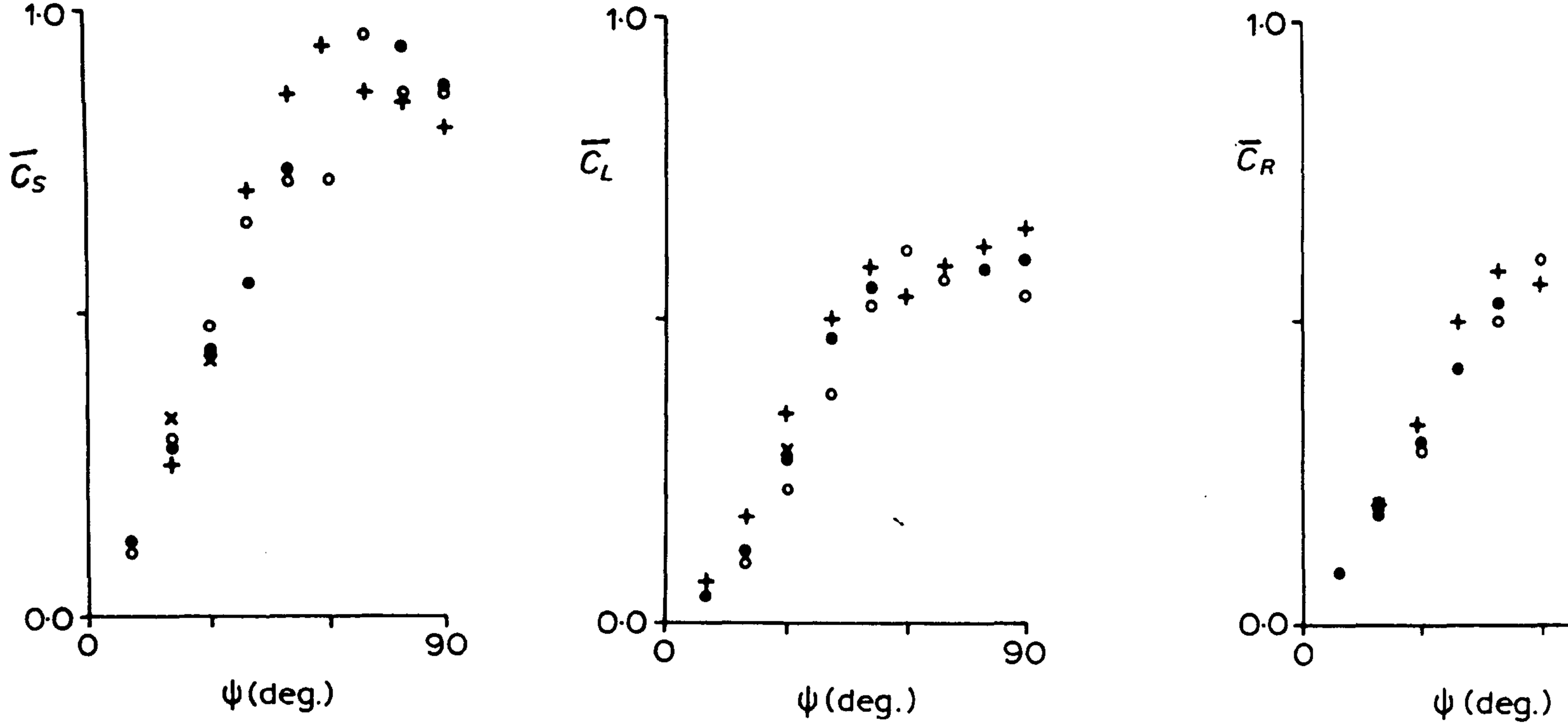

Figure 2.15 APT Car 1 force and moment coefficient data (static models, low turbulence).

+, 1/5th scale, $\bar{V}H/\nu \simeq 16 \times 10^5$;

×, 1/25th scale, $\bar{V}H/\nu \simeq 4 \times 10^5$;

•, 1/35th scale, $\bar{V}H/\nu \simeq 2{\cdot}3 \times 10^5$;

o, 1/50th scale, $\bar{V}H/\nu \simeq 1{\cdot}5 \times 10^5$.

From Baker (1991b)

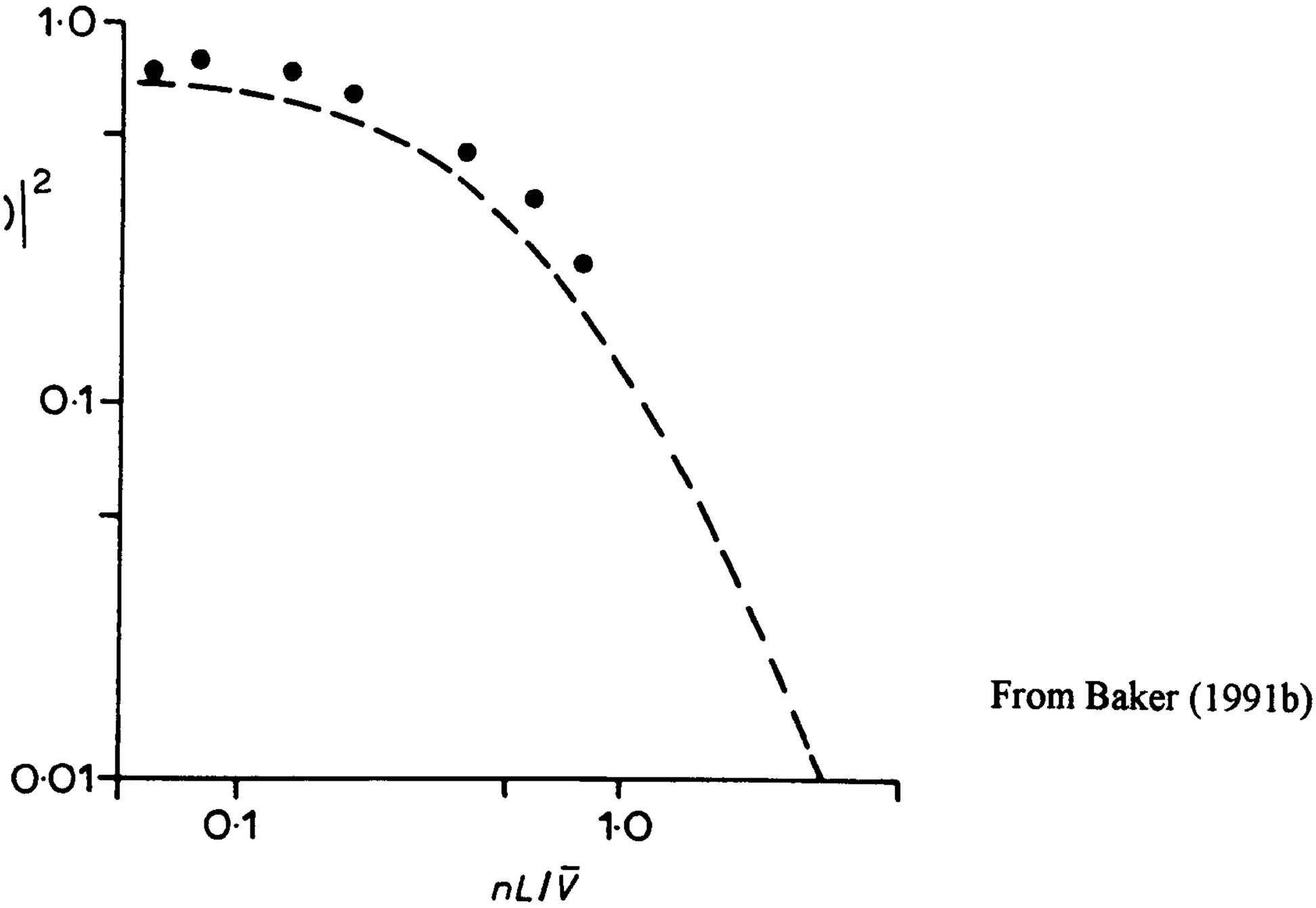

From Baker (1991b)

Figure 2.16 Comparison of theoretical and experimental results for $|X_s(n)|^2$;

Experimental results •, $L/^xL_u = 0{\cdot}903,\ v/\bar{u} = 0{\cdot}0,\ L/H = 7{\cdot}67$;

Theoretical prediction ----

Experimental results obtained from 1/50 th scale APT-S, Baker (1982)

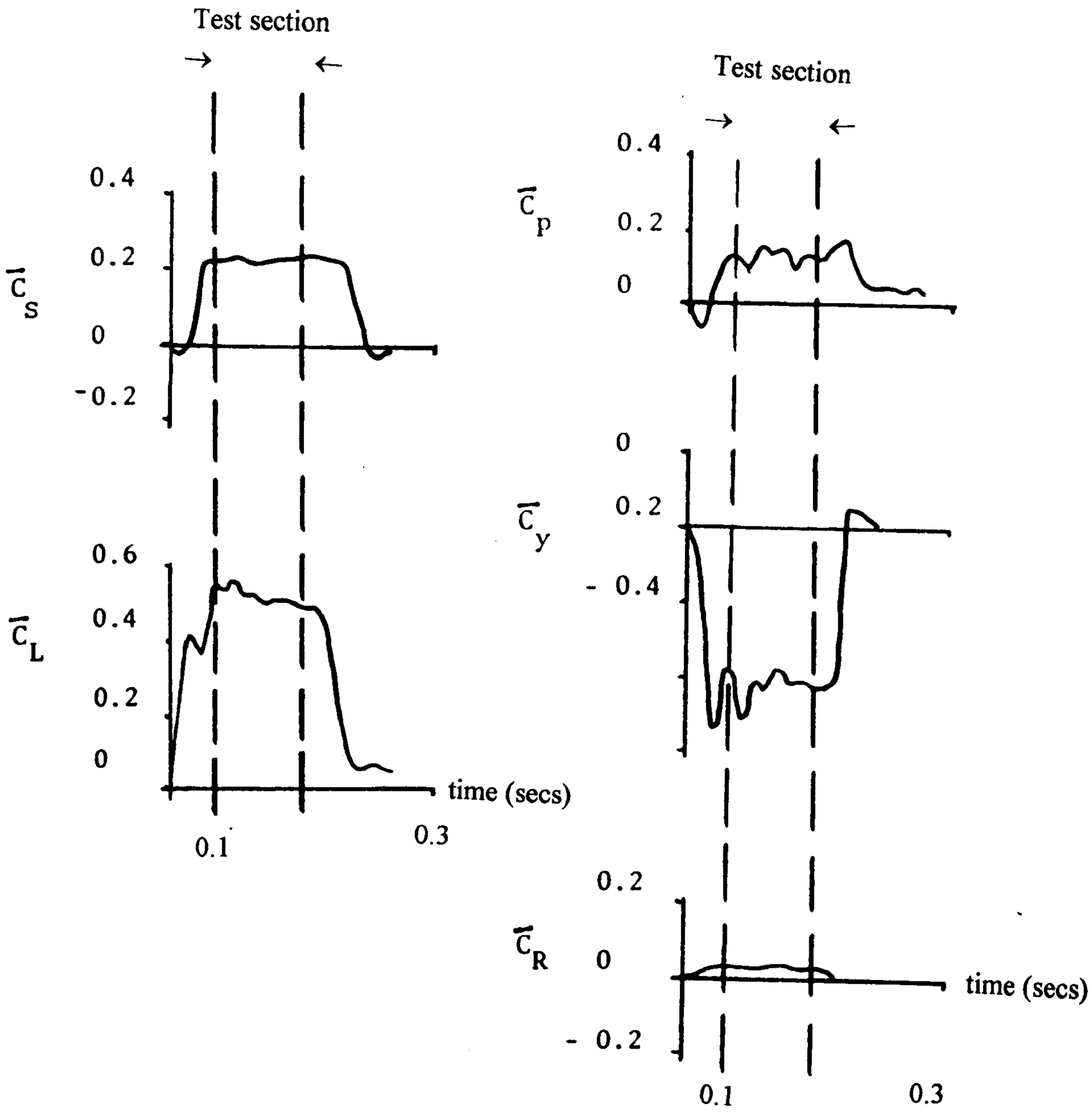

From Baker (1986b)

Figure 2.17 Time histories averaged over 50 runs (analogue filtered at 50Hz prior to measuring) of the $^1/_{50}$ th scale APT-S moving model tests.

Flat ground simulation.

Leading car.

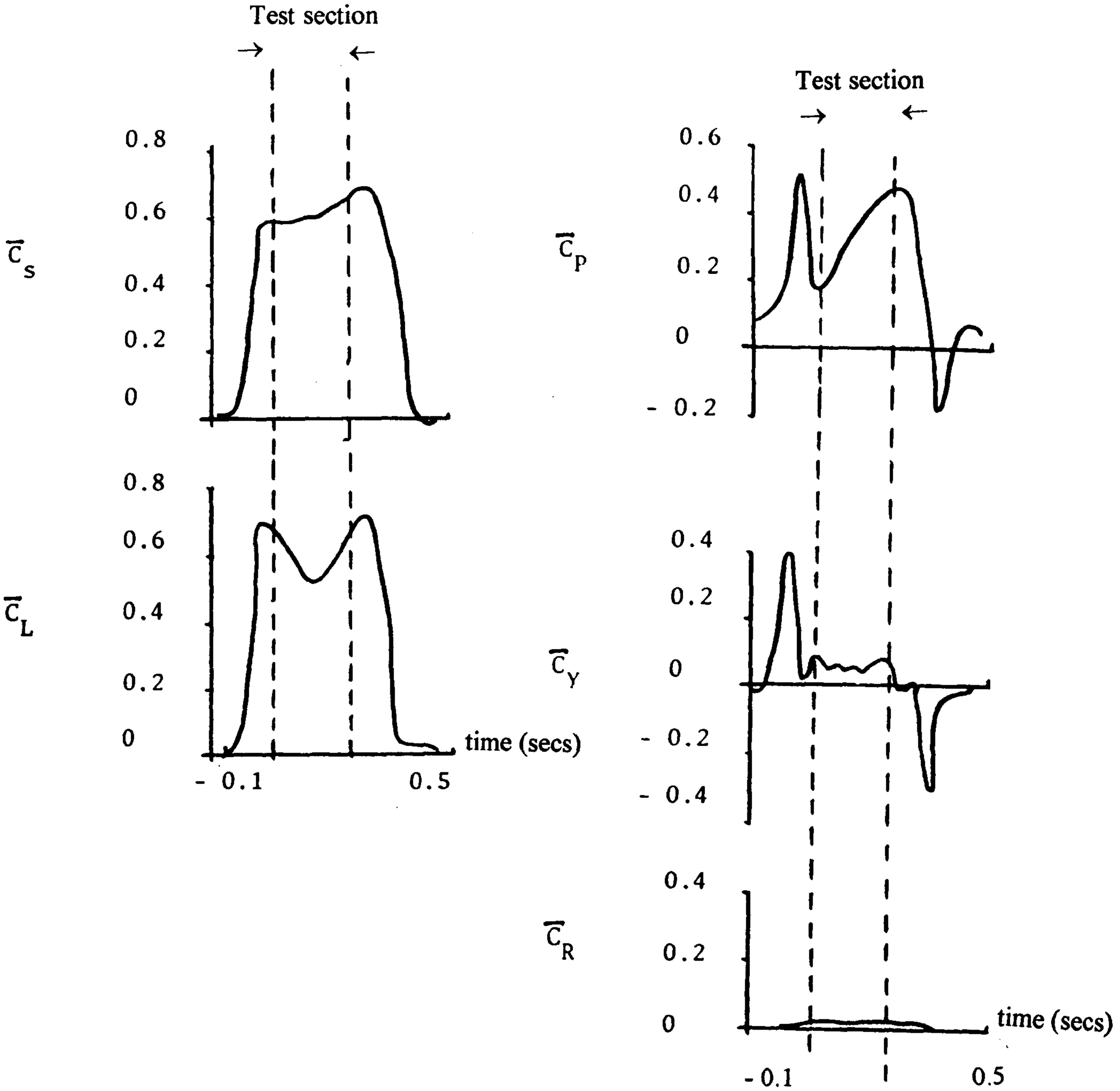

From Baker (1986b)

Figure 2.18 Time histories averaged over 50 runs (analogue filtered at 50Hz prior to recording) of the $^1/_{50}$ th scale APT-S moving model tests.

Embankment simulation.

Second car.

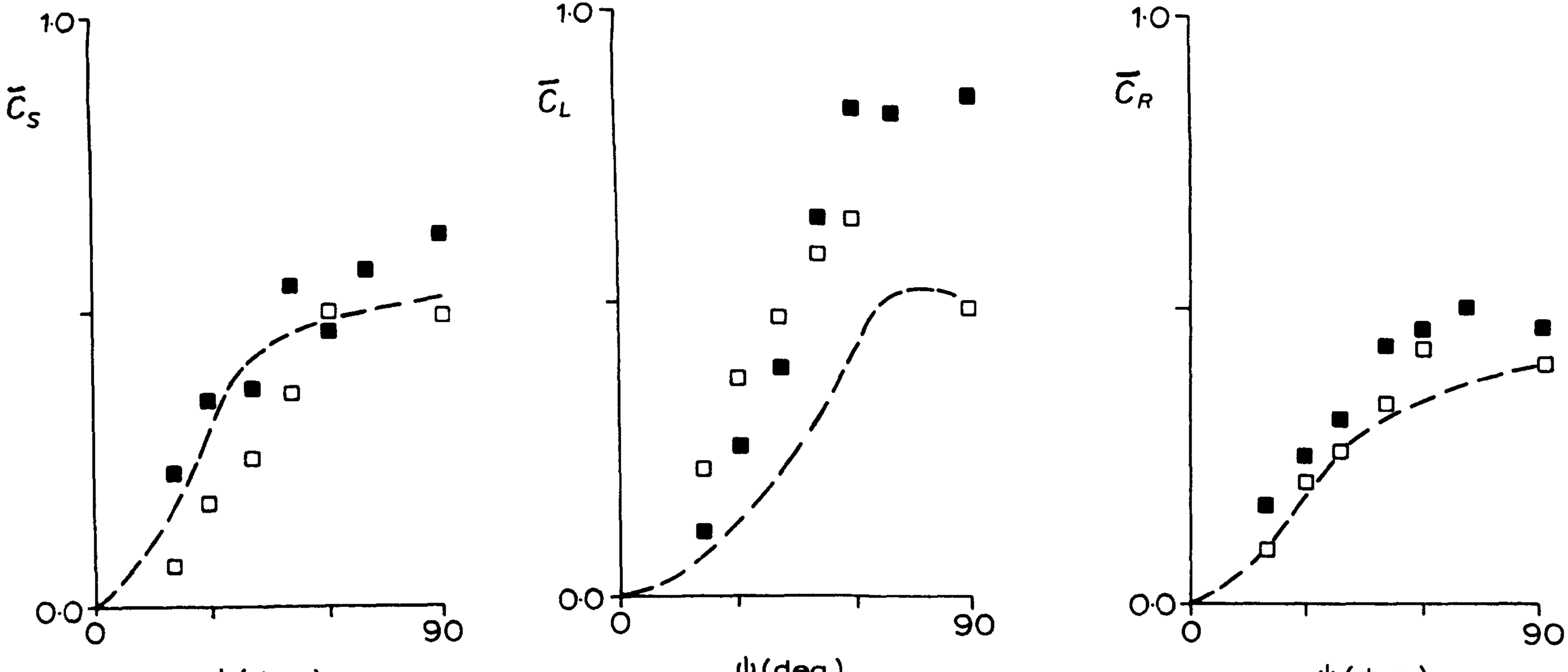

Figure 2.19 APT Car 1 force and moment coefficient data .
$(v/\bar{u}(H)) = 1/\tan\psi$, $\beta = 90°$, $L/^{x}L_u(H) = 3{\cdot}84$, $\sigma_{u0}(\bar{H})/\bar{u}(H) = 0{\cdot}10$, $\bar{V}H/\nu = 10^5$.

□, Level ground simulation

■, Embankment simulation

– – –, Equivalent static level ground results from figure 2.15

From Baker (1991b)

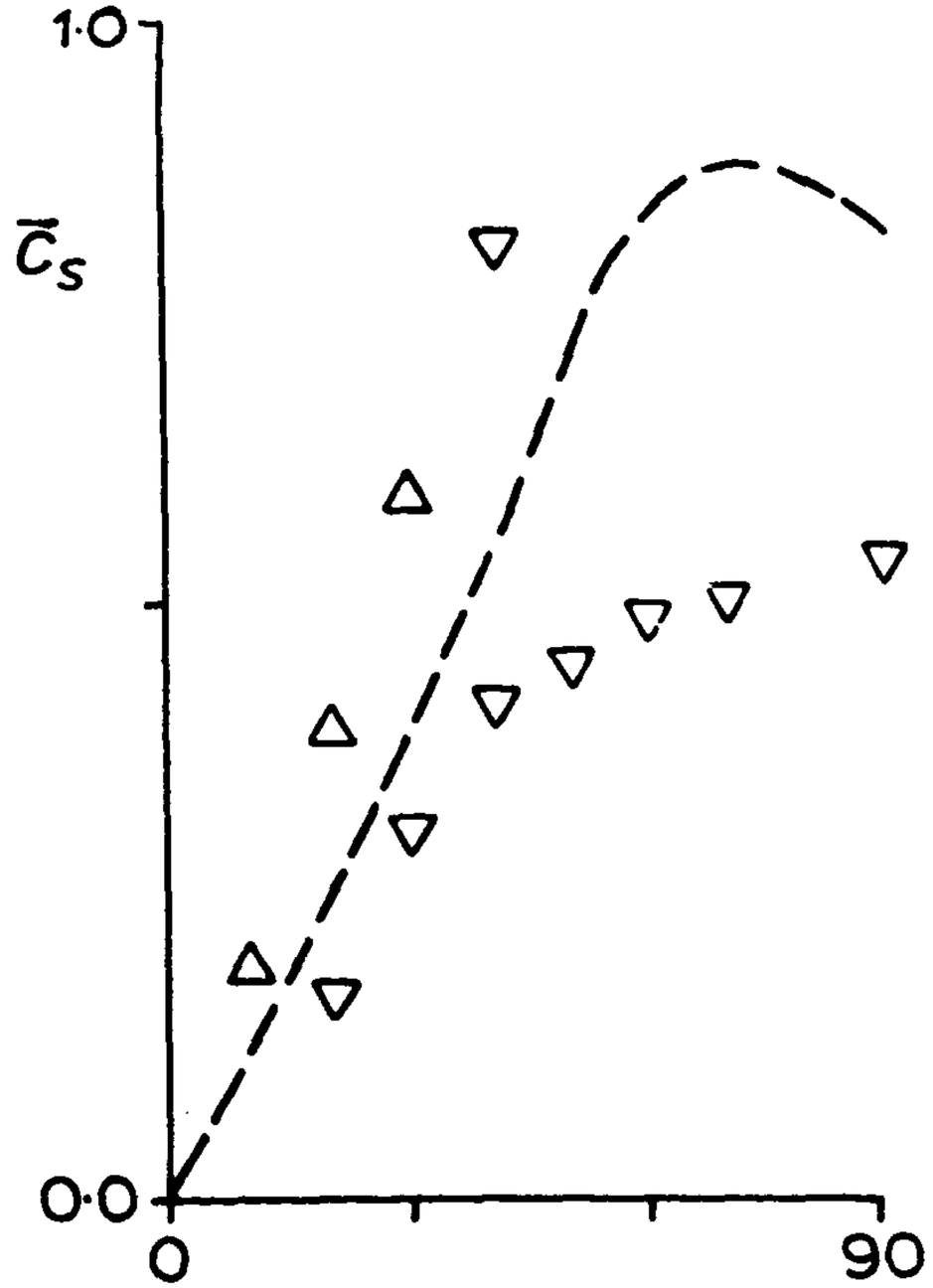

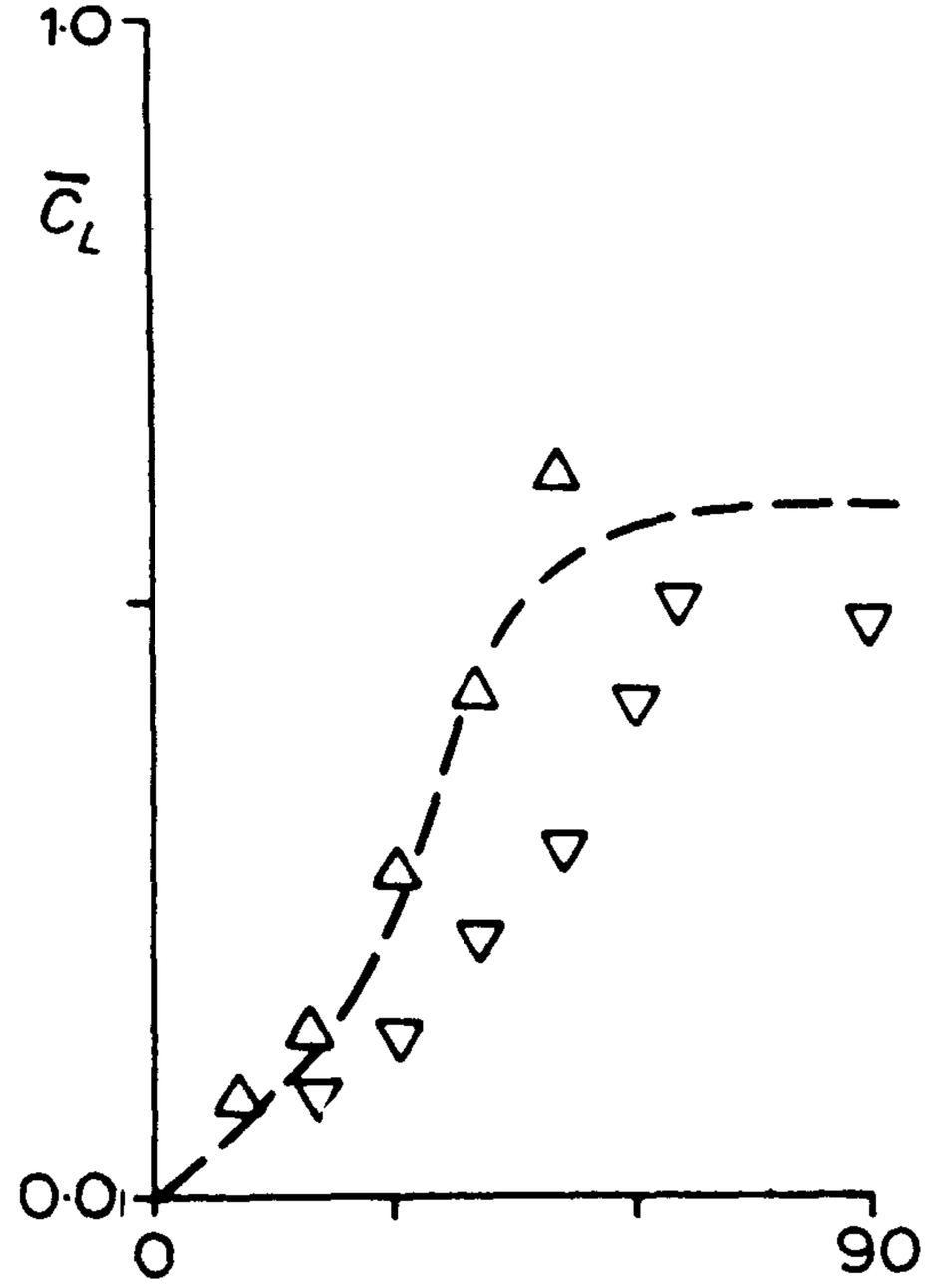

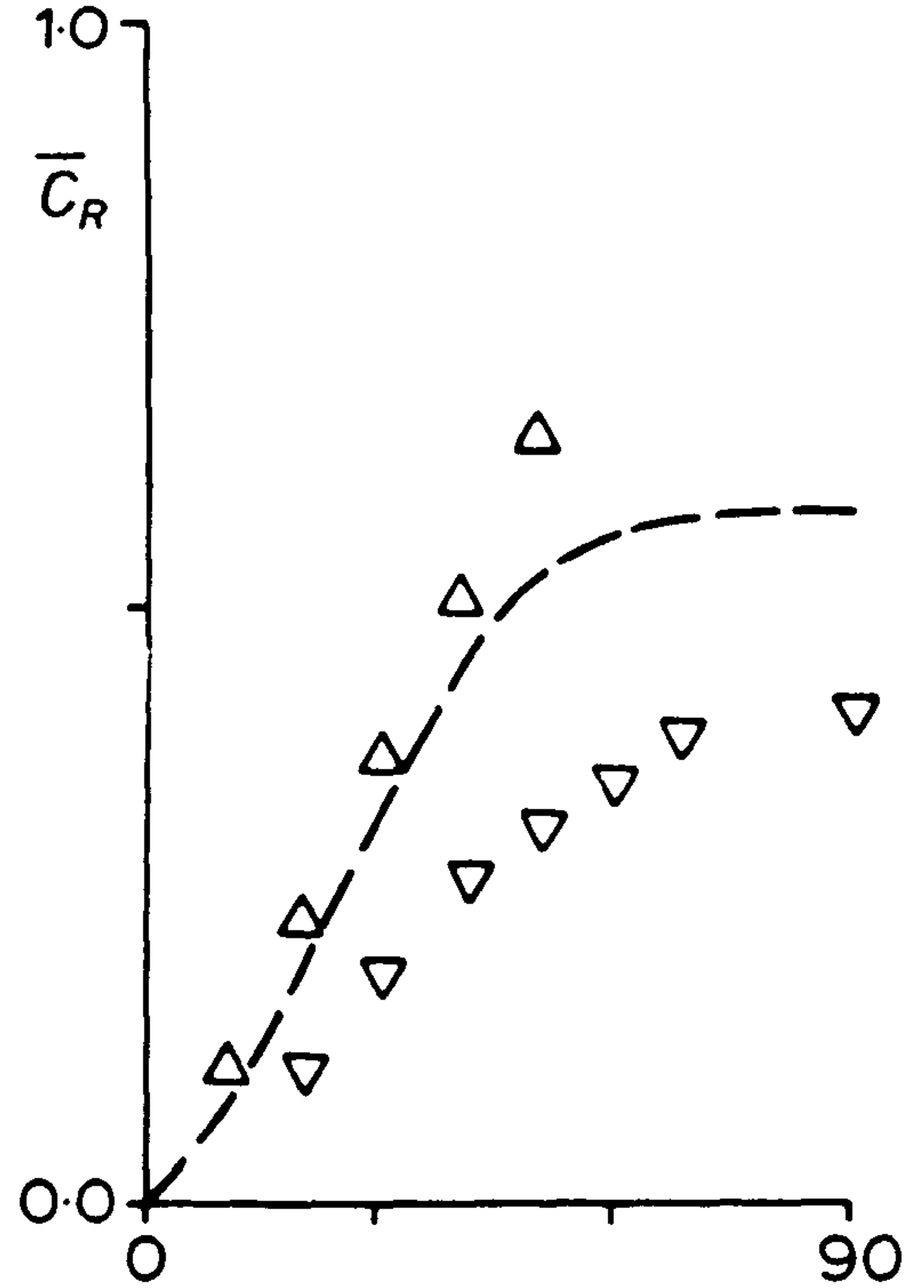

Figure 2.20 APT Car 1 force and moment coefficient data (static models).

△, $L/^xL_u(H) = 0{\cdot}903$, $\sigma_{u0}(H)/\bar{u}(H) = 0{\cdot}21$, $\bar{V}H/\nu = 0{\cdot}5 \times 10^5$;

▽, $L/^xL_u(H) = 3{\cdot}84$, $\sigma_{u0}(H)/\bar{u}(H) = 0{\cdot}10$, $\bar{V}H/\nu = 10^5$;

– – – –, Equivalent data for low turbulence tests from figure 2.15

From Baker (1991b)

3. Review of the Model Scale Testing Requirements and the Full Scale Interpretation.

Aerodynamic similarity between the model wind tunnel tests and the full scale situation is required in order for the forces measured on the model to be correctly scaled to those of the full scale case.

3.1 Basic aerodynamic similarity considerations.

The non dimensional Reynolds number *Re*, is essential to the understanding of aerodynamic similarity. This is defined, in terms of a characteristic length l, and velocity u, to be the ratio of the inertial to the viscous forces present in a fluid :

$$Re = \frac{\rho l u}{\mu} \qquad 3.1$$

where ρ is the density of the fluid and μ is the coefficient of absolute (or dynamic) viscosity of the fluid.

In the absence of other significant forces acting on the fluid, e.g. gravity, electromagnetic etc., this number defines the flow conditions and therefore if this non dimensional value is identical for the full scale case and the model case then the structure of the flow around the bodies will be the same.

The nature of the forces on the body are due the changes in the pressure distribution on its surface. For incompressible flow of relevance to these studies, Bernoulli's equation,

$$p_o = p + \frac{1}{2}\rho u^2 \qquad 3.2$$

relates the fluid velocity u, and static pressure p, to the total pressure p_o. For an isentropic flow there is no loss in total pressure so, considering a fluid accelerating around a body the static pressure reduces as the fluid velocity increases according to equation 3.2. However the situation is much more complicated for real viscous fluids as the flow separates from the body as a large wake flow of recirculating eddies and high turbulence causing a reduction in total pressure. The static pressure is now difficult to calculate in this region as neither the velocity of the fluid or the total pressure is known near to the body. In practice experimental measurements are needed to measure either

the pressure distribution around the body or the net force on the body. In order to relate model scale results of such measurements to a full scale vehicle it is useful to define non dimensional coefficients for the physical quantities that are measured. Forces F, can be non dimensionalised by the product of the dynamic head of the fluid and a reference cross sectional area, A. The latter is chosen for convenience as the absolute magnitude of a coefficient so defined will in any case be a function of the geometric shape of the vehicle. Therefore force coefficients are defined as :

$$C_F = \frac{F}{\frac{1}{2}\rho A u^2} \qquad 3.3$$

This coefficient may only be used for scaling purposes across ranges of body size and air speeds such that the flow characteristics remain unchanged. This is explained in the following paragraphs.

Experimental investigation indicates that there exists several flow regimes as a function of Reynolds number, see Schlichting (1968) (pp 39 - 43) for many references and a full discussion. Of significance to the study of ground vehicles, due to their physical size and wind speeds they encounter, is the supercritical flow regime. In this flow regime the non dimensionalised drag characteristics are constant and the streamwise force coefficient takes its minimum value. This corresponds to a small wake diameter with the flow remaining attached for the largest length along the direction of the flow. (In some cases, depending on the detailed geometry of the body, a smaller wake diameter, and hence lower streamwise drag coefficient, can occur at a slightly lower Reynolds number if the flow reattaches to the body some distance after the initial separation. The final separation is therefore a longer distance from the front stagnation point). The mechanism for these different flow regimes is as follows.

Considering a laminar boundary layer starting from the stagnation point of a bluff body, transition to a turbulent boundary layer occurs at a critical value of Reynolds number, based on the flow velocity and distance from the stagnation point. This means that as the speed of the flow increases, and also the Reynolds number based on a fixed characteristic diameter increases, the point of transition to turbulence moves towards the stagnation point. Noting also that a laminar boundary layer is more unstable than a turbulent boundary layer, then for low flow speeds (and low Reynolds numbers based on a constant diameter) that the point of separation is reached before the critical Reynolds number, based on distance from the stagnation point, for transition to turbulence and the subsequent wake is large. At higher flow speeds (and Reynolds

numbers based on a constant diameter) a turbulent boundary layer is created before the laminar boundary layer separation point and so being more stable, the separation point moves further around the body causing a smaller wake.

Transition of a laminar boundary layer to a turbulent boundary layer can be induced by roughening the body's surface upstream of the point of separation or by an oncoming turbulent flow so that for these conditions supercritical flow is reached at a correspondingly lower fluid speed and hence Reynolds number based on a fixed characteristic dimension. (Schlichting (1968) pp 509 - 515). Considering a laminar boundary layer present on the face of a smooth cylinder, the minimum Reynolds number based on the diameter of the cylinder, for supercritical flow is around 5×10^5. However, for the turbulent boundary layer, aided by a rough surface or a turbulent air stream the value may possibly be up to a factor of 10 smaller depending upon the geometry of the body being tested. Another common technique used in the testing of more streamlined shapes, which works in the same way, is to fix a small wire to their surface near to the stagnation point which again causes the laminar boundary layer to become turbulent. The difference between the forces on a body between the laminar and turbulent boundary layers, due to skin friction, is negligible compared to that due the incorrect positioning of a flow separation line.

It is apparent therefore that it is not necessary in a wind tunnel test of a scale model to achieve the full scale Reynolds number but rather an adequate value to ensure that the test is being undertaken in the correct flow regime. Further in the supercritical flow regime it is possible to scale model test results to full scale using equation 3.3

Experimentalists undertaking scale wind tunnel tests, use this condition of constant force and moment coefficients at supercritical Reynolds numbers to check that the full-scale flow conditions have been reached. These tests are referred to as Reynolds number tests. The applicability of this assumption, for determining the forces on full scale vehicles from the results of model scale tests, i.e. across many magnitudes of supercritical Reynolds number, depends upon the flow to be dominated by inertial fluid effects. The critical Reynolds number value is much lower for very bluff and sharp edged bodies due to the high pressure gradients that exist caused by their sharp edges and these bodies therefore have well defined separation lines along their surfaces. Bearing in mind the general shape of the vehicles, model wind tunnel tests of square shaped lorries and trains can be undertaken at relatively low Reynolds numbers whilst vehicles with highly streamlined form (and certainly cars of complicated shape) need to be tested at much larger Reynolds numbers.

For vehicles which are not dominated by separated flow regimes the effect of surface detail will have a large effect on the forces on a vehicle. Indeed much attention has been given to the necessary detail on small scale model cars designed for the purpose of measuring the forces and moments in a wind tunnel such that the results are representative of the full scale version, see Good (1994) and Cooper et al (1994).

A third characteristic of bluff body aerodynamics of use to this study involves the understanding of the flow in the frequency domain. Again Schlichting (1968) shows that at supercritical Reynolds numbers the flow downstream of a bluff body separates, in time, from alternate sides of the body forming large eddies, similar to the size of the body itself, that propagate downstream in the fluid forming a large wake. The non dimensional number associated with this behaviour is the Strouhal number *St*, that is invariant for a given body, which relates the frequency of vortex shedding *n*, to the physical diameter *d* and flow velocity *u*.

$$St = \frac{n\,d}{u} \qquad 3.4$$

For a supercritical Reynolds number, for a circular cylinder $St = 0.21$, (Schlichting (1968)). More recently Vickery (1966) investigated this further for a square cylinder and obtained $St = 0.12$, relating this, by measurements, to the frequency of the vortex shedding in the wake of the cylinder. The effect was found to produce lateral forces on the cylinder due to the nature of the flow alternatively separating from each side of the cylinder. For a ground vehicle, if this phenomenon was present, this would correspond to alternate vortex shedding from the roof and the underside of the vehicle to produce such a corresponding frequency of oscillation in the measured lift force.

The use of the Strouhal number, for a bluff body, enables the scaling of unsteady forces in the frequency domain between bodies of different sizes and in different air speeds.

In summary, it is clear that any wind tunnel testing of scale vehicles must be conducted in a flow which yields a supercritical Reynolds number. In general any physical quantity which is a function of the general flow structure, if suitably non dimensionalised, can be measured in order to check this criterion.

In practice the minimum scale of the vehicle that may be used in an experiment depends on the maximum wind tunnel wind speed. Previous experiments measuring forces on the 1/50th scale sharp edged lorry in Nottingham University's environmental wind

tunnel (Coleman (1990)) have shown that Reynolds numbers of 4×10^4, based on vehicle height, are acceptable implying a mean wind speed of only 5m/s.

3.2 The atmospheric boundary layer simulation.

In the field of wind engineering, an accepted standard, for describing the characteristics of a mean hourly neutral stable strong wind near the ground are those from E.S.D.U. (1974a,b and 1975). A neutrally stable atmosphere is one which lacks convective currents. The characterisation of strong winds is described in terms of the time period of one hour due to the experimental evidence that little wind energy exists at frequencies corresponding to time periods between 3 and 0.5 hours, see van der Hoven (1957). The energies present at the in lower frequency range, not described by the one mean hourly, ABL correlations, are caused by global air movements which appear, in the context of shorter gusts, as the prevailing mean wind velocity.

The relevant characteristics of the mean hourly atmospheric boundary layer as a function of height above the ground are expressed as the following correlations:

Velocity profile:

$$\frac{\bar{u}\,(z)}{\bar{u}\,(H)} = \frac{\log\,(z/z_0)}{\log\,(H/z_0)} \qquad 3.5$$

Turbulence intensity profile:

$$\frac{\sigma(z)}{\bar{u}\,(z)} = \frac{0.867 + 0.556\,\log z - 0.246\,(\log z)^2}{\ln\,(z/z_0)\,.\;0.76/z_0{}^{0.07}} \qquad 3.6$$

for $z_0 < 0.02$m

Streamwise velocity spectrum, von Karman spectrum:

$$\frac{n\,S(n,z)}{\sigma(z)^2} = \frac{4\,(\,{}^{x}L_u\,(z)\,n/\bar{u}\,(z)\,)}{(1+70.8\,({}^{x}L_u\,(z)\,n/\bar{u}\;(z))^2\;)^{5/6}} \qquad 3.7$$

$$\frac{n_{peak}\;{}^{x}L_u\,(z)}{\bar{u}} = 0.149 \qquad 3.8$$

Streamwise turbulence length scale:

$$^{x}L_u\ (z) = \frac{25\ z^{0.35}}{z_0^{\ 0.063}} \qquad 3.9$$

It should be noted that whist equations 3.5, 3.7and 3.8 are non dimensional equations 3.6 and 3.9 are not. Calculations using these latter equations therefore should be carried out with the full scale values using corresponding values of z and z_0 in metres.

It is seen that equation 3.9 defines the streamwise length scale at a given height above the ground based on the characteristic roughness length, z_0, of the upstream fetch. For example an open countryside simulation has a characteristic roughness length, z_0 = 0.01m which implies a streamwise turbulence length scale of 49m at a height of 3m above the ground. For a 1/50th scale simulation therefore a streamwise turbulence length scale of about 1m would be required for a height of 60mm. From equation 3.9 it is seen that the streamwise turbulence length scale is not very dependent on the value for the surface roughness length.

Similar correlations of the atmospheric boundary layer are shown graphically in Cook (1985) and cover a larger range of surface roughness lengths.

ESDU (1974a,b and 1975) and Cook (1985) express concern at the accuracy of all the correlations at small heights above the ground, say less than 10m. Hoxey and Richards (1992) shows the results of measurements in open countryside type terrain of these wind characteristics at 1m, 3m and 10m above the ground. The major finding was that at the very small heights much of the turbulent energy in the wind velocity spectra was moved to higher frequencies giving a distorted spectrum, see figure 3.1, compared to the calculated von Karman spectrum of equation 3.7. Whilst it is difficult to determine the stream wise turbulence length scale associated with this distorted spectrum by spectral comparisons with the calculated von Karman spectrum it is seen that it is much reduced, probably by around a factor of 2 at a height of 3m.

A concept utilised in the measurement of wind velocity characteristics is that of frozen turbulence and is known as Taylor's hypothesis. This asserts that the structure of the flow changes over time scales much longer than the time scales corresponding to the lengthscales of interest. Lappe and Davidson (1963) from full scale experiments found that this held for lengthscales less than 300m. This allows, for example, the calculation

of wind velocity spectra from measurements at a single point using either autocorrelation or Fourier techniques, see Chapter 5.

The effect of the lateral wind characteristics also need to be considered. The turbulence of the wind has been shown to be close to isotropic (ESDU(1975)). Isotropic turbulence is characterised by having equal fluctuating velocity components but with the lateral turbulence components having a length scale of around half the streamwise value. These lateral components are often referred to as the semi length scales. The effect of isotropic turbulence on bluff bodies has been examined in Tielman and Atkins (1989). From experiments utilising long rectangular bars mounted perpendicular to the oncoming turbulent flow that corresponded to sizes much smaller and much larger than the characteristic turbulence length scales Tielman and Atkins showed that a critical streamwise length scale was reached such that the larger turbulence scales had little effect on the flow structure around bluff bodies. The critical streamwise length scale needed to obtain representative pressures on the bars was found to be twice the model scale of the bodies tested, in this case the body's cross section. Applied to a vehicle this implies that the streamwise turbulence length scale should be twice the vehicle's height, and also, since these tests were conducted with isotropic turbulence, the lateral turbulence semi length scale should be equal to the vehicle's height. The correlation of the gusts across the body is the condition for vortex shedding, discussed in section 3.1, which if present on a vehicle would cause large unsteady lift forces.

For vehicles, the finite nature of their length also needs to be considered. Both the lorry and the DB container, tested in this thesis, have full scale equivalent lengths of 13.5m and 12m, approximately one quarter the streamwise turbulence length scale, (equation 3.9, z_0=0.01m), i.e. $L^x/L_u = 0.25$. Referring to figures 2.4 and 2.5, it is seen that the effect of the finite length of the vehicle is observed in theoretical predictions of the unsteady side force parameters and also the normalised extreme side force parameters (section 2.1). However it is seen that for values of L^x/L_u less than unity these discrepancies are reasonably small. Section 6.2.3 considers this further with reference to the turbulence length scales of the ABL simulated for the tests described in this thesis.

3.3 The model time scale interpretation.

In order to calculate the extreme force values, that is the mean force formed over the period that a vehicle may over turn as discussed in Chapter 1, it is necessary to define the model time period equivalent to a full scale gust. The concept of streamwise eddy

lengthscale is conventionally used in wind engineering for the purpose of determining equivalence between the model wind tunnel tests and the full scale scenario.

It is apparent that the model time scale depends upon the velocity of both the vehicle and the wind, rather than merely their resultant wind speed and yaw angle. As an example, consider the full scale case of a lorry travelling at 30m/s experiencing, at the reference height, a perpendicular cross wind of 30m/s. Utilising the moving model rig in an environmental wind tunnel in which the atmospheric boundary layer has been simulated, this geometry can be represented with a 1/50th scale lorry travelling at 8.5m/s perpendicular to the wind direction of speed 8.5m/s, at the equivalent reference height. The model time period (t_m) corresponding to a full scale 3s gust (t_f) at the reference height and can be calculated as follows:

$$t_m = \frac{t_f}{50} \times \frac{u_f}{u_m} \qquad 3.10$$

For this example the model time scale = 0.21s.

Note that in order to conduct this calculation, only the streamwise wind velocities are needed. Referring to Cooper (1984) it is seen that the above discussion only holds for moving ground vehicles if the two lateral turbulence semi length scales are modelled, in the wind tunnel, in correct proportion to the streamwise length scale as in the full scale case. Experimental data shows that there is some variation in the known values of the lateral semi length scales, see table 3.1, but taking the following values for the lateral semi length scales;

$$^{y}L_u/^{x}L_u = {}^{z}L_u/^{x}L_u = 0.42 \qquad 3.11$$

Cooper (1984) calculated the wind velocity spectra as experienced by a moving vehicle which are moved to higher frequencies as the vehicle's speed increased. For the vehicle moving perpendicular to the wind direction the resultant extreme wind speed $\hat{V}$, at the reference height, experienced by the vehicle was defined to be simply:

$$\hat{V} = \sqrt{v^2 + \hat{u}^2} \qquad 3.12$$

The main effect that was predicted was due to the vehicle encountering the gusts quicker but additionally, also as the vehicle speed increases, with the semi length scales, which are smaller, also increasing the higher frequency energy levels. Figures 3.2 and

3.3 show the results of his calculation. Firstly figure 3.2 shows the overall effect of the resultant spectra, as seen by the vehicle, moving to higher frequencies as vehicle speed increases. Figure 3.3 shows the effect of normalising the spectra by the resultant wind speed experienced by the vehicle therefore showing the effect of the lateral semi length scales alone.

For a direct wind tunnel simulation of a full scale case it is apparent that an additional time scale correction will be needed for any wind tunnel simulation not correctly modelling the full scale lateral semi length scales.

The next two sections utilise this concept of eddy length scale to determine the model time scale for tests in which two common shortcomings are present.

3.3.1 The effect on the model time scale of the incorrect modelling of the turbulence length scales.

The lateral turbulence length scales for wind may be related to the streamwise turbulence lengthscale as this is approximately twice the magnitude of lateral components - indeed as in isotropic turbulence (E.S.D.U. (1975). If this is satisfied then the concept of eddy length scales may be employed to calculate the model time scale as follows. The model time period taken to be equal to the full scale gust is that in which the model experiences the same number of gusts at the correct energy level as the full scale vehicle. As an example, considering the case where the turbulence length scale of a simulated ABL is a factor of 2 too small, and rewriting equation 3.7 as,

$$\frac{n\,S(n,z)}{\sigma(z)^2} = f\left(\frac{{}^{x}L_u(z)\,n}{\bar{u}(z)}\right) \qquad 3.13$$

physically this means that the energy levels of each part of the spectrum are assigned to a frequency twice that of the correct simulation. It is seen therefore that the effect of running a test with the scale turbulence length scale a factor of 2 too small is to move the eddies, at the correct energy at a given wind speed, twice as quickly across the model. The time scale of the model tests is therefore halved, and the model time period taken to be equal to the full scale gust is also reduced to half. This method also corrects the lateral unsteady components of the wind in the same way, so that their energies in the frequency domain are also preserved.

The shortcomings of this method is that at very low frequencies the turbulent energy of the wind is missing but this should be at much longer time scales than the gust times of interest and so should only have an effect similar to the mean wind.

3.3.2 The effect on the model time scale of representing a moving vehicle scenario with a static test.

Now consider using a conventional static wind tunnel test to determine the extreme forces on a moving vehicle. The modelled ABL in the wind tunnel represents the wind as experienced by the would be full scale moving vehicle. Using the results of Cooper (1984) the shift in frequency of the onset wind as experienced by the vehicle for different wind and vehicle velocities can be found. Using the stream wise eddy length scale concept as described in section 3.1 the model time scales can be found for any situation.

In order to give some feel for the effect of using a static test for representing the moving vehicle in a cross wind the example given in section 3.1 is considered further. Positioning the lorry such that the oncoming wind was at the resultant of the vehicle's and the wind velocities, in this case at a yaw angle of 45 degrees, the resultant wind as seen by a full scale vehicle is simulated by the wind tunnel characteristics alone. In this example too small a modelled streamwise turbulence length scale could be seen to be an advantage as the too small streamwise turbulence length scale present in the modelled ABL is representative, in these terms, of that experienced by the vehicle at some speed, in the range of 10 to 30m/s according to the calculations in Cooper (1984) and shown in figure 3.2. As listed in Chapter 1 there are many other shortcomings with this simulation.

3.4 The approach used in this thesis.

From what has been said in sections 3.1 to 3.3 it is apparent that the problems in determining the extreme force that a lorry may experience, by detailed testing in the wind tunnel, are in two categories:

1. The variations in environment and route terrain and exposure.

2. Vehicle velocity relative to the wind velocity.

As discussed in section 3.3 inadequate simulations of the unsteady structure of the wind can be corrected for by choosing an appropriate model time scale but it is unclear as to whether this method is adequate due to the many other shortcomings discussed in Chapter 1.

In order to make progress, this thesis shows the results of calculating the following normalised extreme force parameter from both the conventional static test data and from the moving model test data for a range of model time scales. Thus:

$$\frac{\hat{C}_F}{\bar{C}_F} = \frac{\dfrac{\hat{F}}{\frac{1}{2}\rho A \hat{V}^2}}{\dfrac{\bar{F}}{\frac{1}{2}\rho A \bar{V}^2}} \qquad 3.14$$

where $^-$ and $\hat{}$ indicate the mean and extreme values respectively. Note that the extreme resultant wind speed used in this equation, for a vehicle moving perpendicular to the wind velocity is that defined in equation 3.12.

This thesis sets out to examine the use of this parameter for collapsing the results of:

1. Moving and Static model tests undertaken with a constant ABL simulation.

2. Extreme values derived from a range of model time scales.

It is seen that the normalised extreme force parameter, derived by model testing, can then be used for calculating the extreme force values for any vehicle velocity, terrain etc. using an appropriate value for the streamwise extreme wind value which can be obtained from Cook (1985) or E.S.D.U. (1974a) for various terrain and gust time scales. This parameter is very simple when compared to the complexity between the scenarios concerned and the purpose of this thesis is to test the adequacy of this parameter.

Note that, referring to section 2.1, when this normalised extreme force parameter is unity then this is equivalent to the quasi steady case with no body induced unsteadiness.

One of the main shortcomings of this parameter is that no account is taken of effect of the shorter lateral semi length scales on the resultant extreme wind value as described in Cooper (1984). Referring to section 3.3 it was suggested that these shorter lateral semi length scales would move the wind spectra, as seen by the moving vehicle, further to the higher frequencies than by just the vehicle movement alone.

The justification for using the simple definition for the resultant extreme wind speed lies in the fact that the effect of the smaller lateral semi lengthscales alone as shown in figure 3.3 is small compared to their presently known values for a particular environment, see table 3.1. This area needs further work.

Table 3.1 Experimental estimates of lateral turbulence semi lengthscales.

From full scale experiments estimates for the surface roughness length, $z_0 = 0.03$ at a height, z of 10m for strong winds.

Reference	${}^{y}L_u / {}^{x}L_u$	${}^{z}L_u / {}^{x}L_u$
ESDU (1974a,b and 1975)	0.42	0.3
Flay (1978) *	0.25	0.4
Counihan (1975)	0.35	0.5 -0.6

* This result is based on an estimated ${}^{x}L_u$ value 30% larger than von Karman.

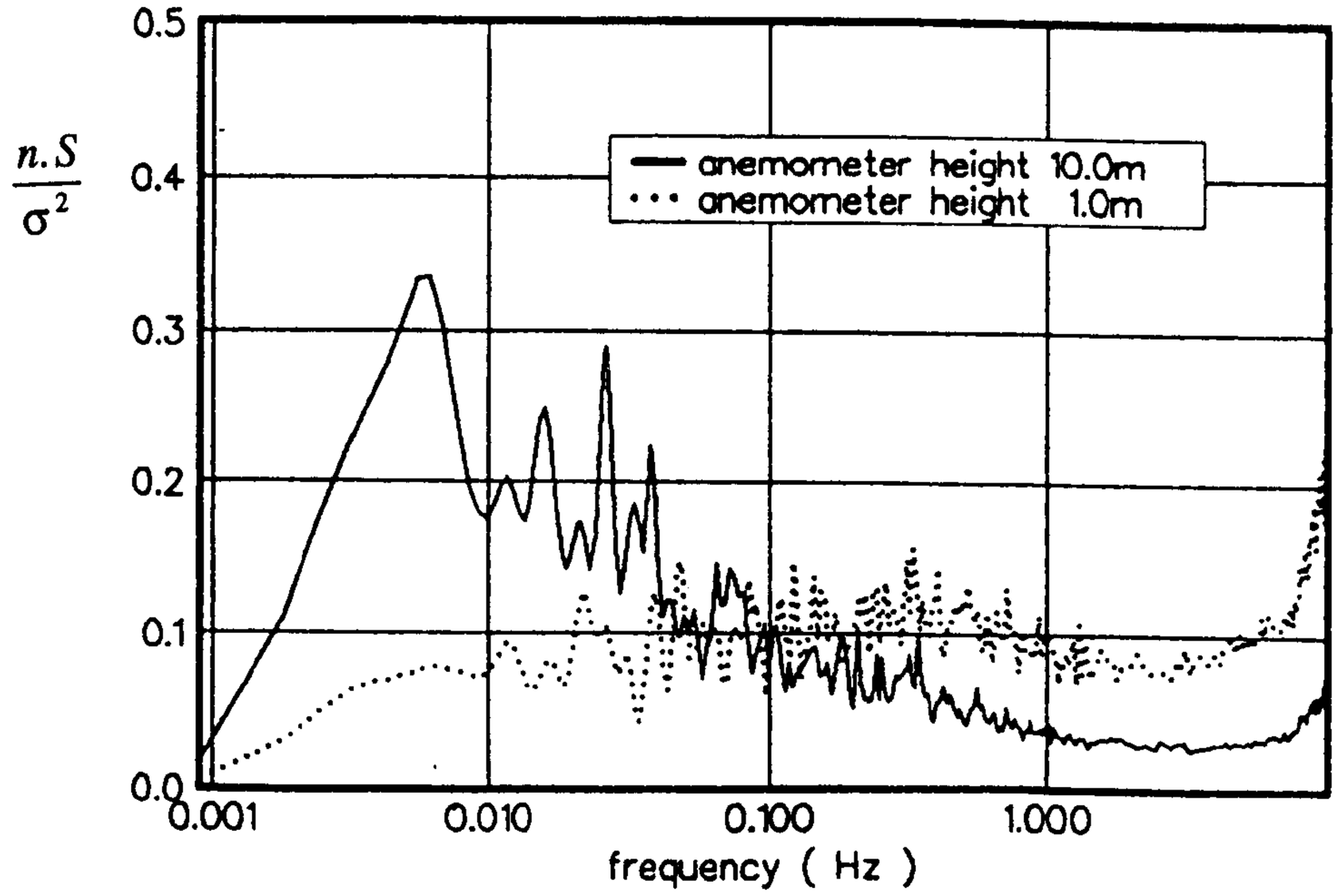

Conventional Wind Engineering log - linear form.

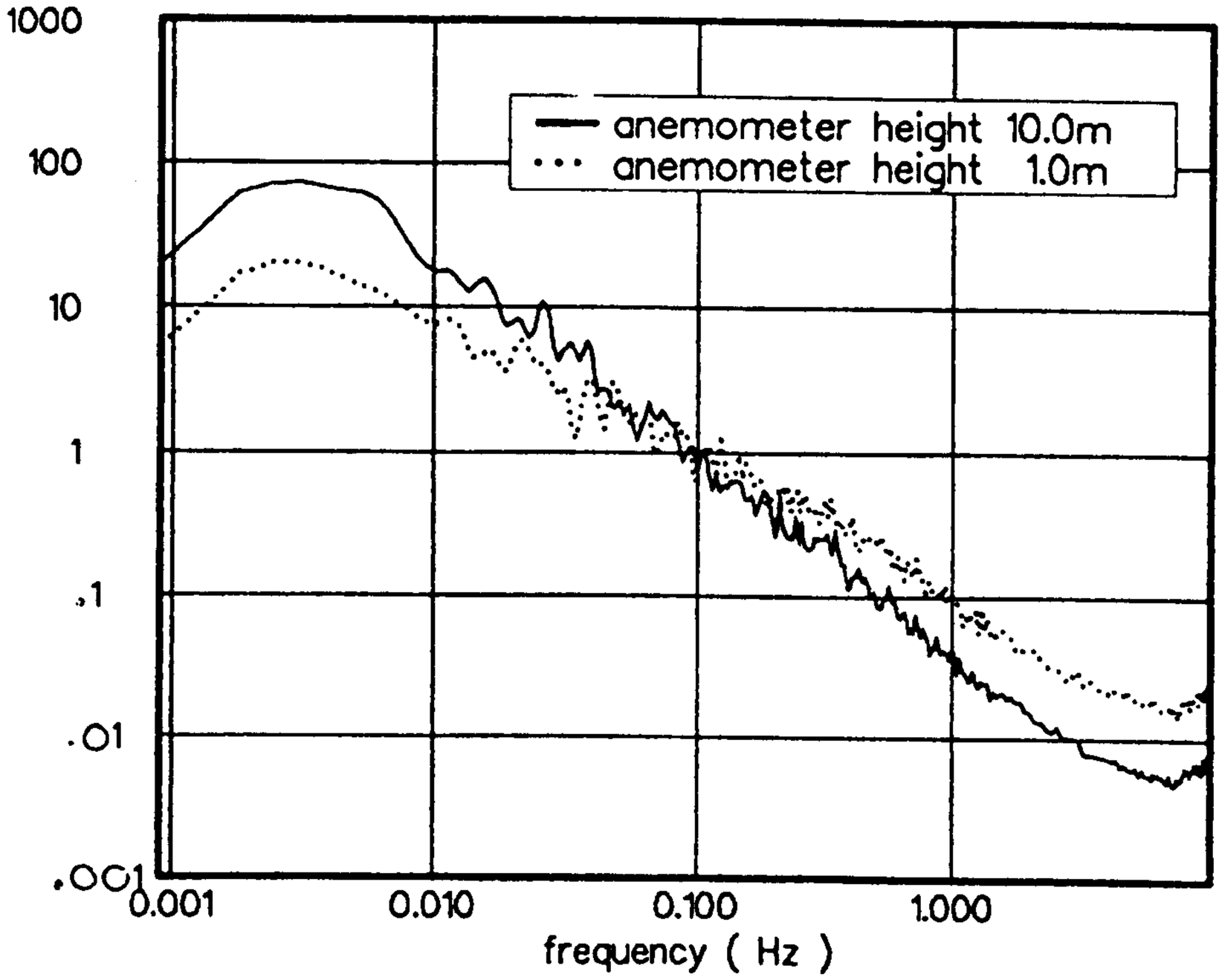

Log - log form showing the gradient of the decay part of the spectra.

Figure 3.1 Comparison of the streamwise wind velocity spectra calculated from measured data at 1.0m and 10.0m heights above the ground, z_0 =0.01m. From Hoxey and Richards (1992).

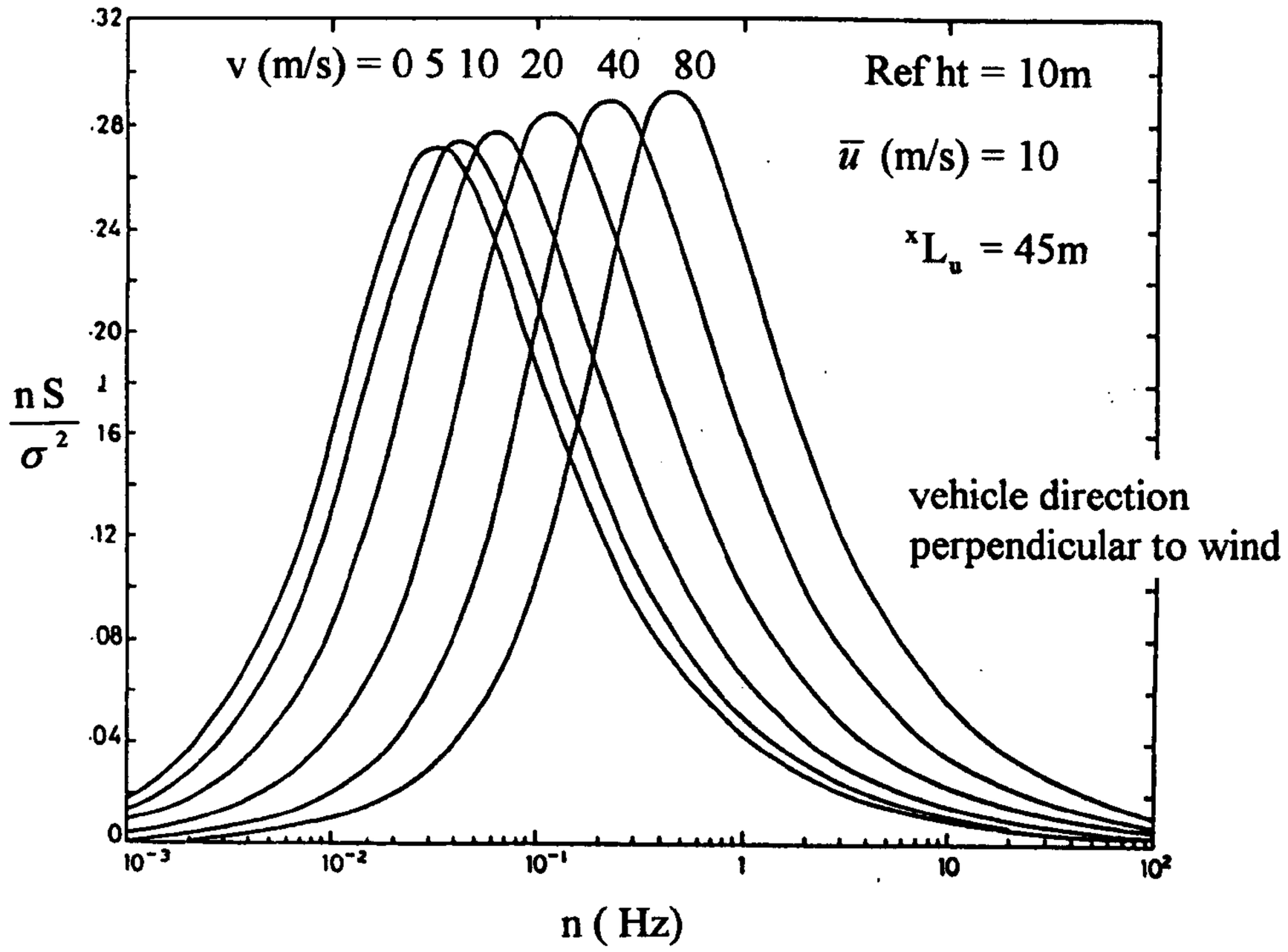

Figure 3.2 Resultant velocity spectra experienced by a moving vehicle calculated using the streamwise wind velocity. From Cooper (1984).

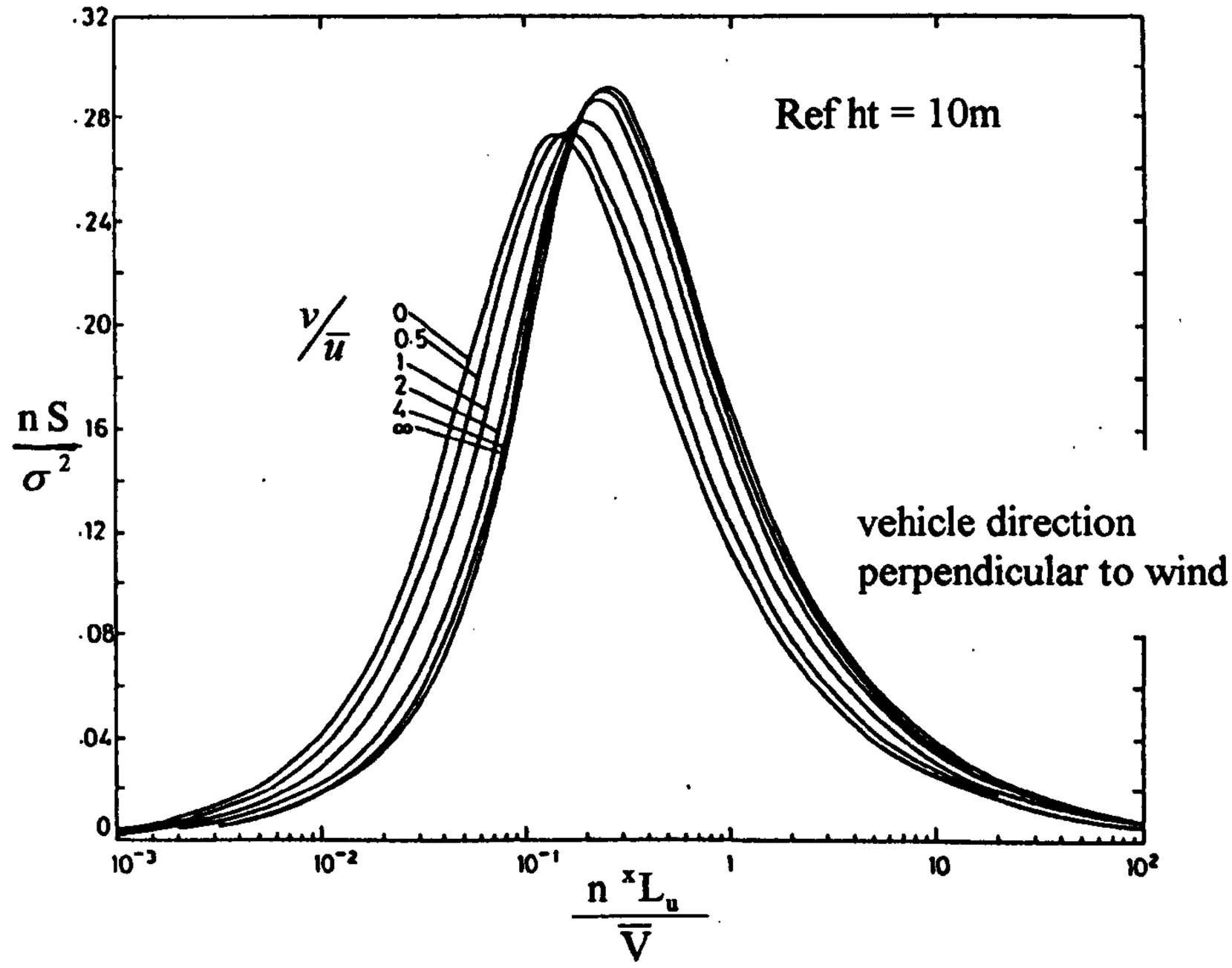

Figure 3.3 Resultant velocity spectra experienced by a moving vehicle calculated using the resultant streamwise wind - vehicle velocity. From Cooper (1984).

4. The Experimental Equipment.

4.1 The wind tunnel.

The Nottingham University environmental wind tunnel occupied the same building, on the university campus, for some 15 years prior to the commencement of these studies. Figure 4.1 shows the configuration of the wind tunnel at the start of the project. It is an open return tunnel occupying around half the height of the building and so allowing plenty of volume for the return flow to move at low velocities.

The working section has a 8 ft x 4 ft (approx. 2.4m x 1.2m) inlet and the original configuration had a working section length of 20ft. The working section is unusual in that it is open but enclosed within a larger room allowing people to stand to the side of the tables of width 9ft which form the working section floor. This is very convenient as access to the working section is available, whilst testing is in progress, due to the relatively slow maximum speed of the wind tunnel of around 17m/s. The wind tunnel is powered by a 42bhp 3 phase electric motor coupled to a 5ft diameter fan of 6 variable pitch blades. The fan rotational speed is therefore controlled by the rotating magnetic field dictated by the 3 phase supply, with some slip depending on the load, i.e. the fan rotates a little slower than that dictated by the 3 phase frequency. The blade pitch is regulated by a vacuum supply such that the natural rest position of the blades with no vacuum, i.e. ambient, is that of full pitch and therefore full wind tunnel speed. As the wind tunnel is powered in this manner the actual maximum speed attainable is controlled by the amount of room leakage, rather than aerodynamic total pressure losses say due to tunnel roughness or intake / exhaust arrangement. That is, the fan motor simply draws more current and hence consumes increasing power until the motor has reached the rotational speed of the 3 phase supply. A maximum current trip is fitted in the motor control system to ensure that the maximum rated power of the motor is not exceeded. If this were reached then the amount of power drawn may be reduced by fitting an exhaust diffuser to the fan.

Measurements of the ambient air temperature in the building that the tunnel occupied showed only an increase of around 0.5 Kelvin per hour of tunnel operation at maximum speed.

As discussed in Chapter 1, one of the requirements of the project was to extend the length of the working section of the wind tunnel to enable a more realistic mean hourly atmospheric boundary layer to be simulated than that achieved during the original tests

at Cranfield Institute at Technology, (see Johnson (1981)). The working section of the tunnel was therefore extended to the maximum size dictated by the building. To give a reasonable distance for the fan exhaust, some 4m as in the original geometry, the working section was extended to 11.7m in length. Figure 4.2 shows the revised wind tunnel, including the installed moving model rig sited 2m from the end of the working section, The building had to be extended at either side to allow for the moving model rig to be incorporated.

Referring to figure 4.2 the new configuration of the wind tunnel at Nottingham University incorporated a control room positioned so that the door to the working section, by the moving model rig, could be conveniently left open whilst the tunnel was operating. The control equipment for the wind tunnel was moved from near the fan outside the tunnel into this room.

It was not expected that the incorporation of the side buildings containing the moving model rig would influence the flow quality or wind tunnel speed significantly providing that the roof and window was sufficiently sealed. As discussed, the losses due to the increase in ground board friction and the length of shear layer development between the open jet and the stationary air to the sides of the working section, manifested themselves in greater current being drawn by the fan. Indeed the current limiting trips had to be reset to allow the fan motor to achieve maximum speed with full blade pitch after the wind tunnel modification had been completed.

It was found that the maximum wind tunnel speed, measured in the working section inlet had now being reduced to 14m/s from 17m/s in the original design, because of the small increase in leakage, particularly in the region round the moving model rig. The modified wind tunnel flow characteristics are described in Chapter 6.

The very sturdy 2m diameter turntable present in the original tunnel was relocated immediately in front of the moving model rig. This could be moved to any location as it is interchangeable with the other working section tops. Another useful feature was that the working section could easily be raised or lowered by up to 300mm or completely removed.

The development of the wind tunnel needed to be co-ordinated with the installation of the major elements of the moving model rig, namely the 2 tonne concrete blocks forming the track base which were aligned perpendicular to the flow direction using a theodolite. Figures 4.3 to 4.7 show the work in progress. These modifications to the

actual wind tunnel and the building took 8 months to complete. The revised wind tunnel was operational in January 1990.

4.2 The moving model rig.

The moving model rig used for these experiments is owned by British Rail Research. It was designed and developed in the late 1970's as a tool for studying the overturning risk of the Advanced Passenger Train, the results of which are described in section 2.2.2. The rig was installed in the 2.4m x 1.2m environmental wind tunnel at the College or Aeronautics, Cranfield Institute of Technology. Prior to the commencement of the present studies the rig was still located at Cranfield although it had not been used since the original tests in 1981. Full details of this previous version of the moving model rig are described in Harrison (1982).

The moving model rig consisted of a high quality guideway on which a trolley carrying the live vehicle and amplifier travelled via high quality bearings. In order to reduce low frequency mechanical vibration the guideway was mounted on a machined steel 'I' beam which in turn was clamped at 200mm intervals on to eight 2m long concrete blocks. The track length was therefore 16m. The main consideration here was that the mechanical noise should be only significant at high frequencies and therefore could be separated from the relatively low frequency aerodynamic signal. With the live vehicle mounted on 6mm square supports the lowest frequency due to mechanical noise was around 125Hz and therefore acceptable as the highest aerodynamic signal of interest was around 70Hz. Figure 4.8 shows details of the live trolley, firing trolley and the track mounting arrangement.

The live trolley was catapulted by a firing trolley by means of rubber bungees and braked using another set of bungees and the application of friction via spring steel hoops applied to brake linings fitted to the trolley sides. The data were captured during the tests by means of a cable hung high above the wind tunnel. A gap was placed in the working section of the tunnel at the moving model rig position to allow this cable to pass during the test. The rig was operated by 4 people with the rig fired and the live trolley retrieved manually.

The next sections describe the installation of the rig at Nottingham University and its development in order to improve its performance compared to its original use at Cranfield.

4.2.1 The rig used for the first series of tests.

The rig described in this section was used for the tests described in Chapter 8. The general layout of the rig is shown in figure 4.9. The components shown in figure 4.8 were used as in their original arrangement at Cranfield.

One of the compromises at Nottingham University was the necessary reduction in track length to 12m due to space considerations. Referring to figure 4.2 the out buildings added to the wind tunnel building were restricted in size due to the presence of a car park road at the firing end and another building at the braking end. Based upon the past experience of using the rig this was not expected to be a problem and this was borne out as adequate vehicle speeds were obtained.

At Nottingham the entire moving model rig was in the same room as the working section which eliminated wind tunnel leakage at the slot needed for the model supports to traverse the ground board because there of the lack of static pressure difference between the working section and underneath its floor. Referring to Bernoulli's formulae, equation 3.2, the static pressure in a wind tunnel working section decreases due to the acceleration of the air through the tunnel inlet. This caused a problem with the original configuration at Cranfield Institute of Technology as the moving model rig was situated underneath but outside the working section creating a strong jet through the slot when the balance and other model supports traversed the working section. This made the interpretation of the lift and pitch components difficult.

The main developments of the rig for the first series of tests, reported in Chapter 8, were:

1. The installation of an automatic firing and trolley retrieval mechanism.

2. The fitting of an automatic data logging system.

3. Improving the model mounting arrangement.

The first modification enabled the running of the moving model rig to become a one person operation rather than four at Cranfield. One hundred runs of the rig were possible in one day's testing.

The second modification was really due to the advancement of portable light weight data loggers since the Cranfield tests. However this was of major benefit as the long cable used in the Cranfield tests was prone to snagging on the entry to the wind tunnel and further was subject to fatigue causing delays to testing.

Referring to figure 4.9, the automatic retrieval system consisted of a continuous loop of steel wire which ran slowly along each side of the rig though a channel with an open slot on the outer face. The wire was fitted with steel lugs which provided the guidance and allowed the system to be powered by wheels at the firing end, into which these lugs fitted. Figure 4.10 shows this and the mechanism and electric motor which powered this retrieval / firing system. The motor powered the wheels independently at the firing end of the rig by means of commercially available V belts and pulley systems. These belts, which slipped if the load was too great, ensured that an equal load was experienced by the two steel loops either side of the track and applied to the trolley. This simple system worked very well with the belts under the tension recommended by the manufacturer. Two larger lugs were fitted, 180 degrees apart on the wire loops, which protruded through the slot of the channel which contained the wire designed to retrieve and fire the live trolley. The firing sequence is as follows, referring to figure 4.9, with the live trolley at point A :

1. The live trolley is retrieved and pushed against the firing trolley through which the bungees pass (figures 4.11 and 4.12).

2. The live trolley is hauled back in turn pushing the firing trolley until released by the lugs moving downwards at the firing point as shown in figure 4.13.

3. The firing trolley accelerating towards the working section pushes the live trolley until it reaches the working section when the light aluminium firing trolley is arrested by the tension in the bungees and the 10kg live trolley crosses the working section at near constant speed until arrested at point C as shown in figure 4.14. The trolley is retrieved quickly by the second set of lugs 180 degrees apart in the loop from the pair which fired the trolley.

The cycle takes around 30 seconds.

The data logging and control hardware, and the associated power source were fitted on to an aluminium platform hanging from the side of the live trolley as shown in figures 4.11 and 4.13. This arrangement was chosen in order to keep the supports of the live

vehicle as short as possible so that the frequency of the mechanical noise would be kept high. Figure 4.15 shows the construction of the working section in the vicinity of the slot.

Figure 4.16 shows the mounting of the live vehicle using 10mm high tensile threaded bar located through slots on 30mm by 30mm by 10mm thick aluminium angle. This enabled vehicles to be fitted much quicker than with the original design which was also tried (Harrison (1982)). Note that for the DB railway container vehicle shown in figure 4.16, only the container was live and the truck beneath it was not touching the container and was supported separately using 2mm screw threaded bar. Figure 4.17 shows a live vehicle, in this case the 1/50th scale lorry, traversing the working section.

Figure 4.13 shows the steel notch that passes through the infrared sensor activating the on board data logger. The infrared sensor was mounted on the underside of the platform and can be seen in figure 4.13. Figure 4.12 shows one of two other notches that enable the position and the speed of the trolley to be calculated from the digital data recorded from the sensor.

The shortcomings of this version of the rig, discussed in detail in Chapter 8, were :

1. Low frequency mechanical vibration, despite the stiffening bars that were used, caused by the low natural frequency of the platform when supporting the data logger and control equipment.

2. The release mechanism was far from smooth due to the slightly different timing of the release of the live trolley by the two lugs on the pull back mechanism fitted either side of the track. This caused two problems:

a) The injection of a large mechanical impulse on the system just prior to release.

b) The release mechanism jammed for trolley speeds above 10m/s, i.e. high tension, after one side of the trolley was released by the pull back mechanism. This left the live trolley stranded under tension at the firing position held by the lug on the other side of track. In this situation the friction was too great for the pull back mechanism to pull the trolley back and enable it to be released.

Despite these problems the pull back mechanism worked reasonably reliably for trolley speeds less than 10m/s. The speed of the trolley was governed by the number and

tension of the bungees which were anchored to rails fitted to the sides of the moving model rig base.

4.2.2 The rig used for the second series of tests.

The rig was developed further in order to overcome the problems encounted during the first series of tests. The full characteristics of this rig are discussed in Chapter 9. Briefly the rig was improved as follows:

1. The release mechanism was improved by the introduction of a third trolley which was used to release both the firing and live trolley smoothly from a single point. This trolley therefore was pulled back by two steel hoops and was only released after the other carriages had been released from it. This third trolley was therefore under low tension and was not released until after the data had been acquired from that particular run.

2. The data logger and control equipment was mounted directly on top of the live trolley removing the low frequency resonance. In order to lift the live vehicle higher above the trolley because of this extra equipment mounted on the trolley an aluminium block was inserted between the live vehicle mounting already described in 4.2.2. This had a negligible effect on the frequency of mechanical vibration.

This final version of the moving model rig is shown in figure 4.18. A description of the working of this rig, starting from point A with the third and firing carriage coupled, is as follows.

1. The trolley is retrieved and pushed against the firing trolley through which the bungees pass, as shown in figures 4.19. As the live and the firing carriage are just pushed together the lugs on the retrieval system release the live trolley and continue past the firing trolley. Note that a spring loaded light magnet situated on the firing trolley ensures that these stay coupled.

2. The lugs of the pull back mechanism engage the third trolley, see figure 4.20, and pulls this towards the firing point, see figure 4.21. The mechanism on the third trolley for holding the firing carriage, under increasing tension, was that used for releasing the trolley originally at Cranfield and is shown in figure 4.22.

3. The firing carriage is released when the handle on the release mechanism on the third carriage is pushed toward the other trolleys. The was done by fixing a post by the side of the track which encounted this handle as the trolley was moved towards it. This is seen in figure 4.23 which shows the situation shortly after the release of the firing and live carriage.

4. Finally the third carriage is released by the lugs in the pull back mechanism by use of dips in their tracks and the third, light, virtually frictionless, carriage is brought back to the firing carriage by another very light bungee, as seen in 4.23. Another post pushes the release handle further in the direction of release, before this trolley is released, so that it does not interfere with the firing trolley release point and to aid its subsequent coupling to the firing trolley.

5. As the jaws of the release mechanism are now fully open as it encounters the firing carriage a second post at the side of the track knocks the release handle to the locking position just after coupling as shown in figure 4.24. These carriages are ready then for the arrival of the live trolley which is done as described in the 4.2.2.

Another minor improvement to the system included fitting a further two notches on the track that the infrared sensor mounted on the trolley could detect, therefore providing information for average speeds to be calculated across three sections, spanning the test section, of the rig. For three trolley speeds, with the wind tunnel operating at maximum speed these sample results are shown in table 4.1 and it can be seen that the deceleration of the live trolley is negligible. It was found that by marking the position of the firing trolley release point for the various trolley speeds tested, tests at repeat yaw angles could easily be conducted.

4.3 Data acquisition equipment.

The Polycorder (700 Series), manufactured by Omnidata International, was chosen as a suitable commercially available data logger. Its prime specification was that it could sample at a reasonably high rate - 2000Hz multiplexing. Thus for 5 channels the sample frequency was 400Hz for each channel. Also it could record a number of digital data channels at the 2000Hz sample rate simultaneously which was used for monitoring the position of the trolley using the infrared sensor arrangement. The first positioning point was at the release point and was used for triggering the logger. The data logger was programmed in machine code by the use of a user friendly utility program (Polytools) installed on the P.C. and downloaded to the

Polycorder via a RS232 cable. The logger had 12 bit resolution (4096 levels) and 256KB RAM and could therefore store data from many runs. In practice 10 runs were conducted before downloading the data as this allowed regular checking of the data whilst the next batch of tests were being conducted.

Five separate amplifiers were used to amplify the signals from the 5 component force balance prior to recording. These were as used in the Cranfield tests and are described in Harrison (1982). In order to avoid possible gain variations of these amplifiers due to temperature changes, the amplifiers were mounted in a wooden box. Wood having a low thermal conductivity would allow the amplifier temperatures to stabilise as the rate of heat flux is proportional to the thermal conductivity. This kept the amplifiers at near constant temperature, which would not be significantly be changed by the sudden ventilation around it caused by the intermittent quick movement of the live trolley. (For the tests at Cranfield the amplifiers were mounted within the body shell of a dummy vehicle.) The variable gain resistors, included in the associated amplifier circuitry, were set to their maximum values, throughout these tests, in order that the output signal matched closely to the input range of 0 to 5V of the Polycorder. The measured signals were checked to ensure that the peaks of the measured unsteady forces and moments were not clipped by the maximum allowable input of 5V of the Polycorder.

The power source for the energising of the force balance, the amplifier and the infrared sensor was done using a dry 12v battery. As the voltage requirements of these sources varied, the 12v supply from the battery was transformed to various outputs in an interchange box :

Force balance amplifiers :	+15v and -15v
Force balance strain gauge energising :	0 and 5v
Infrared sensor :	0 and 3v

As the output from the force balance and the amplifier were proportional to the input voltage, the outputs from the interchange box were fitted with voltage regulators with LEDs displayed through the casing to indicate that the correct voltage was being supplied. (A check on battery condition). This interchange box was designed and manufactured by the Department of Civil Engineering. The battery powering

this system was of large enough capacity to enable some 10 hours of continuous use with this system and was charged overnight between the testing days.

The Polycorder used its own internal battery, sufficient to allow one full day of testing.

4.3.1 Data analysis and storage equipment.

An IBM compatible PC was used for this purpose. This comprised of a 80286 processor fitted with a maths co-processor and 1MB RAM with 40MB hard disk. The data was downloaded from the Polycorder to the PC in binary form via a RS232 cable as shown in figure 4.25. The data was downloaded in separate files each corresponding to a single run of the rig. The Polycorder utility program installed on the PC was used for converting this into ASCII data files (.TBL) which were then pre-processed further as described in Chapter 5.

4.3.2 Wind velocity measurements.

These were made using TSI hot film anemometry equipment including the linearising of the output signal. The general purpose probe, model 1210, was used (figure 4.26) in the end flow mode and held rigidly in a simple manually operated traverse mechanism (Coleman (1990).

4.3.3 Force balance.

This was of the same type as used for the original Cranfield tests, (see Harrison 1992). It was manufactured by NUTEM Ltd and was manufactured from Hiduminium 89, a material that was easy to machine and had a high strength to weight ratio. Figure 4.27 shows the balance and indicates the positions of the strain gauge elements.

4.4 The aerodynamic models.

The geometry of the model vehicles used are shown in figures 1.1 and 1.2.

The 1/50th scale lorry model had already been used before in Coleman (1990) for static tests and was manufactured from balsa wood. The square shape of the model undoubtedly helped in achieving a high rigidity. For measurements in the frequency

domain high rigidity and low mass are important to transmit the rapid aerodynamic fluctuations to the force balance.

The 1/45th scale DB railway container vehicles were made using the same technique as for the lorry and were similar in shape. The scale of these vehicles was chosen to be 1/45th instead of 1/50th in order that the internal force and moment balance would fit in the slightly smaller model container. For the live vehicle, the container was only in contact with the force balance, the wagon beneath it being separately mounted. This was because only the forces and moments on the container were required as on the full scale version these containers are just mounted on vertical lugs, unsecured and are free to lift or rotate.

4.5 Analogue filters.

The following analogue filters were used for filtering the force data prior to digitising when recording data for subsequent extreme value analysis.

1. Barr and Stroud EF5 Series. Filter type, 4 Pole Butterworth. Attenuation rate 48dB per Octave.

2. DISI type 55D25. Unknown filter type. Attenuation rate approximately 24dB per Octave.

Table 4.1 Comparison of the moving model trolley mean speeds across the test section and their repeatability.

Maximum wind tunnel speed = 8.5ms at the reference height of 60mm at moving model test position.

Mean trolley speed calculated over complete 1.5m test section. (m/s). (Repeatability - S.D. over 100 runs.)	Mean speed across 1st 0.5m section (m/s)	Mean speed across 2nd 0.5m section (m/s)	Mean speed across 3rd 0.5m section (m/s)
3.10 (0.02)	3.15	3.10	3.06
6.48 (0.03)	6.53	6.46	6.44
11.15 (0.05)	11.23	11.13	11.09

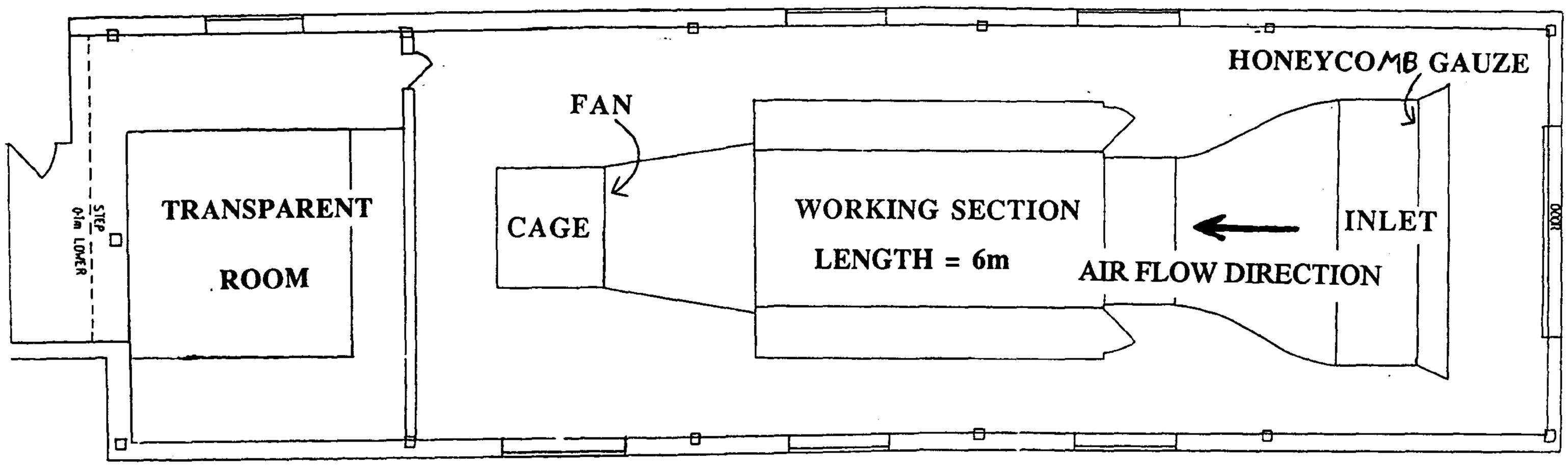

Figure 4.1 Original configuration of Nottingham University's 2.4m x 1.2m environmental wind tunnel.

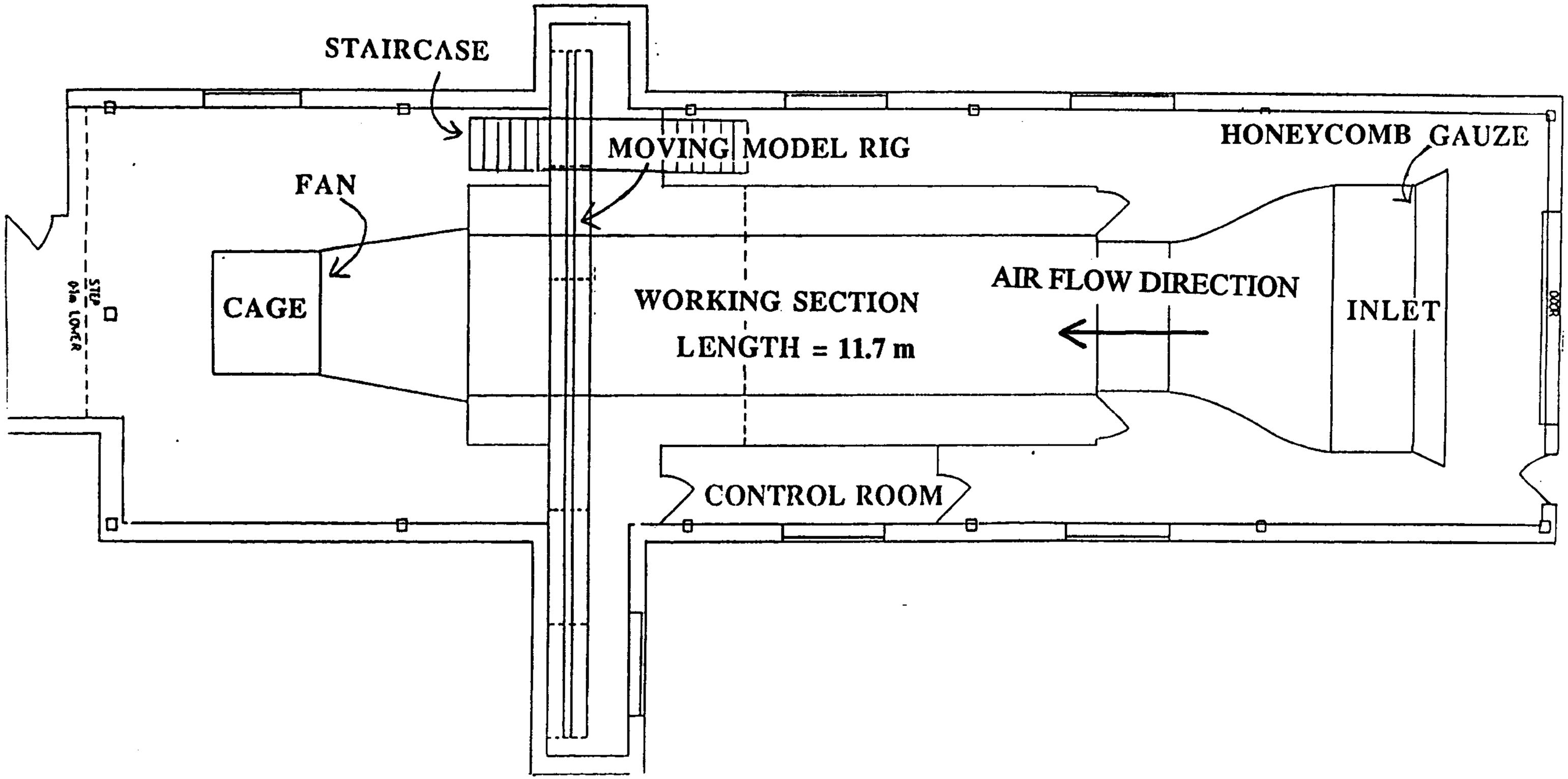

Figure 4.2 Revised (1990) configuration of Nottingham University's 2.4m x 1.2m environmental wind tunnel.

Figure 4.3 Construction of one of the building extensions to accommodate the moving model rig. This shows the firing end.

Figure 4.4 Transporting to the wind tunnel entrance, one of the six 2 tonne concrete blocks forming the base of the moving model rig.

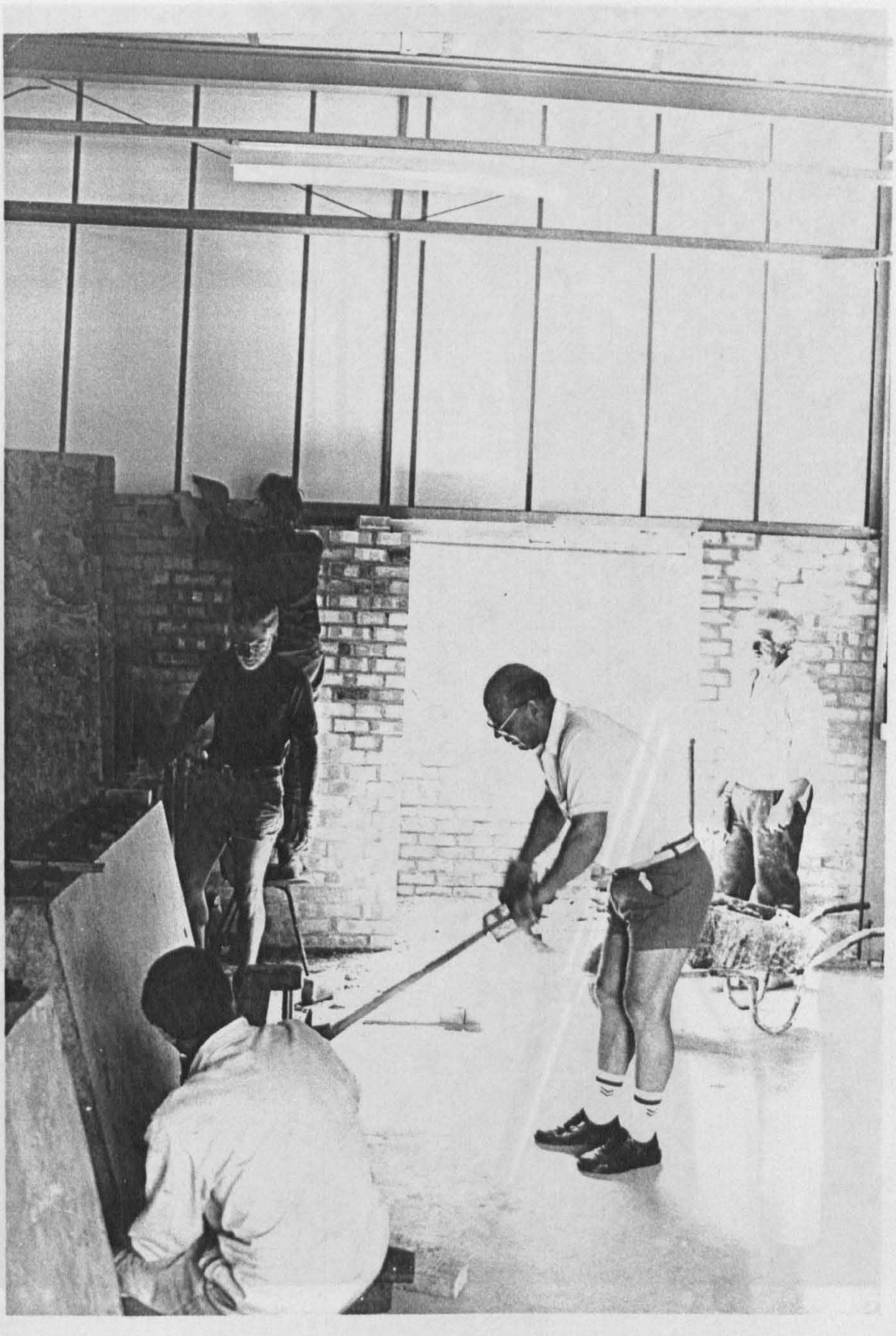

Figure 4.5 Using a hydraulic jack to place the concrete blocks into position. Note that this was done whilst the original wind tunnel had been split in two halves prior to building the extension to the working section.

Figure 4.6 Placing the concrete blocks perpendicular to the wind tunnel flow direction using a theodolite.

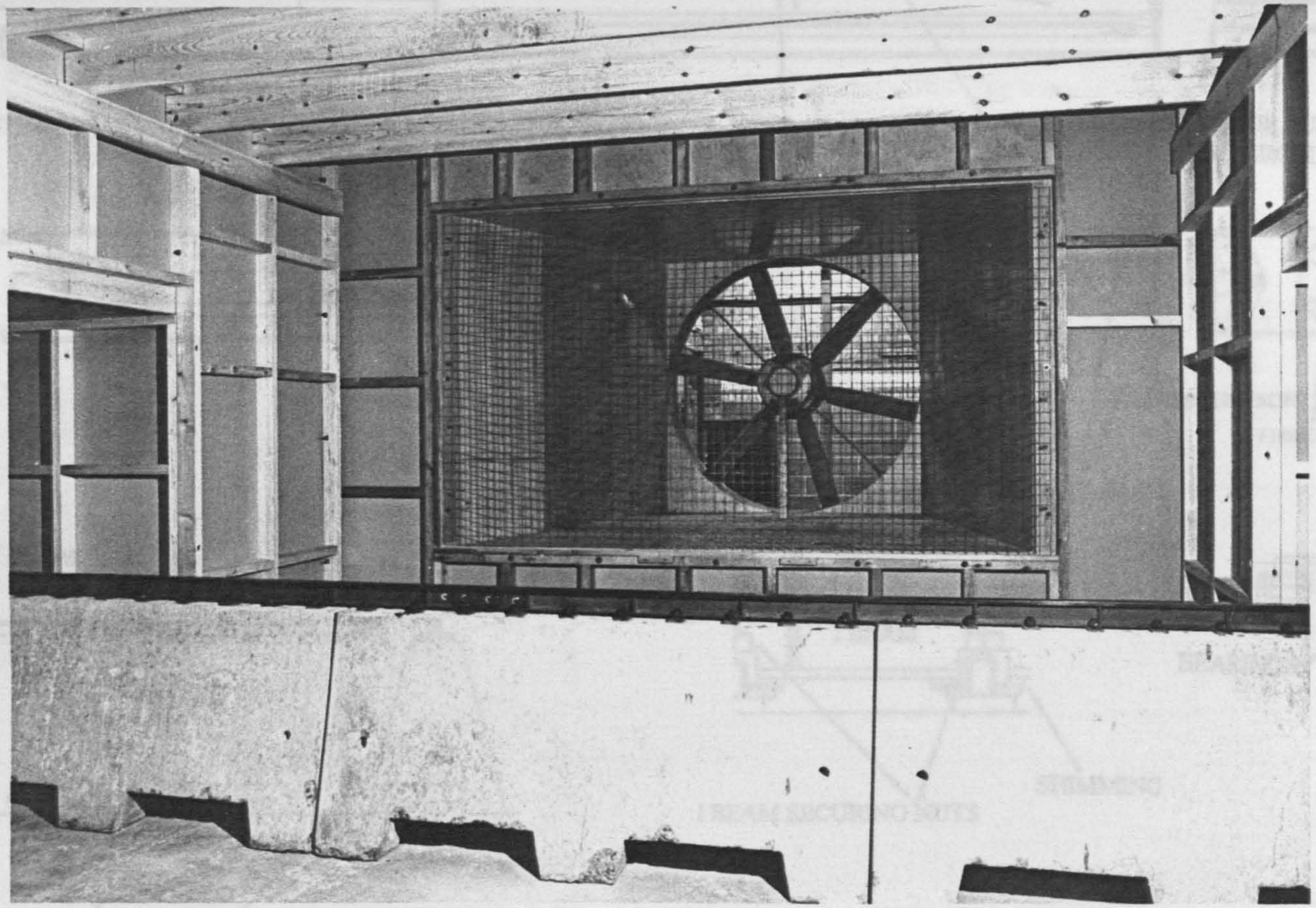

Figure 4.7 The revised wind tunnel working section extension before the installation of the working section floor. The moving model rig track (I beam) is shown installed on the concrete blocks. The flow collector section, fan and motor are from the original tunnel.

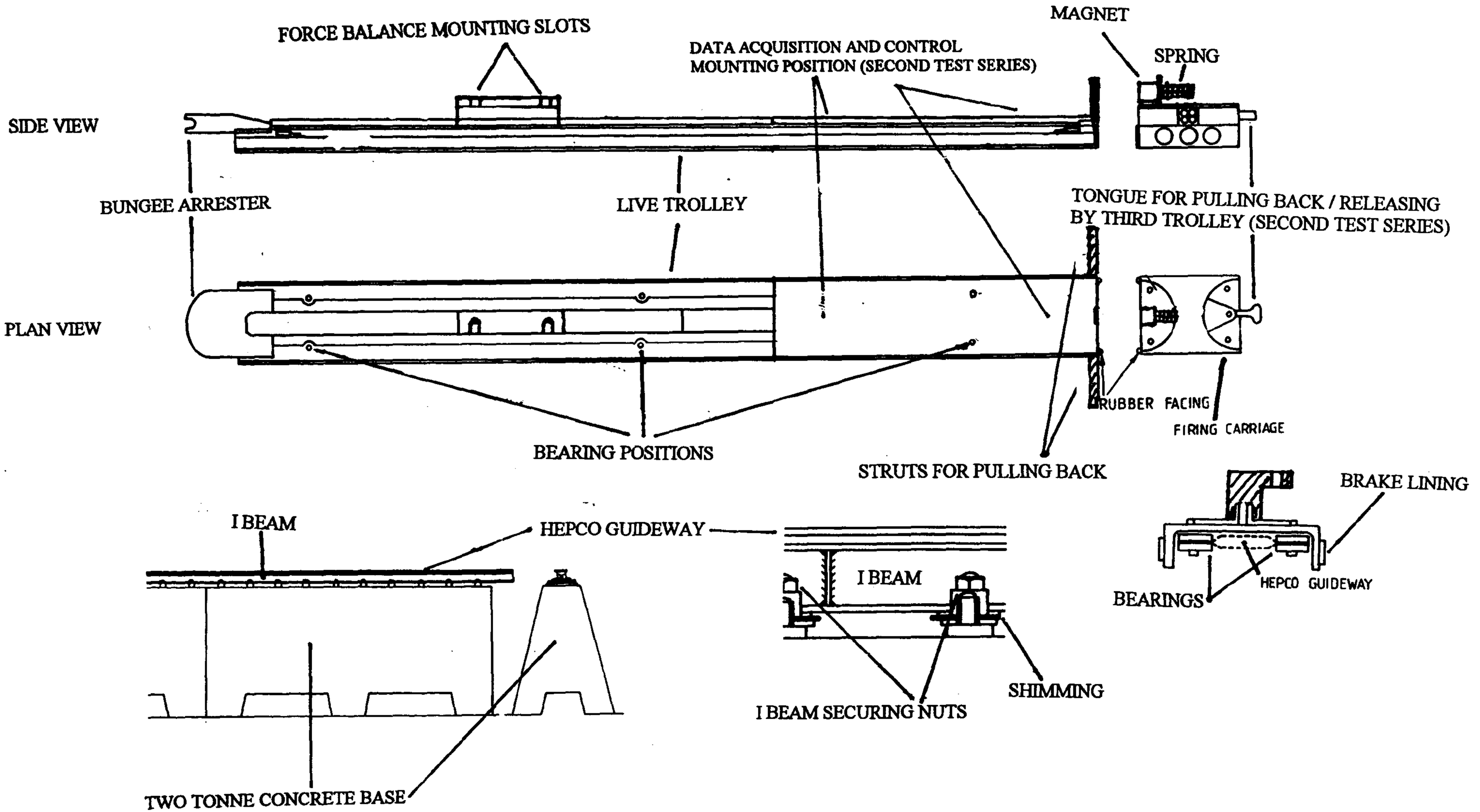

Figure 4.8 The track, live trolley and firing trolley geometries.

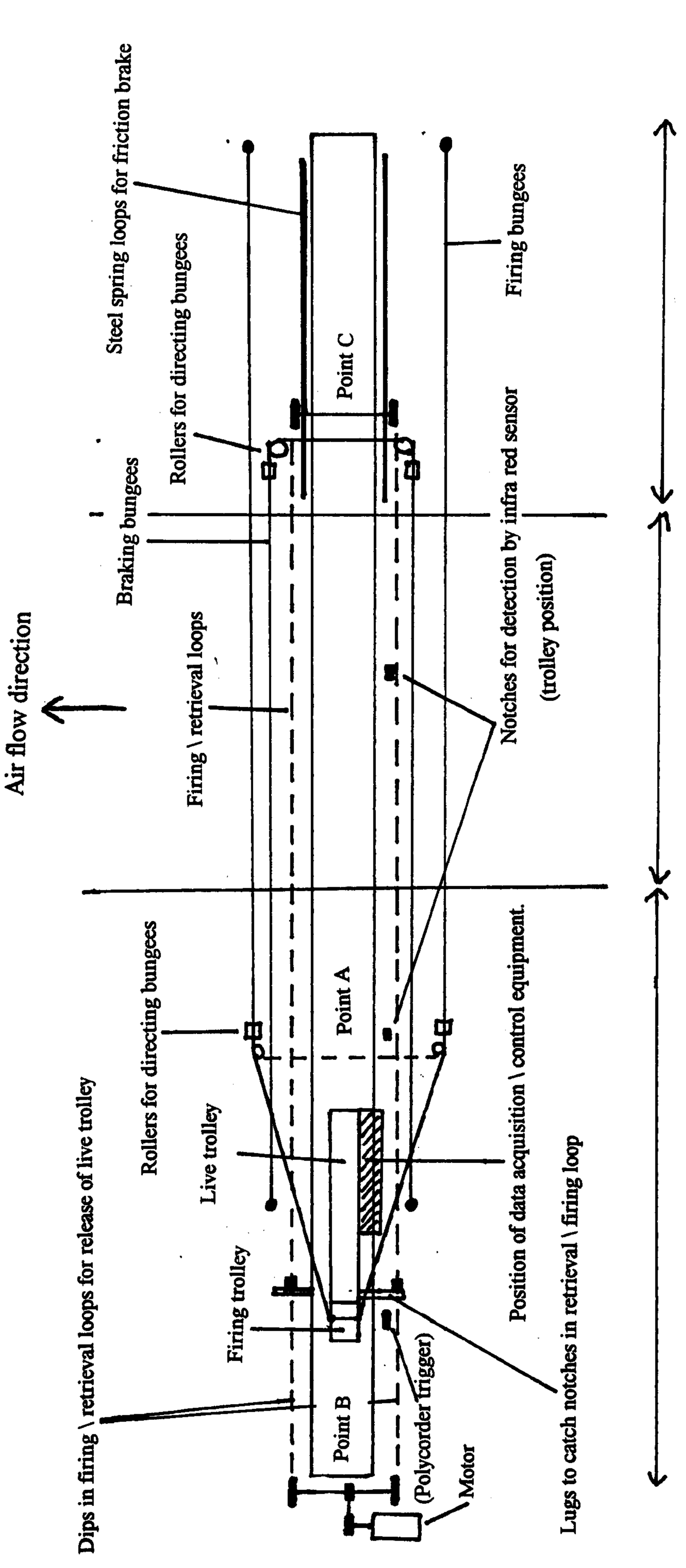

Figure 4.9 General layout of the moving model rig used for the first test series.

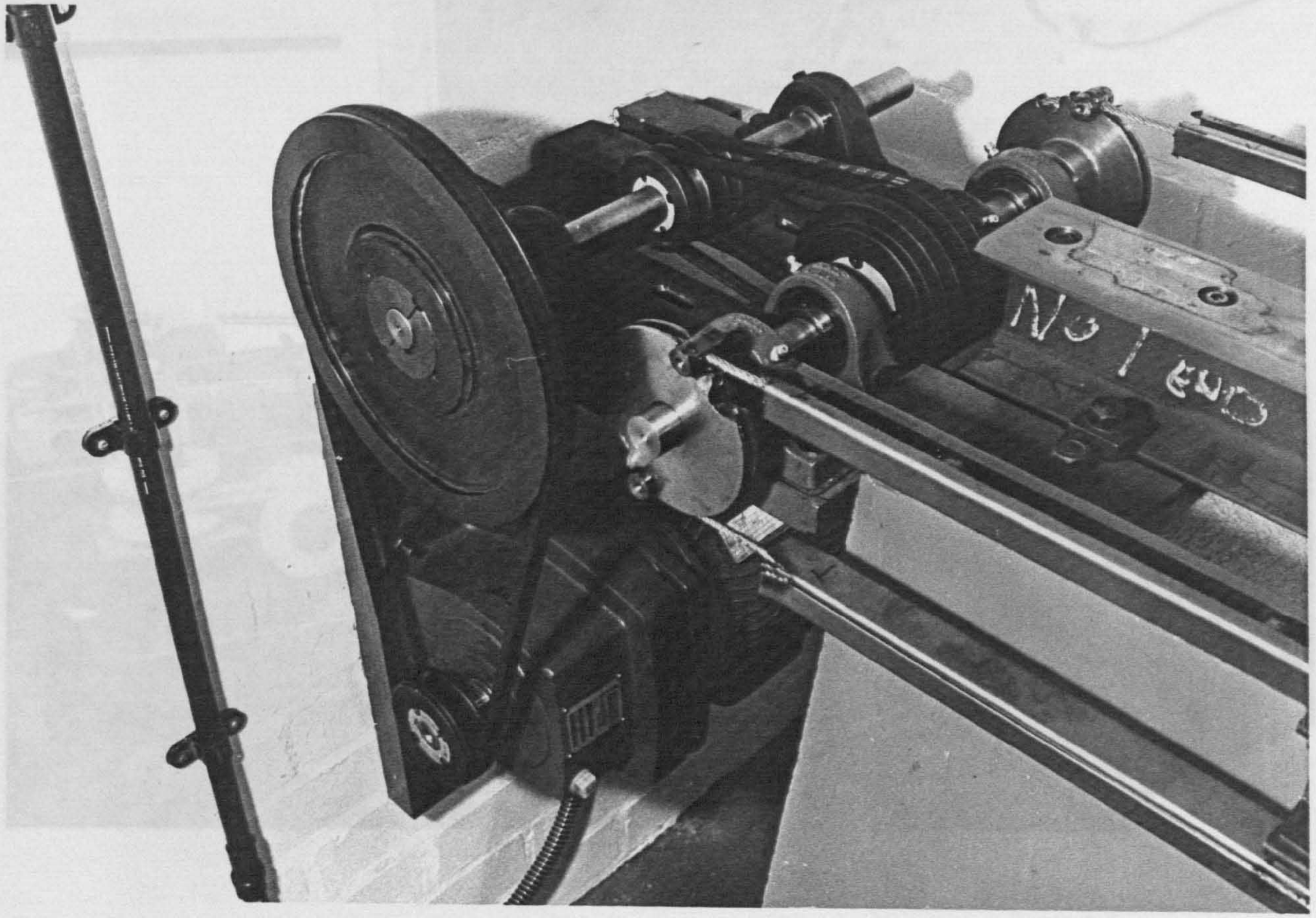

Figure 4.10 The trolley retrieval / firing system drive system.
As used for the second test series.

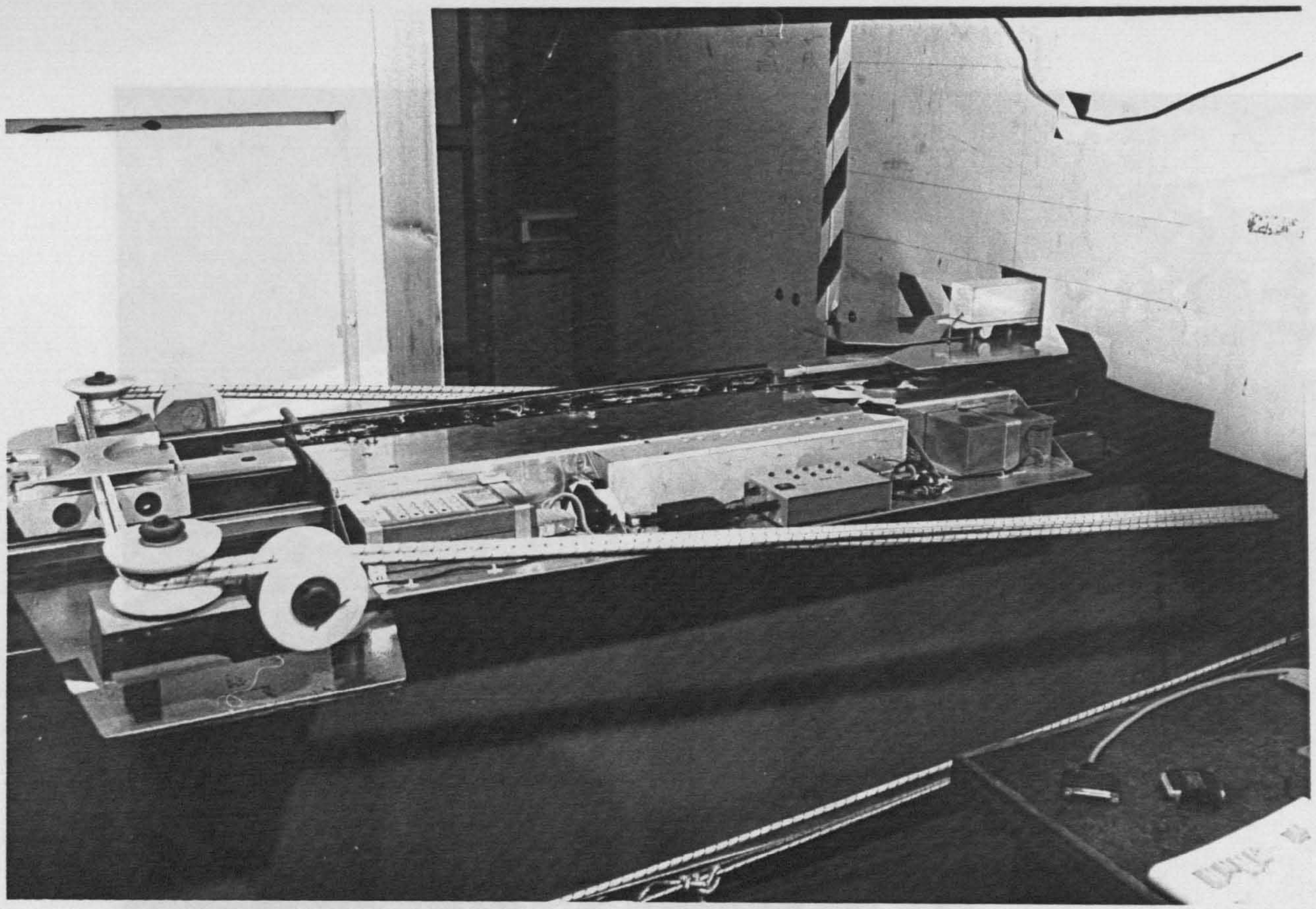

Figure 4.11 The moving model rig used for the first test series.
The live trolley being brought back to the firing trolley.

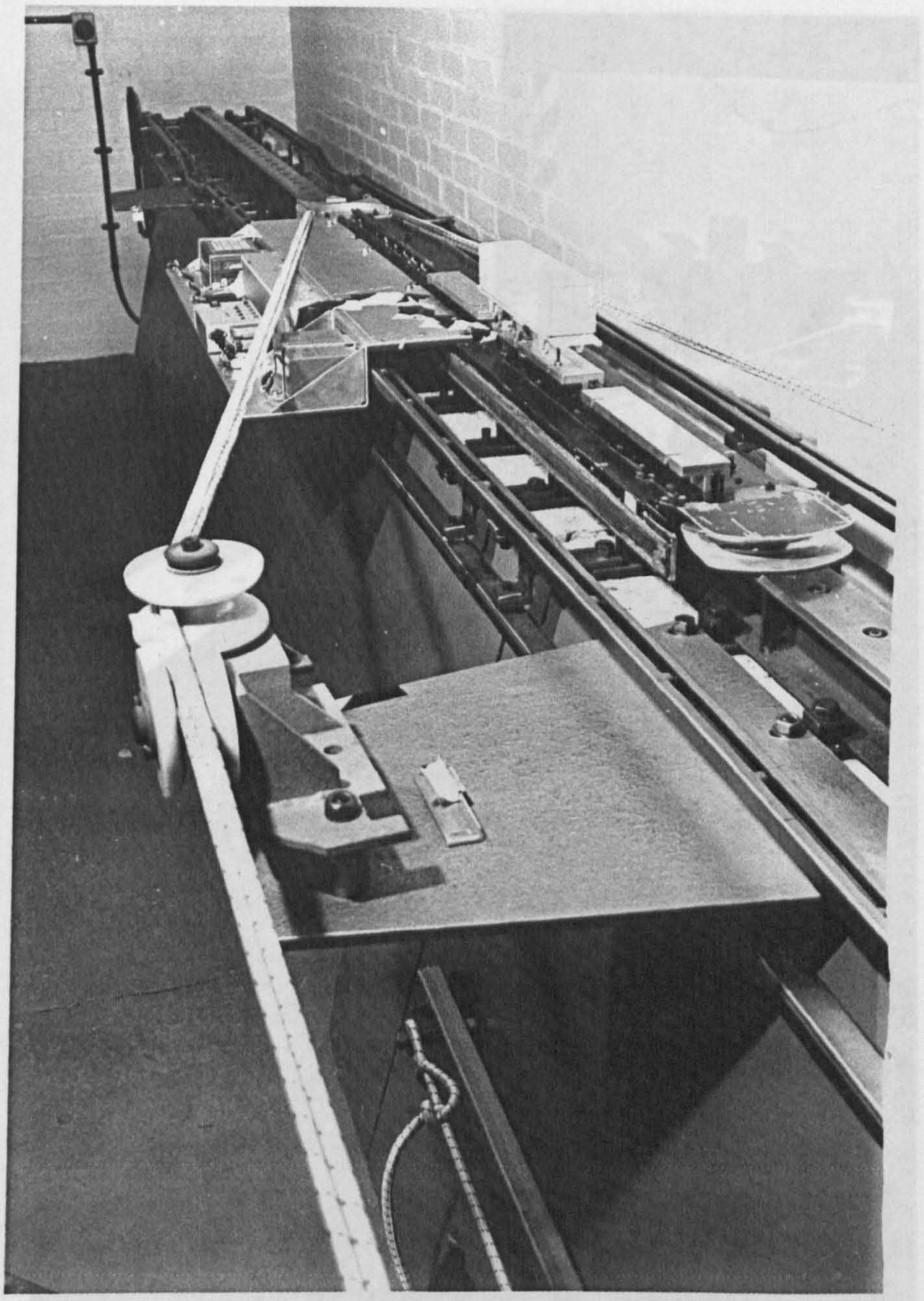

Figure 4.12 The moving model rig used for the first test series.
The live trolley pushing back the firing trolley towards the release point.

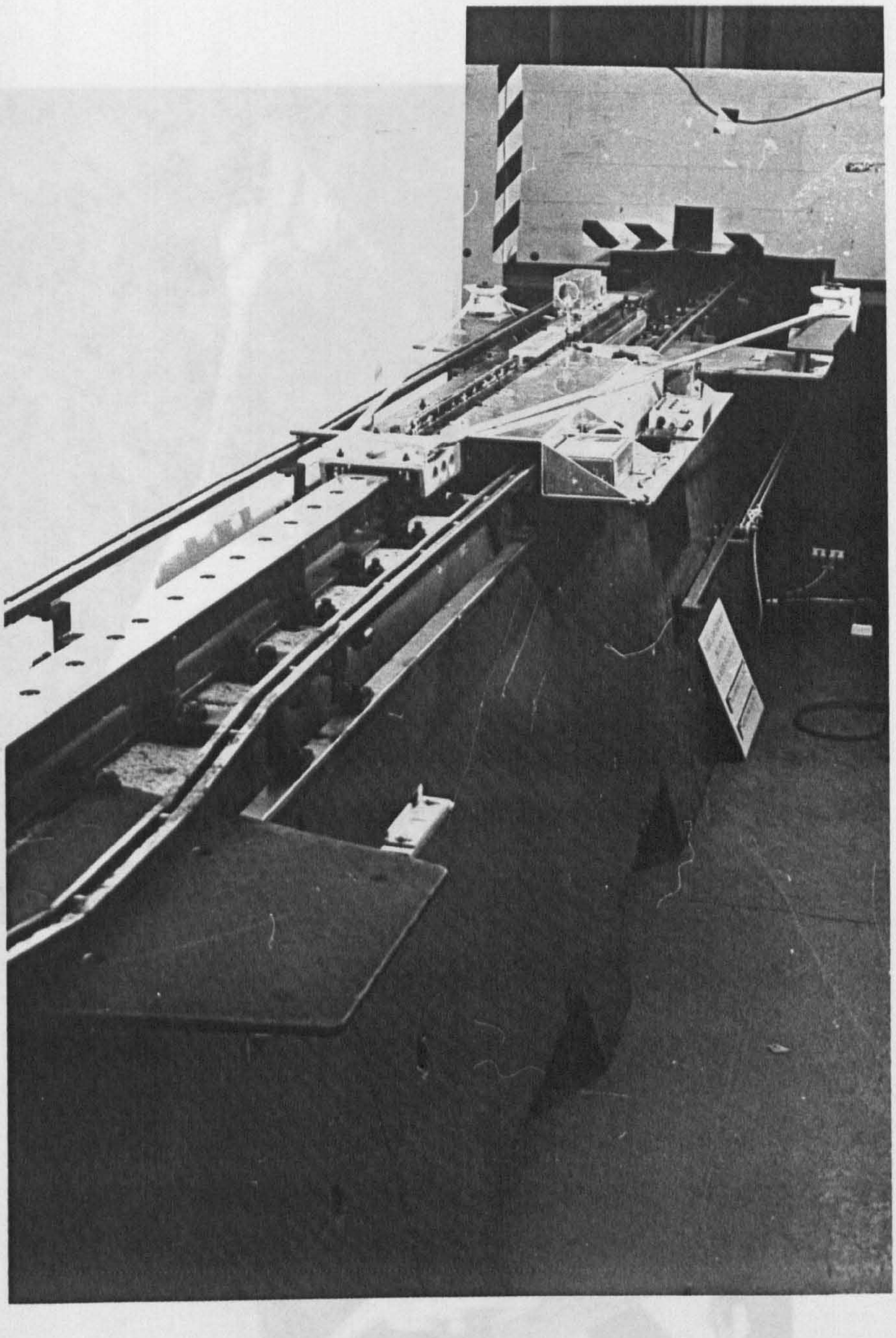

Figure 4.13 The moving model rig used for the first test series.
The live trolley pushing back the firing trolley towards the release point (the dips in the retrieval system track).

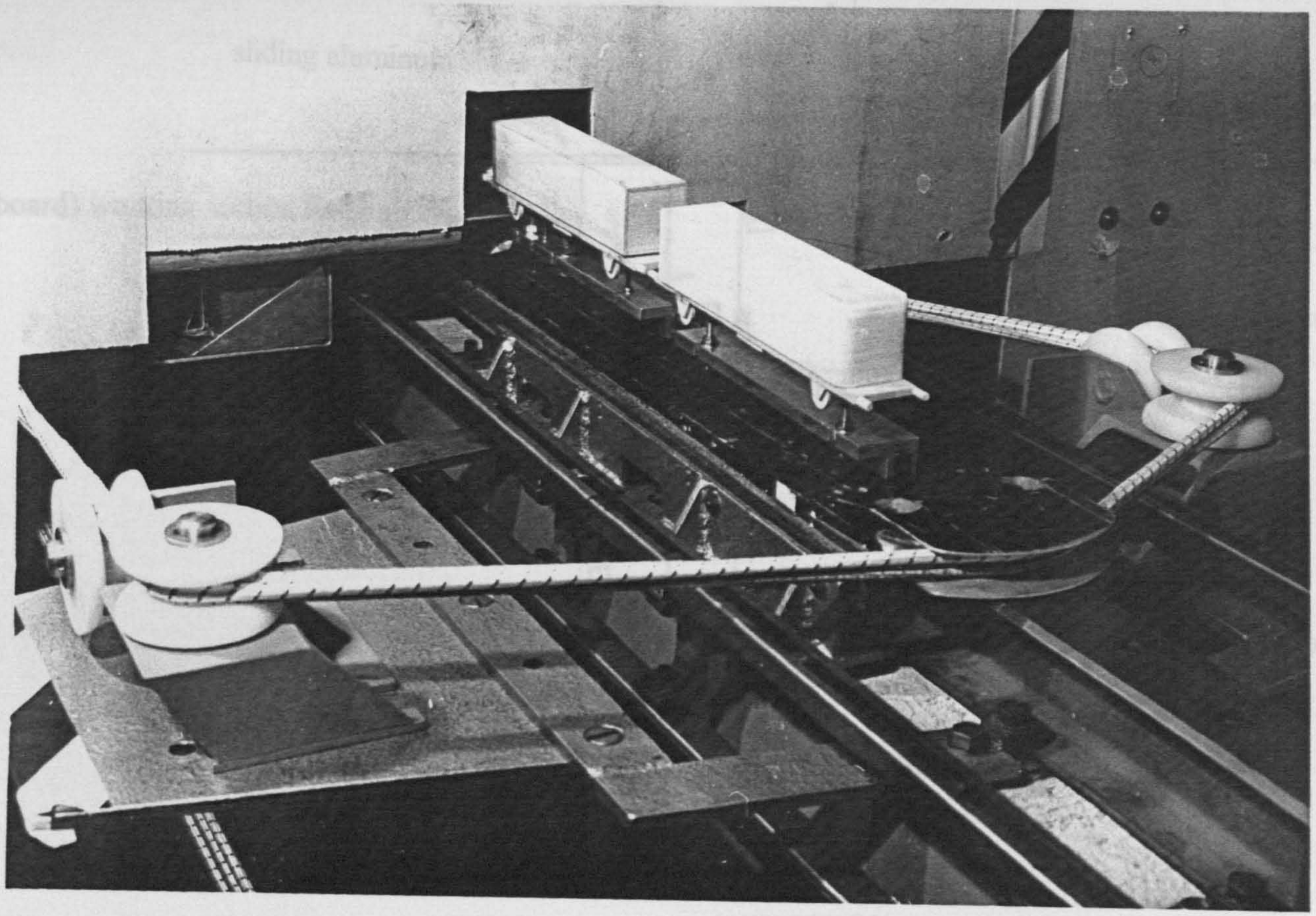

Figure 4.14 The moving model rig used for the first test series.
The live trolley being arrested by friction brakes and rubber bungees soon after leaving the working section.

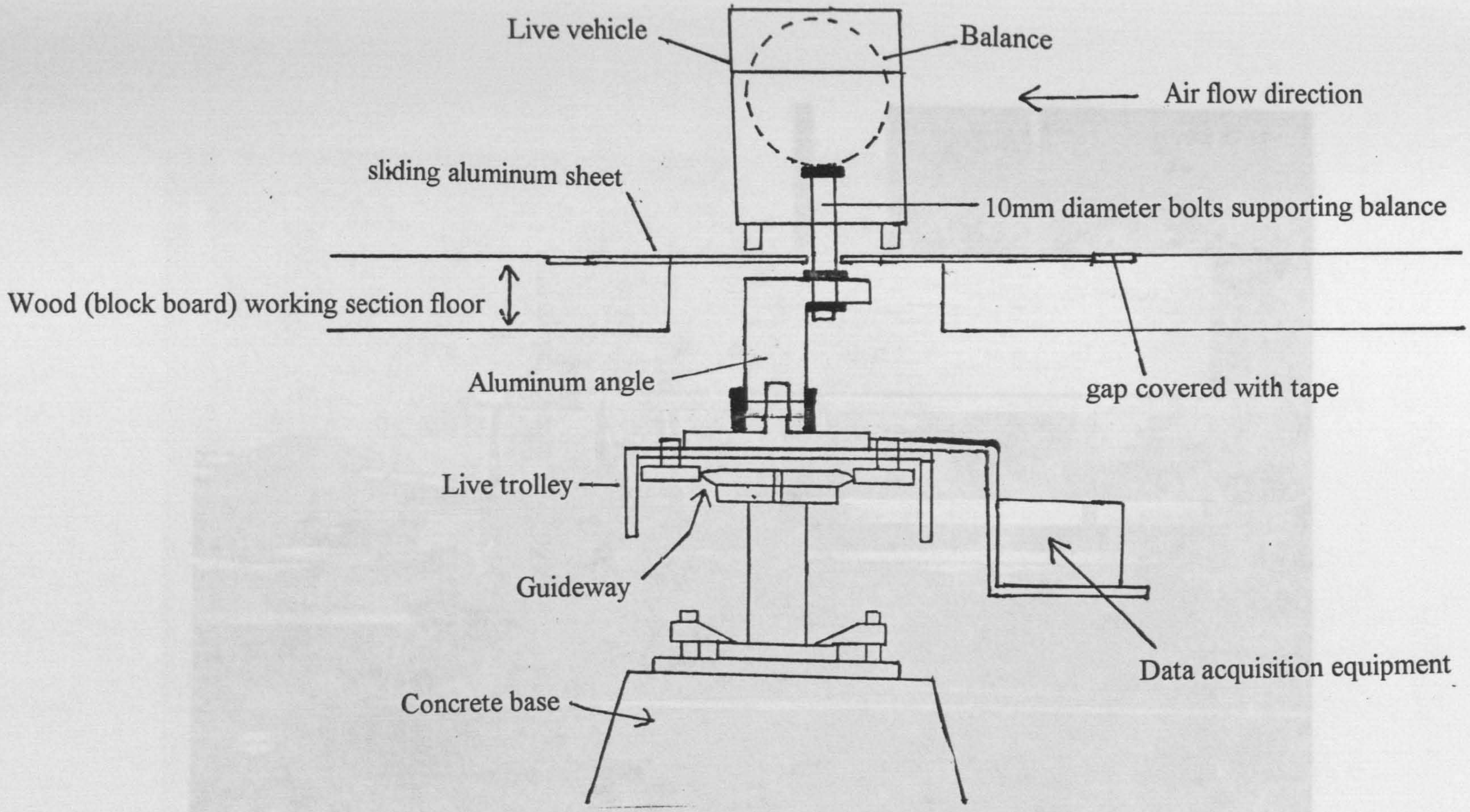

Figure 4.15 Working section slot and model mounting arrangement.
The moving model rig used for the first test series.

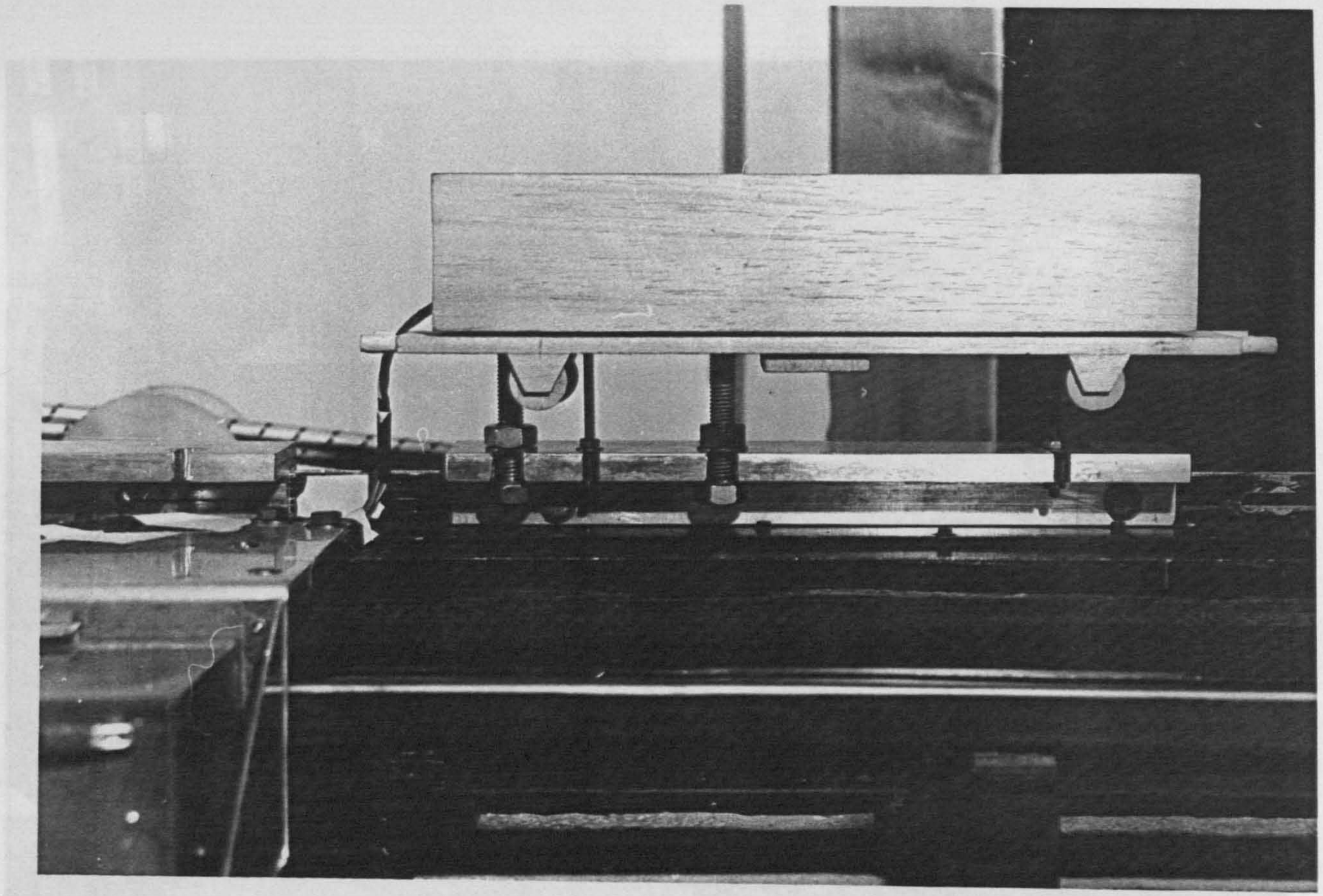

Figure 4.16 Close up of the live D.B. container model and wagon showing their mounting arrangements to the trolley.
The moving model rig used for the first test series.

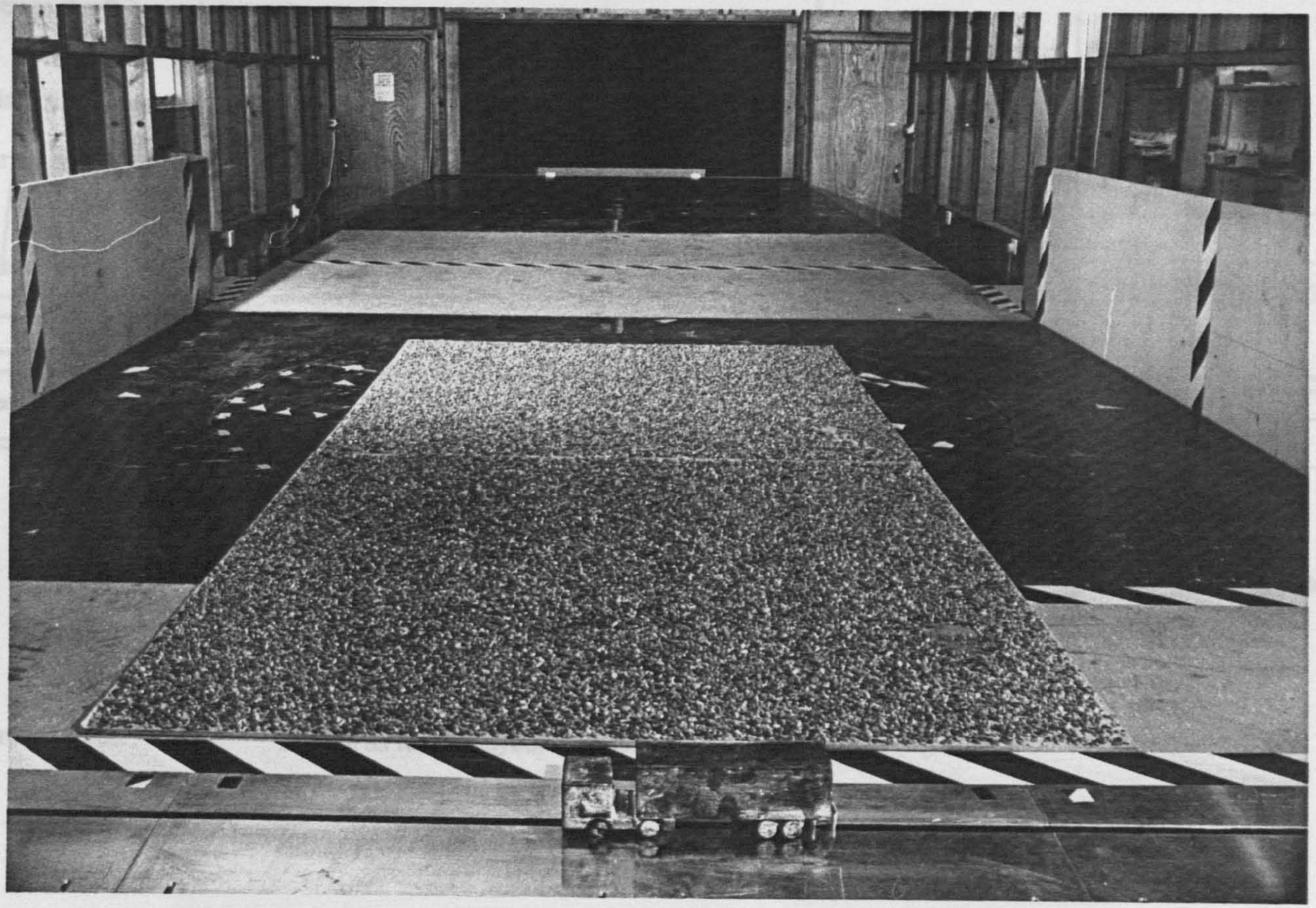

Figure 4.17 Live lorry model traversing the wind tunnel's working section.
As for both the first and the second test series showing the upstream fetch.

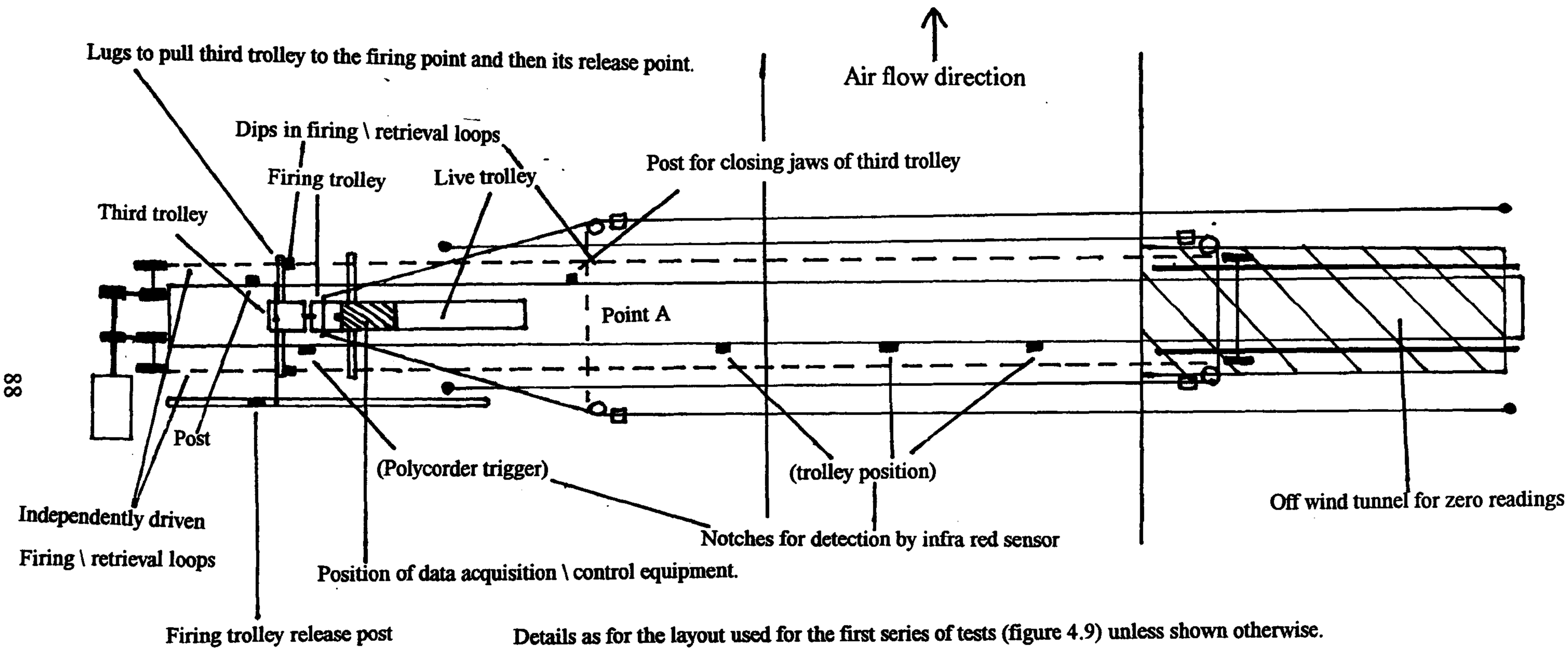

Figure 4.18 General layout of the moving model rig used for the second test series.

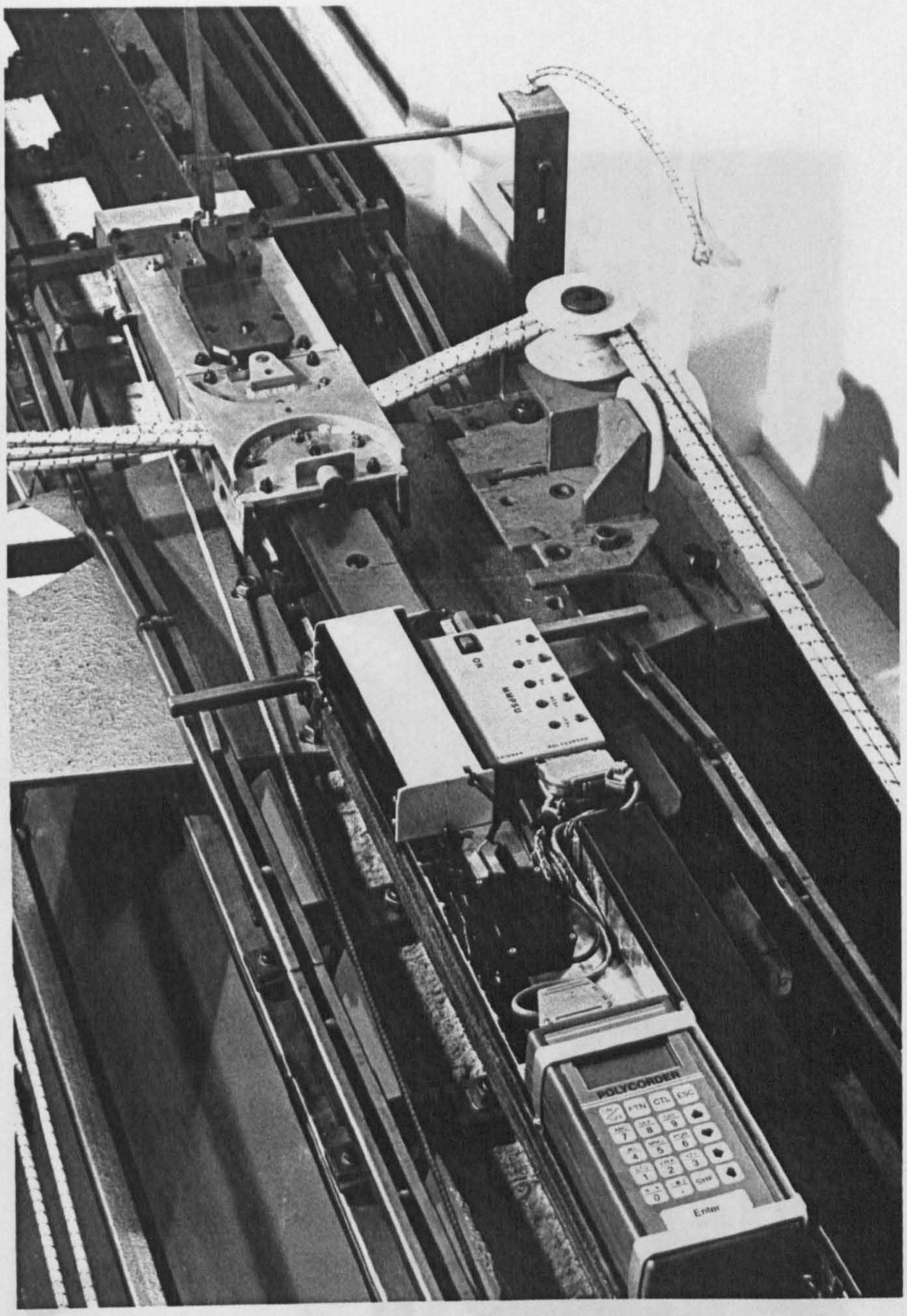

Figure 4.19 The moving model rig used for the second test series.
The live trolley, showing the data acquisition and control equipment, being retrieved prior to coupling to firing trolley.

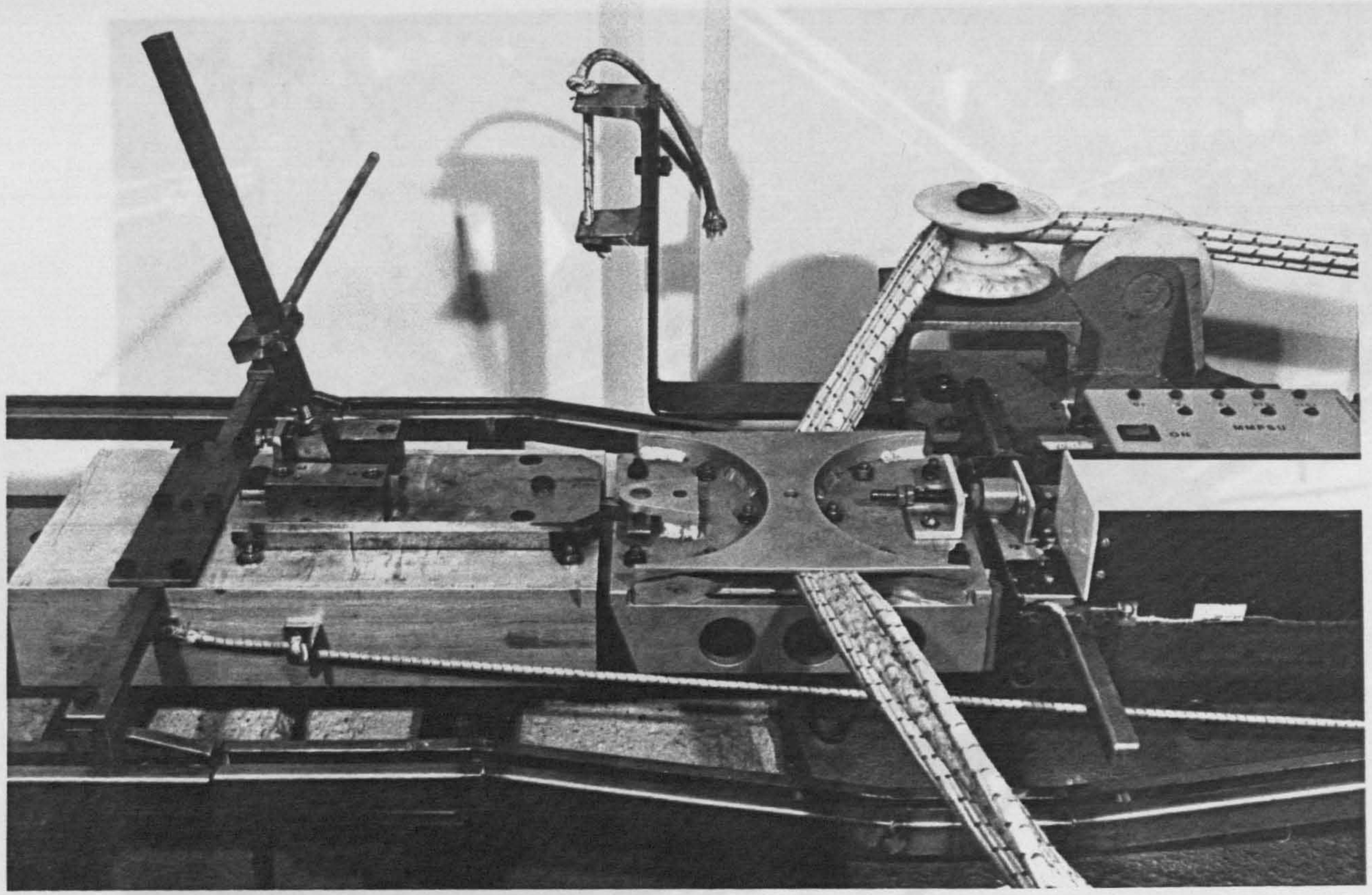

Figure 4.20 The moving model rig used for the second test series.
The 3rd release trolley about to pull back firing and live trolley.

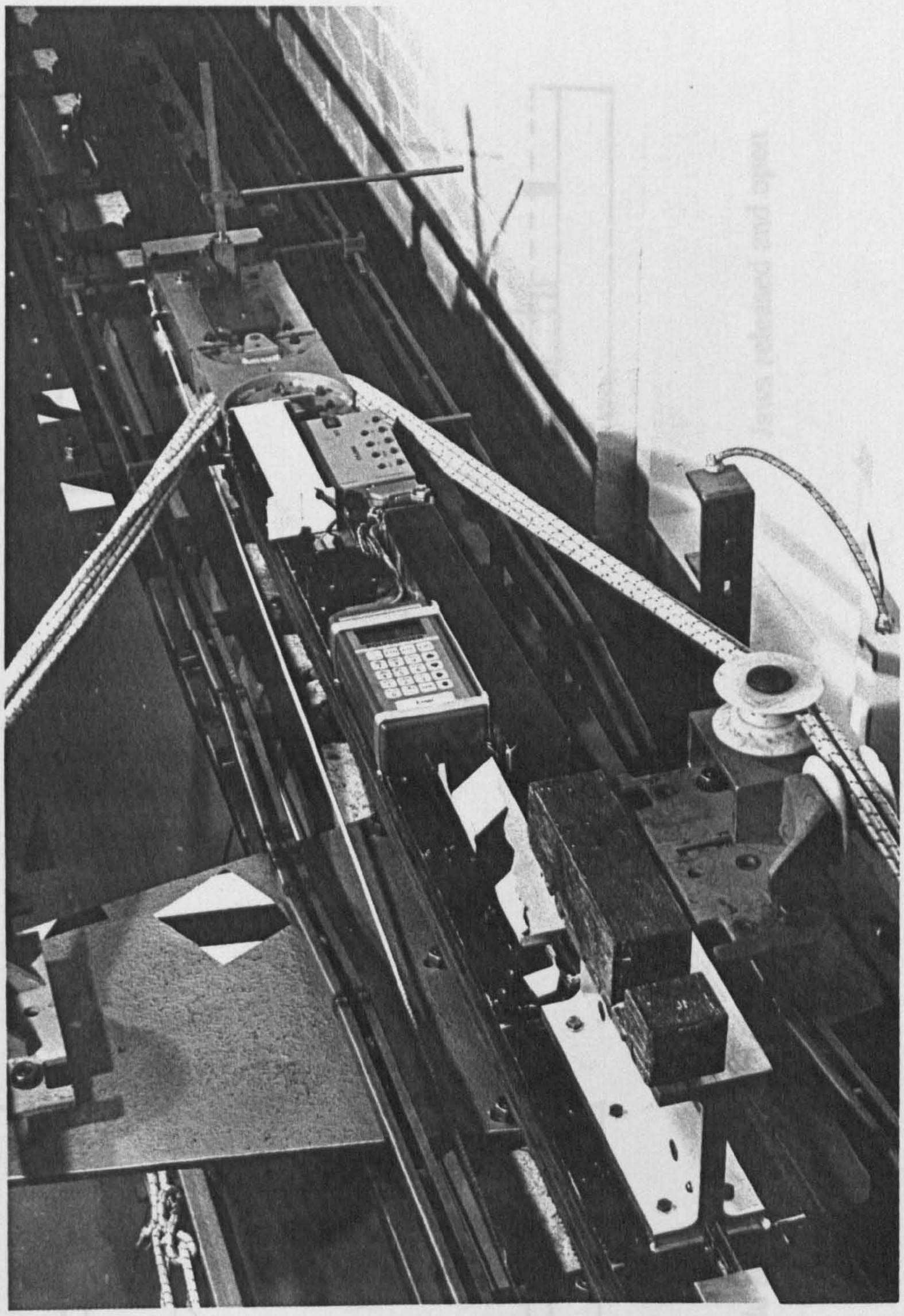

Figure 4.21 The moving model rig used for the second test series.
The 3rd release trolley pulling back the firing and live trolley prior to releasing the firing trolley.

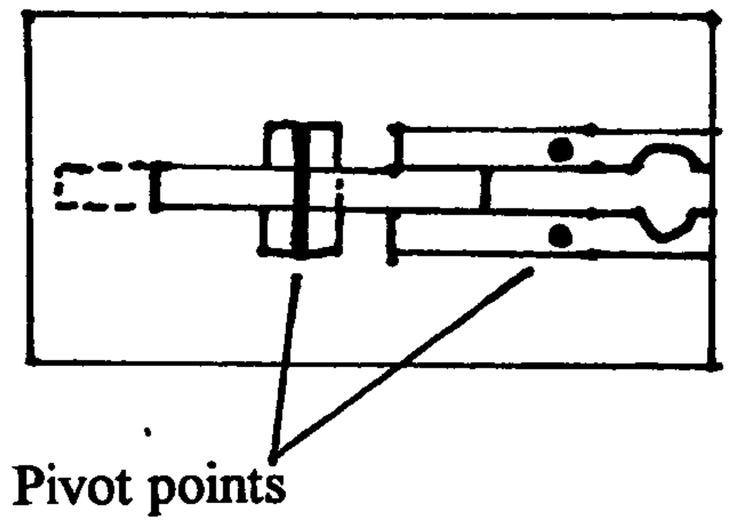

Plan view

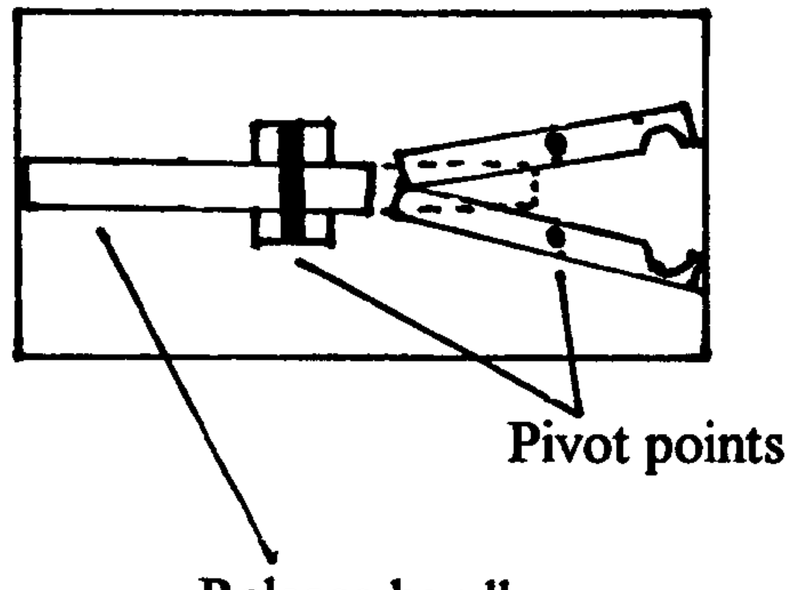

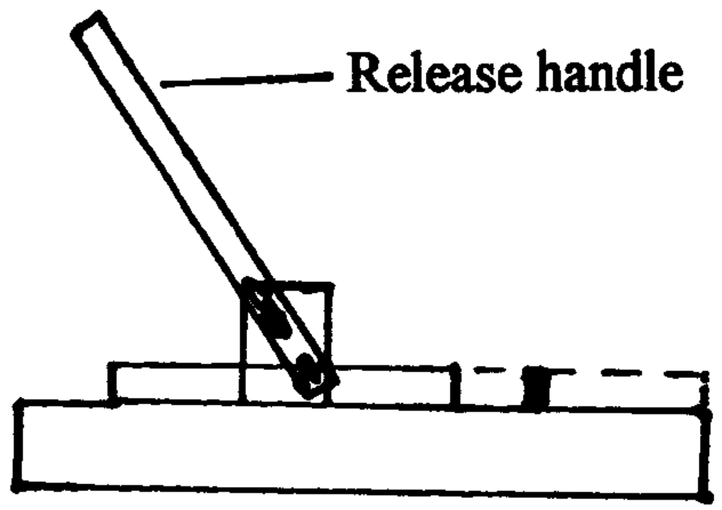

Side view

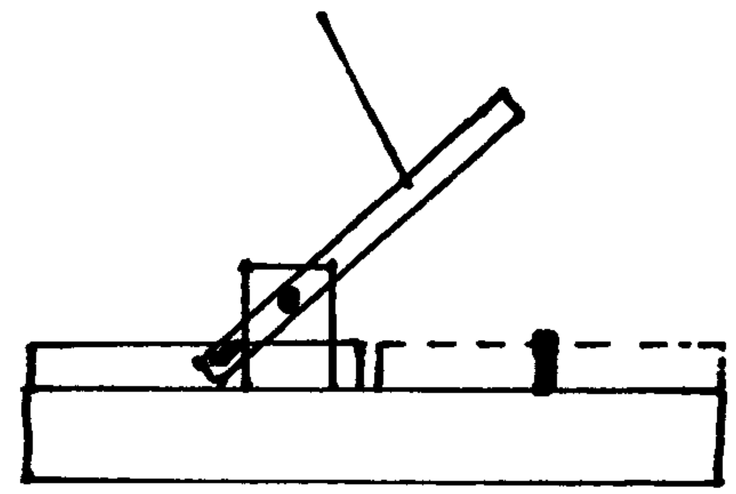

Jaws held shut

Jaws released and open

Figure 4.22 Release mechanism on third trolley.

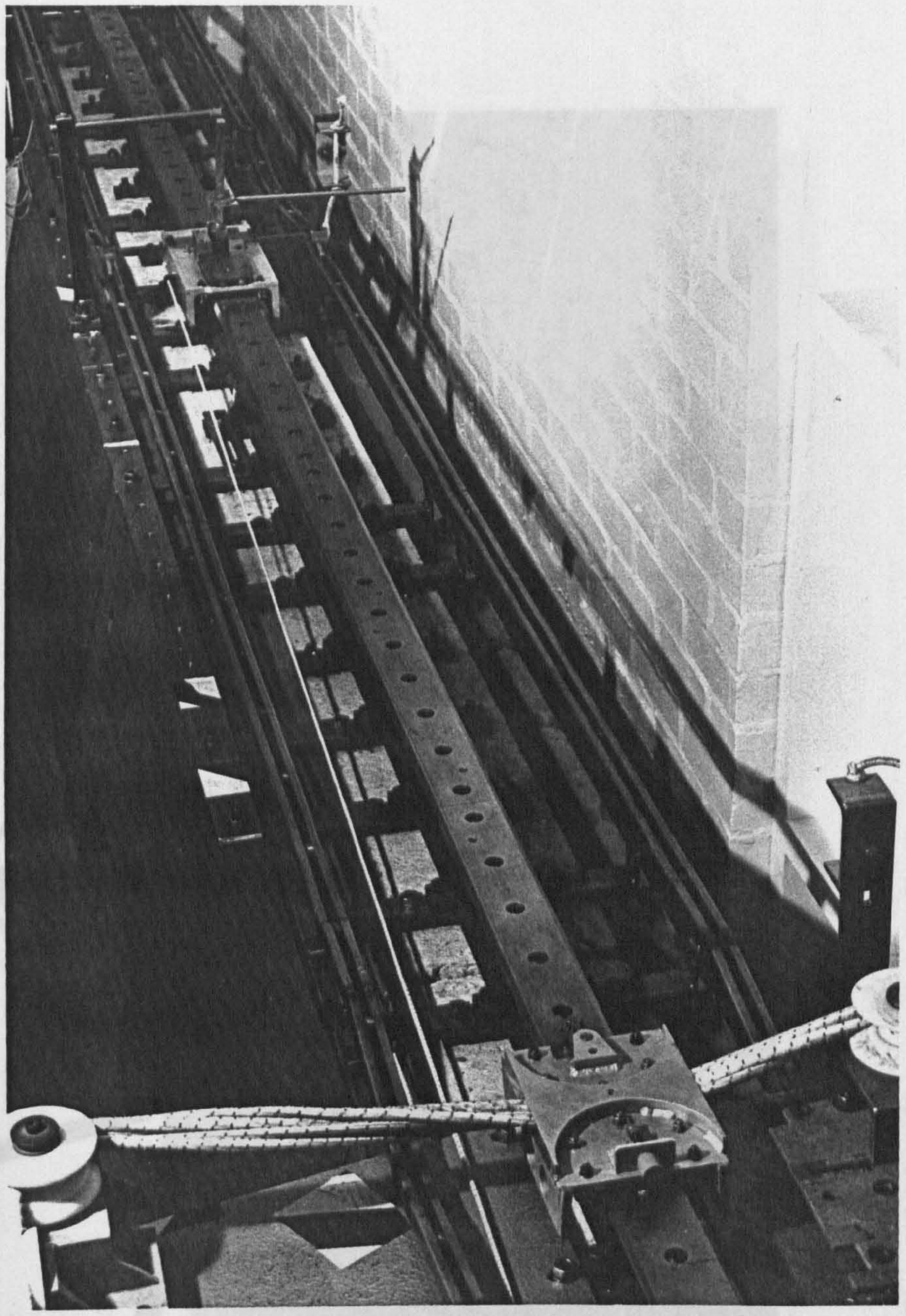

Figure 4.23 The moving model rig used for the second test series.
After firing of the live trolley. The 3rd trolley about to be returned using the small bungee and recoupled to the firing trolley.

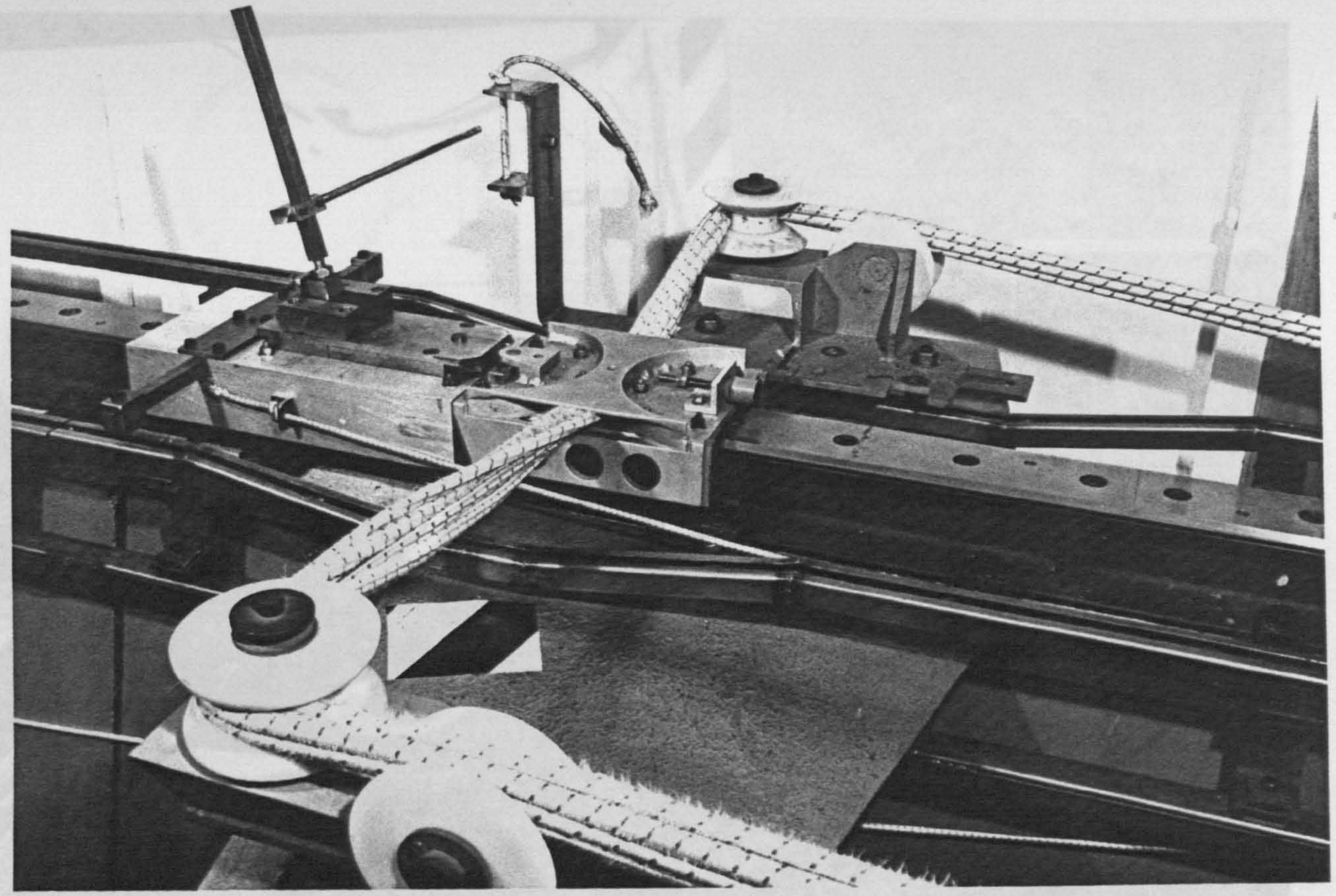

Figure 4.24 The moving model rig used for the second test series.
The 3rd trolley coupled to the firing trolley waiting for the live trolley to be retrieved.

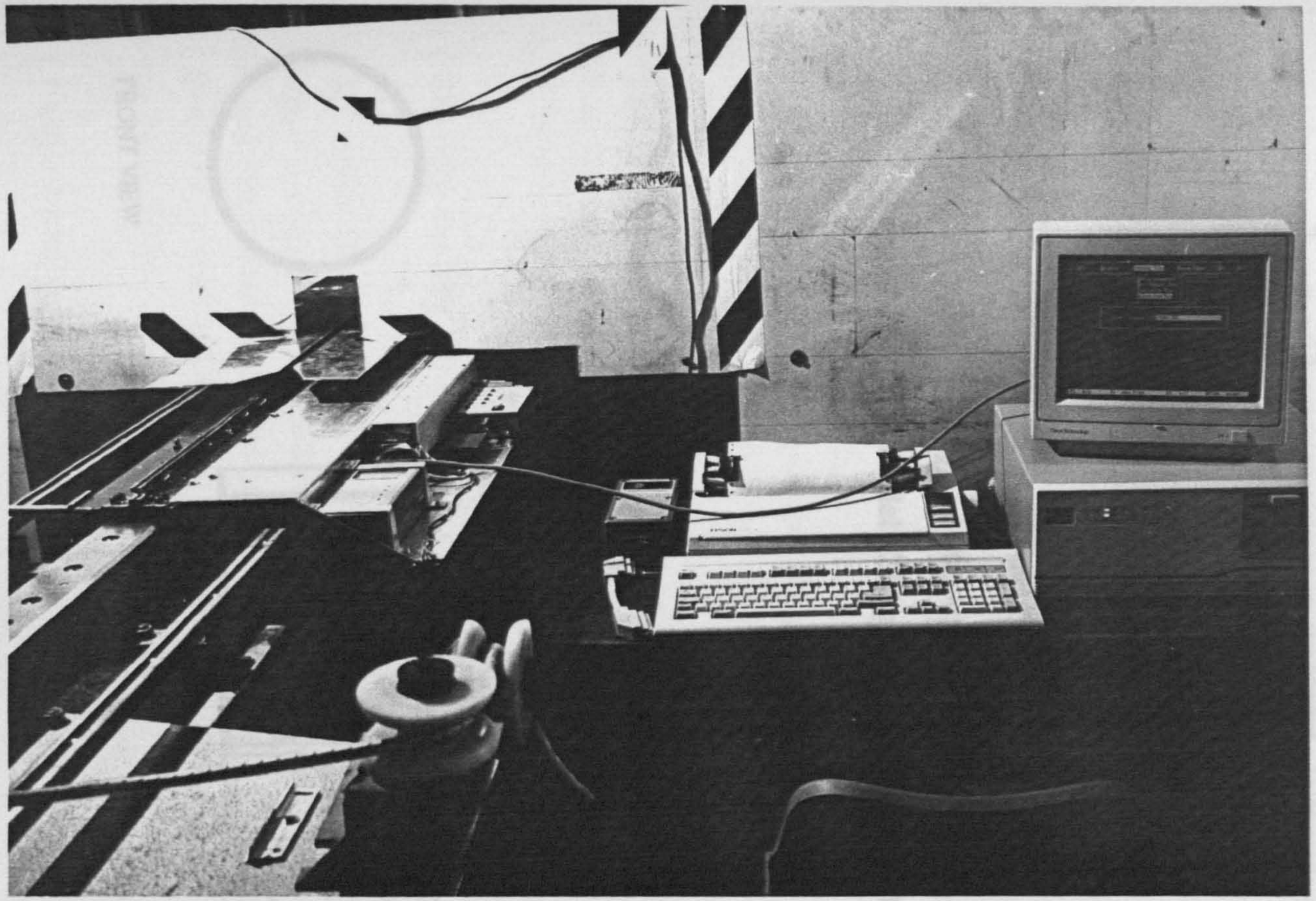

Figure 4.25 Down loading of data from the Polycoorder data logger to the P.C. using an R.S. 232 cable.

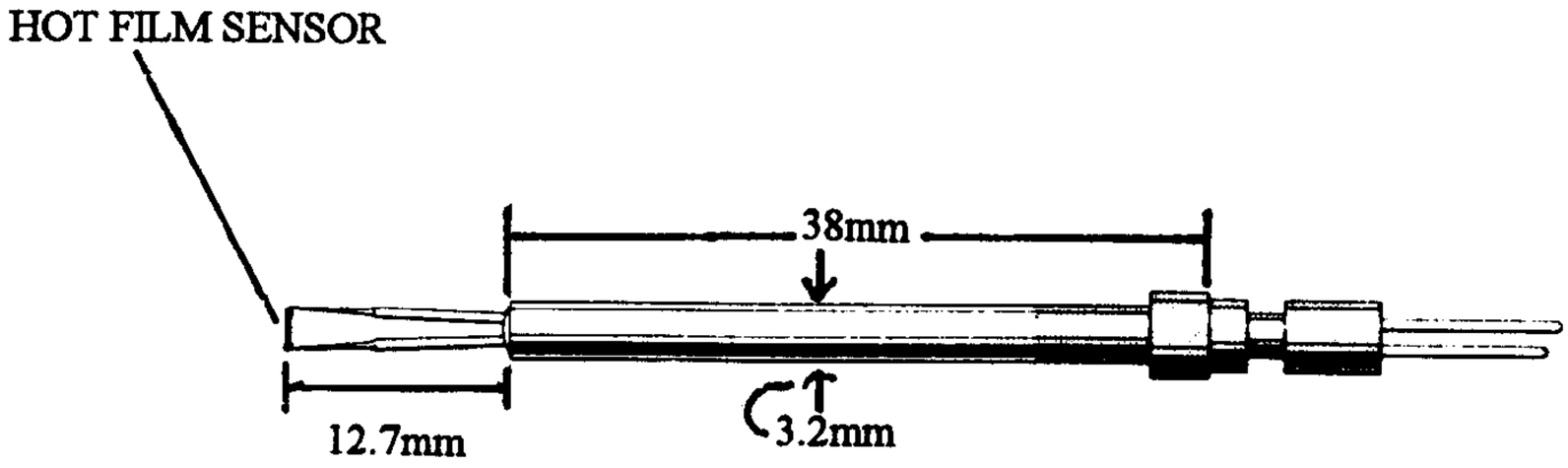

Figure 4.26 TSI model 1210 general purpose hot film probe.

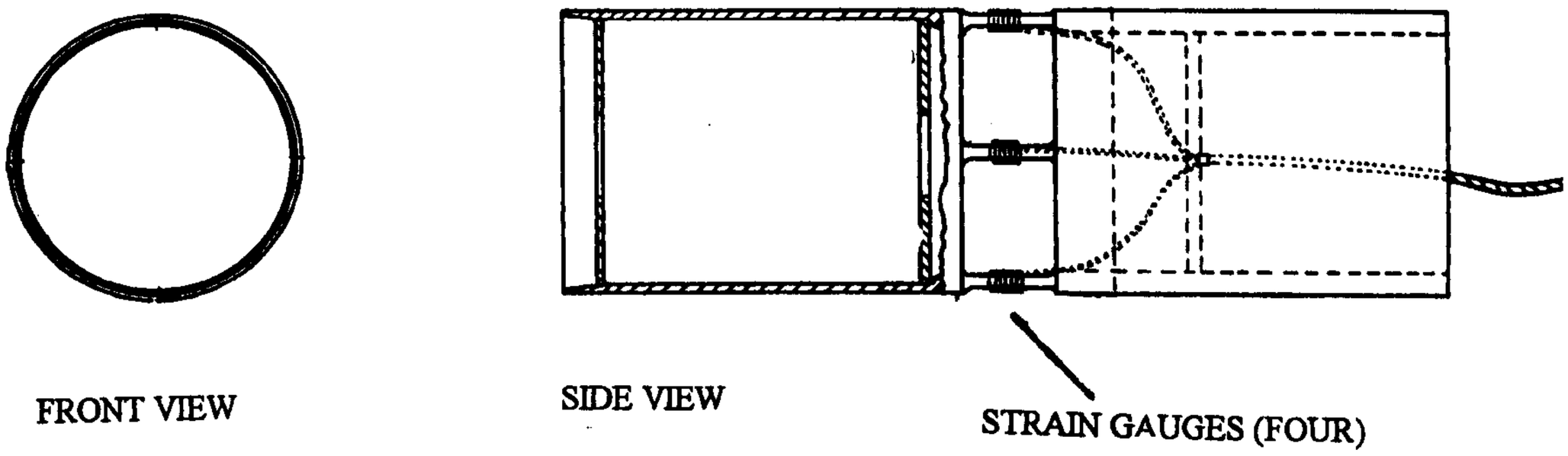

Figure 4.27 5 Component strain gauge balance.

5. Data Acquisition and Analysis.

The first section of this chapter describes the general principles of the numerical methods used for analysing the results shown in this thesis. The following sections deal with acquisition of the recorded data and the application of the numerical methods. The principles of the numerical methods are discussed first because the fundamental concepts of digital signal analysis and their consequences in the design of numerical data analysis methods need to be understood prior to considering the data from the experimental tests.

The numerical methods used in this thesis were developed into a suite of programs written in Prospero FORTRAN, a commercially available 16 bit compiler for IBM compatible personal computers developed from FORTRAN77. Whilst the user runs these programs separately, they were designed to run in sequence with the data transferred via ASCII files complete with header blocks containing test information. Initial processing of the force data provided files which contain the raw test data, zero readings, test and data acquisition information. Subsequent analysis programs were designed to run from these files with the minimum of user input.

Full details of the programs used and input/output data formats are given in Appendix 1. Data analysis was conducted on IBM compatible 80286 (12MHz) and 80386 (20MHz) processor machines fitted with a maths co-processor.

5.1 The data analysis methods.

Whilst measurements of both the force on the vehicle and the wind speed were analogue in nature, the Polycorder data logger (Chapter 4) used for recording both wind and force measurements sampled these signals at a user specified frequency and by means of its own analogue to digital converter subsequently stored them in time series digital form.

5.1.1 Digital time series data.

If information is required in the frequency domain the main concern in the digitising of an analogue signal is that of ailiasing. This phenomena is due to the inadequate sampling frequency of an analogue signal such that high frequency events are misrepresented in the sampled digital signal. As an example consider the case of a 420Hz oscillation in an analogue signal which is sampled at 400Hz. The actual signal

seen in the digital output will be equal to 420Hz - 400Hz ie 20 Hz. Also if the sample frequency of 500Hz had been chosen, which is greater than the analogue variation then a signal of 500 - 420 ie 80Hz would be the resulting digital signal. The Nyquist theorem (Stearns (1975) or Brendat and Piersol (1977)) states that the sample frequency must be equal to or greater than twice the maximum frequency of any significant signal present in the analogue signal in order to represent it correctly as a digital signal.

If possible an analogue low pass filter of half the sample frequency, allowing only oscillations up to this value to pass, should be used prior to digitisation of an analogue signal in order to ensure that ailiasing of the analogue signal does not take place.

It may be thought that greater accuracy can be obtained by sampling at a frequency greater than the Nyquist theorem. However the bandwidth theorem, Wills (1991), demonstrates that an analogue signal can be reconstructed, in the time domain, providing the Nyquist theorem is satisfied and, further, the accuracy obtained is a function of the number of over sampling, in the reconstruction of the data, that is conducted, rather than sampling the data at a rate higher than that satisfied by the Nyquist theorem. This tool is often used to limit the amount of data, once filtered, that needs to be stored.

5.1.2 Mean and standard deviations.

If means are required from the digitised signals, Nyquist's theorem does not need to be adhered to. If low frequency signals are present in the data, repeat measurements should be made and their repeatability checked. These should then be averaged to further increase the repeatability for the final result.

The standard deviation, or root mean square, similarly needs checking for repeatability if Nyquist's theorem is not satisfied.

See Chapter 9 for further discussion of these parameters when the signals are contaminated by additional noise.

5.1.3 Power spectra calculation.

The theory of the method employed is that given in Bendat and Piersol (1977) pp 322 to 330, and was applied to the needs of this project as follows.

1. Subtract the mean signal and calculate the standard deviation.

2. Window the first and last 10% of the data using a cosine squared function.

3. Forward Fourier transform the data. (see below for method used.). Note that the routine used in either the forward or backward direction increases the magnitude of the data by the square root of the number of data. The data is thus divided by this factor after the transform is conducted. (It should be noticed that other conventions are often used such as only increasing the magnitude by the number of data when the backward transform is conducted). Note that the transformed data is composed of real and complex terms. These real and complex pairs of data points correspond to frequencies of 0Hz to half the sample frequency in steps equal to the sample frequency / original number of data points.

4. Calculate the magnitude of the data (square and add the real and complex terms). The phase information is not required.

5. Divide all the data by 0.875 as a correction to the magnitude of the spectral density for applying the cosine squared window function to the first and last 10% of the data.

6. Non dimensionalise the resulting data for plotting in semi log form by multiplying the data points by their corresponding frequency and divide by the standard deviation squared (known as the variance).

This semi log plotting of the data is normally used by wind engineers as it allows for easy comparison of the data at the low frequency end of the spectrum which is often of most interest. The reason for multiplying the magnitude of the data by their frequency, in the calculation of the velocity spectrum, is to ensure that equal areas under the plotted spectrum correspond to equal energy. Sometimes log - log plotting of the data is used when the gradient of the decay part of the spectrum is required, usually to check whether it conforms to a gradient of -5/3 as implied by the correlations, equation 3.7. In this case the calculated spectral density is plotted directly against their

corresponding frequencies. Figure 3.1 shows comparison of the same spectra plotted only using both these conventions.

The Fourier transform employed in these routines is a version of the Cooley - Tukey fast Fourier transform method developed and coded by Norman Brenner, MIT Lincoln Laboratory and published in Brenner (1967). This has the following advantages over the majority of routines.

1. It can deal with an arbitrary number of data points including prime. Most are limited to quantities of data that are 2^N ,where N is integer.

2. A quantity of data points, N, can be transformed in time N*log(N) for N not prime. Simpler methods take a time equal to N^2.

The first advantage is essential if spectra or digital filtering are to be conducted from data measured from the moving model rig where the number of data is dictated by the transit time of the vehicle across the wind tunnel working section and therefore cannot easily be controlled. The second advantage is also useful in the context of this project bearing in mind the some 2000 runs conducted on the moving model rig as the processing was done on IBM compatible PCs. Even PCs utilising a 386 processor of 20MHz clock speed and fitted and with a maths co-processor are relatively slow for such calculations.

5.1.4 Data filtering.

There are two types of data filtering for use with the corresponding signal types,

1. Analogue, usually electronic devices.

2. Digital, usually in the form of a computer code.

Note that ailiasing, as discussed in 5.1.1, is a feature of analogue to digital conversion of a signal. Only the analogue filter is suitable for ensuring the rejection of the high frequency component of the signal prior to digitisation. The digital filter is used for further analysis of part of the signal spectrum present in digitised data.

Because of the location, or because of financial considerations, analogue filtering sometimes cannot be conducted, but it may be possible to reject the high frequency part

of the signal, using digital band pass filtering to remove the ailiased components. This is only really satisfactory if the high frequency components of the original analogue signal are very discrete in nature and can be identified.

An ideal low pass filter would be one which transmits 100% of the signal up to the cut off frequency and then eliminates the rest. However all filters, either analogue or digital vary in performance. It is usual to define the cut off frequency to be at the point at which a 3dB reduction in signal has taken place. The rate of fall off of the filter's capability is also important if very high levels of energy need to be rejected and this attenuation is usually expressed, in log - log form, as dB per octave.

The analogue filters used for the tests of this thesis are described in Chapter 4.

The digital filtering technique employed for further analysis of data in this thesis was developed from the method used for the calculation of the power spectra described in 5.1.3 utilising the non recursive method of Johnson (1978) and using the cosine squared window function for the data cut off. The method is described as follows:

1. to 4. As steps 1 to 4 respectively for power spectrum method in 5.1.3.

5. Apply a cosine squared window function to the frequency domain transformed data, both the real and complex terms, such that at the cut off frequency a 3dB reduction, 50%, in signal strength is obtained.

6. Reverse Fourier transform the data to obtain the time series variations. Note that this is done using both the real and complex terms of the output from the forward Fourier transform in order to preserve the phase information. Note that the routine used in either the forward or backward direction increases the magnitude of the data by the square root of the number of data. The data is thus divided by this factor after the transform is conducted.

7. Note that the complex terms output from the FFT routine are negligible in magnitude, as defined in the original data input into the routine, and discard.

8. Add the mean value of the data, initially removed in step 1.

The performance of this digital filter is shown in figure 5.1. and has an attenuation rate of around 24dB per octave for the first octave past the cut off frequency.

5.1.5 Extreme value analysis.

Extreme value analysis is the subject of statistically predicting the most likely extreme (largest) value in a given, usually longer, period from measurements made over limited periods. For example a civil engineering structure may need to be designed to withstand the maximum wind gust, of a given duration, likely to occur in its design life, say a period of 50 years. Measurements of the wind characteristics at the site over a limited time span would enable, with the aid of extreme value analysis, to determine this maximum likely wind gust over the structures design life, and similarly the corresponding extreme force experienced by the structure can be determined either from scale wind tunnel tests of a limited duration or available tables for standard designs. Cook (1985) details many extreme value analysis methods used in the field of Wind Engineering.

Of relevance to the study of the overturning of large road vehicles and rail vehicles is the determination of a maximum gust of duration 1 to 3s, this being the typical overturning time for these vehicles, see Chapter 2. Overturning prediction methods, discussed in section 2.1, utilise knowledge of the extreme forces and moments formed from averaging data over the gust time periods considered relevant to the size of the vehicle and its environment.

Wind Engineering design methods make use of the most likely extreme value, the mode, corresponding to an hourly extreme mean wind speed for a given time period. This hourly extreme mean wind speed for a given time period is that wind speed averaged over one hour that is only likely to be exceeded once in the given time period. For example ESDU (1974) shows the extreme mean hourly wind speed at a height of 10m that is only likely to be exceeded once in 50 years. The actual extreme wind speed value corresponding to the gust time depends on the terrain, the roughness length and the height above the ground but is derived from these extreme hourly mean wind speeds as described in ESDU (1974).

The averaging period for the mean wind speed of one hour is used due to the spectral gap in the wind spectrum gathered over much longer time periods. This is known as the van der Hoven spectrum and indicates that all wind gusts in the Earth's atmospheric boundary layer are of a duration much less than one hour. See section 3.2 for a full discussion and further references.

In the context of the wind tunnel tests a method would be useful that allows the most likely extreme value corresponding to the extreme hourly mean value to be determined from a time period equivalent to a time scale less than one hour. Such a method is that of Cook and Mayne (1979) and makes use of the quantities mode and dispersion. The mode is the likely extreme calculated from an ensemble of, statistically independent, gust duration maxima. Each maxima is defined to be the maximum gust value from one set of continuously recorded data of a given time period, say 10minutes. The mode thus calculated would be the most likely extreme for a time period of 10 minutes. The dispersion describes the spread of the ensemble of gust duration maxima and using the following formula allows the mode to be extrapolated for longer time periods, say one hour. Thus, from Cook and Mayne (1979) :

$$\text{Mode}_{1\ \text{hour}} = \text{Mode}_t + \frac{\ln(\frac{3600}{t})}{a} \qquad 5.1$$

In this thesis the mode and dispersion from the measured extreme values were calculated using the method of Lieblein (1974). This has the following advantages over Gumbel's original method, see Cook (1985) :

1. Lieblein's analytical method can more accurately determine the mode and dispersion when only a short number of measured extremes are available;

2. Lieblein's analytical method can easily be incorporated into a computer program.

Lieblein's extreme value method, to obtain the mode and dispersion from a set of statistically independent recorded data is as follows:

First determine the equivalent full scale time for the model scale tests using the methods described in section 3.3. The mean wind tunnel speed is taken to be equivalent to the full scale extreme hourly mean value for a given site.

1. Split the continuous data record into a number of blocks. In what follows the model scale observation time is equal to the block time length.

2. For each block calculate the mean values over the model gust periods, these corresponding to the equivalent full scale gust duration.

3. For each block extract the maximum value and rank them according to increasing value.

4. In steps 5 and 6 these are weighted according to their rank by multiplying them by the appropriate value from a set of Best Linear Unbiased Estimators (BLUE numbers). Cook (1985) tabulates these BLUE numbers for blocks of data numbering 10 to 24.

5. For each rank (each block) the product of the corresponding BLUE A number and the maximum value are calculated and then summed to give the mode for the full scale equivalent gust and observation time.

6. For each rank (each block) the product of the corresponding BLUE B number and the maximum value are calculated and then summed to give the dispersion. (Independent of observation time).

This method in conjunction with equation 5.1 is demonstrated with worked examples in sections 5.2.1.3.

As can be seen this method, in common with others (Cook (1985)), relies on the choosing of the equivalent model to full scale time scaling chosen. Section 3.3 has highlighted many of these difficulties which are due to both terrain variations, unknown wind characteristics close to the ground - or reasons of complicated terrain and vehicle movement. Due to these major concerns, the prime role of this thesis was to calculate the extreme values from wind tunnel tests for a range of time scales.

5.2 Application of the methods and data acquisition considerations.

5.2.1 Wind measurements.

5.2.1.1 Mean velocity and turbulence intensity.

The linearised voltage output from the hot film anemometer was calibrated, and checked at regular intervals, by comparison with the output of a pitot static probe connected to a standard N.P.L. design null-reading tilting U-tube micromanometer (see plate 5 of Bryer and Pankhurst (1971)) in the following manner.

Both the hot film anemometer and the pitot static probe were placed in the working section entrance, at 300mm height and spanwise separated by 100mm at positions where a constant reading was obtained with both instruments. The turbulence intensity at this position was 0.7% at full wind tunnel speed increasing to around 1.5% at half this speed indicating that the variance of the measurement signal, sometimes referred to as the turbulence level, was roughly constant. It is essential that the turbulence level is low at the calibration positions due to the mean pressure measured by the pitot static probe being sensitive to large scale turbulence as found downstream of the inlet of the environmental wind tunnel (Bryer and Pankhurst (1971).

The dynamic head recorded by the pitot tube is related to the head of water given by the water manometer:

$$\frac{1}{2}\rho u^2 = \rho_w g h_w \qquad 5.2$$

Also the linearised voltage output from the hot film anemometer is proportional to the mass flow rate per unit area, the product of the air velocity and density which is therefore the quantity to be calibrated. The product of the air velocity and density is determined by rearranging equation 5.2 :

$$\rho u = \sqrt{2\rho\rho_w g h_w} \qquad 5.3$$

Figure 5.2 shows a typical calibration used from which the calibration coefficients were determined. Note the deviation from linearity at very low wind speeds - not used for the tests described in this thesis.

Measurements of the ambient temperature and ambient pressure are used to calculate the air density, using the equation of state, at the time of the data measurement. These were measured using a mercury barometer situated near the exterior of the wind tunnel and a mercury thermometer.

Additionally a further correction to the output voltage was applied due to an additional variation with air temperature. This is recommended by the TSI Hot Film User Manual and is as follows:

$$v_{corrected} = v_{measured} \times \left[\frac{t_{sensor} - t_{calibration}}{t_{sensor} - t_{measurement}} \right]^2 \qquad 5.4$$

Note that the temperature used in equation 5.4 was the average of the ambient temperature in the wind tunnel measured before and after the tunnel was operated from a thermometer situated next to the mercury barometer in the building near to the wind tunnel inlet. Note that the probe experiences the total temperature of the air flow in the tunnel and which is equivalent to the static temperature of the near stationary air in the building, due to the flow from the working section inlet to the probe position in the working section being adiabatic. The static temperature of the flow, as it accelerates into the working section of the wind tunnel, falls proportionally with the static pressure as the air density is constant for these low speeds. The static pressure falls due to two effects:

1. For a given total pressure, which is approximately constant for the flow into the working section the static pressure falls due to the increase in the dynamic head of the fluid as described by Bernoulli's formula, equation 3.2.

2. The static pressure falls directly proportionally with the total pressure reduction due to friction losses. These are caused by the ground roughness and the mixing of the free jet at the sides and top of the flow as it passes through the working section. Again this simple relationship only holds for incompressible flow. In the absence of these losses the flow process would be described as isentropic and the total pressure of the flow in the working section would then be equivalent to the static pressure in the surrounding building.

For the Nottingham University environmental wind tunnel with its maximum speed of 15m/s the ratio of the static to total quantities discussed above are in any case very near unity, to within 0.002%.

Initial wind velocity measurements with the ABL simulation installed were conducted using sample frequencies of 1000Hz, 200Hz and 100Hz sampling from 4096 data points. It was found that 100Hz gave the most repeatable results for the mean value, no doubt due to the long streamwise turbulence length scale and the lack of energy above 50Hz as shown by the wind spectrum. No analogue filter was employed. All wind measurements were conducted using 100Hz sample frequency for 4096 data points. This 41 second recording gave an accuracy of 0.3m/s for the mean wind speed and 1% for the turbulence intensity, these values being the likely error or standard deviation for a single measurement found by analysis of 5 repeat measurements.

5.2.1.2 Velocity spectra.

As the spectra to be calculated are in the non dimensionalised form, and also due to the mean of the signal being removed prior to FFT, the linearised output from the hot film anemometer does not need to be calibrated or corrected for ambient conditions.

These were calculated from an average of 14 individual spectra. Each of these was calculated from a sample of 4096 data points at a frequency at 500Hz utilising the Polycorder's in built low pass analogue filter at 100Hz. The resulting spectrum of 2048 data points therefore extend to 250Hz with a sharp cut off at 100Hz. The resolution of the spectrum is thus 0.122Hz.

The data for the 14 spectra was measured as a single continuous record of 57344 data points corresponding to a measurement time of 115 seconds.

5.2.1.3 Extreme value analysis.

The extreme wind speed corresponding to the gust time divided by the mean wind speed is known as the extreme gust value:

$$G = \frac{\hat{u}}{\bar{u}} \qquad 5.5$$

Extreme gust values were calculated using Leiblien's method utilising 10 blocks of data. As the wind velocity squared is proportional to the aerodynamic force, in the definition of the force coefficient, extreme value analysis for the wind extreme gust values were conducted with these values squared. These 10 blocks were formed from a single measurement of 61440 data points at a sample frequency of 500Hz and analogue filtered at 100Hz.

The methodology described in section 5.1.5 is demonstrated for the static model test position with a mean wind speed of 8.5m/s at an equivalent full scale reference height of 3m and a range of measurement (model) times taken to be equivalent to 3 seconds full scale. The full scale extreme mean hourly wind speed of 30m/s was chosen here as this is typical for the United Kingdom given in ESDU (1974). As this is a typical value it was decided not to correct this value for the difference in reference height between the 3m used in this thesis compared to the 10m used in ESDU (1974). The correction for this difference would only be approximate in any case due to the large variation in the wind characteristics at heights of less than 10m above the ground. However, if

applied, equation 3.5 shows that this correction would be less than 20% for which the methodology of extreme value analysis would not be very sensitive in the predicted extreme gust value. This will be demonstrated in the results obtained for ranges of model time scale varying by many factors.

Considering just one block of data extracted from the continuous record, Table 5.1 illustrates the number of data points that are used to form each gust value, the number of gust values and the equivalent full scale time period from which this maximum is formed. It is seen that this latter time period depends upon the model time period taken to be equal to the 3 second gust and the value of the full scale extreme mean hourly wind speed. Having chosen a model time period equivalent to a 3 second gust, implying a certain full scale time period for the measurement time of a block, the maximum gust value is calculated for each block (in this case 10) from the continuous data record.

Table 5.2 shows these maximum gust values ranked in ascending order with Leiblien's Blue numbers designated A and B indicated alongside.

Table 5.3 continues the calculation first showing the most likely 3s extreme gust values (the mode) and the dispersion for the equivalent full-scale time period of one block of data. Finally 5.3 shows, using equation 5.1 and the calculated mode and dispersion, the 3s extreme gust factor values extrapolated for the full scale time period of one hour. The actual extreme velocity values can be calculated using the extreme mean hourly wind speed. In the wind tunnel this is just the mean wind speed, as the ABL simulated corresponds the mean hourly correlations given in section 3.2.

5.2.2 Force measurements.

The mean force coefficients and moment coefficients were calculated using the definitions described in this section.

The definition of the wind yaw angle and the relative directions of the forces and moments to the oncoming wind used for all tests reported in this thesis are shown in figure 5.3. Note that this sign convention is identical to those previously used for the tests of these vehicles described in sections 2.2.1.1. and 2.2.1.2., as shown in figure 2.3. It should be noted that for the tests described in this thesis, due to the arrangement of the moving model rig, the vehicle was mounted such that the on coming wind approached the vehicle's starboard side rather than the port side as for the previous tests. This arrangement was adhered to for the static turntable tests.

For the DB railway container, it should be remembered that only the forces and moments on the container were measured, as it was mounted above and not touching the wagon below (Chapter 2).

For the lorry and the railway container the mean side and lift force coefficients $\overline{C}_s$ and $\overline{C}_s$, are defined as :

$$\overline{C}_s = \frac{\overline{F}_S}{\frac{1}{2}\rho A \overline{V}^2} \quad , \qquad \overline{C}_L = \frac{\overline{F}_L}{\frac{1}{2}\rho A \overline{V}^2} \tag{5.6}$$

including the resultant mean wind speed $\overline{V}$, formed from the mean vehicle's speed v, and the mean wind speed $\overline{u}$, at the reference height for a vehicle moving perpendicular to the wind direction,

$$\overline{V} = \left(\overline{u}^2 + v^2\right)^{1/2} \tag{5.7}$$

Note that for the lorry the reference area was chosen to be the vehicle's profile frontal area whilst for the DB railway container the container's frontal area is used. These were chosen for consistency with previous tests (sections 2.2.1.1 and 2.2.1.2) and so the results of the previous tests of the same vehicle types could be directly compared.

For the lorry the mean moments were calculated about the lorry's centre of gravity. These were calculated by translating and combining the forces and moments measured and calibrated relative to the centre of the balance to an unladen vehicle's centre of gravity. Considering the contributions due to the pure side and lift forces, the side and lift forces used in forming these coefficients were taken to be acting at the centre of the side and roof coincident with the centre of the force balance. Therefore in forming the pitching moment about the vehicle's centre of gravity, the moment arm used for translating the lift force contribution is from the centre of the balance to the centre of mass. No contribution due to the drag force on the vehicle is included due to this quantity not being measured. However this contribution should be small due to both the relatively low drag and the moment arm. For the yawing moment similarly the side force contribution is from the centre of the balance to the centre of gravity. In forming the rolling moment contributions due to the side and lift forces, only the side force contributes due to the lift force being assumed to be acting directly above the centre of the balance, thus giving a zero value for the moment arm, which is probably not the case. However the resultant error due to this would be expected to be small as both the lift force and the moment arm are much smaller than their side force values.

The mean pitch, yaw and rolling moment coefficients calculated about the lorry's centre of gravity $\overline{C}_P$, $\overline{C}_Y$ and $\overline{C}_R$, are formed in a similar manner to the force coefficients but including a reference length in order to non dimensionalise these moments. For the lorry the reference length used was the lorry's height h, as for the previous tests described in section 2.2.1.1, the moment coefficients are defined as :

$$\overline{C}_P = \frac{\overline{M}_P}{\frac{1}{2}\rho A \overline{V}^2 h_C}, \qquad \overline{C}_Y = \frac{\overline{M}_Y}{\frac{1}{2}\rho A \overline{V}^2 h_C}, \qquad \overline{C}_R = \frac{\overline{M}_R}{\frac{1}{2}\rho A \overline{V}^2 h_C} \qquad 5.8$$

Also in this thesis, for the analysis of the aerodynamic moments acting on the lorry, the non dimensional point of action is defined for the various components, thus:

horizontal non dimensional point of action for side force,

$$X_S = \frac{x_S}{h} = \frac{C_Y}{C_S} \qquad 5.9$$

vertical non dimensional point of action for side force,

$$Y_S = \frac{y_S}{h} = \frac{C_R}{C_S} \qquad 5.10$$

horizontal non dimensional point of action for lift force,

$$X_L = \frac{x_L}{h} = -\frac{C_P}{C_L} \qquad 5.11$$

Note that the vertical non dimensional point of action for the lift force could not be calculated as the drag force (acting in the opposite direction to the vehicle's travel) was not measured.

For the railway container all the definitions were chosen for consistency with the previous tests of this vehicle type (section 2.2.1.2). The only moment calculated, for the tests described in this thesis, was the lee bottom corner rolling moment as the concern was the risk of the container rolling off the wagon on which it was laden. Note that this was formed from the measurement of the side and lift forces taken to be acting at the centre of the container's side and roof respectively (using the moment arm from the centre of the container perpendicular to the bottom corner of the container) and also the rolling moment measured about the container's centre by the balance. The

rolling moment coefficient used a reference height equivalent to the width of the container. (Almost identical to the height of the container (figure 1.2)). Again this was chosen for consistency with the results in section 2.2.1.2. The mean rolling moment for the DB railway container vehicle is defined as :

$$\overline{C}_R = \frac{\overline{M}_R}{\frac{1}{2}\rho A \overline{V}^2 h} \qquad 5.12$$

The extreme side and lift force coefficients $\hat{C}_s$ and $\hat{C}_L$, for both the lorry and the DB container were defined to be :

$$\hat{C}_s = \frac{\hat{F}_s}{\frac{1}{2}\rho A \hat{V}^2}, \qquad \hat{C}_L = \frac{\hat{F}_L}{\frac{1}{2}\rho A \hat{V}^2} \qquad 5.13$$

including the resultant extreme wind speed $\hat{V}$, formed from the mean vehicle's speed v, and the extreme wind speed $\hat{u}$, at the reference height for a vehicle moving perpendicular to the wind direction.

$$\hat{V} = \left(\hat{u}^2 + v^2\right)^{1/2} \qquad 5.14$$

For most of the tests extreme value coefficients were only formed for the pure side and lift forces. It was assumed that these would be adequate to form extreme moment coefficients if needed due to the small contribution of the moments measured about the balance centre in the forming of the mean coefficients. This was checked for the tests described in Chapter 9, where, for the lorry, the extreme moment coefficients were calculated from coincident (at the same time) measured extreme forces and moments.

The extreme lee bottom corner rolling moment for the DB container, for all the DB container tests, was calculated from the sum of the translated extreme side and lift forces and the extreme rolling moment measured simultaneously about the balance centre. The extreme moment coefficients were formed in the same manner as equation 5.13 using both the extreme moment and resultant extreme wind speed.

The use of the 5 component force balance is described in the next section and the details of the data acquisition and analysis for the static and moving tests are described in sections 5.3.2 and 5.3.3 respectively.

5.2.2.1 Using the five component force balance.

The force balance and associated equipment were described in section 4.3.3. The response of the balance, in terms of voltage, is linear with forces and moments that are exerted on it. However the output of each channel includes the effects of other forces and moments, which are termed interactions.

The force balance works in the following way:

v_i is the voltage on channel i. L_i is the load (force or moment) on channel i.

A_i to F_i are the calibration factors.

$$v_1 = A_1 L_1 + B_1 L_2 + C_1 L_3 + D_1 L_4 + E_1 L_5 \qquad 5.15$$

$$v_2 = A_2 L_1 + B_2 L_2 + C_2 L_3 + D_2 L_4 + E_2 L_5 \qquad 5.16$$

$$v_3 = A_3 L_1 + B_3 L_2 + C_3 L_3 + D_3 L_4 + E_3 L_5 \qquad 5.17$$

$$v_4 = A_4 L_1 + B_4 L_2 + C_4 L_3 + D_4 L_4 + E_4 L_5 \qquad 5.18$$

$$v_5 = A_5 L_1 + B_5 L_2 + C_5 L_3 + D_5 L_4 + E_5 L_5 \qquad 5.19$$

The leading diagonal of the matrix of calibration values, A_1 to E_5, are the greatest in magnitude and all the others are termed the interactions.

To calculate the loads from the voltages either the 5 x 5 matrix of calibration coefficients needs inverting for an exact solution or can be found to a specified level of accuracy by use iterative solution methods.

An approximate solution can be made to this, and is often the one recommended by manufactures of such balances. Unfortunately this can only be made if BOTH the following assumptions are valid :

1. If the loads on each channel are similar in magnitude e.g. for equation 5.15, L_1 is similar in magnitude to values L_2 to L_5.

2. If the interactions are small e.g. for equation 5.15, B_1 to E_1 are much smaller than A_1

It is then possible to make the approximation of replacing the force terms in the interactions by a voltage neglecting further interactions e.g. For equation 5.15, L_2 can be replaced, from equation 5.16 using : $v_2 = B_2 L_2$, so that $L_2 = v_2 / B_2$. Applying this approximate method to equations 5.15 to 5.19 gives:

$$L_1 = \frac{1}{A_1}\left(v_1 - \frac{B_1}{B_2}v_2 - \frac{C_1}{C_3}v_3 - \frac{D_1}{D_4}v_4 - \frac{E_1}{E_5}v_5\right) \qquad 5.20$$

$$L_2 = \frac{1}{B_2}\left(v_2 - \frac{A_2}{A_1}v_1 - \frac{C_2}{C_3}v_3 - \frac{D_2}{D_4}v_4 - \frac{E_2}{E_5}v_5\right) \qquad 5.21$$

$$L_3 = \frac{1}{C_3}\left(v_3 - \frac{A_3}{A_1}v_1 - \frac{B_3}{B_2}v_2 - \frac{D_3}{D_4}v_4 - \frac{E_3}{E_5}v_5\right) \qquad 5.22$$

$$L_4 = \frac{1}{D_4}\left(v_4 - \frac{A_4}{A_1}v_1 - \frac{B_4}{B_2}v_2 - \frac{C_4}{C_3}v_3 - \frac{E_4}{E_5}v_5\right) \qquad 5.23$$

$$L_5 = \frac{1}{E_5}\left(v_5 - \frac{A_5}{A_1}v_1 - \frac{B_5}{B_2}v_2 - \frac{C_5}{C_3}v_3 - \frac{D_5}{D_4}v_4\right) \qquad 5.24$$

As was stated earlier this is the standard method often recommended by balance manufacturers. The above equations would be simplified renaming the coefficients proceeding the voltages the 'interactions'. This method was used to calibrate the force balance for the tests described in Coleman (1990) and Baker (1986). In order to verify the adequacy of this method used for these previous tests, calculations of the static forces for the static lorry tests described in this thesis were undertaken using the previously used approximate method. Comparisons of these results with the method used in this thesis which solved equations 5.15 to 5.19 using the Gauss Elimination Method showed that the difference was less than 2% and therefore negligible in the context of these tests.

The force balance was calibrated by hanging weights to various points on a yoke which fitted to the live side of the balance. Referring to equations 5.15 to 5.19 the voltages were measured on all the 5 channels whilst applying a range of positive and negative loads to only one channel. This process was repeated for all 5 channels in turn. The

values A_i to E_i were found from fitting the best straight line fit to manual plotting of these measured voltages against the loads applied. Table 5.4 shows the calibration matrix defined by equation 5.15 to 5.19. The amplifier for each channel was set to maximum gain prior to calibration and also zeroed for zero load on the balance. The actual voltage corresponding to zero load for each vehicle under test, noting that its self weight is small but measurable, was corrected for during post data acquisition analysis.

During the calibration of the balance it was found that the measured voltages corresponding to all the channels responded linearly to the load on any channel thus verifying that equations 5.15 to 5.19 describe the characteristics of the balance adequately. This demonstrates that any combination of loads will be adequately described by the solution of these equations. Due to the linearity of these equations it is seen that in the post data acquisition processing for the determination of the mean and extreme forces over various time scales, the calibration can be conducted on the voltages for each channel that have been averaged over the corresponding time intervals, thus saving a significant amount of processing time. Further, this is essential for the multiplexing data gathering technique employed in these tests as the dominant high frequency noise due to the balance supports etc. may fluctuate over time periods similar or faster than the inter channel frequency of recording the data. This means that over very short time scales, unless this noise were adequately filtered, the voltages being measured on each channel may not be considered synchronous.

The force balance was calibrated prior to the static tests described in Chapter 7 and again before and after the second series of moving model tests described in Chapter 9. It was found that the balance was extremely stable to the accuracy obtainable from this method of calibration, around 2% of the calibration values given in table 5.4.

Coleman (1990) by measuring the transfer function for the balance demonstrated that the balance accurately responded both in magnitude and in the frequency domain to the relatively low frequency forces that were needed to be measured in this thesis.

5.2.2.2 Static tests.

5.2.2.2.1 Mean forces and moments.

These were calculated from multiplex recordings of all 5 channels at a sample frequency of 400Hz per channel. This high sample rate was chosen so that the natural frequency of the balance supports would be averaged out. The number of data recorded per channel was 12288 thus giving a recording time of 31 seconds.

5.2.2.2.2 Extreme force values.

These are calculated in the same manner as those described in section 5.2.1.3 for the extreme wind coefficients. Measurements were made for the side and lift forces only at a sample frequency of 125Hz and 45000 data points per channel. Analogue low pass filtering, using the equipment described in section 4.5, at a frequency of 50Hz of the measured signal was conducted for both channels prior to sampling. Due to wind tunnel occupancy time restrictions no other sample frequencies were tried and the long data records were chosen in order to ensure that the dispersion was suitably small. Table 5.5 summarises the calculation details.

The calculation of the extreme values for each block was based on the mean wind speed and these were extrapolated to give the 1 hour extreme 3s values non dimensionalised by the extreme gust. From these the normalised extreme force parameter and also the unsteady parameters were derived. The data was calibrated using only the diagonal calibration elements for these two channels therefore ignoring any interaction. The calculated mean force coefficients using this method showed up to 5% variation in those calculated using the full matrix of interactions as used for deriving the mean force values in section 5.2.2.2.1. However as the extreme force coefficients are normalised by the mean force coefficients also produced by this program (calibrated in the same manner from the same data), then this error on the normalised extreme force parameter and the unsteady force parameters are greatly reduced and should be considered negligible.

5.2.2.3 Moving model tests.

The data was recorded by the Polycorder data logger which was triggered to record 1.5 seconds of data 0.5 seconds before the rig fired. This delay was necessary due to the time needed for the Polycorder to load the program and compile it prior to

recording the data. The data from each run was downloaded to the PC as a single file. A typical output from a single fire of the moving model rig in its final guise, used for the second series of tests, is shown in figure 5.4. This shows the digital output channel which is used to calculate the speed of the trolley and identify its position across the working section. Also shown at the end of the run is the part of the run used for the zero readings when the trolley has stopped, the mechanical noise being absent, with the live vehicle within a tunnel after exiting the working section.

Output from the earlier test series was similar but did not contain the zero readings and only contained two markers of position on the digital channel. The zeros were taken at the beginning of a test gathering session and at the end (usually 50 runs) and an average taken.

For the main test series only data for which the zeros of that run and the run prior remained similar, within prescribed limits, were accepted.

After 10 runs of the moving model rig, the data for each run was downloaded into the PC and converted into ASCII text (.TBL file). The chosen test data relevant to the test section, with calculated zeros from the data at the end of the run, were then extracted and stored as an ASCII file for further processing (.RAW file). This file also included the mean force coefficients formed from this data and as a header block, the ancillary test data. The actual time histories recorded by the Polycorder were displayed on the PC's screen by the program that undertook this analysis and so each run was visually checked for major problems before being accepted.

5.2.2.3.1 Mean and extreme forces and moments.

Both the mean and extreme force and moment values are calculated from the same data due to discrete nature of gathering data. As discussed in section 3 it is apparent that the model time scales taken to be equivalent to the 3s full scale gust are similar to the transit time of the moving model rig or sub divisions of this time. Rather than calculate extreme values for model time scales of 0.1s, 0.2 and 0.4s etc. as for the static data it was decided that it would be more convenient to take as the time of the trolley transit time of the test section and subdivisions of i.e. half, third, quarter etc.

Each run of the moving model rig lasted between 0.1 and 0.4s depending upon the moving model speed and was constrained by yaw angle and wind tunnel speed. In order to calculate extreme values for time periods comparable to those of the static tests, as

discussed in section 3.3, the data of each run must be split into a number of segments. A chosen segment number of 1 refers to using the data from one whole run, whilst a value of 4 would indicate that four values would be extracted from one run. Analysis was conducted in a similar manner to the static tests with different model time scales to form the extreme values, depending upon the yaw angle in question and thus the transit time of the live model

The overall means and the extreme values for the given number of segments into which each was divided, were calculated from the ensemble of data corresponding to each run, each already pre-processed and stored as an individual data file (.RAW). In the processing of consecutive files of data the zero force measurements made at the end of each run were compared with those of the previous run and the file is only accepted in the analysis if the they were within 2%.

The data could be filtered if required using the method of 5.1.4. Details of this are given with the results of each series of tests in Chapters 8 and 9. If required the software could provide additional mean zero corrections due to mechanical noise described in section 9.1 which is a function of trolley speed. The problem of mechanical noise and the likely error it induces on the mean and extreme results are discussed in section 9.1.

5.2.2.3.2 Force spectra and aerodynamic admittance.

The force spectrum for a particular yaw angle for the moving model tests were formed from the average of the force spectra calculated from the data form each individual run. These were determined in identical manner to the wind velocity spectra described in section 5.2.1.2.

Whilst the aerodynamic admittance may be obtained by dividing the force spectra by the velocity spectra directly using equation 2.8, for such spectra shown in this thesis this would give a resulting aerodynamic admittance spectra which would be very spiky and difficult to interpret. The lack of smoothness of the force and wind velocity spectra is due to the relatively large turbulence length scales compared to the time taken to record the data, even though for the measurements were done over many minutes. Consideration was given to the simpler band pass filtering method in which a mean value of the spectral energy is obtained for each frequency band. Note this is simply the variance of the data averaged over the frequency interval and is the method used for the results shown in figures 2.8, 2.9 and 2.16. Referring to Chapter 9, this method was not

pursued either due to the high level of mechanical noise present in the digital signal throughout the bandwidth of interest seen in the force spectra. This was due to the lack of analogue filtering in the of recording the moving model data resulting in aliasing of the high frequency noise to some other lower frequencies.

If it had been possible to calculate the aerodynamic admittance accurately for the moving model tests then the extreme side and lift forces may have been calculated directly using equations 2.12 to 2.14.

Table 5.1 Wind gust extreme value analysis summary.

Full scale extreme hourly mean value = 30m/s (3m).

Mean wind tunnel reference speed = 8.5m/s at 60mm height = 3m full scale height.

No of data points for 10 blocks =61440. Sample frequency = 500Hz.

Model time period equivalent to 3s gust.	0.05	0.10	0.20	0.30	0.40	0.50	0.60
No of 3s gusts per block of data.	245	122	61	40	30	24	20
Full scale time period equivalent of one block of data.	735	366	183	120	90	72	60

Table 5.2 Worked example of Leiblein's extreme value method.

Static test position gust extreme value analysis based on 10 data blocks and the details in table 5.1. Note analysis conducted on the gust value squared as this is quantity required to non dimensionalise the force coefficient.

Model time period	0.05	0.10	0.20	0.30	0.40	0.50	0.60		
Rank	**Max**	**Gust**	**Sqd**	**Value**	**(G^2)**			**A**	**B**
1	1.904	1.729	1.597	1.459	1.288	1.221	1.204	0.2229	-0.3478
2	1.931	1.745	1.604	1.464	1.287	1.221	1.207	0.1623	-0.0912
3	1.943	1.761	1.611	1.469	1.287	1.222	1.209	0.1338	-0.0192
4	1.943	1.774	1.619	1.472	1.286	1.223	1.211	0.1129	0.0222
5	1.945	1.787	1.627	1.472	1.285	1.223	1.212	0.0956	0.0487
6	1.961	1.802	1.634	1.473	1.285	1.224	1.214	0.0806	0.0661
7	1.987	1.822	1.640	1.473	1.285	1.224	1.214	0.0670	0.0770
8	2.011	1.842	1.642	1.474	1.284	1.226	1.215	0.0542	0.0828
9	2.022	1.855	1.643	1.476	1.281	1.227	1.215	0.0417	0.0836
10	2.023	1.856	1.643	1.477	1.288	1.229	1.215	0.0289	0.0779
								Σ 0.9999	0.0001

Table 5.3 Worked example of Leiblein's extreme value method continued.

Model time period equivalent to 3s gust (s)	0.05	0.10	0.20	0.30	0.40	0.50	0.60
Equivalent full scale time (s). 1 data block.	735	366	183	120	90	72	60
3 s Mode (ΣA.Max. G^2)	1.95	1.78	1.62	1.47	1.28	1.22	1.21
Dispersion (ΣB.Max. G^2)	0.040	0.045	0.020	0.008	0.005	0.003	0.006
Extrapolated 3s mode for 1 hour of G^2 value	2.01	1.88	1.68	1.50	1.30	1.24	1.23

Table 5.4 Force balance calibration matrix.

Coefficients as defined in equation 5.15 to 5.19.

Channel i	A_i	B_i	C_i	D_i	E_i
1	7.50	-0.23	0.13	0.01	-0.01
2	0.21	7.93	0.13	0.00	0.02
3	0.13	-0.03	55.0	0.00	-0.02
4	-0.05	-0.44	-0.29	0.83	0.05
5	0.00	-0.07	-0.36	-0.02	0.80

Table 5.5 Static lorry extreme value analysis summary.

Full scale extreme hourly mean value = 30m/s (3m).

Mean wind tunnel reference speed = 8.5m/s at 60mm height = 3m full scale height.

No of data points for 10 blocks =45000. Sample frequency = 125Hz.

Model time period equivalent to 3s gust	0.05	0.10	0.20	0.30	0.40	0.50	0.60
No. of 3s gusts per block of data.	750	346	180	121	90	72	60
Full scale time period equivalent of one block of data	2250	1038	540	363	270	216	180

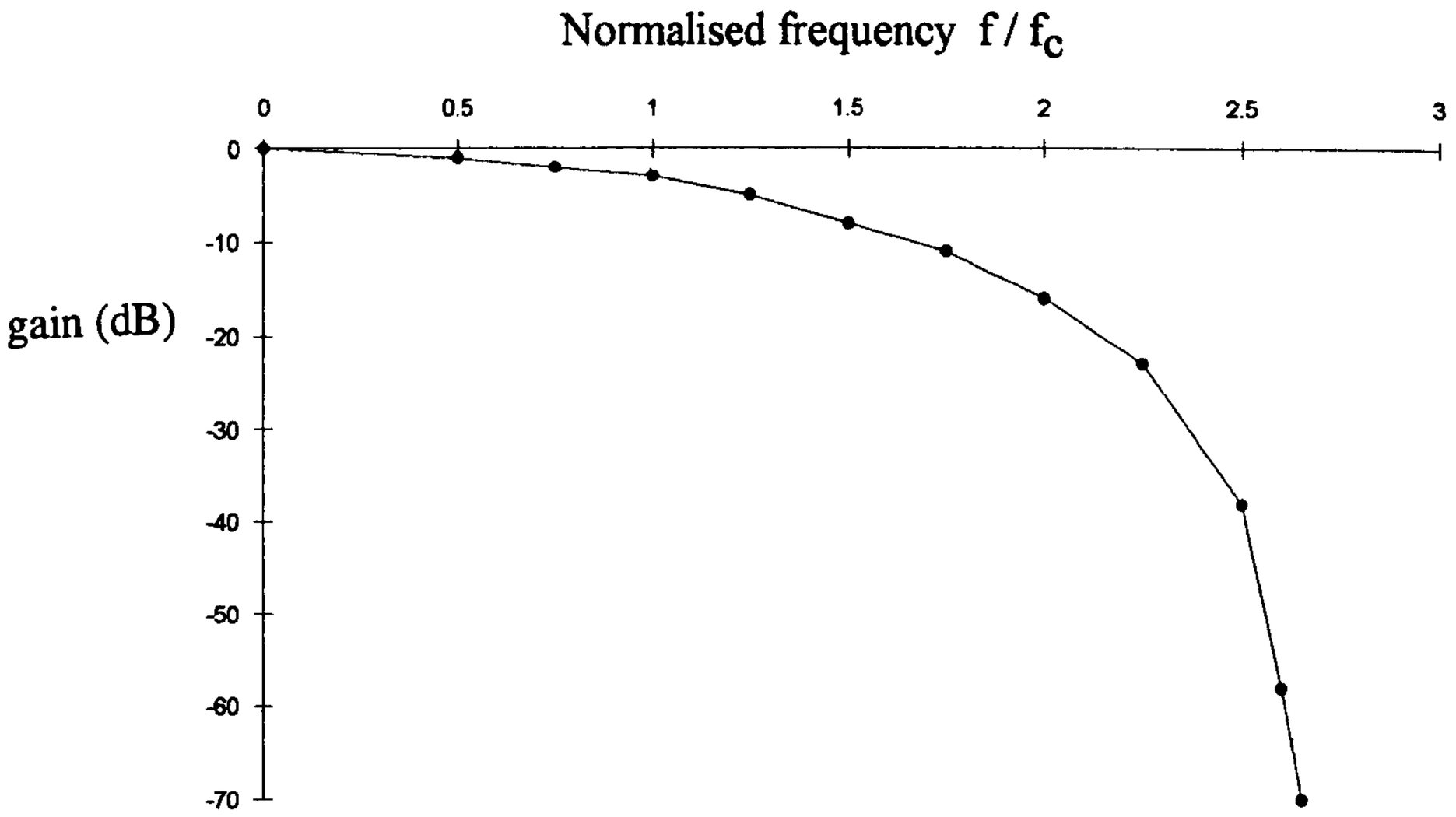

Figure 5.1 Characteristics of low pass cosine squared cut off digital filter.

From Johnson (1978).

At cut off frequency f_c, gain = -3dB

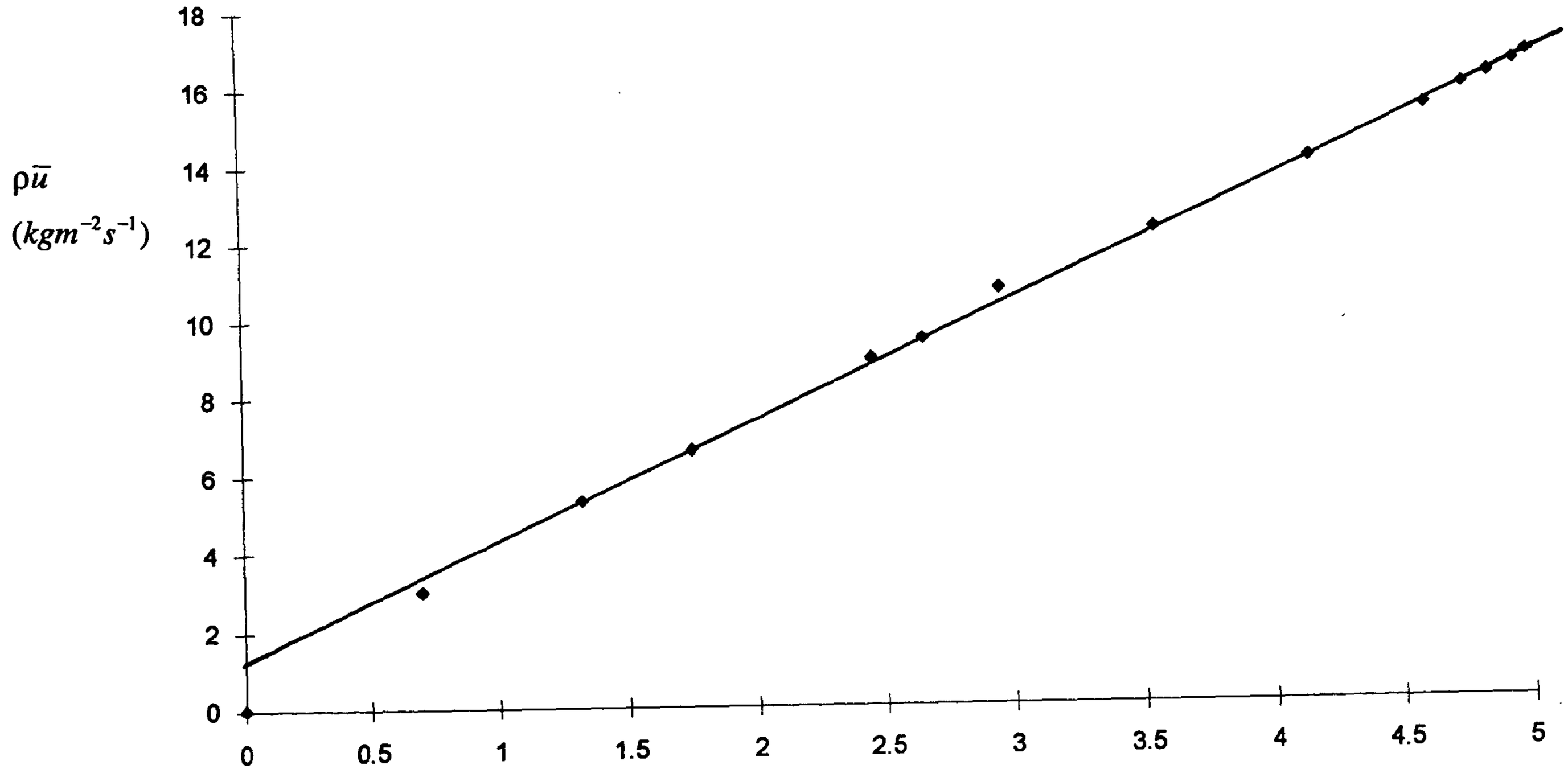

Figure 5.2 Hot film anemometer calibration.

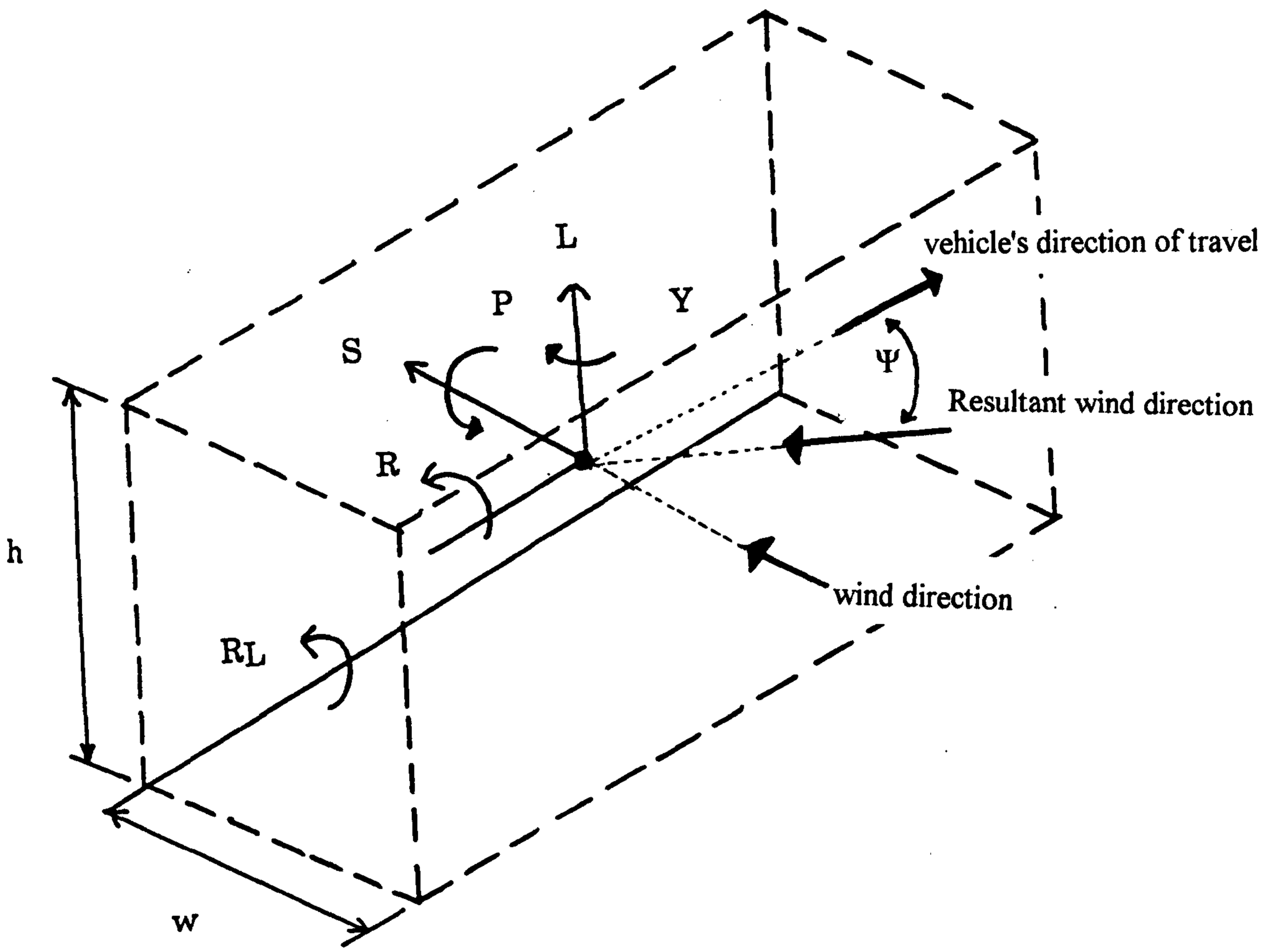

Figure 5.3 Relative direction for aerodynamic forces amd moments, vehicle direction of travel and wind direction for vehicle tests described in this thesis.

Ψ = Yaw angle

S = side force

L = lift force

P = pitching moment

Y = yawing moment

R = rolling moment

R_L = lee bottom corner rolling moment.

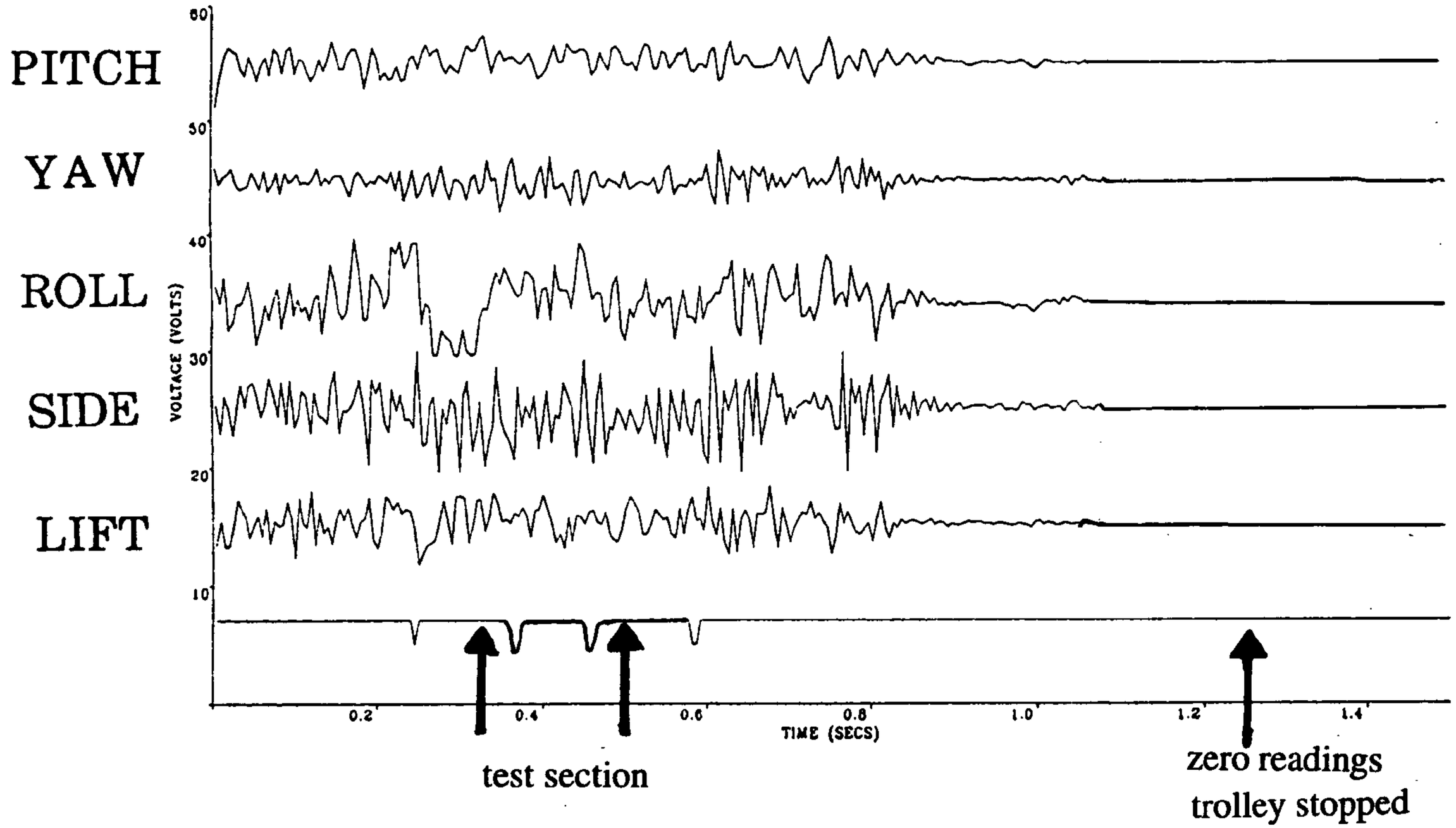

Figure 5.4 Raw data recorded by polycorder for 1.5 seconds operation.
5 force and moment channels from balance.
1 channel for polycorder control, trolley position and velocity.

6. The Atmospheric Boundary Layer Simulation.

The aim of the wind tunnel simulation was to achieve a mean hourly atmospheric boundary layer (ABL), typical of strong winds with a target roughness length corresponding to that of an open countryside. Section 3.2 describes the correlations between the streamwise velocity and turbulence intensity profiles and streamwise turbulence length scales used in this section for generating target values. Initial wind measurements were taken to gain experience of the extended wind tunnel and in the creation of a realistic atmospheric boundary layer (ABL). These tests, undertaken during April, 1990 are described in section 6.1. Described in section 6.2 is the final ABL, used for both the first and second series of model vehicle tests, obtained from tests during June and July, 1990.

Using equations 3.5 to 3.8 the target ABL characteristics at model scale were calculated. These are based on a model scale of 1/50th and a wind tunnel velocity at 0.2m above the surface of the working section floor (equivalent to 10m full scale) of 10m/s. This latter value was thought to be achievable based on the maximum wind tunnel speed of 14m/s with no roughness elements present. The full scale target roughness length, z_0, for the open countryside simulation (Cook (1985)), was 0.01m.

The target quantities calculated were those that would be measured in the wind tunnel and used in this thesis to assess the ABL generated :

1. Streamwise velocity and turbulence intensity vertical profiles.

2. Streamwise velocity spectrum.

The target streamwise wind velocity vertical profile is shown in figure 6.1. It is seen that this gives a wind velocity of 8.3m/s at the reference height, equivalent to 3m full scale, that is used in this thesis. The vertical streamwise turbulence intensity profile is shown in figure 6.2. It is seen that the turbulence intensity is around 20% at the reference height nearly twice the value achieved in the experiments of Coleman (1990).

Rearranging equation 3.5:

$$\frac{\overline{u}\,(z)}{\overline{u}\,(H)} = \text{constant}\,(\log_{10}z - \log_{10}z_0) \qquad 6.1$$

so that when $\frac{\bar{u}(z)}{\bar{u}(H)} = 0$, then $z = z_0$.

Referring to figure 6.3, a graph of $\frac{\bar{u}(z)}{\bar{u}(H)}$ versus $\log_{10}z$, it is seen that z_0 can be found from the intercept on the z axis for data which behaves as equation 6.1. This graphical technique was used to determine z_0, from measured streamwise wind velocity values at various heights above the wind tunnel working section floor described in section 6.1.

Finally the streamwise velocity spectrum, shown in figure 6.4, corresponds to a streamwise lengthscale of 1m, which is equivalent to 50m full scale. This value is some 8 times larger than that modelled in Coleman (1990) and Johnson (1981).

Note that the streamwise length scale is not a strong function of either the roughness length or the height above the ground, equation 3.8, and so during the initial experiments to determine an adequate ABL the streamwise lengthscale was only determined at one height, with reasonable confidence that it would not vary much for quite large changes in the roughness element height. This assumption would be checked for the final simulation as discussed in section 6.2.

6.1 The initial experiments.

The physical devices used for producing the experimental ABLs were as follows and are based on the advice in Cook (1978) :

1. Arrays of 200mm, 100mm and 50mm cubes to a 12% plan density. For each size a fetch, of working section width, of 2.5m was constructed. See figures 6.5 and 6.6.

2. Gravel boards. 1.2m square of gravel size approximately 3mm diameter.

3. A 70mm high barrier placed at the working section inlet.

4. A grid shown in figure 6.7 for placing at the working section inlet. This was used as the turbulence generator for previous vehicle overturning studies described in Coleman (1990).

The fetch described is on the basis of the entire 9ft width of the working section being covered as shown in figure 6.5. Various combinations of the turbulence generators were tried as listed in table 6.1.

The measurements were taken in the centre of the working section 50mm forward of the moving model rig. The results of the corresponding ABL parameters from this data are given in table 6.2. The actual measurements and corresponding spectra are shown in Humphreys (1990).

It was found that the target velocity and turbulence intensity profiles, figures 6.1 and 6.2, could be modelled quite easily but, as expected, the velocity spectrum was more difficult. This was due to the inadequate length of the available fetch. The best velocity spectrum was shifted to higher frequencies by a factor of 2 when compared with the target shown in figure 6.3. Note, however, that this spectrum is similar to that shown in Hoxey (1992) for measurements made at similar small heights above the ground.

The wind velocity spectrum for all the simulations tried were dominated by a low frequency peak, around 2Hz. A low frequency contribution was expected because the wind velocity spectrum measured in the original wind tunnel had a similar feature, reported in Coleman (1990). Coleman traced this to the presence of a separation bubble in the roof of the collector section just forward of the fan. The presence of this low frequency oscillation in the flow actually aided the generation of a 1/50th scale velocity spectrum. This provided a low frequency component to the velocity spectrum that would not be possible to generate using conventional roughness elements over the relatively short fetch of the Nottingham University environmental wind tunnel. The normalising velocity relevant to the frequency of oscillation of the separation bubble (Strouhal number dependence) is that of the wind jet at the roof of the working section. As the wind speed at the roof of the tunnel is not very dependent on the ABL simulation it follows that the frequency of the low frequency component present in the measured spectra is roughly constant. It is seen, referring to the discussion in section 3.2, that the streamwise turbulence length scale is proportional to the wind speed. In order to create the largest possible turbulence length scale near the floor of the working section it was therefore necessary to choose turbulence generating devices which did not reduce the maximum wind tunnel speed too greatly in this region of interest, i.e. the first 200mm above the ground.

The horizontal streamwise velocity and turbulence intensity profiles along the length of the working section were initially investigated by Yang (1990) working on another

project. As was expected the horizontal profiles became worse down the length of the working section due to the mixing in the shear layer wind between the wind jet and the stationary air to the sides of the test room. The spanwise characteristics were improved by fitting some side walls and a secondary flow collector of height 600mm to the last 6.6 metres of the working section spanning the moving model rig.

6.2 The final atmospheric boundary layer simulation.

The ABL simulation used for all the tests described in this thesis used the following devices:

1. 70mm high barrier of length 1.5m situated in the centre if the working section inlet.

2. Two 1.2m x 1.2m gravel boards, average gravel size 3mm, placed in the centre of the working section 100mm forward of the test position, either the static position or the moving test slot.

3. Inclusion of 600mm high side walls to the last 6.6m of the working section.

Figure 6.8 shows the layout of the devices for the moving model experiments.

6.2.1 Moving test position streamwise profiles.

It was found that placing these devices only in the centre of the working section produced reasonably uniform horizontal profiles for the central 1.5m of the working section, and data analysis was constrained to data sampled from this central section. The initial 600mm that the moving model travelled through the wind, prior to the central 1.5m section from which the data was analysed, was thought to be useful as it may enable the flow pattern around the moving vehicle to stabilise. This was checked, see Chapter 9. The wind measurements were carried out 50mm forward of the working section slot needed for the moving model supports. Figures 6.9 and 6.10 show the spanwise velocity and turbulence intensity profiles for the moving model position.

The reference height for the wind measurement position shown in this section was 60mm, equivalent to 3m for a 1/50th scale model. Measurements at the moving model and static positions were made at the maximum attainable wind speed, 8.5m/s and the lowest used for the tests reported in this thesis, 5.0 m/s.

Figures 6.11 and 6.12 show the spanwise averaged streamwise velocity and turbulence intensity profiles compared to the target values based on a 1/50th scale simulation of a full scale roughness length, z_0 = 0.03m, and 3m reference height from Cook (1985). Note that the value of the target z_0 has been slightly changed as it better fits the attainable data but it is still representative of an open country simulation. Generally the comparisons are good and importantly the comparisons between the measured values and the target are independent of the wind speed considered, which demonstrates Reynolds number independence for the ABL.

Next the streamwise velocity spectrum are compared with the target von Karman spectrum, equation 3.7. Figures 6.13 and 6.14 show the comparison for wind speeds of 8.5m/s and 5.0m/s at the reference 3m full scale height. These show a consistent (i.e. Reynolds independence) mismatch by a factor of around 2, the measured length scale being about half that of the target. The length scale of the measured data is about 0.5m, rather than the target of 1m, i.e. 1/50th of 50m full scale for z_o = 0.03m. These spectra however are similar to those of Hoxey and Richards (1992), discussed in section 3.2, from measurements made at similar heights above the ground.

Figures 6.15 and 6.16 show the spectral comparisons for measurement full scale equivalent heights of 1.5m and 10m at the working section centre, again showing the consistency between measurement and target. Similarly figures 6.17 to 6.19 show comparisons for measurements at the start and end of the data sampling region along the moving vehicle's test position.

Figure 6.20 shows the average non dimensionalised longitudinal wind velocity spectrum from all the spectra measured at a height equivalent to 3m full scale, at 5 positions spanwise along the moving model test position. As with all the spectral calculations in this thesis the spectrum at each position was averaged from 14 calculated. This spectrum therefore was formed from 70 individually analysed spectra. This average spectrum is representative of that experienced by the moving vehicle over a large number of test runs.

6.2.2 Static test position streamwise profiles.

Figures 6.21 to 6.23 show the velocity, turbulence intensity and a streamwise velocity spectrum at the static test position. The comparisons between the measured and target profiles show the same relationship as those for the moving test positions, thus enabling valid comparisons to be made between moving and static tests.

6.2.3 Lateral wind characteristics.

It was not possible to measure the lateral wind characteristics during the commissioning of the ABL described in this chapter due to the lack of suitable equipment. In order to measure the lateral length scales, a cross correlation has to be conducted of the signals from two anemometers (usually hot wires) positioned in the direction of the axis of the lateral component that is being measured. However it is known (Schlichting (1968) pp 531 to 539) that a conventional zero pressure gradient turbulent boundary layer is characterised by lateral velocity components similar to the magnitude of the streamwise components and therefore approximate to isotropic turbulence. Further, ESDU (1975) notes that the Earth's ABL turbulence is near isotropic characterised by lateral turbulence semi length scales of around half the streamwise length scale. As the mechanism for the simulated ABL generated by the roughness blocks in the environmental wind tunnel is physically the same as these turbulent boundary layers it was expected that the simulated ABL would be characterised by turbulent semi length scales in the correct ratio to their streamwise component. As discussed in section 6.1, part of the ABL simulation described here was created, not by conventional roughness blocks, but by the low frequency streamwise oscillation due to separation in the roof of the tunnel. Fortunately this component would be expected to have high lateral spanwise correlation and therefore should serve to increase the lateral correlation across the length of the vehicle.

Noting that the streamwise turbulence length scale, using the ABL modelled, is 0.5m it is seen that the semi length scales should be around 0.25m. The characteristic dimension that is important from the point of view of vortex shedding is the height of the vehicle. Both the model Lorry and the Container with wagon are around 0.08m high (4m full scale) and therefore the condition of Tielman and Atkins (1989) discussed in section 3.1, that the streamwise length scale modelled in a wind tunnel test should at be least twice the model scale of the bodies tested is satisfied. Note that the lateral length scales of the simulated ABL are roughly three times the height of the models tested.

As the vehicles under study are 3 dimensional in nature and finite in length the condition of Tielman and Atkins may not be considered adequate to fully represent the unsteady effects on a vehicle. Referring to figures 2.4 and 2.5, it is seen that the effect of the finite length of the vehicle is observed in theoretical predictions of the unsteady side force parameters and also the normalised extreme side force parameters computed (section 2.1) for vehicle height to length ratios similar to those described and tested in

this thesis. Noting the ratio of the length of the vehicle to the streamwise length scale L/L_u, for the lorry $L/L_u = 0.54$, and the DB container $L/L_u = 0.53$, these figures show that both extreme parameters obtained from these wind tunnel tests should be representative of such tests conducted with a much longer simulated turbulence scales. It is seen that the values of L/L_u obtained for the vehicles tested in this thesis correspond to the condition of Tielman and Atkins applied to the length of the vehicle as well as its height. The semi lateral length scales are very nearly equal to the length of the vehicles and therefore the large scale turbulence is correlated across the length of these vehicles.

The lateral length scales have since been measured in the environmental wind tunnel at the University of Nottingham (King (1994)). At a position near to the moving model rig and with the ABL simulation used in this thesis and the following ratios to the streamwise component were obtained, ${}^{y}L_u/{}^{x}L_u = 0.35$ and ${}^{z}L_u/{}^{x}L_u = 0.35$. These verify that the condition of Tielman and Atkins, applied to both the height and the length of the vehicles tested in this thesis, was satisfied. The ABL modelled, for these vehicles tested, was therefore an adequate simulation of the full scale mean hourly ABL for the purpose of determining the gust loads on these vehicles in a high cross wind.

Referring to the wind velocity measurements of Hoxey and Richards (1989), discussed in section 3.2, it may be that the ABL simulation obtained at Nottingham University is representative of the full scale mean hourly ABL at small heights, less than 10m. In this case, no additional streamwise length scale corrections would be necessary to the model time scale. Further, the lateral correlation of the gusts over the model in the wind tunnel are representative of the full scale situation. More full scale wind measurements are needed at these small heights.

6.2.4 Extreme values and time scaling.

One of the aims of this thesis is to explore the concept of time scaling for the moving model tests particularly with reference to an inadequately modelled ABL. Indeed, even for a static test, as discussed in section 3.4, the interpretation of the ABL simulation is needed in order to decide on the time scaling required to produce representative full scale 3 second extreme values.

In order to explore this topic further a range of 1 hourly 3 second extreme wind speed values have been calculated from the same set of measured wind data by taking different model time periods equal to the 3s full scale values. The method was

described in 5.1.5 and an example given in 5.2.1.3. Figure 6.24 shows the calculated extreme values against the model time period taken equal to the 3 second full scale value for data measured at both the static and moving model test positions.

6.3 Summary of the final atmospheric boundary layer simulation.

1. The ABL simulations measured at the moving model and the static model positions are comparable.

2. For the moving model tests the measured profiles and analysed spectra are reasonably uniform over the central 1.5m working section width.

3. The mean measured vertical velocity and turbulence intensity profiles compare with accepted target correlations for a full scale roughness length of 0.03m.

4. The analysed velocity spectra from the measured wind data remain consistent compared to the target von Karman correlation for all the vertical, and in the case of the moving model tests, also for the spanwise measurements. In all cases the implied streamwise turbulence length scale, from the analysed spectra, is approximately half that predicted by the von Karman correlation. However the analysed spectra are similar to the recent results in Hoxey (1992) from measurements made at similar low heights.

5. The atmospheric boundary layer generated for the tests reported in this thesis is a much better full scale representation than that achieved for the original version of this rig featuring the Advanced Passenger Train, Johnson (1981). The latter tests showed the streamwise turbulence length scale was a factor of 8 too small compared to the von Karman spectrum.

6. The lateral turbulence length scales of the ABL simulated were around three times the height of the 1/50th scale vehicles tested and therefore adequate model the possible full scale unsteady forces due to vortex shedding in the wake of a vehicle.

7. The lateral turbulence length scales of the ABL simulated were around the same order as the length of the vehicle. Therefore, this should enable the values of subsequently calculated normalised extreme value parameters and the unsteady parameters to be representative of much longer turbulence length scales.

TEST	PROBE HEIGHT FOR SPECTRA (m)		ABL SIMULATION CONFIGURATION
	Model scale	Full scale	
SPEC1	0.24	12	Empty Wind Tunnel
SPEC2	0.24	12	2 rows of 8" cubes
SPEC3	0.24	12	2 rows of 8" cubes, 2 rows of 4" cubes
SPEC 4	0.24	12	2 rows of 8" cubes, 2 rows of 4" cubes, 2 rows of 2" cubes
SPEC5	0.24	12	8ft gap, 2 rows of 4"cubes
SPEC6	0.80	40	Empty wind tunnel
SPEC7	0.24	12	Grid
SPEC8	0.24	12	Grid, 2 rows of 8" cubes, 2 rows of 4" cubes
SPEC9	0.06	3	Grid
SPEC10	0.06	3	8" cube placed in solid wall across working section inlet
SPEC11	0.06	3	As SPEC 10 but 50% density wall. (Every other block removed)
SPEC12	0.06	3	0.07m wall at working section inlet, 6m gap, 2 rows of 2" blocks, 1 row of gravel boards

Table 6.1 Configurations of turbulence generating devices tested in order to produce the target atmospheric boundary layer.

Test	$\overline{u}$ (10m) (m/s)	$\overline{u}$ (3m) (m/s)	$\sigma/\overline{u}$ (3m) %	z_o (m)	^xL_u from spectra (m)	Anemo-meter height for spectra (m)	Air speed at anemo-meter for spectra (m/s)
SPEC1	10.5	9.3	22	$1x10^{-3}$	30	12	10.6
SPEC2	7.7	7.0	19	$2x10^{-2}$	20	12	7.7
SPEC3	7.0	6.2	22	$1x10^{-1}$	15	12	7.1
SPEC4	7.4	6.2	23	$2x10^{-1}$	20	12	8.5
SPEC5	8.2	7.3	19	$5x10^{-2}$	20	12	8.0
SPEC6	10.5	9.3	22	$1x10^{-3}$	30	40	12.1
SPEC7	8.2	7.6	26	$5x10^{-4}$	20	12	8.4
SPEC8	9.0	7.5	23	$5x10^{-4}$	20	12	9.2
SPEC9	8.3	7.5	28	$1x10^{-3}$	15	3	7.3
SPEC10	2.0	1.8	47	$1x10^{-1}$	1	3	1.7
SPEC11	7.7	7.2	21	$1x10^{-4}$	20	3	7.0
SPEC12	7.2	5.7	29	$5x10^{-2}$	15	3	5.5

Table 6.2 Analysed results from measurements made of the various configurations of the turbulence generating devices given in table 6.1.

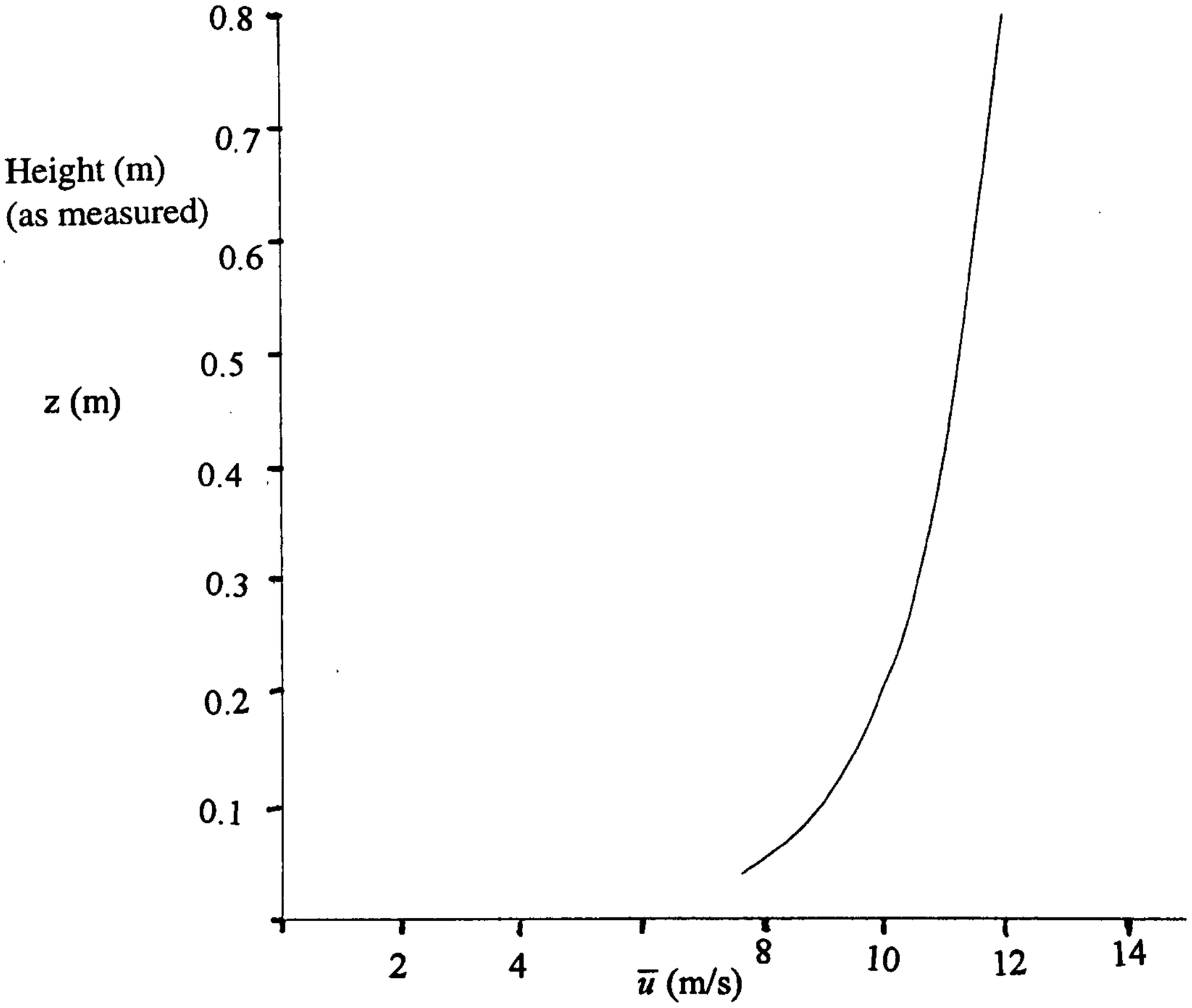

Figure 6.1 Target vertical streamwise wind velocity profile.

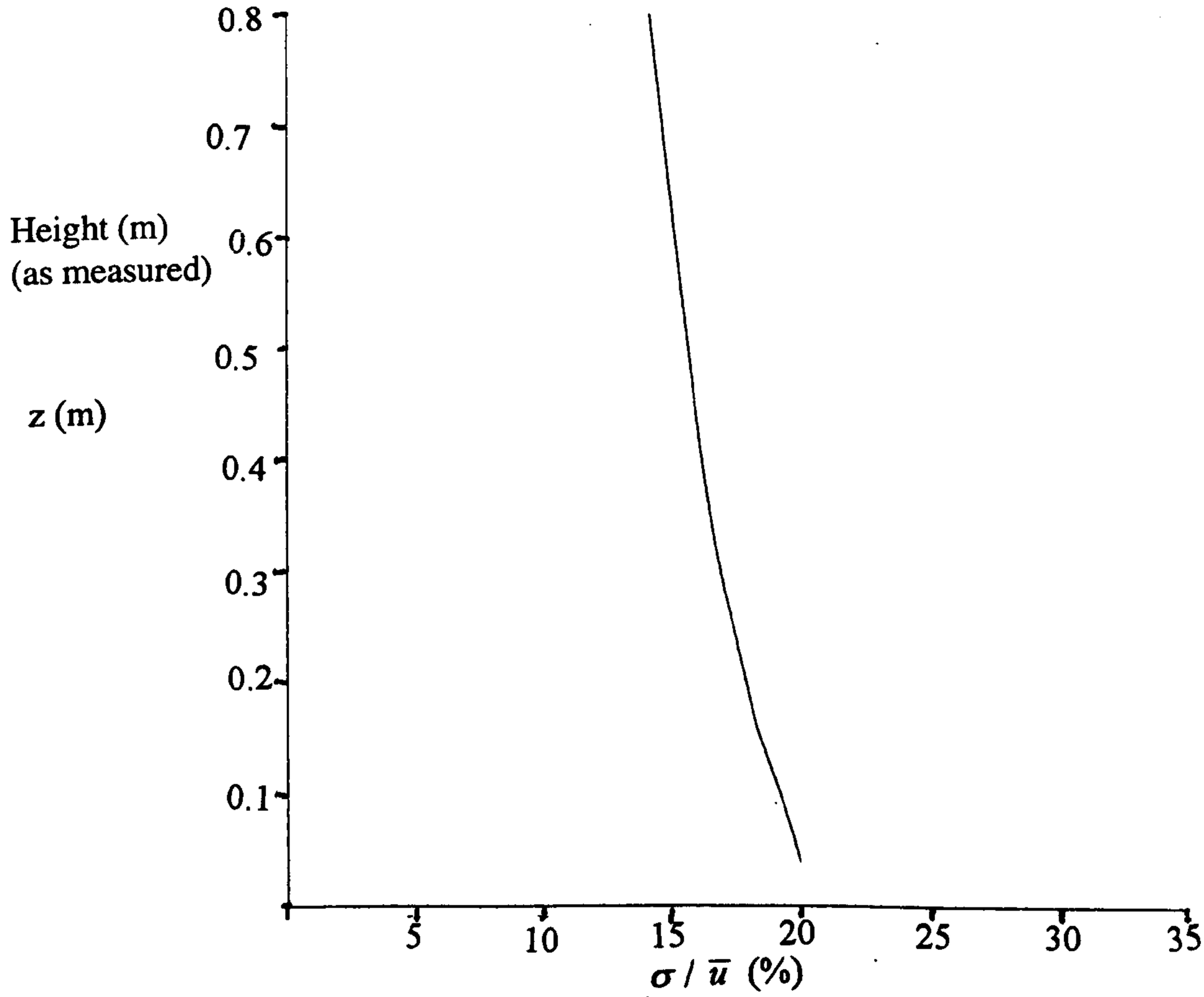

Figure 6.2 Target vertical streamwise wind turbulence intensity profile.

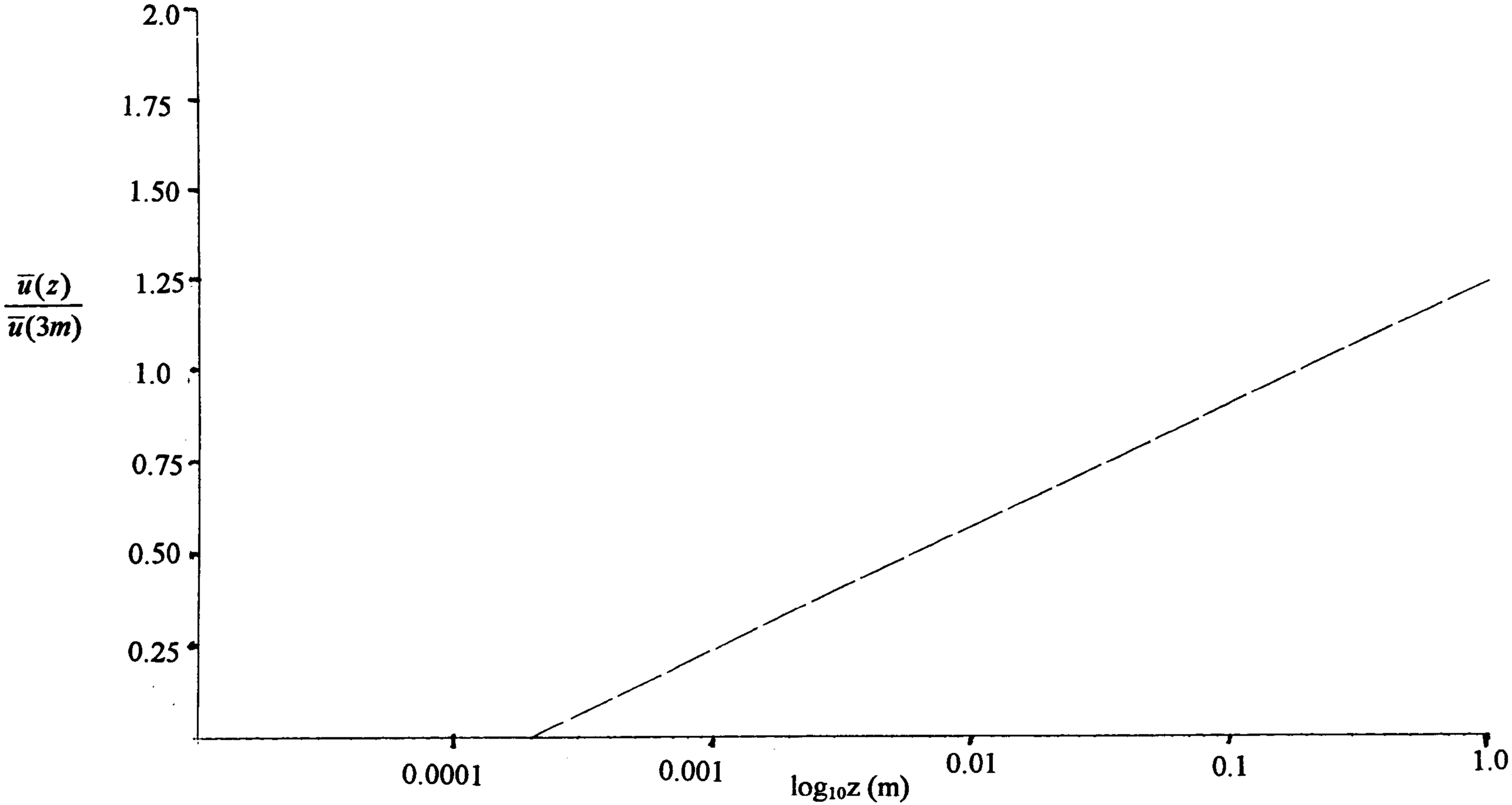

Figure 6.3 Target semi-log vertical streamwise wind velocity profile.

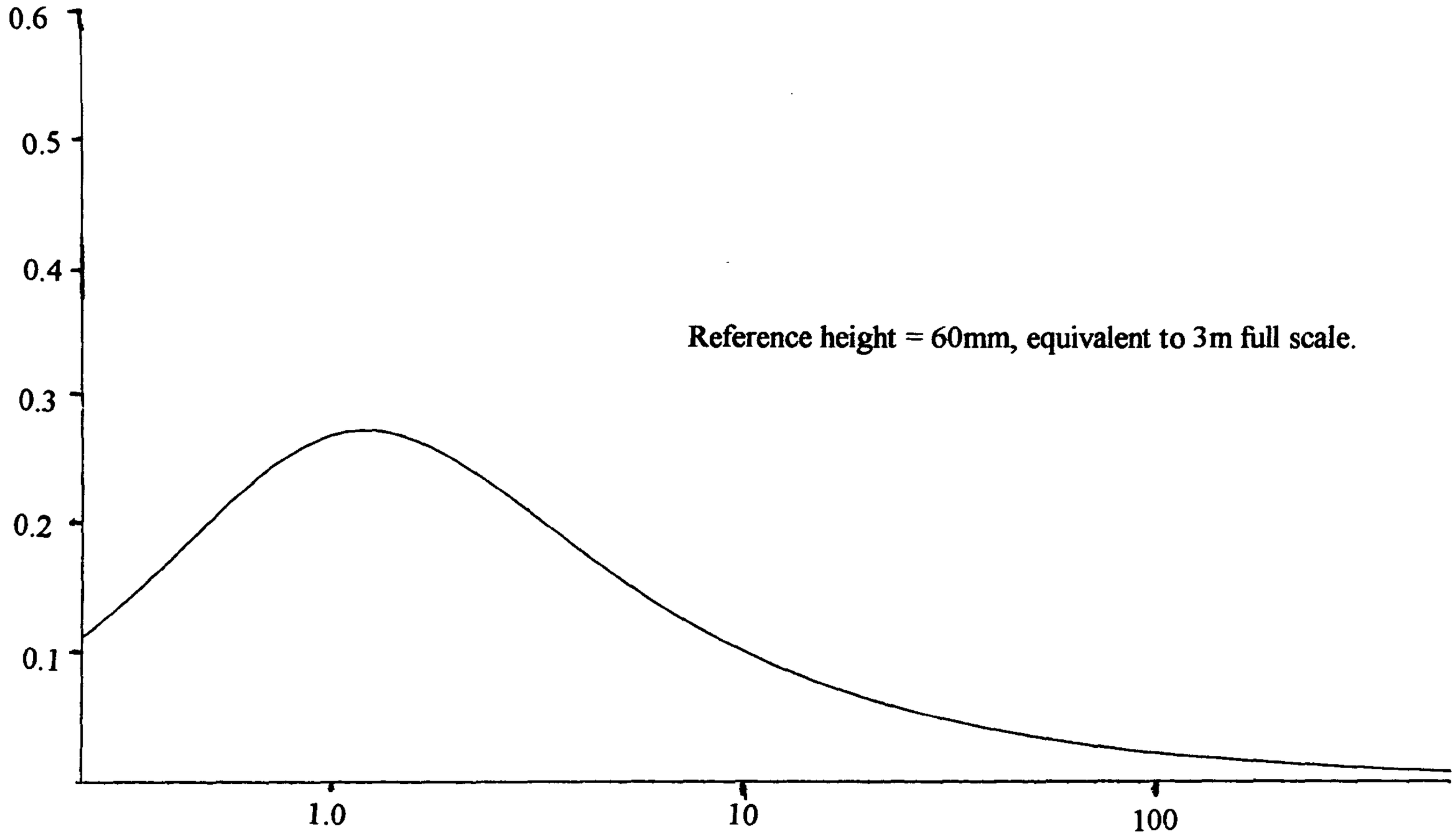

Reference height = 60mm, equivalent to 3m full scale.

Figure 6.4 Target non dimensionalised streamwise wind velocity spectrum

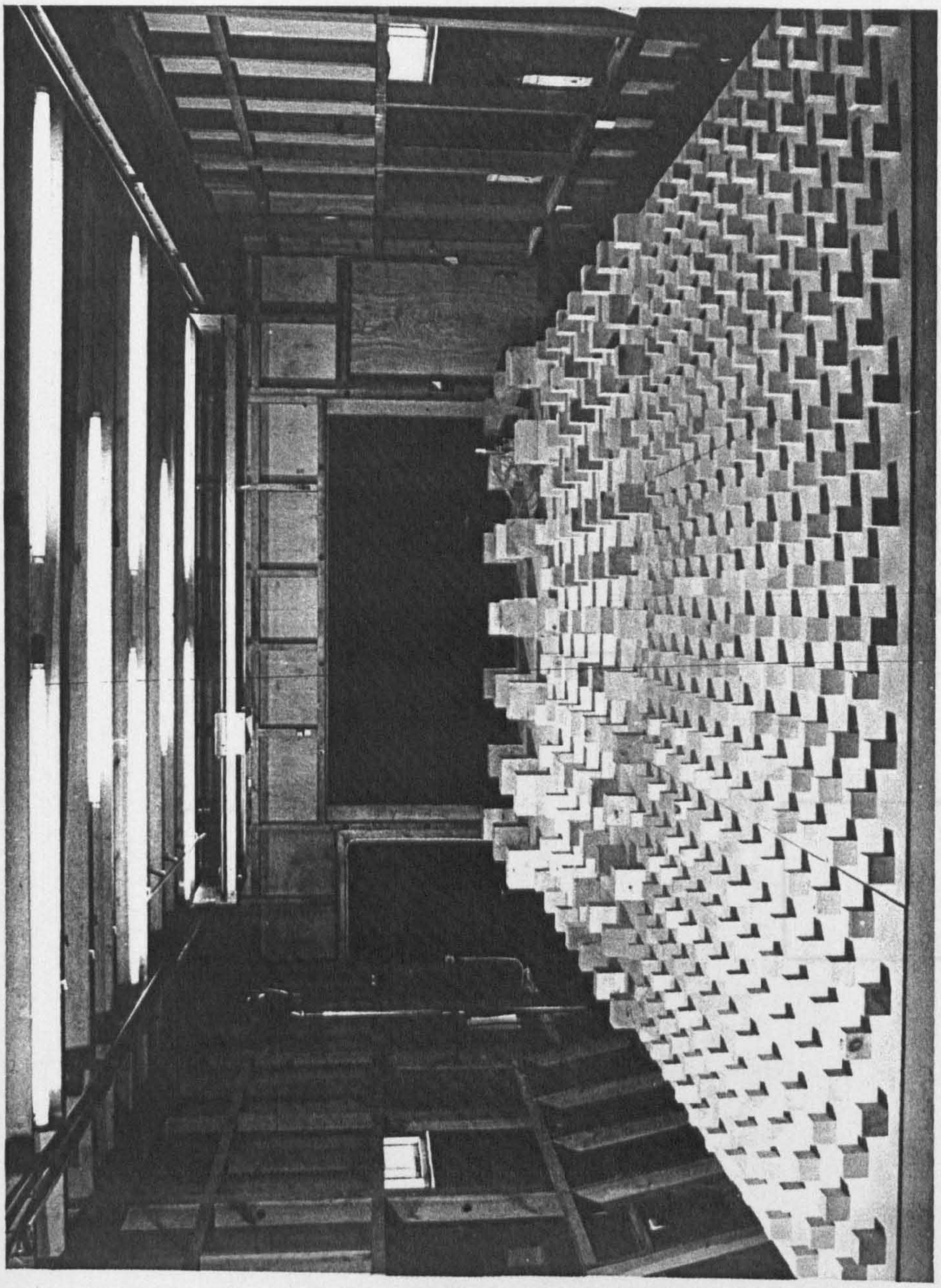

Figure 6.5 Upstream view of wind tunnel working section from near moving model test position. Configuration is as SPEC 4 detailed in table 6.1.

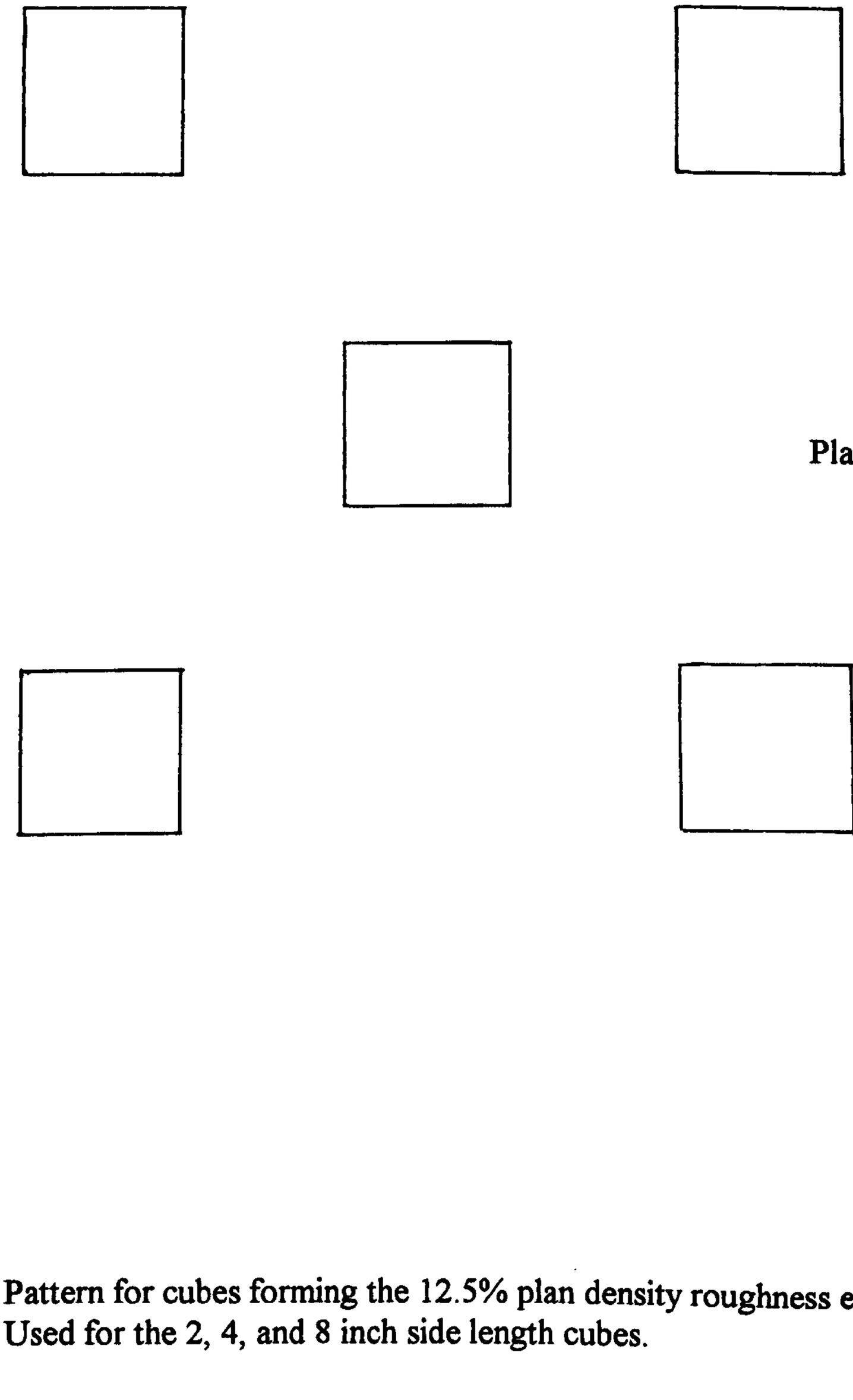

Plan view.

Figure 6.6 Pattern for cubes forming the 12.5% plan density roughness elements. Used for the 2, 4, and 8 inch side length cubes.

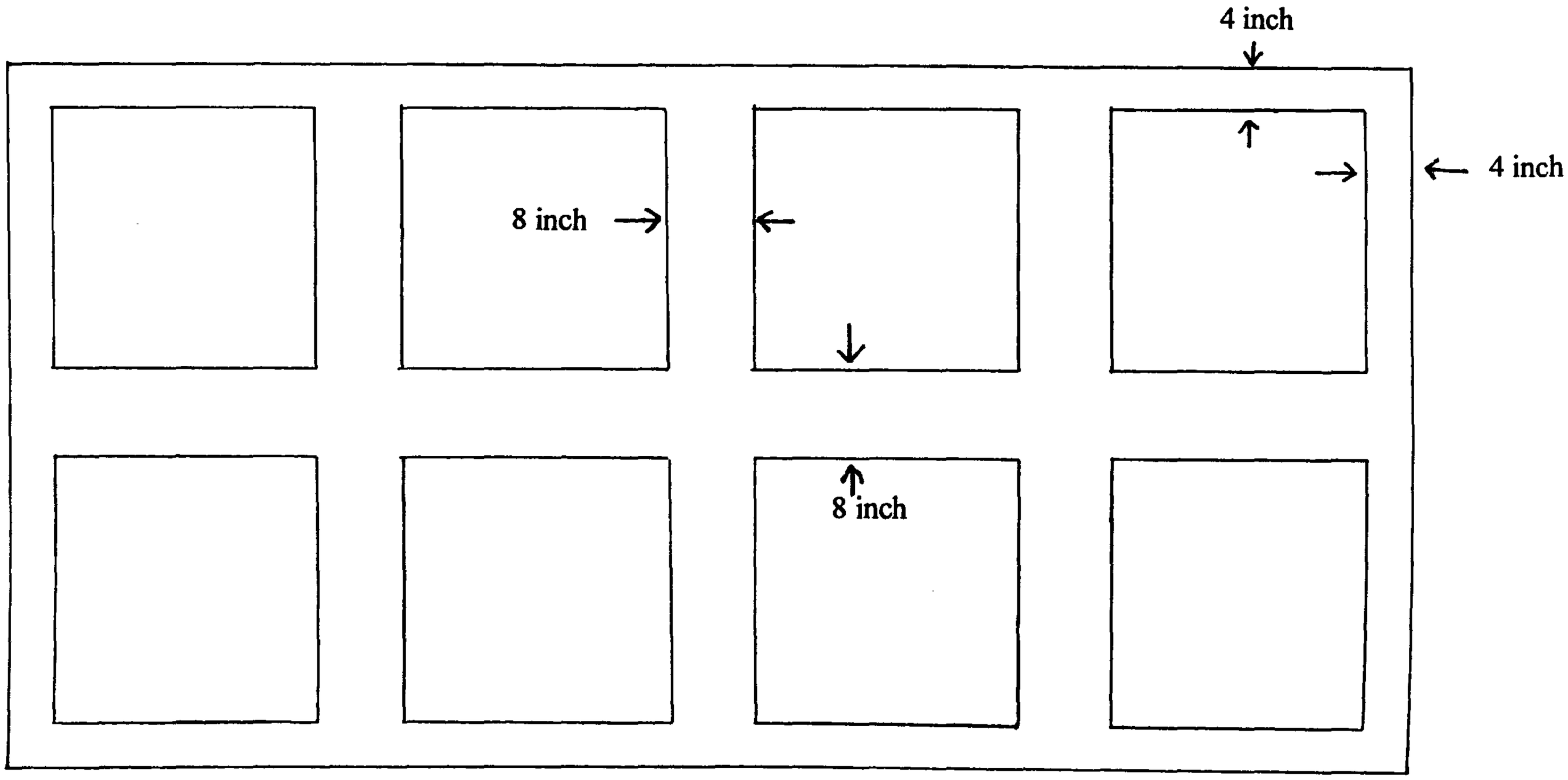

Figure 6.7 Turbulence grid (8ft by 4ft) for fitting at working section inlet.

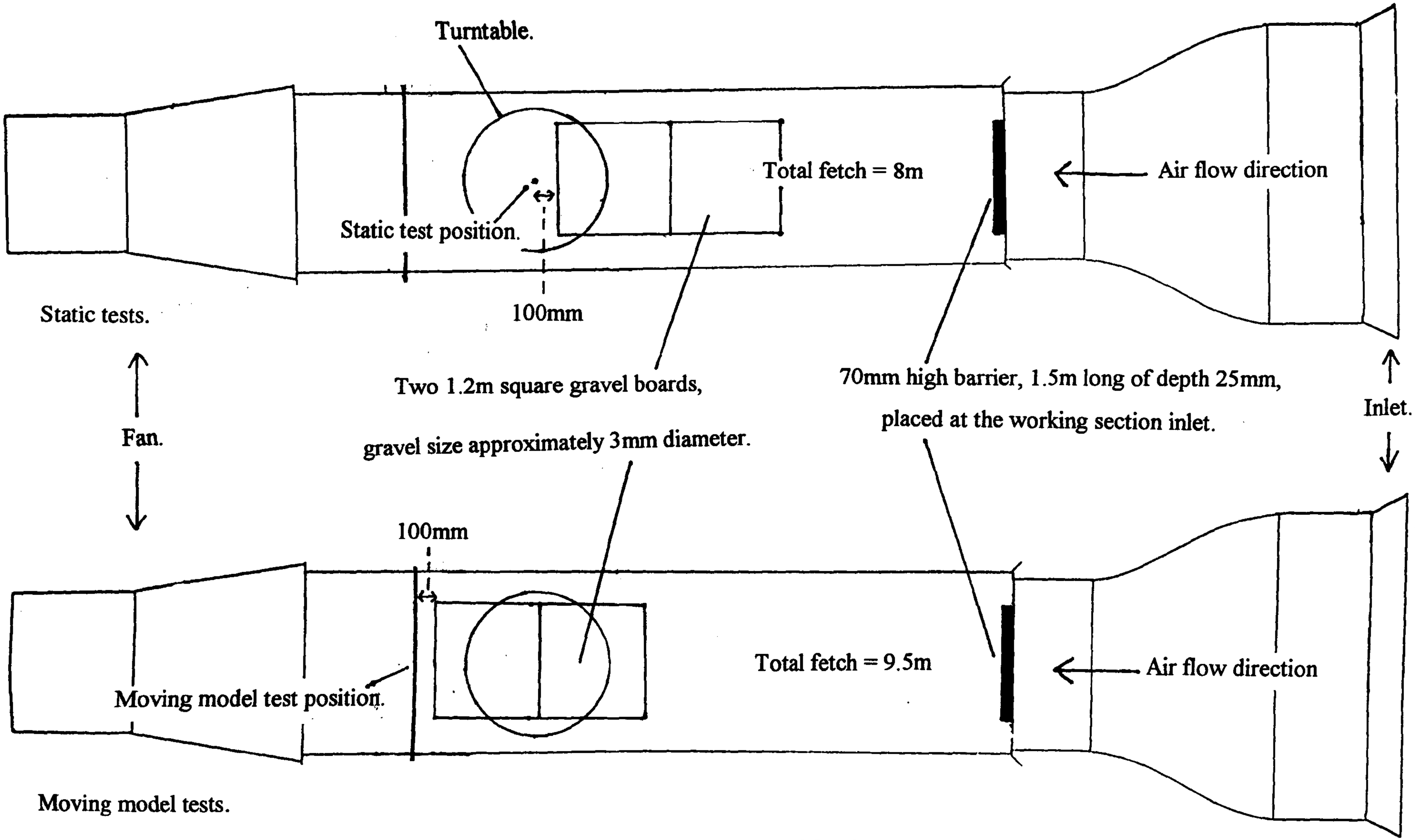

Figure 6.8 Layout of the turbulence generators used for the final ABL simulation. These layouts were used for all tests described in this thesis.

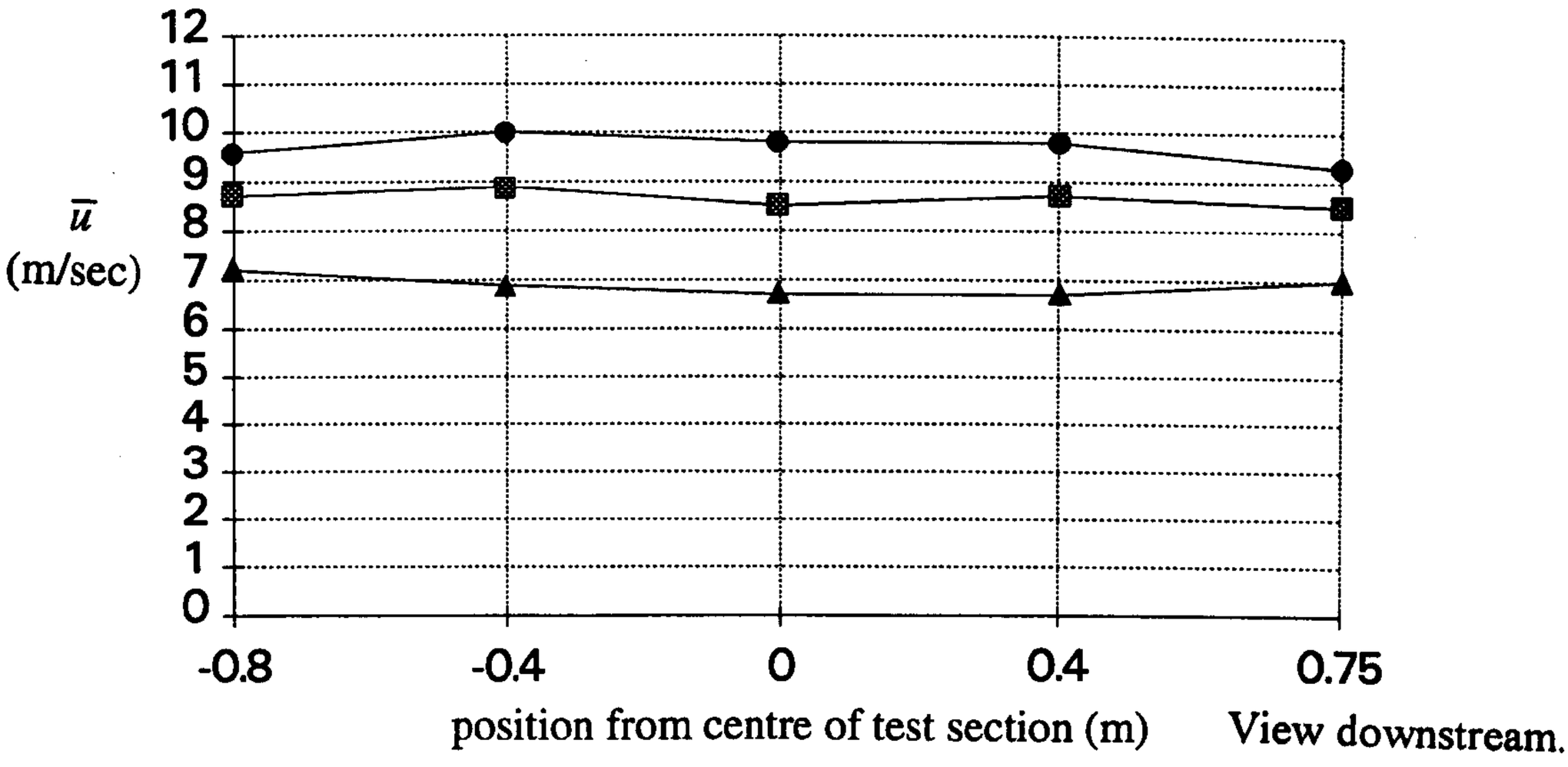

Figure 6. 9 Spanwise streamwise mean wind velocity profiles at the moving model test position.

▲ equivalent 1.5 m full scale height,
■ equivalent 3 m full scale height,
● equivalent 10m full scale height

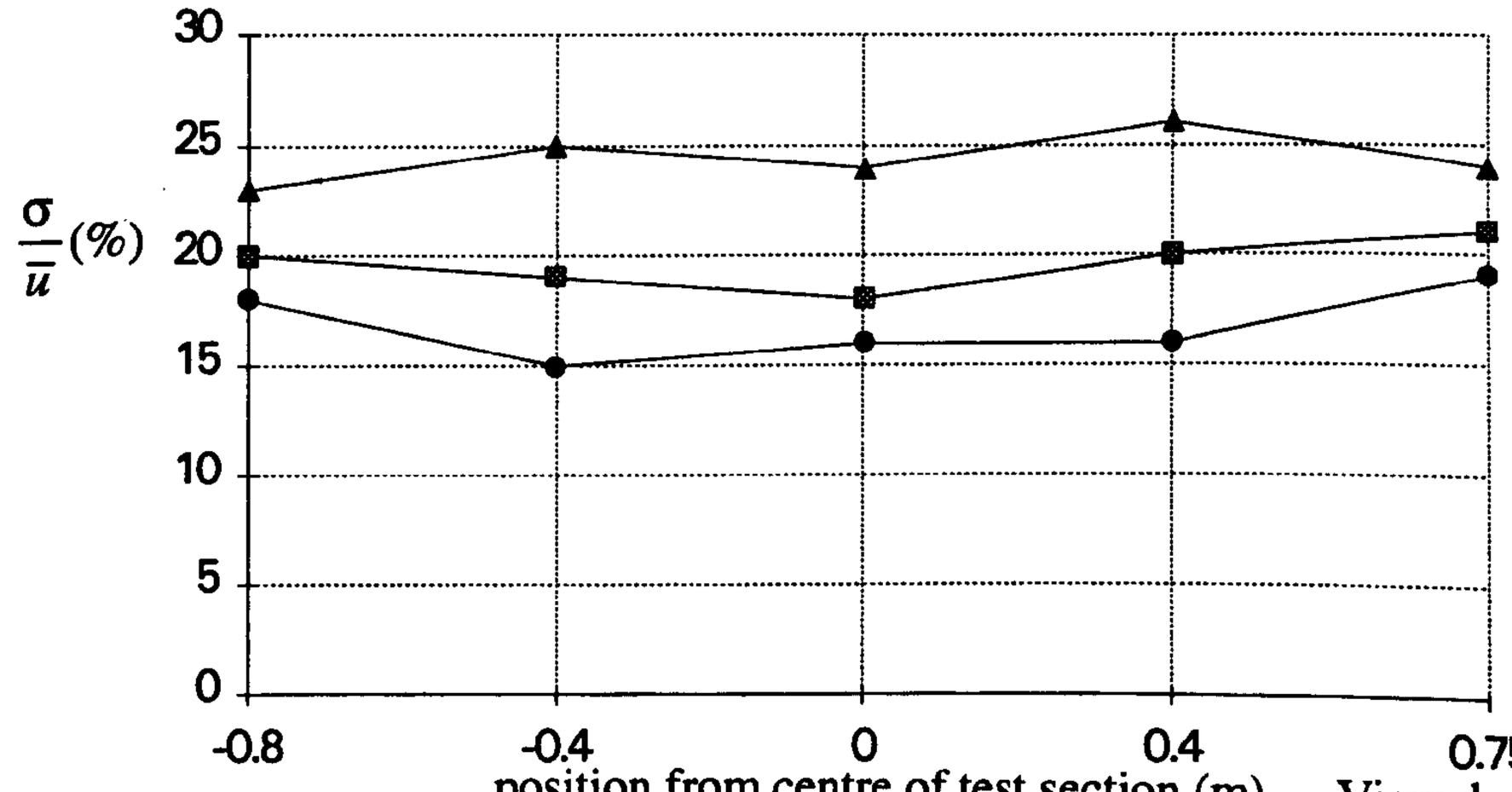

Figure 6. 10 Spanwise streamwise turbulence intensity profiles at the moving model test position.

▲ equivalent 1.5 m full scale height,
■ equivalent 3 m full scale height,
● equivalent 10m full scale height

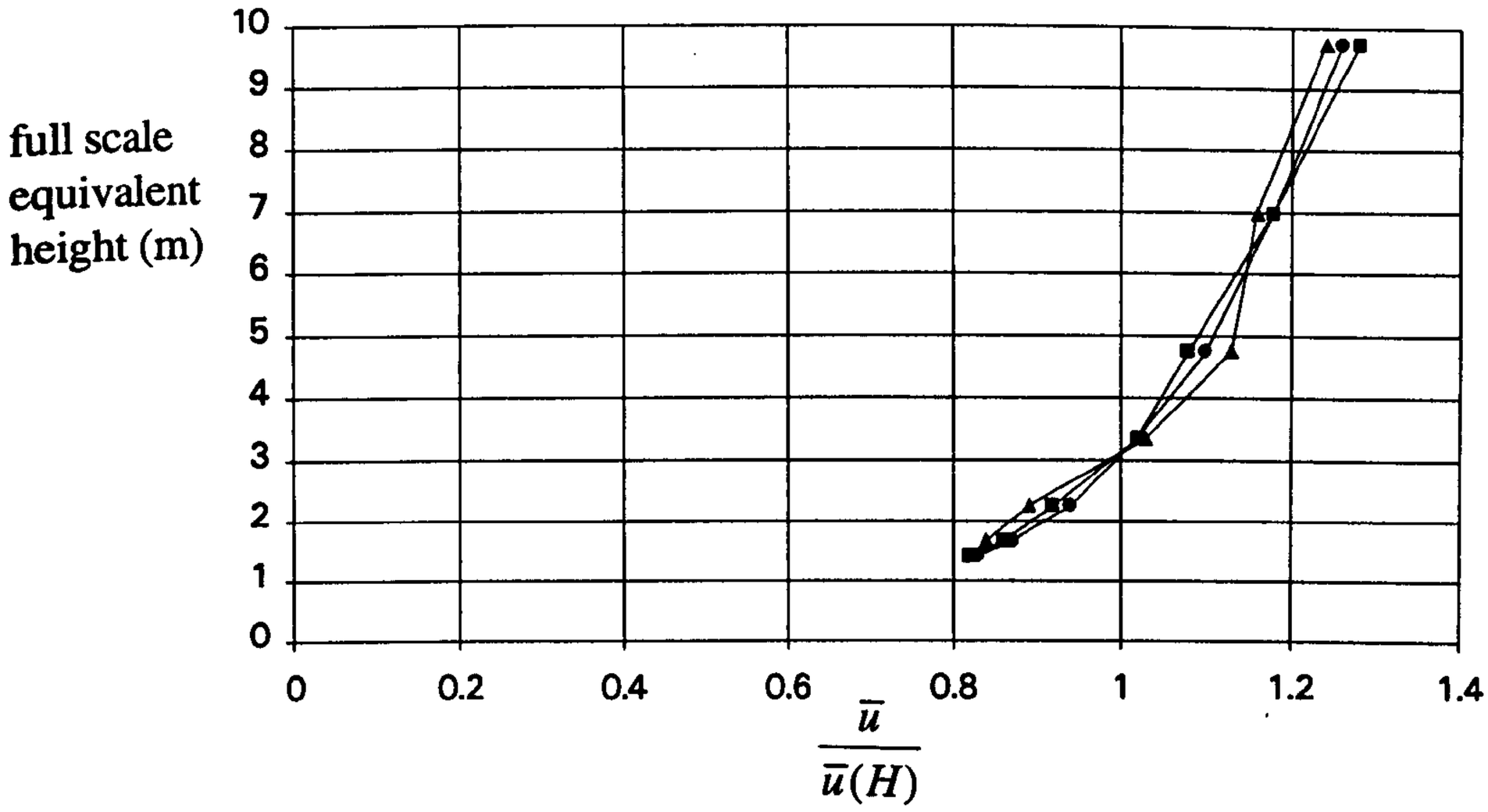

Figure 6. 11 Spanwise averaged vertical mean wind velocity profile compared with the target value at the moving model test position.

■ u = 8.5 m/s

▲ u = 5 m/s

● target (z_o = 0.03m fullscale equivalent)

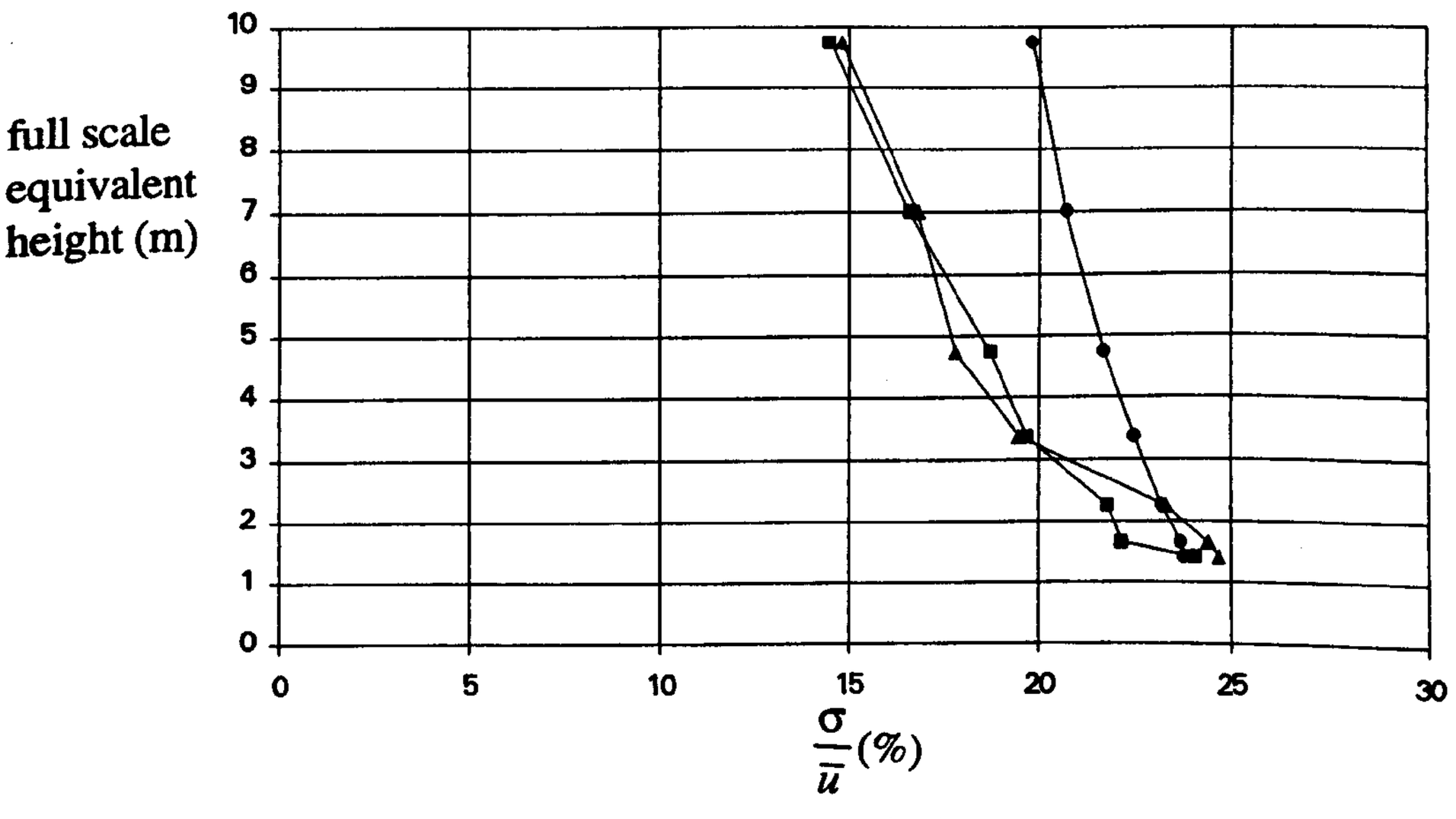

Figure 6 .12 Spanwise averaged vertical streamwise turbulence intensity profile compared with the target value at the moving model test position.

■ u = 8.5 m/s

▲ u = 5 m/s

● target (z_o = 0.03m fullscale equivalent)

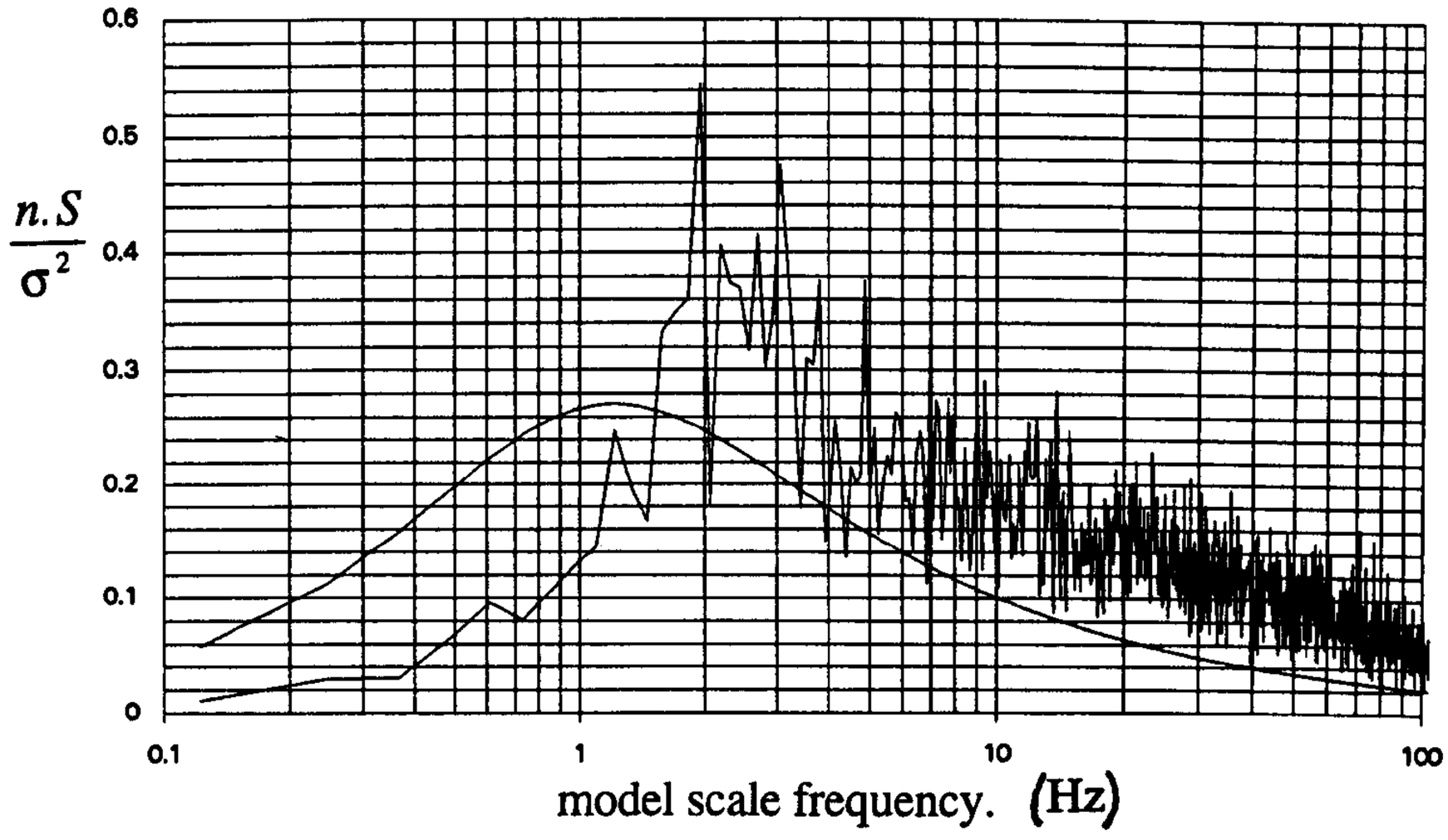

Figure 6.13 Streamwise wind velocity spectrum compared with the target von Karman spectrum (smooth line) for a $\bar{u}$(3m) = 8.5 m/s (full scale equivalent height) at the centre of the moving model test position. Spectrum measurement height 60mm equivalent to 3m fullscale.

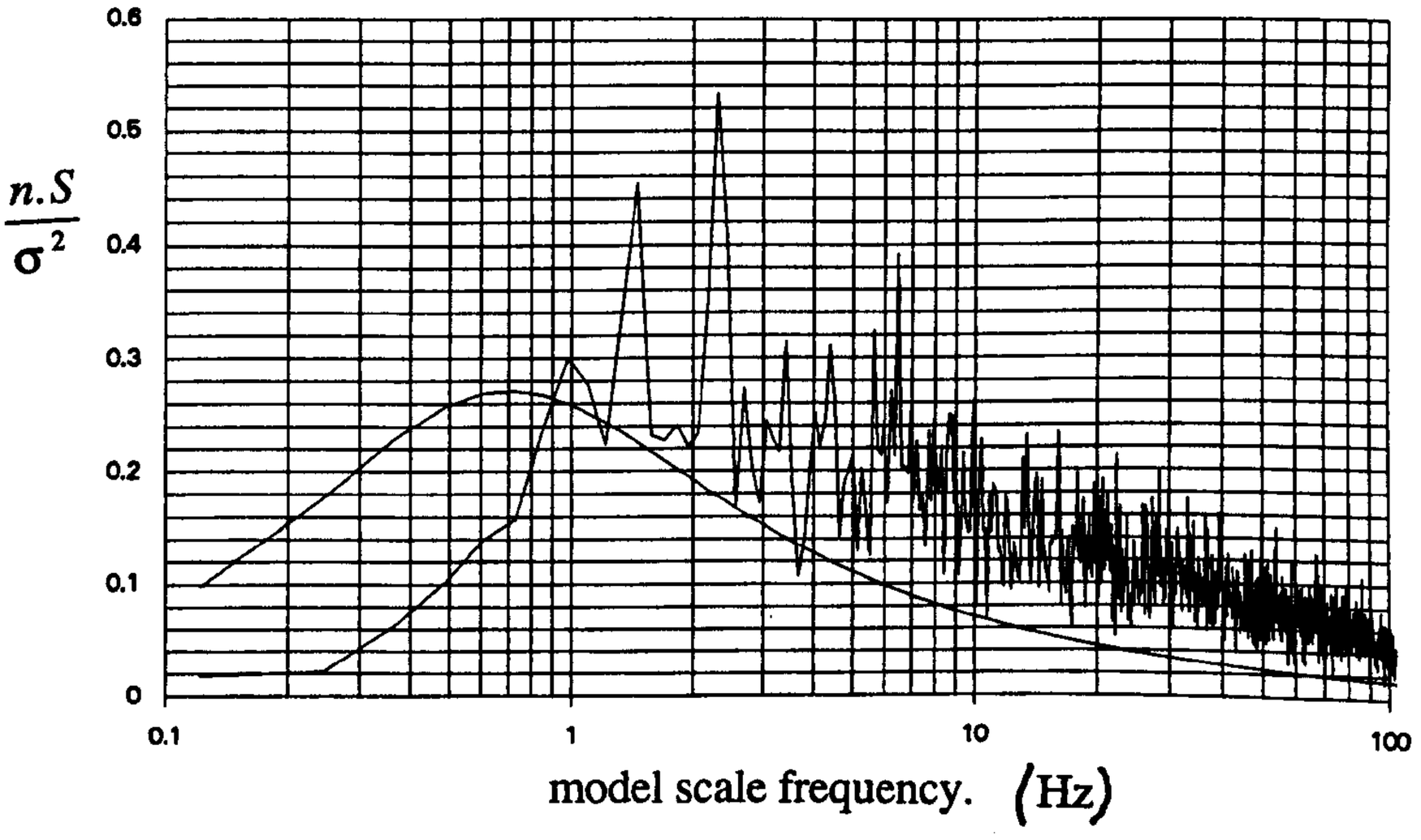

Figure 6.14 Streamwise wind velocity spectrum compared with the target von Karman spectrum (smooth line) for a $\bar{u}$(3m) = 5 m/s (full scale equivalent height) at the centre of the moving model test position. Spectrum measurement height 60mm equivalent to 3m fullscale.

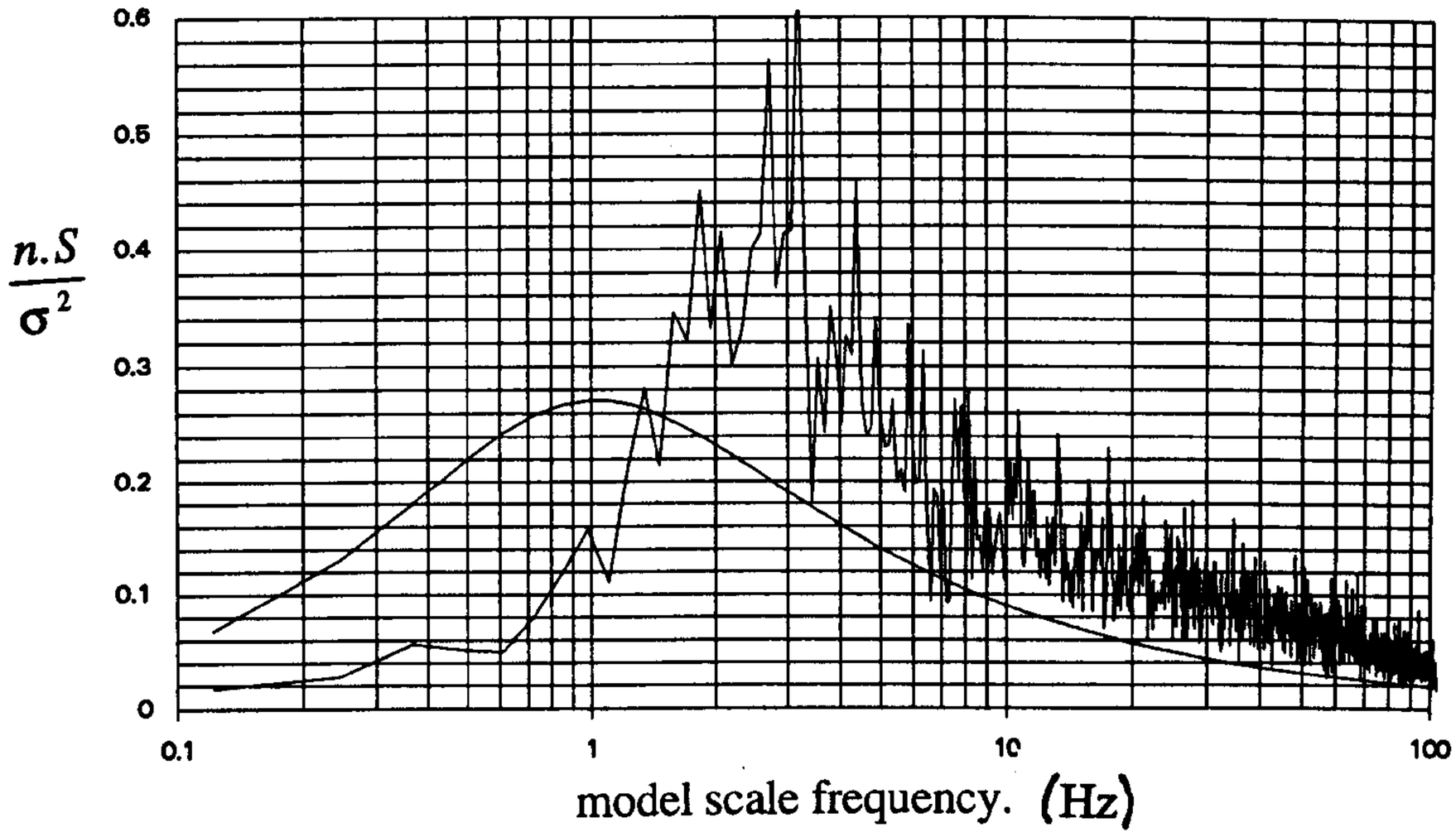

Figure 6.15 Streamwise wind velocity spectrum compared with the target von Karman spectrum (smooth line) for a $\bar{u}(3\text{m}) = 8.5$ m/s (full scale equivalent) at the centre of the moving model test position. Spectrum measurement height at 200mm equivalent to 10m fullscale.

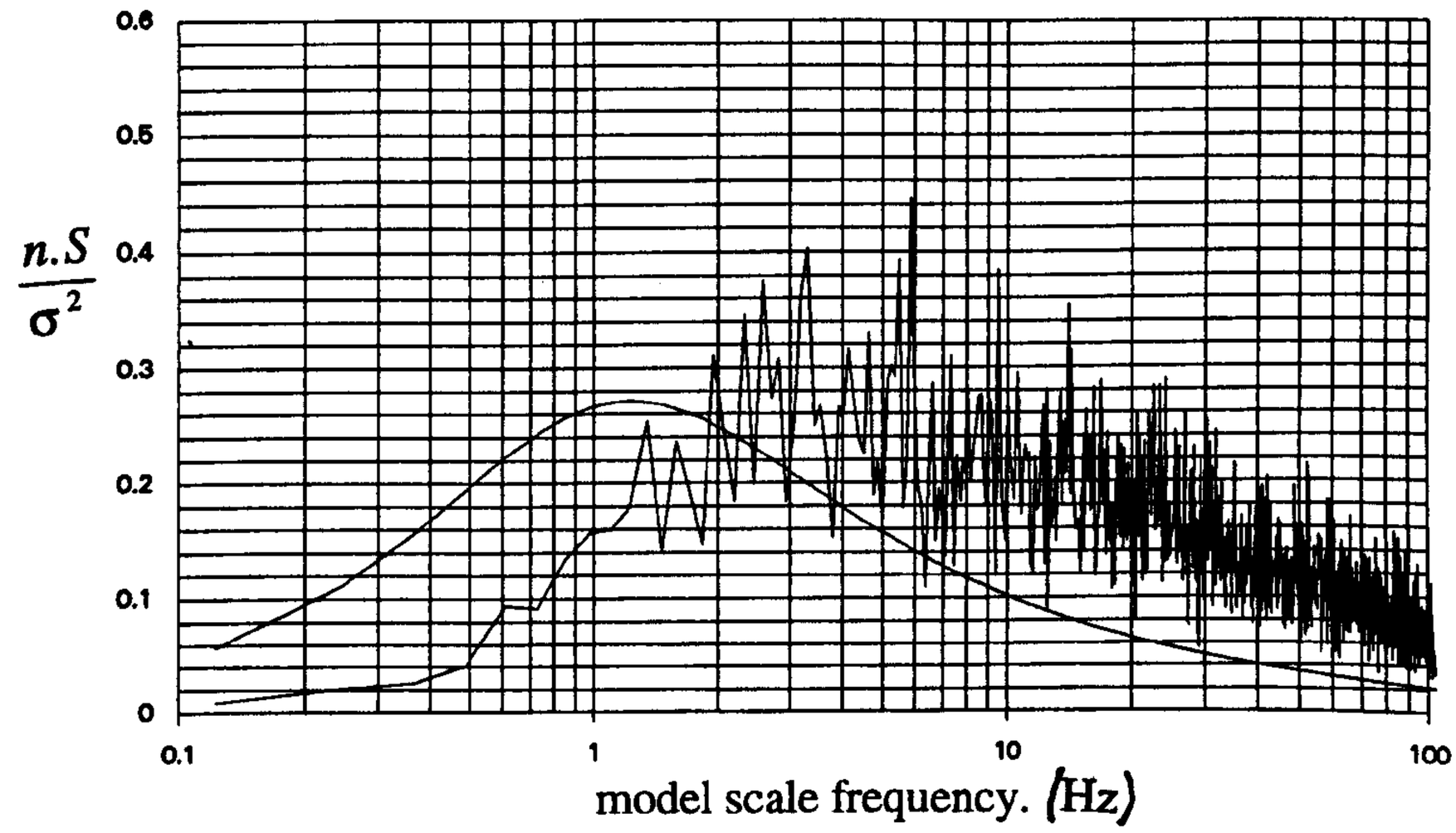

Figure 6.16 Streamwise wind velocity spectrum compared with the target von Karman spectrum (smooth line) for a $\bar{u}(3\text{m}) = 8.5$ m/s (full scale equivalent) at the centre of the moving model test position. Spectrum measurement height 30mm equivalent to 1.5m fullscale.

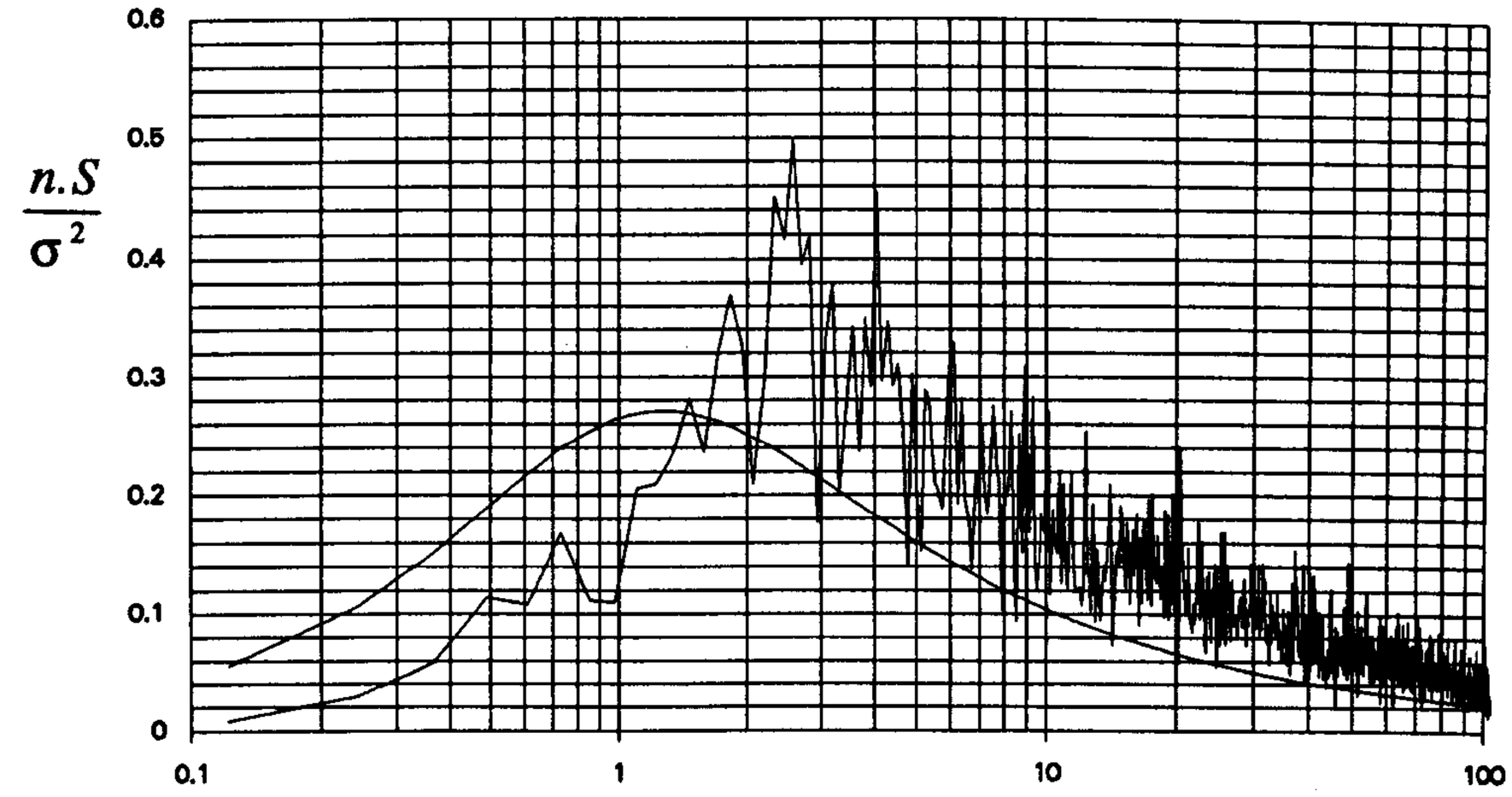

Figure 6 .17a Streamwise wind velocity spectrum compared with the target von Karman spectrum (smooth line) for a $\overline{u}(3\text{m}) = 8.5$ (full scale equivalent) at the start of the moving model test position, 0.75m before centre of working section. Spectrum measurement height 60mm equivalent to 3m fullscale.

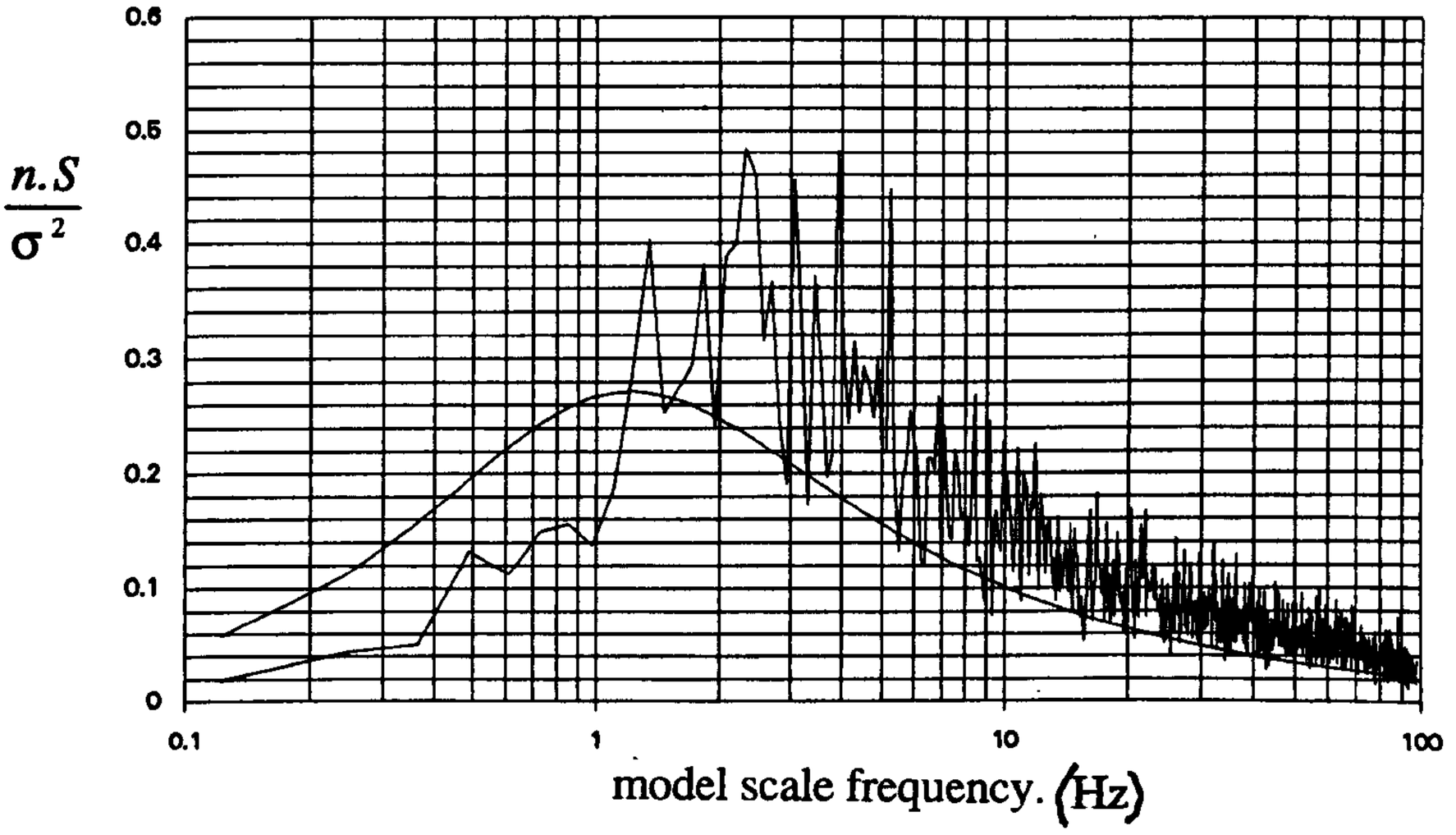

Figure 6. 17b Streamwise wind velocity spectrum compared with the target von Karman spectrum (smooth line) for a $\overline{u}(3\text{m}) = 8.5$ m/s (full scale equivalent) at the end of the moving model test position, 0.75m after centre of working section. Spectrum measurement height 60mm equivalent to 3m fullscale.

Figure 6.18a Streamwise wind velocity spectrum compared with the target von Karman spectrum (smooth line) for a $\bar{u}$(3m) = 8.5 m/s (full scale equivalent) at the start of the moving model test position. Anenometer height 200mm equivalent to 10m fullscale.

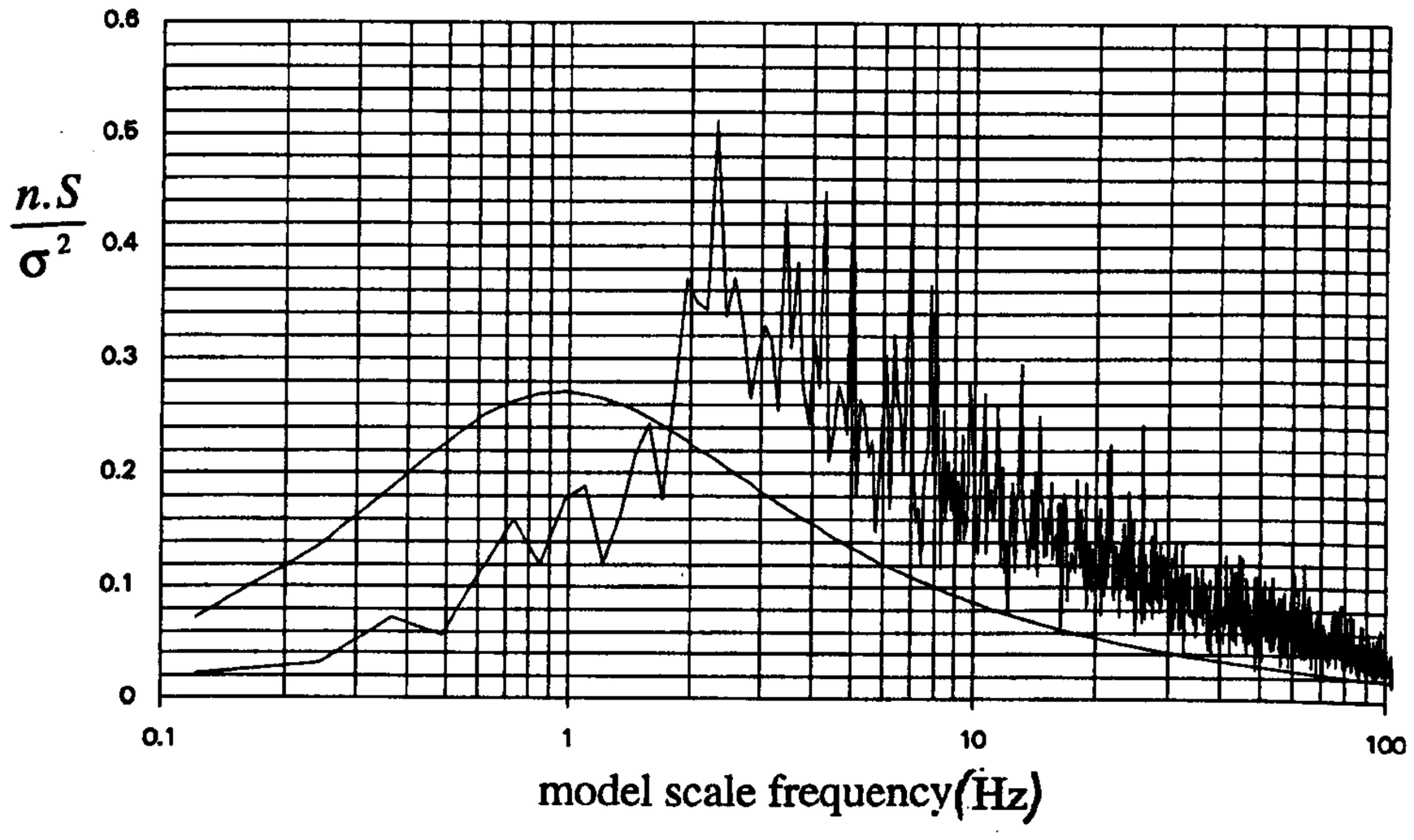

Figure 6.18b Streamwise wind velocity spectrum compared with the target von Karman spectrum (smooth line) for a $\bar{u}$(3m) = 8.5 m/s (full scale equivalent) at the end of the moving model test position. Anemometer height 200mm equivalent to 10m fullscale.

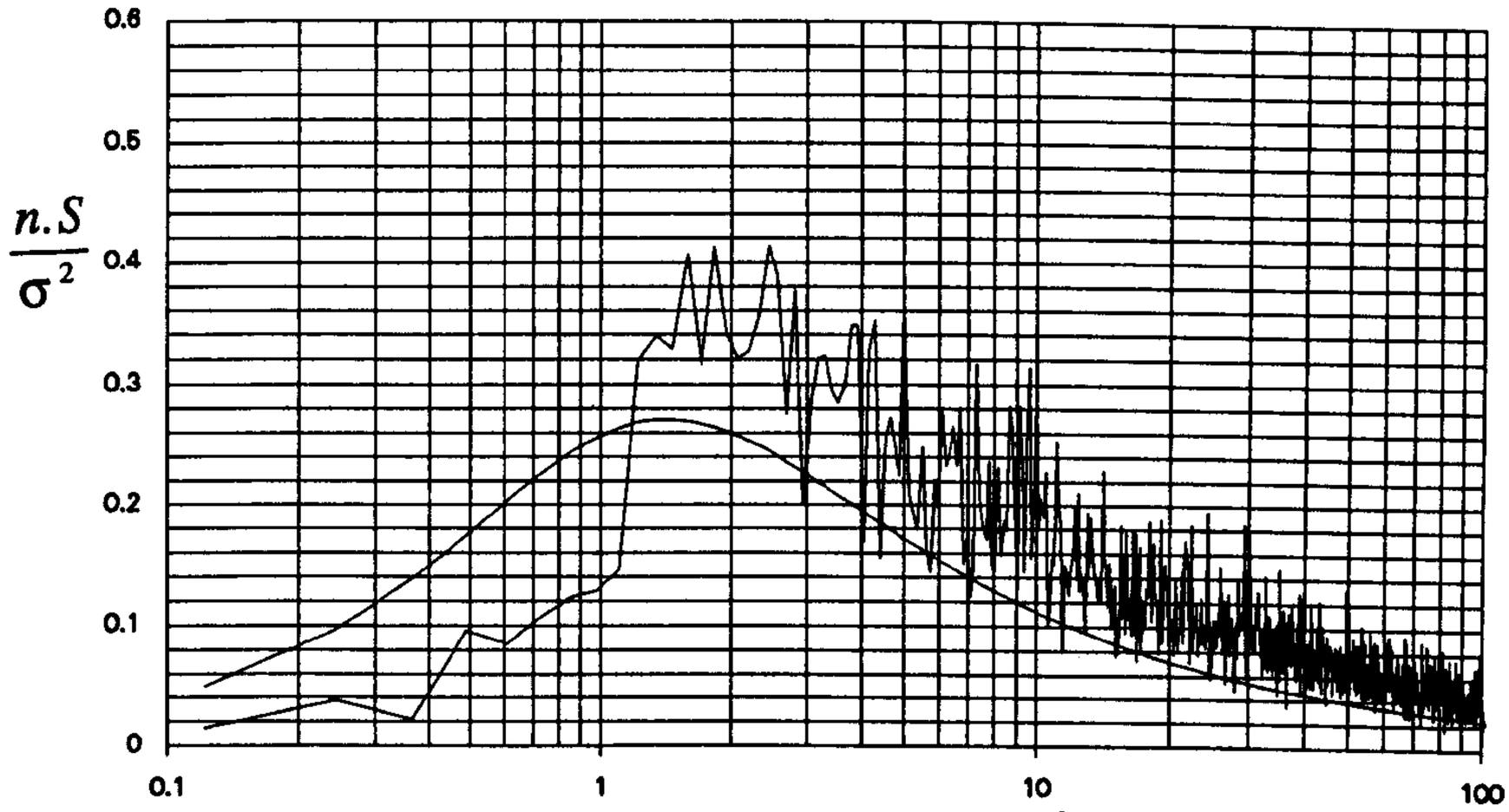

Figure 6.19a Streamwise wind velocity spectrum compared with the target von Karman spectrum (smooth line) for a $\bar{u}$(3m) = 8.5 m/s (full scale equivalent height) at the start of the moving model test position. Anemometer height 30mm equivalent to 1.5m.

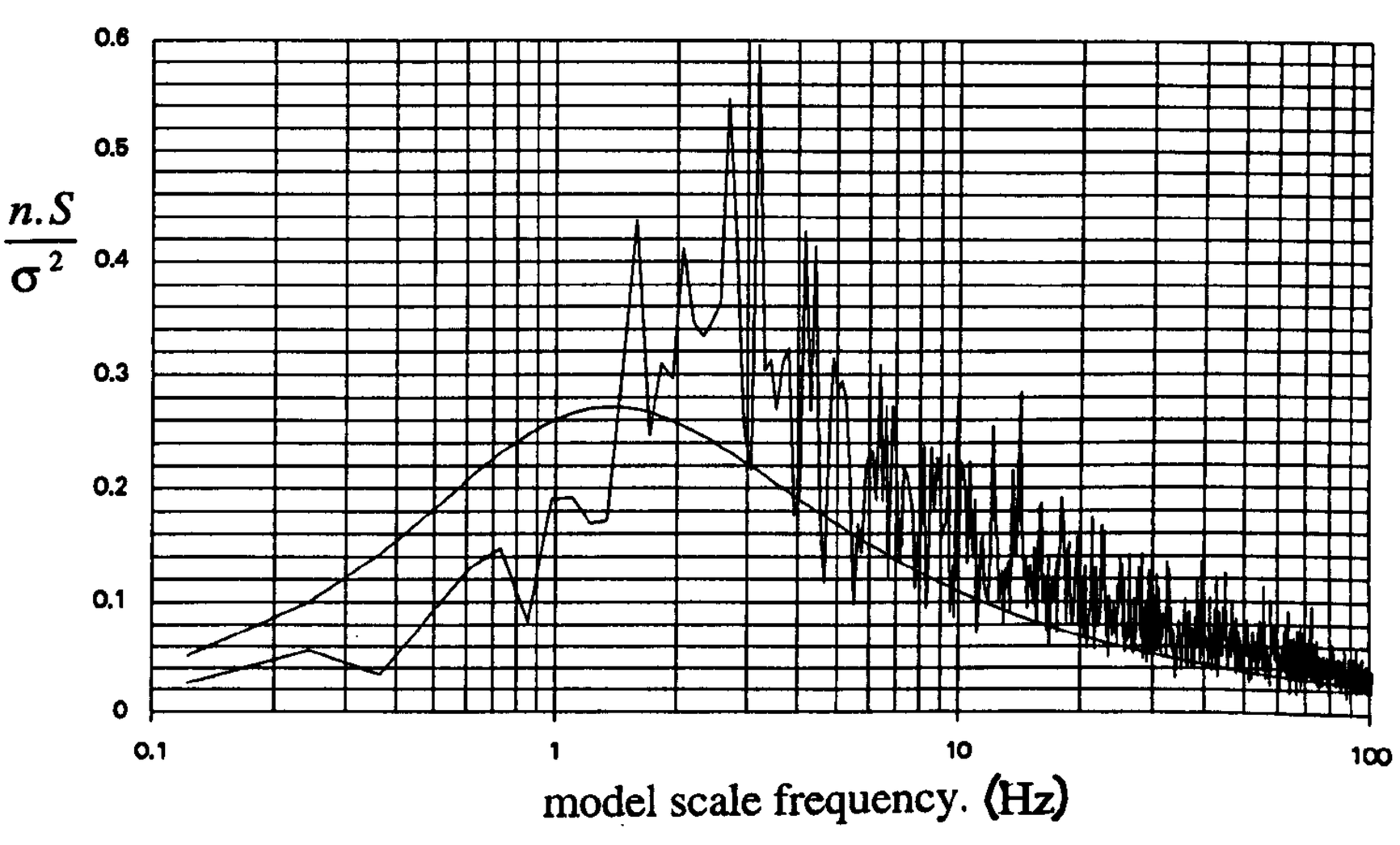

Fig 6.19b Streamwise wind velocity spectrum compared with the target von Karman spectrum (smooth line) for a $\bar{u}$(3m) = 8.5 m/s (full scale equivalent height) at the end of the moving model test position. Anemometer height 30mm equivalent to 1.5m fullscale.

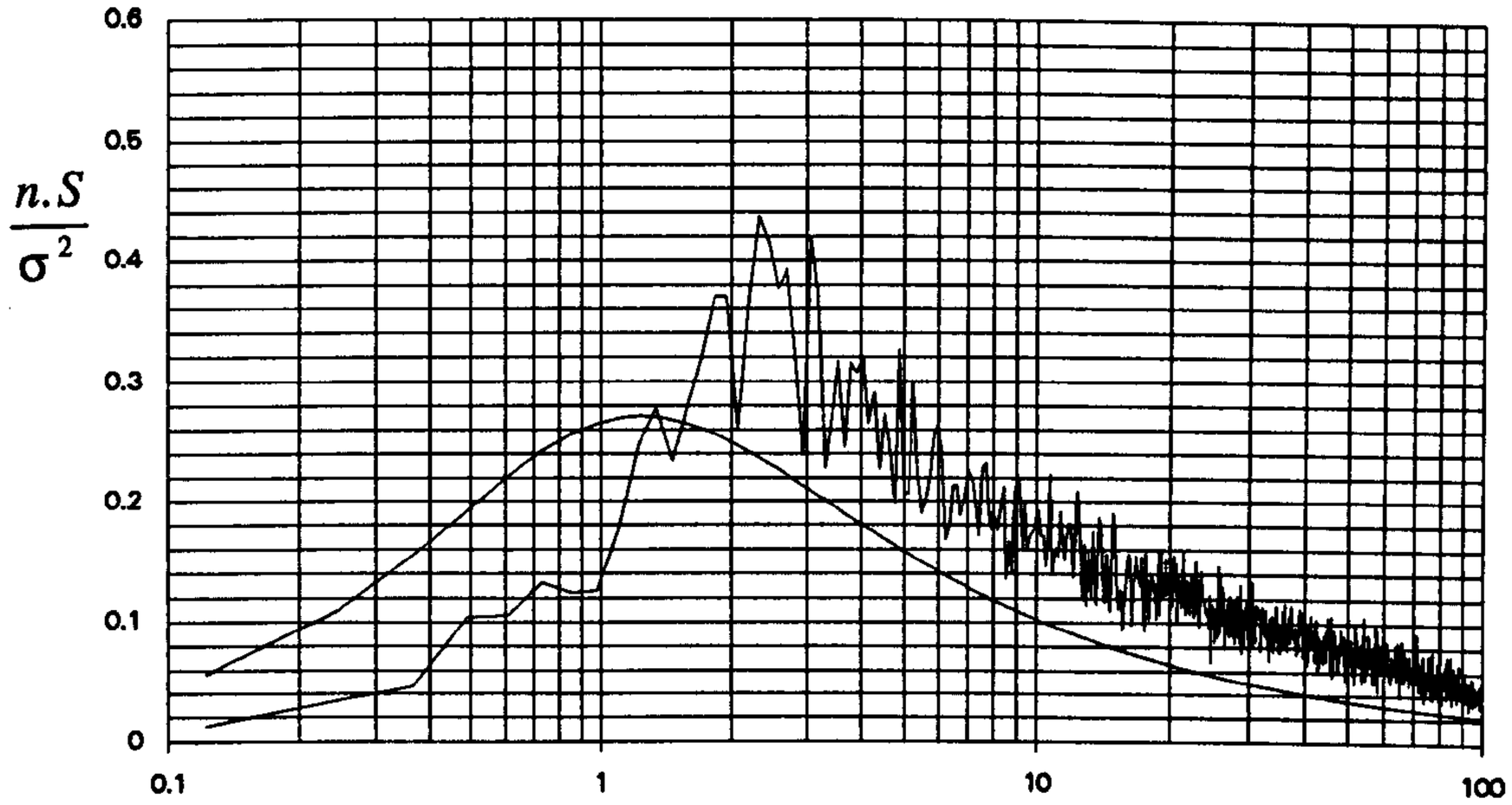

Figure 6.20 Average streamwise wind velocity spectrum from 5 spanwise positions along the moving model test position.
Measurement height 60mm equivalent to 3m full scale.
$\bar{u}$(3m) = 8.5 m/s (full scale equivalent).

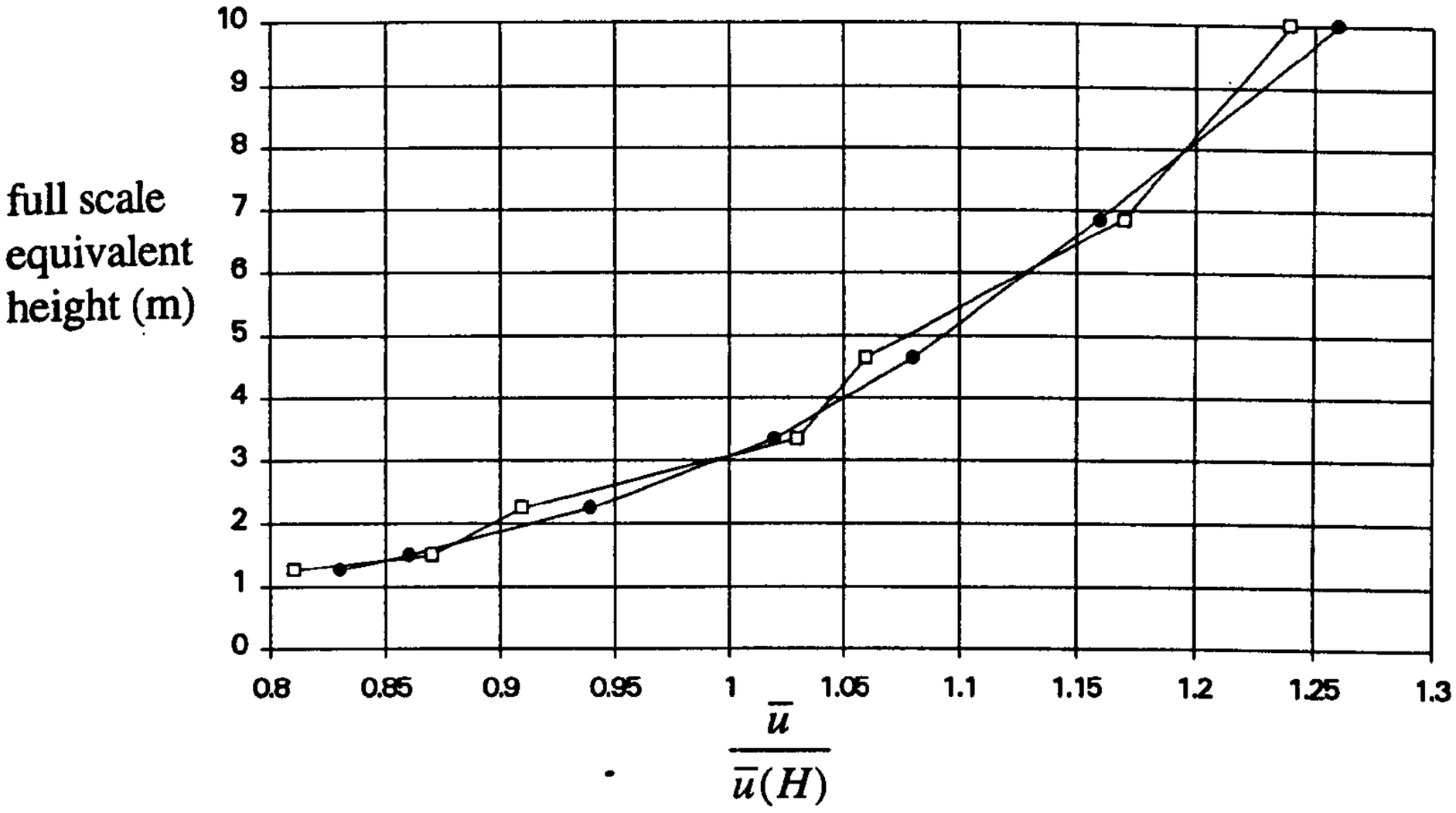

Figure 6.21 Vertical streamwise mean wind velocity profile compared with the target value at the static model test position.

- • target (fullscale $z_0 = 0.03$m)
- □ measured values, $\overline{u}$ = 8.5 m/s.

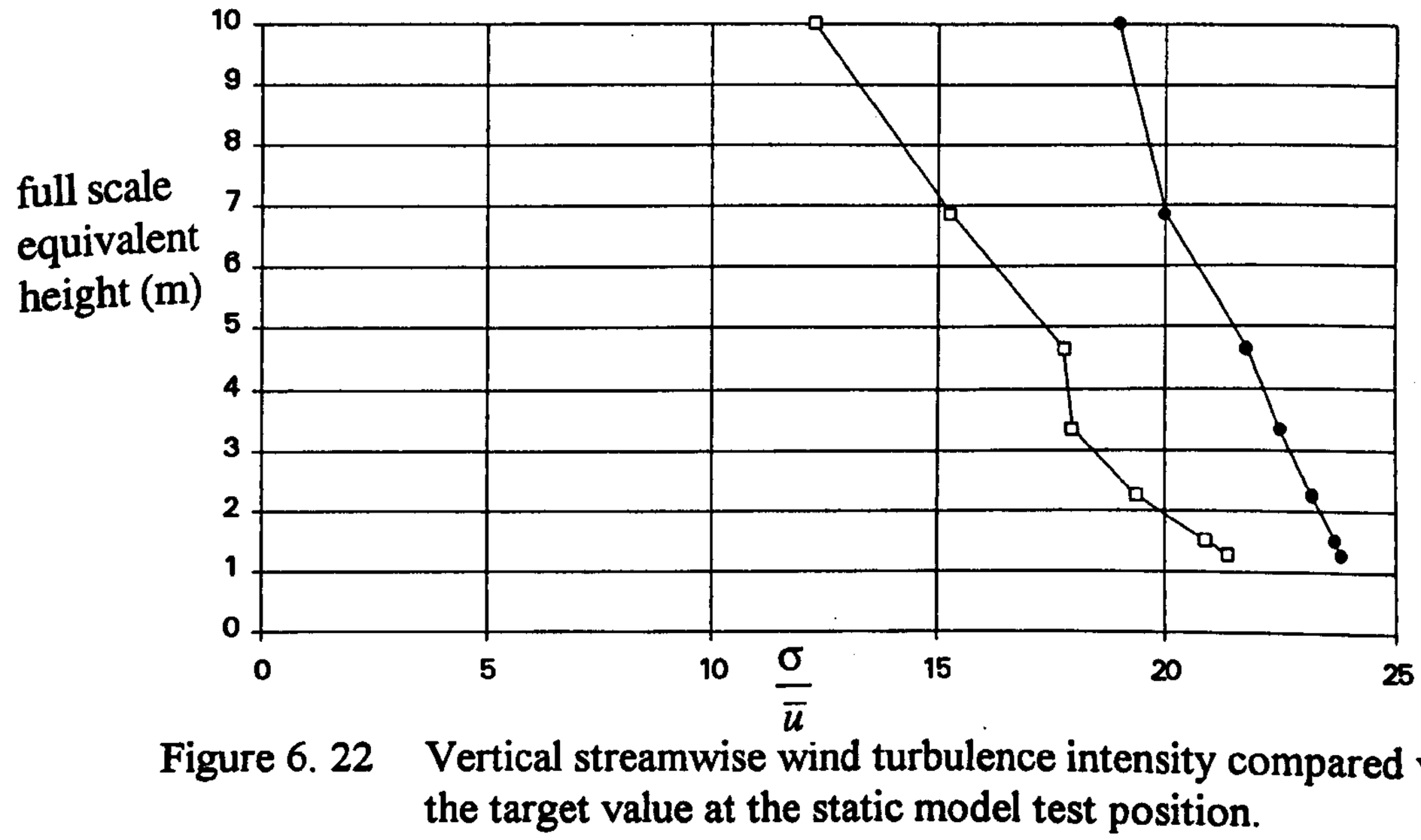

Figure 6. 22 Vertical streamwise wind turbulence intensity compared with the target value at the static model test position.

- • target (fullscale $z_0 = 0.03$m)
- □ measured values, $\overline{u}$ = 8.5 m/s.

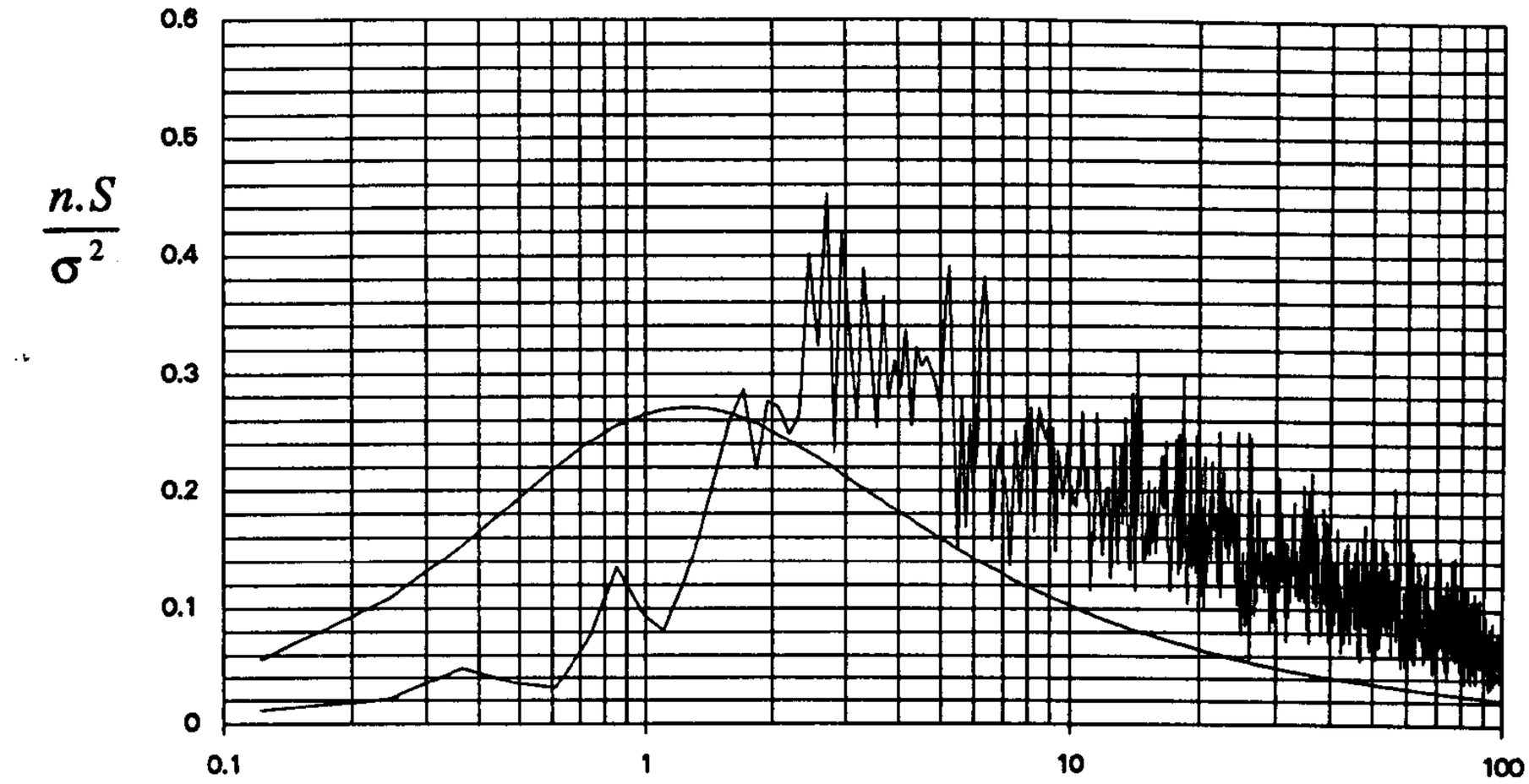

Figure 6.23 Streamwise wind velocity spectrum compared with the target von Karman spectrum (smooth line) for a $\overline{u}$ (3m) = 8.5 m/s (full scale equivalent height) at the static moving model test position. Measurement height 60mm equivalent to 3m.

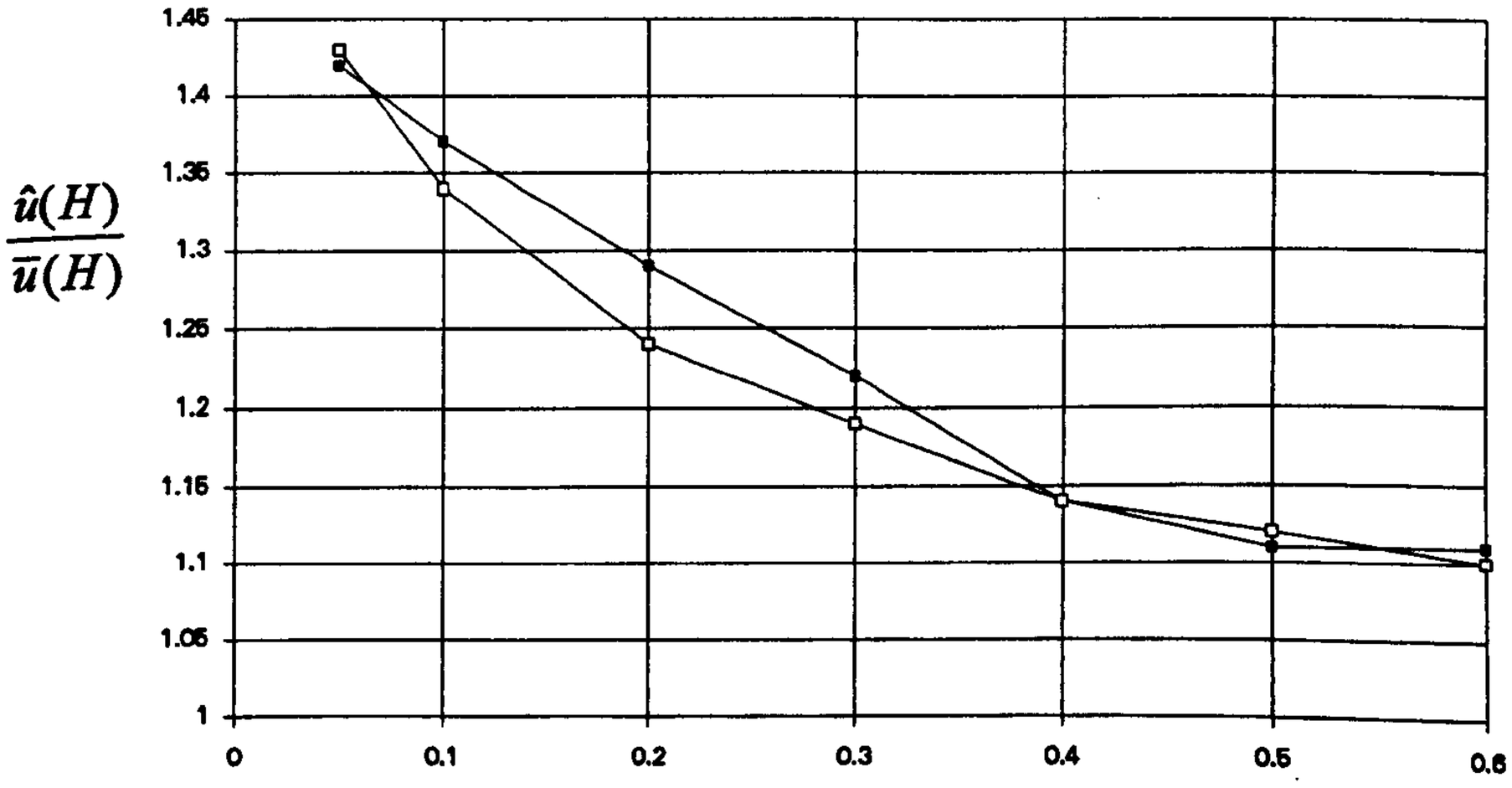

Figure 6.24 Calculated extreme wind velocity values as a function of model time period, taken to be equal to the 3s full scale value at the reference height.

- ■ static model test position.
- □ moving model, centre of test position.

7. The Static Tests.

Static tests were conducted with the 1/50th scale lorry and four configurations, see section 7.3, of the 1/45th railway container vehicles. These tests were undertaken during October and November 1990.

The live model was situated in the centre of the turntable as shown in figure 7.1. All the models were mounted so that the wheels of the vehicle were 1mm above the ground surface. The reference wind speed was measured at an equivalent full scale height of 3m above the ground; i.e. 60mm for the 1/50th scale lorry tests and 66mm for the 1/45th scale railway container vehicles. All tests were conducted at maximum wind tunnel velocity giving a reference wind velocity of 8.5m/s for the lorry tests and 8.7m/s for the container vehicles.

The yaw angle range tested was from 0 to 90 degrees, the turntable positioned at 15 degree intervals. These were chosen as they were close to the intended yaw angles for the moving model tests, which needed to be limited in number due to the large number of runs required to acquire a representative data sample for each yaw angle.

7.1 Reynolds number tests.

These were conducted by measurement and analysis of mean side and lift forces from tests of the lorry at a range of wind tunnel speeds at yaw angles of 60 and 90 degrees. The results, in terms of force coefficients, are shown in figures 7.2 a and b.

It is seen that, in general, both the side and lift force coefficients remain reasonably constant above Reynolds number of 3.0×10^4, based on the lorry's height. However the side and lift coefficient values at 3.7×10^4 show a marked deviation, which is difficult to explain. Suffice to say that this reading was taken in the middle of the test series so ruling out a possible calibration drift. Further, the side force coefficient at this Reynolds number has decreased whilst the lift force coefficient has increased therefore indicating that it may be a real effect. For example it could not be due to an error in the measurement or analysis of the corresponding normalising wind velocity as this would have affected both the side and lift results in the same manner.

7.2 The lorry results.

The Reynolds number of these tests, based on the lorry's height and the reference wind speed (at equivalent full scale height of 3m), was 4.3×10^4.

7.2.1 Mean forces and moments.

Figures 7.3 to 7.7 show the analysed mean force and moment coefficients, the latter translated to the vehicles centre of mass compared with previous tests (Coleman (1990)) of the same model. In Coleman (1990) the model was mounted on a bridge deck in uniform flow with two turbulence simulations tested; low turbulence and grid turbulence of streamwise length scale, ${}^{x}L_u = 0.15$m and turbulence intensity of 10%. Comparison of the non dimensional force and moment coefficients between Coleman's experiments and these present tests was not straight forward due to the latter tests being conducted using an ABL. The magnitude of the calculated force coefficients from tests with an ABL present depends upon the reference height chosen for the wind velocity measurement.

It is seen that the side force coefficient is not very sensitive to the turbulence simulation providing a suitable reference height is taken for the sheared ABL simulation. The plot of the lift force coefficient demonstrates the sensitivity of this parameter to the turbulence simulation, although the recent results compare favourably with the shorter turbulence length scale results of Coleman (1990).

Before considering the mean moment coefficients alone it is instructive to consider also the non dimensional points of actions. Figures 7.8 to 7.10 show the non dimensional point of actions for the side and lift forces again compared with the results of Coleman (1990). Firstly it is seen that the point of action of both the side and lift forces are greatly affected by the turbulence simulation. Considering the yawing moment coefficient shown in figure 7.6 and the horizontal point of action of figure 7.8, it is seen that the yawing moment coefficient is greater for the recent tests compared to Coleman (1990), that is the centre of pressure moves further away from the vehicle's centre of mass towards the rear of the vehicle. This may not be surprising as in the most recent tests, with the simulated ABL, the rear part of the lorry, being higher, is exposed to a higher velocity flow than the front compared to the uniform flow tests of Coleman (1990). However the rolling moment coefficient of figure 7.7, for the recent tests is considerably less than that for the uniform flow tests, which is only in part due to the decrease in side force coefficient. The pitching moment coefficient of figure 7.5, shows

a similar character to the shorter turbulence lengthscale results of Coleman (1990) but again show a translation of the point of action towards the rear of the vehicle.

7.2.2 Extreme force values.

Tables 7.1a to c show the calculated normalised extreme force parameters and the unsteady parameters for a number of reasonable model time periods taken to be equal to the full scale 3 second gust period for yaw angles of 15, 60 and 90 degrees. These were calculated using the Lieblein's extreme value analysis method described in section 5.1.5. A worked example is given in 5.2.2.2.2

It is seen that the normalised force coefficients were reasonably independent of the model time scale chosen to represent the 3s gust, for the model gust values chosen. This demonstrates the correlation between the extreme force and the extreme streamwise wind velocity for the gust times relevant to the overturning of large ground vehicles.

Due to the invariance of the normalised extreme force parameters with model gust time scale, and the length of time needed to undertake the analysis of each case, the analysis of the remaining yaw angle tests were undertaken for one model time scale. Table 7.2 shows the normalised extreme force values and the unsteady parameters for the side and lift cases from analysis using a model, as measured, gust time of 0.2 seconds, this being taken to be equivalent to a full scale 3 second gust. It is seen that the quasi steady state (coefficients around unity) exists for most of the yaw angle range, that is both the side and lift normalised extreme force parameters taking the value of unity. Only at low yaw angles, demonstrated by the normalised extreme force parameters taking larger values than unity for 15 and 30 degrees, was there evidence of body induced unsteadiness of the side and lift forces.

Figures 7.11 to 7.14 compare these results with those using uniform flow and grid turbulence as described in section 2.2.1.1. (Coleman 1990). It should be noticed that the time scaling used in Coleman (1990) was based upon the ratio of the wind speeds and model scale only neglecting the mismatch in turbulence lengthscale which was considerable for these tests of Coleman (1990). The grid turbulence produced a streamwise lengthscale, ${}^{x}L_{u} = 0.15$m compared with 1m required for the 1/50th scale simulation. This means that the streamwise lengthscale was a factor of 8 too small so that the model gust time period ought to be reduced by this factor. This is noted in Coleman (1990) but was not applied in the analysis of the data. In any case with such a

disparity in lengthscales it is unlikely that the eddy lengthscale correction method would be valid, due to the corresponding magnitude of the modelled lateral semi lengthscales being much smaller than both the vehicle's height and length thus causing a poor correlation of the streamwise gusts across the vehicle for such small time scales. It is interesting therefore that, for this vehicle, the magnitude of the normalised extreme force parameters are similar for the recent tests compared with the grid turbulence of Coleman (1990).

7.3 The DB railway container vehicle results.

These vehicles were tested due to the interest in this project by the German State Railways (DB) and the vulnerability of such vehicles currently in operation. As part of this collaboration DB provided the results of detailed model 1/3rd scale tests of these vehicles undertaken in the DNW wind tunnel, Peters (1989). These tests were undertaken in low turbulence flow without the presence of a vertical wind velocity profile. The results of the tests at Nottingham University are compared initially with Peters (1989) in the following sections as was done at the time of the analysis of the results described in this thesis. Following these, further comparisons are then conducted with the results from the tests of Peters (1992) and Kronke and Sockel (1992), discussed in section 2.2.1.2. These latter tests were done around the same time as the Nottingham University tests but the results only became available after the Nottingham University project had been completed.

For these railway vehicle tests the container, fastened to the tunnel floor via the internal balance mounted in the geometric centre of the container, was not touching the wagon beneath it. The wagon (figure 1.2) is of an open construction such that changes in pressure beneath the wagon will also affect the container to some extent. The container was mounted so that its base was 1mm clear of the top of the wagon.

Various configurations, involving dummy vehicles were tested shown in figure 7.15. and labelled A to D. These configurations were:

Configuration A : Isolated container on flat wagon with wagon side fence. Identical geometry to the container and wagon tested in Peters (1989).

Configuration B : Isolated container on flat wagon with no side fence.

Configuration C : Container on flat wagon with no side fences with containers on wagons in front and behind.

Configuration D : Container on flat wagon with no side fences, with container on wagon in front and empty wagon behind.

Configurations C and D were intended to simulate a live vehicle situated well aft of the front of the train. Whilst only one vehicle aft of the live vehicle is probably adequate for such a simulation the effect of a vehicle travelling in front is more complicated. The sharp edged container in front of the live container would probably provide a large, unrealistic separation of the flow down the sides and over the roof of the live container. On a full scale train, the reduced pressure underneath the train tends to bleed the boundary layer in the gaps between the wagons. This results in wagons rear of the locomotive experiencing a similar flow field. In order to simulate the mid train position, in a simple manner, for configurations C and D, the front corners on the dummy container mounted fore of the live container were rounded with 10mm radii.

In operation on the full scale railway these containers are not fastened to the wagons but are located by vertical pins at the corners. These tests were designed to evaluate the likely overturning risk of these containers from the wagon. Considering the mounting arrangement already discussed, the forces and moments derived from these tests refer to the container only. Further, the rolling moment of the container was redefined to be about the bottom leeward corner of the container. As defined in Chapter 5, this was calculated using both the moments formed from the action of the side and lift forces acting on the centre of the container and the rolling moment measured about the container's centre. The rolling moment calculated about the lee bottom corner of the container were therefore formed from nearly equal contributions of the side and lift forces, (noting that their perpendicular moment arms are very similar) and additionally the rolling moment measured about the balance centre.

Whilst the mean rolling moment about the lee bottom corner of the container can be calculated from the overall mean values of the side and lift forces and rolling moment, more care is needed in the formation of the extreme rolling moment coefficients. The extreme rolling moment was calculated from extreme value analysis of values of the rolling moment, averaged over the gust periods, found from simultaneously measured side and lift force and the rolling moment values.

Section 5.2.2. defines the force and moment coefficients used for these tests. Briefly though, as with Peters (1989), these use the container end area as the reference area and the container width (almost identical to the height) for the reference vehicle height.

As the containers are sharp edged and similar to the 1/50th scale lorry and of a very similar model size it was considered that the Reynolds number tests undertaken for the lorry discussed in section 7.1 were also adequate for these vehicles. The Reynolds' number of these tests, based on the container length, and the wind speed at the reference height (equivalent to 3m full scale) was 1.3×10^5. Note this is similar to the Reynolds number definition used in the other tests of this vehicle described in section 2.2.1.2. Whilst there is no difference between the definitions used for the Nottingham University ABL tests and for the steady flow tests of Peters (1989) and Peters (1992), a slight discrepancy is present for the ABL tests of Kronke and Sockle (1992). In these tests the wind speed height used was that of the roof of the container, equivalent to 3.9m full scale, a little higher than used for the Nottingham University tests. Referring to the wind velocity profiles shown in Chapter 6 this discrepancy is reasonably small in this context, around 5%.

Pitching and yawing moments as well as the non dimensional points of action were not analysed for these tests due to time considerations.

7.3.1 Mean forces and moments.

Figures 7.16 and 7.17 compare the mean side and lift force results of the configuration A tests with the results of 1/3rd scale DNW low turbulence tests of the same configuration from Peters (1989). It can be seen that the results for the side force coefficient are in good agreement whilst the lift force coefficient for the smaller scale tests lie below the 1/3rd scale DNW tests. The agreement in the side force results should be viewed as being coincidental due to the large difference in the test conditions particularly that of the vertical wind profile present in these Nottingham University tests. The absolute magnitude of these coefficients therefore depend on the height chosen for the reference wind velocity used in the formation of these coefficients. The other important difference between the tests is the turbulence simulation. Coleman (1990) has already shown the large and complicated effect that the turbulence simulation has on the lift force of the, similar in geometry, lorry (figure 7.4.). However undertaking side force measurements of vehicles using this ABL simulation, using a 3m equivalent reference height for the wind measurements, produces side force coefficients that are equivalent to those from tests in a uniform wind velocity. Further it could

therefore be argued that wind measurements with this ABL simulation at an equivalent 3m height produces values equivalent to the value of a uniform wind velocity used in a low turbulence test.

Figures 7.18 to 7.20 compare the mean side and lift force coefficients of all the four configurations tested. It is seen, from an initial comparison, that the form of all the results are similar.

Comparing first the results from comparisons of the isolated container with the wagon with side fences configuration A, and without side fences configuration B it is seen that the side force coefficient, for those with the side fence on the wagon, are lower than those without the side fence. This is as expected as the area of the container exposed to the oncoming wind is reduced by the side fences for configuration A. Comparison of the lift forces between these two vehicles shows that the lift force is also reduced for configuration A. Speculatively this may be due to the effect of the fence, blocking the flow between the wagon and the underneath of the container. This flow when present, for configuration B, perhaps increases the pressure on the underside of the container and therefore a higher net increase in lift force, compared to configuration A. The flow over the roof of the container would be expected to be unaltered by these minor changes in the flow. Overall this results in the lee bottom corner rolling moment for the container on the wagon with side fences to be up to be 60% to 75%, depending on yaw angle, of the value when loaded on a wagon without the fences.

Comparisons of the side and lift forces for various configurations of containers and wagons without wind fences, configurations B, C and D are more complicated. It is seen that the largest values of the side force coefficient occur at all yaw angles for the isolated container, configuration B. However at the larger yaw angles this difference is less and the side force coefficient is very similar for all the container configurations B, C and D. Comparisons of the lift force coefficients show that the configurations with the dummy container and wagon leading the live container C and D, have values that are similar and some 20% to 30% larger than the isolated container configuration B. Comparing the rolling moment coefficients it is seen that these resultant values for configurations B, C and D are similar with the largest value, at each yaw angle, occurring for configuration C, with the dummy containers loaded on wagons both in front and behind.

Next to be described are the comparison of the results of these tests with those of Peters (1992) and Kronke and Sockle (1992), described in detail in section 2.2.1.2. In

these papers results are given of mean side and lift force coefficients from various tests of the isolated container and wagon fitted with side fences for a range of model scales and Reynolds numbers. In Peters (1992) these are from steady flow tests and the Reynolds number ranges from 1.7×10^5 to 1.0×10^6. From Kronke and Sockle (1992) in various turbulence flow simulations the Reynolds number was 2.5×10^4. Referring to figures 2.10 and 7.16 is seen that the side force coefficients all agree with each other as well as with the results from the Nottingham University tests, even though the container tested in Kronke and Sockle (1992) was of only half the full scale equivalent length (20 foot). Remembering that the lift force coefficient for the lorry model was very sensitive to the turbulence simulation, the results from Peters(1992) and Kronke and Sockel (1992) showed that the lift force coefficient was very similar between the turbulence simulations and the steady flow tests at a similar Reynolds number even though the container of the latter tests was only half the full scale equivalent length. Further these tests demonstrated, figure 2.11, a clear Reynolds number dependency with the lift force coefficient increasing with Reynolds number, independent of the turbulence simulation. Speculatively this may be a Reynolds number effect due to varying underbody flow conditions for which the local Reynolds number is sub critical. Comparing figure 7.17 with figure 2.11 it is seen that the Nottingham University tests of this same vehicle, configuration A, agree with the set of lift coefficient data for tests at a similar Reynolds number.

7.3.2 Extreme force values.

These results were analysed in the same manner as the static lorry tests discussed in 7.2.2. but for only one model time period of 0.02s taken to be equivalent to the equivalent full scale 3s gust. Similarly these calculations used a full scale extreme hourly mean value of 30m/s at the reference height, equivalent to 3m full scale.

As extreme force values were not available for the 1/3rd scale DNW tests (Peters(1989)) due to these tests being undertaken in low turbulence, extreme value analysis was not conducted for this configuration, with side fences fitted to the wagon (configuration A) of the Nottingham University tests. This configuration was indicated by DB to be not of primary interest but useful only for mean value comparisons with the larger scale DNW tests. Due to the large time needed to perform extreme value analysis this was only conducted at all the yaw angles tested for configuration B, the isolated container without side fences fitted to the wagon. For configurations C and D extreme value analysis was conducted for the yaw angles of 15, 60 and 90 degrees only.

Figures 7.21 and 7.22 shows the normalised extreme side and lift force parameters for configurations B, C and D. Firstly it is seen that the results are similar for both the side and lift forces and also for all the configurations with configuration C having normalised extreme force parameters slightly higher than the other configurations. Therefore configuration C with the dummy containers for and aft is the most likely to cause a container to roll, slip or lift from its wagon. Generally, for all configurations, comparing the values of the normalised extreme force coefficients with unity, the value which signifies a quasi steady force on the container, it is seen that some evidence of unsteadiness is present at the lowest yaw angles. This is particularly in evidence for the isolated container wagon at 15 degrees, the only configuration for which these values were calculated. However configuration C also shows evidence of unsteadiness at the yaw angle of 30 degrees in the side and lift forces. The general conclusions are very similar to those of the lorry tests described in section 7.2.2.

From Kronke and Sockle (1992), for the 20 foot long equivalent full scale isolated container, the only extreme values published were the extreme rolling moment coefficients calculated about the lee bottom corner of the container. Figure 2.13 shows these results, for a range of ABL simulations, normalised by the mean rolling moment coefficients also published. Note that the ABL simulation of Kronke and Sockle (1992) that most closely matches that ABL simulated at Nottingham University is that characterised by a turbulence intensity of 22% and a spectral decay power exponent of 0.23. Figure 7.23 shows the extreme lee bottom corner rolling moments calculated from the Nottingham University measurements, for configurations B, C and D, conducted in an identical manner to those of Kronke and Sockle (1992) and described in section 5.2.2. The first conclusion is that the results are very similar for all the configurations tested and therefore do not follow the results of the mean rolling moment coefficients which showed that configuration C was most at risk. Kronke and Sockle (1992) limit their tests to the isolated container case (although only half the length) based on the fact that this was deemed to be most at risk from the results of steady flow tests of Peters (1992) and Peters (1989). Extreme lee bottom corner rolling moment comparisons of the isolated container test of Nottingham University, configuration B, with the results of Kronke and Sockle (1992), with the similar ABL, show very good agreement. It is seen that the quasi - steady case is seen to exist at most of the higher yaw angles with a departure at the lower yaw angles, particularly below 20 degrees, where body induced unsteadiness is clearly seen.

Table 7.1 Static lorry hourly extreme values for various model time periods taken to be equivalent to a full scale 3s gust.

Full scale extreme hourly mean value = 30m/s (3m).

Mean wind tunnel reference speed = 8.5m/s at 60mm height = 3m full scale height.

No of data points for 10 blocks =45000. Sample frequency = 125Hz.

a) Yaw angle=15 degrees

Model time equivalent to full scale 3s gust (s).	0.05	0.1	0.2	0.4	0.6
Unsteady side force parameter.	4.26	3.92	3.33	5.00	5.07
Normalised extreme side force parameter.	1.38	1.31	1.18	1.31	1.26
Unsteady lift force parameter.	4.20	3.11	3.00	3.34	4.24
Normalised extreme lift force parameter.	1.37	1.15	1.12	1.13	1.19

b) Yaw angle=60 degrees

Model time equivalent to full scale 3s gust (s).	0.05	0.1	0.2	0.4	0.6
Unsteady side force parameter.	1.84	1.84	1.42	1.84	1.82
Normalised extreme side force parameter.	0.88	0.89	0.84	0.97	0.97
Unsteady lift force parameter.	2.94	2.57	2.06	2.66	1.88
Normalised extreme lift force parameter.	1.11	1.04	0.96	1.06	0.97

c) Yaw angle=90 degrees

Model time equivalent to full scale 3s gust (s).	0.05	0.1	0.2	0.4	0.6
Unsteady side force parameter.	2.80	2.80	2.90	3.61	3.35
Normalised extreme side force parameter.	1.08	1.08	1.11	1.16	1.11
Unsteady lift force parameter.	4.81	3.50	2.68	2.87	3.80
Normalised extreme lift force parameter.	1.50	1.22	1.07	1.08	1.15

Table 7.2 Summary of static lorry hourly extreme values for a model time period of 0.2s taken to be equivalent to the full scale 3s gust.

Full scale extreme hourly mean value = 30m/s (3m).

Mean wind tunnel reference speed = 8.5m/s at 60mm height = 3m full scale height.

No of data points for 10 blocks =45000. Sample frequency = 125Hz.

Yaw angle	15	30	45	60	75	90
Unsteady side force parameter.	3.33	2.28	1.85	1.42	1.64	2.90
Normalised extreme side force parameter.	1.18	1.00	0.92	0.84	0.88	1.11
Unsteady lift force parameter.	3.00	2.97	2.48	2.06	2.43	2.68
Normalised extreme lift force parameter.	1.12	1.12	1.03	0.96	1.02	1.07

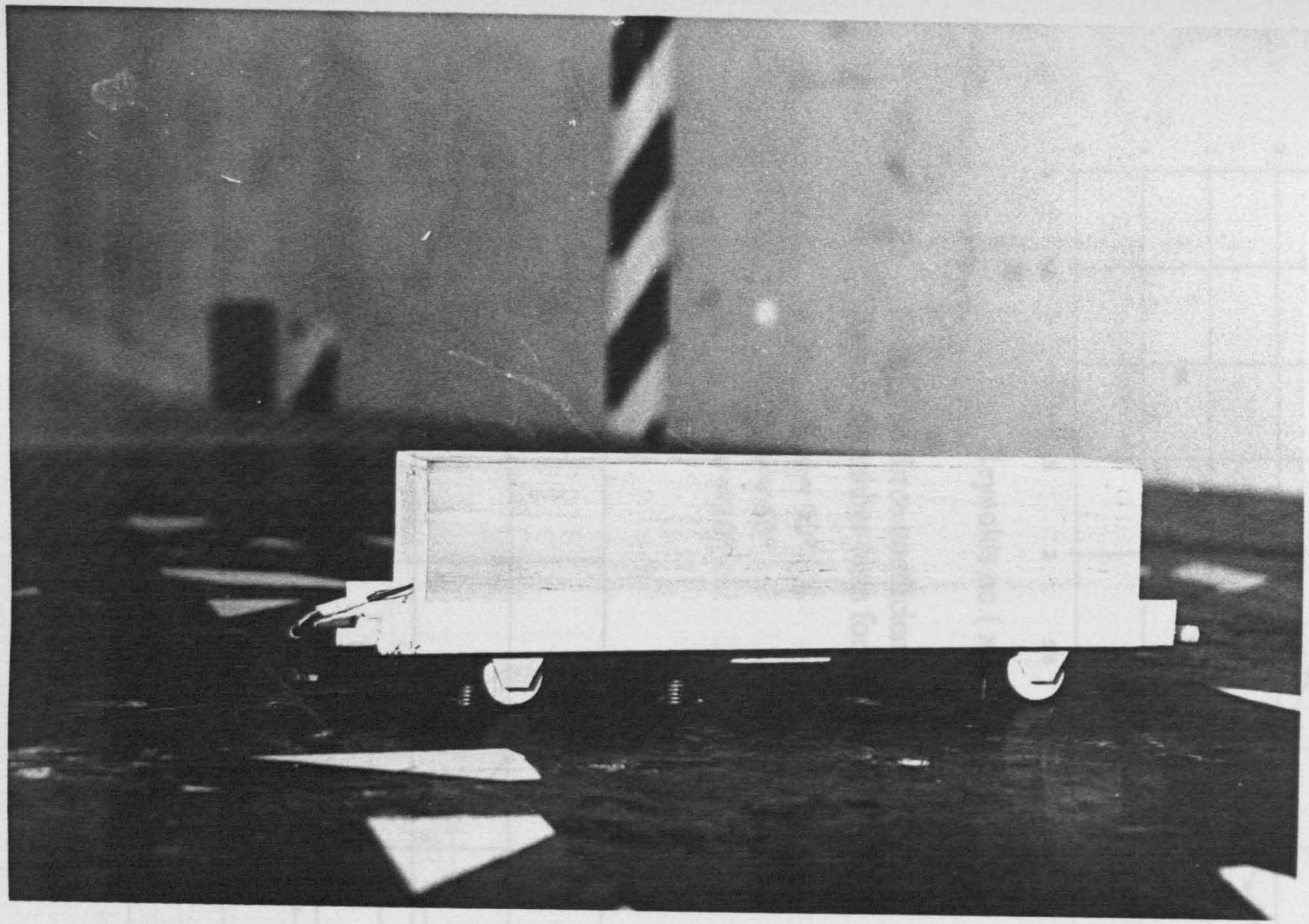

Figure 7.1 DB container and railway wagon with side fences, configuration A, mounted on turntable for static tests. Note small leads exiting from rear of live container for strain gauge excitation and measurement.

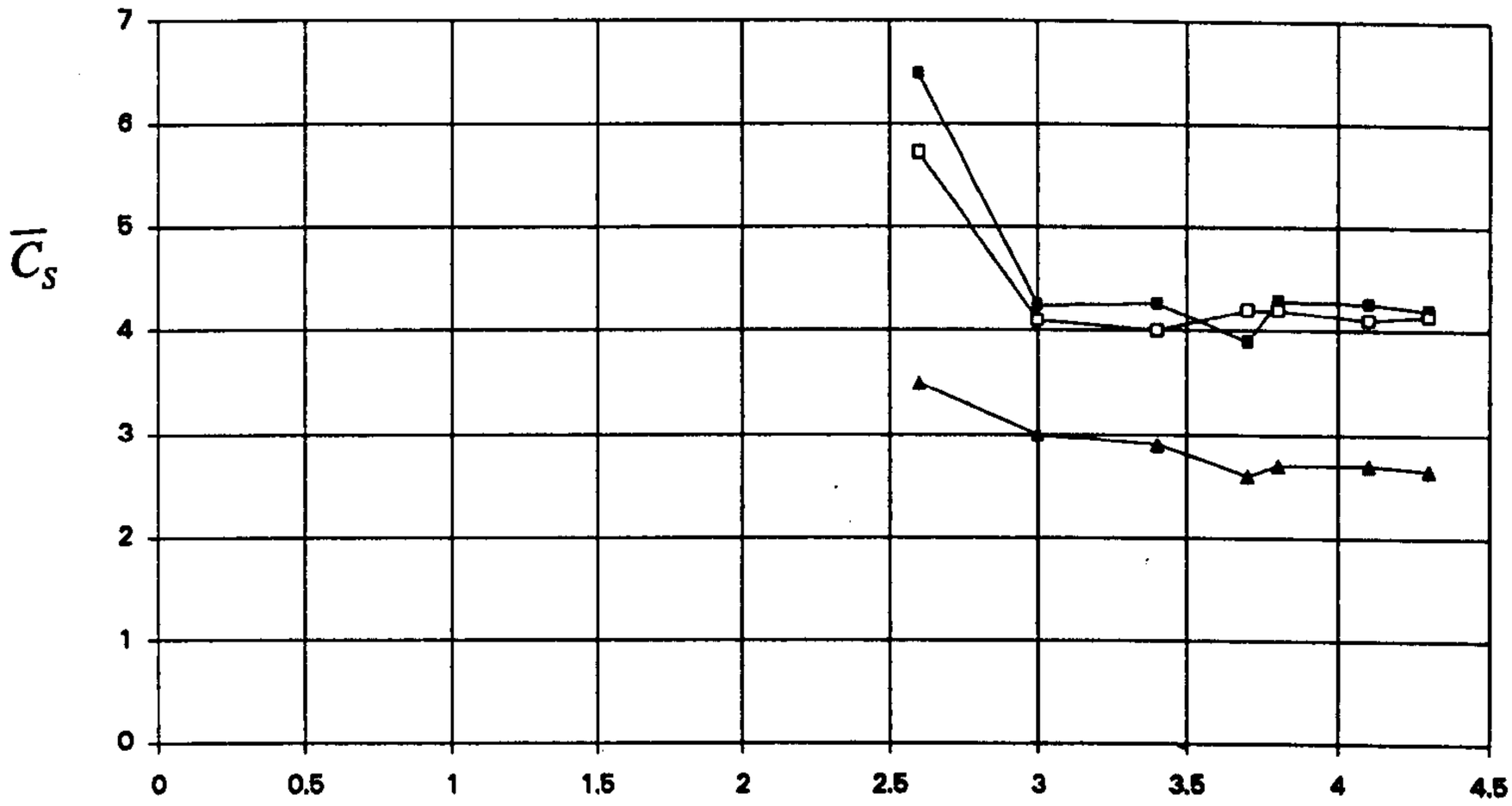

Figure 7.2a Mean side force coefficient.
Reynolds number tests for static lorry.

- ■ Yaw = 90°
- □ Yaw = 60°
- ▲ Yaw = 30°

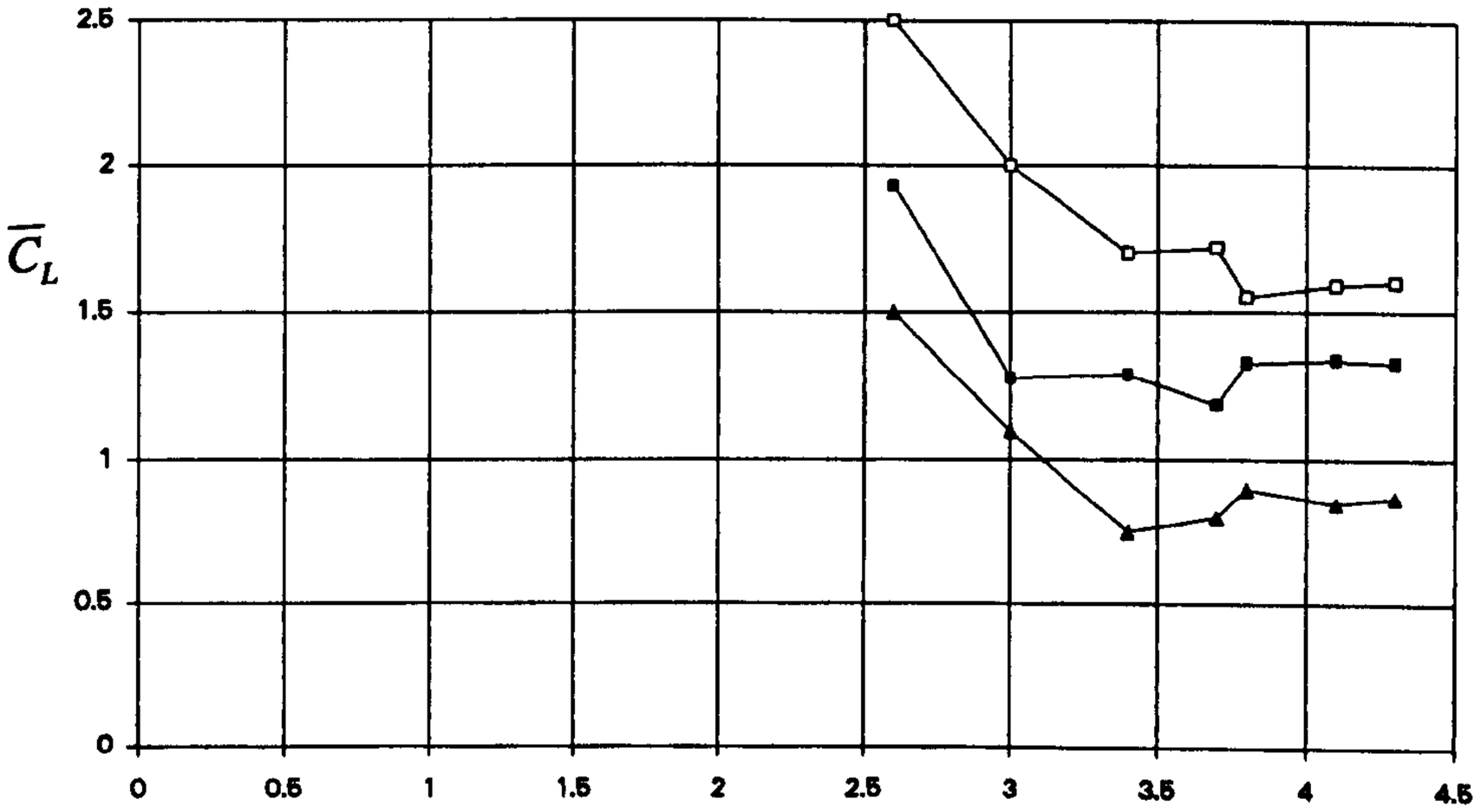

Figure 7.2b Mean lift coefficient.
Reynolds number tests for static lorry.

- ■ Yaw = 90°
- □ Yaw = 60°
- ▲ Yaw = 30°

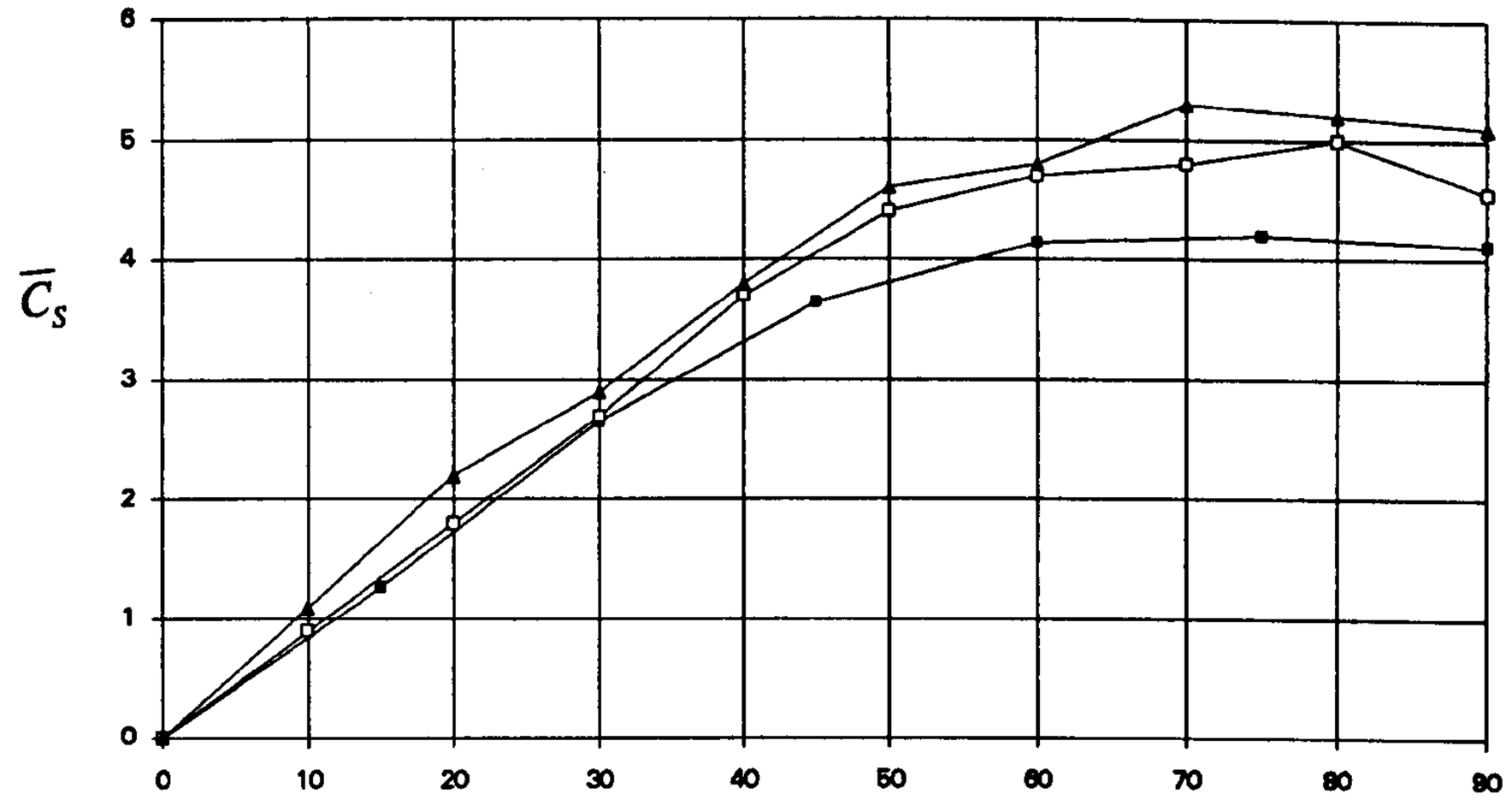

Figure 7.3 Mean side force coefficient.
Static lorry tests.

- ■ Flat ground ABL simulation.
- □ Coleman (1990), low turbulence.
- ▲ Coleman (1990), Turbulence: ${}^{x}L_u = 0.15\text{m}$, $\sigma = 10\,\%$

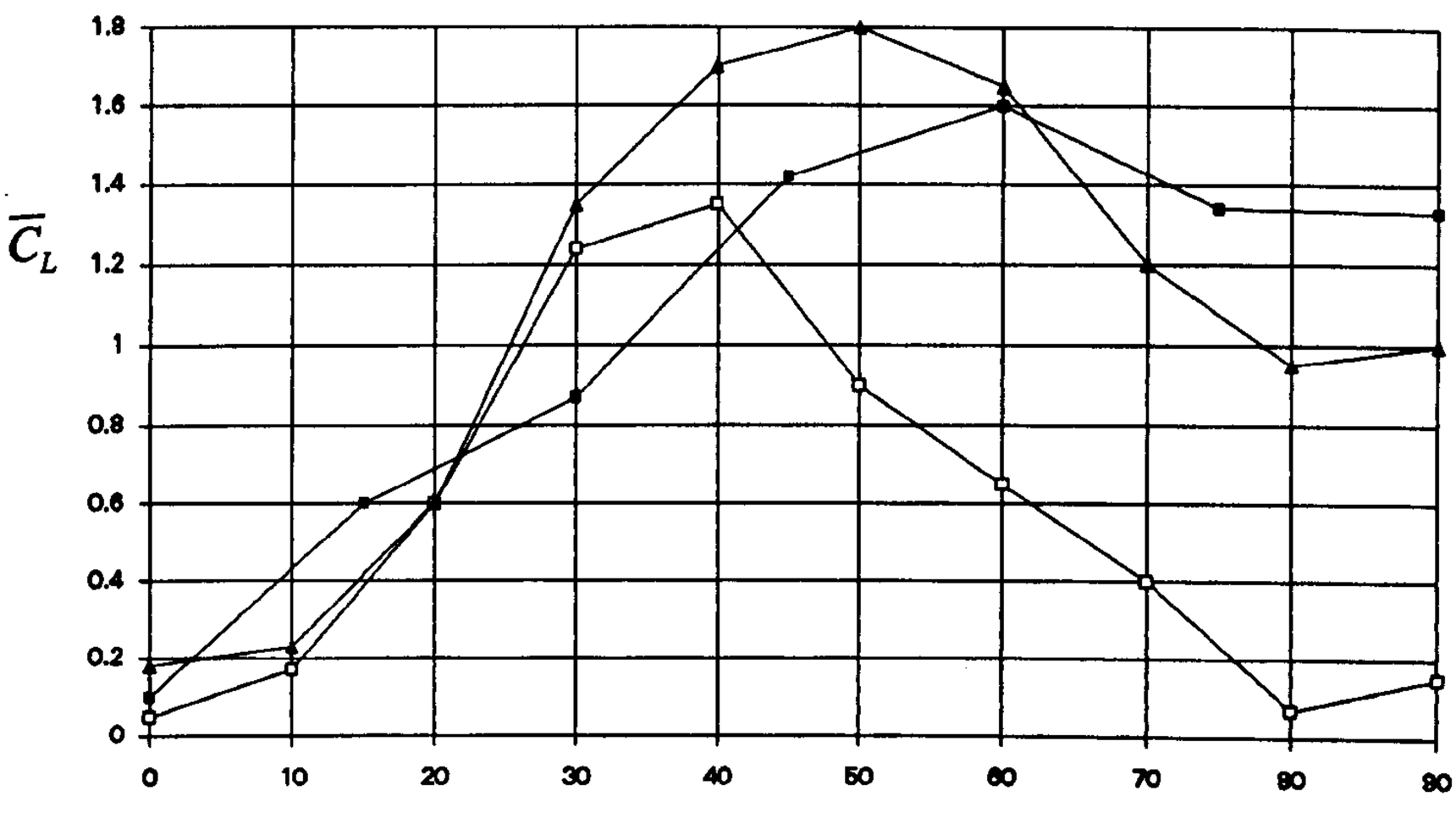

Figure 7.4 Mean lift force coefficient.
Static lorry tests.

- ■ Flat ground ABL simulation.
- □ Coleman (1990), low turbulence.
- ▲ Coleman (1990), Turbulence: ${}^{x}L_u = 0.15\text{m}$, $\sigma = 10\,\%$

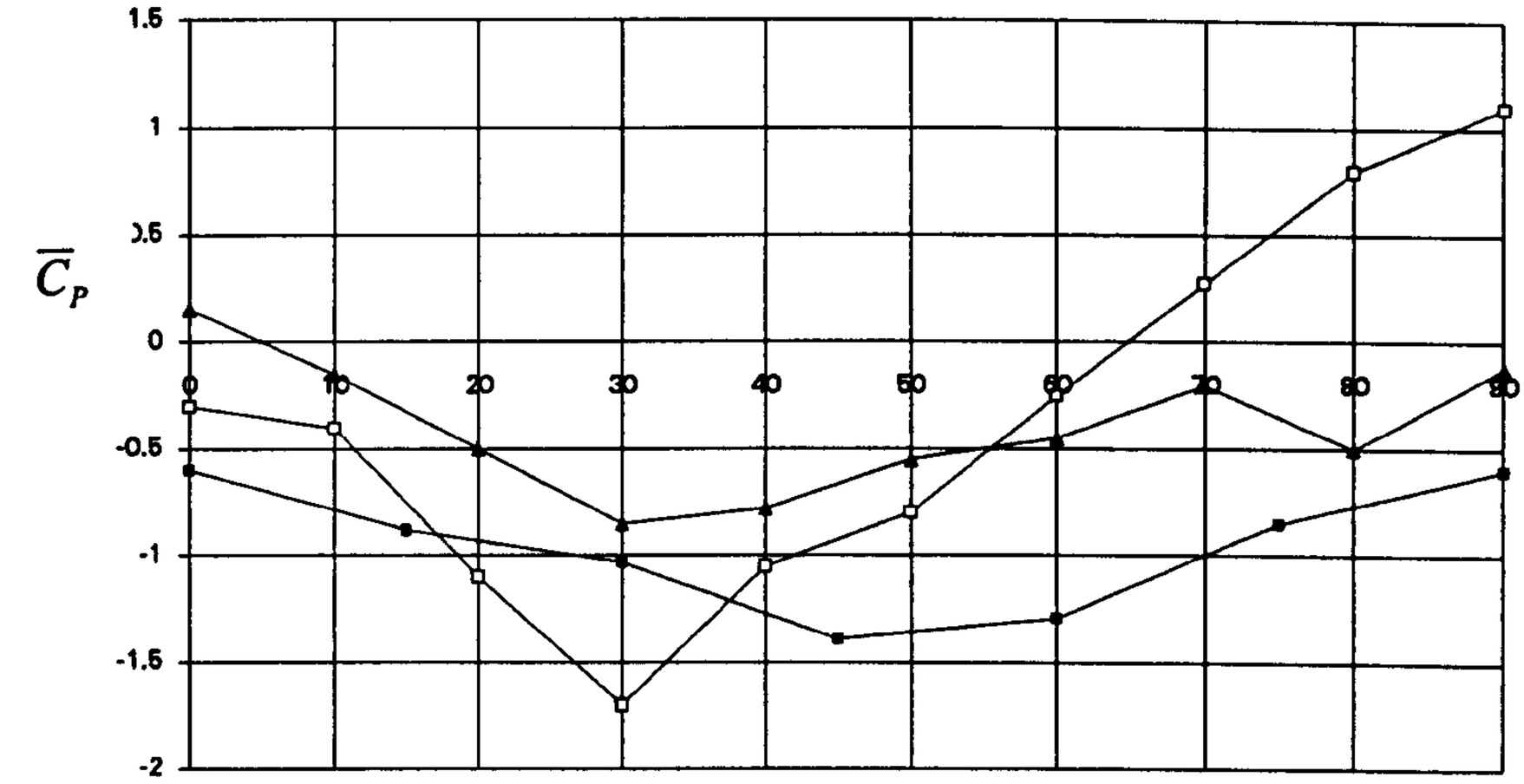

Figure 7.5 Mean Pitching moment coefficient.
Static lorry tests.

- ■ Flat ground ABL simulation.
- □ Coleman (1990), low turbulence.
- ▲ Coleman (1990), Turbulence: ${}^{x}L_u = 0.15\text{m}$, $\sigma = 10\ \%$

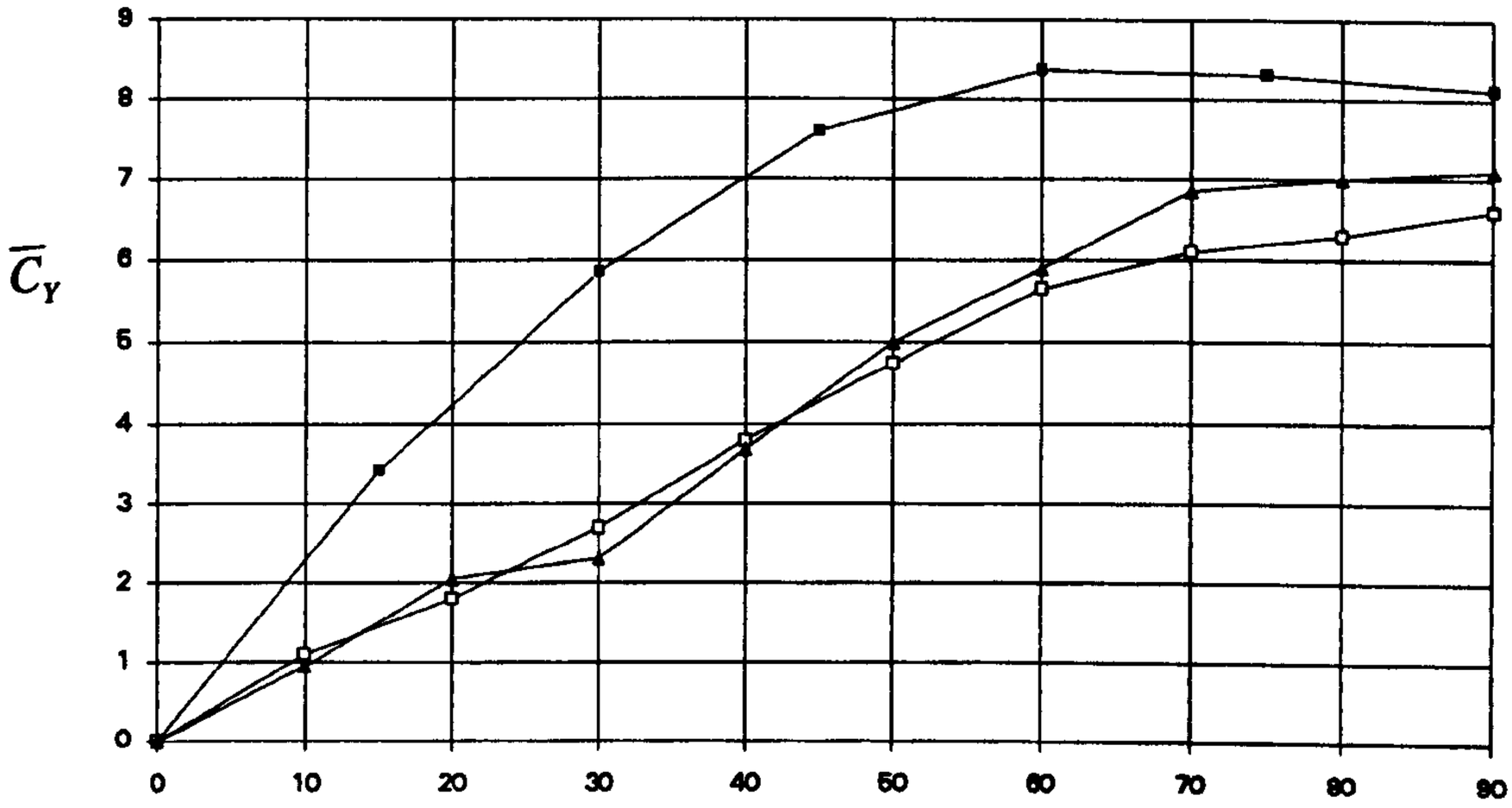

Figure 7.6. Mean yawing moment coefficient.
Static lorry tests.

- ■ Flat ground ABL simulation.
- □ Coleman (1990), low turbulence.
- ▲ Coleman (1990), Turbulence: ${}^{x}L_u = 0.15\text{m}$, $\sigma = 10\ \%$

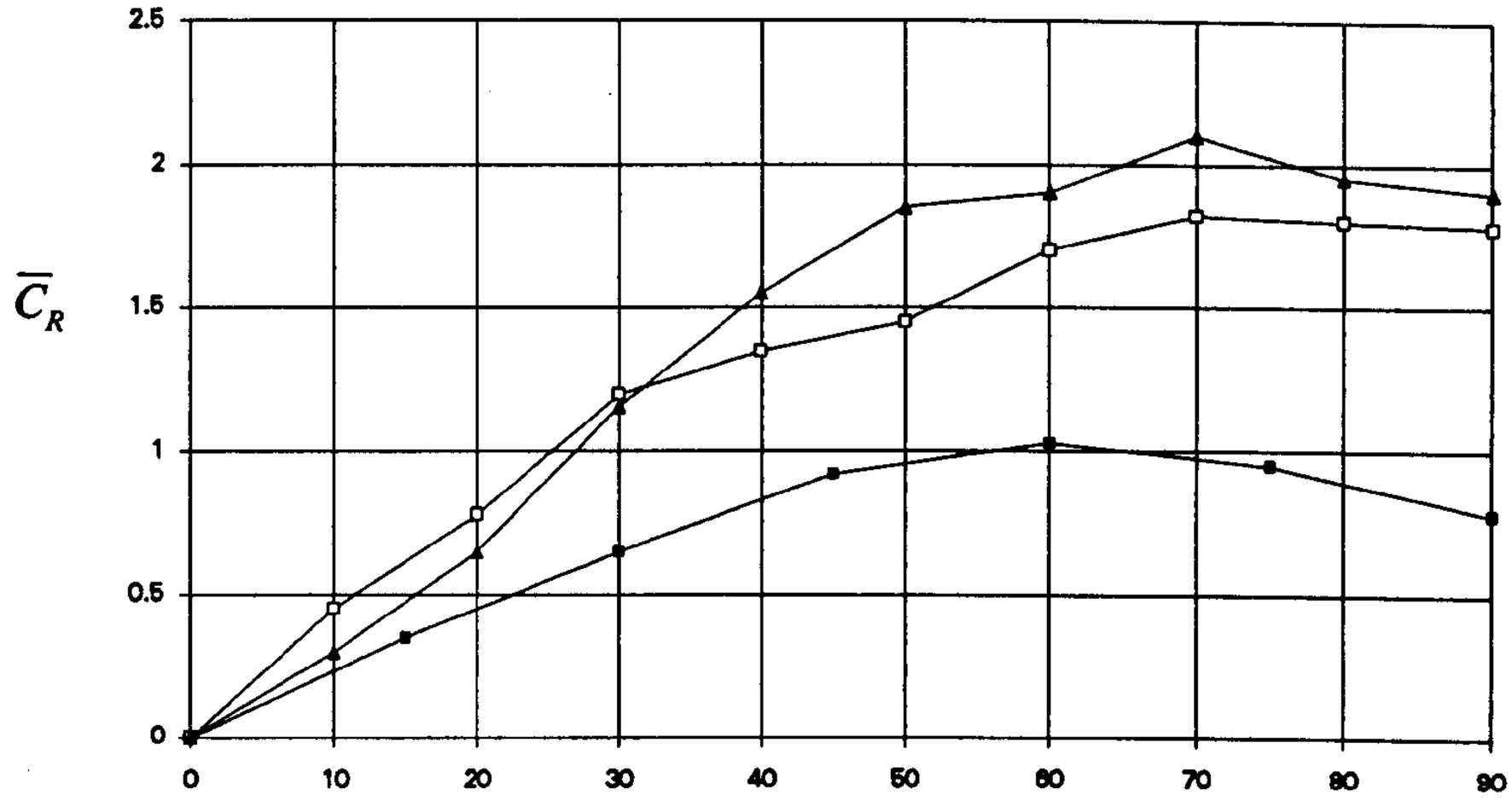

Figure 7.7 Mean rolling moment coefficient.
Static lorry tests.

- ■ Flat ground ABL simulation.
- □ Coleman (1990), low turbulence.
- ▲ Coleman (1990), Turbulence: ${}^{x}L_u = 0.15\text{m}$, $\sigma = 10\ \%$

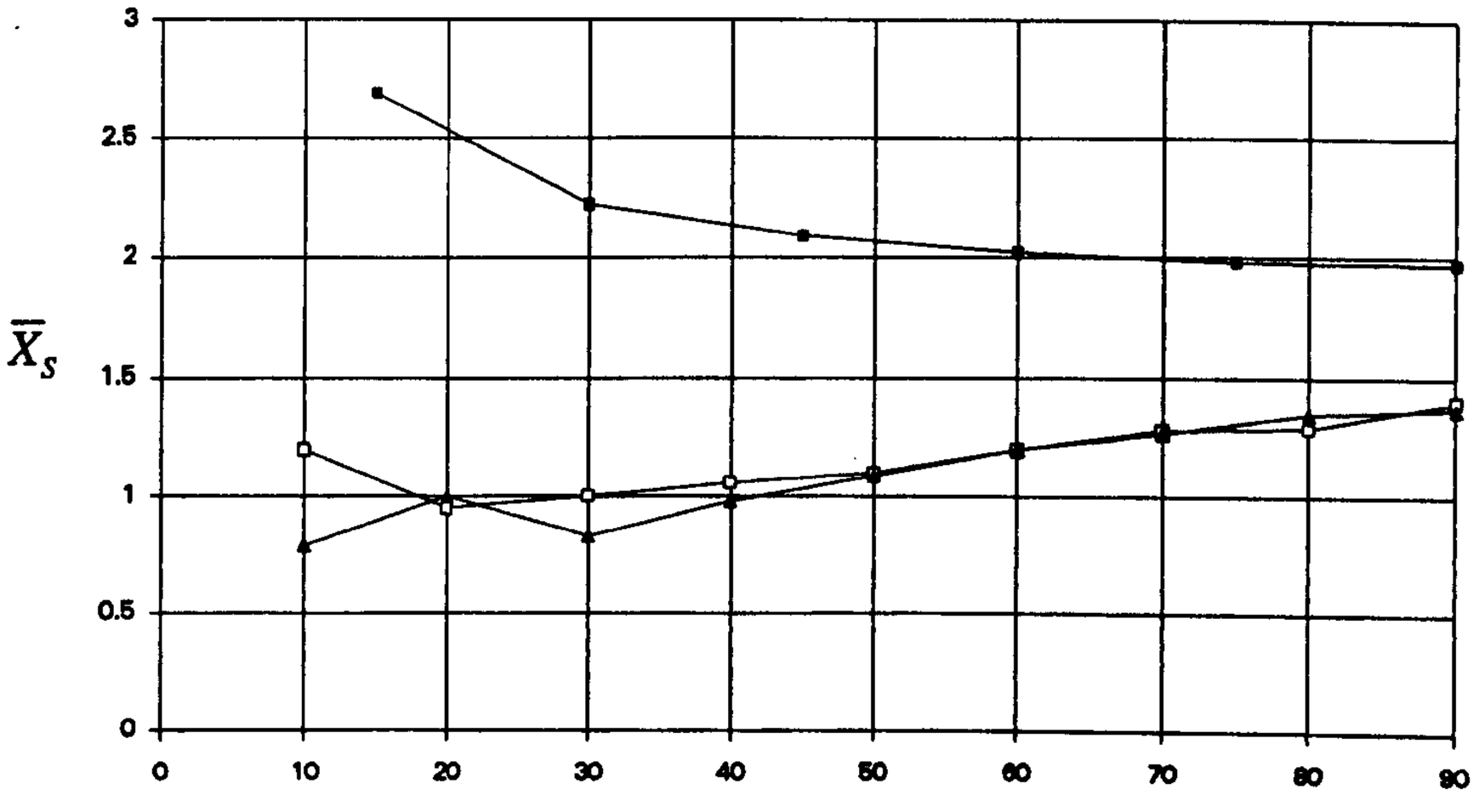

Figure 7.8 Horizontal non-dimensional point of action of side forces.
Static lorry tests.

- ■ Flat ground ABL simulation.
- □ Coleman (1990), low turbulence.
- ▲ Coleman (1990), Turbulence: ${}^{x}L_u = 0.15\text{m}$, $\sigma = 10\ \%$

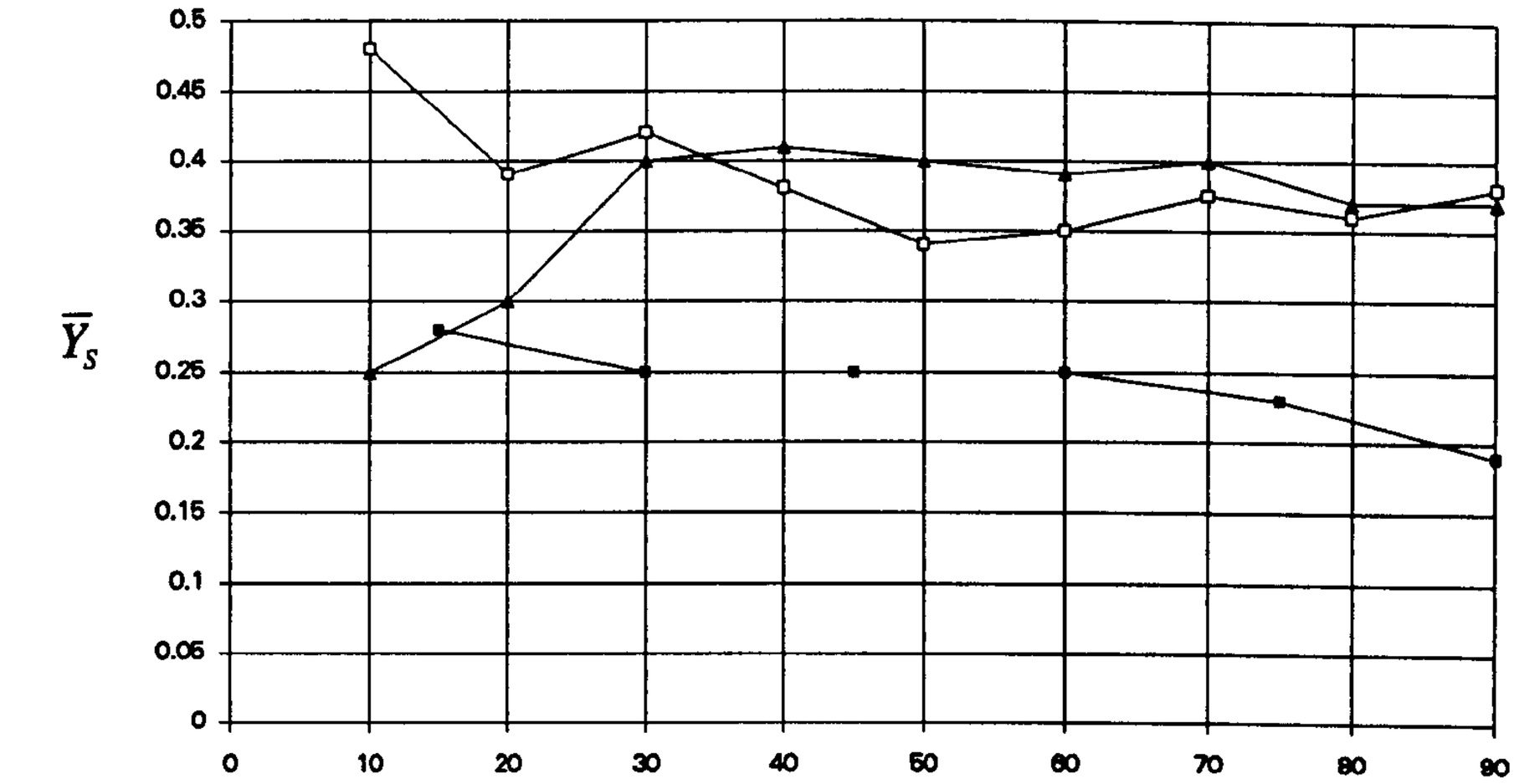

Figure 7.9 Vertical non-dimensional point of action of side force. Static lorry tests.

- ■ Flat ground ABL simulation.
- □ Coleman (1990), low turbulence.
- ▲ Coleman (1990), Turbulence: ${}^{x}L_u = 0.15\text{m}$, $\sigma = 10\ \%$

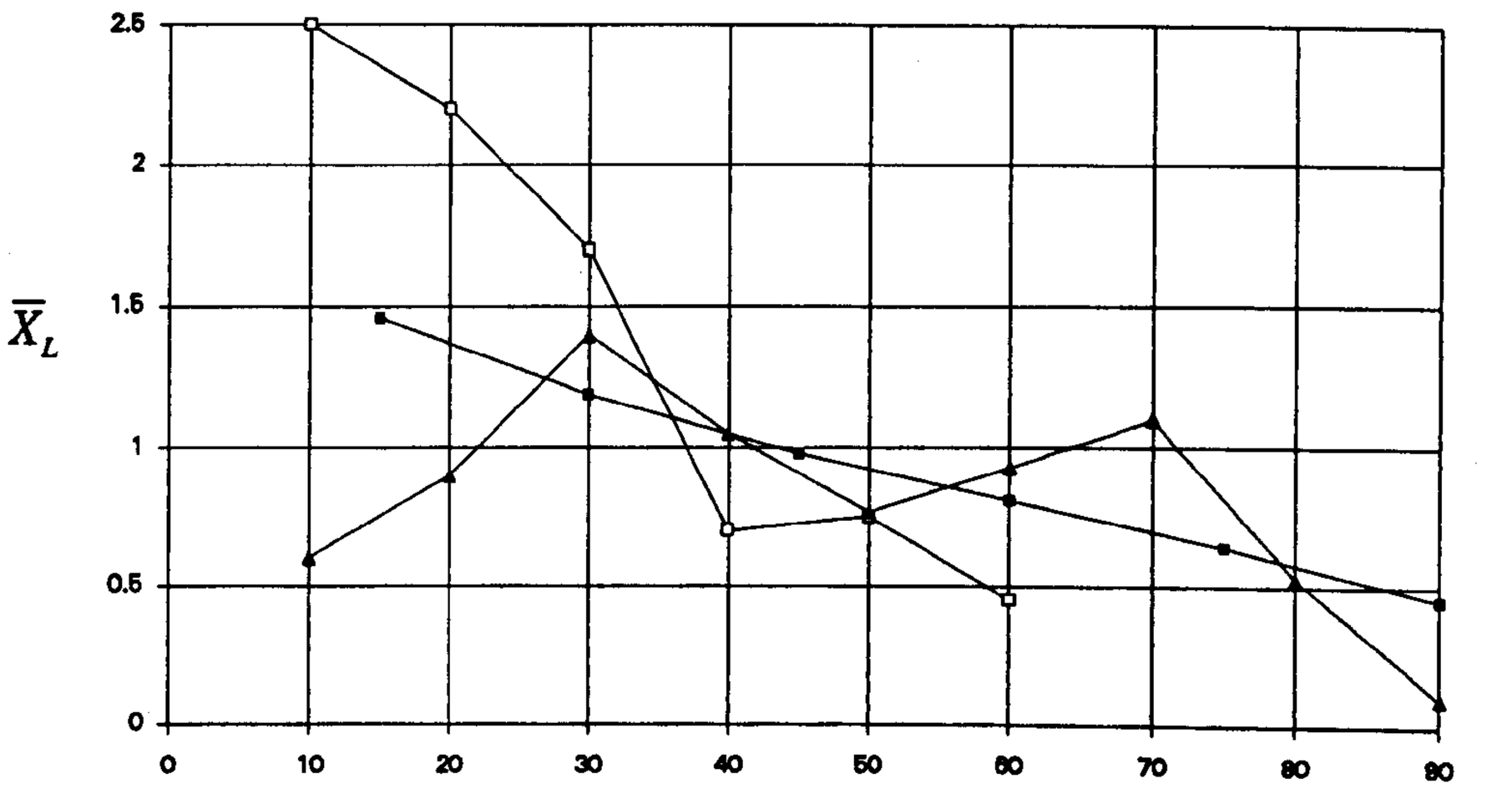

Figure 7.10 Horizontal non-dimensional point of action of lift force. Static lorry tests.

- ■ Flat ground ABL simulation.
- □ Coleman (1990), low turbulence.
- ▲ Coleman (1990), Turbulence: ${}^{x}L_u = 0.15\text{m}$, $\sigma = 10\ \%$

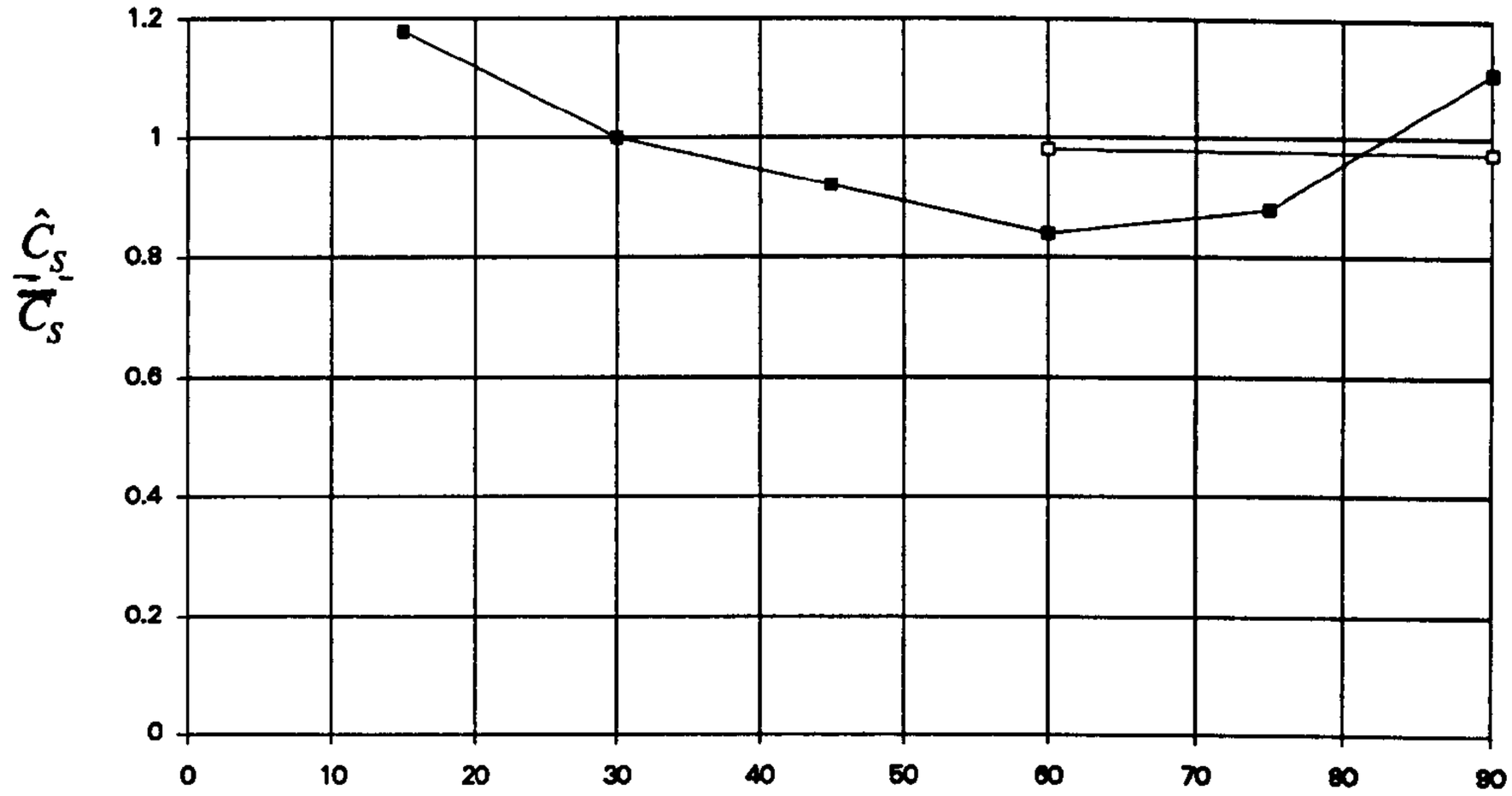

Figure 7.11 Normalised extreme side force parameter.
Static lorry tests.

- ■ Flat ground ABL simulation.
- □ Coleman (1990), low turbulence.
- ▲ Coleman (1990), Turbulence: ${}^{x}L_u = 0.15\text{m}$, $\sigma = 10\ \%$

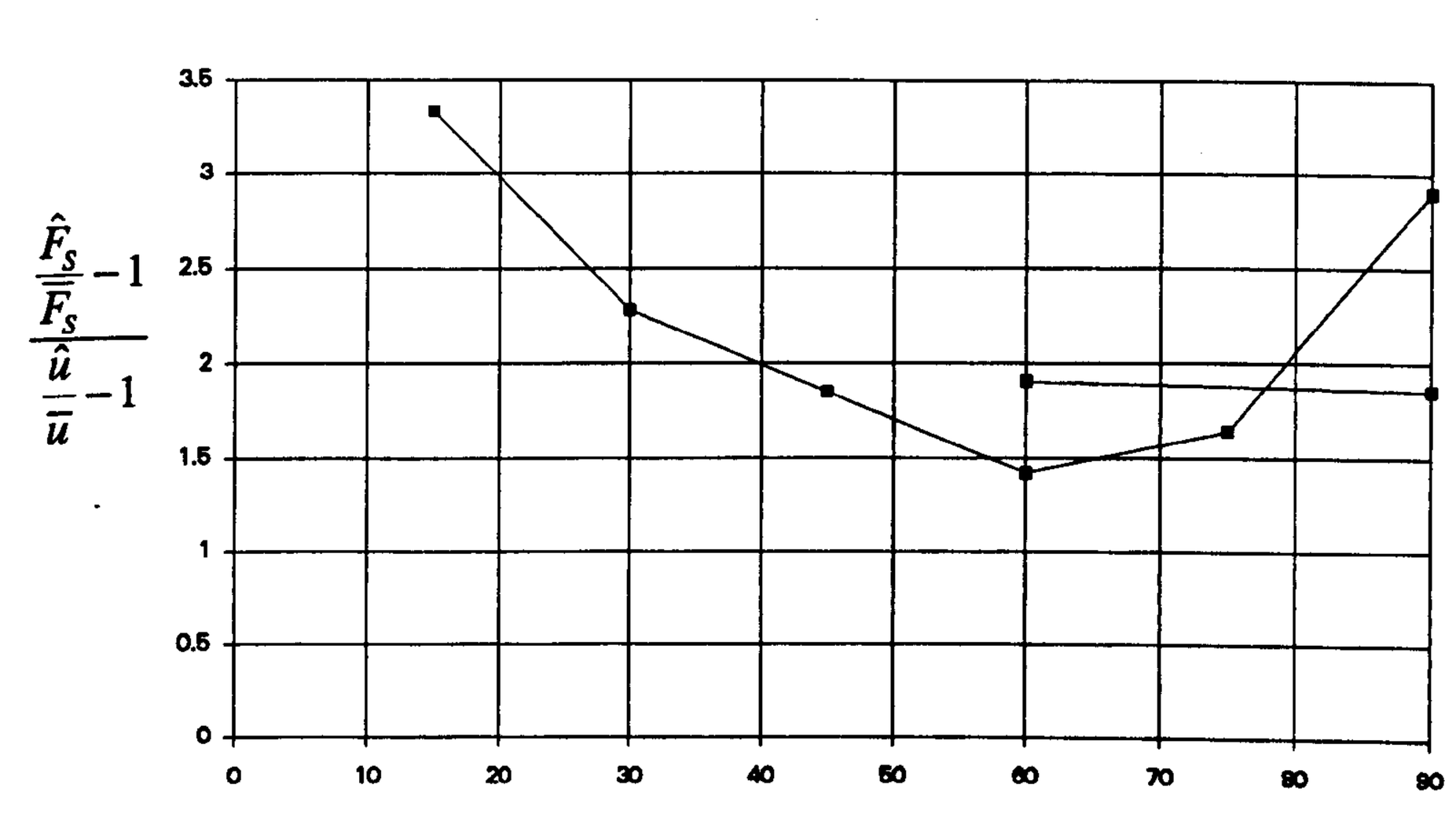

Figure 7.12 Unsteady side force parameter.
Static lorry tests.

- ■ Flat ground ABL simulation.
- □ Coleman (1990), low turbulence.
- ▲ Coleman (1990), Turbulence: ${}^{x}L_u = 0.15\text{m}$, $\sigma = 10\ \%$

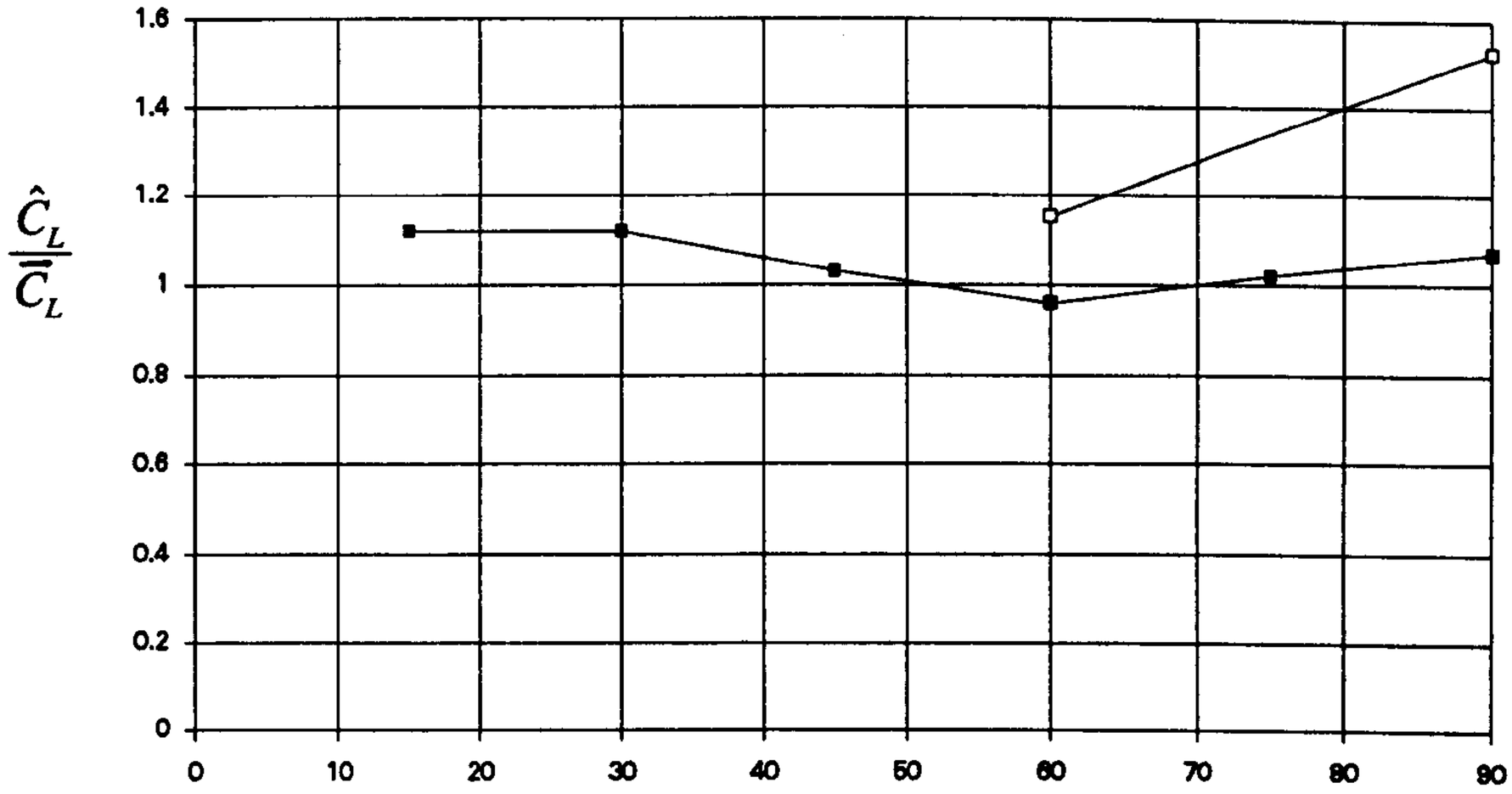

Figure 7.13 Normalised extreme lift force parameter.
Static lorry tests.

- ■ Flat ground ABL simulation.
- □ Coleman (1990), low turbulence.
- ▲ Coleman (1990), Turbulence: ${}^{x}L_u = 0.15\text{m}$, $\sigma = 10\ \%$

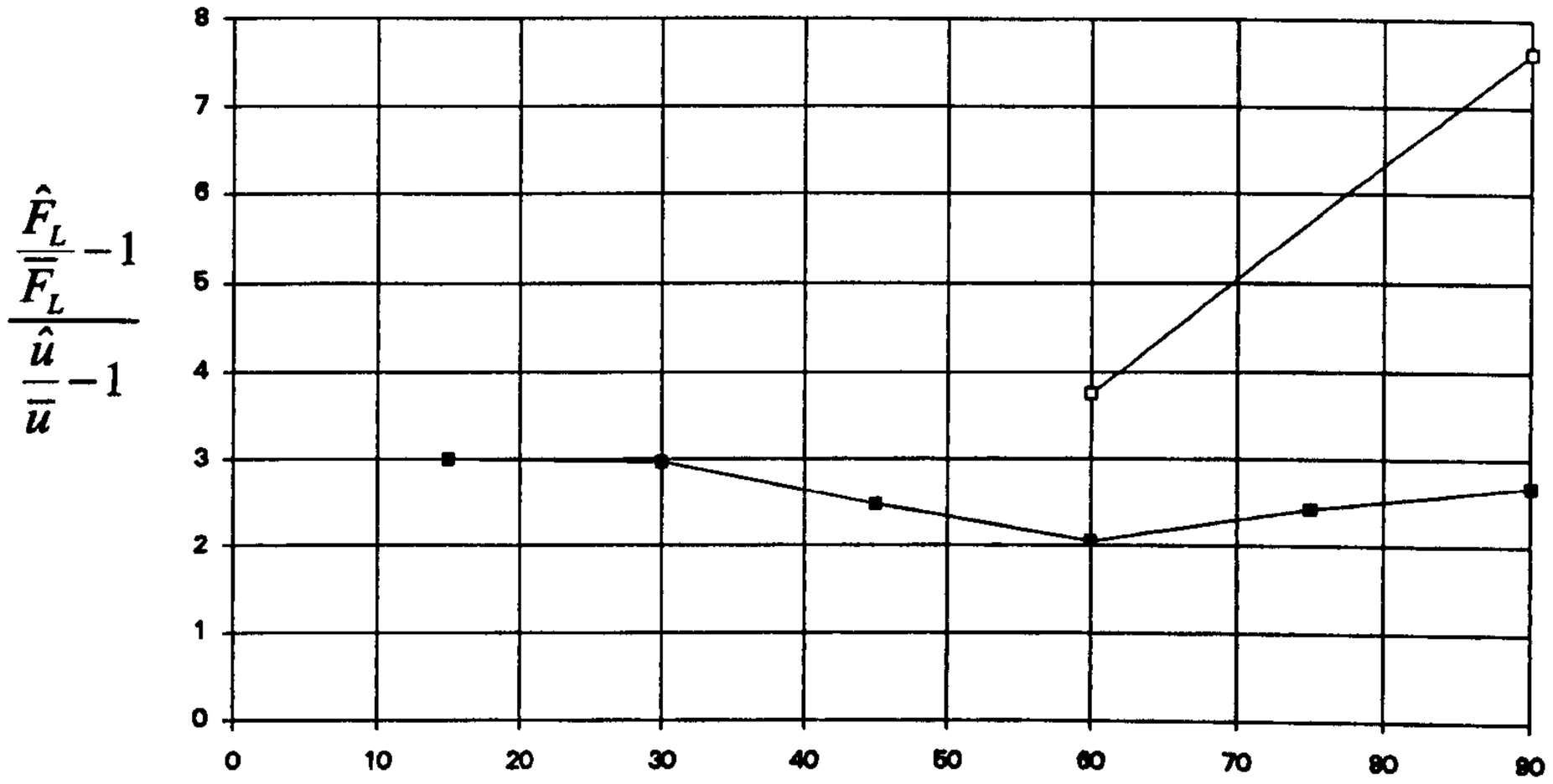

Figure 7.14 Unsteady lift force parameter.
Static lorry tests.

- ■ Flat ground ABL simulation.
- □ Coleman (1990), low turbulence.
- ▲ Coleman (1990), Turbulence: ${}^{x}L_u = 0.15\text{m}$, $\sigma = 10\ \%$

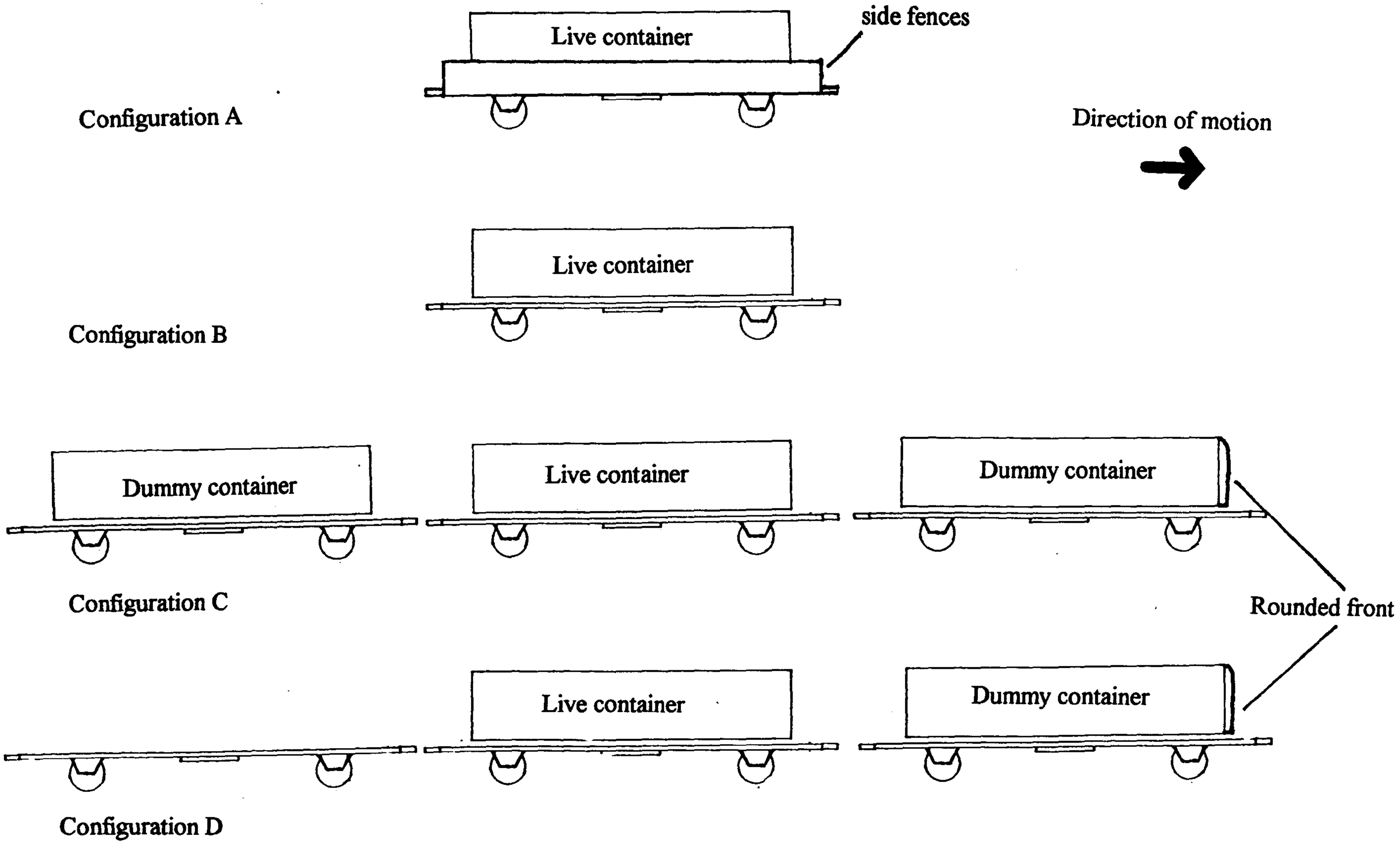

Figure 7.15 Configurations of DB railway container vehicles tested.

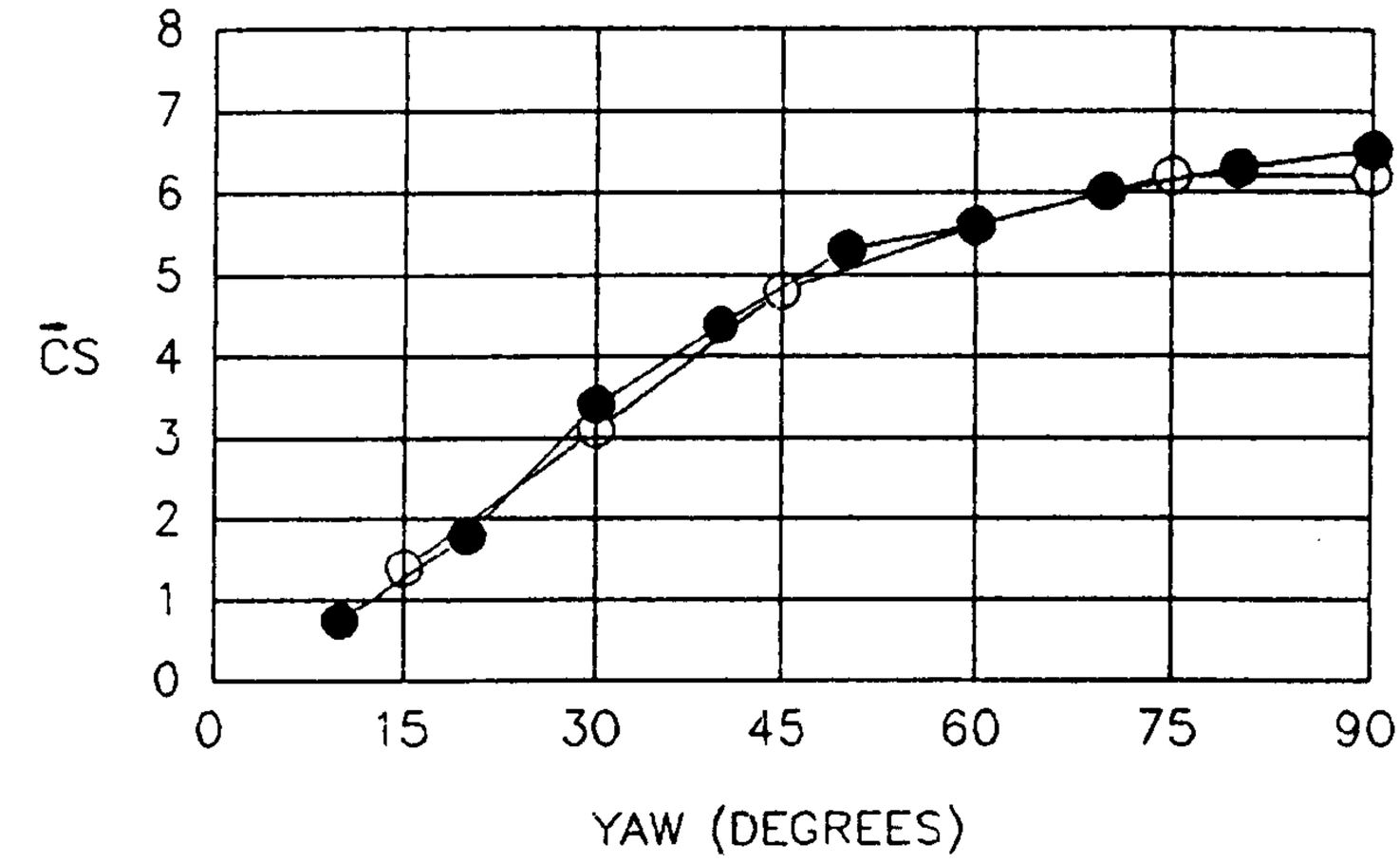

Figure 7.16 Mean side force coefficients for DB container.
Configuration A.
Static level ground simulation.

○ Nottingham University, ABL simulation.
● Peters (1992), steady flow, $^1/_3$ scale DNW.

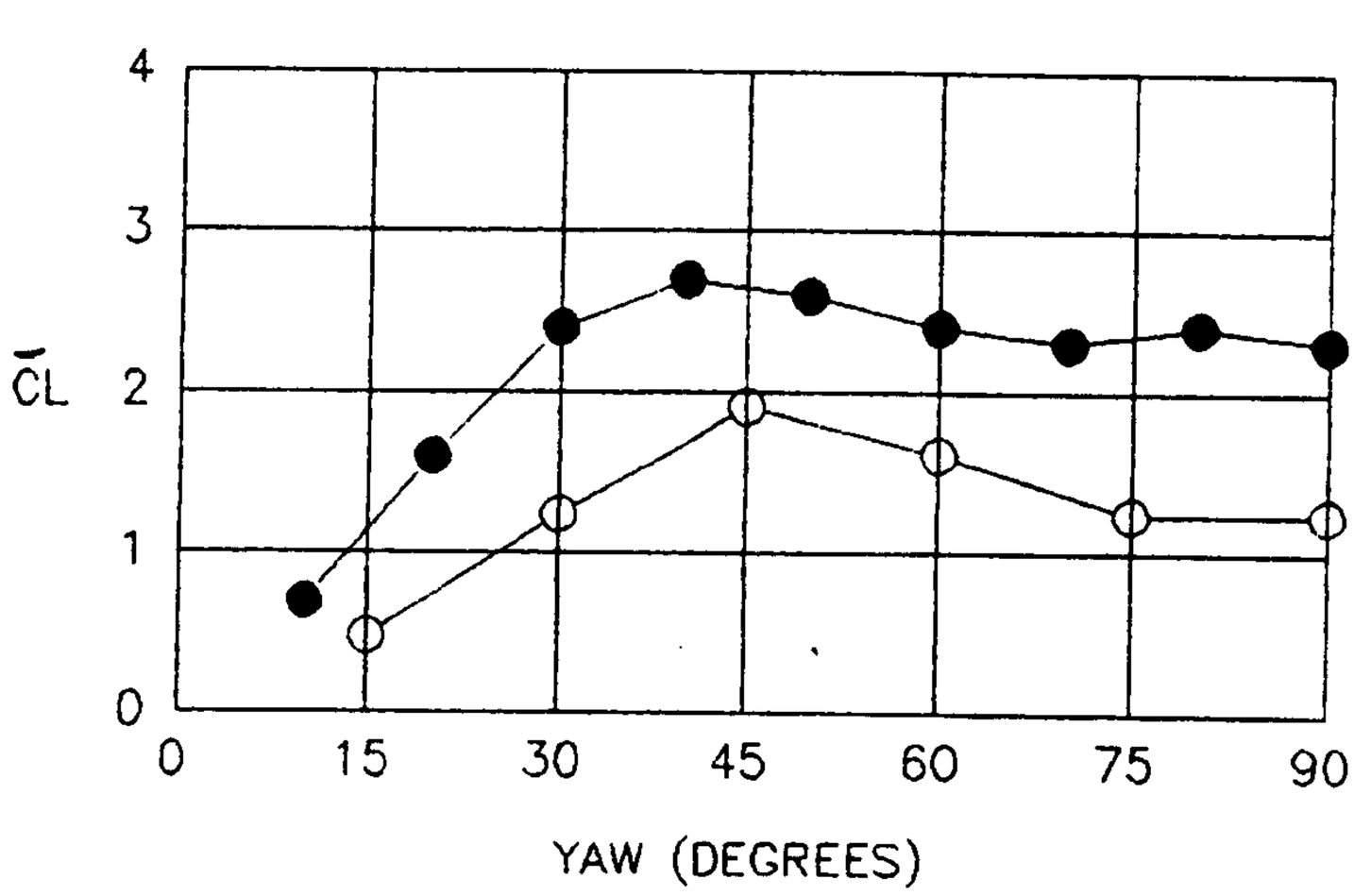

Figure 7.17 Mean lift force coefficients for DB container.
Configuration A.
Static level ground simulation.

○ Nottingham University, ABL simulation.
● Peters (1992), steady flow, $^1/_3$ scale DNW.

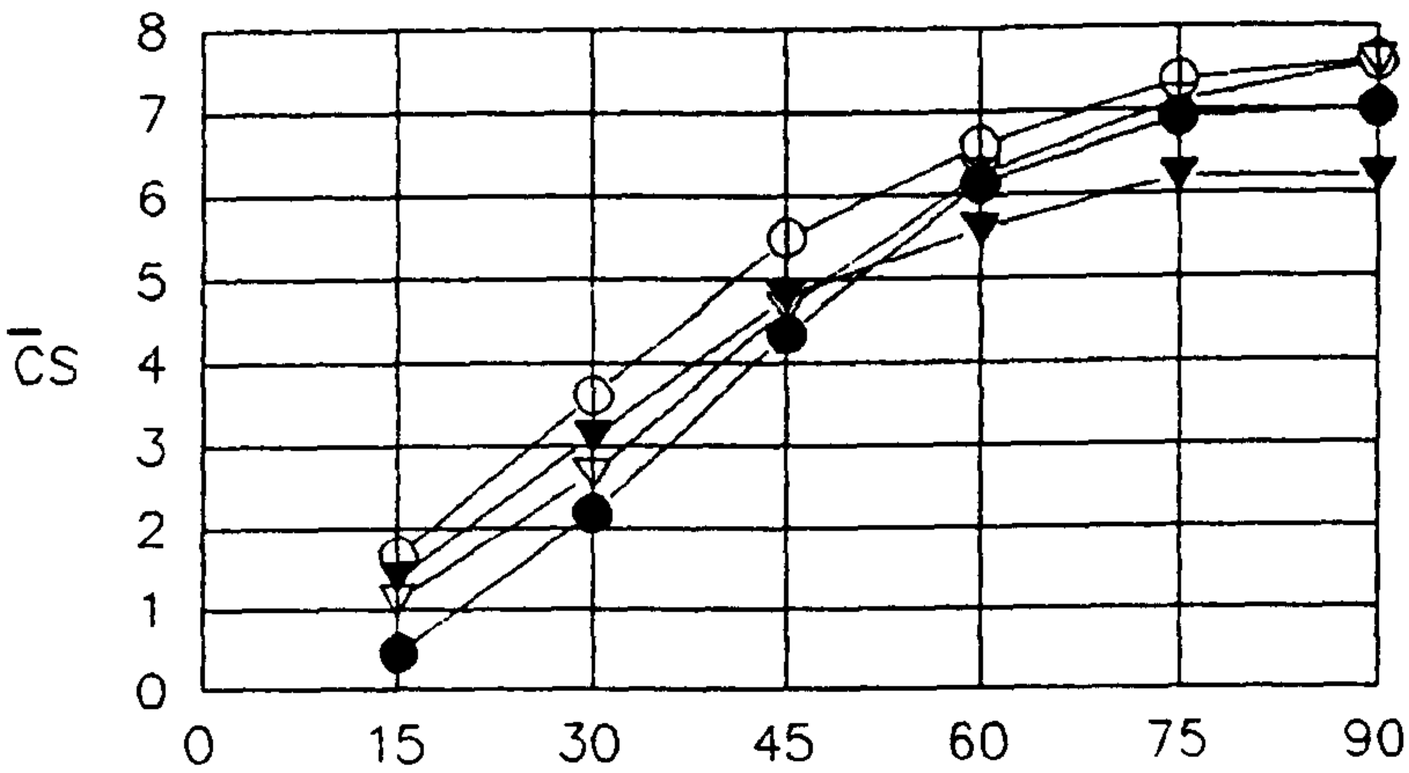

Figure 7.18 Mean side force coefficients for DB containers.
Configurations A to D.
Static level ground simulation with ABL.

▼ config. A, o config. B , ● config. C, ▽ config. D.

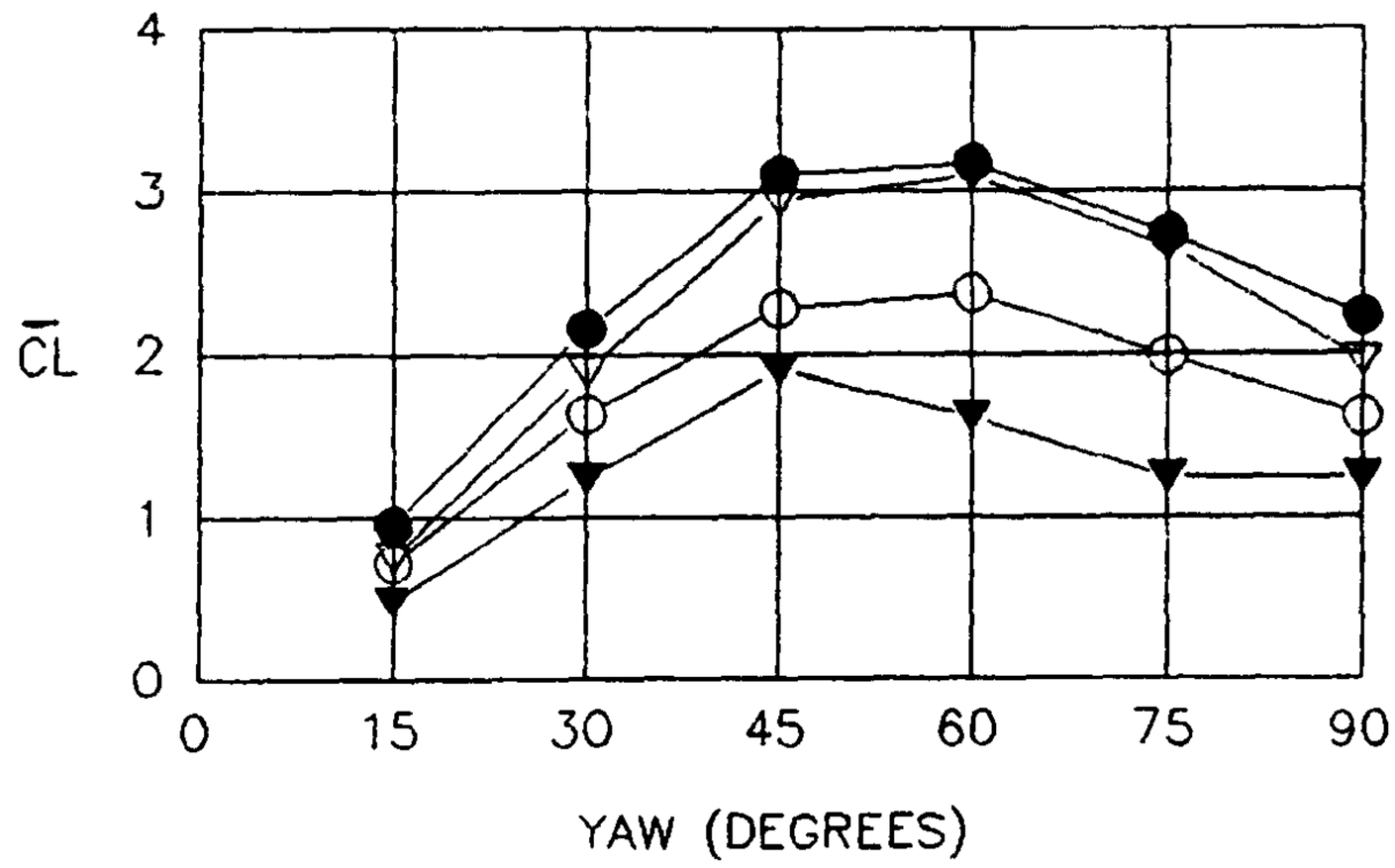

Figure 7.19 Mean lift force coefficients for DB containers.
Configurations A to D.
Static level ground simulation with ABL.

▼ config. A, o config. B , ● config. C, ▽ config. D.

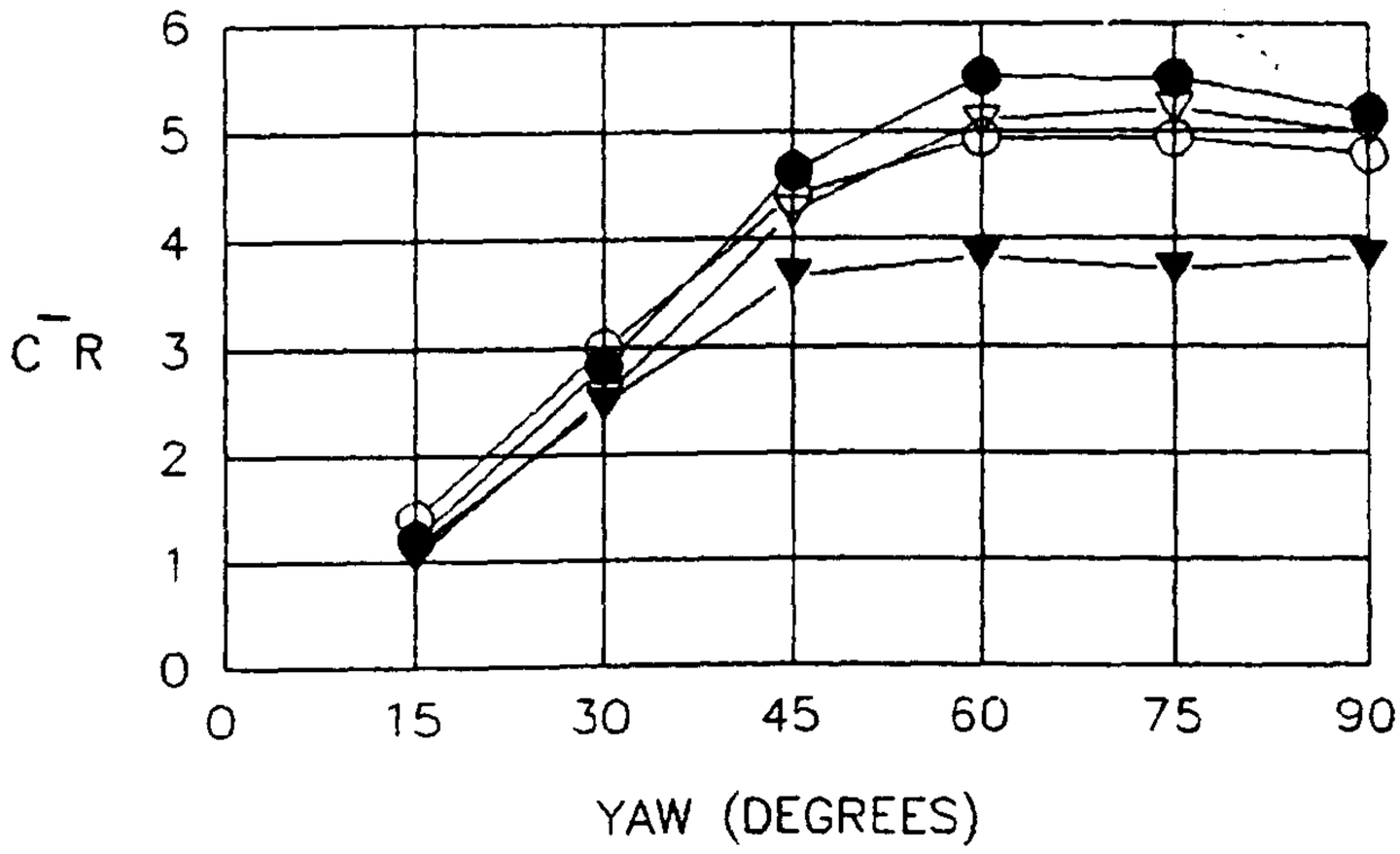

Figure 7.20 Mean lee bottom corner rolling moment coefficients for DB containers.
Configurations A to D.
Static level ground simulation with ABL

▼ config. A, o config. B , ● config. C, ▽ config. D.

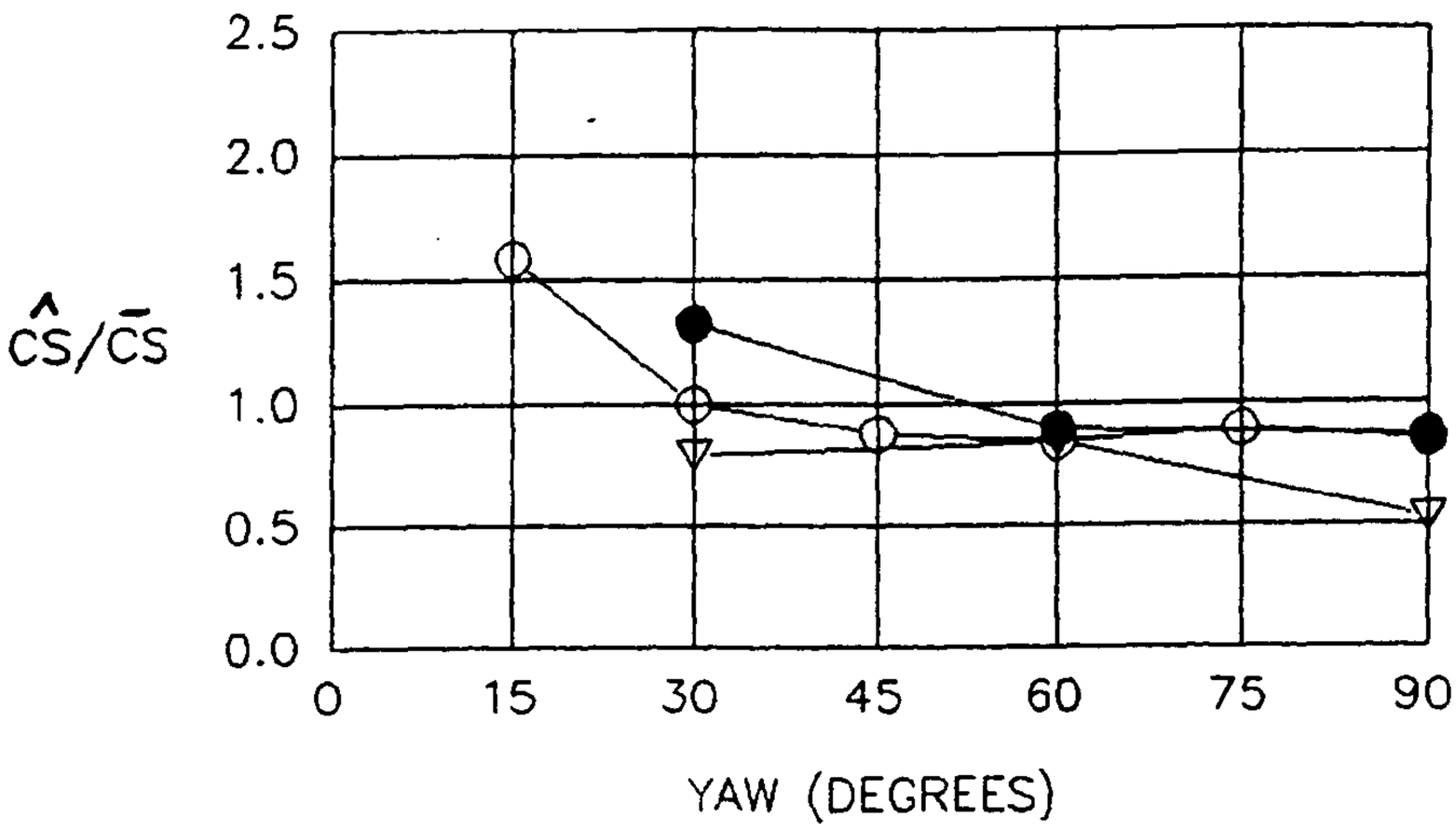

Figure 7.21 Normalised extreme side force parameter for DB containers.
Configurations B to D.
Static level ground simulation with ABL.

o config. B , ● config. C, ▽ config. D.

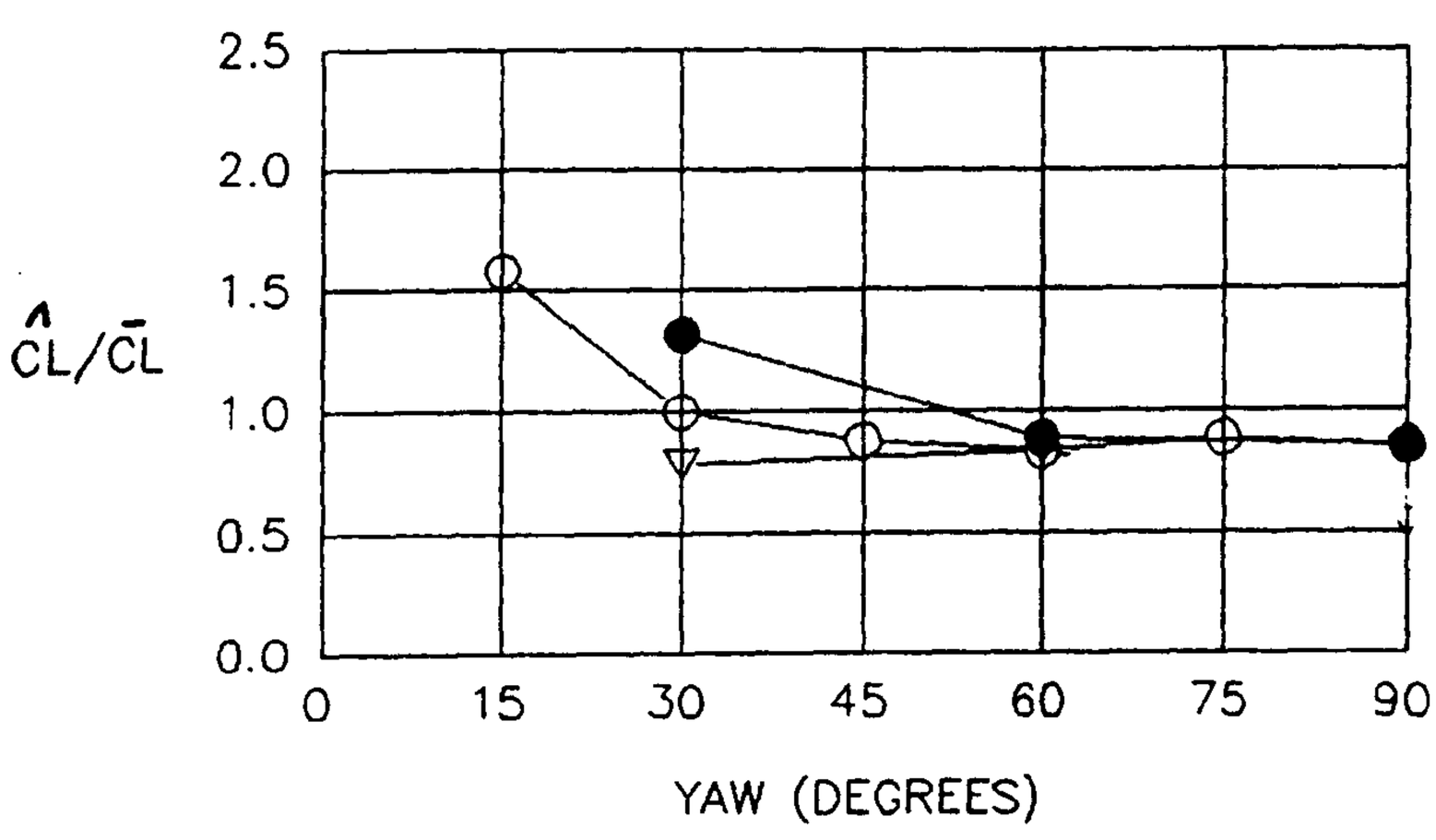

Figure 7.22 Normalised extreme lift force parameter for DB containers.
Configurations B to D.
Static level ground simulation with ABL.

o config. B , ● config. C, ▽ config. D.

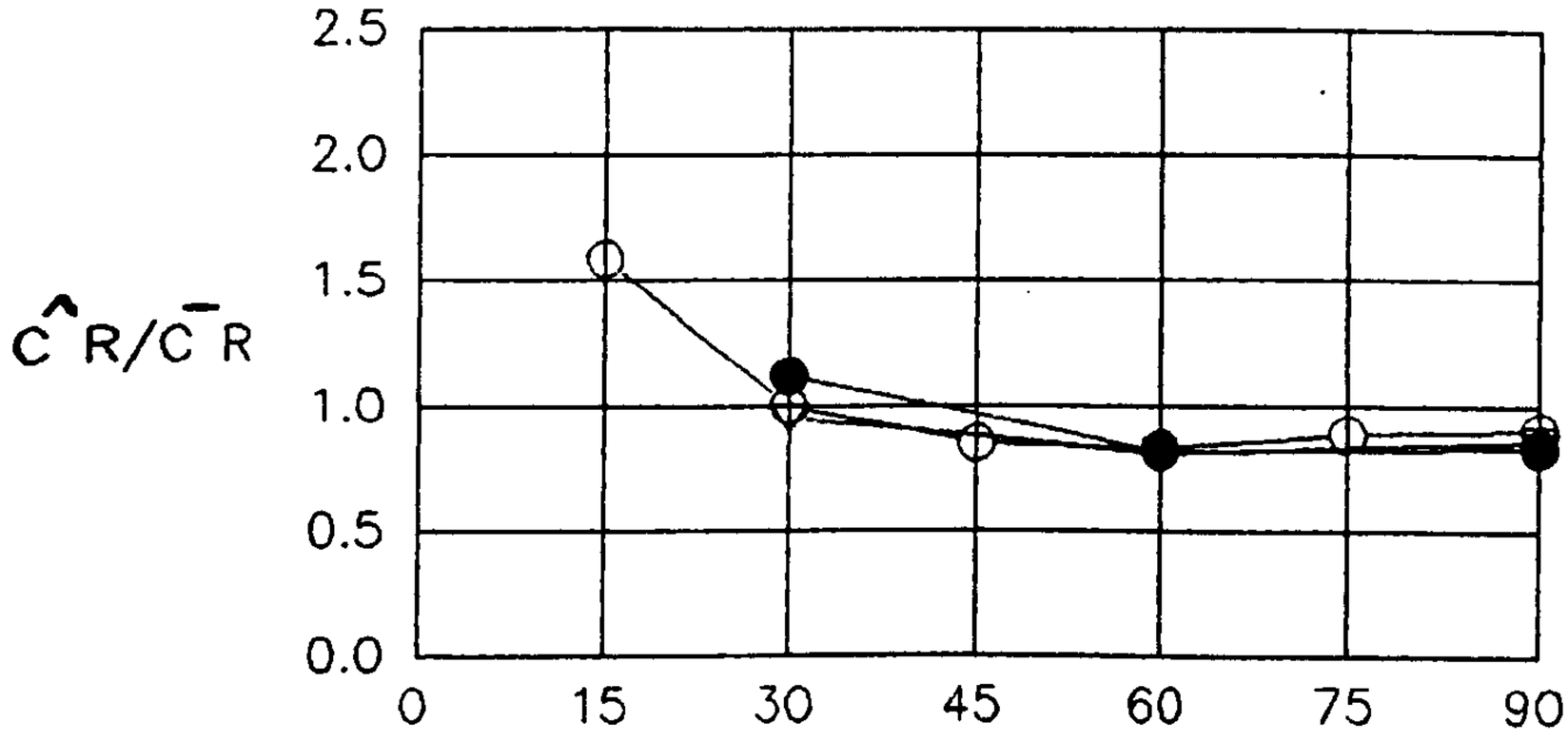

Figure 7.23 Normalised extreme lee bottom corner rolling moment parameter.
Configurations B to D.
Static level ground simulation with ABL.

o config. B , ● config. C, ▽ config. D.

8. The First Series of Moving Model Tests.

These tests were undertaken in January and February 1991. The 1/50th scale lorry and various configurations of the 1/45th scale DB railway container vehicles were tested using the level ground simulation.

Details of the moving model rig used for these tests are described in section 4.2.2 including photographs of the live vehicles traversing the working section. Tables 8.1 to 8.2 detail the moving model rig and wind speeds used for these tests. For each yaw angle 50 runs of the moving model rig was conducted. The zero force readings were conducted every 10 runs with the tunnel operating with the fan blades feathered, at zero wind speed and the live vehicle at the firing end of the rig i.e. not in the working section.

For these moving model tests only data from the central 1.5m of the 2.7m working section width were extracted to ensure a reasonable consistency of the wind characteristics. Also all wind velocities used for calculating the non dimensionalised force and moment coefficients were averages of measurements made in 5 positions across the central 1.5m test section. The wind velocity measurements and the calculation of the average values used are described in Chapter 6.

Analysis was conducted as described in section 5.2.2.3 for the mean and extreme force and moment coefficients, their non dimensional points of action and the extreme values. For these initial tests the model time period taken to be equivalent to a 3s full scale gust was simply the transit time of the vehicle across the central 1.5m of the working section. The corresponding extreme wind speed was that calculated for the same sample time as described in Chapter 6 and the results shown in figure 6.20. The model time period obtained in this way varied between 0.1 and 0.4s which is of the correct order for a full scale gust of 3s as described using the scaling method described in section 3.3. Noting that the methods for extreme value analysis are only available for a continuous time series of measured data, the actual extreme force value was taken to be simply the largest of the ensemble of forces obtained from the 50 runs of the moving model rig. This was justified, without further analysis for this first test series, on the grounds that the dispersion of the extreme values formed from the static tests were very low. Therefore even a rigorous analysis should not return extreme values very different to the simple method. This was considered further for the data measured in the second moving model test series.

As it turned out, many problems concerning the quality of the data, due to mechanical noise, were encounted during the processing of the extreme values from these initial tests and therefore the analysis of the results was limited in favour of spending time on modifying the rig for the second series of tests. Further, no specific tests were undertaken to accurately assess the mechanical noise as it seem to dominate the signals recorded during the aerodynamic tests. After the initial analysis of the results presented in this chapter were completed, some further investigation of the moving model trolley was conducted: With a live model mounted and the trolley pushed along by hand, and the wind tunnel not operating, it was apparent that there was a large low frequency oscillation in the system that one could actually detect the in the live vehicle body simply by touching it. This was traced to the mounting arrangement of the data acquisition equipment as this resonated at a similar frequency. Also by tapping the data acquisition platform one could feel the oscillation transmitted to the live vehicle. This simple vibration check was repeated without the platform present and indeed the large amplitude low frequency component disappeared.

This chapter describes the results of these tests discussing the effect of mechanical noise on the processed extreme values. Chapter 4 deals with the modifications undertaken afterwards prior to the second series of tests in which specific tests to determine the level of mechanical noise were undertaken.

8.1 The lorry results.

For this vehicle only the force data were analysed due to the problems with mechanical noise as it was decided to repeat the measurements with the improved rig, see Chapter 9.

8.1.1 Mean forces.

Figures 8.1 and 8.2 show the analysed mean force coefficients compared with the static test results of Chapter 7. Included in these plots are the standard deviation of the force coefficients calculated for each run. The side force coefficients show excellent agreement at all yaw angles whilst the lift force coefficient for the moving model tests shows a much higher value including the value for the yaw angle of 90 degrees, i.e. the moving model stationary. This was investigated further by repeating the measurement during the second series of tests, see Chapter 9.

The standard deviation of both the side and lift force coefficients is seen to be very large. This is discussed further in the next section.

8.1.2 Extreme force values.

Figures 8.3 and 8.4 show the normalised extreme side and lift force parameters. It is seen that the values for the moving model tests are much larger than the static test results for all yaw angles as indicated by the standard deviations of the ensemble of extremes indicated in figures 8.2 and 8.3. This is especially apparent for the lift force coefficients at the lowest yaw angles. This is in agreement with the effect of mechanical noise as this will certainly increase as the moving model speed increases for the low yaw angle tests. The suspicion at this time was that the mechanical noise of the system was dominating the measured signals as discussed in the opening section of this chapter.

8.2 The DB railway container vehicle results.

Moving model tests were conducted of only configurations B, C and D that is the same wagon type without the side walls fitted as shown in Chapter 7. As for the static tests the means and extreme values were calculated for the side and lift forces and the rolling moment of the container about its leeward corner. These coefficients are defined in Chapter 5.

8.2.1 Mean forces and moments.

Figures 8.5 to 8.13 show the mean side and lift force and the lee bottom corner rolling moment coefficients for the configurations tested each configuration compared with the static test results. It can be seen that in general the side force coefficient values are similar at all yaw angles. The lift force coefficients are however generally larger for the moving model tests, particularly at the two lowest yaw angles. As with the lorry tests the standard deviations are large particularly for the lift force coefficients at the lowest yaw angles where the discrepancy seems to be the largest. This is discussed further in section 8.2.2.

Figures 8.14 to 8.16 show the comparison between the moving model mean results for configurations B, C and D. These are very similar but with configuration C, as with the static tests, producing the largest values for the mean lee corner rolling coefficient.

8.2.2 Extreme force values.

Figures 8.17 to 8.19 shows the normalised extreme force coefficients for all the configurations. As with the lorry tests, and as indicated by the large standard deviations of the ensemble of means formed for each run as shown in figures 8.5 to 8.13, these values are similar for each configuration tested and are extremely large particularly at the low yaw angles. Comparing these with the static test results shown in figure 7.23, it is only at the highest two yaw angles that the normalised extreme force coefficients are similar where the standard deviations are smaller. This indicates the increasing effect of the mechanical noise at the highest trolley speeds.

Table 8.1 Flat ground lorry moving model tests (1st test series).

50 runs at each yaw angle.

Moving model speed. (m/s)	Reference Wind tunnel speed. (m/s)	Yaw angle. (degrees)	Model transit time. (s)	Reynolds number.
3.1	8.7	70	0.48	4.1×10^4
6.8	8.7	52	0.22	4.9×10^4
8.4	7.2	41	0.18	4.9×10^4
8.4	4.5	28	0.18	4.2×10^4

Table 8.2 Flat ground DB container moving model tests (1st test series).

50 runs at each yaw angle.

Config - uration	Moving model speed. (m/s)	Reference Wind tunnel speed. (m/s)	Yaw angle. (degrees)	Model transit time. (s)	Reynolds number.
B,C & D	3.1	8.7	70	0.48	4.1×10^4
B,C & D	6.8	8.7	52	0.22	4.9×10^4
C & D	8.4	7.7	43	0.18	5.0×10^4
B	8.4	7.2	41	0.18	4.9×10^4
B,C & D	8.4	4.5	28	0.18	4.2×10^4

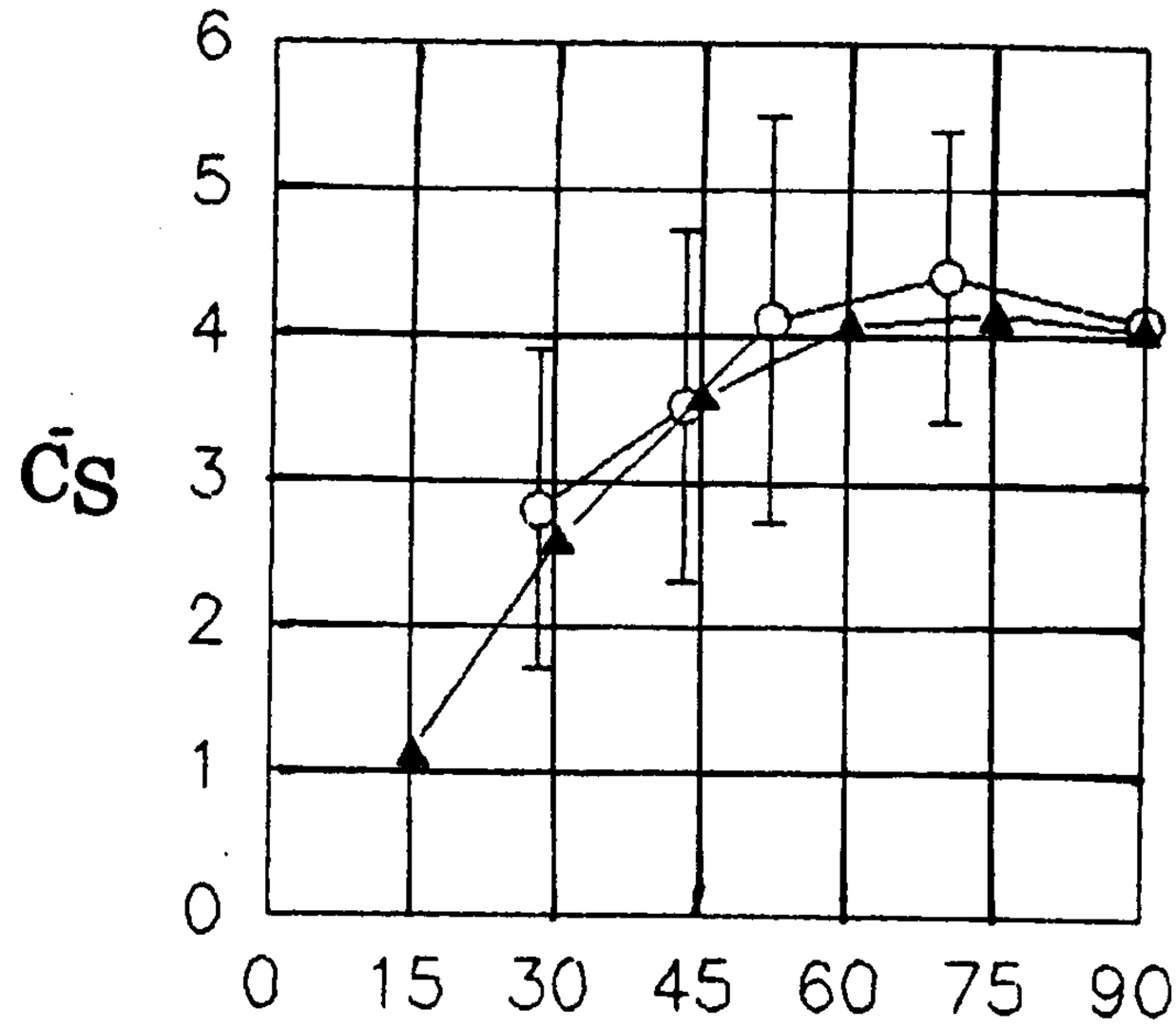

Figure 8.1 Mean side force coefficients for lorry.
Level ground ABL simulation.
o moving model tests, Δ static tests
vertical bars indicate the standard deviation of the coefficients.

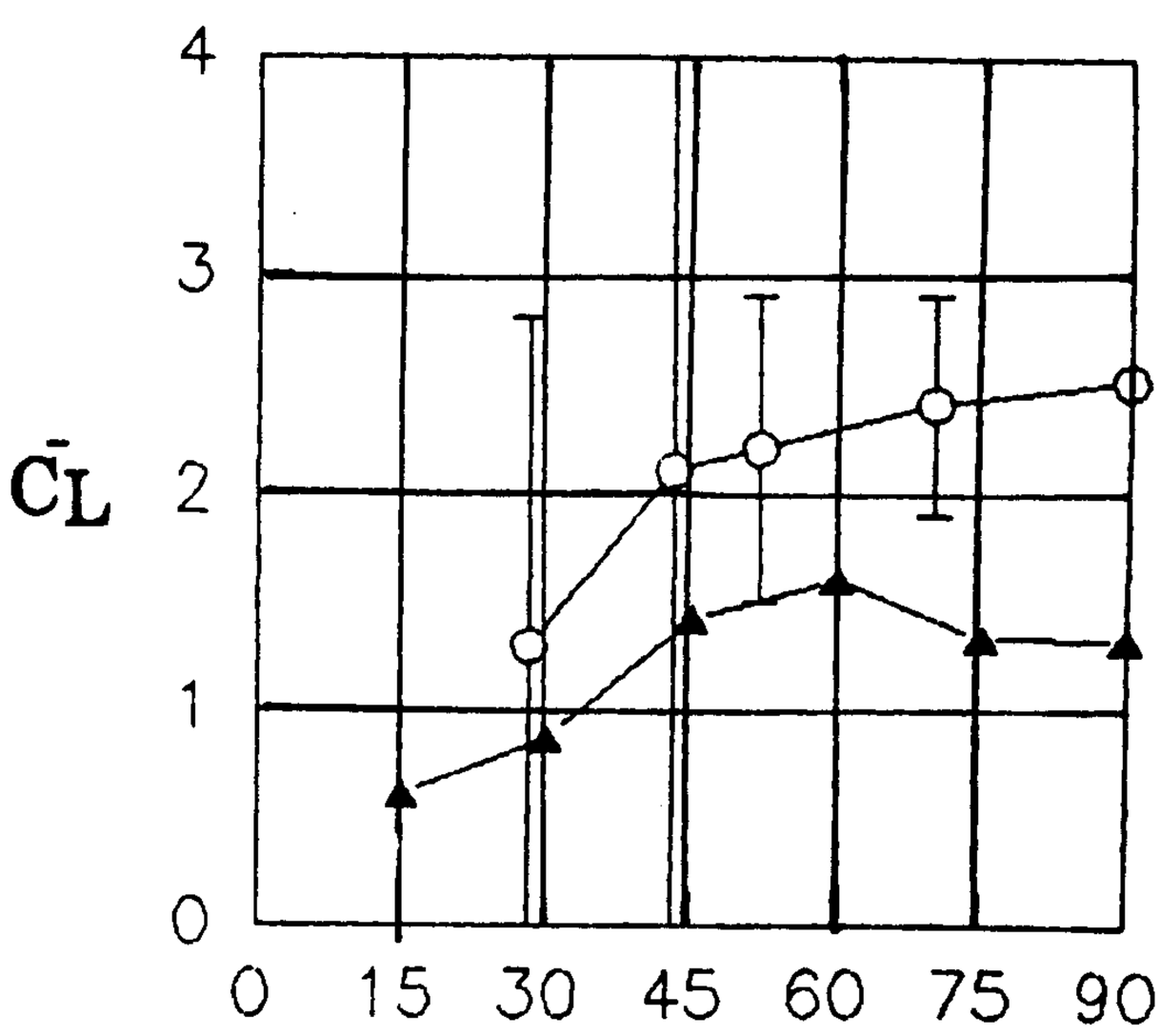

Figure 8.2 Mean lift force coefficients for lorry.
Level ground ABL simulation.
o moving model tests, Δ static tests
vertical bars indicate the standard deviation of the coefficients.

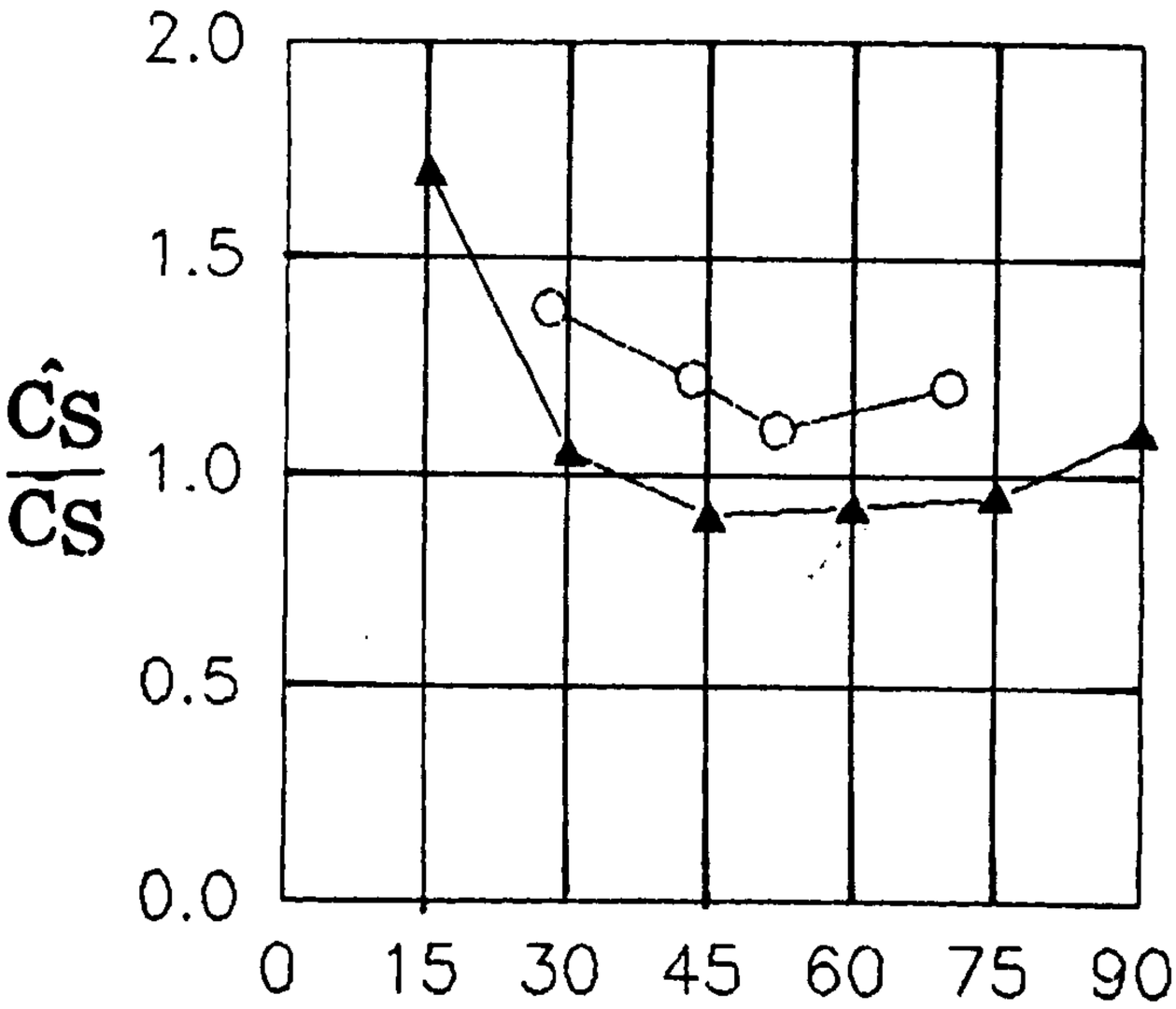

Figure 8.3 Normalised extreme side force parameters for lorry. Level ground ABL simulation.
o moving model tests, Δ static tests

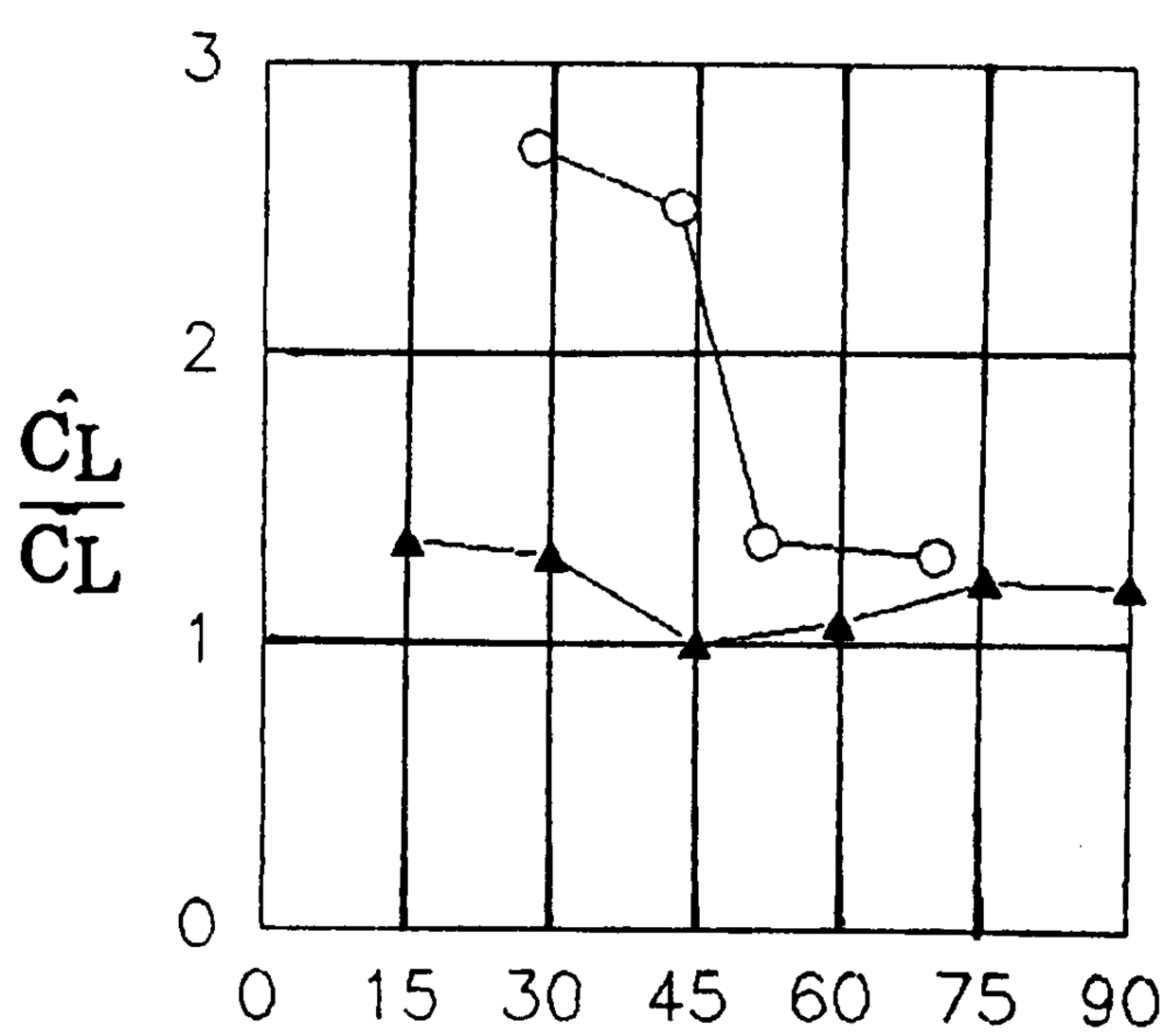

Figure 8.4 Normalised extreme lift force coefficients for lorry. Level ground ABL simulation.
o moving model tests, Δ static tests

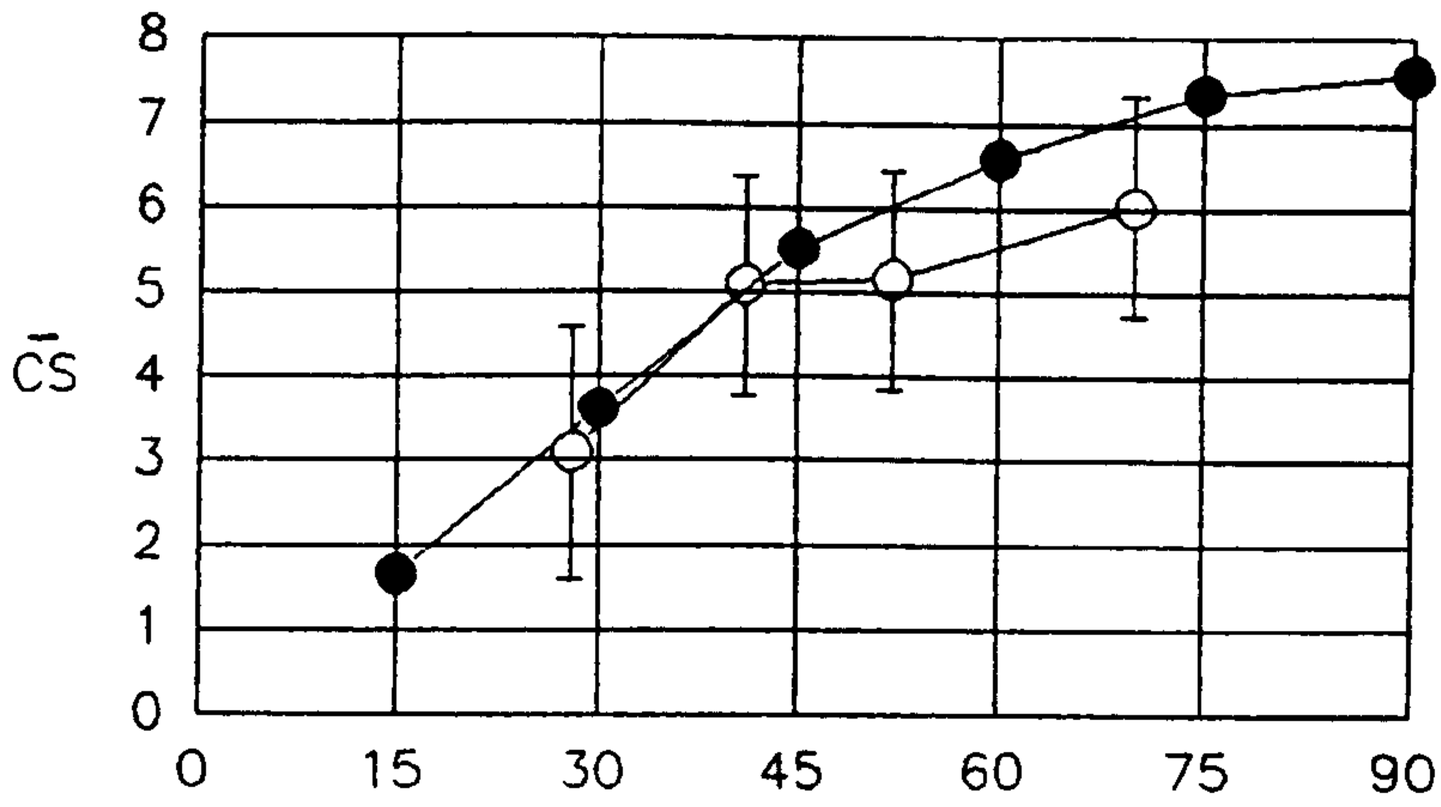

Figure 8.5 Mean side force coefficient for DB container - config. B.
Level ground ABL simulation.

● static tests, o moving model rig tests (1st series)
Vertical bars indicate the standard deviation of the coefficients.

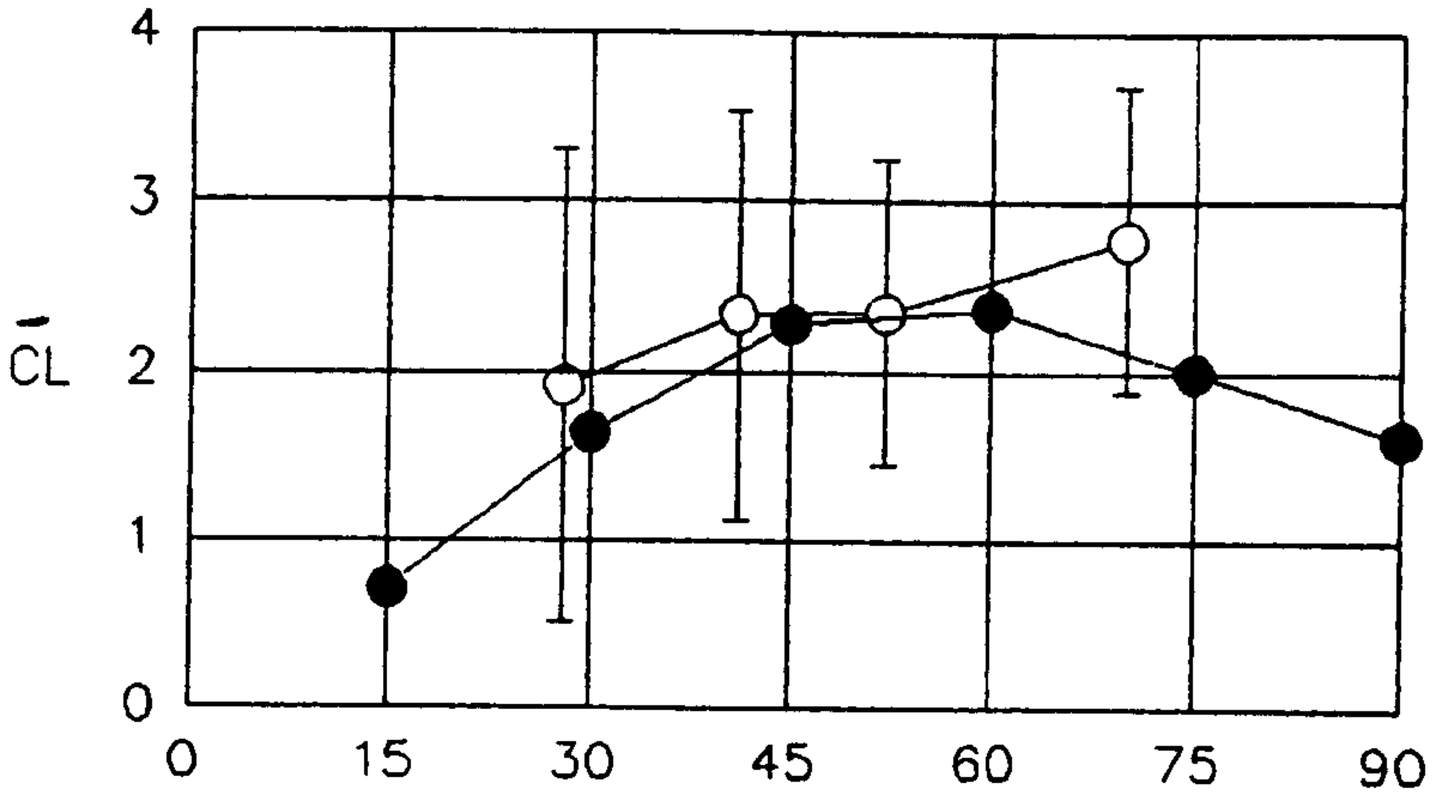

Figure 8.6 Mean lift force coefficient for DB container - config. B.
Level ground ABL simulation.

● static tests, o moving model rig tests (1st series)
Vertical bars indicate the standard deviation of the coefficients.

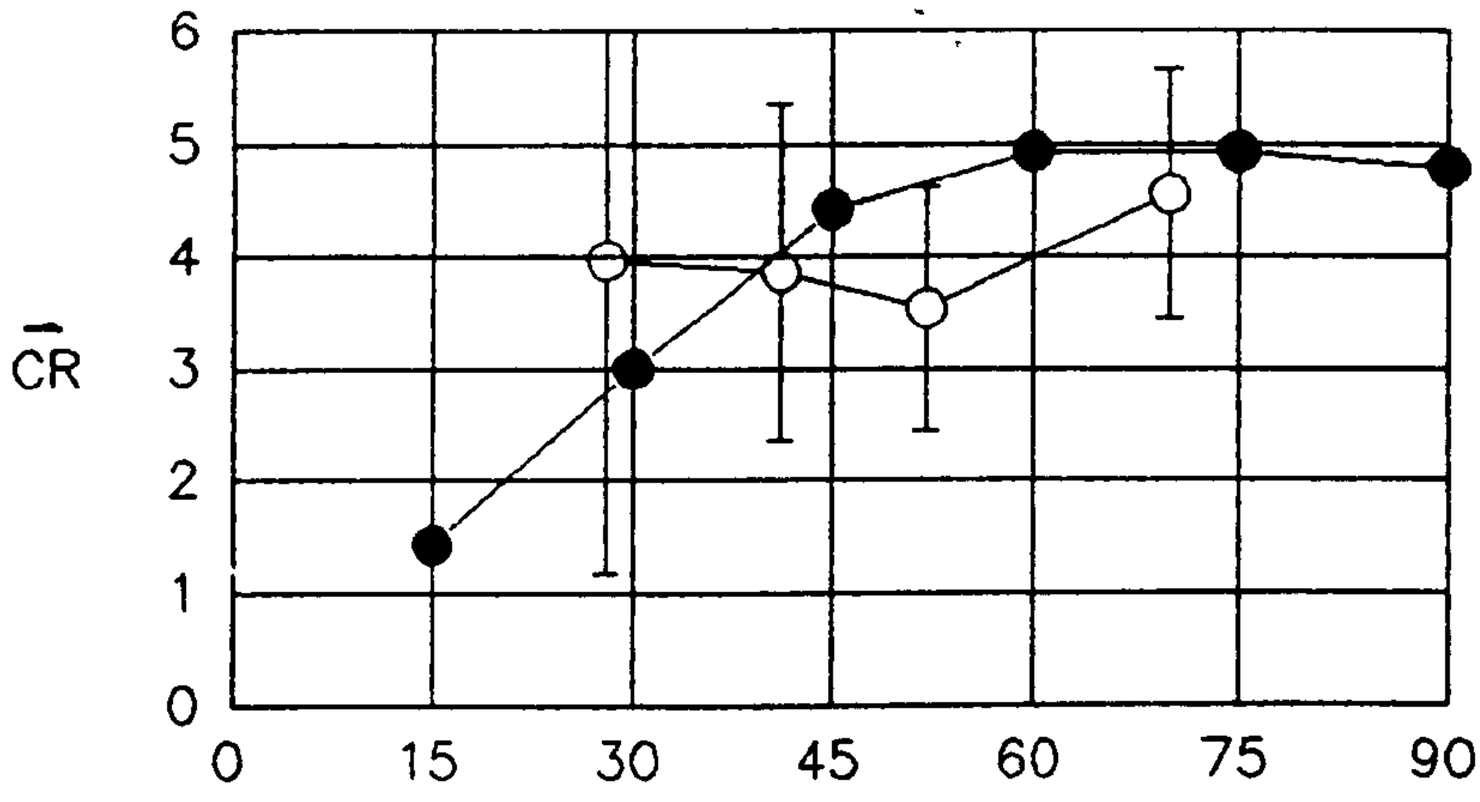

Figure 8.7 Mean lee bottom corner rolling moment coefficient for DB container - config. B.
Level ground ABL simulation.

● static tests, o moving model rig tests (1st series)
Vertical bars indicate the standard deviation of the coefficients.

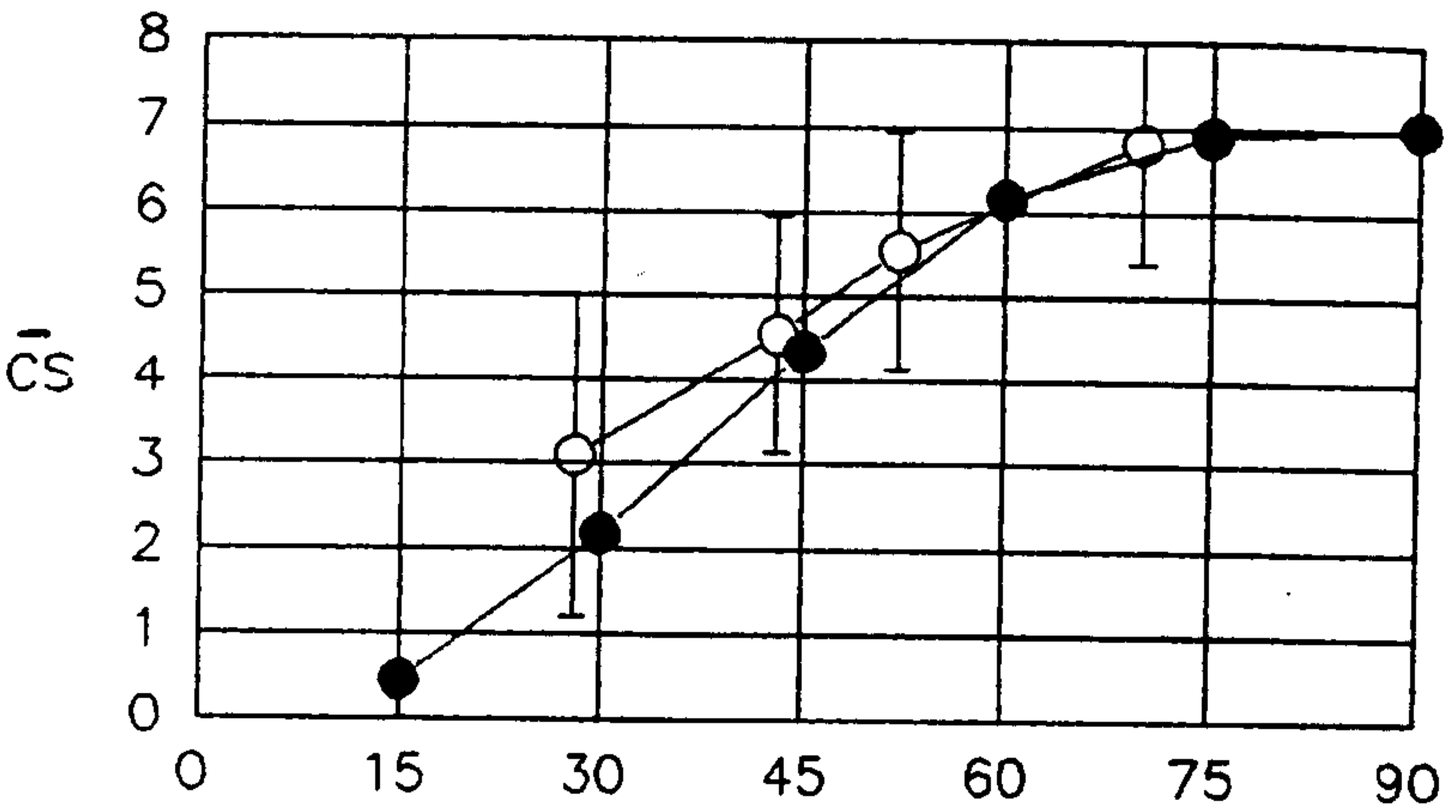

Figure 8.8 Mean side force coefficient for DB container - config. C.
Level ground ABL simulation.
● static tests, o moving model rig tests (1st series)
Vertical bars indicate the standard deviation of the coefficients.

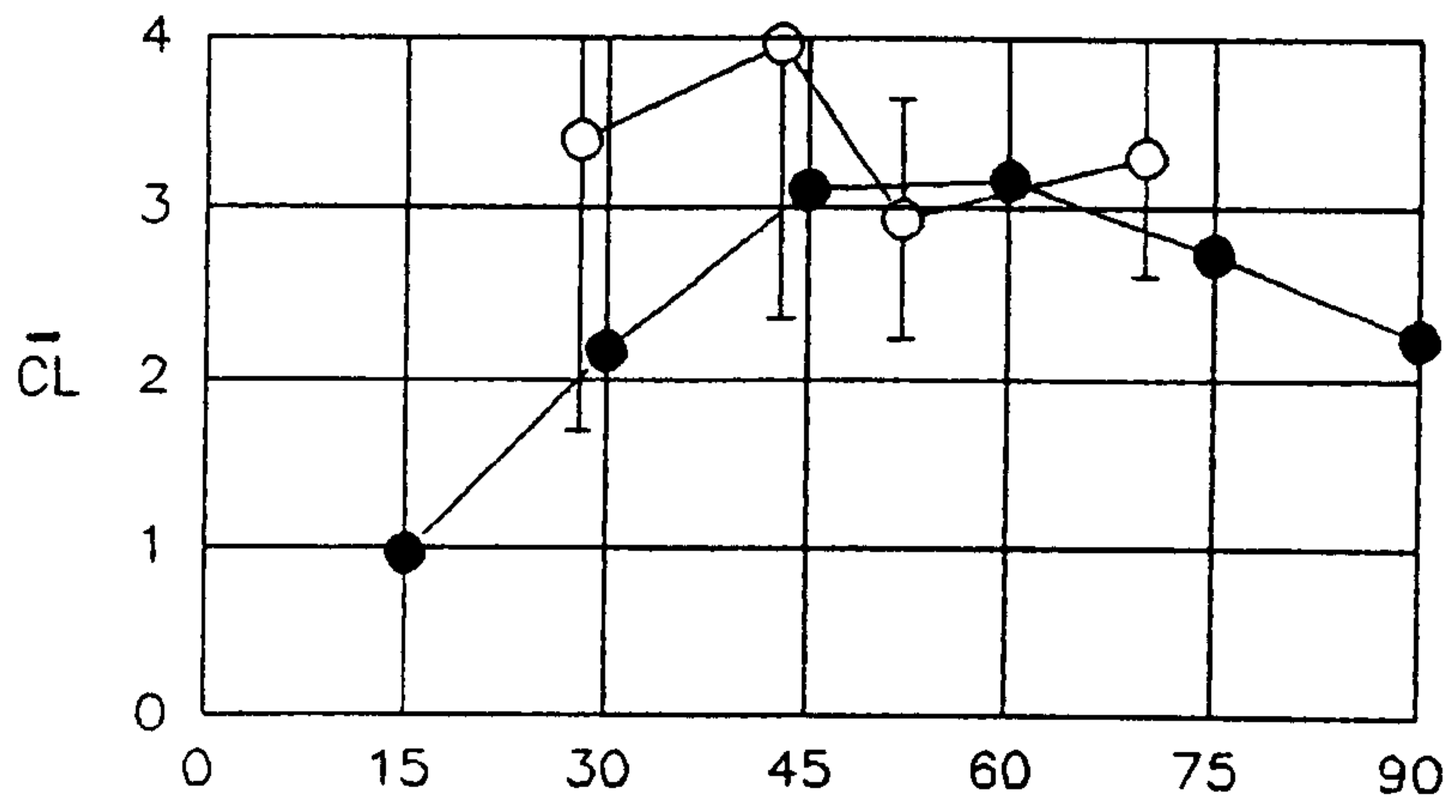

Figure 8.9 Mean lift force coefficient for DB container - config. C.
Level ground ABL simulation.
● static tests, o moving model rig tests (1st series)
Vertical bars indicate the standard deviation of the coefficients.

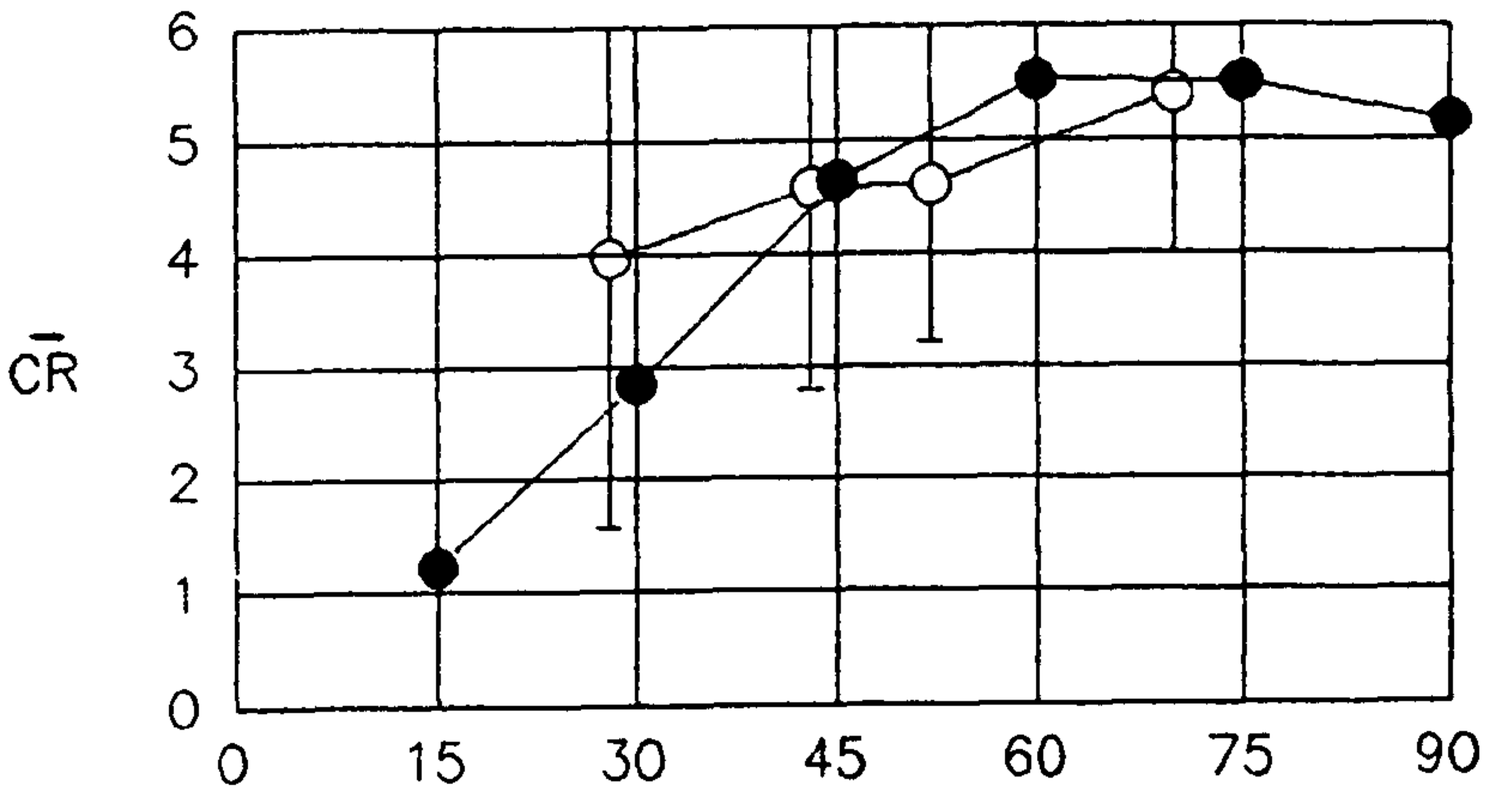

Figure 8.10 Mean lee bottom corner rolling moment coefficient for DB container - config. C.
Level ground ABL simulation.
● static tests, o moving model rig tests (1st series)
Vertical bars indicate the standard deviation of the coefficients.

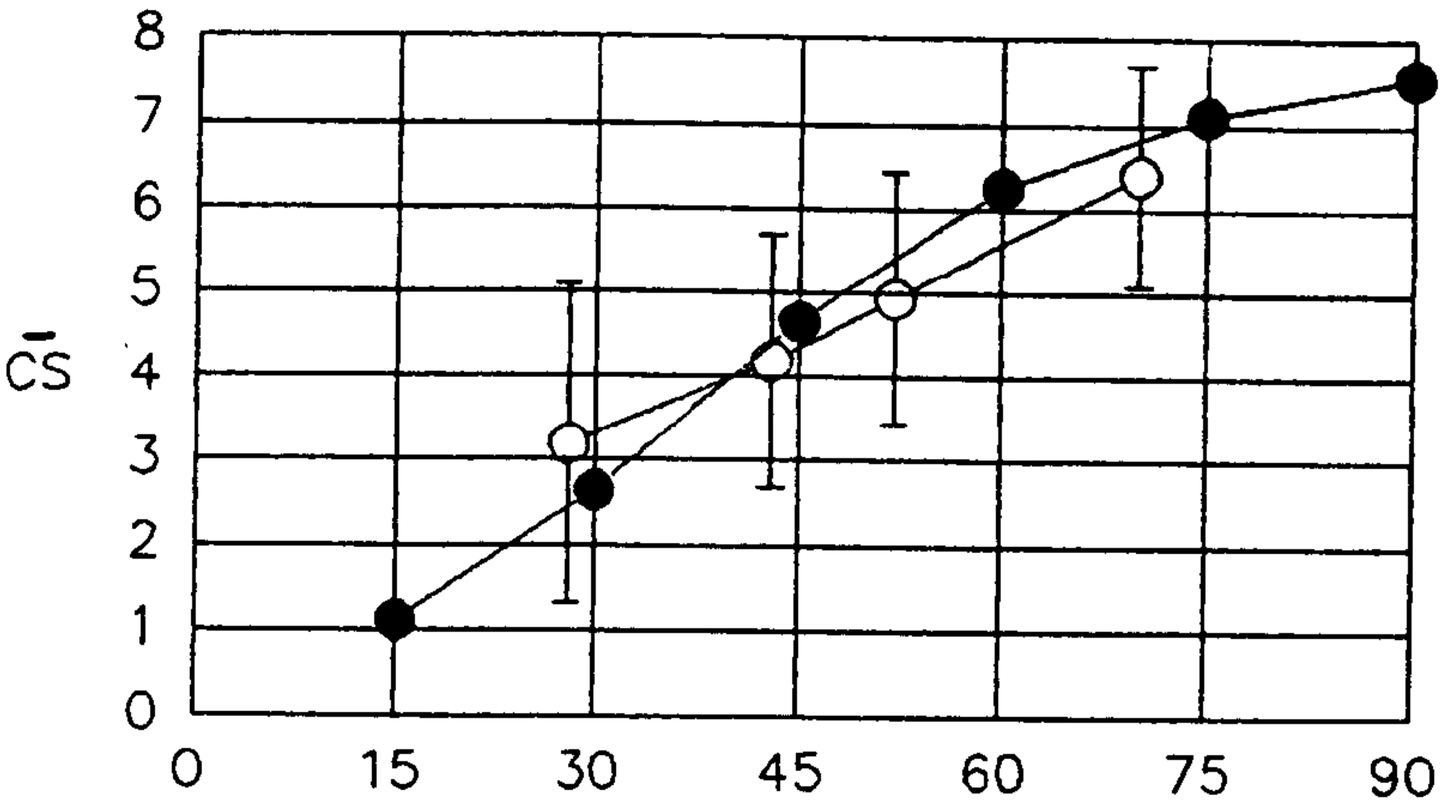

Figure 8.11 Mean side force coefficient for DB container - config. D.
Level ground ABL simulation.
● static tests, o moving model rig tests (1st series)
Vertical bars indicate the standard deviation of the coefficients.

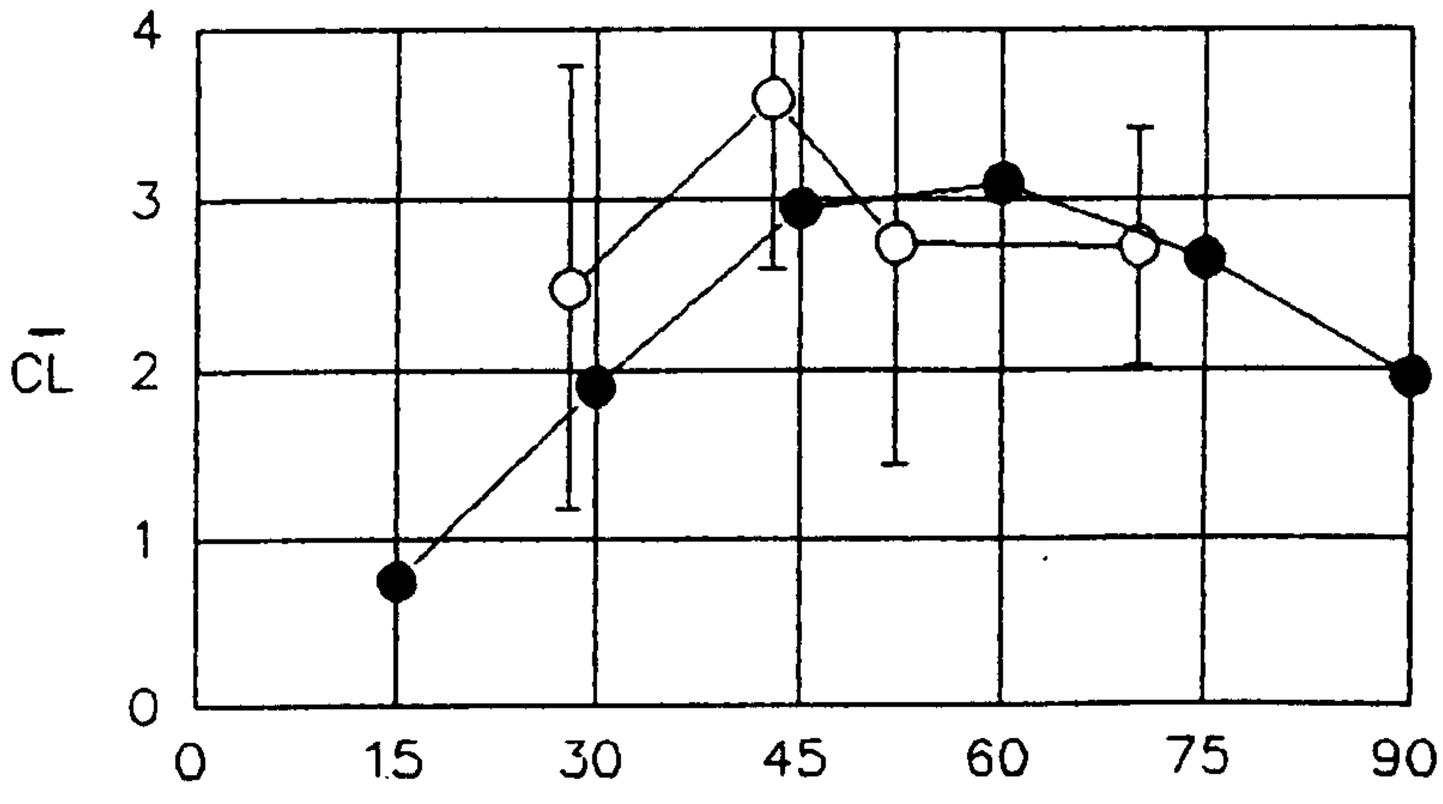

Figure 8.12 Mean lift force coefficient for DB container - config. D.
Level ground ABL simulation.
● static tests, o moving model rig tests (1st series)
Vertical bars indicate the standard deviation of the coefficients.

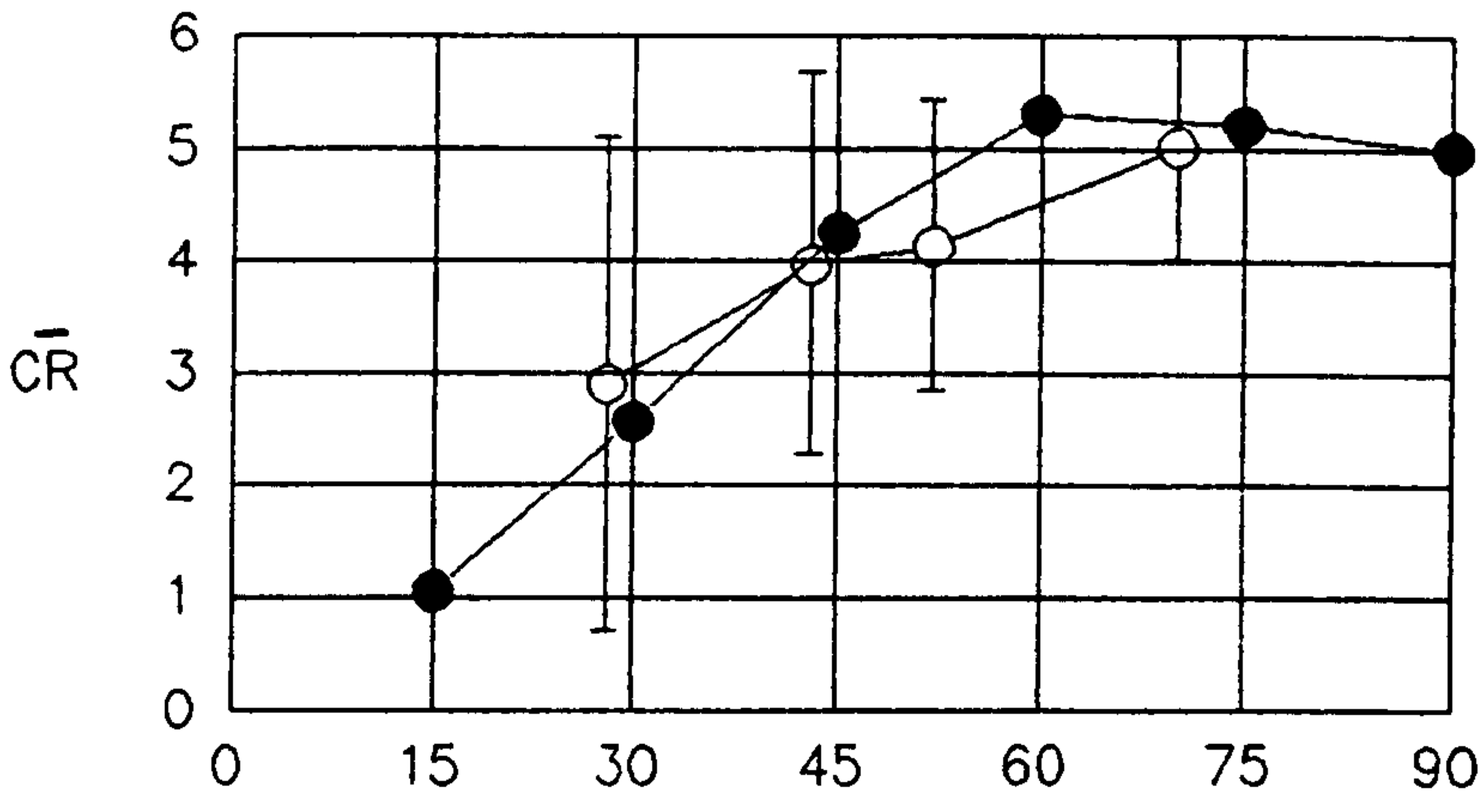

Figure 8.13 Mean lee bottom corner rolling moment coefficient for DB container - config. D.
Level ground ABL simulation.
● static tests, o moving model rig tests (1st series)
Vertical bars indicate the standard deviation of the coefficients.

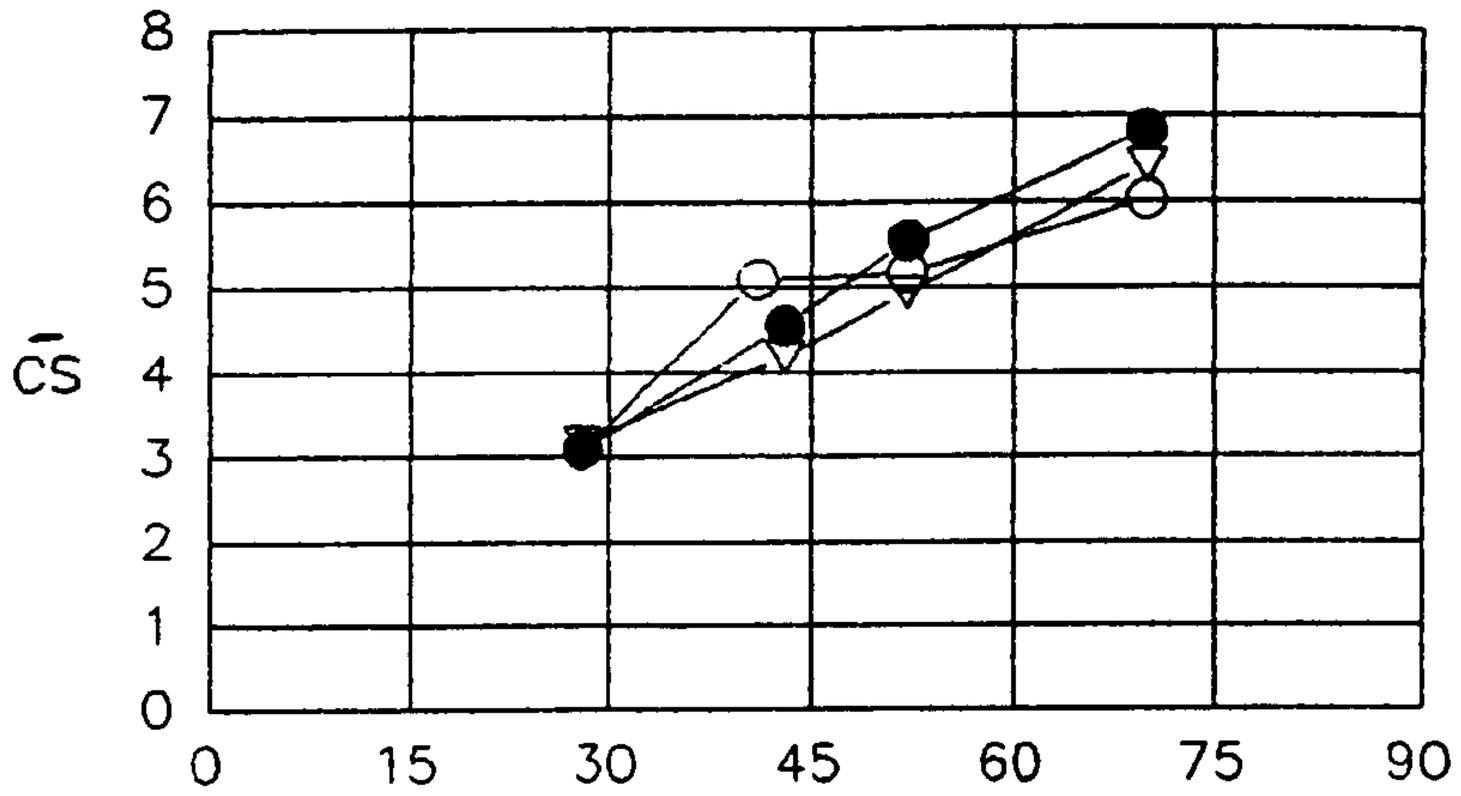

Figure 8.14 Mean side force coefficient for first series of moving model DB containers.
Level ground ABL simulation.
o config. B , ● config. C, ▽ config. D.

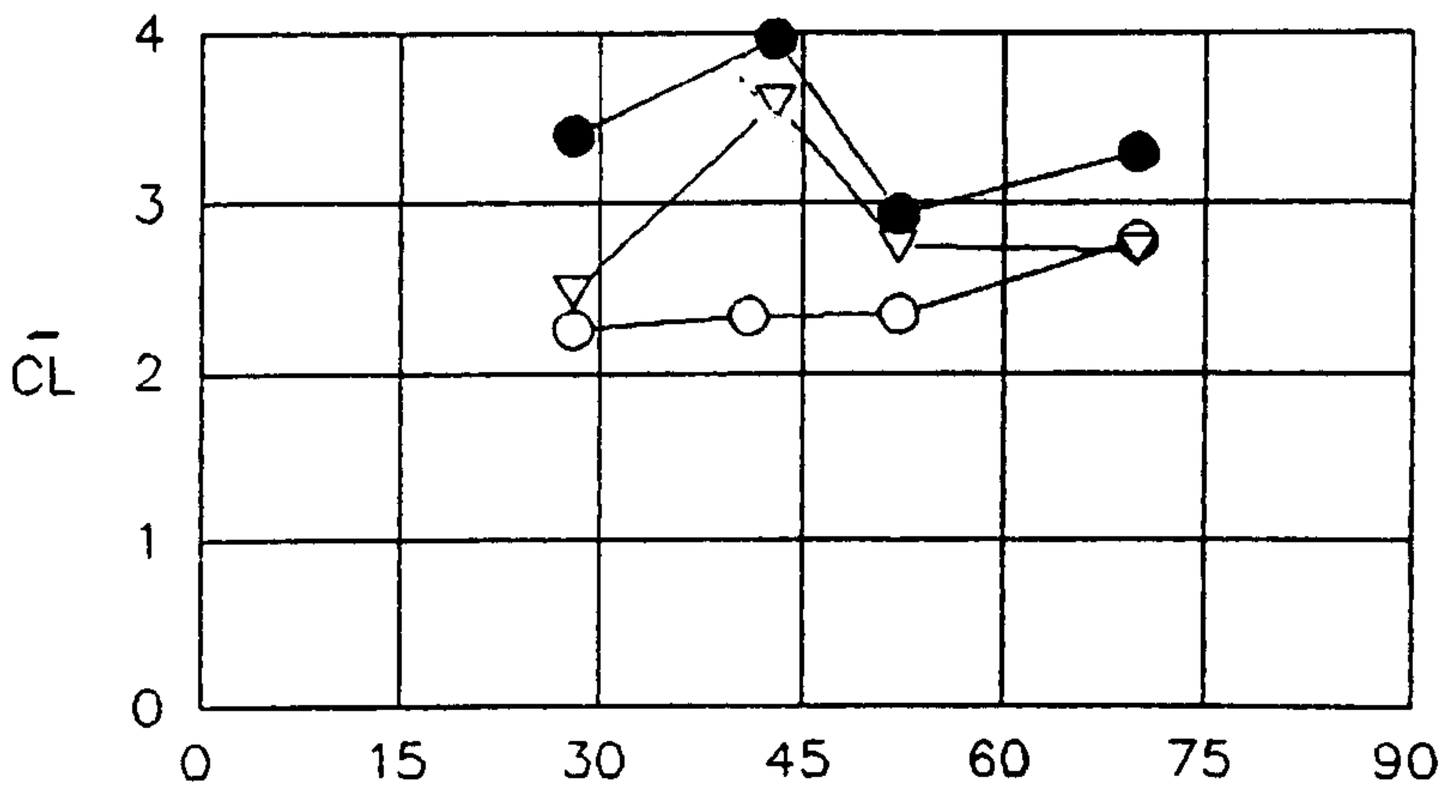

Figure 8.15 Mean lift force coefficient for first series of moving model DB containers.
Level ground ABL simulation.
o config. B , ● config. C, ▽ config. D.

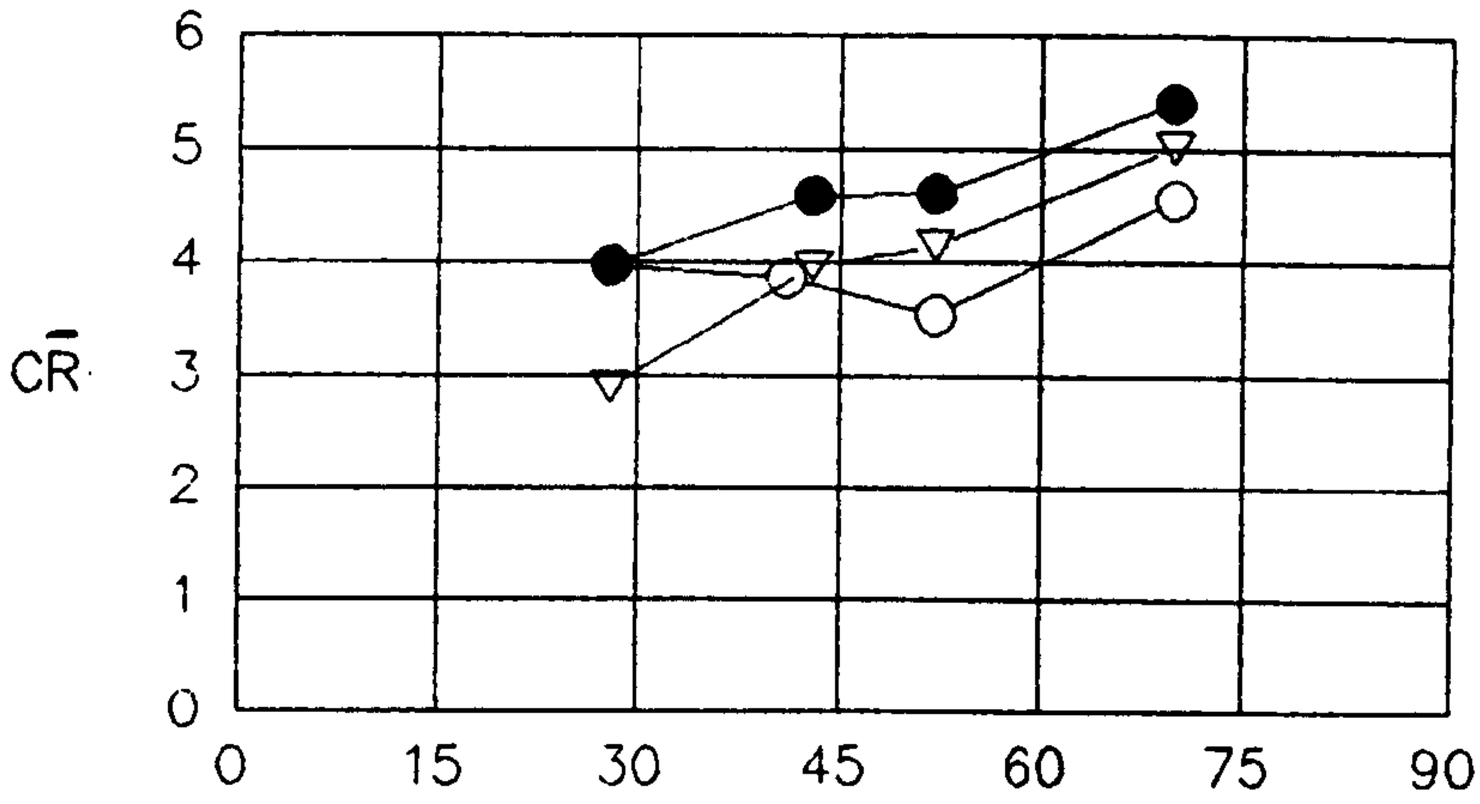

Figure 8.16 Mean lee bottom corner rolling moment coefficient for first series of moving model DB containers.
Level ground ABL simulation.
o config. B , ● config. C, ▽ config. D.

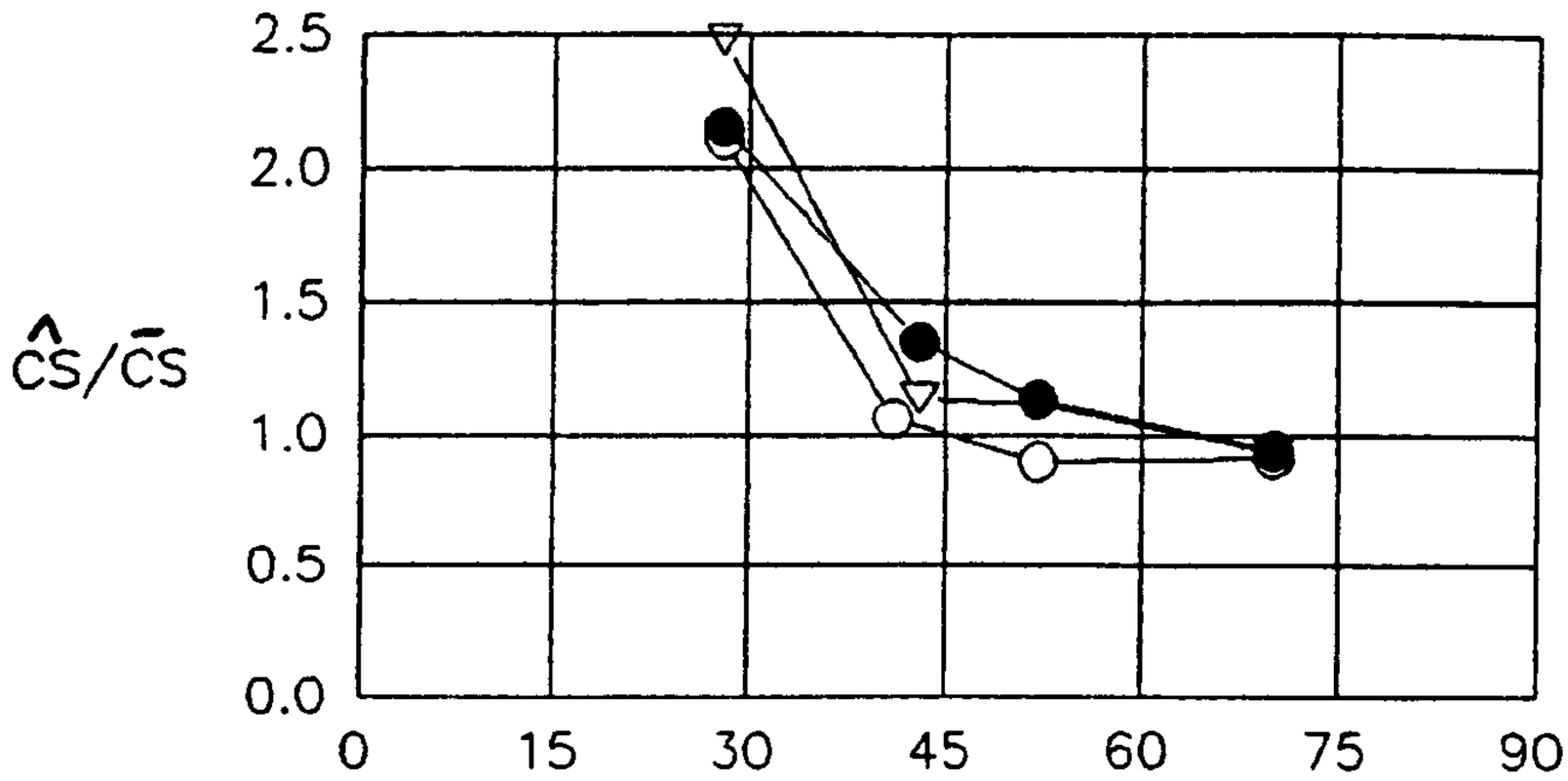

Figure 8.17 Normalised extreme side force parameters for first series of moving model DB containers.
Level ground ABL simulation.
o config. B , ● config. C, ▽ config. D.

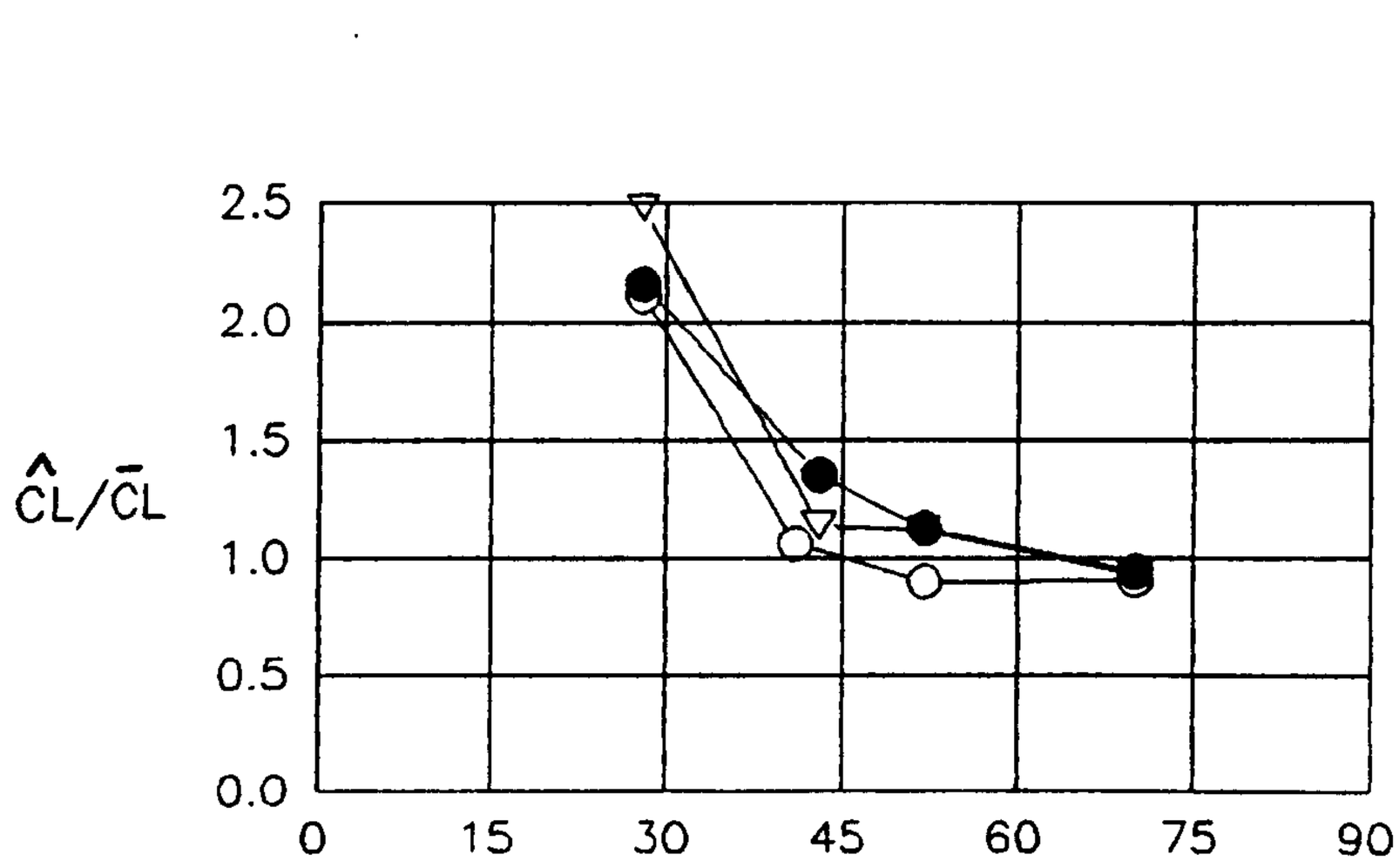

Figure 8.18 Normalised extreme lift force parameters for first series of moving model DB containers.
Level ground ABL simulation.
o config. B , ● config. C, ▽ config. D.

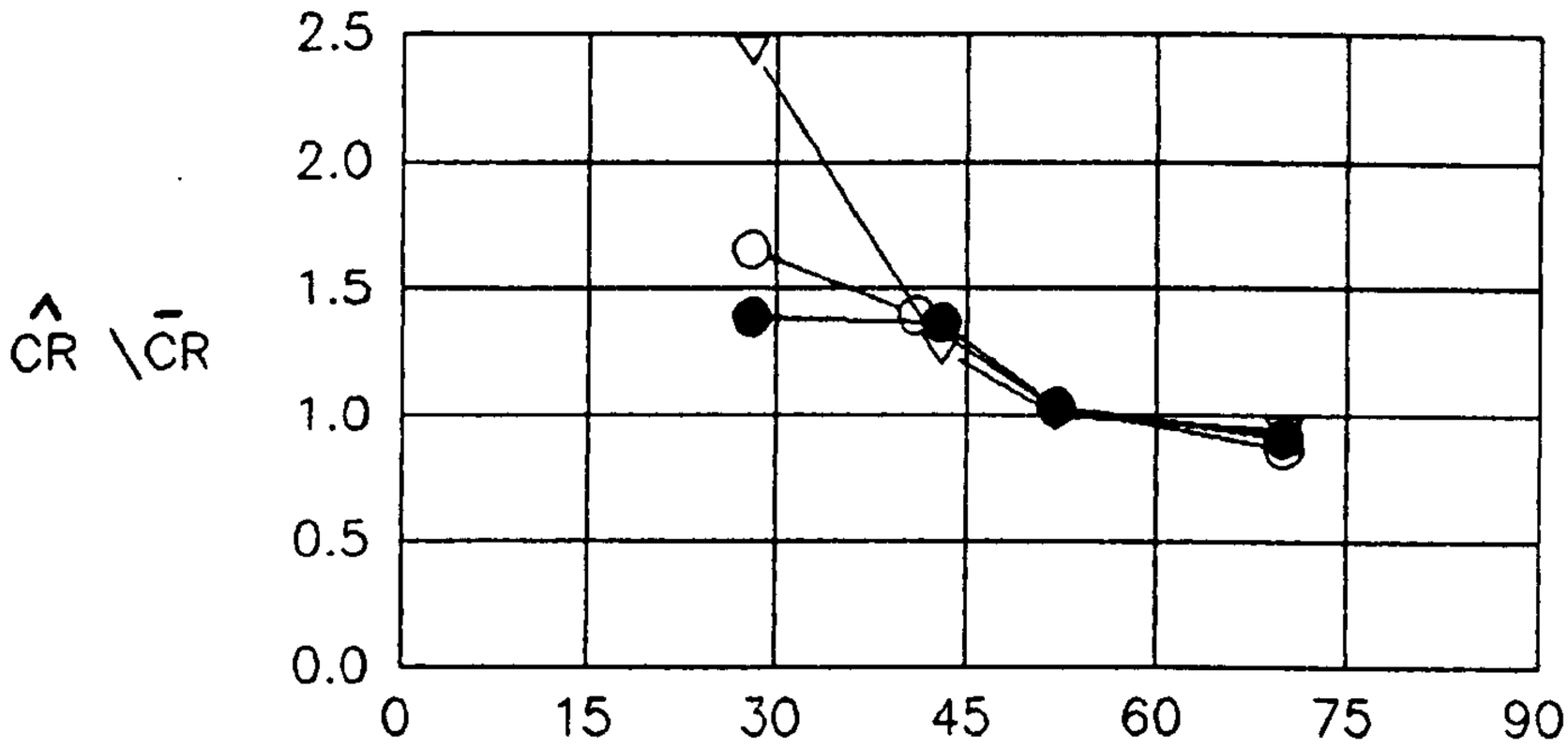

Figure 8.19 Normalised extreme lee bottom corner roliing moment parameter for first series of moving model DB containers. Level ground ABL simulation.
o config. B , ● config. C, ▽ config. D.

9. The Second Series of Moving Model Tests.

These tests, using the modified moving model rig described in section 4.2.3, took place as a continuous test series which started in November 1991 and was completed at the end of January 1992. Four geometries, with the 1/50th scale lorry, were tested, all with the common upstream ABL as described in section 6.2, as follows:

1. Flat ground as for the first test series and for direct comparison with the static test results.

2. Escarpment, equivalent to a full scale height of 5m.

3. Escarpment with a 50% porosity slatted fence upstream of moving model.

The full results and details of the geometry and wind conditions at the test position for each of the above geometries are given in sections 9.2 to 9.5 respectively. Tables 9.1 to 9.3 give details of the test conditions used for these geometries.

Using the flat ground simulation some runs were conducted at repeat yaw angles using both a lower vehicle speed and a lower wind speed in order to validate the extreme value analysis method and check for Reynolds number effects by comparison of the mean values. (Table 9.1.)

For all the moving model tests only data from the central 1.5m of the 2.7m working section width were extracted to ensure a reasonable consistency of the wind characteristics. Also all wind velocities used for calculating the non dimensionalised force and moment coefficients were averages of measurements made in 5 positions across the central 1.5m test section. (Chapter 6).

The effect of the mechanical noise, generated during the moving model tests, is discussed in section 9.1. and the likely errors due to this on the calculated overall mean forces and moments, and the extreme force values, are quantified.

Analysis was conducted as described in section 5.3.3 for the mean force and moment coefficients, their non dimensional points of action, extreme values and unsteady parameters for a model time scale of around 0.1s, this time being taken to be equivalent to a 3s full scale gust. Note that this is not a precise value as it was decided to split the data from each run into an integer number of segments rather than waste

data. The extreme forces and unsteady parameters were calculated using the resultant extreme velocity for the corresponding model time period. For some of the level ground simulation tests where the duration of the run across the test section was an integer value longer than the nominal 0.1s, typically for the larger yaw angles, the extreme values and unsteady parameters were additionally calculated for these longer time scales. This was done in order to assess the sensitivity of these parameters with model time scale as discussed in section 3.4. Tables 9.1 to 9.4 indicate the number of segments the data of individual runs were divided into prior to the analysis and the corresponding model transit time across the central 1.5m of the working section. Note that the model gust time of 0.1s was not adhered to for the escarpment tests, see section 9.4.

A full extreme value analysis procedure such as Liebliens', as used for the static tests and described in section 5.1.5, has not been developed for dealing with the discrete average values such as obtained from the moving model rig. Experience of calculating extreme values from the static test data described in Chapters 4 and 7 showed that in the engineering context of this research this was no detriment upon the accuracy of the hourly extreme values that were calculated because the dispersion of the analysed ensembles was found to be so low as to make such analysis unnecessary compared to the uncertainty due to the mechanical noise of the moving model rig. Both the data analysis method used and the justification for this simplified extreme value analysis method are described fully in section 9.2.2.

9.1 Moving Model Rig Data Quality and Data Analysis Discussion.

Figure 9.1 shows a typical set of raw data recorded from the 5 component balance during a run of the moving model rig with the wind tunnel operating at maximum speed. It is clear that the recorded signals were contaminated by high frequency mechanical noise. Figure 9.2 shows the results of transforming this sampled data into the frequency domain. Probably some of the low frequency energy shown in the spectra were ailiaised higher frequencies due to the relatively low, 400Hz, sample frequency of the data logger. Ideally these signals should be passed through an electronic low pass analogue filter before being digitally recorded. Unfortunately the Polycorder data logger could not do this and reliance was placed in designing the rig such that the mechanical noise was only present at very high frequencies so that it could be averaged out over the much longer time scales of interest. Post data acquisition digital filtering by computational methods was also tried in an attempt to remove some of this mechanical noise and this is also described in what follows.

It is clear that the shorter the time period for which the data was averaged the greater the influence of the relatively high frequency mechanical noise. For an actual mean force or moment calculation the signal for the relevant channel was averaged over 50 or 100 runs whilst the extreme values, depending upon the chosen time scale were calculated from signals averaged over a quarter, a half or over one run. These extreme values were taken to be equivalent to a full scale gust of 3s. It is seen that in order to achieve a high signal to noise ratio for the calculated extreme values then it is important to ensure that the mechanical noise is only *apparent* at high frequencies, i.e. not only ensuring that the mechanical noise is present at high frequencies but also that the ailiaised components of these frequencies are also allocated to the high frequencies in the digitisation process.

Tests were conducted with a box fitted around, but not touching, the live model, in order to determine the influence of the mechanical noise on the analysed data. These are referred to as the 'off wind' tests. Ten runs of the moving model rig were conducted at the 4 different trolley speeds that were used for the aerodynamic moving model tests.

For each set of 10 'off wind' runs, at each of the 4 trolley speeds, the ensemble of equivalent 3s gust moment and force coefficients were formed for the different time scales required. The force and moment coefficients, the extreme force coefficients and the normalised extreme force parameters were calculated from this data. These coefficients were for direct comparison with the aerodynamic tests and so were formed for each of the resultant wind (mean and extreme values) and trolley speeds used in the aerodynamic tests. Further the mean and standard deviation of these calculated coefficients were formed. The calculated mean values are given in table 9.4. Two tables are shown for the calculated standard deviations; table 9.5 utilising a mean wind speed for the normalisation and table 9.6 utilising the extreme wind speed. The calculations made use of the zero, non moving, measurements taken at the end of the run and rejected data if a drift of 2% or greater was found as for the aerodynamic tests described in sections 9.2, 9.3 and 9.4.

The derivation of the means and standard deviations given in tables 9.4, 9.5 and 9.6 were repeated with the raw data that had been digitally filtered at 10Hz, this being the highest frequency of interest in the formation of the extreme values using the time domain method. However the means were only altered by up to 1% and the standard deviations lowered by less than 5%. This lack of significant improvement in the aerodynamic signal to mechanical noise ratio was due to the inevitable ailiasing in the

digitising of the original analogue signal. As the filtering program took several seconds, due to the forward and reverse FFT of 'unfriendly' numbers of data (i.e. not a power of 2 and sometimes prime, see section 5.3.3), the simpler analysis of averaging the data over the time periods of interest was considered adequate. This simple method was also used for the aerodynamic tests.

The mechanical noise was quantified as a mean value and the standard deviation. The mean is an additional zero correction that should be applied to the aerodynamic test results. The standard deviation represents the likely error on the repeatability of a value. Note that both the mean and the standard deviation of a set of values calculated in the same manner, in this case a constant time scale, from a random set of data is independent of the number of values from which it is formed and so these values calculated from the 10 'off wind' tests, shown in tables 9.4 and 9.6, can be applied directly to the extreme value coefficients formed from the aerodynamic tests which took place over 50 or 100 runs.

It should be noticed that whilst the means calculated for the mean force coefficients and the extreme force coefficients can be applied directly to the aerodynamic tests, only the standard deviation values for the extreme force coefficients, shown in table 9.6, should be used directly as the likely error on the aerodynamic results due to mechanical noise. The mean force coefficients are formed from further averaging of all the test data and thus the likely error will be much lower. This is demonstrated by referring to table 9.5 where it is seen that the calculated standard deviations of the mean force coefficients from a given test series reduce as the number of segments a run is divided into reduces, i.e. the time scale increasing. Indeed this may be thought to apply to the calculated extreme value force coefficients derived over longer time periods. However the values of relevance here are those shown in table 9.6 where this effect is not noticeable due to the variation of the normalising extreme velocity. The extreme velocity reduces as the time period extends resulting in a fairly constant extreme value force coefficient standard deviation.

The likely error, defined to be the standard deviation, due to mechanical noise of the mean force coefficients determined over runs of 50 to 100 runs can be calculated from the standard deviations already formed, shown in table 9.5, in the following manner:

$$S.D.(N) = \frac{1}{\sqrt{N}}\sqrt{\sum_{i=1}^{N}(S.D.(i))^2} \qquad 9.1$$

Noting that the standard deviation due to mechanical noise, for each yaw angle, for each run of the moving model run is a constant value, say $S.D.(i=1)$, i.e. one value from table 9.5, then equation 9.1 can be written as:

$$S.D.(N) = \frac{1}{\sqrt{N}}(S.D.(i=1)) \qquad 9.2$$

Therefore it is seen that the standard deviation of the mechanical noise on mean force and moment values calculated over a number of runs falls inversely with the square root of the number of runs. Table 9.4 shows that the standard deviation for one run is generally less than 4% of the value of the mean force or moment and therefore the likely error will be less than 0.5% for calculations of mean values for 50 runs and over.

Similarly this equation can be applied to calculate the likely error on the mean correction due to mechanical noise over the 10 runs for each trolley speed Again referring to table 9.5 it is seen that these errors will be similar in magnitude to the mean values given in table 9.4. Therefore as these mean force and moments due to mechanical noise lie within the likely error of their measurement they were not used for further correcting the aerodynamic data.

9.2 Flat ground tests.

One of the main problems of moving model tests is the attainment of aerodynamic equilibrium in the short transit time of the moving model across the wind tunnel working section. As described in section 9. the additional time that the model spends in the wind, along the 0.6m upstream length before data to be analysed is extracted, should aid this. Although the wind conditions in the region nearest the wind tunnel wall vary compared with those measured in the centre of the working section they are similar enough to enable the flow pattern around the moving vehicle to stabilise. Figures 9.3 and 9.4 show the calculated mean force coefficients, filtered at 50Hz over 100 runs for the highest and lowest trolley speeds. It is seen that aerodynamic equilibrium has been reached prior to entry of the test section.

In Chapter 6 it was shown that the measured characteristics of the ABL for the moving model tests are very similar to those provided for the static tests described in Chapter 7 enabling comparisons to be made between the static tests and these moving model tests.

9.2.1 Mean forces and moments.

Figures 9.5 to 9.9 show the mean forces and moments, the latter translated to the vehicles centre of mass, compared to the static results of Coleman (1990). These include the additional moving model tests indicated in table 1 as Reynolds number tests. The side force coefficient results show excellent agreement but a problem with the lift force coefficients is evident by their non agreement at the yaw angle of 90° degrees, i.e. with the moving model stationary in the centre of the working section. Repeat measurements at these positions indicated that this was a real effect and may be therefore due to the effect of the slot through which the moving model supports travel. Although the moving model rig is also fully enclosed in the working section and so no pressure difference exists across the slot it could stop the development of a possible low pressure region under the floor of the vehicle and therefore allow the high suction above the vehicle's roof, to dominate and give rise to a greater lift force. The high suction on the roof of the lorry is caused by delta wing vorticies, starting from the front sharp edged windward corner of the container roof, for most of the yaw angle range, see Coleman(1990). Interestingly the high lift force coefficients, measured from the tests described in this thesis, are similar to those measured on a 1/25th scale identical vehicle type in uniform low turbulence flow at a much higher Reynolds number of 2.4×10^5, see Chapter 2 and Baker (1987). The low turbulence static tests of Coleman (1990), see Chapter 2, also show a much lower lift force compared to Baker (1987); Coleman (1990) offers a reasonable explanation of this discrepancy based on possible bending of the model's supports, with the effect of such vehicle camber experimentally demonstrating a very similar effect. However Peters (1993) shows the results of low turbulence static sharp edged container wagon tests, see Chapter 7, showing an increase in lift force with increasing wind speed and model size. Further Peters (1993) shows that the lift forces increases with increasing Reynolds number. Although satisfactory Reynolds number tests were conducted of the model vehicle for the tests described in this thesis the evidence suggests that the explanation for this poor agreement may be the very low local Reynolds number of the passage of air, attenuated in these tests by the modelling of a sheared flow, under the model vehicle. Comparisons of the moment coefficients for the static and moving tests also indicate something aerodynamically significantly different. As expected the pitching moment, which is calculated in part using the lift force value, is altered drastically. However the lift force does not contribute in the calculation of the yawing and rolling moment coefficients about the vehicle's centre of mass but for the moving model tests, the yawing moment is much reduced and the rolling moment reduced at low yaw angles and increased at high yaw angles.

Figures 9.10 to 9.12 show the non dimensional points of action for the side and lift forces compared with the static test results. These further illustrate the observations already made. For the moving model tests both the horizontal points of action of the side and lift forces are slightly (a few millimetres) nearer the vehicle's centre of gravity than found for the static tests.

9.2.2 Extreme force values.

Tables 9.9a and b lists the top 10 normalised extreme force values for the side and lift forces derived from the 100 runs of the moving model rig. Note that the equivalent full scale time of 100 runs is between 5 and 20 minutes depending on the number of segments each run is divided. (Each segment corresponding to 3s full scale gust). There are two points to note:

1. The difference between the values for each channel is much less than those indicated from the mechanical noise standard deviation values shown in table 9.6.

2. In the context of the extreme value analysis, the dispersion (defined in section 5.1.5), as for the static tests in Chapters 7 and 8, was small.

Therefore it is reasonable to merely take one of these values as the most likely extreme value, say the maximum, to be the mode corresponding to the total sample time. Thus no further extrapolation was used in the calculation of the hourly extreme value justified by the very low dispersion. In summary the hourly extreme values and the unsteady parameters were therefore obtained by simply taking the maximum value from the ensemble of 0.1s values produced by the moving model rig.

In the following sections of this chapter, in the description of the extreme force values analysed from the moving model tests, no difference between the measured extreme value, the mode corresponding to the sample time or the ensuing extreme value over one hour periods will be emphasised. All these extreme values will be similarly described.

Tables 9.8a and b show the calculated normalised extreme force parameters and the unsteady parameters against model time periods, taken to be equal to the full scale 3 second gust period. These were calculated for the yaw angles of 53 and 70 degrees only as these were the only yaw angles for which the trolley transit time was long enough to enable such an analysis to be conducted. (Section 9.1 and table 9.1.) These

were calculated using the method of section 5.3.3.1 It is seen, as for the static tests described in Chapter 7, that the normalised extreme force parameter is independent of the model time scale, over the range shown, and the mechanical noise small in comparison.

Table 9.9 shows the extreme values of the normalised extreme force parameters and the unsteady parameters for taking the full scale 3 second value to be equal to 0.12 seconds for all yaw angles. This value of 0.12s was attainable for all yaw angles without the waste of any data. Also included in this table are the Reynolds number tests and the mechanical noise standard deviation from table 9.6 for the extreme force parameters. In interpreting the accuracy of the data, bearing in mind the many values similar to these maxima present in the distribution, it is probably safe to interpret these as an upper limit and that the true extremes are in the region of the value given minus up to one standard deviation. Figures 9.13 to 9.16 compare these results with those obtained from the static turntable simulation. For both the static and the moving tests the quasi steady state is seen to exist at most yaw angles except at the very lowest where some evidence of unsteadiness is apparent.

It may be expected that the normalised extreme force parameters for the pitching moment about the lorry's centre of gravity would be similar to that of the lift force as the latter is the dominant contribution. Likewise the yawing and rolling moment normalised extreme values can be compared with those of the side force. Table 9.10 shows the calculated normalised extreme values and the unsteady parameters for the moments for each yaw angle for a model time period of around 0.12s. Comparing the results with table 9.9 it is seen that, as expected, these normalised extremes are similar; to within the experimental error as suggested by the mechanical noise standard deviation which are also shown in these tables. Only the side and lift extreme force parameters were calculated for the other geometries tested.

9.3 Escarpment tests without wind fences.

The escarpment simulation, with the live model mounting arrangement, is shown in figure 9.17. This includes the wind fence position used for the tests to be described in section 9.4. Figure 9.18 shows a photograph of the simulated escarpment (with the wind fence in place). The escarpment is of an equivalent full scale height of 5m with a bank 5m full scale upstream of gradient 30°. The escarpment continues for an equivalent full scale distance of 50m behind the moving model and therefore gives a good representation of a typical 3 lane (in each direction) motorway embankment with

the lorry travelling in the nearest lane to the oncoming wind. One difference however is the lack of camber, usually provided for rain run off, on the full scale version. This will be discussed further in what follows.

The geometry of the ABL devices were identical to that used for the flat ground tests and so the ABL modelled just upstream of the escarpment is similar to the flat ground simulation. Unless stated otherwise, the reference wind speed for calculating the resultant mean and extreme values are made from measurements at a height of 60mm, equivalent to 3m full scale, above the top of the escarpment at the moving model position. The wind characteristics at the moving model position are shown in figures 9.19 to 9.24. All these values are measured and calculated in the same manner as those in Chapter 6.

Note that the flow is more uniform, with height, compared to the level ground simulation shown in Chapter 6 and that the extreme wind velocity values are also much reduced.

9.3.1 Mean forces and moments.

Figures 9.25 to 9.29 show the mean forces and moments compared with the level ground moving results of section 9.2.1. Due to a problem with data collection on channel 1 which caused large fluctuations in the raw data the pitching moment data was calculated only using the lift force data. From knowledge of the contributions from the lift force and measured pitching moment towards the pitching moment about the centre of gravity for the static tests it is expected that the pitching moment about the C. of G. derived only from the lift data will be in error by less than 10%. Similarly the error in the calculation of the other force coefficients due to the lack of correction due to interaction of the balance with the pitch channel is less than 2%.

Comparisons of the data with those of the level ground simulation show very similar results, the largest differences, being for the lift coefficient, the lift coefficient for the embankment tests increasing at lower yaw angles but reducing a little for the higher. This may be attributable to the likely change in flow direction that this simulation produces. The flow streamlines are likely to have some vertical component at the roof of the vehicle.

Figures 9.30 and 9.31 show the non dimensional point of actions for the side forces again compared well with the level ground results. The non dimensional point of

actions for the lift force could not be calculated due to lack of accurate pitch information.

9.3.2 Extreme force values.

Figures 9.32 to 9.35 show the normalised extreme force values and the unsteady parameters for the side and lift forces compared with the level ground moving results. As for the level ground tests these extremes were calculated using a model gust time of around 0.12s. Comparisons of the values for the case without wind fences with those for the level ground simulation show excellent agreement. The quasi steady case for body induced unsteadiness is seen to exist at all yaw angles except at the lowest where some body unsteadiness is present.

9.4 Escarpment with wind fence tests.

The wind fence used for these tests is of a simple sharp edged slatted design of 50% porosity and it is situated at the top of the bank a distance of 5m upstream of the near side of the moving lorry. Figure 9.36 shows the geometrical details of the fence. The layout of the ABL simulation is identical to that described in section 9.3.

The aim of these tests was to investigate the effect of the wind fence compared to that if there were no fence present and so the magnitude of the reference wind velocities are those defined in section 9.3, i.e. as if the wind fence were absent. Of course it was not possible to measure the wind velocity at this position accurately with the wind fence present or calibrate an anemometer at this position accurately to another reference anemometer due to its proximity to the wind fence. The detailed construction of the fence and its slatted nature caused the wind characteristics to vary enormously with small differences in the measurement position as shown in figure 9.37. Instead a calibration to the wind velocity measured in section 9.3, that is without the wind fences, in the centre of the working section at the moving model position, was provided by means of an additional anemometer reading at a height of 200mm and 600mm forward of the embankment. The definition of yaw angle, also uses this wind velocity. See table 9.3 for the normalising mean wind speeds. The use of the force and moment coefficients calculated for the wind fence tests are limited to the direct comparison with the data without the fences.

The measured wind speeds, turbulence intensity variations with height at the moving model position with and without the wind fences present are shown in figures 9.37 and

9.38. The wind speeds are not needed for the calculation of the results in this section, but nevertheless of interest to aid their understanding. Figures 9.39a to c shows the streamwise wind velocity spectra measured at the moving model test position with the fence present at a range of heights. It is seen that, comparing these figures with 9.23, without the wind fence present, the slatted wind fence breaks up the large, low frequency, eddies into much smaller high frequency components. Chapter 6 shows that the simulated ABL, without the fences present, did not vary very much with height above the ground over the range considered.

Bearing in mind the 3D nature of turbulence, the spanwise lateral semi lengthscale will also be similarly reduced, possibly by a factor of 20, for these wind fences. This effect will break up the correlation of the fluctuating extreme forces on the lorry, as the lorry, behind the fence, will be of much larger dimensions than the characteristic eddy size. Consequently the effect of the wind fences on the extreme forces on a lorry may be marked. Indeed the extreme forces could well be reduced by amounts larger than that predicted from consideration of the mean forces alone.

Due to the large reduction in wind speed caused by the wind fences, from Reynolds number considerations, only the yaw angles utilising the maximum wind tunnel speed were tested.

9.4.1 Mean forces and moments.

Figures 9.40 to 9.44 show the mean forces and moments compared with the results without the wind fence present described in section 9.3.1. Identical problems with the measured pitch channel as in section 9.3 were encountered which degrades the accuracy of the pitch channel about the lorry's C. of G. to 10% and the other forces and moments to 2%. See section 9.3.1 for further details.

The presence of the wind fences reduce the side force coefficient and hence the rolling and yawing moment coefficients to values of only 20% of the value without the fences present. The lift force, and therefore the pitching moment also, are only reduced to around 50% of the value without the fences. This is to be expected as the lift forces are dominated by the roof flow, as discussed in section 2.2.1.1, which is above the height of the fence.

Figures 9.45 and 9.46 show the non dimensional point of actions for the side forces again compared with the static test results. The non dimensional point of action for the

lift force is not shown due to the lack of accurate pitch information. It is seen that the non dimensional point of action of the side force is increased compared to the value without the wind fences which is expected due to the top part of the lorry being above the top part of the fence. The non dimensional horizontal point of action for the side force however is reduced a little at high yaw angles.

Coleman (1990) also undertook similar measurements of this vehicle using wind fences of identical geometry as well as other wind fence types. In these tests the vehicle was mounted static on a bridge deck and experienced uniform flow with the grid turbulence characteristics described in section 2.2.1.1. As a comparison of these different testing techniques table 9.11 shows comparisons of the mean side and lift force coefficient reductions due to wind fences from Coleman (1990) and the moving model tests with the simulated ABL described in this thesis. Table 9.11 expresses the results in terms of the mean side or lift force coefficient ratio, defined to be the ratio of the mean force coefficient with the fences to the mean force coefficient without the fences. It is seen that the mean side force coefficient ratio between the tests are very similar but that the mean lift force reductions of the tests of Coleman (1990) show much larger reductions. The reduction in the mean lift force coefficient for the recent moving model tests, due to the wind fences, is around 40% whilst it is around 90% to 120%, i.e. producing negative lift, for the tests of Coleman (1990).

9.4.2 Extreme force values.

The normalised extreme force values and unsteady parameters taking the model gust time to be 0.12s are shown compared to the embankment results without the wind fence in figures 9.47 to 9.50. Note again that these extremes have been calculated using the wind velocities and the extreme / mean velocity ratio as if the wind fences were absent. The extreme / mean velocity ratio was therefore read from figure 9.23, which was also used for the results without the wind fence.

The effect of the wind fence is seen to increase the normalised extreme side force parameter whilst this parameter for the lift force remains identical for the case without the wind fences present. Table 9.12 compares the extreme side and lift forces with and without the wind fences with those of Coleman (1990). Coleman's tests, for extreme value analysis, were limited to yaw angles of 60 and 90 degrees. Generally it is seen that the moving model escarpment tests with the ABL simulation show normalised extreme side and lift force parameters a little over unity compared to values slightly less from the uniform gird turbulence static bridge deck tests of Coleman (1990).

Considering the magnitude of the extreme side forces first, it is seen that the moving model escarpment tests with the ABL simulation give the larger results due to the similar results for the side forces between this test series without the fences present, referring to figures 7.3, 9.5 and 9.13, and the similar reduction due to the fences including the geometry difference, table 9.11. However the actual magnitude of the extreme lift force values is complicated due to the differences between the mean values of the lift forces of these two test series. With the aid of figures 7.4, 9.6 and 9.14, it is seen that the moving model tests produced unexpected large lift forces, compared to Coleman (1990) without the presence of the fences but referring to table 9.11 the tests of Coleman (1990) show large and difficult to explain reductions due to the fences.

Table 9.1 Flat ground moving model test series.

100 runs at each yaw angle.

Moving model speed. (m/s)	Wind tunnel speed. (m/s)	Yaw angle. (degrees)	Model transit time. (s)	Reynolds number.	No. of segments for which analysis conducted.
3.06	8.5	70.2	0.49	4.0×10^4	1, 2, 4
6.40	8.5	53.0	0.24	4.8×10^4	1, 2
10.51	8.5	39.0	0.14	6.3×10^4	1
12.19	5.1	22.7	0.12	5.6×10^4	1
6.40 #	5.3	39.6	0.24	3.4×10^4	2
6.40 #	6.4	45.0	0.24	4.0×10^4	2
3.06 #	6.4	64.4	0.49	2.5×10^4	4

These were extra tests conducted for Reynolds number checks and are of 50 runs. Extreme value analysis was limited to a single segment number chosen to correspond to a model time scale of around 0.12s.

Table 9.2 Escarpment moving model test series.

50 runs at each yaw angle.

Moving model speed. (m/s)	Reference Wind tunnel speed. (m/s)	Yaw angle. (degrees)	Model transit time. (s)	Reynolds number.	No. of segments for which analysis conducted.
2.81	10.5	75.1	0.54	4.8×10^4	4
6.15	10.5	59.8	0.24	5.4×10^4	2
10.79	10.5	44.1	0.14	6.7×10^4	1
10.95	7.2	33.5	0.14	5.8×10^4	1

Table 9.3 Escarpment with wind fence moving model test series.

50 runs at each yaw angle.

Moving model speed. (m/s)	Reference Wind tunnel speed. (m/s)	Yaw angle. (degrees)	Model transit time. (s)	Reynolds number.	No. of segments for which analysis conducted.
3.02	10.5	74.2	0.50	4.8×10^4	4
6.05	10.5	53.0	0.25	5.4×10^4	2
10.71	10.5	44.1	0.14	6.6×10^4	1

Table 9.4 Mean mechanical noise as a function of trolley speed.

Mean force and moment mean coefficients from 10 runs at 4 trolley speeds.
Calculations of the coefficients are given for normalising velocities identical to those of the aerodynamic tests given in tables 9.1 to 9.4.

Moving model speed (m/s)	Ref. wind speed (ref. ht = 3m) (m/s)	Pitching moment coefficient	Yawing moment coefficient	Rolling moment coefficient	Side force coefficient	Lift force coefficient
3.06	8.5	-5.0×10^{-2}	1.1×10^{-1}	6.8×10^{-3}	4.8×10^{-2}	4.0×10^{-2}
3.06	6.4	-7.4×10^{-2}	1.2×10^{-1}	5.2×10^{-3}	5.3×10^{-3}	5.9×10^{-2}
6.40	8.5	2.2×10^{-2}	4.5×10^{-1}	3.7×10^{-2}	1.5×10^{-1}	-1.7×10^{-2}
6.40	6.4	5.9×10^{-2}	4.5×10^{-1}	3.9×10^{-2}	1.5×10^{-1}	-4.7×10^{-2}
6.40	5.3	8.4×10^{-2}	4.9×10^{-1}	4.1×10^{-2}	1.6×10^{-1}	-6.6×10^{-2}
10.51	8.5	2.4×10^{-1}	5.8×10^{-1}	8.7×10^{-2}	1.7×10^{-1}	-1.9×10^{-1}
12.19	5.1	-3.8×10^{-1}	3.8×10^{-1}	3.0×10^{-2}	1.5×10^{-2}	3.0×10^{-1}

Table 9.5 Mechanical noise standard deviation normalised by the mean resultant wind speed as a function of trolley speed and analysis time scale.

Coefficients given in this table are normalised by the mean resultant wind speed corresponding to the test case and segment number. i.e. that of the mean wind speed at the equivalent full scale reference height of 3m and the moving model speed.

Moving model speed (m/s)	Reference mean wind speed. (ref. ht. = 3m) (m/s)	Number of segments	Pitching moment coefficient	Yawing moment coefficient	Rolling moment coefficient	Side force coefficient	Lift force coefficient
3.06	8.5	4	3.3×10^{-1}	3.2×10^{-1}	8.6×10^{-2}	1.9×10^{-1}	2.6×10^{-1}
3.06	8.5	2	2.3×10^{-1}	1.9×10^{-1}	4.6×10^{-2}	1.1×10^{-1}	1.8×10^{-1}
3.06	8.5	1	2.1×10^{-1}	1.4×10^{-1}	3.5×10^{-2}	4.7×10^{-2}	1.6×10^{-1}
3.06	6.4	4	3.7×10^{-1}	3.9×10^{-1}	9.0×10^{-2}	2.0×10^{-1}	2.9×10^{-1}
3.06	6.4	2	2.5×10^{-1}	2.8×10^{-1}	4.8×10^{-2}	1.3×10^{-1}	1.9×10^{-1}
3.06	6.4	1	2.8×10^{-1}	2.3×10^{-1}	3.7×10^{-2}	5.3×10^{-2}	1.8×10^{-1}
6.40	8.5	2	5.0×10^{-1}	3.8×10^{-1}	1.2×10^{-1}	2.1×10^{-1}	4.1×10^{-1}
6.40	8.5	1	2.8×10^{-1}	2.5×10^{-1}	9.7×10^{-2}	1.4×10^{-1}	2.3×10^{-1}
6.40	6.4	2	5.5×10^{-1}	4.1×10^{-1}	1.2×10^{-1}	2.2×10^{-1}	4.3×10^{-1}
6.40	6.4	1	3.5×10^{-1}	2.8×10^{-1}	9.9×10^{-2}	1.5×10^{-1}	2.5×10^{-1}
6.40	5.3	2	5.5×10^{-1}	4.3×10^{-1}	1.2×10^{-1}	2.3×10^{-1}	4.4×10^{-1}
6.40	5.3	1	3.2×10^{-1}	3.1×10^{-1}	1.0×10^{-1}	1.5×10^{-1}	2.8×10^{-1}
10.51	8.5	1	2.4×10^{-1}	5.3×10^{-1}	1.1×10^{-1}	2.8×10^{-1}	1.9×10^{-1}
12.19	5.1	1	3.9×10^{-1}	3.9×10^{-1}	6.4×10^{-2}	2.4×10^{-1}	3.1×10^{-1}

Table 9.6 Mechanical noise standard deviation normalised by the extreme resultant wind speed as a function of trolley speed and analysis time scale.

Coefficients given in this table are normalised by the extreme resultant wind speed corresponding to the test case and segment number quantifying the model time scale. i.e. the extreme wind speed is calculated by taking the mean wind speed at the equivalent full scale reference height of 3m multiplying it by the gust factor given in figure 6.21 corresponding to the model time implied by the segment number previously shown in table 9.1. The normalising wind speed is calculated using the extreme wind speed and the moving model speed. These figures should be used for quantifying the likely error of the aerodynamic extreme value force and moment coefficients.

Moving model speed. (m/s)	Reference mean wind speed. (ref. ht. = 3m) (m/s)	Number of segments	Pitching moment coefficient	Yawing moment coefficient	Rolling moment coefficient	Side force coefficient	Lift force coefficient
3.06	8.5	4	2.0×10^{-1}	2.0×10^{-1}	5.2×10^{-2}	1.2×10^{-1}	1.6×10^{-1}
3.06	8.5	2	1.7×10^{-1}	1.3×10^{-1}	3.0×10^{-2}	7.1×10^{-2}	1.2×10^{-1}
3.06	8.5	1	1.8×10^{-1}	1.1×10^{-1}	2.9×10^{-2}	3.8×10^{-2}	1.4×10^{-1}
3.06	6.4	4	2.3×10^{-1}	2.4×10^{-1}	5.4×10^{-2}	1.2×10^{-1}	1.8×10^{-1}
3.06	6.4	2	1.8×10^{-1}	2.1×10^{-1}	3.4×10^{-2}	9.0×10^{-2}	1.4×10^{-1}
3.06	6.4	1	1.9×10^{-1}	1.9×10^{-1}	2.8×10^{-2}	4.1×10^{-2}	1.4×10^{-1}
6.40	8.5	2	3.5×10^{-1}	2.6×10^{-1}	8.0×10^{-2}	1.4×10^{-1}	2.8×10^{-1}
6.40	8.5	1	2.2×10^{-1}	1.9×10^{-1}	7.5×10^{-2}	1.1×10^{-1}	1.8×10^{-1}
6.40	6.4	2	3.9×10^{-1}	3.0×10^{-1}	7.9×10^{-2}	1.6×10^{-1}	3.0×10^{-1}
6.40	6.4	1	2.8×10^{-1}	2.5×10^{-1}	7.8×10^{-2}	1.2×10^{-1}	2.2×10^{-1}
6.40	5.3	2	3.7×10^{-1}	2.8×10^{-1}	8.1×10^{-2}	1.5×10^{-1}	2.9×10^{-1}
6.40	5.3	1	2.5×10^{-1}	2.2×10^{-1}	7.6×10^{-2}	1.1×10^{-1}	2.0×10^{-1}
10.51	8.5	1	1.9×10^{-1}	4.2×10^{-1}	8.6×10^{-2}	2.2×10^{-1}	1.5×10^{-1}
12.19	5.1	1	3.5×10^{-1}	3.5×10^{-1}	5.7×10^{-2}	2.2×10^{-1}	2.8×10^{-1}

Table 9.7 The 10 maximum normalised extreme force parameters produced from 100 runs of the moving model rig.

All for equivalent full scale 3s gust.

a) Normalised extreme side force parameters.

Moving model speed (m/s)	3.06	3.06	3.06	6.40	6.40	10.51	12.19
Ref. wind speed (m/s)	8.5	8.5	8.5	8.5	8.5	8.5	5.1
No. of segments	1	2	4	1	2	1	1
	1.05	0.94	0.95	0.95	0.99	1.11	1.30
	1.05	0.93	0.89	0.93	0.98	1.10	1.30
	1.02	0.91	0.88	0.91	0.92	1.10	1.23
	1.00	0.91	0.87	0.88	0.90	1.02	1.21
	0.99	0.90	0.84	0.87	0.89	1.01	1.21
	0.99	0.88	0.83	0.86	0.85	1.00	1.18
	0.99	0.88	0.82	0.83	0.85	1.00	1.18
	0.99	0.88	0.82	0.82	0.83	0.99	1.12
	0.98	0.88	0.82	0.81	0.79	0.97	1.10
	0.98	0.87	0.81	0.81	0.77	0.96	1.08

b) Normalised extreme lift force parameters.

Moving model speed (m/s)	3.06	3.06	3.06	6.40	6.40	10.51	12.19
Ref. wind speed (m/s)	8.5	8.5	8.5	8.5	8.5	8.5	5.1
No. of segments	1	2	4	1	2	1	1
	1.04	1.00	1.10	1.09	1.15	1.10	1.42
	0.91	0.96	0.99	1.08	1.12	0.99	1.40
	0.85	0.95	0.99	1.04	1.09	0.82	1.37
	0.80	0.95	0.98	0.98	0.98	0.78	1.34
	0.78	0.89	0.98	0.92	0.92	0.76	1.31
	0.77	0.87	0.98	0.91	0.90	0.75	1.26
	0.75	0.87	0.98	0.88	0.89	0.73	1.20
	0.71	0.86	0.93	0.86	0.88	0.72	1.17
	0.63	0.84	0.89	0.83	0.88	0.66	1.17
	0.61	0.82	0.87	0.81	0.86	0.65	1.14

Table 9.8 Flat ground 3s equivalent full scale gust extreme values as a function of model time scale.

Mean wind tunnel reference speed = 8.5m/s (60mm = 3m full-scale).

a) Yaw angle = 53 degrees

Model time scale equivalent to 3s gust.	0.12	0.24
Unsteady side force parameter.	0.72	0.92
Normalised extreme side force parameter.	0.99	0.95
Mechanical noise S.D.	0.04	0.03
Unsteady lift force parameter.	1.88	1.68
Normalised extreme lift force parameter.	1.15	1.09
Mechanical noise S.D.	0.13	0.09

b) Yaw angle = 70 degrees

Model time scale equivalent 3s gust. (s)	0.12	0.24	0.49
Unsteady side force parameter.	0.67	0.61	1.54
Normalised extreme side force parameter.	0.95	0.94	1.05
Mechanical noise S.D.	0.03	0.02	0.01
Unsteady lift force parameter.	1.42	1.08	1.38
Normalised extreme lift force parameter.	1.10	1.01	1.04
Mechanical noise S.D.	0.07	0.05	0.05

Table 9.9 Summary of flat ground extreme force values for a model time period of around 0.12s equivalent to a full scale 3s gust.

Yaw angle (degrees)	26.9	39.0	39.6	45.0	53.0	64.4	70.2
Unsteady side force parameter.	6.51	2.41	1.98	1.44	0.72	1.23	0.67
Normalised extreme side force parameter.	1.30	1.11	1.09	0.97	0.99	1.06	0.95
Mechanical noise S.D.	0.10	0.07	0.05	0.04	0.04	0.03	0.03
Unsteady lift force parameter.	9.16	2.67	1.16	1.17	1.88	1.13	1.42
Normalised extreme lift force parameter.	1.42	1.10	1.24	1.10	1.15	1.13	1.10
Mechanical noise S.D.	0.31	0.11	0.20	0.17	0.13	0.08	0.07

Table 9.10 Summary of flat ground extreme moment values for a model time period of around 0.12s equivalent to a full scale 3s gust.

Yaw angle (degrees)	26.9	39.0	39.6	45.0	53.0	64.4	70.2
Normalised extreme pitching moment parameter.	1.51	1.10	1.14	1.08	1.09	1.04	1.01
Mechanical noise S.D.	0.24	0.12	0.23	0.19	0.16	0.09	0.08
Normalised extreme yawing moment parameter.	1.17	1.05	1.06	0.97	0.99	1.19	1.01
Mechanical noise S.D.	0.10	0.09	0.07	0.06	0.05	0.05	0.04
Normalised extreme rolling moment parameter.	1.29	1.08	1.15	1.11	0.95	1.13	0.95
Mechanical noise S.D.	0.14	0.10	0.10	0.09	0.08	0.05	0.04

Table 9.11 Comparison of mean side and lift force coefficient ratio with and without fences with previous grid turbulence, uniform profile, tests of Coleman (1990).

These yaw angles are approximate as they are formed from repeat moving model test series with and without the fences present, see tables 9.2 and 9.3. (* Static test)

Mean side force coefficient ratio.

Moving model tests.

Yaw angle (degrees)		44#	55#		75#		90.0*
Mean side force coefficient ratio. Escarpment simulation.		0.31	0.30		0.25		0.25

Coleman (1990).

Yaw angle (degrees)	30.0	40.0	50.0	60.0	70.0	80.0	90.0
Mean side force coefficient ratio. Bridge deck simulation.	0.39	0.33	0.28	0.27	0.22	0.20	0.18

Mean lift force coefficient ratio.

Moving model tests.

Yaw angle (degrees)		44#	55#		75#		90.0*
Mean lift force coefficient ratio. Escarpment simulation.		0.45	0.53		0.66		0.61

Coleman (1990).

Yaw angle (degrees)	30.0	40.0	50.0	60.0	70.0	80.0	90.0
Mean lift force coefficient ratio. Bridge deck simulation.	-0.20	-0.08	-0.02	0.03	0.13	0.01	-0.02

Table 9.12 Comparison of the normalised extreme side and lift force parameters for wind fence tests with previous grid turbulence, uniform profile, tests of Coleman (1990).

All for equivalent full scale 3s gust.

Moving model tests.

Yaw angle (degrees)	44.1	53.0	74.2	
Normalised extreme side force parameter. Escarpment simulation.	1.03	1.08	1.07	

Coleman (1990).

Yaw angle (degrees)		60.0		90.0
Normalised extreme side force parameter. Bridge deck simulation.		0.93		0.79

Moving model tests.

Yaw angle (degrees)	44.1	53.0	74.2	
Normalised extreme lift force parameter. Escarpment simulation.	1.50	1.30	1.20	

Coleman (1990).

Yaw angle (degrees)		60.0		90.0
Normalised extreme lift force parameter. Bridge deck simulation.		1.00		0.84

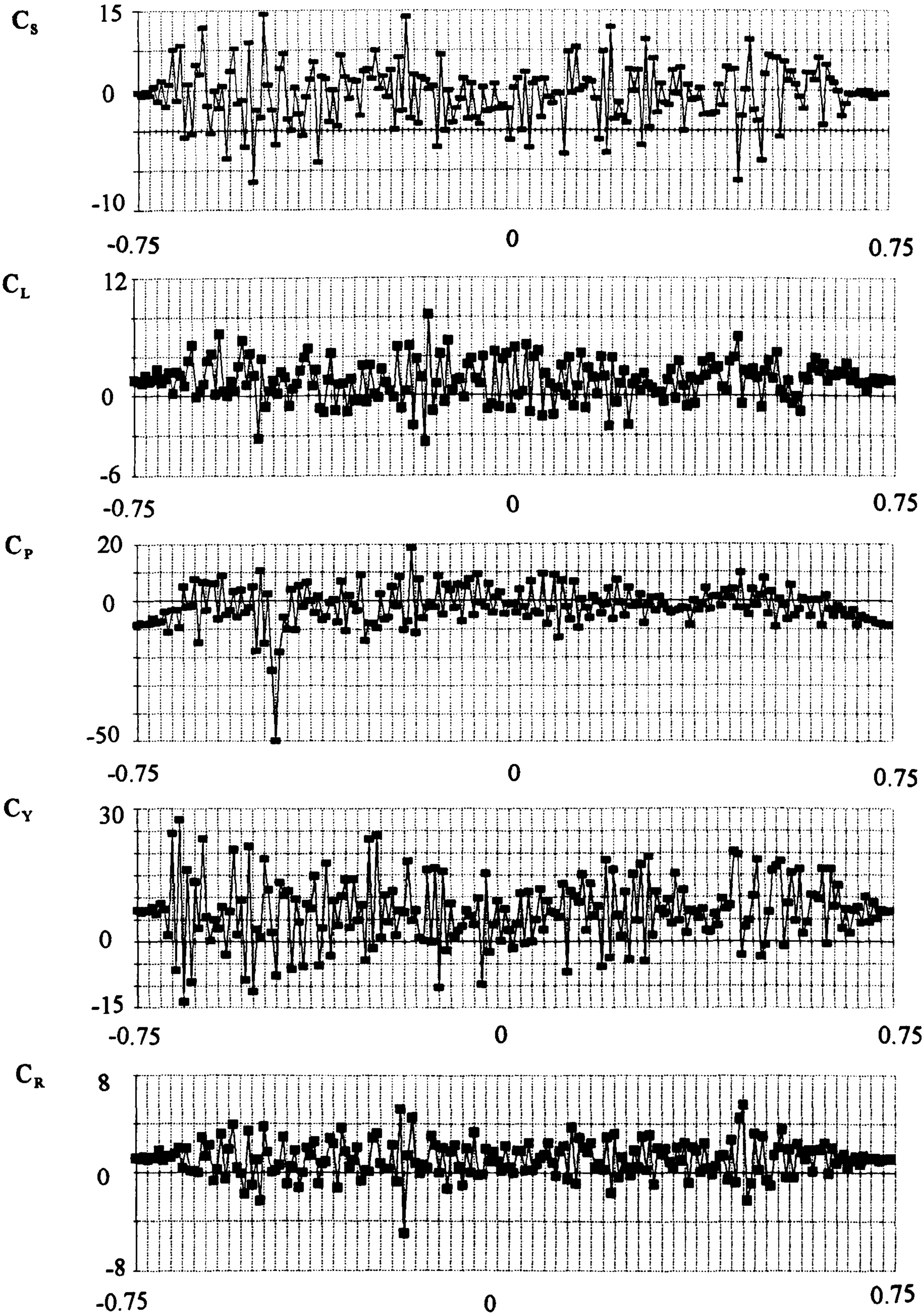

Figure 9.1 Time history from 1 run of moving model rig. Lorry on flat ground simulation, v = 3.06m/s, u (60mm) = 8.5m/s.

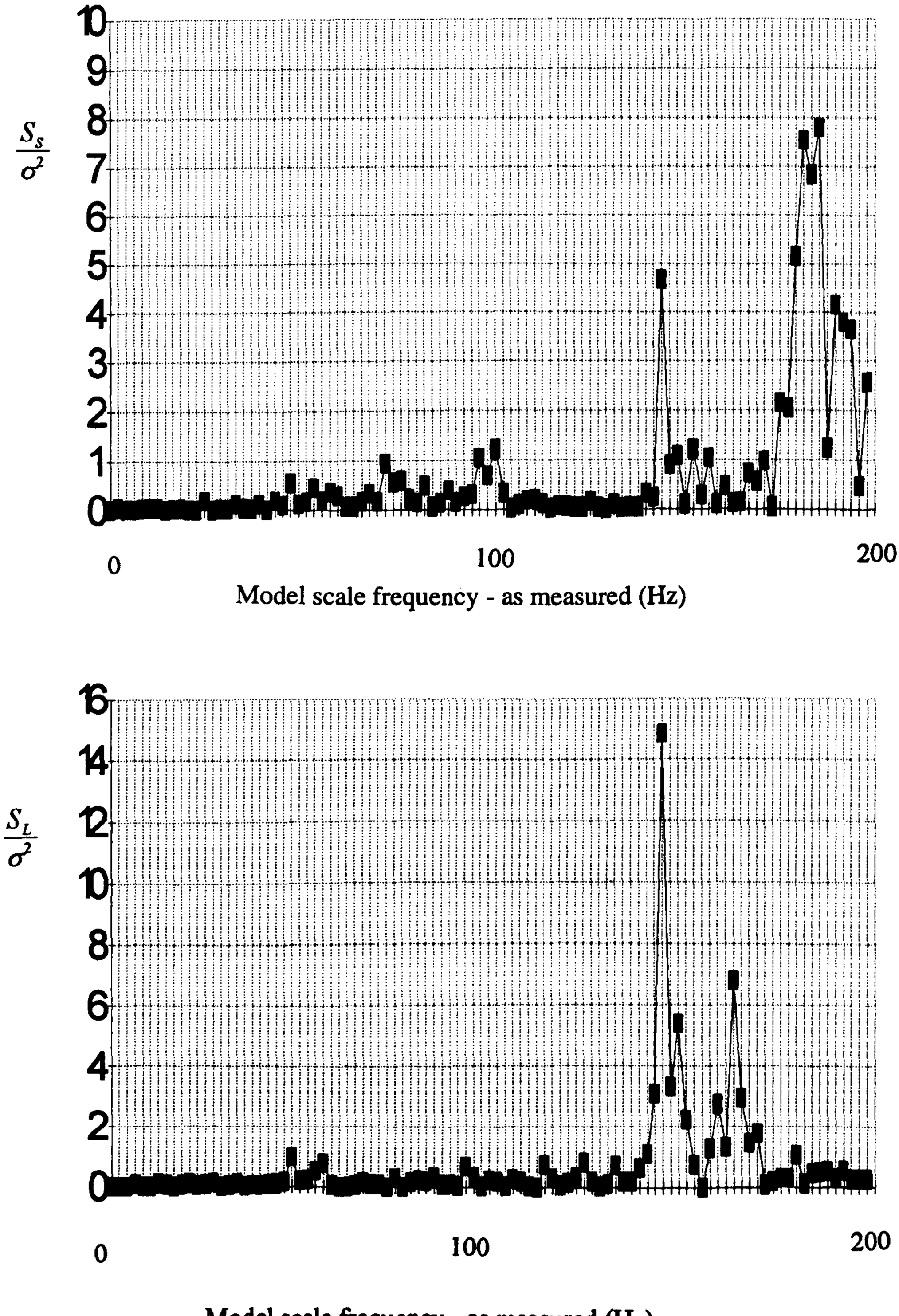

Figure 9.2 Force spectra from 1 run of moving model rig. Lorry on flat ground simulation, v = 3.06m/s, u (60mm) = 8.5m/s.

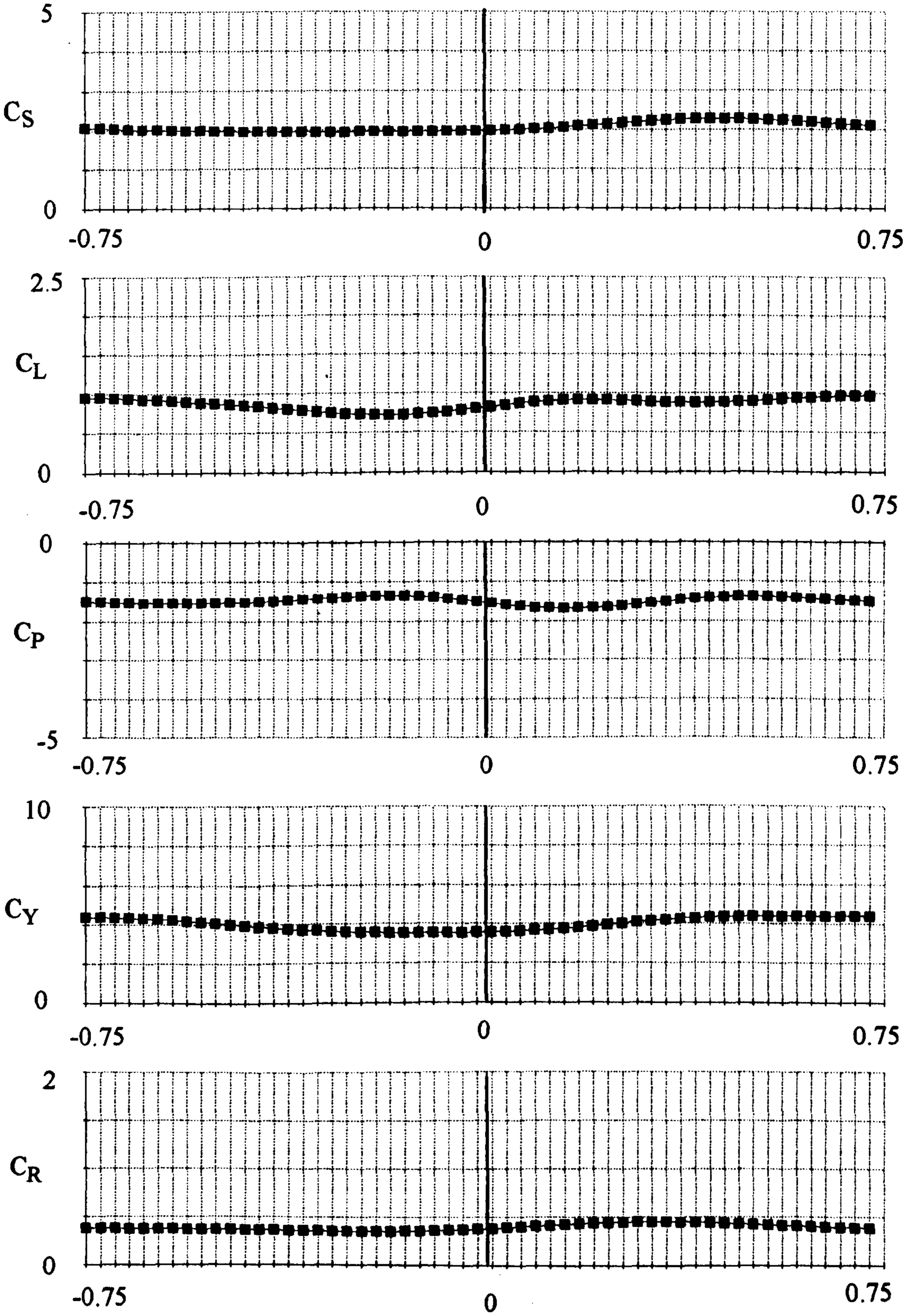

Position relative to centre of test section (metres) - facing downstream.

Figure 9.3 Average time history over 100 runs for flat ground simulation.
v = 12.19m/s, u (60mm) = 5.1m/s.

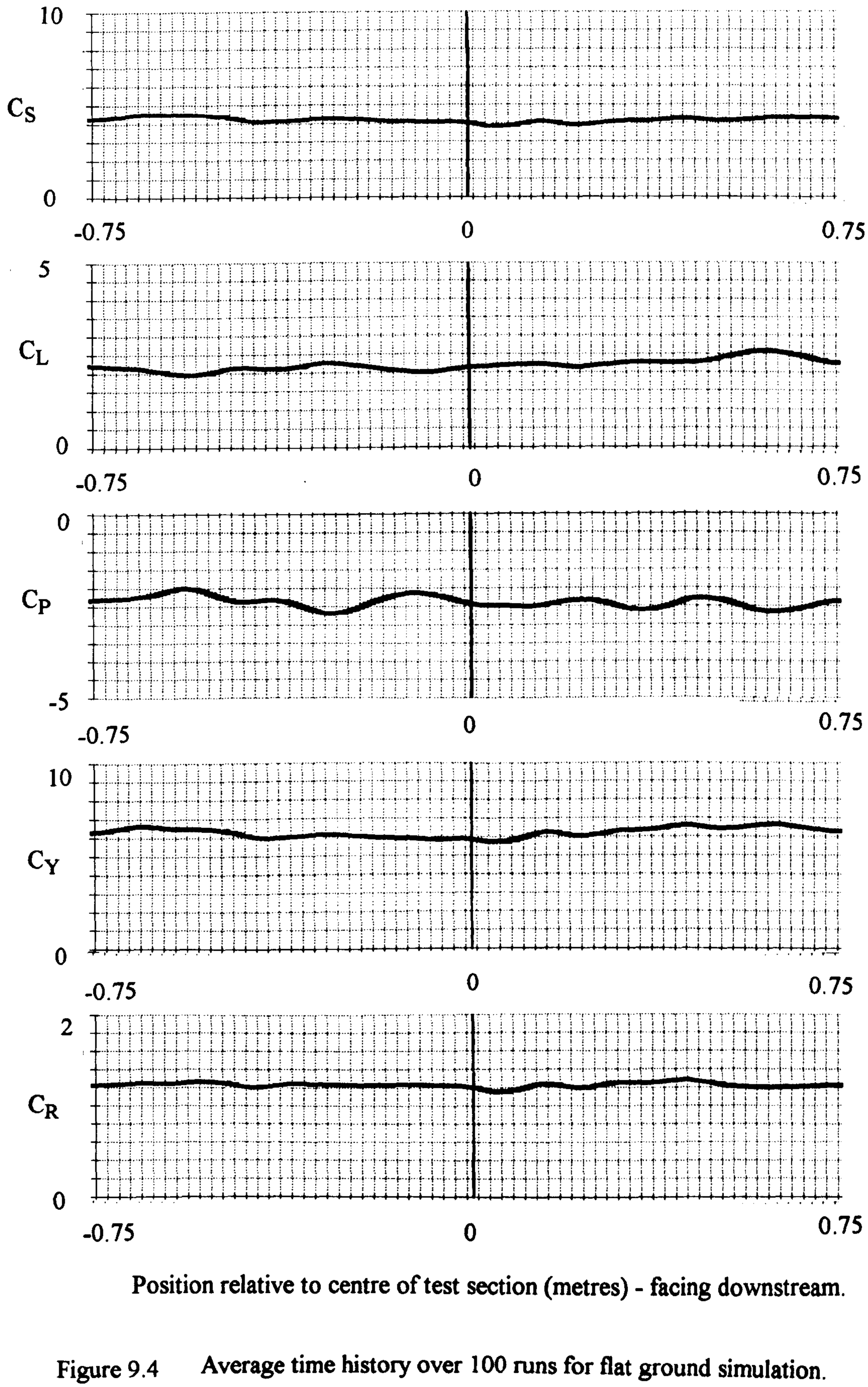

Position relative to centre of test section (metres) - facing downstream.

Figure 9.4 Average time history over 100 runs for flat ground simulation.

v = 3.06m/s, u (60mm) = 8.5m/s.

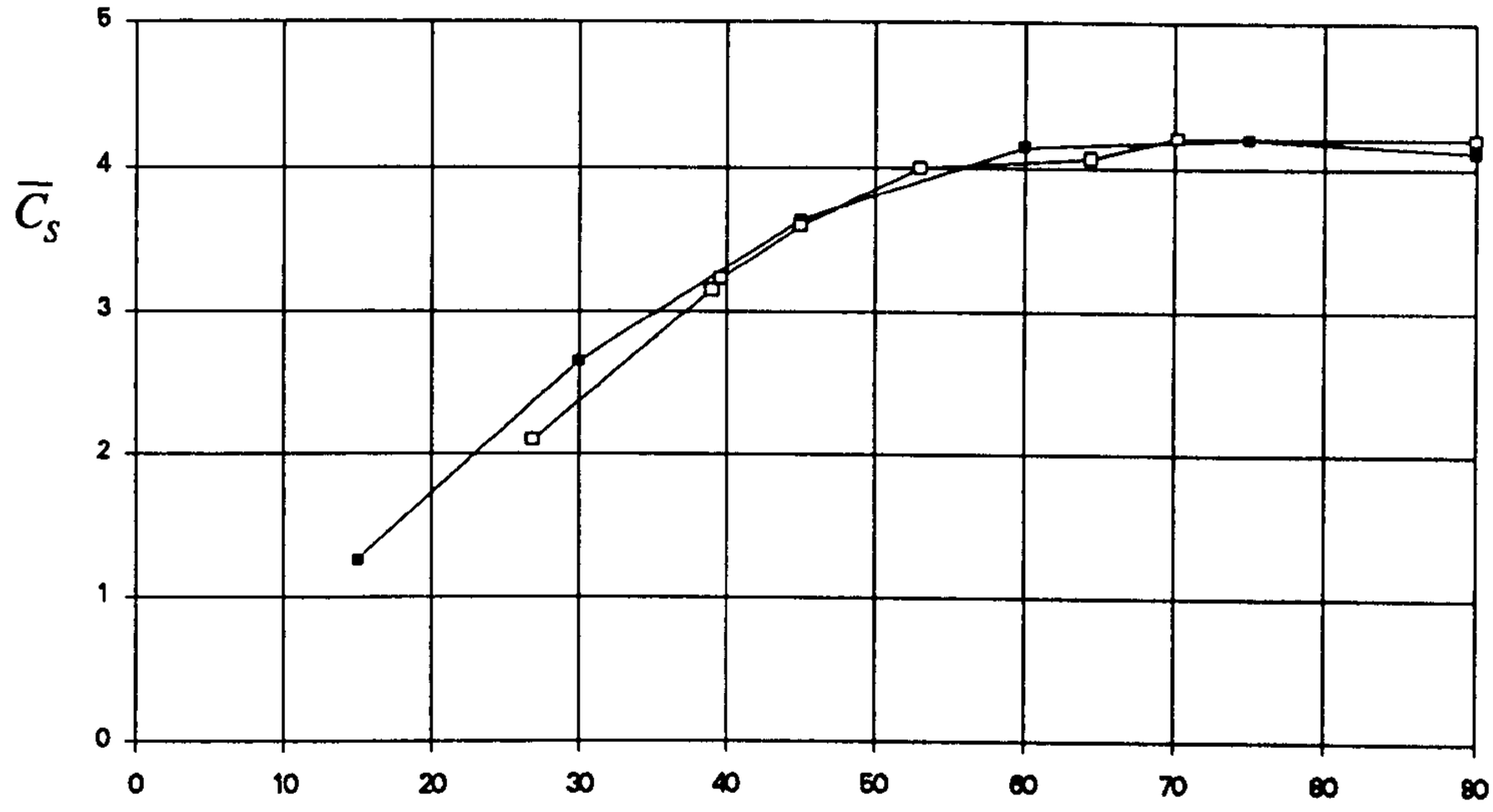

Yaw angle (degrees)

Figure 9.5 Mean side force coefficient.
Flat ground simulation for moving and static lorry tests.

■ Static Test, □ Moving Test

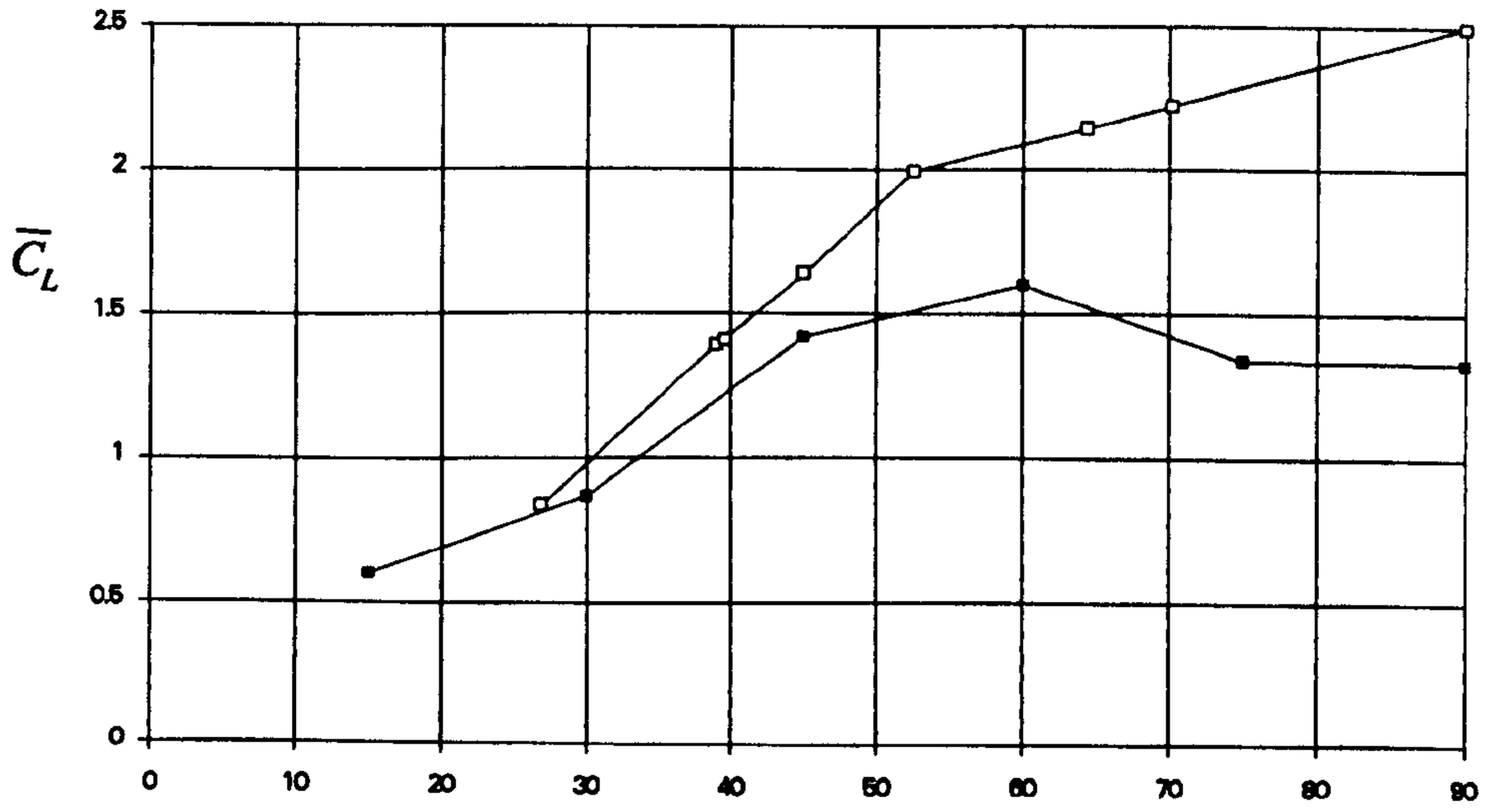

Yaw angle (degrees)

Figure 9.6 Mean lift force coefficient.
Flat ground simulation for moving and static lorry tests.

■ Static Test, □ Moving Test

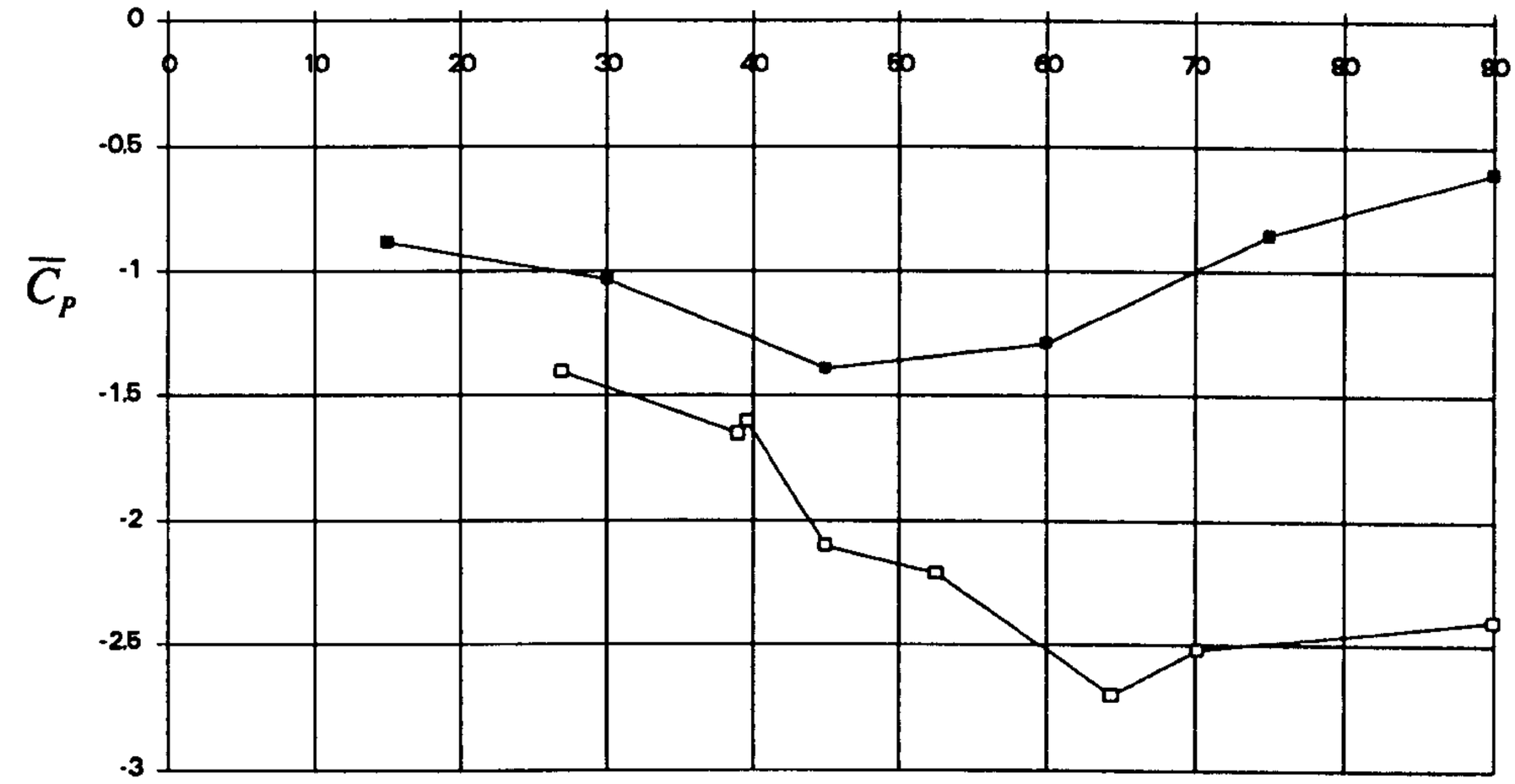

Figure 9.7 Mean pitching moment coefficient.
Flat ground simulation for moving and static lorry tests.

■ Static Test, □ Moving Test

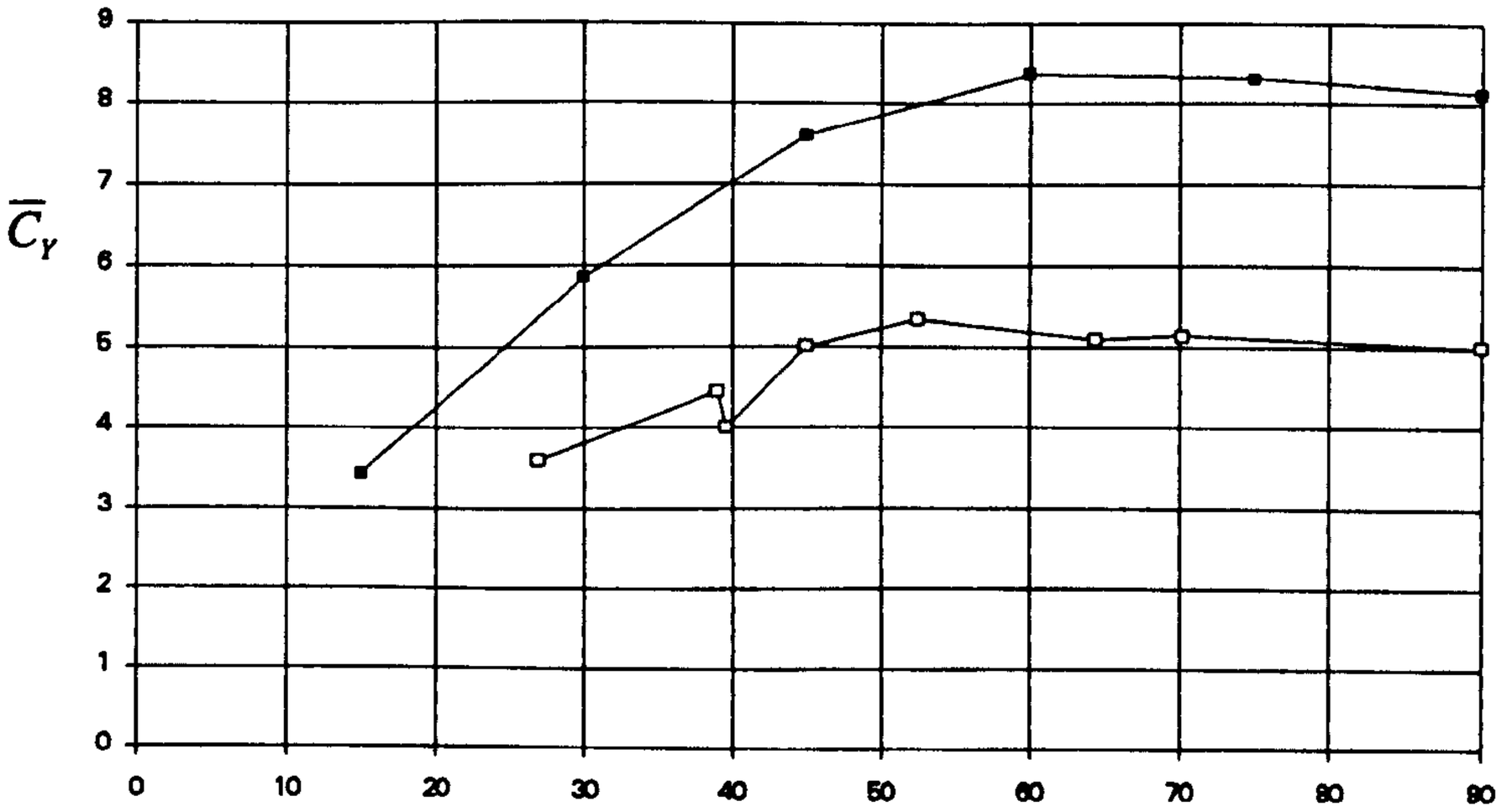

Figure 9.8 Mean yawing moment coefficient.
Flat ground simulation for moving and static lorry tests.

■ Static Test, □ Moving Test

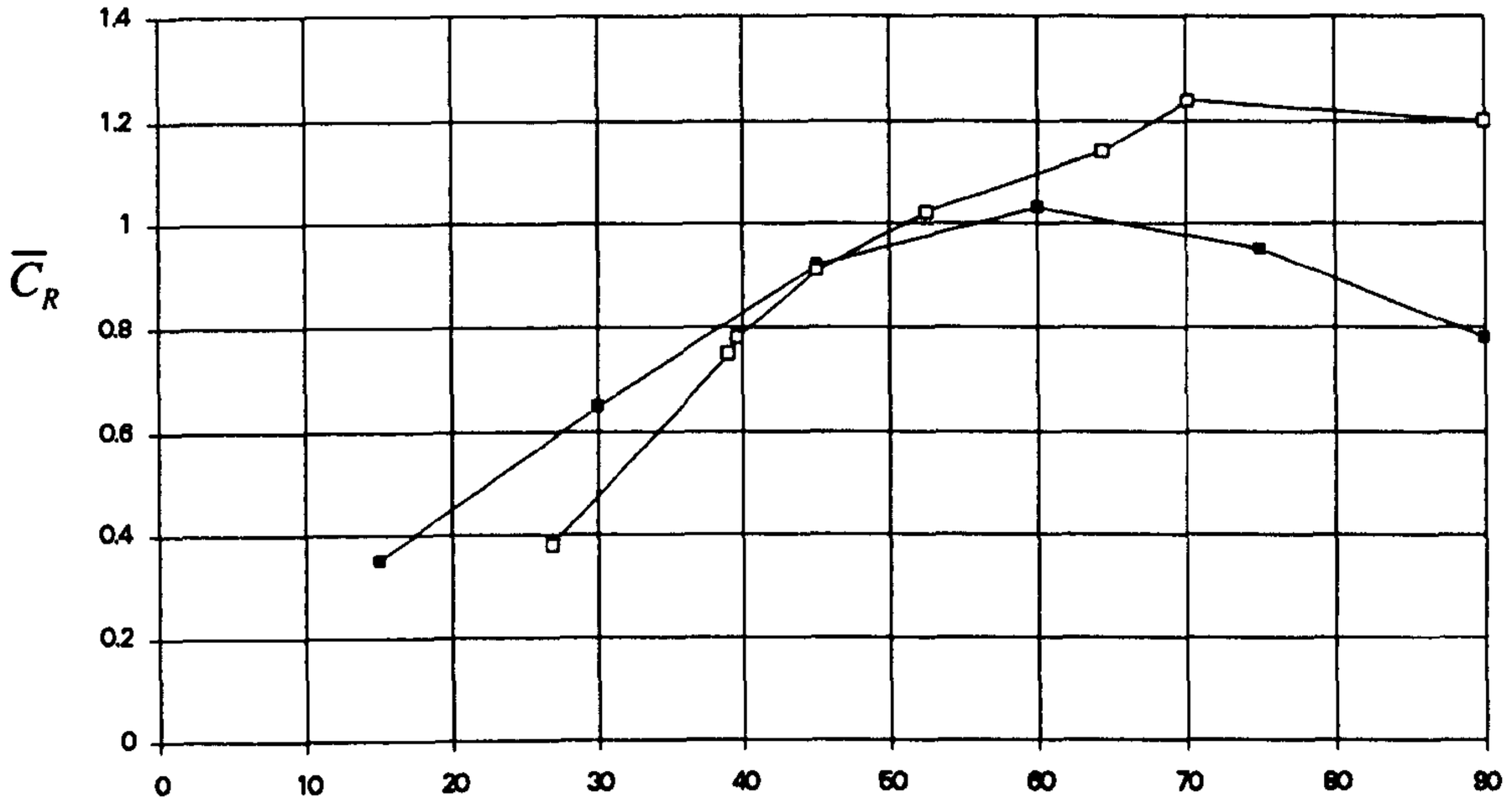

Figure 9.9 Mean rolling moment coefficient.
Flat ground simulation for moving and static lorry tests.

■ Static Test, □ Moving Test

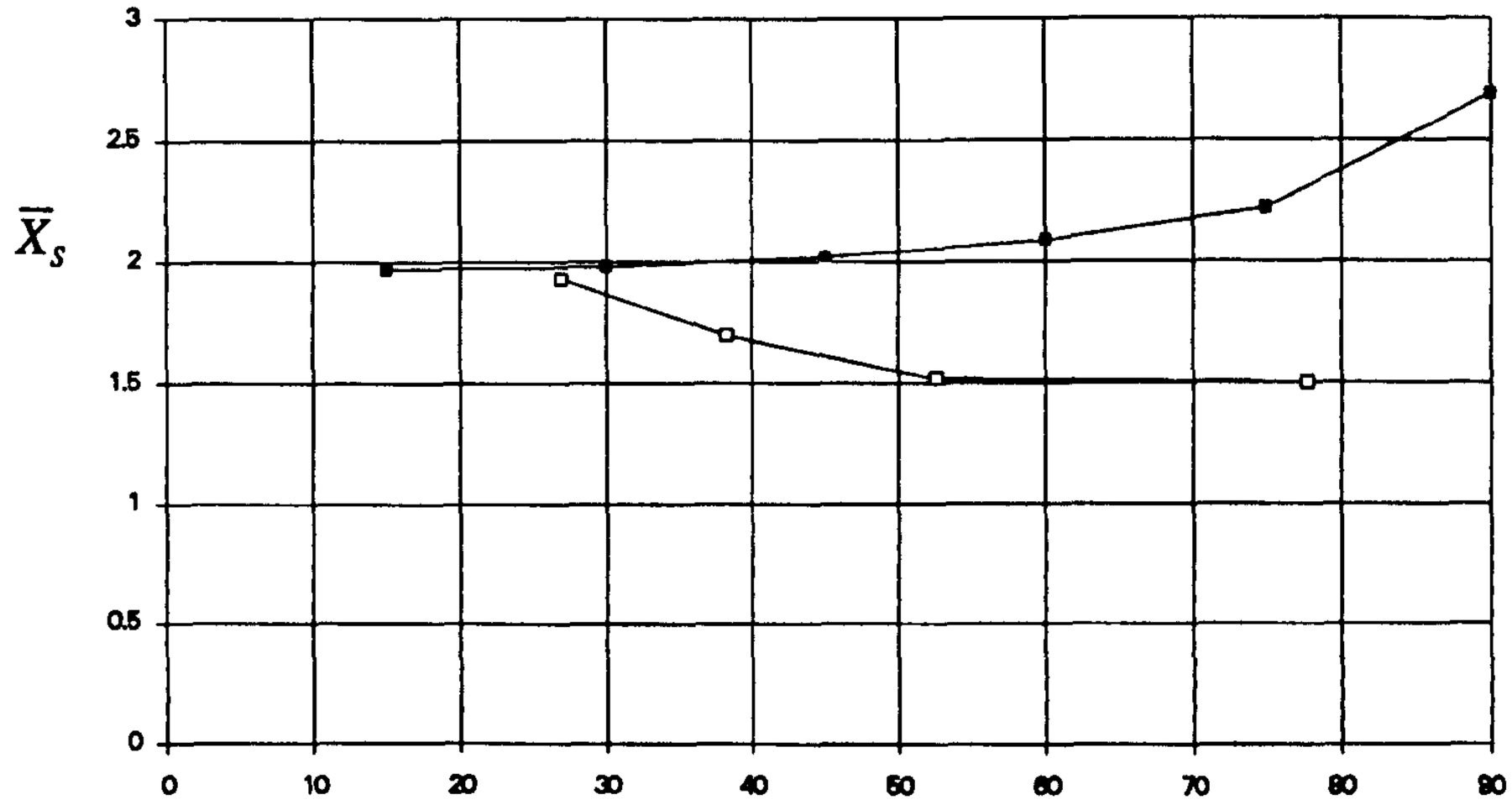

Figure 9.10 Horizontal non-dimensional point of action of side force.
Flat ground simulation for moving and static lorry tests.

■ Static Test, □ Moving Test

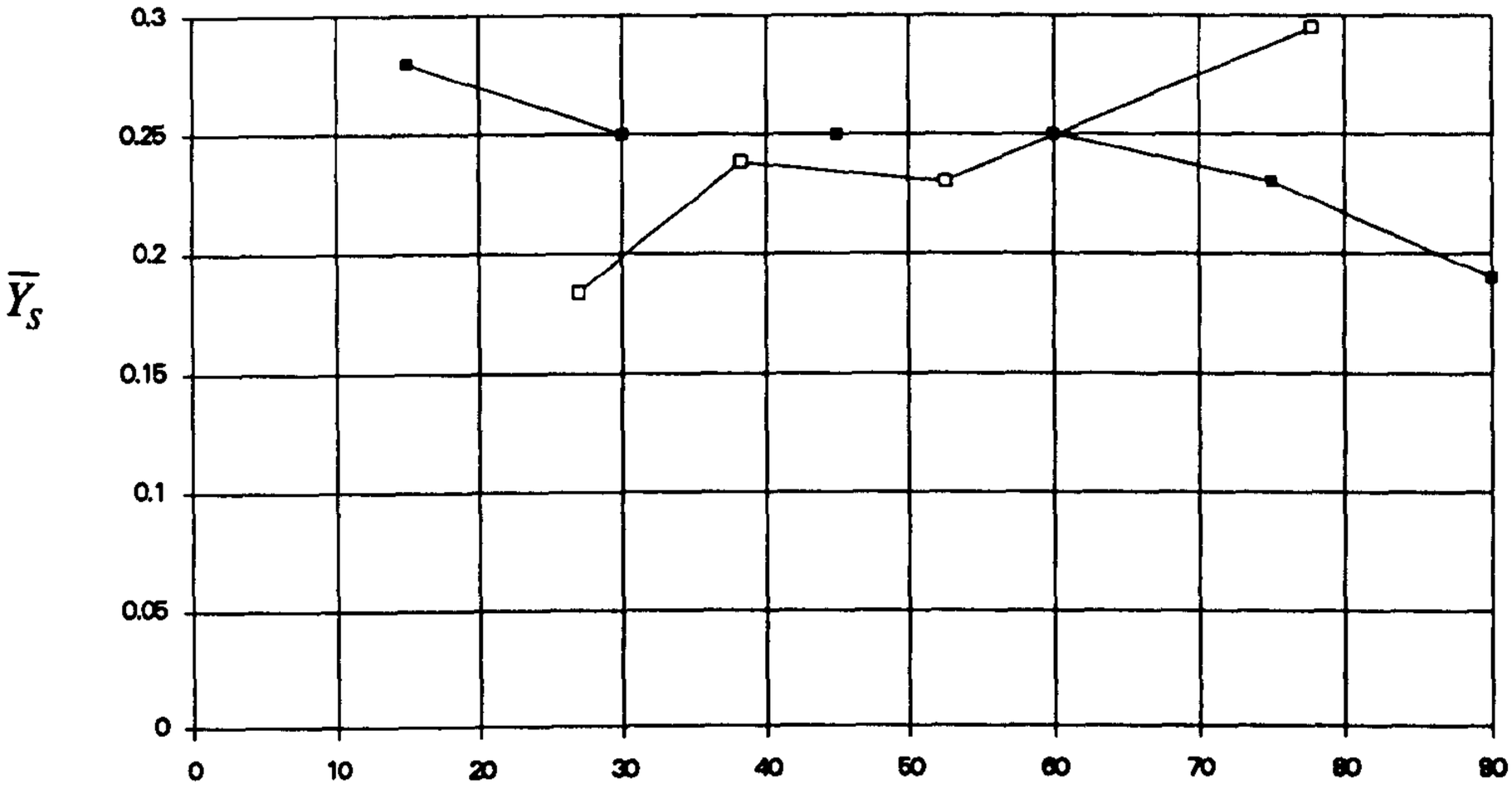

Figure 9.11 Vertical non-dimensional point of action of side force. Flat ground simulation for moving and static lorry tests.

■ Static Test, □ Moving Test

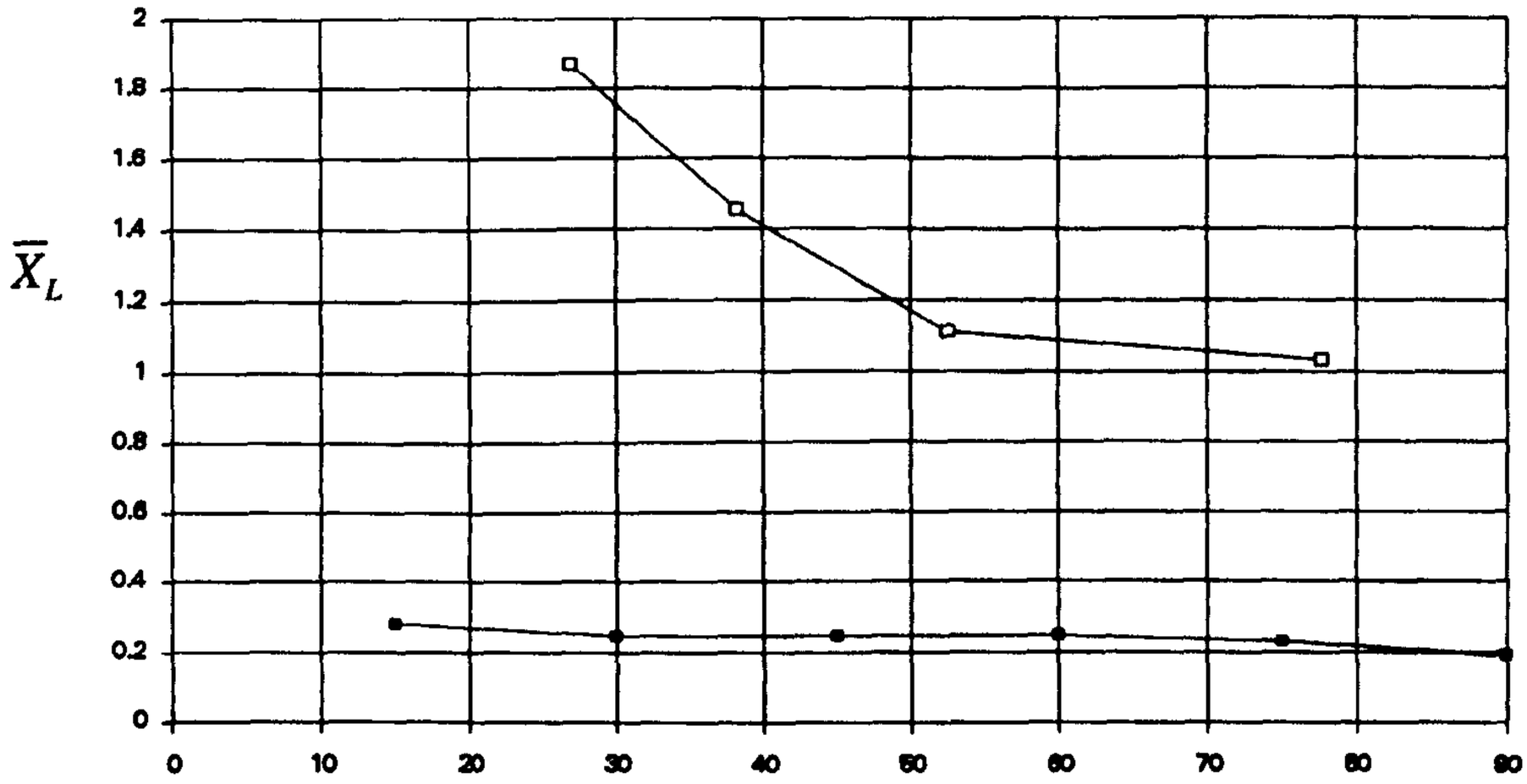

Figure 9.12 Horizontal normalised point of action of lift force. Flat ground simulation for moving and static lorry tests.

■ Static Test, □ Moving Test

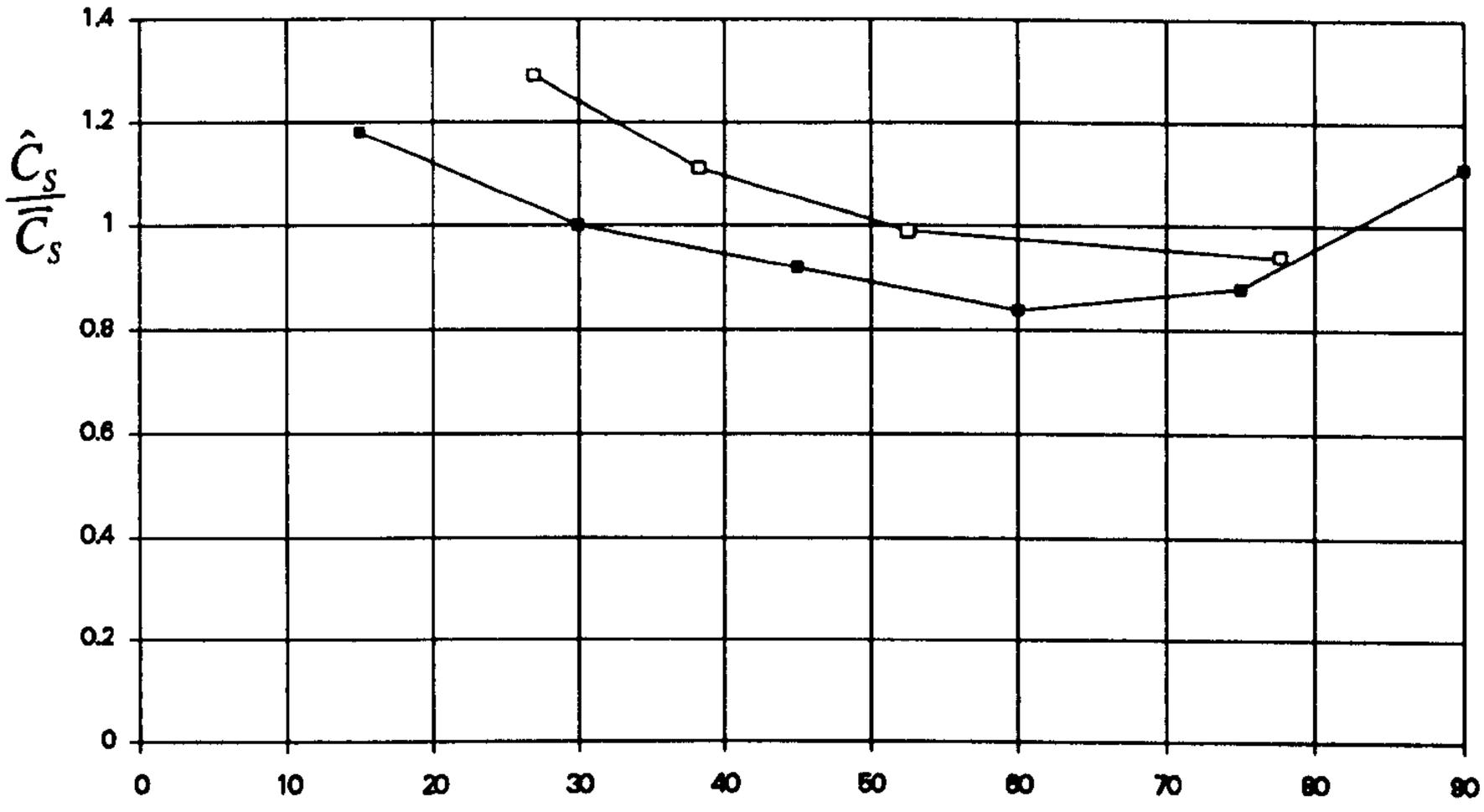

Figure 9.13 Normalised extreme side force parameter.
Flat ground simulation for moving and static lorry tests.

■ Static Test, □ Moving Test

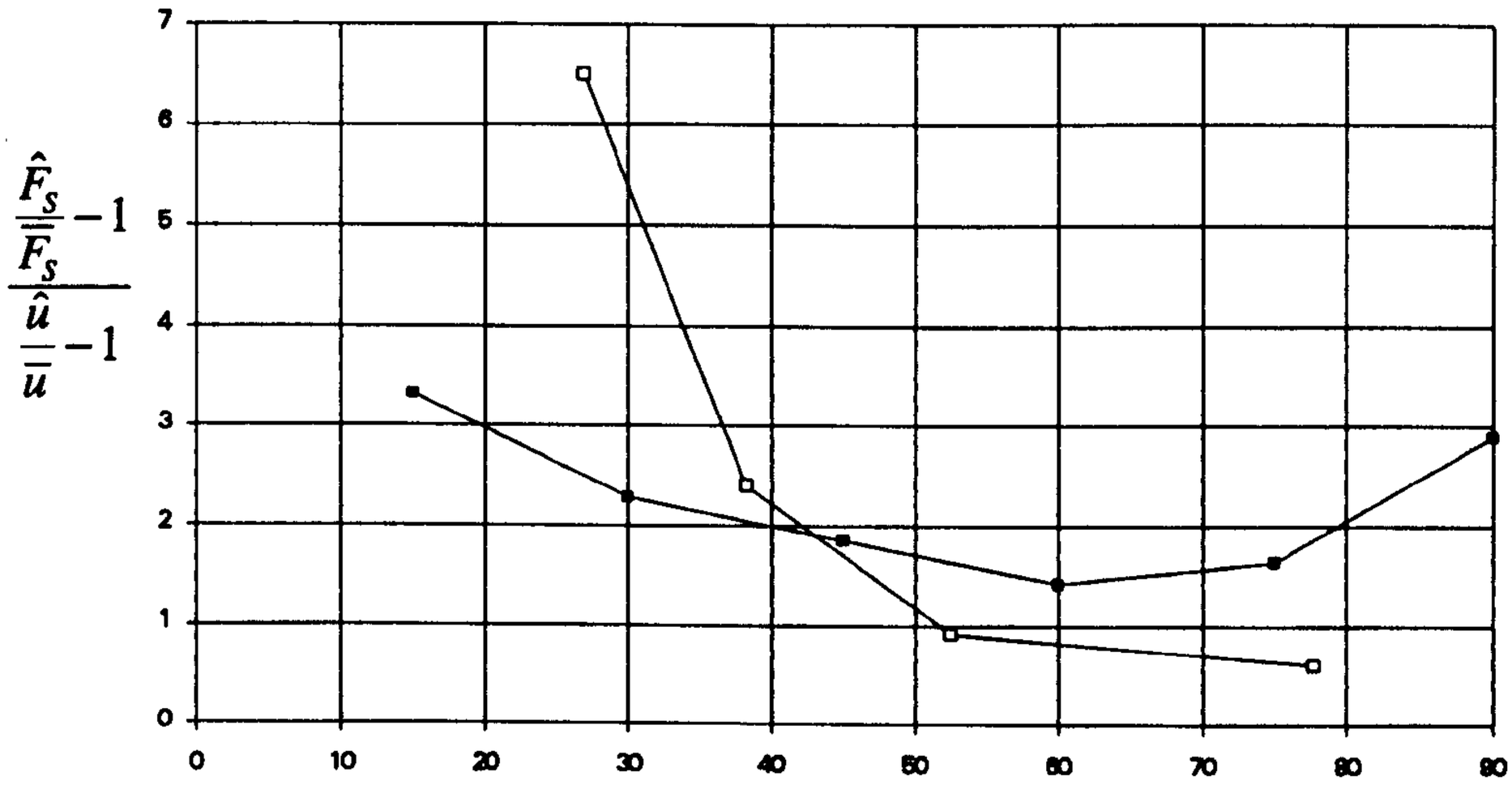

Figure 9.14 Unsteady side force parameter.
Flat ground simulation for moving and static lorry tests.

■ Static Test, □ Moving Test

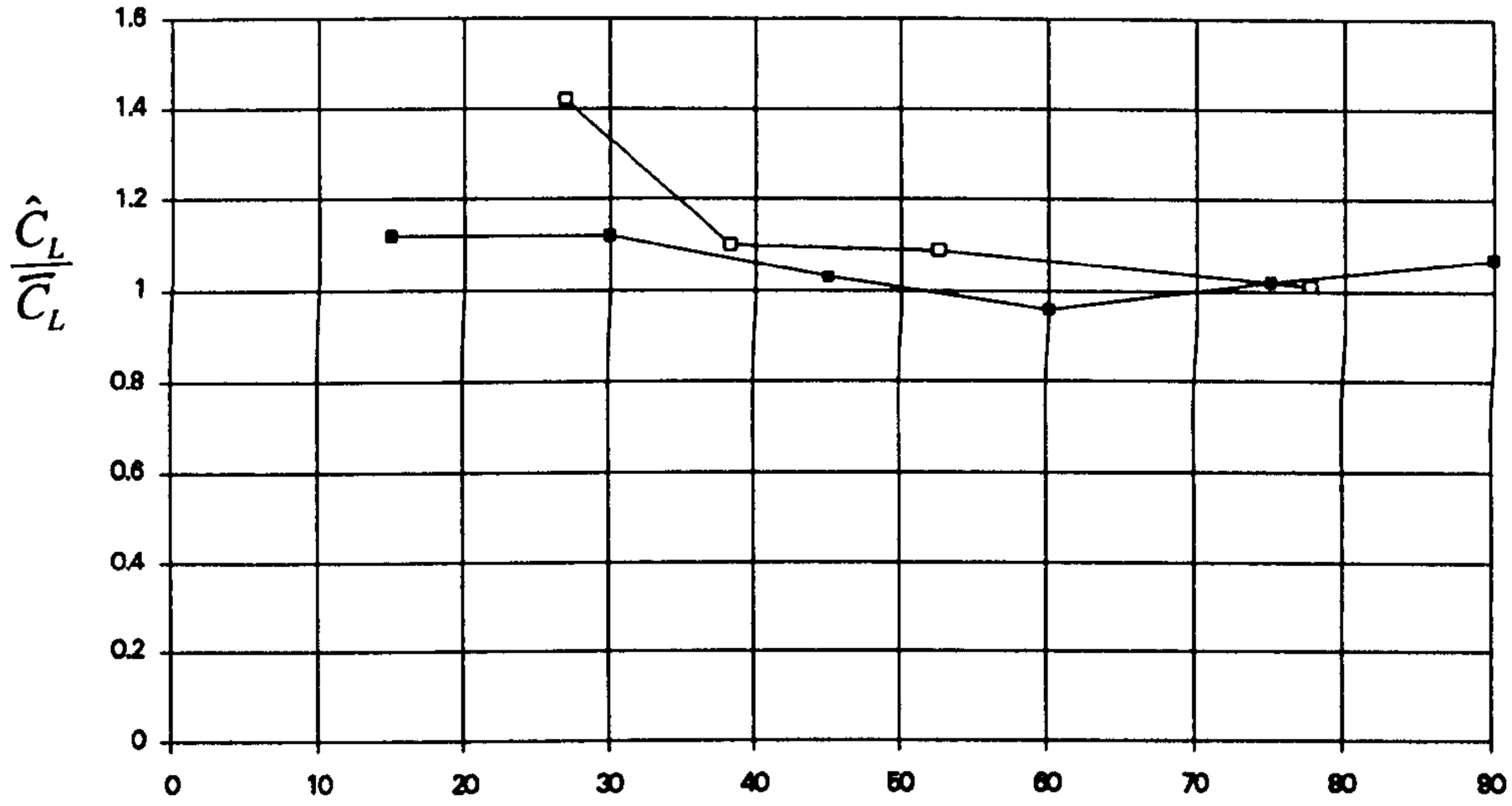

Figure 9.15 Normalised extreme lift force parameter.
Flat ground simulation for moving and static lorry tests.

■ Static Test, □ Moving Test

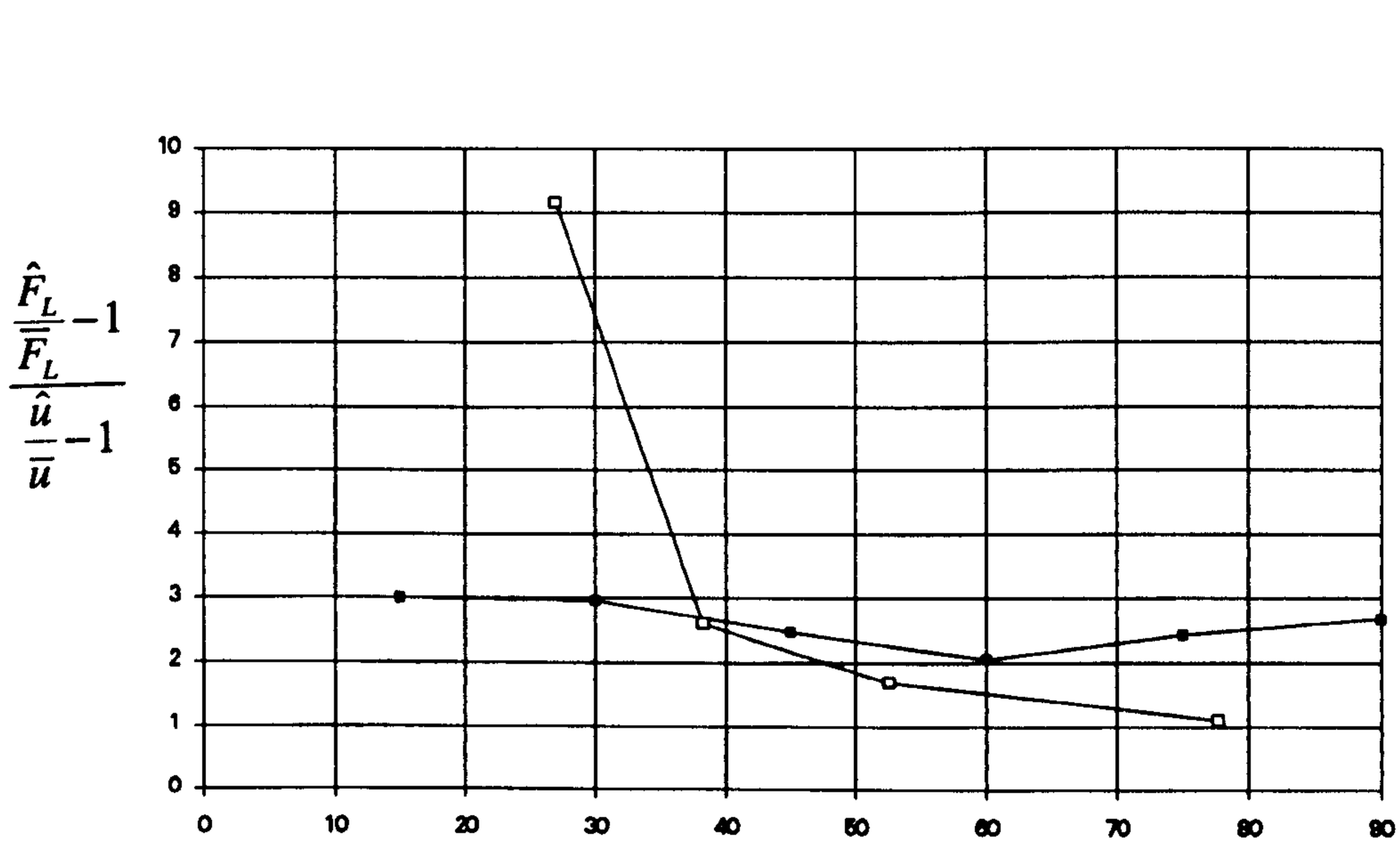

Figure 9.16 Unsteady lift force parameter.
Flat ground simulation for moving and static lorry tests.

■ Static Test, □ Moving Test

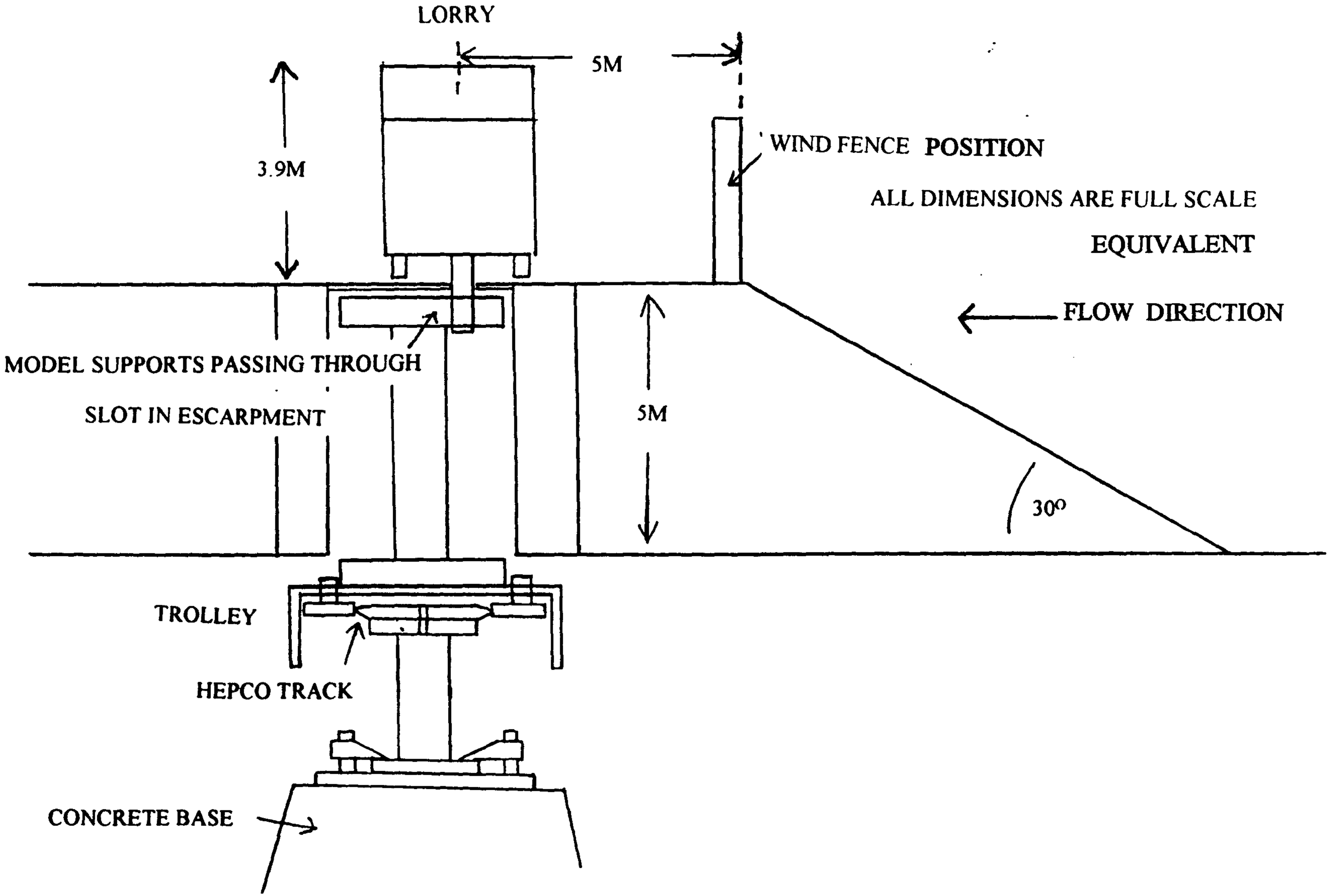

Figure 9.17 Escarpment simulation geometry showing the moving model (lorry) mounting arrangement, its position on the escarpment and also the wind fence position.

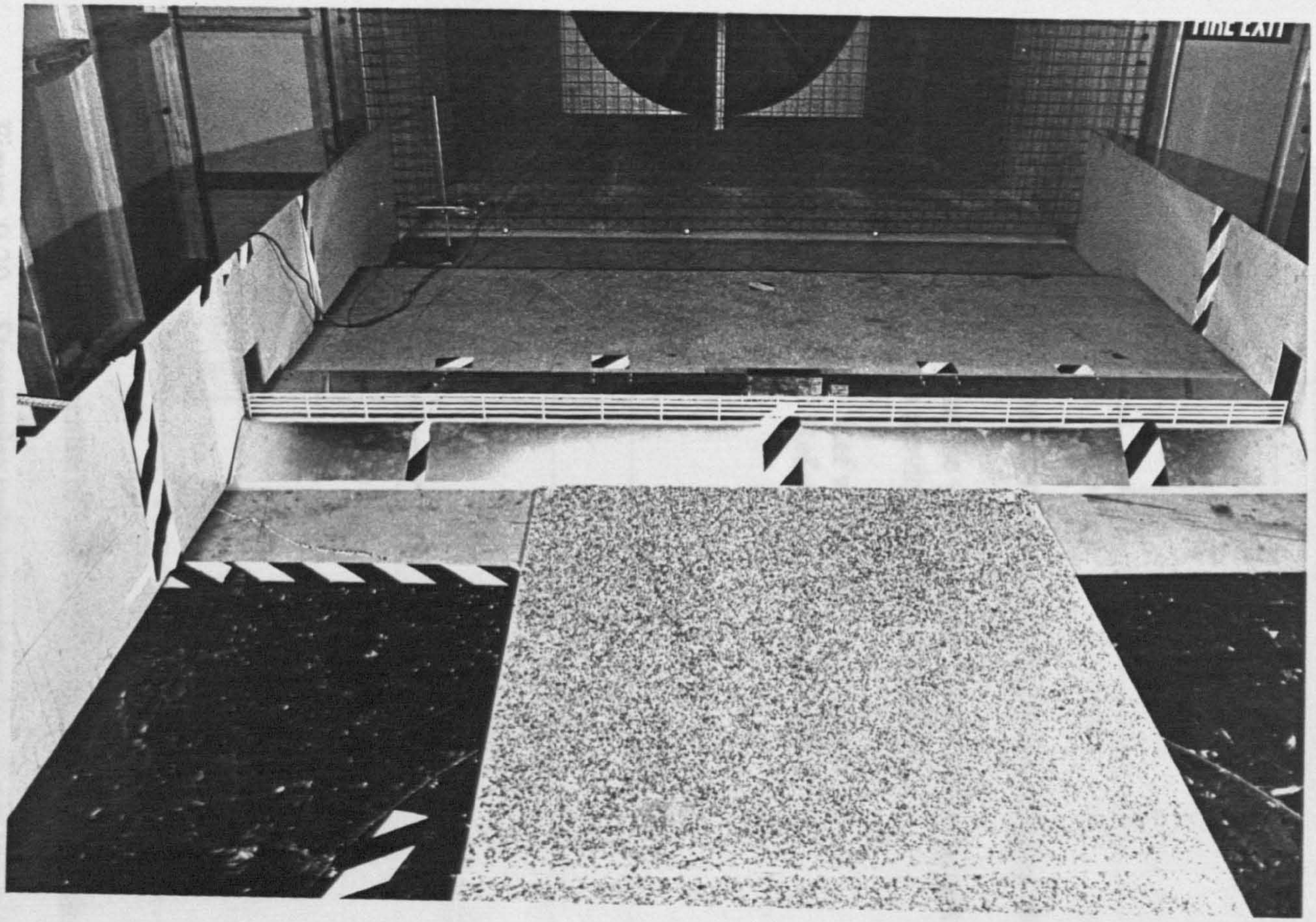

Figure 9.18 Live articulated lorry model traversing the escarpment simulation behind the wind fence during a run of the moving model rig. Note the holes in the side walls where the vehicle enters and exits the working section.

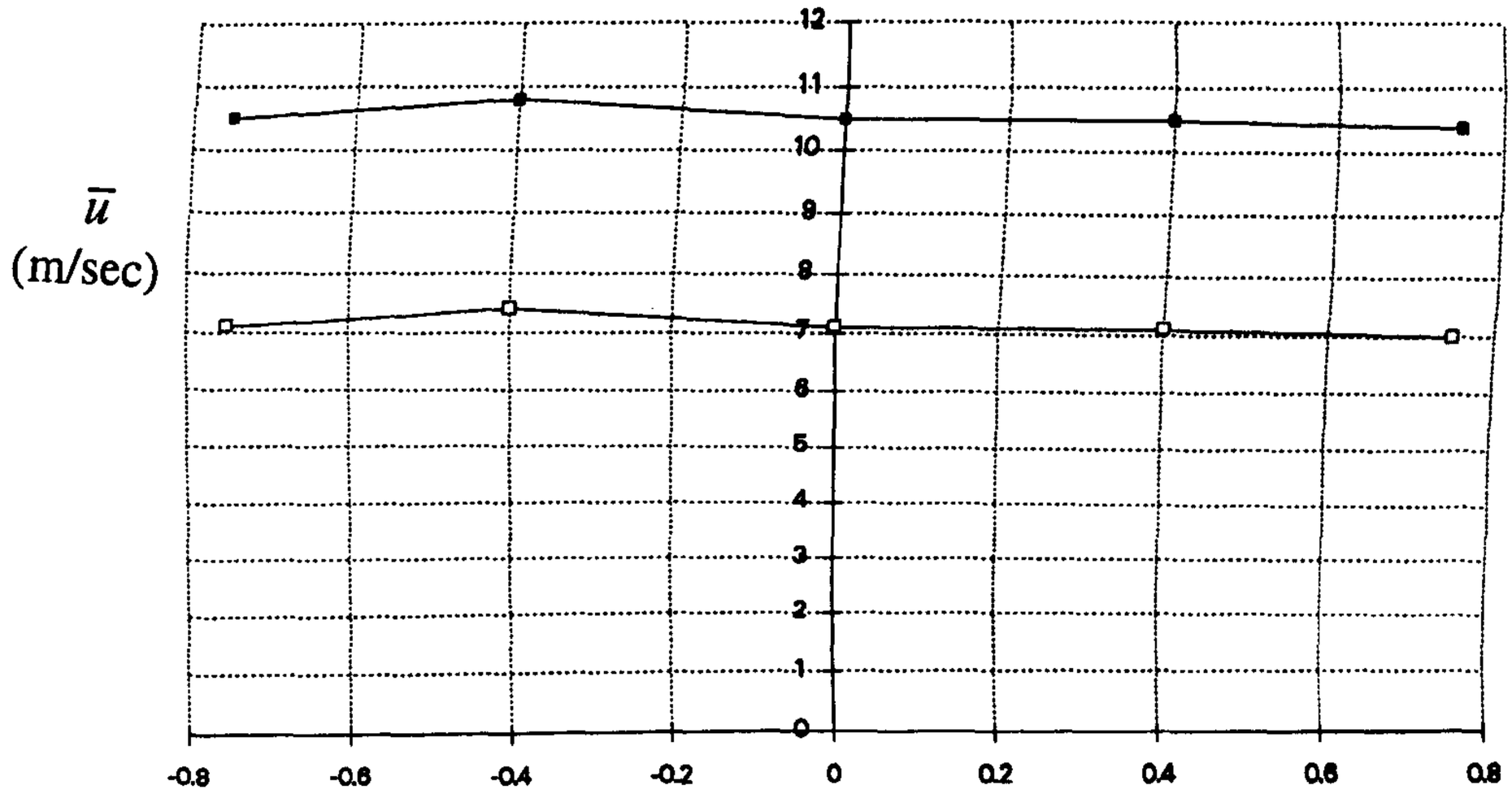

Figure 9.19 Streamwise wind velocity 60mm above height of escarpment across moving model test section.

■ Ref wind speed = 10.5 m/s
□ Ref wind speed = 7.2 m/s

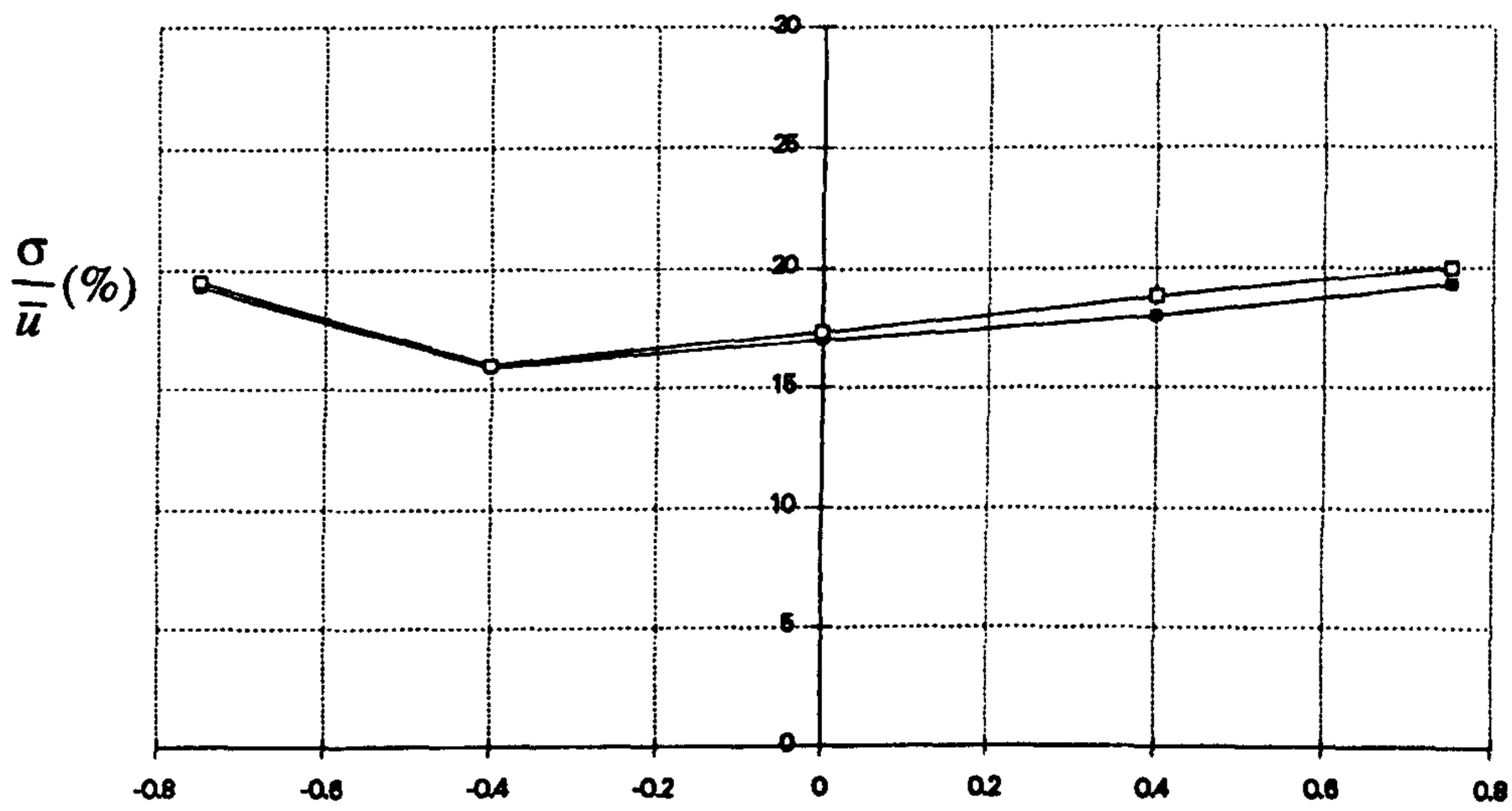

Figure 9.20 Streamwise turbulence intensity 60mm above height of escarpment across moving model test section.

■ Ref wind speed = 10.5 m/s
□ Ref wind speed = 7.2 m/s

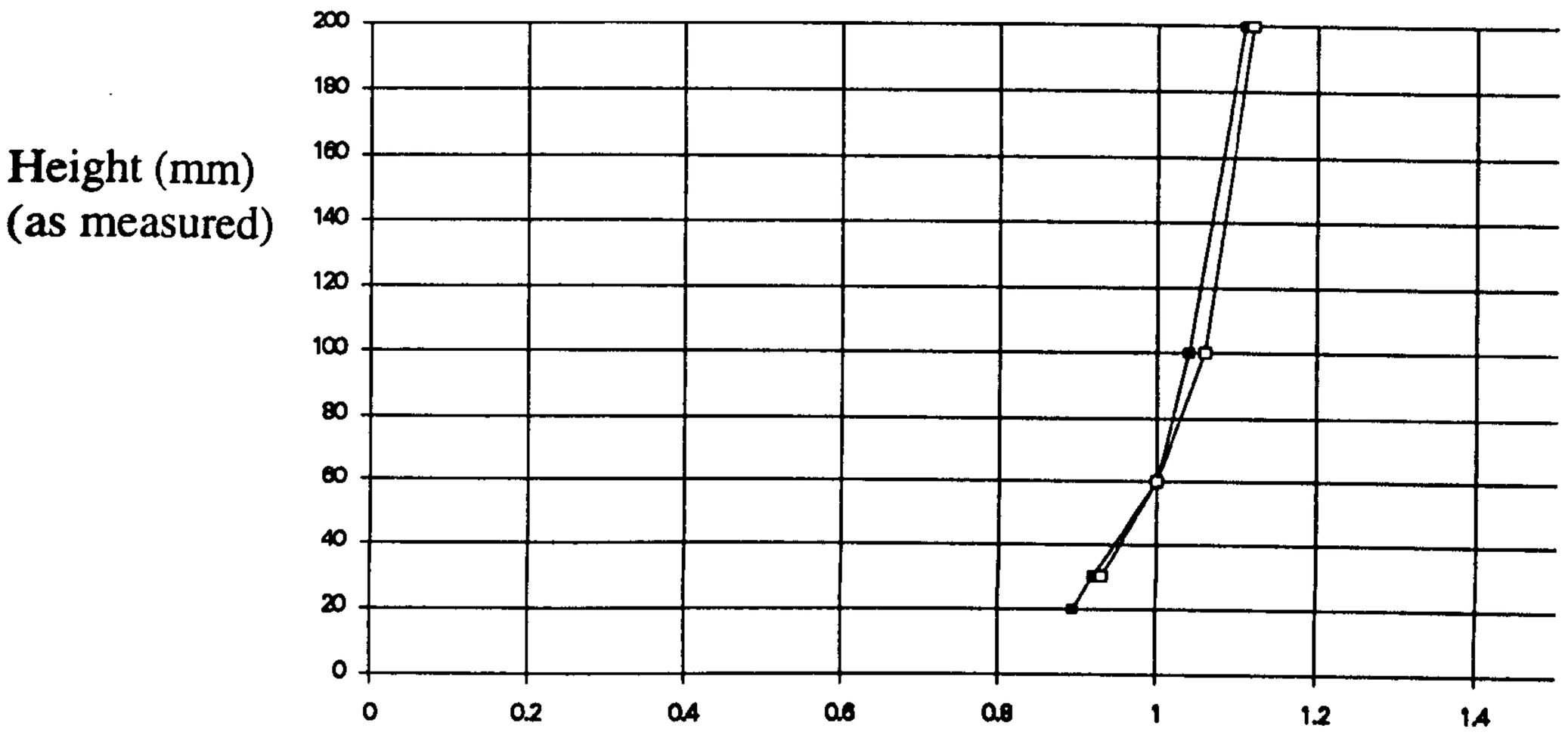

Streamwise wind velocity/ reference wind velocity at 60mm
(equivalent to 3m full scale)

Figure 9.21 Streamwise wind velocity profile with height measured from escarpment surface at centre of test section.

■ Ref wind speed = 10.5 m/s
□ Ref wind speed = 7.2 m/s

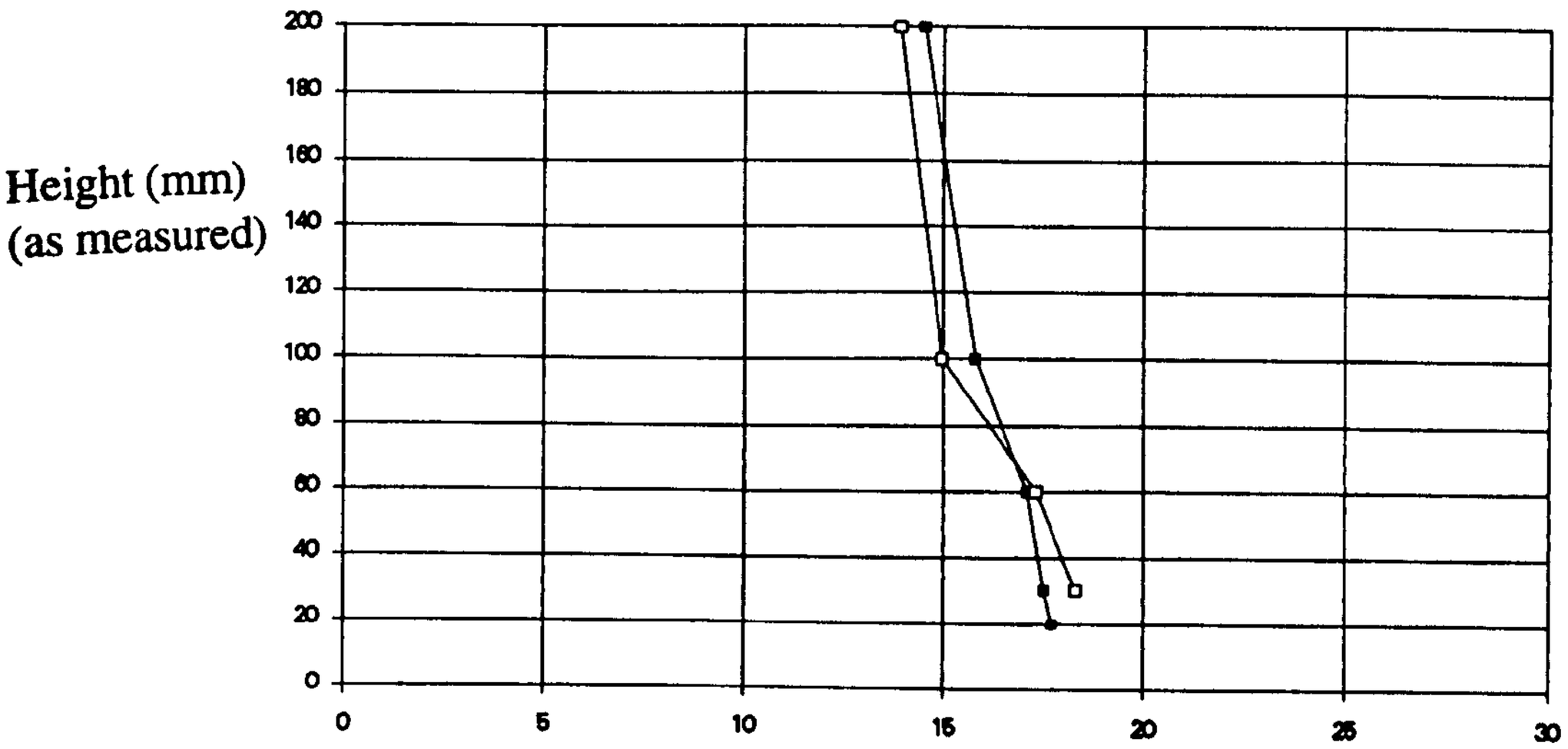

Streamwise turbulence intensity (%)

Figure 9.22 Streamwise turbulence intensity profile with height measured from escarpment surface at centre of test section.

■ Ref wind speed = 10.5 m/s
□ Ref wind speed = 7.2 m/s

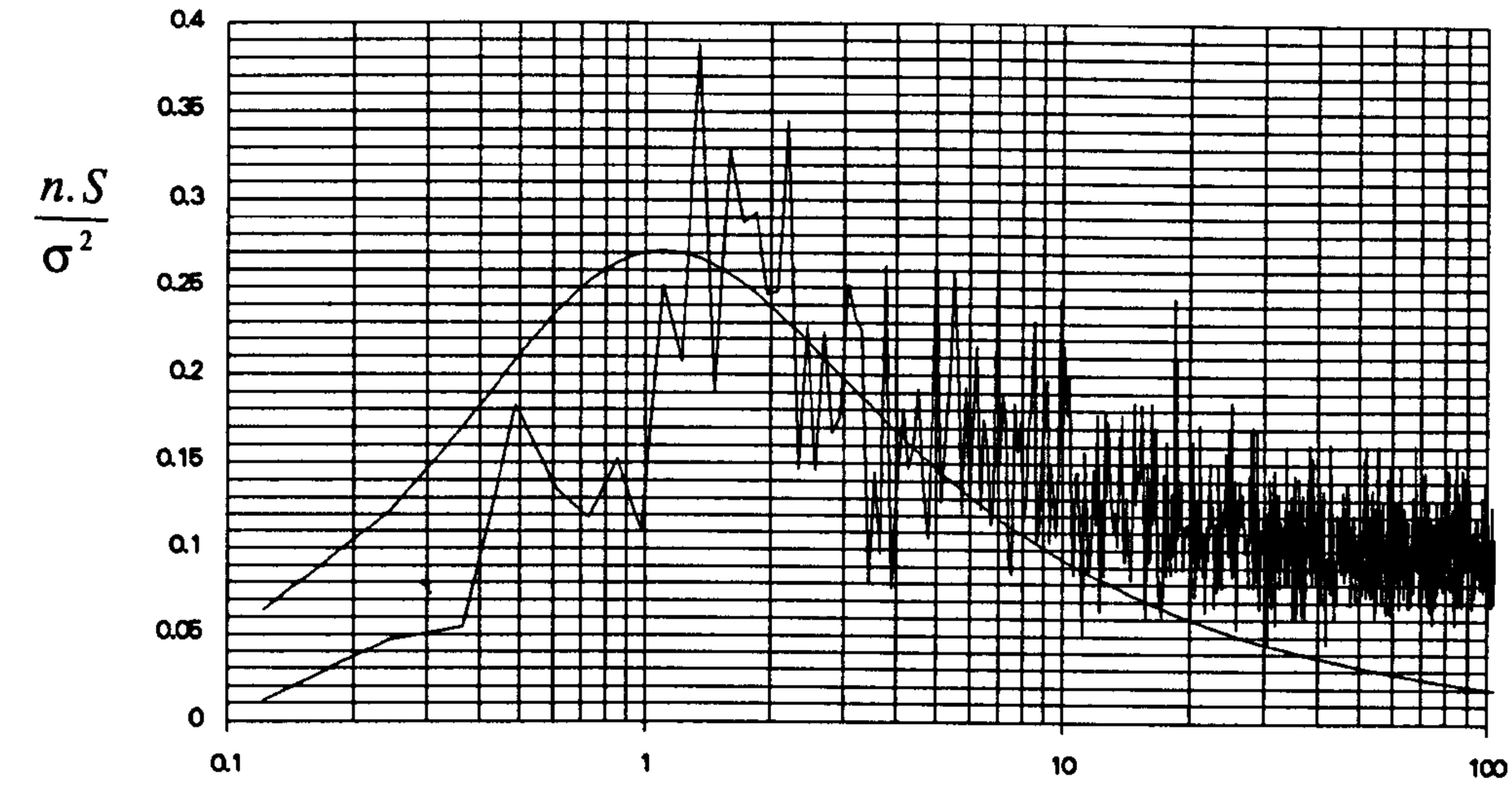

Figure 9.23 Streamwise velocity spectrum measured 60mm (equivalent to 3m full scale) above escarpment surface at centre of test section. Reference wind speed = 7.2 m/s. Smooth line is target von Karman spectrum for a full scale roughness length of 0.03m at the reference wind speed.

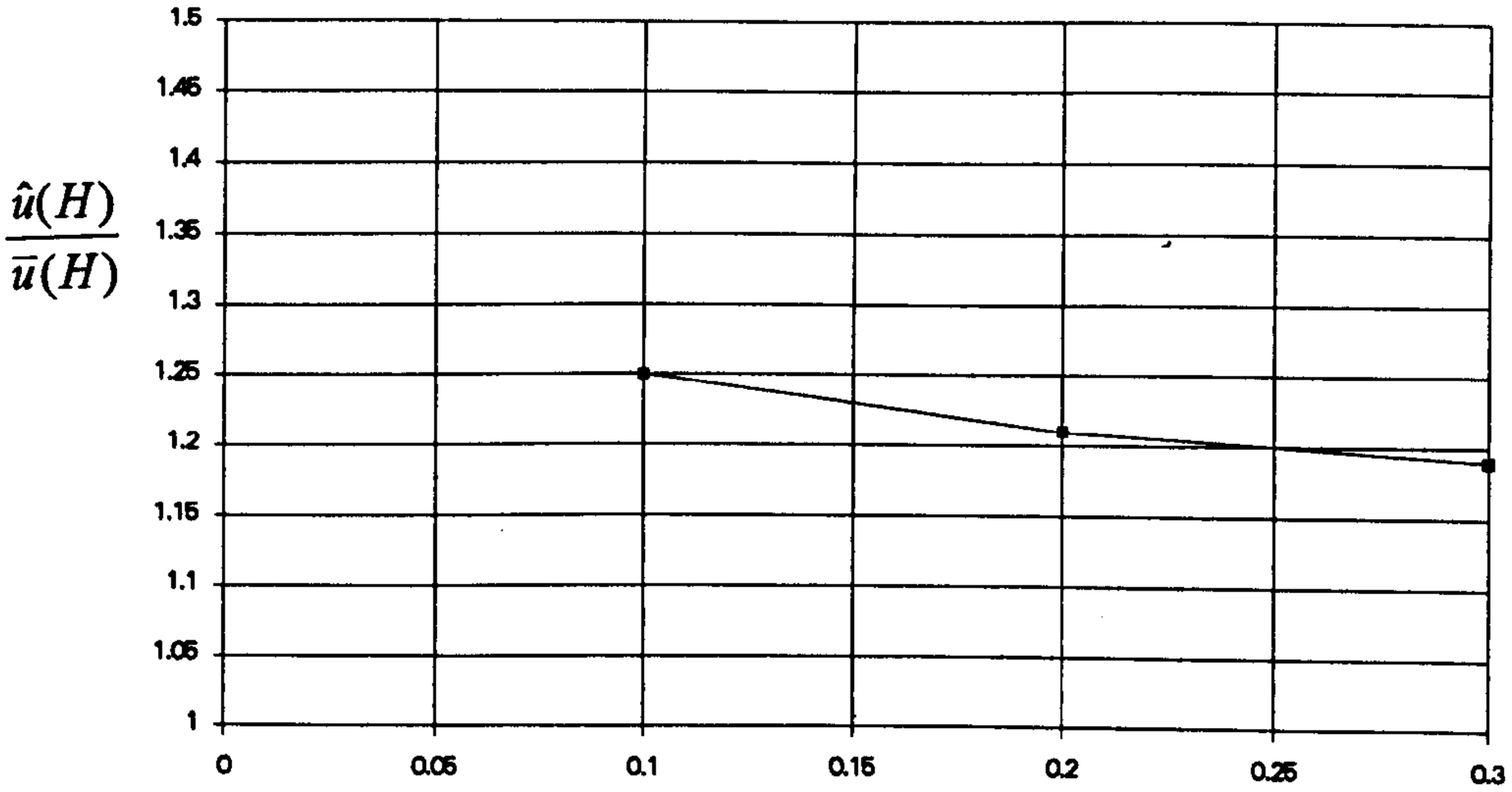

Figure 9.24 Extreme wind velocity / mean wind velocity as a function of model time equivalent to 3s full scale gust for escarpment simulation. Reference wind speed = 10.5 m/s at measurement height of 60mm (equivalent to 3m full scale).

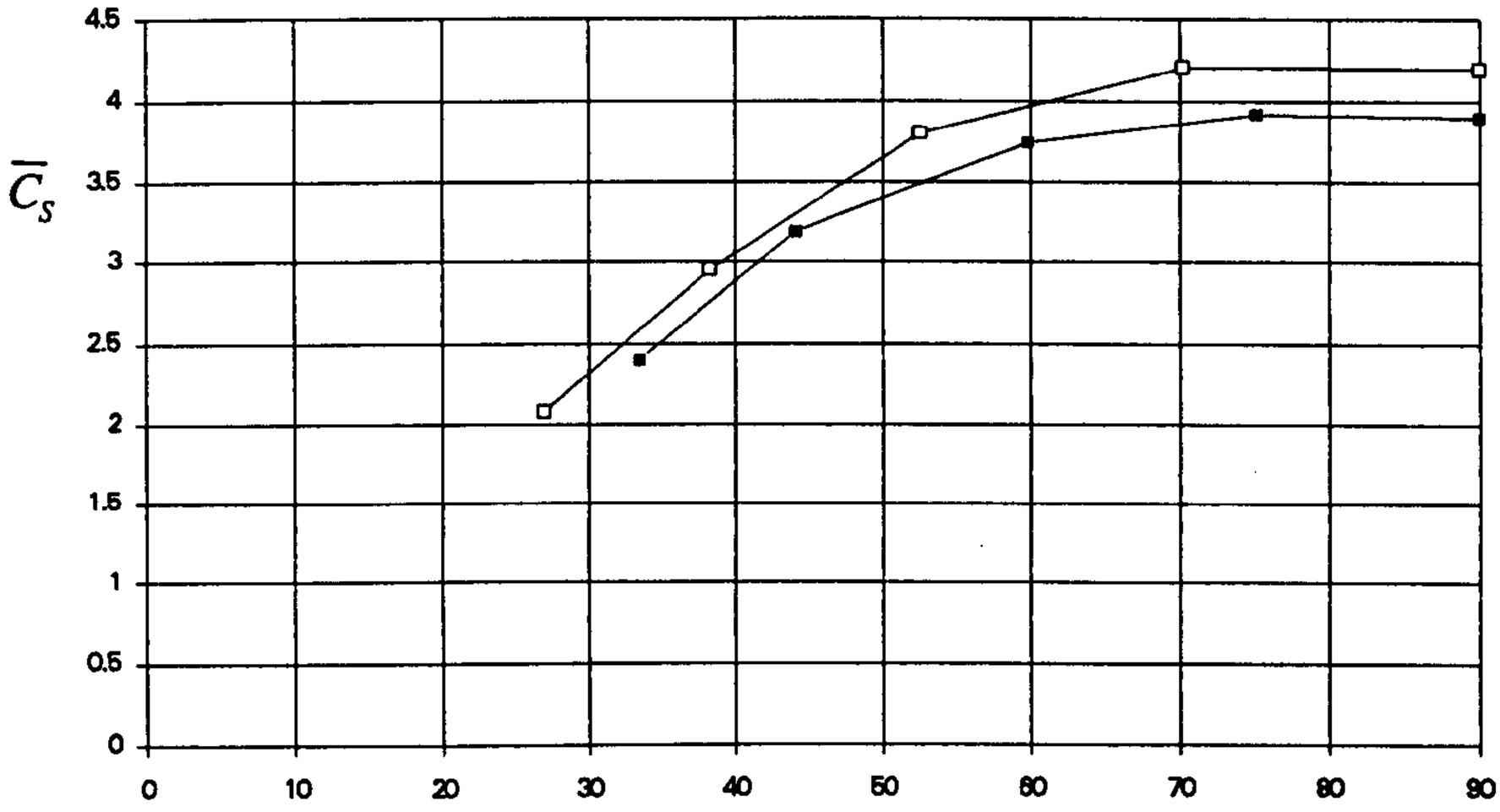

Figure 9.25 Mean side force coefficient.
Flat ground and escarpment simulation for moving lorry tests.

□ Flat Ground Simulation
■ Escarpment Simulation

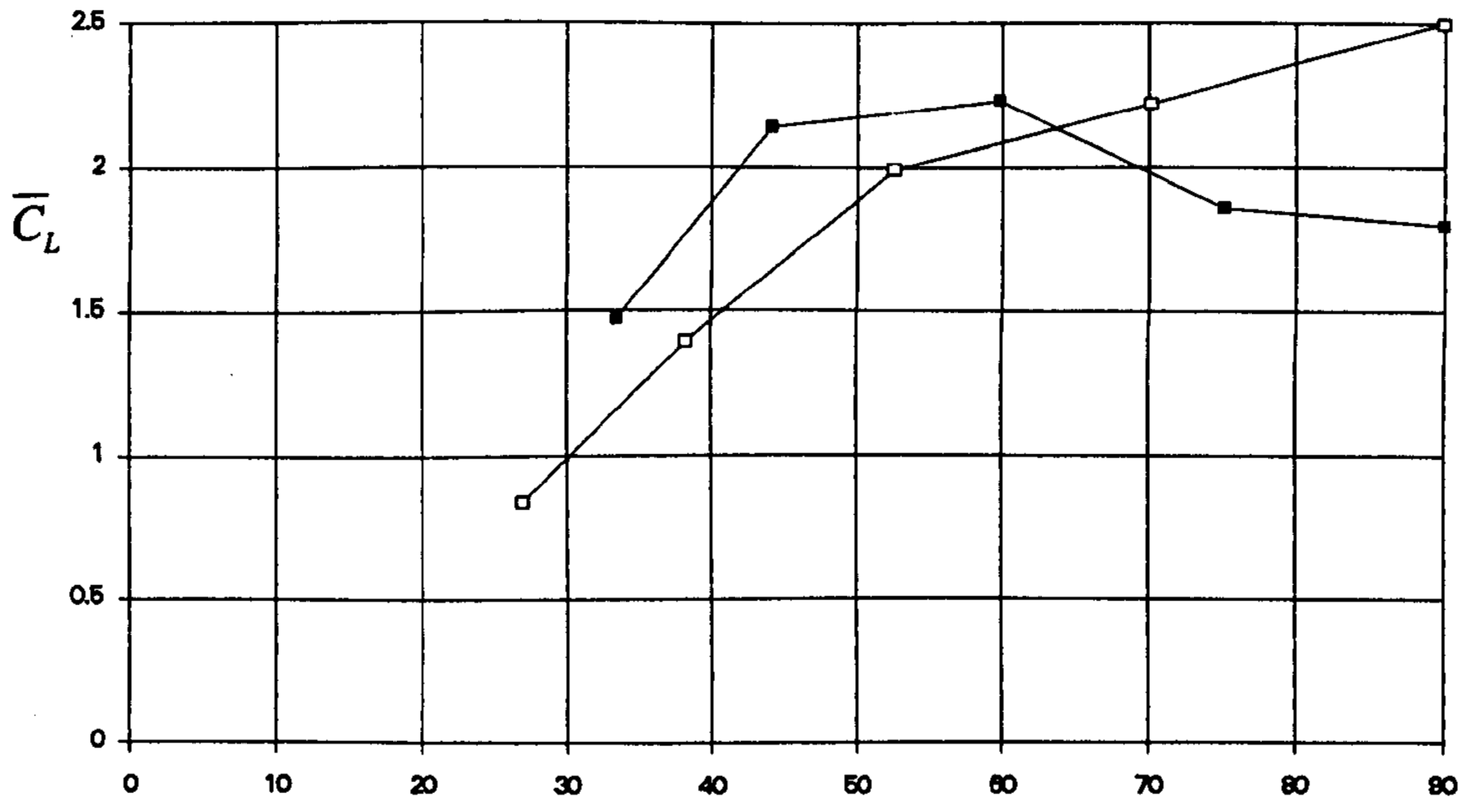

Figure 9.26 Mean lift force coefficient.
Flat ground and escarpment simulation for moving lorry tests.

□ Flat Ground Simulation
■ Escarpment Simulation

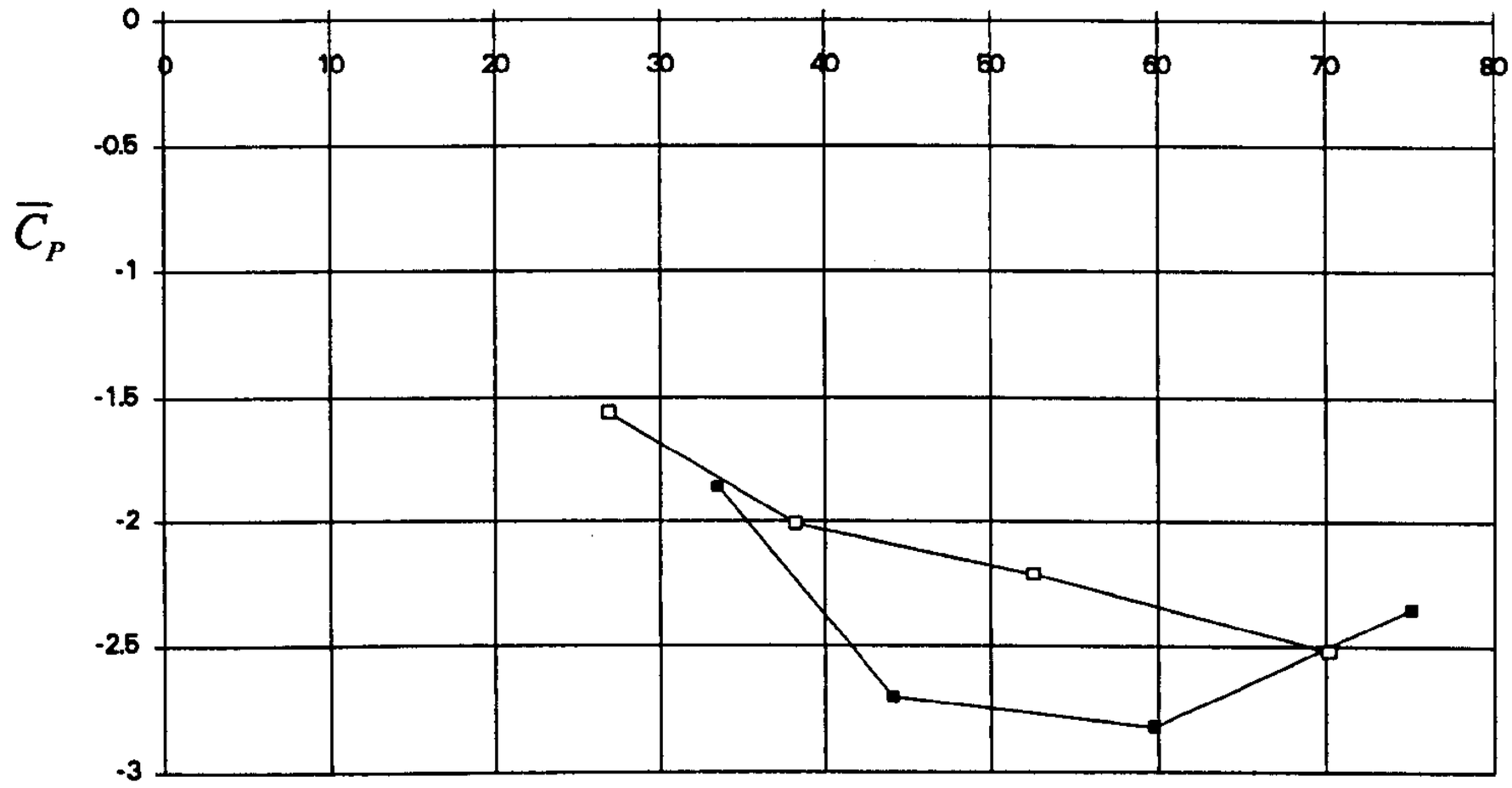

Figure 9.27 Mean pitching moment.
Flat ground and escarpment simulation for moving lorry tests.

□ Flat Ground Simulation
■ Escarpment Simulation

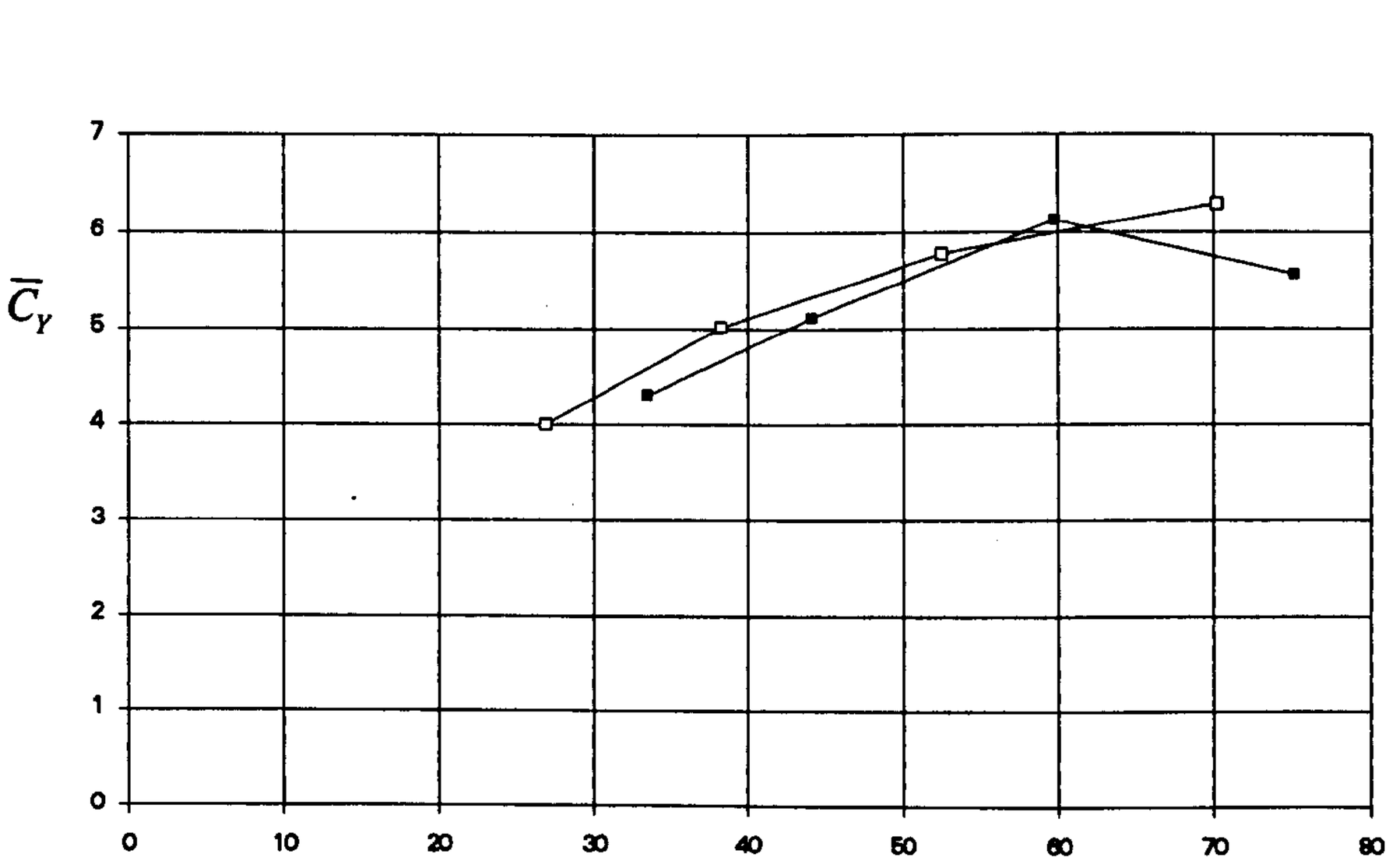

Figure 9.28 Mean yawing moment.
Flat ground and escarpment simulation for moving lorry tests.

□ Flat Ground Simulation
■ Escarpment Simulation

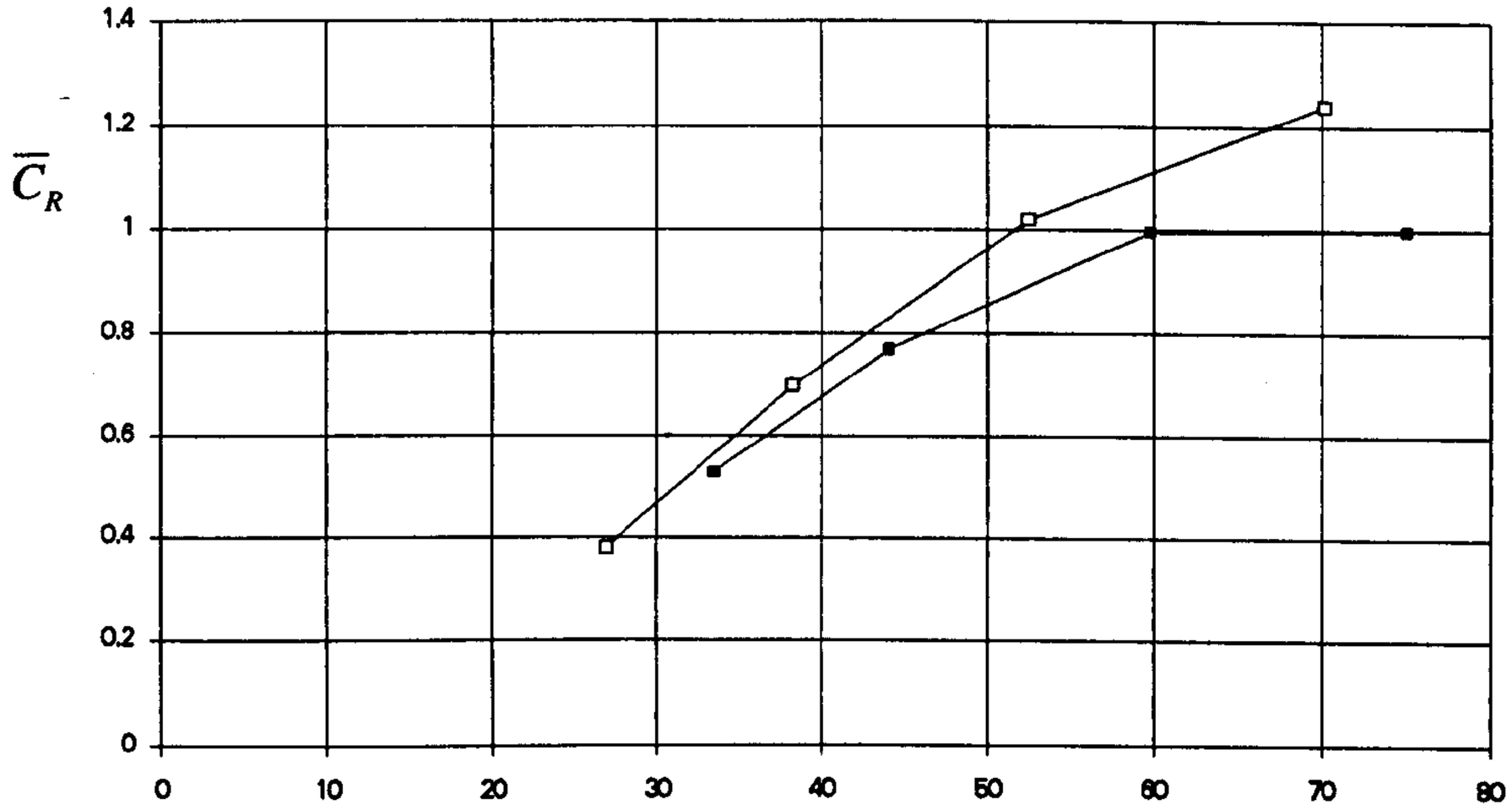

Figure 9.29 Mean rolling moment.
Flat ground and escarpment simulation for moving lorry tests.

□ Flat Ground Simulation
■ Escarpment Simulation

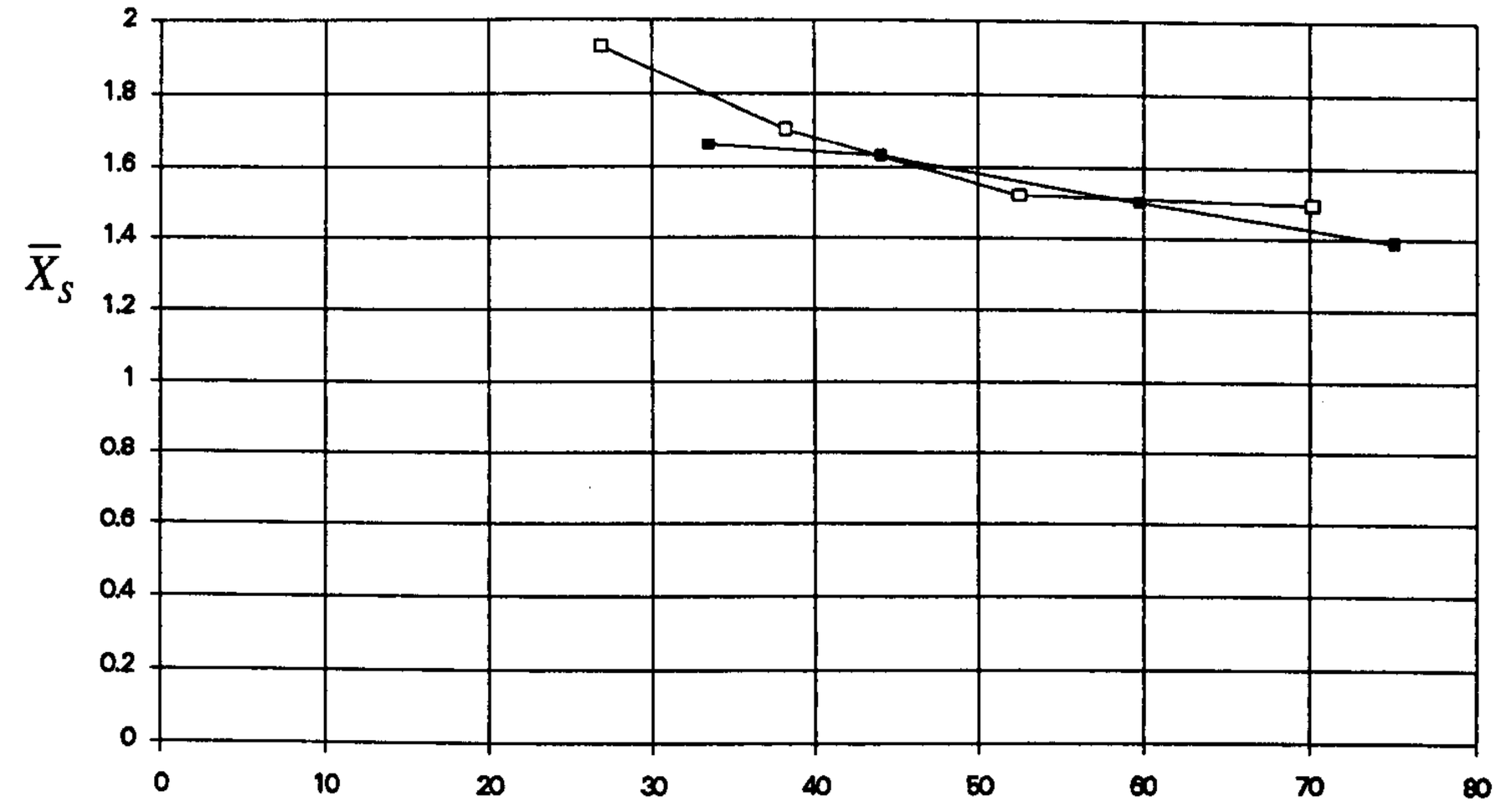

Figure 9.30 Non-dimensional horizontal point of action of side force.
Flat ground and escarpment simulation for moving lorry tests.

□ Flat Ground Simulation
■ Escarpment Simulation

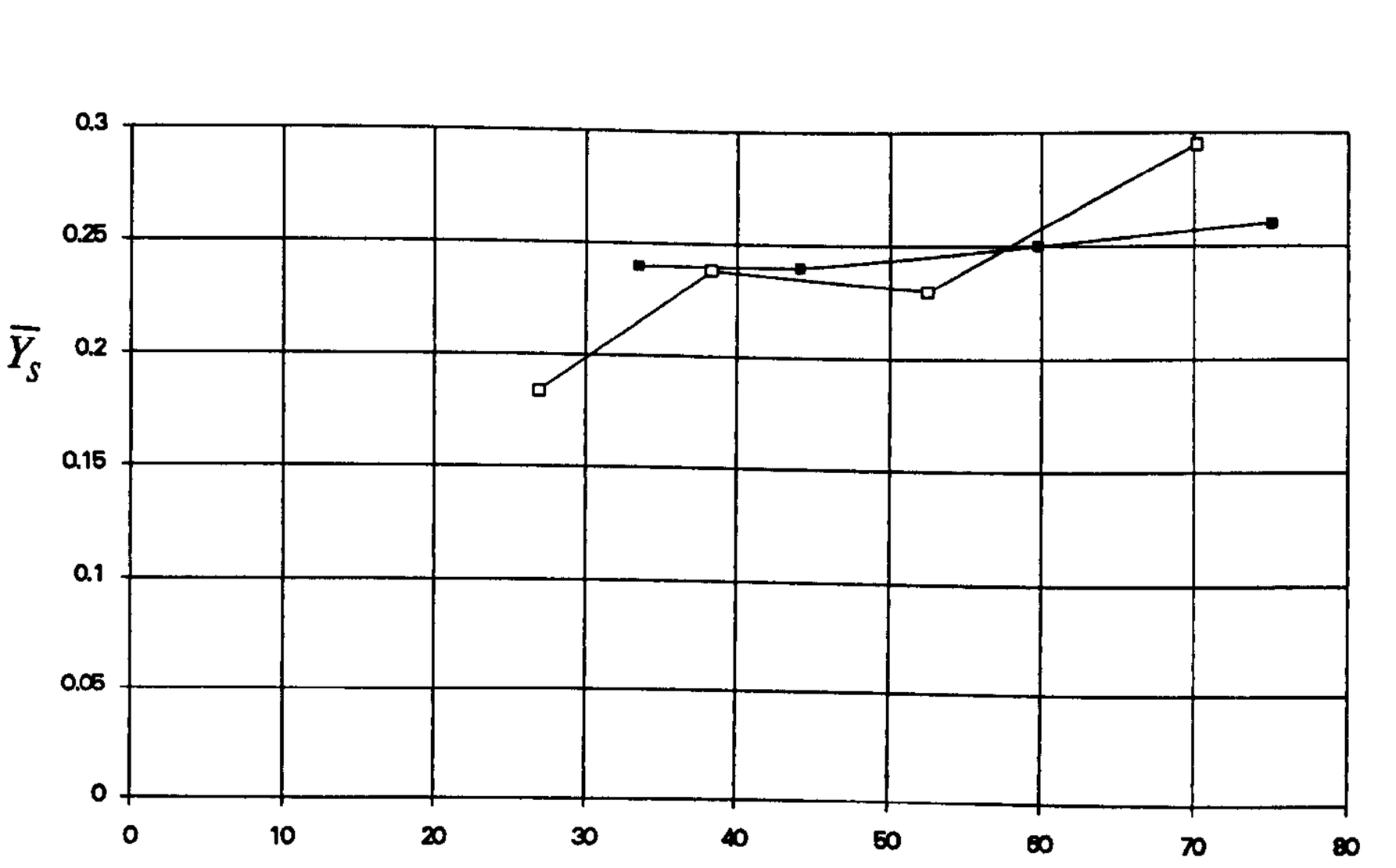

Figure 9.31 Non-dimensional vertical point of action of side force.
Flat ground and escarpment simulation for moving lorry tests.

□ Flat Ground Simulation
■ Escarpment Simulation

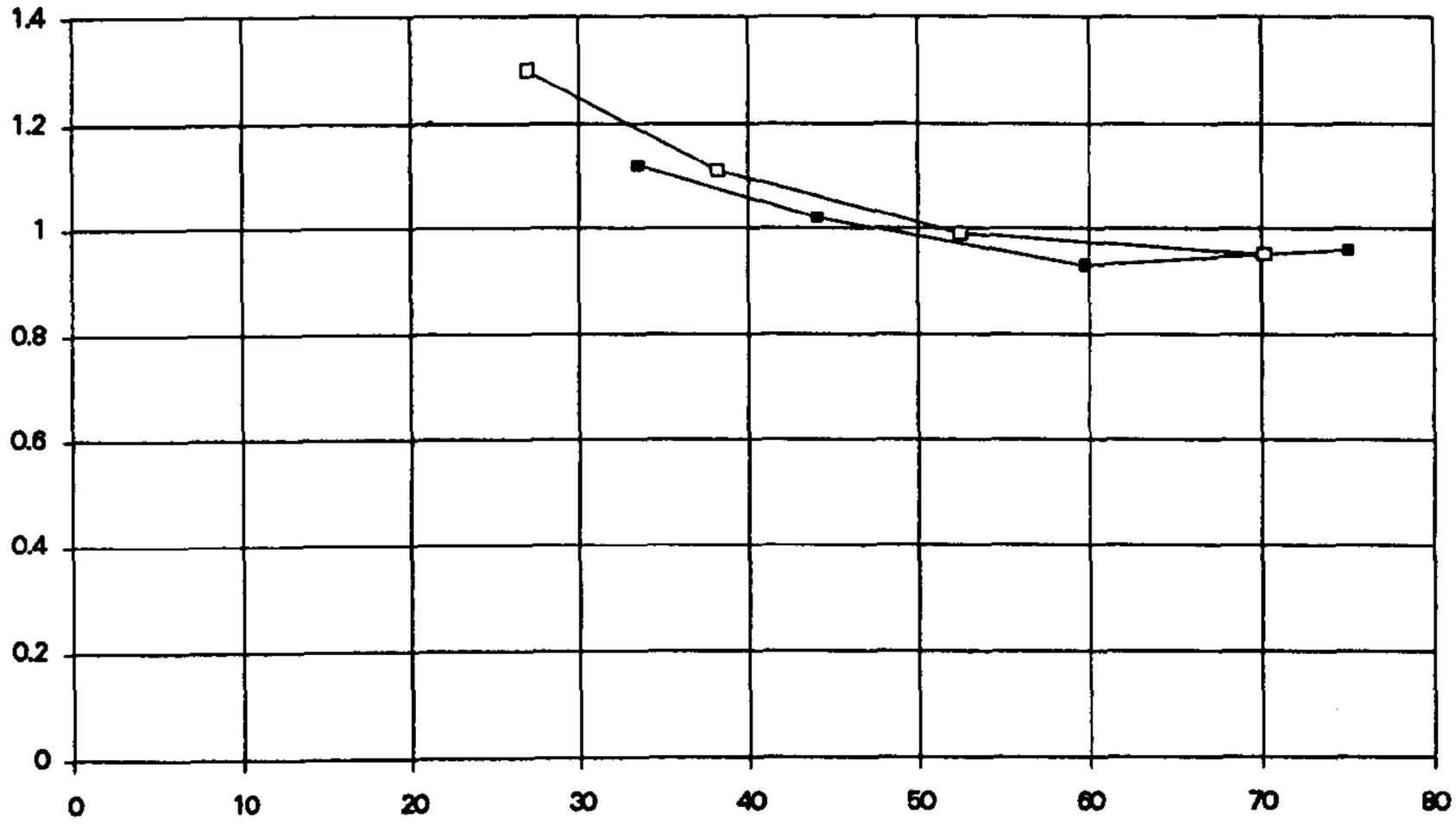

Figure 9.32 Normalised extreme side force parameter.
Flat ground and escarpment simulation for moving lorry tests.

□ Flat Ground Simulation
■ Escarpment Simulation

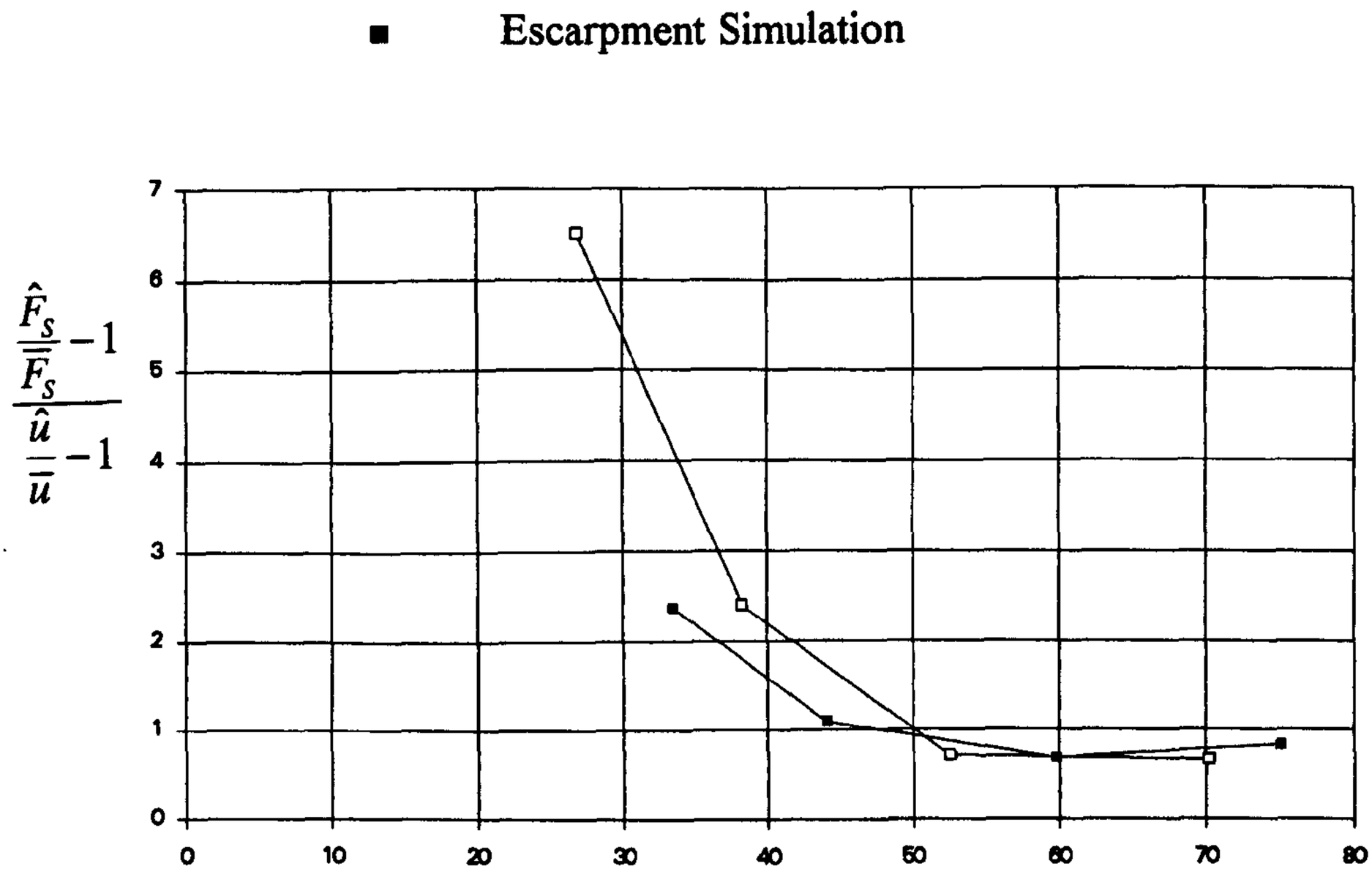

Figure 9.33 Unsteady side force parameter.
Flat ground and escarpment simulation for moving lorry tests.

□ Flat Ground Simulation
■ Escarpment Simulation

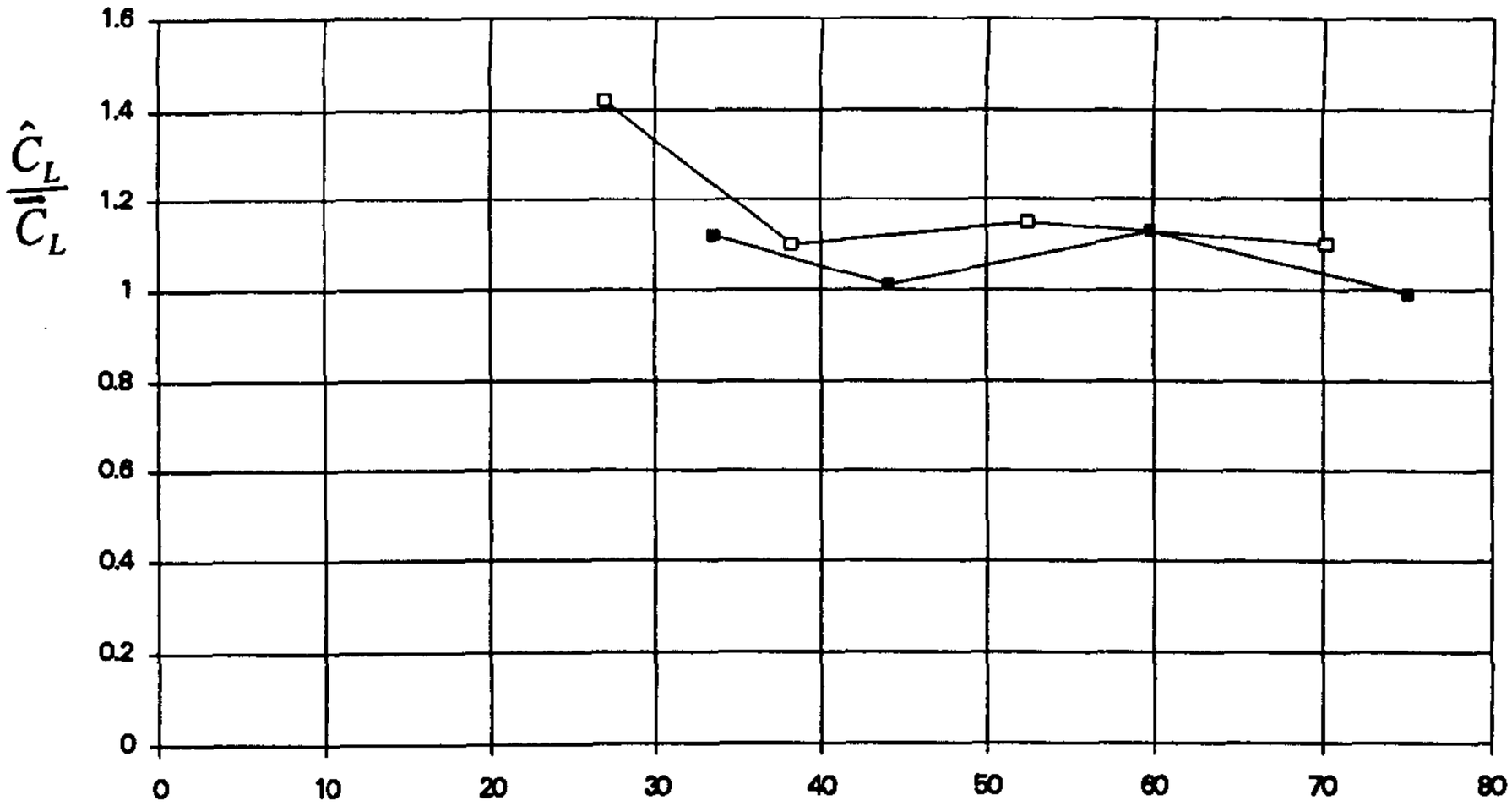

Figure 9.34 Normalised extreme lift force parameter.
Flat ground and escarpment simulation for moving lorry tests.

□ Flat Ground Simulation
■ Escarpment Simulation

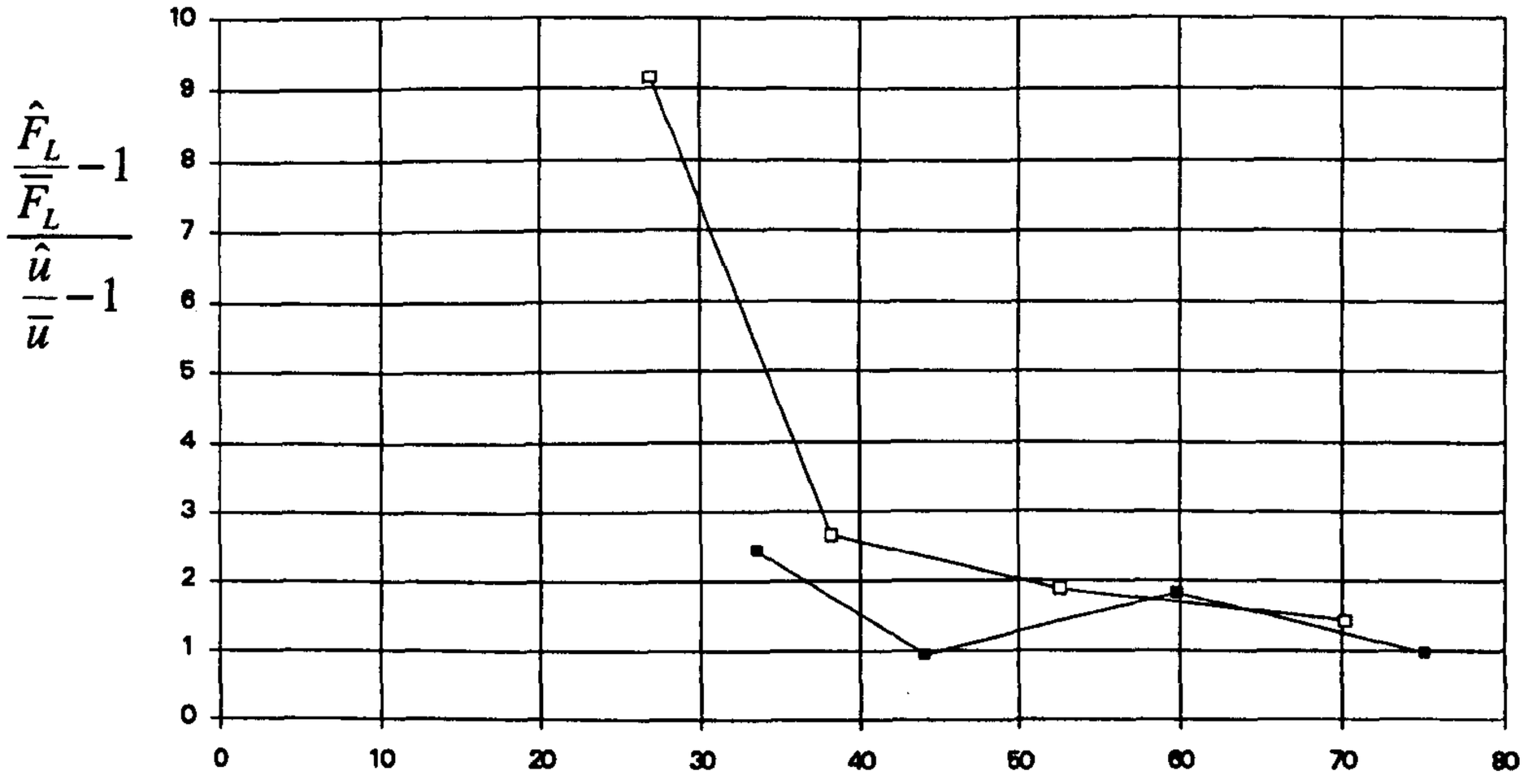

Figure 9.35 Unsteady lift force parameter.
Flat ground and escarpment simulation for moving lorry tests.

□ Flat Ground Simulation
■ Escarpment Simulation

FENCE LENGTH WAS THE FULL WIDTH OF WORKING SECTION

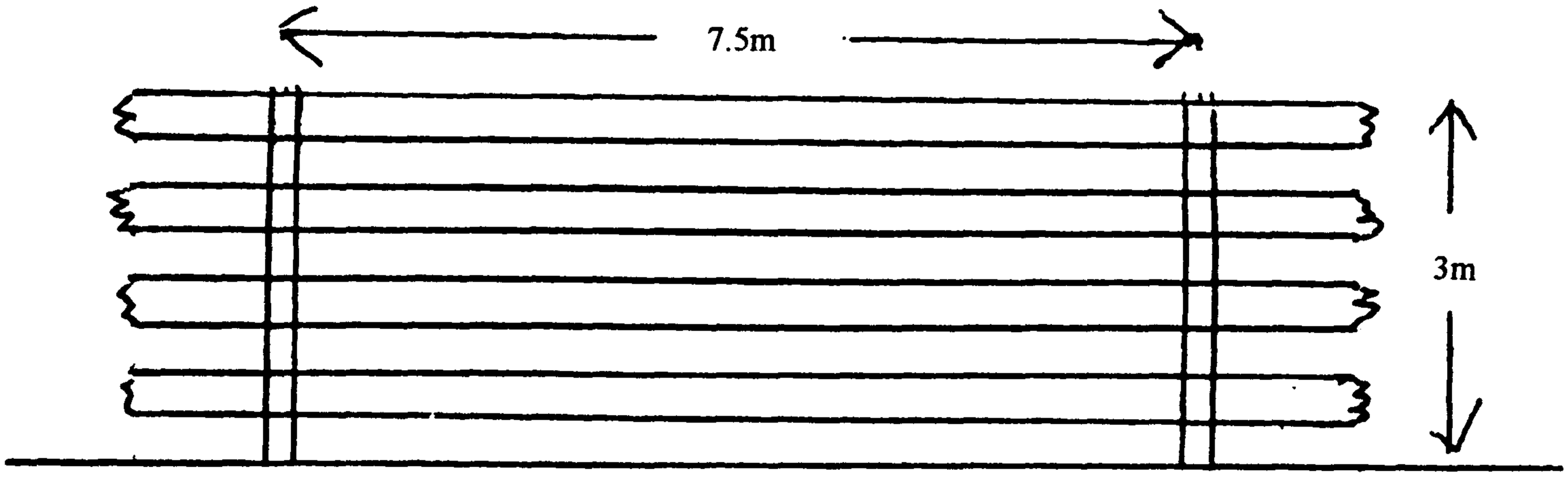

50% POROSITY WIND FENCE

DIMENSIONS ARE FULL SCALE EQUIVALENT

Figure 9.36 Wind fence model geometry.

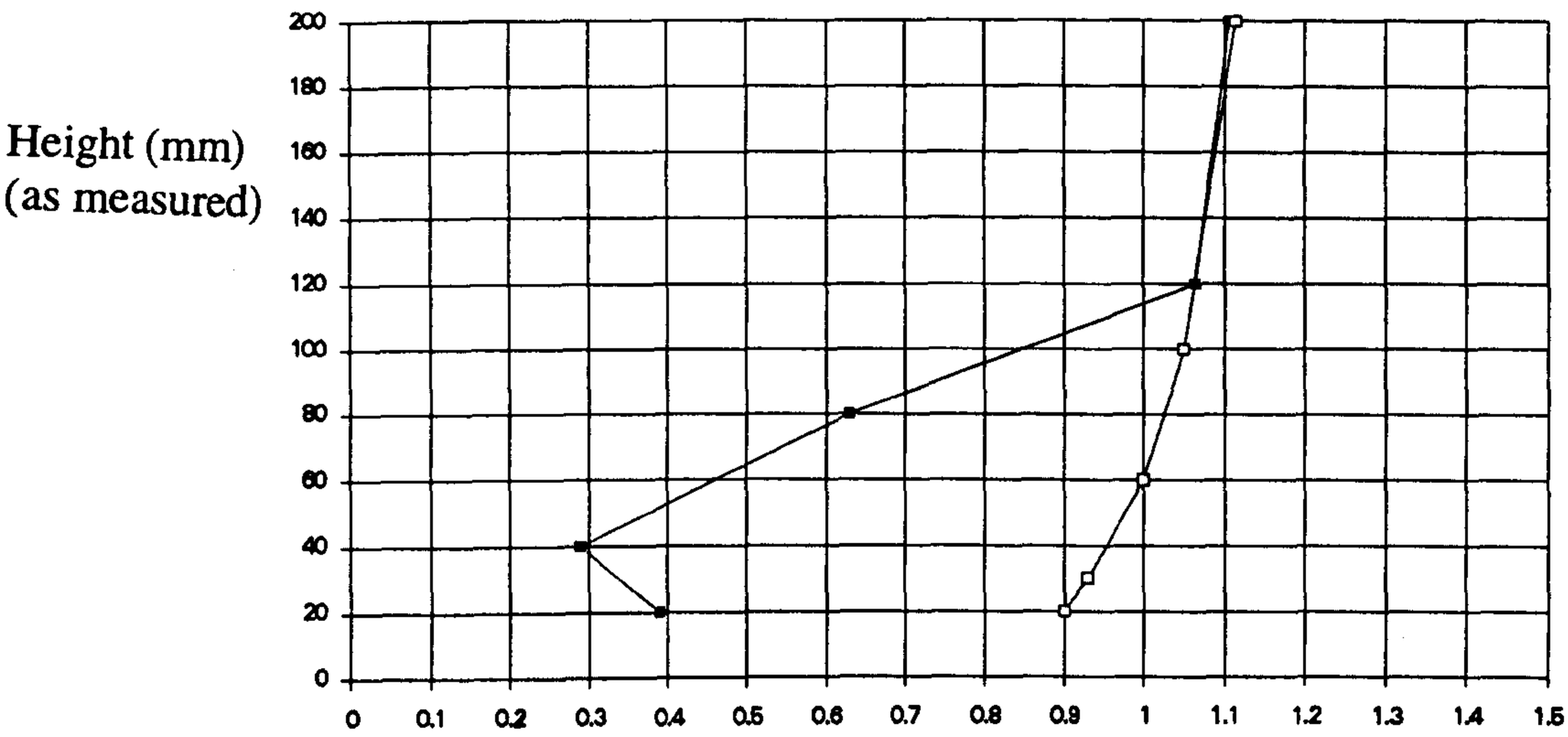

Figure 9.37 Streamwise wind velocity profile with height measured from escarpment surface, 100mm downstream of the wind fence at the centre of the moving model test section.

□ without fences, ■ with fences

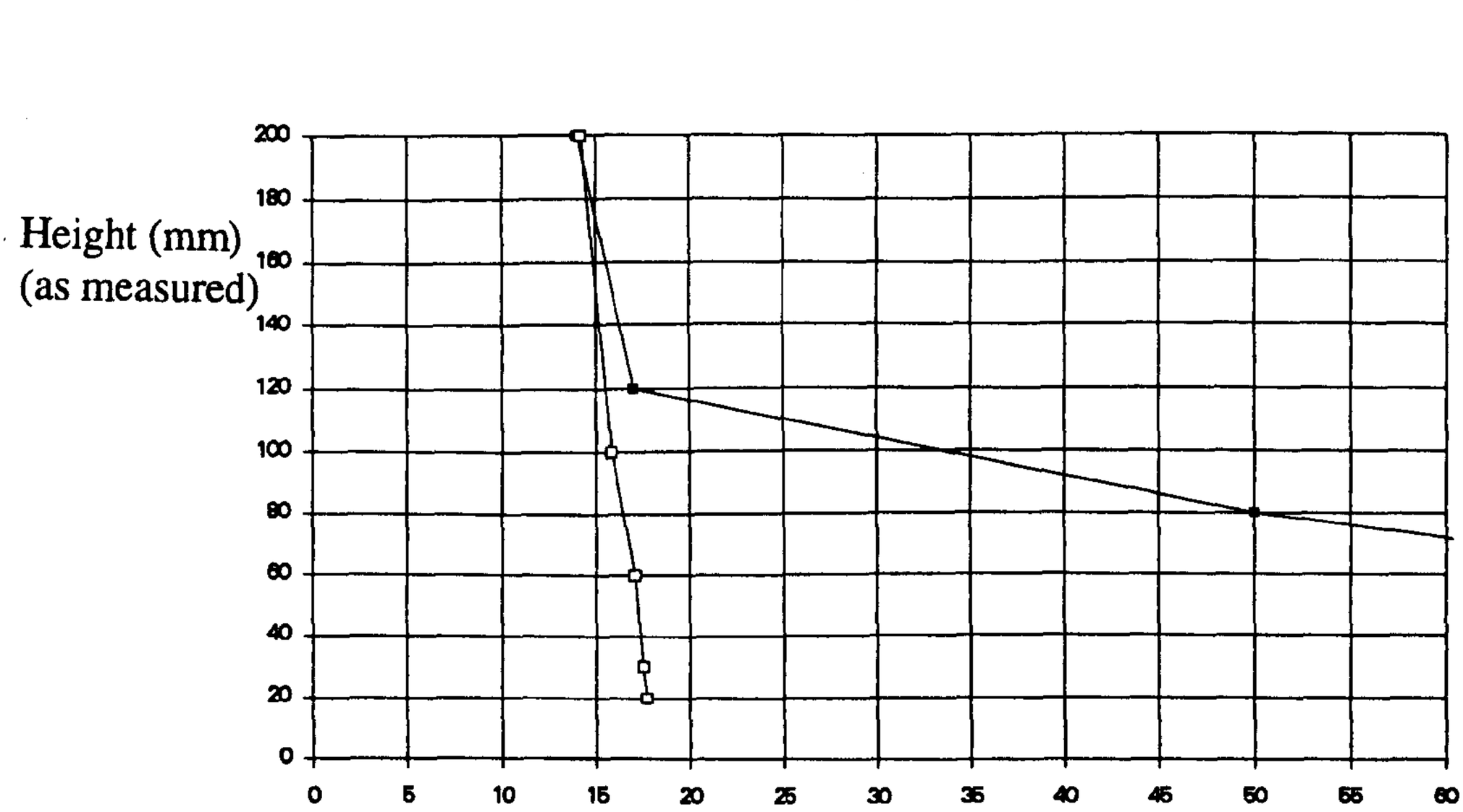

Figure 9.38 Streamwise turbulence intensity profile with height measured from escarpment surface, 100mm downstream of the wind fence at the centre of the moving model test section.

□ without fences, ■ with fences

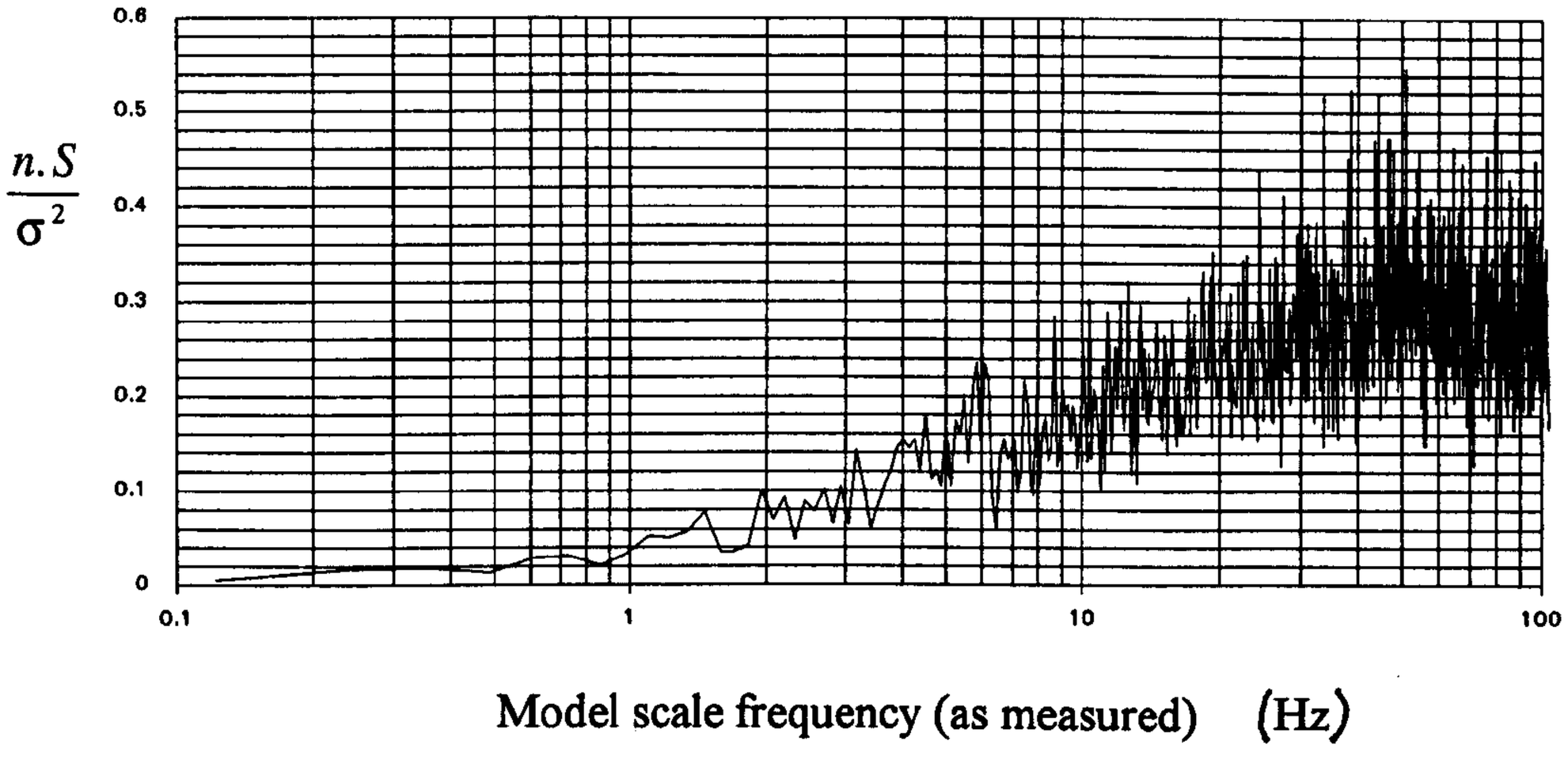

Figure 9.39a 40mm (equivalent to 2m full scale) above surface of escarpment. Streamwise wind velocity spectrum downstream of wind fence at centre of moving model test section.

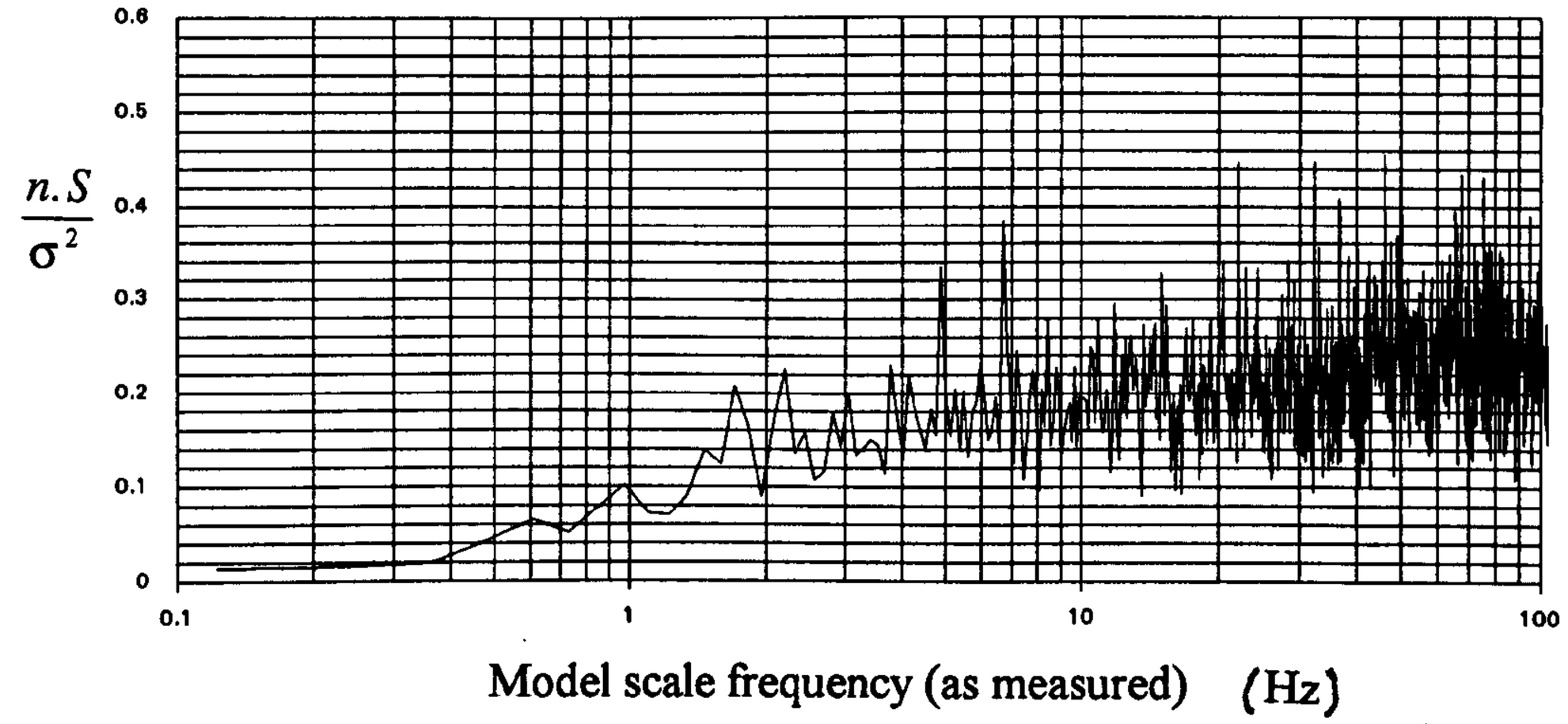

Figure 9.39b 80mm (equivalent to 4m full scale) above surface of the escarpment. Streamwise wind velocity spectrum downstream of wind fence at centre of moving model test section.

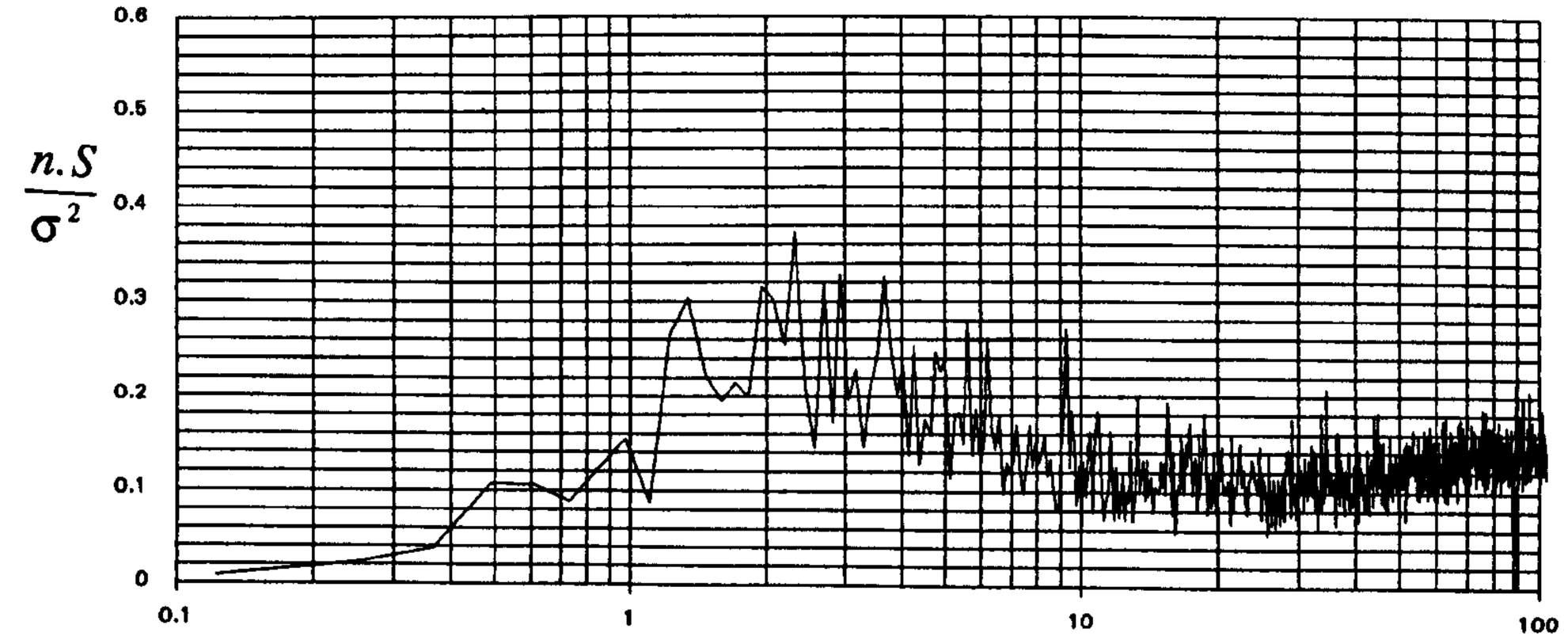

Figure 9.39c 120mm (equivalent to 6m full scale) above escarpment. Streamwise wind velocity spectrum downstream of wind fence at centre of moving model test section.

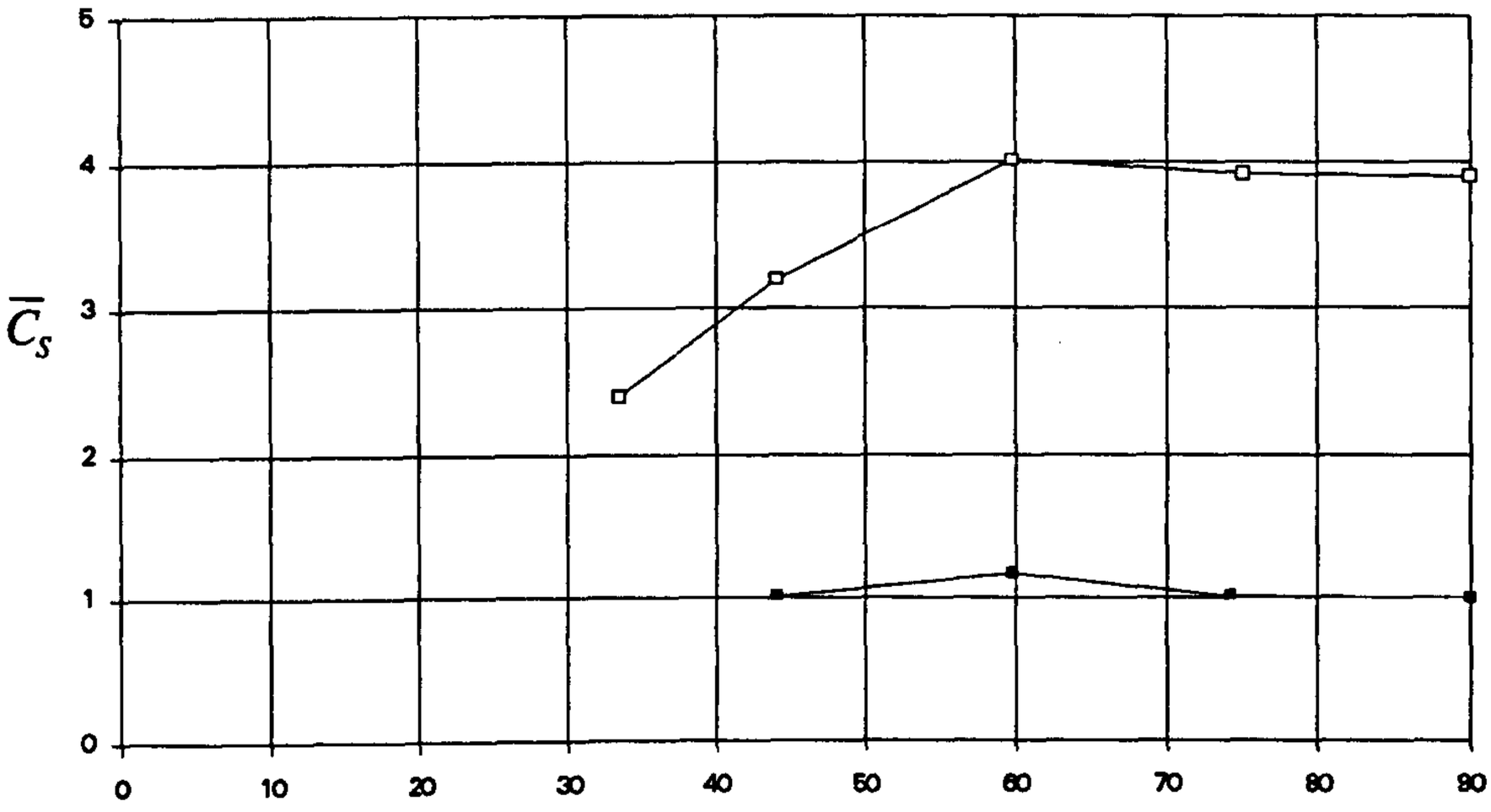

Figure 9.40 Mean side force coefficient.
Escarpment simulation for moving lorry tests with and without fences.

□ without fences, ■ with fences

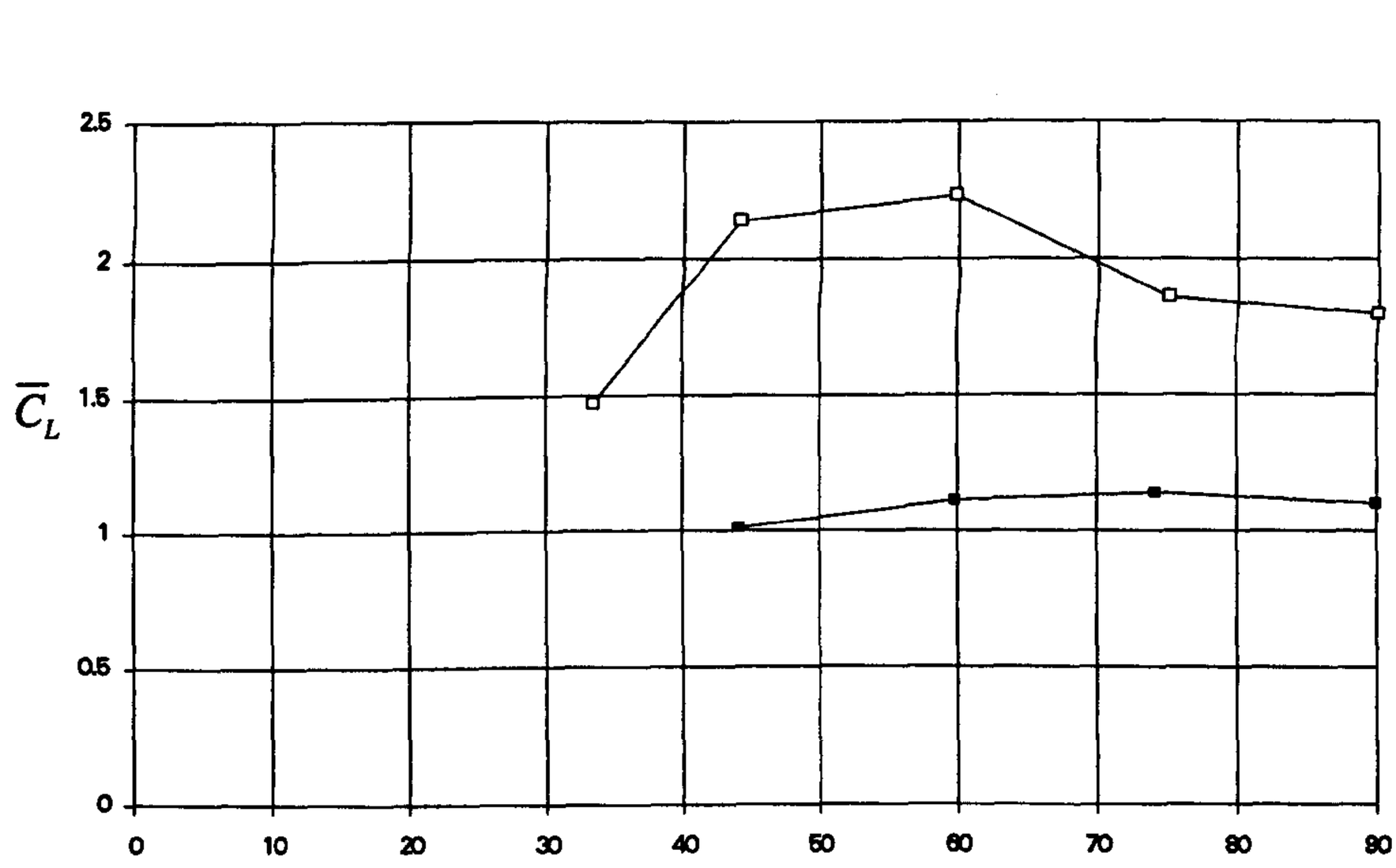

Figure 9.41 Mean lift force coefficient.
Escarpment simulation for moving lorry tests with and without fences.

□ without fences, ■ with fences

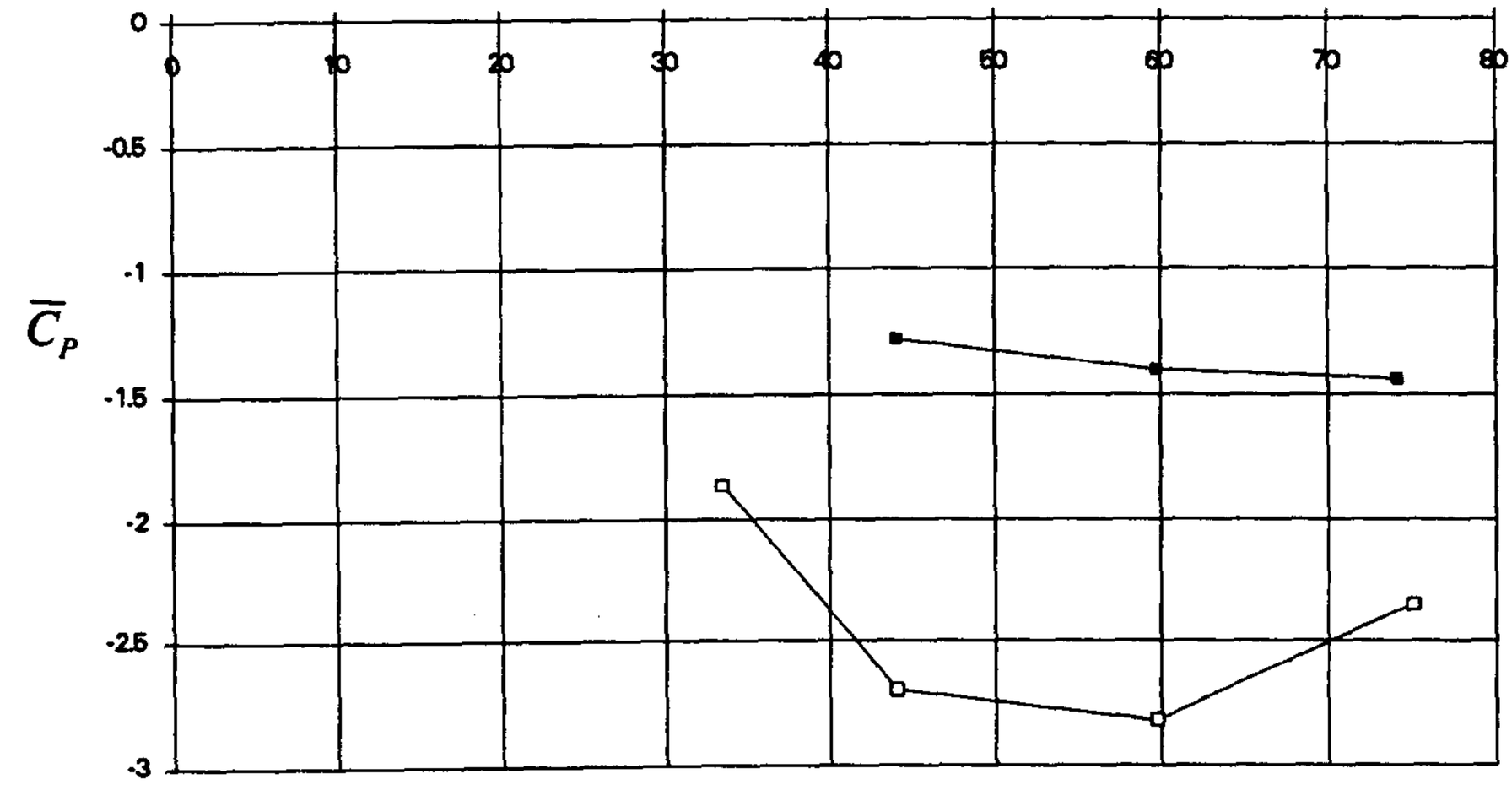

Figure 9.42 Mean pitching moment coefficient.
Escarpment simulation for moving lorry tests with and without fences.

□ without fences, ■ with fences

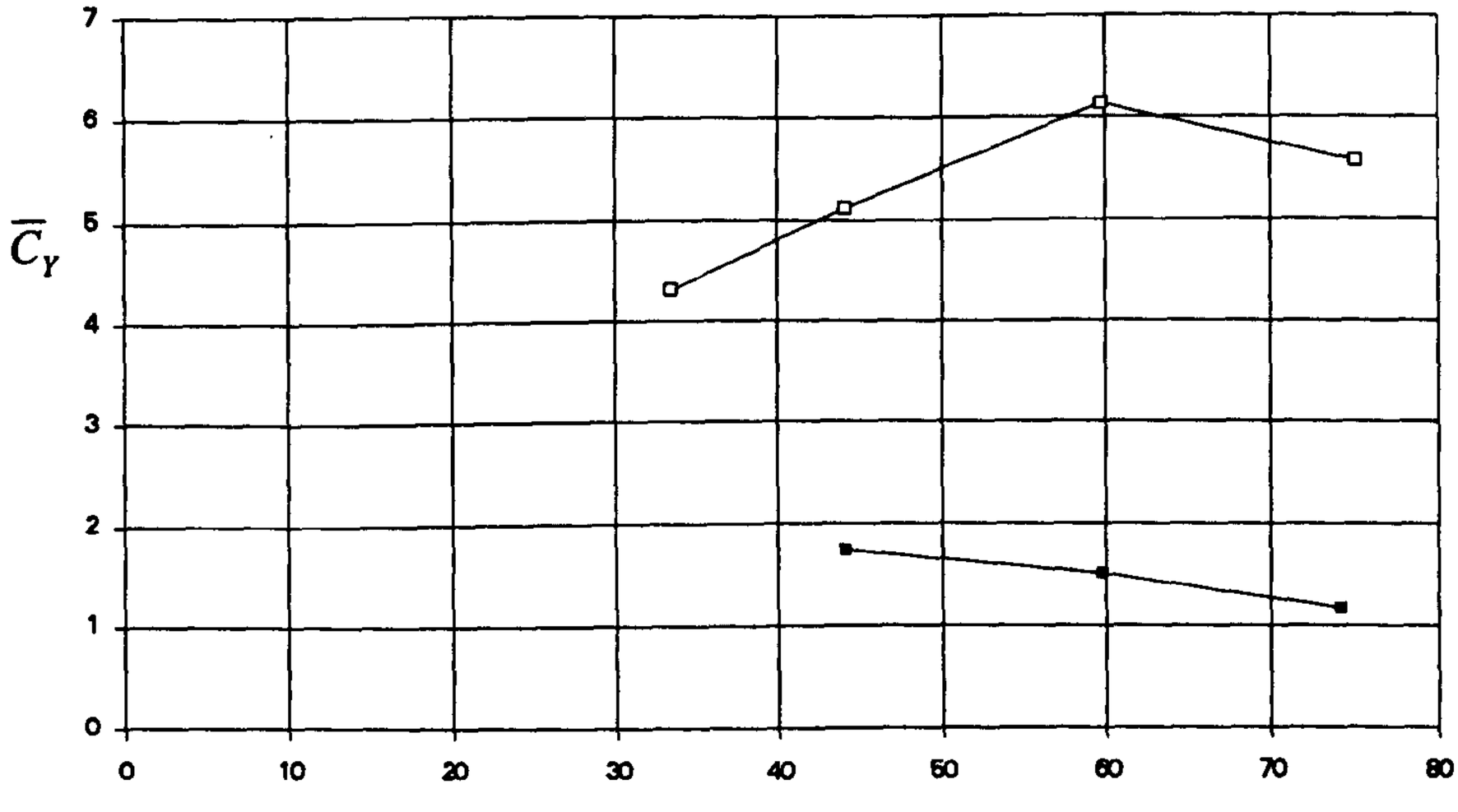

Figure 9.43 Mean yawing moment coefficient.
Escarpment simulation for moving lorry tests with and without fences.

□ without fences, ■ with fences

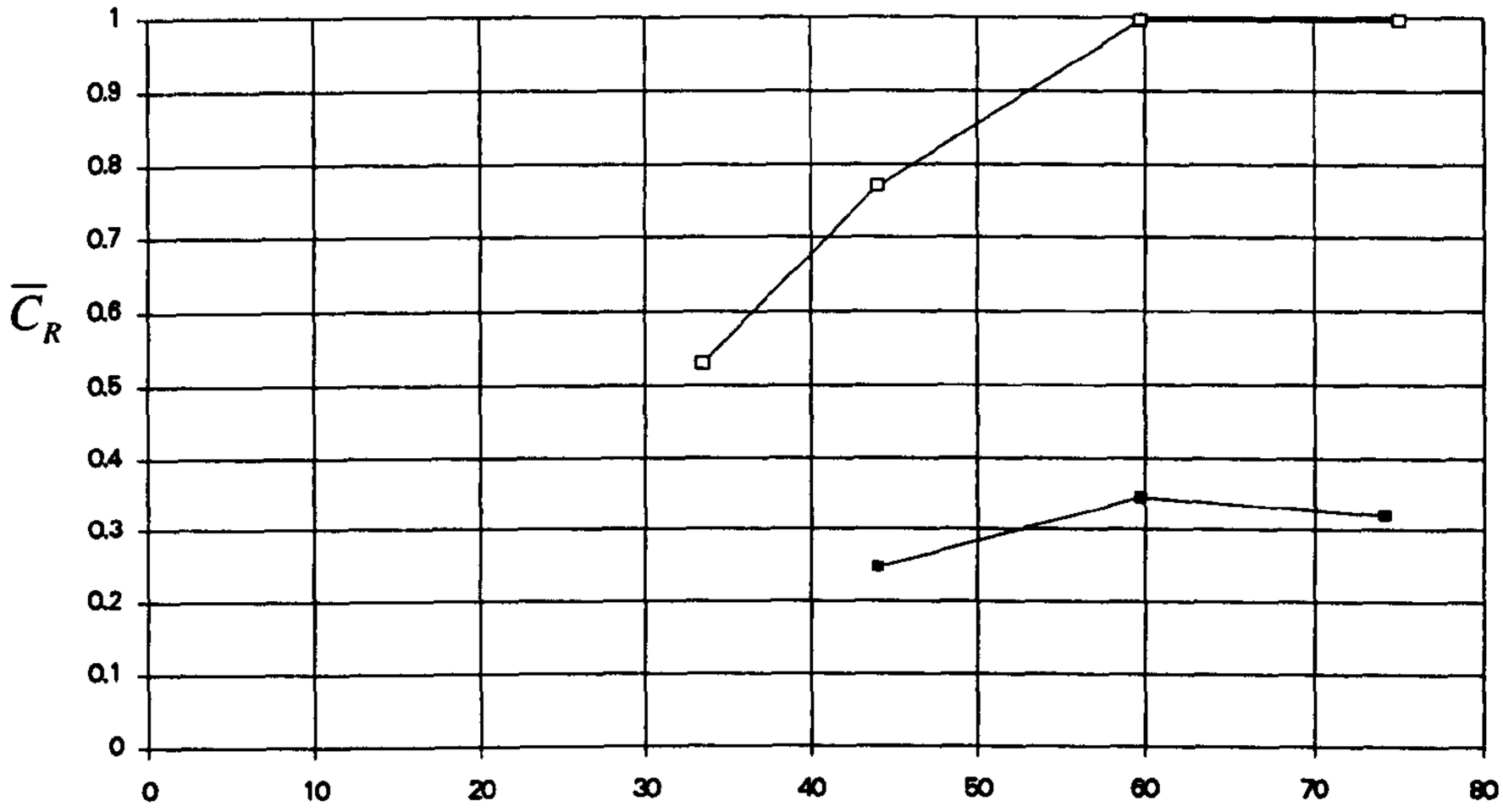

Figure 9.44 Mean rolling moment coefficient.
Escarpment simulation for moving lorry tests with and without fences.

□ without fences, ■ with fences

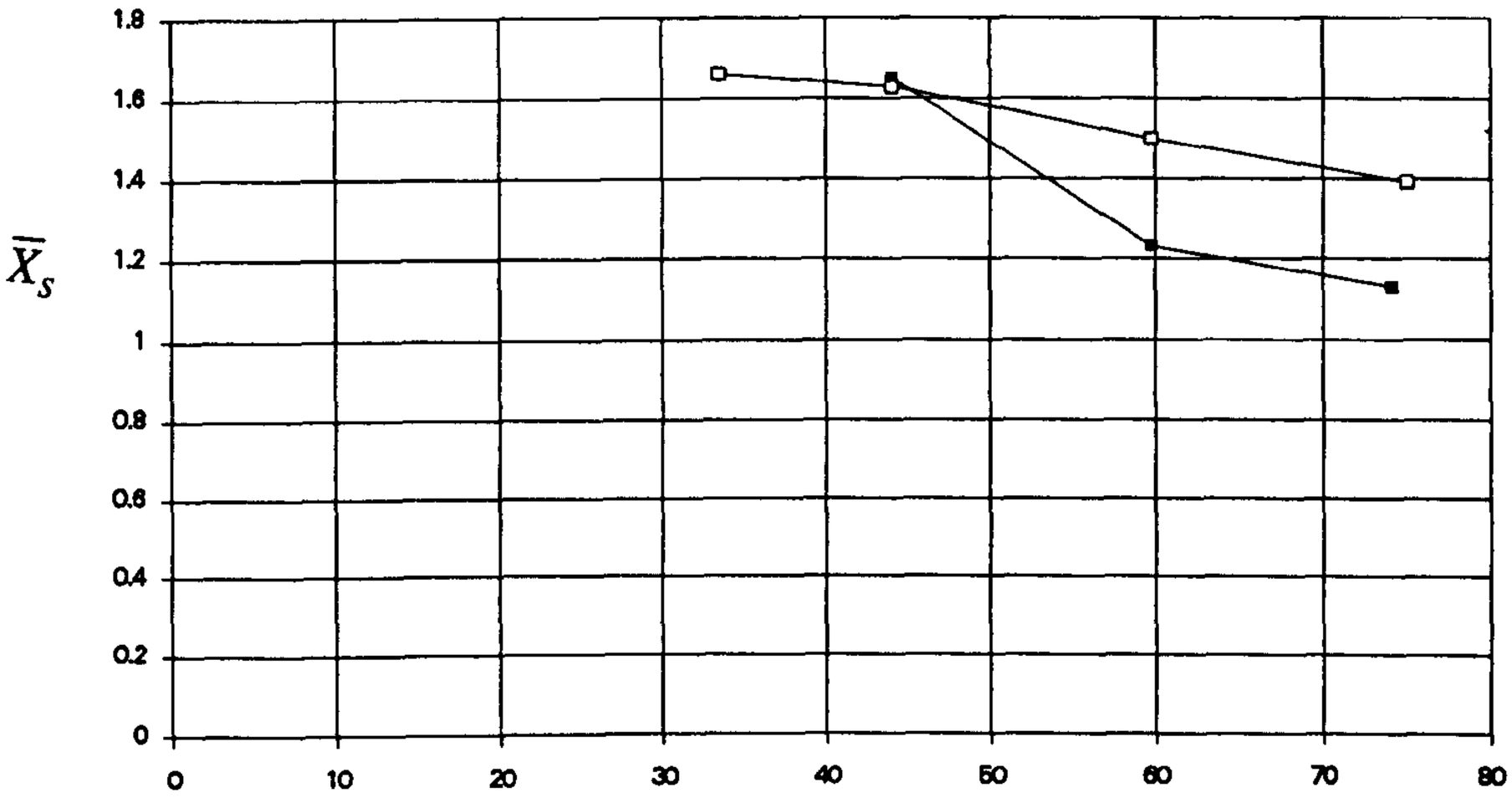

Figure 9.45 Non-dimensional horizontal point of action of side force. Escarpment simulation for moving lorry tests with and without fences.

□ without fences, ■ with fences

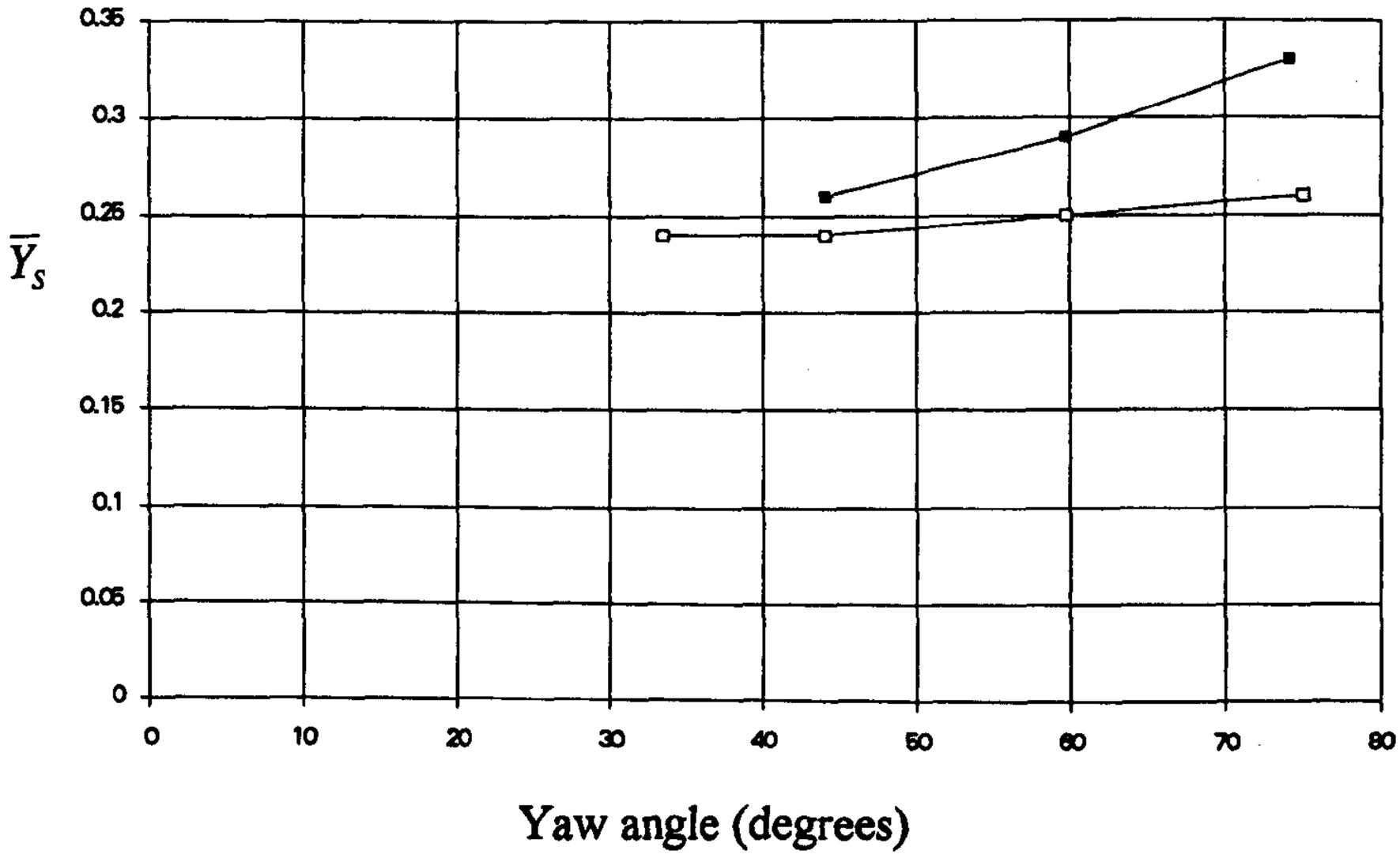

Figure 9.46 Non-dimensional vertical point of action of side force. Escarpment simulation for moving lorry tests with and without fences.

□ without fences, ■ with fences

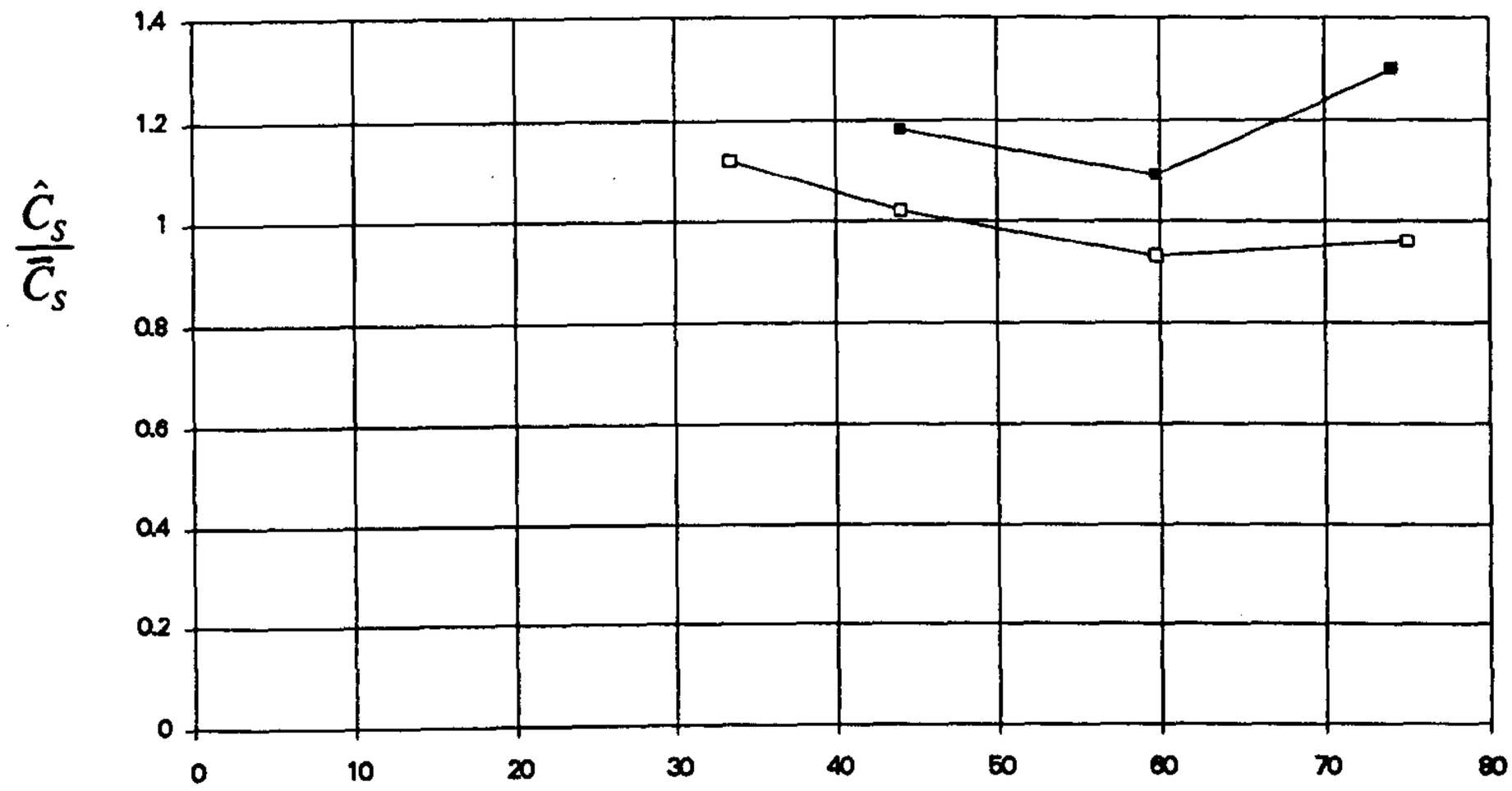

Figure 9.47 Normalised extreme side force parameter.
Escarpment simulation for moving lorry tests with and without fences.

□ without fences, ■ with fences

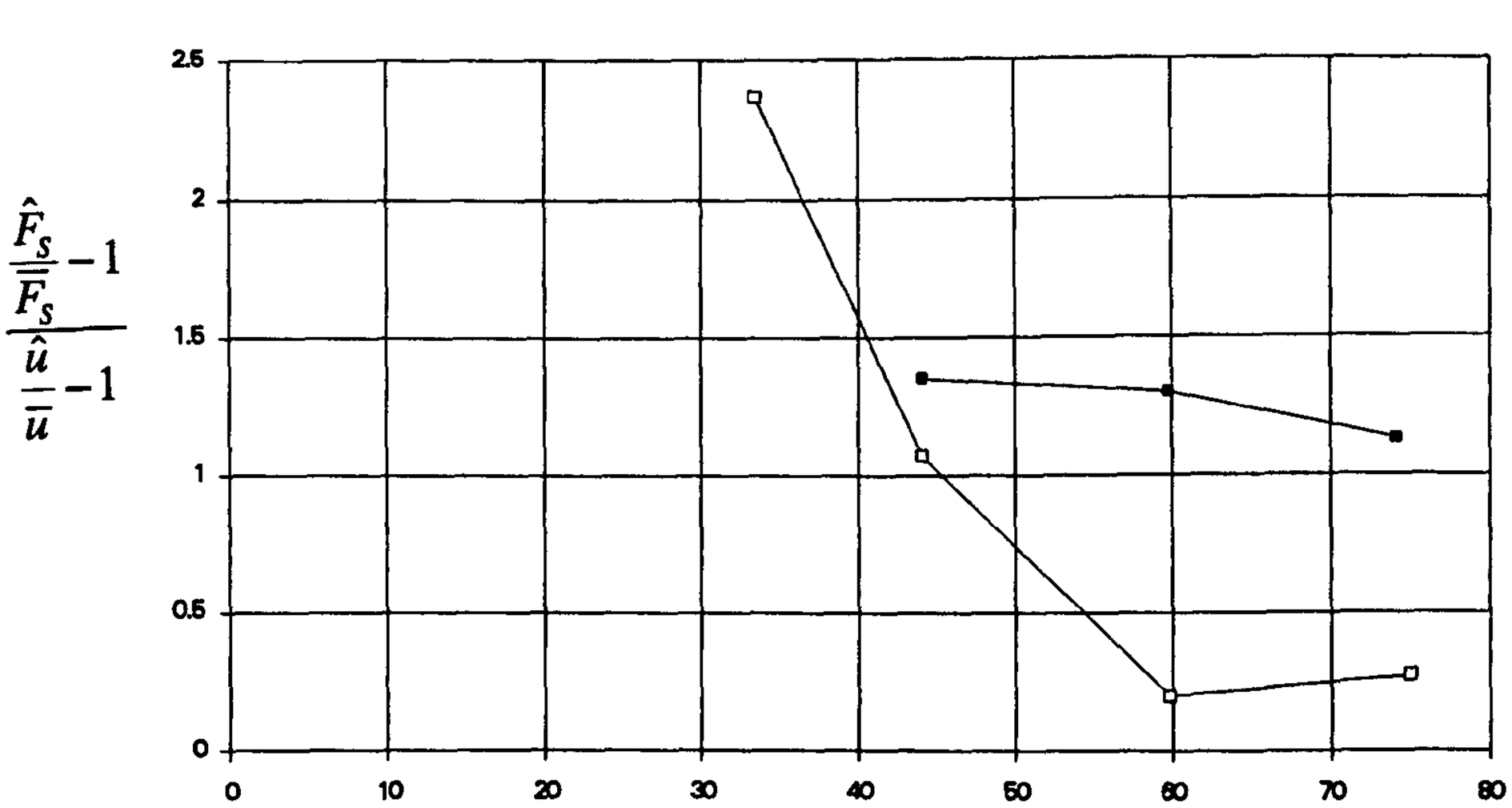

Figure 9.48 Unsteady side force parameter.
Escarpment simulation for moving lorry tests with and without fences.

□ without fences, ■ with fences

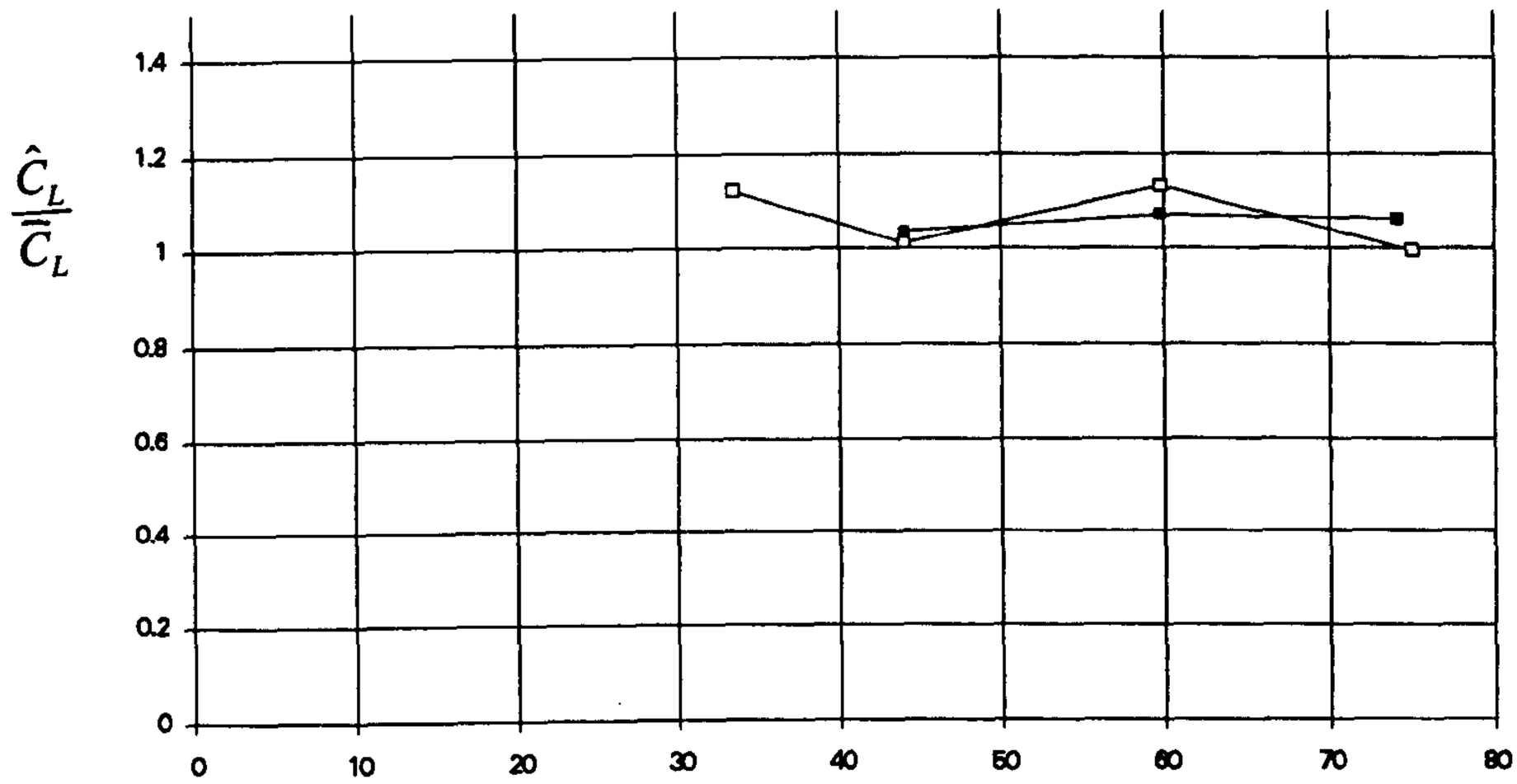

Figure 9.49 Normalised extreme lift force parameter.
Escarpment simulation for moving lorry tests with and without fences.

□ without fences, ■ with fences

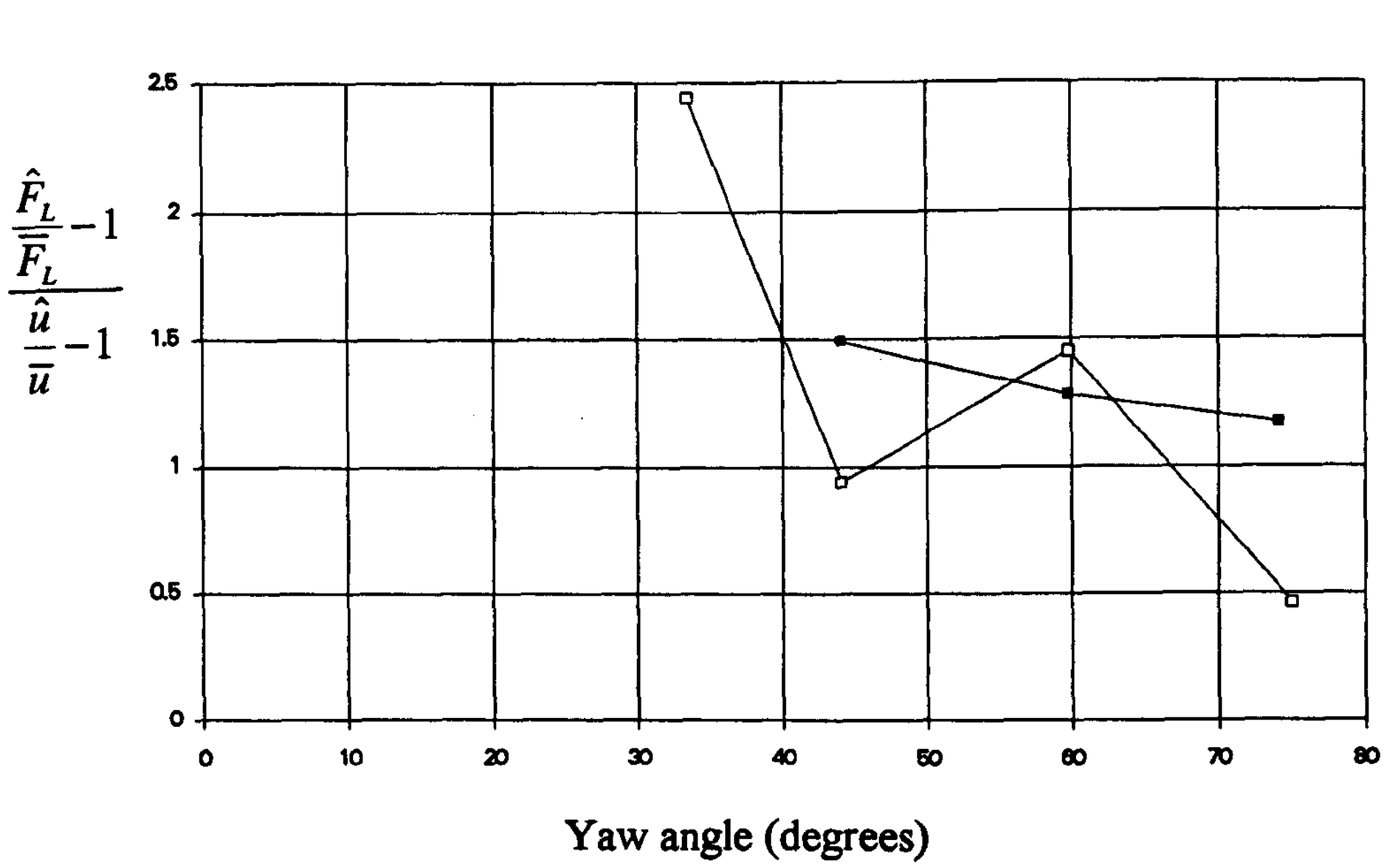

Figure 9.50 Unsteady lift force parameter.
Escarpment simulation for moving lorry tests with and without fences.

□ without fences, ■ with fences

10. Conclusions.

1. A mean hourly atmospheric boundary layer was simulated that was adequate for the determination of full scale representative normalised extreme force parameters and unsteady parameters from wind tunnel tests of 1/50th scale high sided sharp edged ground vehicles.

2. The moving model rig was shown to produce data of a reasonably high quality adequate for the determination of both mean and extreme aerodynamic forces.

3. The development of the automatic retrieval and firing mechanism was successful allowing one hundred runs of the rig to be undertaken in one day by one person.

4. The normalised extreme force parameter appears to be independent of the model time scale for both the static and moving wind tunnel tests.

5. For yaw angles above 30 degrees the normalised extreme force parameter takes the value of unity implying the quasi steady case for body induced unsteadiness. This was shown for the both the static and moving model tests on level ground and additionally the moving model tests on the escarpment.

6. For yaw angles less than 30 degrees, body induced unsteadiness was implied with the normalised extreme force parameters taking values up to 1.3. Again this was shown for both the static and moving model tests on level ground and additionally the moving model tests on the escarpment.

7. The side force coefficients for the static tests and both the flat ground and the escarpment moving model tests show excellent agreement. Additionally these values show similar trends with yaw angle as previous tests in low turbulence and simulated short turbulence length scale undertaken in uniform flow. The absolute values however depend upon the reference height chosen for the tests in which a vertical wind profile has been measured.

8. The lift force coefficients were found to be very sensitive to changes in geometry and turbulence length scale. Of concern, was the much larger value of the lift force coefficient measured at the moving model position, but stationary i.e. 90 degrees, compared with the same geometry at the static test position. The reason for this is

unclear but suspicion is cast at the presence of the slot beneath the moving model which may alter the pressure beneath the vehicle. However reference to previous static higher Reynolds number tests may indicate that the fault could lie with the recent static tests for which the Reynolds number appropriate for the underbody gap may be inadequate. More work is needed in this area.

9. The 50% porosity wind fences reduced the side force such that for some yaw angles its value is only 20% of the value without the fences. Such reductions of the lift force however were not found, the maximum being 50%, due to the top of the vehicle being above the height of the fence.

10. The normalised extreme force parameters were calculated for tests behind the wind fence and provide useful data but caution should be taken in relating their values to states of body induced unsteadiness due to the unknown effects of the wind fence on the mean and extreme wind velocity values.

11. The invariance of the normalised extreme force parameter with model time scale (over the range of concern) implies that it is possible to calculate full scale extreme force values based on this parameter and knowledge of the full scale extreme wind velocity. Further, whilst wind tunnel tests are needed to measure data in order to determine the magnitude of the normalised extreme force parameters, conclusions 4 and 5 indicate that this parameter does not appear to be too sensitive to either the geometric or ABL simulation. This latter point is due to the agreement of both the static and moving tests.

12. For a given full scale scenario, in general a static measured wind gust value at the site (at say 3m height) will provide an overestimated extreme wind velocity value, for calculating the extreme force based on a known normalised extreme force parameter, for a vehicle moving perpendicular to it. Indeed the results of these wind tunnel tests indicate, to the accuracy considered, that the extreme wind velocity to be used for a moving vehicle is the resultant of the vehicle's velocity and the wind velocity. Caution should be applied in using this result for the full scale case as differences in the lateral components of the ABL may be important.

13. Recently Hoxey (1992) from measurements at heights of up to 10m above ground level has derived wind velocity spectra which were found to be distorted, with some energy transferred to the higher frequencies. This implies, therefore, a lower extreme wind velocity value than predicted by Cook (1985). This latter reference does

indicate the lack of knowledge of wind data at these small heights. Extreme force values calculated from use of the normalised extreme force parameter and the results of Cook (1985) for level ground situations ought to be conservative if the results of Hoxey (1992) are generally applicable. That is the effect of possibly over estimating the extreme streamwise wind speed due to using the results of Cook (1985) or E.S.D.U. (1974a,b and 1975), compared to the recent results of Hoxey and Richards (1992), leads to an over prediction to the extreme forces.

14. If the prime aim of future tests, using the moving model rig and the existing hardware, is the determination of the aerodynamic admittance for the side and lift forces, it is recommended that these are recorded from separate tests. The Polycorder data logger can facilitate analogue filtering providing that only one channel is utilised and this would aid the reduction of the mechanical noise present at low frequencies. This noise may be mainly due to the ailiasing of the mechanical noise which dominates the high frequency part of the measured force spectra, as shown in this thesis. Further, the use of the Polycorder in this manner should also increase the accuracy of any extreme values calculated using the time domain method demonstrated in this thesis.

15. Noting the problems with the measured lift force measurement, using the moving model rig, it is recommended that for subsequent tests, designed to measure this component, that the model be mounted in front of the slot through which the balance supports pass. For example, the balance support struts could pass through the lee ward side of the vehicle, before turning and passing through the slot which would be downstream of the vehicle's track. However these struts would have to be suitably rigid in order to keep the mechanical noise to the high frequency part of the force spectrum. For future side force measurements, the mounting arrangement used for the tests described in this thesis is adequate.

References.

Baker, C.J. (1981a) : *The Cranfield moving model experiment : part III results and discussion,* British Rail Research Division Technical Memorandum TMAERO 52.

Baker, C.J. (1981b) : *Tests on a 1/50th scale APT-S in low a low turbulence wind tunnel,* British Rail Research Division Technical Memorandum TMAERO 58.

Baker, C.J. (1983a) : *Wind tunnel tests on a 1/35th scale model APT-S,* British Rail Research Division Technical Memorandum TMAERO 69.

Baker, C.J. (1983b) : *Wind tunnel tests on a 1/50th scale model APT-S in the Oxford University Wind Tunnel,* British Rail Research Division Technical Memorandum TMAERO 69.

Baker, C.J. (1986a) : *A simplified analysis of various types of wind induced road vehicle accidents,* Journal of Wind Engineering and Industrial Aerodynamics 22, 1, 69-85.

Baker, C.J. (1986b) : *Train aerodynamic forces and moments from moving model experiments,* Journal of Wind Engineering and Industrial Aerodynamics 24, 227-251.

Baker, C.J. (1987) : *Measures to control vehicle movement at exposed sites during windy periods,* , Journal of Wind Engineering and Industrial Aerodynamics 25, 2, 151-161.

Baker, C.J. (1988) : *High -sided articulated road vehicles in strong cross winds,* Journal of Wind Engineering and Industrial Aerodynamics 31, 67-85.

Baker, C.J. (1989) : *Private communication with Coleman, S.A.,* Dept. of Civil Engineering, University of Nottingham.

Baker, C.J. (1991a) : *Ground vehicles in high cross winds - part I: Steady aerodynamic forces,* Journal of Fluids and Structures 5, 69-90.

Baker, C.J. (1991b) : *Ground vehicles in high cross winds - part II: Unsteady aerodynamic forces,* Journal of Fluids and Structures 5, 91-111.

Baker, C.J. (1991c) : *Ground vehicles in high cross winds - part III: The interaction of aerodynamic forces and the vehicle system,* Journal of Fluids and Structures 5, 221-241.

Baker, C.J. (1993) : *The behaviour of road vehicles in unsteady cross winds,* Journal of Wind Engineering and Industrial Aerodynamics 49, 439-448.

Baker, C.J. and Gawthorpe, R.G. (1983) : *The effect of turbulence simulation on the wind induced loads on ground vehicles.* ASME : Aerodynamics of Transportation II (eds T. Morel and J. Miller), pp.1-9. New York.

Bearman, P.W. and Mullarkey, S.P. (1994) : *Aerodynamic forces on road vehicles due to steady side winds and gusts,* Proceedings RAeS Conference on Vehicle Aerodynamics, Loughborough, 1994.

Brendat, J. and Piersol, A. (1977) : *Random Data: Analysis and Measurement Procedures,* Wiley-Interscience.

Brenner, N. (1967) : *The fast Fourier transform,* IEEE Transactions on Audio and Electroacoustics, June 1967.

Bryer, D.W. and Pankhurst, R.C. (1971) : *Pressure - probe methods for determining wind speed and flow directions.* National Physical Laboratory, London 1971, HMSO

Cairns, R.S. (1994) : *The lateral aerodynamic characteristics of motor vehicles in cross winds.* PhD Thesis, Cranfield University, 1994.

Coleman, S.A. (1990) : *The aerodynamics of ground vehicles in cross winds,* Ph.D. Thesis, University of Nottingham, 1990.

Coleman, S.A. and Baker, C.J. (1989) : *High sided road vehicles in cross winds,* Proceedings of the 6th US Wind Engineering Conference, Houston 1989, also Journal of Wind Engineering and Industrial Aerodynamics 36, 1383-1397.

Coleman, S.A. and Baker, C.J. (1992) : *Reduction of accident risk for high sided vehicles in cross winds,* Proceedings of the 8th International Conference on Wind Engineering 1991, also Journal of Wind Engineering and Industrial Aerodynamics 41-44, (1992) 2685-2695.

Coleman, S.A. and Baker, C.J. (1994) : *An experimental study of the aerodynamic behaviour of high sided lorries in cross winds,* Journal of Wind Engineering and Industrial Aerodynamics.

Counihan, J. (1975) : *Adiabatic atmospheric boundary layers: a review and analysis of data from the period 1880 - 1972.* Atmospheric Environment 9, 871 - 905.

Cook, N.J. (1985) : *The designers guide to wind loading of building structures - Part I.* Butterworths, London.

Cook, N.J. (1978) : *On simulating the atmospheric boundary layer in wind tunnels.* Building Research Establishment Current Paper, CP71/78.

Cook and Mayne (1989) : *A novel working approach to the assessment of wind loading for equivalent static structures.* Journal of Industrial Aerodynamics 2, 149-161.

Cooper, R.K. (1977) *: The aerodynamic forces on a 3-car APT model at low angles of yaw.* British Rail Research Division Technical Memorandum TMAERO 14.

Cooper, R.K. (1978) : *Tests on a 1/5th scale APT-P in the MIRA wind tunnel.* British Rail Research Division Technical Memorandum TMAERO 28.

Cooper, R.K. (1979) : *Tests on a 1/5th scale model APT-P moving through a cross wind,* British Rail Research Division Technical Memorandum TMAERO 35.

Cooper, R.K. (1982) : *Wind tunnel tests on a 1/25th scale APT-P model,* British Rail Research Division Technical Memorandum TMAERO 43.

Cooper, R.K. (1981) : *The effect of cross winds on trains.* ASME Journal of Fluids Engineering, 103, 170 - 178.

Cooper, R.K. (1984) : *Atmospheric turbulence with respect to moving ground vehicles,* Journal of Wind Engineering and Industrial Aerodynamics, 17, 215-238.

Cooper, K.R., Fediw, A.A. and Garry, K.P. (1994) : *Development of a moving belt system for the study of vehicle aerodynamics,* Proceedings RAeS Conference on Vehicle Aerodynamics, Loughborough, 1994.

Cowperthwaite, N (1986) : *An investigation of the effect of rear body pitch on aerodynamic characteristics of a simplified tractor - trailer model,* Journal of Wind Engineering and Industrial Aerodynamics, 22, 2-3, 215-226.

Dominy, R.G. and Docton, M.K.R. (1994) *Passenger vehicles in unsteady cross winds,* Proceedings RAeS Conference on Vehicle Aerodynamics, Loughborough, 1994.

E.S.D.U. (1974a) : *Characteristics of wind speed in the lower layers of the atmosphere near the ground: strong winds (neutral atmosphere).* Engineering Science Data Unit item 72026.

E.S.D.U. (1974b) : *Characteristics of atmospheric turbulence near the ground. Part 2: Single point data for strong winds.* Engineering Science Data Unit item 74031.

E.S.D.U. (1975) : *Characteristics of atmospheric turbulence near the ground. Part 3: Variations in space and time for strong winds.* Engineering Science Data Unit item 75001.

E.S.D.U. (1980) : *Blockage corrections for bluff bodies in confined flows.* Engineering Science Data Unit item 80024.

E.S.D.U. (1982) : *Strong winds in the atmospheric boundary layer, part 1: Mean hourly wind speeds,* Engineering Science Data Unit item 82026.

Flay, R.G.J. (1978) : *Structure of a rural atmospheric boundary layer near the ground,* Ph.D. Thesis, University of Canterbury, Christchurch, New Zealand, 1978.

Garry, K.P. (1984) : *Private communication to C.J. Baker.*

Garry, K.P. and Cooper, K.R. (1986) : *Comparison of quasi-static and dynamic wind tunnel measurements on simplified tractor-trailer models,* Journal of Wind Engineering and Industrial Aerodynamics, *22, 185-194.*

Garry, K.P., Macklin, A.R. and van Opstal, E.P.E. (1994) : *Measurement of transient aerodynamic loads on bluff bodies at extreme yaw angles,* Proceedings RAeS Conference on Vehicle Aerodynamics, Loughborough, 1994.

Good, G.M.le (1994) : *Passenger car wind tunnel testing: The correlation of 1/4 scale model to full scale results,* Proceedings RAeS Conference on Vehicle Aerodynamics, Loughborough, 1994.

Greenway, M. (1979) : *An analytic approach to wind velocity gust factor,* Journal of Industrial Aerodynamics 5, 61-91.

Harrison, D. (1982) : *The Cranfield moving model experiment, part 1. Experimental apparatus & procedure.* British Rail Research and Development Division Technical Memorandum, TMAERO 51.

van der Hoven, I (1957) : *Power spectrum of horizontal wind speed in the frequency range from 0.0007 to 90Hz,* Journal of Meteorology, 14, 160, 1957.

Howell, J. (1986) : *Aerodynamic response of maglev train models to a cross wind gust.* Journal of Wind Engineering and Industrial Aerodynamics 22, 205 - 231.

Hoxey, R.P. and Richards, P.J. (1992) : *Structure of the atmospheric boundary layer below 25m and implications to wind loading on low rise buildings.* Journal of Wind Engineering and Industrial Aerodynamics 41-44.

Humphreys, N.D. (1990) : *Initial studies of the atmospheric boundary layer simulation for the British Rail moving model rig installed in the University of Nottingham Environmental Wind Tunnel.* University of Nottingham, Dept of Civil Engineering Report No FR90024.

Johnson, R. (1981) : *The Cranfield moving model equipment, part II : atmospheric boundary layer simulation.* Technical Report of the Environmental Aerodynamics Group, College of Aeronautics, Cranfield Institute of Technology.

Johnson, T. (1978) : *A brief survey of digital filtering techniques,* British Rail Research and Development Division. Dynamics Group Internal Memorandum, IMAERO 104.

King, D.M. (1994) : *Wind \ Wave Interactions in the Surf Zone,* Ph.D. Thesis, University of Nottingham, 1994.

Kronke, I. and Sockel, H. (1992) : *Model tests about cross wind effects on containers and wagons in atmospheric boundary layers,* Proceedings 1st Wind Engineering Conference, Cambridge 1992, also Journal of Wind Engineering and Industrial Aerodynamics 52 (1994), 109-119.

Lappe, U.O. and Davidson, B. (1963) : *On the range of validity of Taylor's hypothesis and the Kolmogoroff spectral law,* Journal of Atmospheric Science, 20, 569-576.

Lieblein (1974) : *Efficient methods of extreme value methodology.* Report NBSIR 74-602, Washington National Bureau of Standards.

Peters, J. L. (1989) : *Bestimmung der wind - und geschwindigkeits - grenzen fur containertransport auf rungenwagen durch Messungen im DNW windkanal,* Krauss Maffei report, 1989.

Peters, J. L. (1992) : *Effect of Reynolds number on the aerodynamic forces on a container model.* Proceedings 2nd Conference on Bluff Body Aerodynamics and its Applications, Melbourne 1992, also Journal of Wind Engineering and Industrial Aerodynamics 49 (1993), 431-438.

Rigby, P. (1973) : *Overturning moment studies for APT-E,* British Rail Research and Development Division Technical Memorandum IMAERO 32.

Robinson, C.G. (1987) : *The effect of atmospheric turbulence on trains,* PhD Thesis, University of Nottingham.

Schlichting, H. (1968) : *Boundary Layer Theory. 6th Edition,* McGraw - Hill.

Stewart, M.J. (1977) : *Transient aerodynamic forces on simple road vehicle shapes in simulated cross-wind gusts.* MIRA Report 77/5.

Tieleman, H and Atkins, R. (1989) : *Effects of incident turbulence on pressure distributions on rectangular prisms,* (ed. A. Kareem), Proceedings of the 6th US Wind Engineering Conference, Houston 1989.

Vickery, B.J. (1965) : *On the flow behind a coarse grid and its use as a simulation of atmospheric turbulence in studies relating to wind loads on buildings,* National Physical Laboratory Aero Report 1143.

Vickery, B.J. (1966) : *Fluctuating lift and drag on a cylinder in a smooth and turbulent flow*, Journal of Fluid Mechanics, 25 -3, 481-494.

Wills, J.A.B. (1991) : *Data Sampling and Data Recovery*, Experiments in Fluids, 12, 23-28.

Yang, X. (1990) : *Private Communication.*

Appendix 1. Data Analysis Programs and Files.

This appendix gives details of the programs written by the author used for the analysis of the data shown in this thesis. All programs were written in PROSPERO FORTRAN for use on IBM compatible PCs. Additionally many were modified for use on the Nottingham University Cripps Computing Centre VME mainframe and these versions were modified to use standard NAGRA library subroutines and the appropriate control language for user and file interface. The use of both sets of programs operate in a similar manner, with common input and output formats. All programs, unless stated, use files containing ASCII characters with the 'space' acting as the delimiter. Both formatted and unformatted files are used. Chapter 5 details the methods used in these programs. The programs are listed according to their application with many designed to be run in this order.

For both the static and the moving model tests a common procedure was used for the recording of the raw test data and its subsequent storage for further processing. These files used the .TBL and .RAW format given in section A.1.4

The raw data was obtained in the format of a .TBL file direct from Polytools, the PC software package for programming and downloading of data to / from the Polycorder data logger. The final processed data, for each individual test, was stored in the format of a .RAW file for which further data analysis programs use. These files include full details of the test conditions as well as the extracted raw data corresponding to the test section. Mean forces and moments are also stored in this file.

A.1.1. Wind analysis programs.

MEANWIND.

Calculates the mean wind speed and turbulence intensity using the method of 5.2.1.1.

User Input: Ambient temperature and pressure.

File Input: .TBL containing linearised voltage output from TSI hot film anemometer (1 channel only).

Program defined values: Hot film anemometer calibration coefficients A and B as defined in section 5.2.1.1.

Output to screen: mean wind speed and turbulence intensity.

SPLITDAT.

Splits one file into a user defined number of equal length shorter files. Used for creating a set of file for spectral analysis which will be subsequently used for creating average spectra.

User Input: Number of files to be created, total number of data in original file and sample frequency.

File Input: As MEANWIND.

Output to user defined files: Number of data in file, sample frequency and data.

CALCSPEC.

Calculates non dimensional spectral density using method of section 5.1.3. Can be used with files output from SPLITDAT.

File Input: Output files from SPLITDAT.

File Output: Frequency and non dimensional spectra.

This program was also used for calculating the force spectra.

MEANSPEC.

Calculates the mean of spectra created by CALCSPEC and also if requested the corresponding von Karman spectra.

User input: Number of files to be input, each containing one spectra. If von Karman spectra requested then supply model scale height and wind velocity corresponding to wind velocity measurement height.

File input: Output files from CALCSPEC.

File output: Frequency, mean non dimensional spectra and von Karman spectra.

CONVSPEC.

Creates file identical to that input but using ',' as the delimiter between the columns of data suitable for reading by Microsoft EXCEL and subsequent plotting.

File input: Output file from CALCSPEC.

File output: Identical to input but using ',' as delimiter between columns.

WINDEVAL.

Divides a set of input data into a number of blocks and calculates gust values according to the user defined model time period of the gust. The maximum gust from each block is output. See section 5.1.5 and 5.2.1.3.

User input: Number of data per gust, Number of blocks to be calculated. (These together imply a model time period for a gust).

File Input: As for MEANWIND.

Output to screen: Mean wind speeds for each block and the maximum gust value, for the implied time period, for each block.

WINDMODE.

Calculates the Mode and Dispersion of 10 extreme values using Leiblien's method, see section 5.1.5 and 5.2.1.3, for the time period corresponding to one block of data. The mode for 1 hour is extrapolated and output.

User input: The 10 gust values corresponding to the maximum from each block, and the model time period corresponding to one block.

Output to screen: The mode corresponding to the full scale time period of one block of data, the dispersion and the full scale hourly mode.

A.1.2 Static force analysis programs.

STATCOEF.

Calculates the 5 mean force and moment coefficients and the non dimensional points of action using the definitions and methods of 5.2 and 5.2.2.2.1

User input: Reference wind speed, ambient temperature and pressure.

File input: .TBL file containing 5 channels of data from the amplifier and force balance in multiplex format (as measured), see A.1.4

Program defined values: Force balance calibration matrix, vehicle reference area and reference height. Relative position of centre of rotation relative to balance centre. (For the lorry this is the centre of mass and for the DB container this is the lee bottom corner).

Output to screen : Mean force and moment coefficients (about the centre of the balance and the centre of rotation) and non dimensional points of action.

SPROCESS.

Reads one .TBL file containing 5 channels of data from the amplifier and force balance in multiplex format. The data is saved in a .RAW file with other relevant test ancillary data input by the user including zero force corrections. Additionally some preliminary analysis is conducted and the results also saved. The output form of the .RAW file is identical to that produced by the program MPROCESS which performs a similar pre processing task for the moving model data.

User input: Reference wind speed, ambient temperature and pressure.

File input: .TBL file.

Program defined values: Force balance calibration matrix, vehicle reference area and reference height. Relative position of centre of rotation relative to balance centre.

File out: .RAW file.

STATEVAL.

As WINDEVAL but for 2 channels.

File input: .RAW file containing two channels of force data.

Output to screen: Mean force values and the normalised extreme force parameters for the implied time period, for each block.

STATMODE.

As WINDMODE but for two channels. (Only side and lift force usually required). Additionally calculates the unsteady parameters.

A.1.3 Moving force analysis programs.

MPROCESS.

Reads one .TBL file containing 5 channels of data from the amplifier and force balance in multiplex format and one continuous digital channel corresponding to the trigger channel (as measured). All channels are shown on the screen as shown in figure 5.4.

The data from the central 1.5m test section is extracted, zero values are calculated from the data at the end of the run and saved in a .RAW file with other relevant test ancillary data. Additionally some preliminary analysis is conducted and the results also saved.

User input: Reference wind speed, ambient temperature and pressure. Also user selects the window of data for which the aerodynamic data and zero force and moment calibration are subsequently extracted. The aerodynamic data then automatically extracted from this window, one it has been checked visually, by reference to the markers present in the digital channel.

File input: .TBL file.

Program defined values: Force balance calibration matrix, vehicle reference area and reference height. Relative position of centre of rotation relative to balance centre. (For the lorry this is the centre of mass and for the DB container this is the lee bottom corner).

Screen output : All recorded data (5 channels and 1 digital channel).

File output: .RAW file.

CALC1.

This calculates mean and extreme parameters from an ensemble of .raw files input into this program using the method of 5.2.2.3.1.

User input: Number of files, extreme / mean wind speed for model time period corresponding to trolley transit time across the 1.5m test section.

File input: ensemble of .RAW files.

Output to screen: mean yaw angle, wind speed, extreme wind speed, average trolley speed, mean trolley transit time, overall mean force and moment coefficients (about the balance centre and the centre of rotation), standard deviation of these mean coefficients, standard deviation of the zero coefficient values, extreme force coefficients, non dimensional unsteady force parameters.

TIMEHIST.

This program is a developed version of CALC1 and additionally:

a) Filters the raw data to remove high frequency mechanical noise using the method of 5.1.4.

b) As the files are read in to the program the zeros for each channel are compared

c) Extremes are formed integral portions of the extracted data corresponding to the test section. This is in order to investigate the effect of changing the model time scale on the calculated extreme values.

d) Provides additional mean zero corrections due to mechanical noise described in section 9.1 which is a function of trolley speed.

e) Outputs to user specified files the overall averaged filtered time histories of for each force and moment channel.

f) Outputs to user specified files the overall averaged force and moment spectra formed from each channel.

A.1.4 File Formats.

These files are used extensively in the transfer and storage of data.

The .TBL files are created by the Polytools (Polycorder software) program after downloading the data from the Polycorder.

The .Raw files are intended as a permanent record of the test data. These files include the processed force and moment data corresponding to the test section, all calibrations used and other test conditions.

<u>.TBL File Format (e.g. 5 analogue and 1 digital channels).</u>

TIME(1)	CH1(1)			DIGITAL(1)
TIME(2)		CH2(1)		DIGITAL(2)
TIME(3)			CH3(1)	DIGITAL(3)
TIME(4)			CH4(1)	DIGITAL(4)
TIME(5)				CH5(1) DIGITAL(5)
TIME(6)	CH1(2)			DIGITAL(6)
TIME(7)		CH2(2)		DIGITAL(7)
TIME(8)			CH3(2)	DIGITAL(8)

Notes. TIME corresponds to the inter channel sampling frequency. CH1 to CH5 represent the data digitised by the multiplex sampling of the strain gauge balance and DIGITAL is the continuously sampled digital channel used for control of the logger, and marking the position of the data record relative to the track.

.RAW File Format.

NDATA AVESPEED SAMPFREQ WINDVEL AREF

TAMB PAMB REFHT XREF ZREF

A(1,1) A(2,2) A(3,3) A(4,4) A(5,5)

CH1(1), CH1(2), CH1(3), CH1(4), CH1(5), CH1(6) ----------

CH2(1), CH2(2), CH2(3), CH2(4), CH2(5), CH2(6) ----------

CH3(1), CH3(2), CH3(3), CH3(4), CH3(5), CH3(6) ----------

CH4(1), CH4(2), CH4(3), CH4(4), CH4(5), CH4(6) ----------

CH5(1), CH5(2), CH5(3), CH5(4), CH5(5), CH5(6) ----------

RHO

AVEDATA (1 TO 5)

AVEZERO (1 TO 5)

RMEANCOEF (1 TO 8)

ZEROCOEF (1 TO 8)

Notes. This file may be considered to consist of two sections. The first section stores the test data, reference wind and ambient conditions. Also included are the main balance calibration factors so that the original calibration may be traced. The second section stores the calculated values from this input data.

Input data :

NDATA is the number of data. AVESPEED is the mean speed of the trolley. SAMPFREQ is the sample frequency of the recorded data. WINDVEL is the reference wind velocity and PAMB and TAMB are the ambient pressure and temperature. AREF and REFHT are the reference area and reference height of the vehicle. XREF and ZREF are the co-ordinates of the centre of rotation of the vehicle relative to the balance centre. A(1,1) to A(5,5) give the diagonal (main) calibration factors of the force balance. CH1 to CH5 list the extracted data for each channel corresponding to the test section.

Calculated values :

RHO is the density of the air. AVEDATA gives the mean measured values for each recorded channel. AVEZERO gives the corresponding zero values previously calculated from the end of each run. RMEANCOEF gives the calibrated mean forces and moments (about the centre of the balance and the centre of rotation). ZEROCOEF gives the corresponding calibrated zeros of the mean forces and moments from the data previously calculated at the end of each run.